

STAR 14 MAY 21 1985

NASA Conference Publication 2373

Eng # 17081

Thirteenth NASTRAN[®] Users' Colloquium

(NASA-CP-2373) THIRTEENTH NASTRAN USERS'
COLLOQUIUM (Computer Software Management and
Informatics) 469 p HC \$20/EF \$01; also
available from COSMIC, CSCI 20K

NS5-25663
THEU
NS5-25891
Unclas

C3/39 17081

*Proceedings of a colloquium held in
Boston, Massachusetts
May 6-10, 1985*

NASA

NASA Conference Publication 2373

Thirteenth NASTRAN[®] Users' Colloquium

Proceedings of a colloquium held in
Boston, Massachusetts
May 6-10, 1985

NASA
National Aeronautics
and Space Administration
Scientific and Technical
Information Branch

1985

FOREWORD

NASTRAN® (NASA STRUCTURAL ANALYSIS) is a large, comprehensive, nonproprietary, general purpose finite element computer code for structural analysis which was developed under NASA sponsorship and became available to the public in late 1970. It can be obtained through COSMIC® (Computer Software Management and Information Center), Athens, Georgia, and is widely used by NASA, other government agencies, and industry.

NASA currently provides continuing maintenance of NASTRAN through COSMIC. Because of the widespread interest in NASTRAN, and finite element methods in general, the Thirteenth NASTRAN Users' Colloquium was organized and held at the Back Bay Hilton Hotel, Boston, Massachusetts, May 6-10, 1985. (Papers from previous colloquia held in 1971, 1972, 1973, 1975, 1977, 1978, 1979, 1980, 1982 and 1983, are published in NASA Technical Memorandums X-2378, X-2637, X-2378, X-2893, X-3278, X-3428, and NASA Conference Publications 2018, 2062, 2131, 2151, 2249, 2284 and 2328.) The Thirteenth Colloquium provides some comprehensive general papers on the application of finite element methods in engineering, comparisons with other approaches, unique applications, pre- and post-processing or auxiliary programs, and new methods of analysis with NASTRAN.

Individuals actively engaged in the use of finite elements or NASTRAN were invited to prepare papers for presentation at the Colloquium. These papers are included in this volume. No editorial review was provided by NASA or COSMIC; however, detailed instructions were provided each author to achieve reasonably consistent paper format and content. The opinions and data presented are the sole responsibility of the authors and their respective organizations.

NASTRAN® and COSMIC® are registered trademarks of the National Aeronautics and Space Administration.

CONTENTS

	Page
FOREWORD	iii
1. NEW ENHANCEMENTS IN APRIL 85 NASTRAN RELEASE	1
by Gordon C. Chan (Sperry Systems Management Group)	
2. IMPROVED ACCURACY IN SOLID ISOPARAMETRIC ELEMENTS USING SELECTIVELY REDUCED INTEGRATION (abstract only)	31
by W. R. Case, R. S. Mitchell and R. E. Vandegrift (NASA/Goddard Space Flight Center)	
3. CRACK ELEMENTS FOR COSMIC/NASTRAN	32
by P. J. Woytowicz and R. L. Citerley (Anamet Laboratories, Inc.)	
4. A FOUR-NODE BILINEAR ISOPARAMETRIC ELEMENT IN ROCKWELL NASTRAN	47
by C. Liao and R. E. Allison (Rockwell International)	
5. LAYERED COMPOSITE ANALYSIS CAPABILITY FOR NASTRAN	67
by R. (Swami) Narayanaswami and J. G. Cole (Computerized Structural Analysis and Research Corporation)	
6. NPLOT: AN INTERACTIVE PLOTTING PROGRAM FOR NASTRAN FINITE ELEMENT MODELS	110
by Gary K. Jones and Kelly J. McEntire (NASA/Goddard Space Flight Center)	
7. CGSMIC/NASTRAN - PATRAN INTERFACE	133
by Daron H. Libby (PDA Engineering)	
8. TWO INTERACTIVE GRAPHICS POSTPROCESSORS FOR NASTRAN	152
by Robert R. Lipman (David W. Taylor Naval Ship R&D Center)	
9. AN UNUSUAL APPLICATION OF NASTRAN CONTOUR PLOTTING CAPABILITY	164
by S. Mittal, M. Gallo and T. Wang (Bell Aerospace Textron)	
10. ISOPARAMETRIC 3-D FINITE ELEMENT MESH GENERATION USING INTERACTIVE COMPUTER GRAPHICS	172
by Cuneyd Kayrak and Tulga Ozsoy (Lehigh University)	
11. A NEW NASTRAN CAPABILITY FOR DATA REDUCTION	177
by Michael Gallo and S. Mittal (Bell Aerospace Textron)	

	Page
12. AUTOMATIC DYNAMIC AIRCRAFT MODELER (ADAM) FOR THE COMPUTER PROGRAM NASTRAN	188
by Hugh Griffis (Wright-Patterson Air Force Base)	
13. CADS - A COMPUTER AIDED DESIGN SYSTEM	199
by Victoria A. Tischler and Elizabeth M. Copenhaver (Wright-Patterson Air Force Base) and Michael C. Less and Susan Manuel (Rockwell International)	
14. RITZ PROCEDURE FOR COSMIC/NASTRAN	225
by R. I. Citerley and F. J. Woytcowitz (Anamet Laboratories, Inc.)	
15. SYMMETRIC COMPOSITE LAMINATE STRESS ANALYSIS	234
by T. Wang, K. F. Smolinski and S. Gellin (Bell Aerospace Textron)	
16. ON THE INTERCONNECTION OF INCOMPATIBLE SOLID FINITE ELEMENT MESHES USING MULTIPOINT CONSTRAINTS	245
by Gary L. Fox (Hughes Drilling Equipment)	
17. NASTRAN'S APPLICATION IN AGRICULTURAL ENGINEERING TEACHING AND RESEARCH	273
by Garrett L. Van Wicklen (University of Georgia)	
18. USE OF COSMIC NASTRAN IN A DESIGN DEPARTMENT	289
by Richard C. Coddington and Jose O. Nazario (John Deere Lubuque Works)	
19. AN ELASTIC ANALYSIS OF A PLATED BONE TO DETERMINE FRACTURE GAP MOTION	308
by Francis W. Cooke and William H. Vannah (Clemson University)	
20. LEARJET MODEL 55 WING ANALYSIS WITH LANDING LOADS	320
by Robert R. Boroughs (Gates Learjet Corporation)	
21. FILLET WELD STRESS USING FINITE ELEMENT METHODS	341
by Terry F. Lehnhoff and Gerald W. Green (University of Missouri-Rolla)	
22. THE STRUCTURAL FINITE ELEMENT MODEL OF THE C-5A	364
by Gisela W. McClellan (Lockheed-Georgia Company)	
23. USING NASTRAN TO MODEL MISSILE INERTIA LOADS (abstract only)	377
by Ron Marvin and Craig Porter (Naval Weapons Center)	

	Page
24. EXPERIENCE WITH FREE BODIES	378
by T. C. Butler (Butler Analyses)	
25. NASTRAN ANALYSIS COMPARISON TO SHOCK TUBE TESTS USED TO SIMULATE NUCLEAR OVERPRESSURES	389
by T. K. Wheless (Wright-Patterson Air Force Base)	
26. FINITE ELEMENT PREDICTION OF LOSS FACTORS FOR STRUCTURES WITH FREQUENCY-DEPENDENT DAMPING TREATMENTS	419
by Gordon C. Everstine and Melvyn S. Marcus (David W. Taylor Naval Ship R&D Center)	
27. DIRECT TRANSIENT ANALYSIS OF A FUZE ASSEMBLY BY AXISYMMETRIC SOLID ELEMENTS	431
by Chung C. Dai and Jackson C. S. Yang (Advanced Technology and Research, Inc.) and John Titus (Harry Diamond Laboratory)	
28. TRANSIENT ANALYSIS OF A MAGNETIC HEAT PUMP	453
by Erwin A. Schroeder (David W. Taylor Naval R&D Center)	

N85-25864

NEW ENHANCEMENTS IN APRIL 85 NASTRAN RELEASE

by Gordon C. Chan
Sperry Systems Management Group
Huntsville, Alabama

INTRODUCTION

Several new features have been added to COSMIC NASTRAN, along with some enhancements to improve or update existing capabilities. Most of the new features and enhancements were not developed by COSMIC; they have been provided by industry users to be incorporated into NASTRAN for wider use. The major new features and enhancements are discussed here.

NEW FEATURES

1. DIAG 48

DIAG 48 has been added to provide a synopsis of the significant developments in the past NASTRAN releases (April 83, April 84, and April 85) and to provide an index listing of all Diagnostic Output Messages and Operation Requests (DOMOR). The synopsis provides a timely communication between COSMIC NASTRAN and its users, and keeps the latter better informed. The synopsis also indicates references where additional materials can be found. The diagnostic index listing gives users complete, accurate, and up-to-date information about Diagnostic Requests currently available. The DOMOR is also listed in the Users' Manual, but the manual is infrequently updated. Therefore, if there is any discrepancy between the two sources, the listing from DIAG 48 should be used.

DIAG 48 will be updated in each future NASTRAN release.

2. VOLUME AND SURFACE COMPUTATION OF THE 2-D AND 3-D ELEMENTS

The volumes and the surface areas of the 2-dimensional and 3-dimensional elements can be requested for output by the PARAM card, as follows:

PARAM VOLUME m
PARAM SURFACE n

where m and n are scale factors, greater than zero. The calculations are actually done in the Element Matrix Generation (EMG) module, with the results tabulated and printed before the termination of the module.

In the April 85 NASTRAN release, the EMG module has been expanded to include one more output data block such that the element ID's volumes, surface areas and associated grid points and their coordinates can be saved. This new output data block can be a GINO written file, to be used internally within the NASTRAN system, or a FORTRAN binary file, intended for external use. The contents of this output data block, the choice of GINO or FORTRAN file, and the definitions of the surface areas are presented in Appendix A, pages 2.4-222 and 2.4.222b.

3. NOLIN5 INPUT CARD

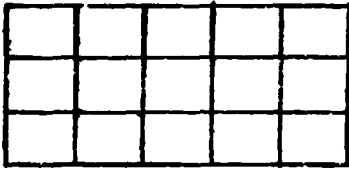
A new non-linear load, NOLIN5, has been added to the family of NOLINi bulkdata cards. The first four (NOLIN1 through NOLIN4) are applications of the non-linear loads as functions of the displacement, and they are described in the User's manual. The new NOLIN5 card offers non-linear load as a function of both displacement and velocity; thus allowing wider application of the non-linear load including damping. See Appendix A, pages 2.4-205a and 2.4-205b, for the formulation and specification of this new load.

4. NASTRAN PLOTOPT=N (where N=2,3,4 or 5)

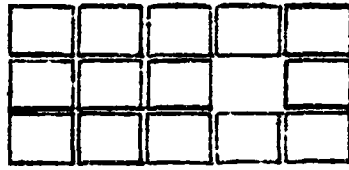
The undeformed plot of a NASTRAN model is particularly useful in pre-analysis structure checking. However, in all previous NASTRAN releases, such a plot can be obtained only if there is no error in the input deck. A missing material card, for example, which is practically not needed in plotting, would terminate a NASTRAN run. A new Plot Option has been added to the NASTRAN card in the April 85 release. The new NASTRAN PLOTOPT has a default value of zero (N=0) if there is no plot tape assigned in a NASTRAN job, or one (N=1), if a plot tape has been assigned. The other options (N=2 through 5) can be used for various error conditions in the Bulk Data and in plot commands as indicated in the Appendix A, page 2.1-5.

5. SHRINK-ELEMENT PLOTS

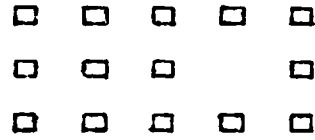
A new Shrink-Element option has been added to the plotting capability. The user can specify that all elements in a plot are to "shrink in place" by a given percentage. This option should be very useful in pre-analysis structure checking, or in graphic presentation of the structure model. The following diagrams illustrate the use of Shrink-Element plotting. The model is a simple panel, supposedly made up of 15 CQUAD1 elements. The plot on the left side is a NASTRAN regular plot. The plot on the right side clearly shows a missing element. The middle plot can be used in model presentation; it gives a better definition of the connecting elements. The command for Shrink-Element plots is included in Appendix A, pages 4.2-25, 4.2-29 through 4.2-31.



NASTRAN Regular Plot



Shrink-Element plot (SHRINK=.90)



Shrink-Element Plot (Shrink=.35)

6. OUTPUT SCAN

A new output SCAN feature has been added to NASTRAN. This is a major contribution to the April 85 release, and can significantly reduce the amount of output that an analyst must review. Using this SCAN feature, the user can indicate only the top "n" (and bottom "n") values, or values above "x" (or below "y") of stresses and/or forces which are to be printed. The user can also request SCAN on any element SET, in any SUBCASE, SUBCOM, or in the master set (i.e. above all subcases). Both SORT1 and SORT2 types of data blocks can be scanned. Any number of the SCAN cards can be used in a NASTRAN job, and are placed in the Case Control section of the Bulk Data. A SCAN request in the Master Set is common to all Subcases. However, unlike the ELSTRESS or ELFORCE cards, a SCAN request in a Subcase level will not override a SCAN request in the Master Set. The final results are sorted and printed in a descending order. The description of the SCAN input card is presented in Appendix A, pages 2.3-41a through 2.3-41f.

The Output Scan operation is driven by a new SCAN module which has the following DMAP specification:

```
SCAN CASECC,OESi,OEF1/OESF1/C,N,ELEMENT/C,N,COMPONENT/C,N,TOPN/
C,N,MAX/C,N,MIN/C,N,LCS1/C,N,LCS2/C,N,COMPONENTX $
```

where:

i = 1 (for SORT1 output data blocks), or 2 (SORT2 data),
ELEMENT is an element BCD name,
COMPONENT is a coded word whose bit(s) is set to correspond to the field number(s) (1 through 31) of the output page whose values are to be scanned,
TOPN is the number of "top" and "bottom" values to be printed,
MAX,MIN define a range of values; values outside this range only are printed,
LCS1,LCS2 are the beginning and ending element ID's to be scanned (SORT1); or SUBCASE ID's (SORT2),
COMPONENTX is same as COMPONENT, except for field number(s) 32 through 62.

The SCAN module has been incorporated in all WASTRAN rigid formats. Since the SCAN input card in the Case Control section has been decoded by the Input File processor (IFP), and all useful information stored in the CASECC data block, the DMAP for SCAN in the rigid format takes on a simpler form, with most of the parameters not needed:

```
SCAN CASECC,OESi,OEf1/OESF1/C,N,*RF* $
```

On the other hand, if the SCAN module is called by the user via DMAP-alter, and no SCAN input card is used in the Bulk Data (therefore no SCAN data saved in CASECC), the following form should be used for a "stress-Scan":

```
SCAN, ,OESi,/OESX/C,N,ELEMENT/C,N,COMPONENT/C,N,TOPN/  
C,N,MAX/C,N,MIN/C,N,LSC1/C,N,LSC2/C,N,COMPONENTX $
```

and for a "force-SCAN":

```
SCAN, ,,OEf1/OEFX/C,N,ELEMENT/C,N,COMPONENT/C,N,TOPN/  
C,N,MAX/C,N,MIN/C,N,LSC1/C,N,LSC2/C,N,COMPONENTX $
```

Normally, the Output File Processor (OFP) should be called immediately to print the scanned data in OESX, or OEFX.

The SCAN module actually re-processes the data blocks originally generated for the OFP - e.g. the stress data block OESi, and force data block OEf1. It is obvious then that SCAN cannot operate on data which has not been generated. For example, if the stresses for elements 1 through 100 were requested to be output from an ELSTRESS card, a SCAN request for elements 101 through 200 would produce zero values (not a fatal error condition). It is also obvious that there is a need for a NOPRINT option in the STRESS and FORCE request cards to eliminate massive output printing and make SCAN much more useful. See the NOPRINT option described below for more details.

In a special case where the user requests SCAN on the element stresses, and there is no ELSTRESS (or STRESS) card in the Case Control deck, the IFP module would automatically generate internally a STRESS input card with the following arguments:

```
ELSTRESS (SORT1,NOPRINT,REAL) = ALL
```

Similar, an ELFORCE card would be generated.

Currently SCAN handles only the stress and force output data blocks. It is possible in the near future that other output data blocks, such as displacement, velocity, PSD, etc., might be included in the Scan Operation.

IMPROVEMENTS

1. NOPRINT OPTION ON STRESS AND FORCE OUTPUT REQUEST CARDS

A new NOPRINT option has been added to the output request PRINT or PUNCH of the STRESS (or ELSTRESS) and FORCE (or ELFORCE) cards. This new option allows NASTRAN to compute, save data in the output data block, and not to print (by OFF). This is not the same option as NONE, which instructs NASTRAN to skip over stress or force computation and not to write an output data block. The new NOPRINT option is particularly useful in the SCAN and PLOT operations, where the user can compute without massive printout all of the element stresses or forces and have the results scanned, and/or plotted. See the update pages in Appendix A, pages 2.3-17 and 2.3-18.

2. AUTOMATED FIND AND NOFIND OPTIONS ON THE PLOT CARD

The April 85 NASTRAN release will provide an automatic FIND for plot SCALE, ORIGIN, and VANTAGE POINT. Thus, for each PLOT SET n command, the scale will be determined such that the elements in SET n will fill the image area of a plot. This automatic option can be disabled by the NOFIND keyword on the PLOT command. The PLOT NOFIND will produce an image using the immediately preceding SCALE, ORIGIN, and VANTAGE POINT. See the update pages in Appendix A, pages 4.2-25, 4.2-29 through 4.2-31.

3. IMPROVED FULLY-STRESSED DESIGN

TRIM6, QDMEM1, QDMEM2, and IS2D8 have been added to the element list that can be included in the fully-stressed design computation and iteration process.

Previously, the fully stressed design process altered the element properties by use of a linear ratio of calculated stress to the allowable stress. That is, in the case of a BAR or ROD element, the cross sectional area was changed to force the applied stress to equal the allowable stress. This process could yield non-convergent results for a case of pure bending of the QUAD2 element, where the altered property is the thickness. In the April 85 release, the program has been changed to provide more rapid convergence that includes the situation of equal stresses of opposite sign, on upper and lower extreme fibers of the plate elements. This improved process is only active if the user does not specify a value for the iteration factor gamma on the POPT card.

4. HIGH-LEVEL PLATE ELEMENTS

The thickness calculations of the triangle for the high-level

elements (TRIM6, TRPLT1, and TRSHL) are presented in the Theoretical Manual, page 5.8-45, equations 16 and 17 and in the Programmer's Manual, page 8.24-6, equations 35 and 37. These simple equations were evaluated incorrectly in the manuals, and the results were repeatedly used in these high-level element formulations. Equation 28 of the Theoretical Manual, page 8.24-8 is also incorrect, where (-b) should be (b). This may partially explain why these elements never produced good answers in the past. In addition, the Grid Point Weight-and-Balance tables verified the fact that the consistent mass matrices of these high-level elements gave extremely bad results. These errors have been corrected in the April 85 release for the calculations in stiffness matrices, thermal loads, and stress recoveries, and the consistent mass matrices have been replaced by the lumped mass formulation; these high-level plate elements begin to yield reasonable results. It is hoped that the consistent mass matrices will be corrected in the near future.

5. EIGENVALUE MESSAGES

The real eigenvalue extraction procedures have been enhanced by including an automatic matrix topology analysis, and by the addition of user information messages. During the matrix decomposition of the dynamic matrix, the leading principal minors in the Sturm's sequence are counted each time the sign changes. This, in turn, indicates the number of roots below the eigenvalue shift-point, a property of the Sturm's sequence. The importance of this information is then translated into useful messages and provides for a more complete evaluation of the eigenvalue results. The messages (#3307, #3308, and #3309) indicate whether or not the lowest eigenvalue has been found, or if there is a missing mode in the frequency range the user specified. However, occasionally no conclusive message can be issued due to lack of basic information during the decomposition process.

The printout of these messages can be suppressed by the use of DIAG 43.

6. ANSI 77 FORTRAN CODE

All FORTRAN source code of COSMIC NASTRAN has been upgraded to the ANSI 77 standard. This began with the UNIVAC ASCII version of NASTRAN in the April 84 release. (The UNIVAC FORTRAN V version is no longer supported.) In this new April 85 release, the CDC version of NASTRAN is upgraded from FORTRAN 4 to the FORTRAN 5, a subset of ANSI 77 FORTRAN. Previously, the VAX version required many custom changes; especially in the source code that handles character-word (byte) manipulation. A set of character-word functions is standardized in the ANSI 77 source code, such that all four machines (CDC, IBM, UNIVAC, and VAX) will operate identically. In addition, the labeled commons that carry the open-core working space in all ANSI 77 FORTRAN source code have been standardized, so that the NASTRAN 15 links are similar

structured in all four machines. At present, only a very few routines remain machine-dependent.

CONCLUSION

The input card descriptions for the new features SCAN, NOLIN5, Shrink-Element Plot, FIND, and NOFIND, VOLUME, SURFACE are presented in Appendix A. The pages in this appendix are written in KASTRAN Users' Manual format, so that they can be copied and moved directly into the users' own manual for future reference. The page numbers at the bottoms of these pages indicate where they should be inserted in the NASTRAN Users' Manual as published in September 1983.

APPENDIX A

**A Collection of NASTRAW User's
Manual Update Pages**

THE NASTRAN CARD

2 (default)	Print two copies of the full title page.
3	Print a one-line comment (which can be modified by the user by updating subroutine TTLPGE) followed by the short title items on the same page.
4	Read <u>another card immediately following</u> the NASTRAN card, print its contents on one line and follow it by the short title items on the same page.
>4	Do not print any title page (same as TITLEPT = 0).
-2	(UNIVAC only) Print a short title page and suppress the alternate logfile assignment which is not allowed in real-time environment.

As can be seen, when TITLEPT = 4 is specified on the NASTRAN card, the user must supply another card immediately following the NASTRAN card to be read by the program. The user can therefore utilize this feature to print one-line individual comments (along with the short title) for individual runs.

22. PLOTPT - defines the action to be taken by NASTRAN in the case where plottings are requested and error(s) exists in Bulkdata. The default is zero (PLOTPT = 0) only if there is no plot tape assigned in a NASTRAN job, or one (PLOTPT = 1) if plot tape has been assigned. The plot option (0 through 5) are listed below:

PLOTPT	BULKDATA	PLOT COMMANDS	NASTRAN ACTION
N=0	no error	no error	executes all links, no plots
	error	error	stops after link1 data check
N=1	error	err or no err	stops after link1 data check
	no error	no error	executes all links, and plots
N=2	error	error	stops after link1 data check
	no error	err or no err	stops after link1 data check
N=3	err or no err	no error	stops after undef. plots in link2
	err or no err	error	stops after link1 data check
N=4	err or no err	err or no err	attempts to plot; stops in link2
	no error	no error	executes all links, and plots
N=5	no error	error	attempts to plot; stops in link2
	error	no error	stops after undef. plots in link2
N=6	error	error	stops after link1 data check

2.1-5 (4/30/85)

NASTRAN DATA DECK

N=5	no error	no error	executes all links, and plots
	no error	error	executes all links, but no plots
	error	no error	stops after undef. plots in link2
	error	error	stops after link1 data check

Examples

Following are some examples of the use of the NASTRAN card.

Example 1

NASTRAN BUFFSIZE = 900, SYSTEM(2) = 3, CONFIG = 3

The above card changes the 1st, 2nd and 28th words of /SYSTEM/. SYSTEM(2) = 3 changes the system output unit from 6 (default) to 3.

Example 2

NASTRAN SYSTEM(4) = 4, NLINES = 40

The above card changes the 4th and 9th words of /SYSTEM/. SYSTEM(4) = 4 changes the system input unit from 5 (default) to 4. This means that all subsequent input data must be present on unit 4.

Example 3

NASTRAN TITLE@PT = -1, FILES = (UMF,NPTP)

The above card requests a short title page and establishes the UMF and NPTP files as executive files.

Example 4

NASTRAN SYSTEM(14) = 30000, SYSTEM(79) = 16384

The above card changes the 14th and 79th words in /SYSTEM/. SYSTEM(14) = 30000 changes the maximum number of output lines from 20000 (default) to 30000. (See the description of the MAXLINES card in Section 2.3) SYSTEM(79) = 16384 turns on DIAG 15 thereby requesting the tracing of GIN@ OPEN/CLOSE operations. (See the description of the DIAG card in Section 2.2.)

THE NASTRAN CARD

Example 5

NAS.RAN BANDPCH = 1, BANDTRUN = 1

The above card requests the punchin_ of the new SEQGP cards unconditionally generated by the BANDIT procedure and the subsequent termination of the NASTRAN job.

Example 6

NASTRAN BANDIT = -1

The above card requests the unconditional skipping of the BANDIT operations.

MASTRAM DATA DECK

REFERENCE

1. **Everstine, G.C., BANDIT User's Guide, COSMIC Program No. DOD-C0033, May 1978.**

CASE CONTROL DECK

Case Control Data Card ELFØRCE - Element Force Output Request

Description: Requests form and type of element force output.

Format and Example(s):

$$\text{ELFØRCE} \left[\left(\begin{array}{ccc} \text{SØRT1} & \text{PRINT} & \text{REAL} \\ \text{SØRT2} & \text{PUNCH} & \text{IMAG} \\ & \text{NØPRINT} & \text{PHASE} \end{array} \right) \right] = \left\{ \begin{array}{c} \text{ALL} \\ n \\ \text{NØNE} \end{array} \right\}$$

ELFØRCE = ALL

ELFØRCE(REAL, PUNCH, PRINT) = 17

ELFØRCE = 25

ELFØRCE(SØRT2, NØPRINT) = ALL

Option

Meaning

SØRT1	Output will be presented as a tabular listing of elements for each load, frequency, eigenvalue, or time, depending on the rigid format. SØRT1 is not available in Transient problems (where the default is SØRT2).
SØRT2	Output will be presented as a tabular listing of load, frequency, or time for each element type. SØRT2 is available only in Static Analysis, Transient and Frequency Response problems.
PRINT	The printer will be the output media.
PUNCH	The card punch will be the output media.
NØPRINT	FØRCE output will not be printed nor punched.
REAL or IMAG	Requests real and imaginary output on Complex Eigenvalue or Frequency Response problems.
PHASE	Requests magnitude and phase ($0.0^\circ \leq \text{phase} < 360.0^\circ$) on Complex Eigenvalue or Frequency Response problems.
ALL	Forces for all elements will be output.
NØNE	Forces for no elements will be output.
n	Set identification of a previously appearing SET card. Only forces of elements whose identification numbers appear on this SET card will be output (Integer > 0).

- Remarks:
1. Both PRINT and PUNCH may be requested.
 2. An output request for ALL in Transient and Frequency response problems generally produces large amounts of printout. An alternative to this would be to define a SET of interest.
 3. In Static Analysis or Frequency Response problems, any request for SØRT2 output causes all output to be SØRT2.
 4. FØRCE is an alternate form and is entirely equivalent to ELFØRCE.
 5. ELFØRCE = NØNE allows overriding an overall request.
 6. In heat transfer analysis, ELFØRCE output consists of heat flow through and out of the elements.

2.3-17 (04/30/85)

NASTRAN DATA DECK

Case Control Data Card ELSTRESS - Element Stress Output Request

Description: Requests form and type of element stress output.

Format and Example(s):

$$\text{ELSTRESS} \left[\left(\begin{array}{ccc} \text{SORT1} & \text{PRINT} & \text{REAL} \\ \text{SORT2} & \text{PUNCH} & \text{IMAG} \\ & \text{NOPRINT} & \text{PHASE} \end{array} \right) \right] = \left\{ \begin{array}{c} \text{ALL} \\ n \\ \text{NONE} \end{array} \right\}$$

ELSTRESS = 5

ELSTRESS = ALL

ELSTRESS(SORT1, PRINT, PUNCH, PHASE) = 15

ELSTRESS(SORT2, NOPRINT, REAL) = ALL

Option

Meaning

SORT1	Output will be presented as a tabular listing of elements for each load, frequency, eigenvalue, or time, depending on the rigid format. SORT1 is not available in Transient problems (where the default is SORT2).
SORT2	Output will be presented as a tabular listing of load, frequency, or time for each element type. SORT2 is available only in Static Analysis, Transient and Frequency Response problems.
PRINT	The printer will be the output media.
PUNCH	The card punch will be the output media.
NOPRINT	STRESS output will not be printed nor punched.
REAL or IMAG	Requests real and imaginary output on Complex Eigenvalue or Frequency Response problems.
PHASE	Requests magnitude and phase ($0.0^\circ \leq \text{phase} < 360.0^\circ$) on Complex Eigenvalue or Frequency Response problems.
ALL	Stresses for all elements will be output.
n	Set identification of a previously appearing SET card (Integer > 0). Only stresses for elements whose identification numbers appear on this SET card will be output.
NONE	Stresses for no elements will be output.

- Remarks:
1. Both PRINT and PUNCH may be requested.
 2. An output request for ALL in Transient and Frequency response problems generally produces large amounts of printout. An alternative to this would be to define a SET of interest.
 3. In Static Analysis or Frequency Response problems, any request for SORT2 output causes all output to be SORT2.
 4. STRESS is an alternate form and is entirely equivalent to ELSTRESS.
 5. ELSTRESS = NONE allows overriding an overall request.

(Continued)

2.3-18 (04/30/85)

CASE CONTROL DECK

ELSTRESS (Cont.)

6. If element stresses in material coordinate system are desired (only for TRIA1, TRIA2, QUAD1 and QUAD2 elements and only in Rigid Format 1), the parameter STRESS (see the description of the PARAM bulk data card in Section 2.4.2) should be set to be a positive integer. If, in addition to element stresses in material coordinate system, stresses at the connected grid points are also desired, the parameter STRESS should be set to 0.

NASTRAN DATA DECK

Case Control Data Card SCAN - Output Scan Request.

Description: Scan output data and eliminate values that do not meet the specification set by this SCAN card.

Format and Example(s):

$$\text{SCAN} \left(\begin{array}{l} \text{STRESS} \\ \text{FORCE} \\ \text{HELP} \\ \text{ON-LINE} \end{array} \right), \text{ element, component} = \left(\begin{array}{l} \text{topn} \\ \text{max,min} \end{array} \right) \left[\text{, SET } i \right]$$

```
SCAN (STRESS, CBAR, AXIAL) = 10
SCAN (STRESS, BAR, AXIAL, SA-MAX) = 15, SET 102
SCAN (FORCE, RBD, 2, 3) = 17
SCAN (FORCE, 3, CRBD, 2) = +2000., -1500., SET 102
SCAN (RBD, SHEAR, FORCE, TORQUE) = 5000., 400.
SCAN (HELP)
```

Option

Meaning

STRESS	Request scan on Stress file, of SORT1 or SORT2 format. (BCD).
FORCE	Request scan on Force file, of SORT1 or SORT2 format. (BCD).
element	Any NASTRAN element name, with or without the leading letter "C".
component	One or more components specified by keywords, or by numeric codes. The numeric codes are the field numbers on the heading of the output page, whose values are to be scanned. (Each element has its own page heading.) See Remark 11 for the keywords and their corresponding field numbers. (BCD(s) or Integer(s) > 0).
topn	The highest n values, and the lowest n values, found by SCAN in the field(s) specified by component are printed out; e.g., top n tension and top n compression stresses. (Integer > 0).
max,min	Values exceeding max, and below min, in the field(s) specified by component are printed out. (Real).
SET i	Element set identification of a previously appearing SET card. Only forces or stresses of elements whose identification numbers appear on this SET card will be scanned for output (Integer > 0).

(Continued)

2.3-41a (04/30/85)

CASE CONTROL DECK

SCAN (Cont.)

HELP A table of the component keywords and their corresponding field numbers will be printed immediately before the Bulk Data echo, and job continues.

@N-LINE Request SCAN operation to be run on-line under real-time environment.

- Remarks:**
1. Multiple SCAN cards can be requested in a NASTRAN run. They do not override one another.
 2. A SC/N card specifies only one element type; an element type can have more than one SCAN card.
 3. More than one component field can be requested in a SCAN card. However, these fields will be scanned together as a group.
 4. SCAN sorts and prints the scanned values in descending order. All fields of the same output line are printed.
 5. If the component keyword is misspelled, a list of the valid names and their corresponding fields will be printed automatically. Job will be flagged for fatal error termination.
 6. Some component keywords imply multi-field scan; e.g., "AXIAL" may imply axial forces for grid points 1, 2, 3, etc.
 7. Component numeric code specifies field numbers 1 through 62 only.
 8. Normally SCAN will scan only data already generated for the Output File Processor (OFP). That is, SCAN cannot scan data that have not been created. However, if no ELSTRESS (or STRESS) card is specified before a stress SCAN card, a STRESS card is generated internally in the following form:

STRESS (SORT1, NOPRINT, REAL) = ALL

Forces are handled similarly.
 9. The Label line (after TITLE and SUBTITLE) is limited to 36 characters. The rest of the line is replaced by SCAN header.
 10. When the @N-LINE option is requested, all other input parameters are not needed on the SCAN card. These parameters will be prompted on the CRT screen by the computer system when the SCAN module is executed.

(Continued)

2.3-41b (04/30/85)

NASTRAN DATA DECK

SCAN (Cont.)

11. The component keywords for stress and force, and their corresponding output field numbers, are listed below:

<u>FORCE/STRESS</u>	<u>KEYWORD</u>	<u>COMPONENT (OUTPUT FIELD NO.)</u>
ROD, TUBE, CONROD		
STRESS	AXIAL	2
STRESS	TORSIONAL	4
STRESS	MARGIN	3, 5
FORCE	AXIAL	2
FORCE	TORQUE	3
SHEAR, TWIST		
STRESS	MAX-SHR	2
STRESS	MARGIN	4
STRESS	AVG	3
STRESS	MAX	2
FORCE	FORCE-1	2
FORCE	FORCE-2	3
FORCE	MOMENT-1	2
FORCE	MOMENT-2	3
TRIA1, TRIA2, QUAD1, QUAD2, TRBSC, TRPLT, QDPLT		
STRESS	NORM-X	3, 11
STRESS	NORM-Y	4, 12
STRESS	SHEAR-XY	5, 13
STRESS	MAJOR	7, 15
STRESS	MINOR	8, 16
STRESS	MAX-SHR	9, 17
FORCE	MOMENT-X	2
FORCE	MOMENT-Y	3
FORCE	SHEAR-X	5
FORCE	SHEAR-Y	6
TRMEM, QMEM, QMEM1, QMEM2		
STRESS	NORM-X	2
STRESS	NORM-Y	3
STRESS	SHEAR-XY	4
STRESS	MAJOR	6
STRESS	MINOR	7
STRESS	MAX-SHR	8

(Continued)

CASE CONTROL DECK

SCAN (Cont.)

FORCE/STRESS KEYWORD COMPONENT (OUTPUT FIELD NO.)

ELAS1, ELAS2, ELAS3, IS2D8

STRESS	OCT-SHR	2
FORCE	CIRCUM	2
FORCE	FORCE-1	4, 9
FORCE	FORCE-2	3, 6
FORCE	FORCE-3	5, 8
FORCE	FORCE-4	2, 7

BAR, ELBOW

STRESS	SA-MAX	7, 8
STRESS	SB-MAX	14, 15
STRESS	MARGIN	9, 16
STRESS	AXIAL	6
FORCE	AXIAL	8
FORCE	TORQUE	9
FORCE	SHEAR	5, 6
FORCE	MOMENT-A	2, 3
FORCE	MOMENT-B	4, 5

CONEAX

STRESS	NORM-U	4, 22
STRESS	NORM-V	5, 23
STRESS	SHEAR-UV	6, 24
STRESS	MAJOR	8, 26
STRESS	MINOR	9, 27
STRESS	MAX-SHR	10, 28
FORCE	MOMENT-U	3
FORCE	MOMENT-V	4
FORCE	SHEAR-XY	6
FORCE	SHEAR-YZ	7

TRIARG

STRESS	RADIAL	2
STRESS	CIRCUM	3
STRESS	AXIAL	4
STRESS	SHEAR	5
FORCE	RADIAL	2, 5, 8
FORCE	CIRCUM	3, 6, 9
FORCE	AXIAL	4, 7, 10

(Continued)

2.3-41d (04/30/85)

NASTRAN DATA DECK

SCAN (Cont.)

<u>FORCE/STRESS</u>	<u>KEYWORD</u>	<u>COMPONENT (OUTPUT FIELD NO.)</u>
TRAPRG		
STRESS	RADIAL	2, 6, 10, 14 ... 22
STRESS	CIRCUM	3, 7, 11, 15 ... 23
STRESS	AXIAL	4, 8, 12, 16 ... 24
STRESS	SHEAR	5, 9, 13, 17 ... 25
STRESS	SHR-FORC	6, 10, 14, 18 ... 26
FORCE	RADIAL	2, 5, 8, 11
FORCE	CIRCUM	3, 6, 9, 12
FORCE	AXIAL	4, 7, 10, 13
TORDRG		
STRESS	MEM-T	2, 7, 12
STRESS	MEM-C	3, 8, 13
STRESS	FLEX-T	4, 9, 14
STRESS	FLEX-C	5, 10, 15
STRESS	SHR-FORC	6, 11, 16
FORCE	RADIAL	2, 8
FORCE	CIRCUM	3, 9
FORCE	AXIAL	4, 10
FORCE	MOMENT	5, 11
FORCE	CURV	7, 13
IHEX1, IHEX2		
STRESS	NORM-X	3, 22, 41, 60 ... ETC.
STRESS	SHEAR-XY	4, 23, 42, 61 ... ETC.
STRESS	PRINC-1	5, 24, 43, 62 ... ETC.
STRESS	MEAN	9, 28, 47, 66 ... ETC.
STRESS	NORM-Y	11, 30, 49, 68 ... ETC.
STRESS	SHEAR-YZ	12, 31, 50, 69 ... ETC.
STRESS	PRINC-2	13, 31, 49, 67 ... ETC.
STRESS	NORM-Z	17, 36, 55, 74 ... ETC.
STRESS	SHEAR-ZX	18, 37, 56, 75 ... ETC.
STRESS	ESTRESS	19, 38, 57, 76 ... ETC.

(Continued)

CASE CONTROL DECK

SCAN (Cont.)

<u>FORCE/STRESS</u>	<u>KEYWORD</u>	<u>COMPONENT (OUTPUT FIELD NO.)</u>
IHXS		
STRESS	NORM-X	3, 23, 43, 63 ... 643
STRESS	SHEAR-XY	4, 24, 44, 64 ... 644
STRESS	PRINC-1	5, 25, 45, 65 ... 645
STRESS	MEAN	9, 29, 49, 69 ... 649
STRESS	NORM-Y	12, 32, 52, 72 ... 652
STRESS	SHEAR-YZ	13, 33, 53, 73 ... 653
STRESS	PRINC-2	14, 34, 54, 74 ... 654
STRESS	NORM-Z	18, 38, 58, 78 ... 658
STRESS	SHEAR-ZX	19, 39, 59, 79 ... 659
STRESS	ESTRESS	20, 40, 60, 80 ... 660
TRIAAX, TRAPAX		
STRESS	RADIAL	3, 11, 19
STRESS	AXIAL	4, 12, 20
STRESS	CIRCUM	5, 13, 21
STRESS	MEM-C	6, 14, 22
STRESS	FLEX-T	7, 15, 23
STRESS	FLEX-C	8, 16, 24
FORCE	RADIAL	3, 7, 11
FORCE	CIRCUM	4, 8, 12
FORCE	AXIAL	5, 9, 13

Use output field numbers(s) to specify component(s) for elements or keywords not listed above. See sections 2.3.51 and 2.3.52 of the NASTRAN Programmer's Manual for additional element stress and force component definitions.

NASTRAN DATA DECK

Input Data Card NONLINS - Nonlinear Transient Response Dynamic Load

Description: Defines nonlinear transient forcing functions of the form.

$$P_i(t) = S T(x_j(t)) \begin{cases} \dot{x}_j(t) & \text{if } CJ \leq 6 \\ x_j(t) & \text{if } CJ \geq 10 \end{cases}$$

Format and Example:

	1	2	3	4	5	6	7	8	9	10
NONLINS	SID	GI	CI	S	GJ	CJ	T			
NONLINS	21	3	4	2.1	3	1	6			

Field

Contents

SID	Nonlinear load set identification number (Integer > 0)
GI	Grid or scalar or extra point identification number at which nonlinear load is to be applied (Integer > 0)
CI	Component number if GI is a grid point (0 < Integer ≤ 6); blank or zero if GI is a scalar or extra point
S	Scale factor (Real)
GJ	Grid or scalar or extra point identification number (Integer > 0)
CJ	Component number if GJ is a grid point (0 < Integer ≤ 6; 11 ≤ Integer ≤ 16); blank or zero or 10 if GJ is a scalar or extra point (See Remark 4 below)
T	Identification number of a TABLEDi card (Integer > 0)

- Remarks:
1. Nonlinear loads must be selected in the Case Control Deck (NONLINEAR=SID) to be used by NASTRAN.
 2. Nonlinear loads may not be referenced on a DLOAD card.
 3. All coordinates referenced on NONLINS cards must be members of the solution set. This means the u_e set for modal formulation and the $u_d = u_e + u_a$ set for direct formulation.
 4. The permissible values for the component number CJ are given in the following table:

\dot{x}_j or x_j \ CJ	Grid point	Scalar or extra point
Displacement (x_j)	1 ≤ Integer ≤ 6	0 or blank
Velocity (\dot{x}_j)	11 ≤ Integer ≤ 16	10

(Continued)

2.4-205a (04/30/85)

BULK DATA DECK

NONLINS (Cont.)

Note that velocity components are represented by integers ten greater than the corresponding displacement components.

5. Velocity (\dot{x}_j) is determined from the relation

$$\dot{x}_{j,t} = \frac{x_{j,t} - x_{j,t-1}}{\Delta t} ,$$

where Δt is the time increment and $x_{j,t}$ and $x_{j,t-1}$ are the displacements at time t and at the previous time step respectively.

6. Since the forcing functions $P_i(t)$ is a product of TABLEDi, displacement, velocity and the scale factor S, any zero value of these quantities will make $P_i(t)$ equal to zero. This condition may occur when initial displacement or velocity are zeros, and no other load applied to the structure

BULK DATA DECK

PA:JM (Cont.)

- am. **STRESS** - optional in static analysis (rigid format 1). This parameter controls the transformation of element stresses to the material coordinate system (only for TRIA1, TRIA2, QUAD1 and QUAD2 elements). If it is a positive integer, the stresses for these elements are transformed to the material coordinate system. If it is zero, stresses at the connected grid points are also computed in addition to the element stresses in the material coordinate system. A negative integer value results in no transformation of the stresses. The default value is -1.
- an. **STRAIN** - optional in static analysis (rigid format 1). This parameter controls the transformation of element strains/curvatures to the material coordinate system (only for TRIA1, TRIA2, QUAD1 and QUAD2 elements). If it is a positive integer, the strains/curvatures for these elements are transformed to the material coordinate system. If it is zero, strains/curvatures at the connected grid points are also computed in addition to the element strains/curvatures in the material coordinate system. A negative integer value results in no transformation of the strains/curvatures. The default value is -1.
- ao. **MINPTS** - optional in static analysis (rigid format 1). A positive integer value of this parameter specifies the number of closest independent points to be used in the interpolation for computing stresses or strains/curvatures at grid points (only for TRIA1, TRIA2, QUAD1 and QUAD2 elements). A negative integer value or 0 specifies that all independent points are to be used in the interpolation. The default value is 0.
- ap. **VOLUME** - optional in all rigid formats. The volume computations for the 2-D and 3-D elements are activated by this parameter when they are generated in ENG. The results are multiplied by the real value of this parameter. If the 7th output data block of the ENG module were specified (via DMAP-alter), the element ID's, volumes, surface areas (see (aq) below), SIL, and grid point coordinates would be saved in the data block, a GIND written file. If the 7th output data block were one of the INPI (I=1,2,3,...,9,T) files, the same element data would be saved, in a FORTRAN binary written file. The following table summarizes the data being saved.

RECORD	WORDS	CONTENTS
0	1,2	Header record, begins with GIND BCD name
	3-34	Title, BCD
	35-66	Sub-title, BCD
	67-98	Label, BCD
	99-101	Date, BCD

(Continued)

2.4-222 (04/30/85)

NASTRAN DATA DECK

PARAM (Cont.)

```

1      1,2  Element name of the first element, BCD
      2      Element ID, Integer
      3      Volume (multiplied by scale factor n), or zero, real
      4      (No. of surfaces)*100 + (No. of grid points), Integer f
      5      Surface area of first surface real
      :      :
      4+N    Surface area of N-th surface, real
      4+N+1  SIL of the first grid point, Integer
      4+N+2,3,4  x,y,z coordinates of the first grid point, real
      :      Repeat last 4 words for other grid points
      2      A record similar to record 1 for the second element.
      :      :
LAST   Last record for the last element.
    
```

The trailer of the output data block has the following information:

Word 1 = LAST (No. of records written, header excluded).

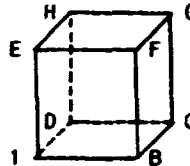
Words 2 thru 6 contain no useful information.

eq. SURFACE - optional in all rigid formats. The computations of the external surface areas for the 2-D and 3-D elements are activated by this parameter when they are generated in ENG. The results are multiplied by the real value of this parameter. See (ap) for the case where the surface areas are to be saved in an output file. The surface areas of the 3-D elements are defined below:

SURFACE AREA NO. CORNER GRID POINTS USED

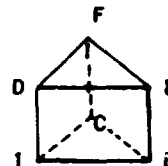
Brick (8 or more grid points):

1	1,B,C,D
2	1,B,F,E
3	B,C,G,F
4	C,D,H,G
5	D,I,E,H
6	E,F,G,H



Wedge (6 grid points):

1	1,B,C
2	1,B,E,D
3	B,C,F,E
4	C,I,D,F
5	D,E,F



(Continued)

2.4-222a (04/30/85)

BULK DATA DECK

PARAM (Cont.)

Tetrahedron (4 grid points):

1	1,2,3
2	1,2,4
3	2,3,4
4	3,1,4



STRUCTURE PLOTTING

Structure Plot Data Card PL0T - Plot Generation

Description: Specifies all plot parameters so as to cause plots to be generated for the selected plotter.

Format:

$$\text{PL0T} \left[\left\{ \begin{array}{l} \text{STATIC} \\ \text{MODAL} \\ \text{CMODAL} \\ \text{FREQUENCY} \\ \text{TRANSIENT} \end{array} \right\} \right] \left[\left\{ \begin{array}{l} \text{DEFORMATION} \\ \text{VELOCITY} \\ \text{ACCELERATION} \end{array} \right\} \right] [\text{CONTOUR}] [i1, i2 \text{ THRU } i3, \text{ etc.}] \left[\left\{ \begin{array}{l} \text{RANGE } f1, f2 \\ \text{RANGE } \lambda1, \lambda2 \\ \text{TIME } t1, t2 \end{array} \right\} \right] \left[\left\{ \begin{array}{l} \text{PHASE LAG } \phi \\ \text{MAGNITUDE} \end{array} \right\} \right] , \\
 \text{[MAXIMUM DEFORMATION } d],$$

$$\text{[SET } j1][\text{ORIGIN } k1] \left[\left\{ \begin{array}{l} \text{SYMMETRY} \\ \text{ANTISYMMETRY} \end{array} \right\} \right] * \left[\left\{ \begin{array}{l} \text{PEN} \\ \text{DENSITY} \end{array} \right\} \right] P \text{ [SYMBOLS } m[, n] \left[\begin{array}{l} \text{LABEL} \\ \text{GRID POINTS} \\ \text{ELEMENTS} \\ \text{BOTH} \\ \text{EPID} \end{array} \right] \right] ,$$

$$\left[\left\{ \begin{array}{l} \text{SHAPE} \\ \text{VECTOR } v \\ \text{SHA-C, VECTOR } v \\ \text{OUTLINE} \\ \text{HIDDEN} \\ \text{SHRINK } s \end{array} \right\} \right] , \text{ [NOFIND]} .$$

[SET j2][ORIGIN k2] etc.

Option

Meaning

- | | |
|----------------|---|
| 1. STATIC | Plot static deformations in Rigid Formats 1, 2, 4, 5, 6 and 14; Heat Rigid Formats 1 and 3; Aero Rigid Format 11. |
| MODAL | Plot mode shapes in Rigid Formats 3, 5, 13 and 15. |
| CMODAL | Plot mode shapes in Aero Rigid Format 10. |
| FREQUENCY | Plot frequency deformations in Rigid Formats 8 and 11 and Aero Rigid Format 11. |
| TRANSIENT | Plot transient deformations in Rigid Formats 9 and 12; Heat Rigid Format 9; Aero Rigid Format 11. |
| 2. DEFORMATION | Nonzero integers(i) following refer to subcases that are to be plotted. Default is all subcases. See SHAPE and VECTOR for use of "G" command. |
| VELOCITY | Nonzero integers(i) following refer to subcases that are to be plotted. Default is all subcases. |
| ACCELERATION | Nonzero integers(i) following refer to subcases that are to be plotted. Default is all subcases. |
| 3. CONTOUR | Refers to stress or displacement contour lines and values. If deformed plots are requested, then the contours will be drawn on the deformed shape. If an underlay is requested (via "0" in the subcase string), the contours will be drawn on the undeformed shape. |

(Continued)

STRUCTURE PLOTTING

PLØT (Cont.)

RXY or RXZ or RYZ - requesting vector sum of two components

R - requesting total vector deformation

N - used with any of the above combinations to request no underlay shape be drawn.

All plots requesting the VECTØR option shall have an underlay generated of the undeformed shape using the same sets, PEN 1 or DENSITY 1, and symbol 2 (if SYMBOLS is specified). If SHAPE and VECTØR are specified, the underlay will depend on whether "0" is used with DEFØRMATION. It will be the deformed shape when not used and will be both deformed and undeformed shapes when it is used. The part of the vector at the grid point will be the tail when the underlay is undeformed and the head when it is deformed. If the "N" parameter is used with VECTØR, no shape will be drawn but other options such as SYMBOLS will still be valid.

16. ØUTLINE Connecting lines between grid points that lie on the boundary of the structural model will be plotted. The outline will reflect the deformed shape unless "0" is included in the subcase string. The ØUTLINE option will be ignored if the ØONTØUR option is not also requested.
17. HIDDEN Provides a hidden image plot of the elements in the plot set. The HIDDEN option will be ignored if the ØONTØUR option is also requested. The LABEL option should not be used with the HIDDEN option.
18. SHRINK s The real value (s) is the factor used to shrink or reduce elements within connecting grid points. The value s is limited to 0.1 to 1.0 with a default value of 0.75.
19. NØFIND Disenables the automatic FIND for this plot. That is, the SET defined for the present plot will be drawn using the SCALE, VANTAGE PØINT and ØRIGIN from the previous PLØT command.

- Remarks:
1. The plot card is required to generate plots. Each logical card will cause one picture to be generated for each subcase, mode or time step requested, using the current parameter values.
 2. If only the word PLØT appears on the card, a picture of the undeformed structure will be prepared using the first defined set and the first defined origin.
 3. If no FIND card is given after the previous PLØT card, the specified set on the PLØT card is used to perform an Automatic Find operation.

Examples:

Following are some examples illustrating the use of the PLØT card:

1. PLØT

Undeformed SHAPE using first defined SET, first defined ØRIGIN and PEN 1 (or DENSITY 1).

2. PLØT SET 3 ØRIGIN 4 PEN 2 SHAPE SYMBOLS 3 LABEL

Undeformed SHAPE using SET 3, ØRIGIN 4, PEN 2 (or DENSITY 2) with each grid point of the set having a + placed at its location, and its identification number printed adjacent to it.

(Continued)

PLOTTING

PL0T (Cont.)

3. PL0T MODAL DEF0RMATION 5 SHAPE

Modal deformations as defined in subcase 5 using first defined SET, first defined 0RIGIN, and PEN 1 (or DENSITY 1). Subcases must have previously been defined in the Case Control Deck via the use of MODES cards, otherwise all modes will be in an assumed subcase 1.

4. PL0T STATIC DEF0RMATION 0, 3 THRU 5, 8 PEN 4, SHAPE

Static deformations as defined in subcases 3, 4, 5 and 8, deformed SHAPE; drawn with PEN 4, using first defined SET and 0RIGIN, underlayed with undeformed SHAPE drawn with PEN 1. This command will cause four plots to be generated.

5. PL0T STATIC DEF0RMATION 0 THRU 5,

SET 2 0RIGIN 3 PEN 3 SHAPE,

SET 2 0RIGIN 4 PEN 4 VECT0RS XYZ SYMB0LS 6,

SET 35 SHAPE

Deformations as defined in subcases 1, 2, 3, 4 and 5, undeformed underlay with PEN 1, consisting of SET 2 at 0RIGIN 3, SET 2 at 0RIGIN 4 (with an * placed at each grid point location), and SET 35 at 0RIGIN 4. Deflected data as follows: SHAPE using SET 2 at 0RIGIN 3 (PEN 3) and SET 35 at 0RIGIN 4 (PEN 4); 3 VECT0RS (X, Y and Z) drawn at each grid point of SET 2 at 0RIGIN 4 (PEN 4) (less any excluded grid points), with 0 placed at the end of each vector.

6. PL0T STATIC DEF0RMATIONS 0, 3, 4,

SET 1 0RIGIN 2 DENSITY 3 SHAPE,

SET 1 SYMMETRY Z SHAPE,

SET 2 0RIGIN 3 SHAPE,

SET 2 SYMMETRY Z SHAPE

Static deformations as defined in subcases 3 and 4, both halves of a problem solved by symmetry using the X-Y principal plane as the plane of symmetry. SET 1 at 0RIGIN 2 and SET 2 at 0RIGIN 3, with the deformed shape plotted using DENSITY 3 and the undeformed structure plotted using DENSITY 1. The deformations of the "opposite" half will be plotted to correspond to symmetric loading. This command will cause two plots to be generated.

7. PL0T TRANSIENT DEF0RMATION 1, TIME 0.1, 0.2, MAXIMUM DEF0RMATION 2.0, SET 1, 0RIGIN 1, PEN 2,

SYMB0LS 2, VECT0R R

Transient deformations as defined in subcase 1 for time = 0.1 to time = 0.2, using SET 1 at 0RIGIN 1. The undeformed shape using PEN or DENSITY 1 with an * at each grid point location will be drawn as an underlay for the resultant deformation vectors using PEN or DENSITY 2 with an * typed at the end of each vector drawn. In addition, a plotted value of $d_{max}/2.0$ (where d_{max} is the value specified on the

MAXIMUM DEF0RMATION card) will be used for the single maximum deformation occurring on any of the plots produced. All other deformations on all other plots will be scaled relative to this single maximum deformation. This command will cause a plot to be generated for each output time step which lies between 0.1 and 0.2.

(Continued)

STRUCTURE PLOTTING

PLØT (Cont.)

8. PLØT CMØDAL DEFORMATIØN PHASE LAG 90., SET 1 VECTØR R

The imaginary part of the complex mode shape will be plotted for SET 1.

9. PLØT CØNTØUR 2

PLØT CØNTØUR 2 ØUTLINE

CØNTØUR MINPRIN

PLØT STATIC DEFORMATIØN CØNTØUR 1 ØUTLINE

The first PLØT card will cause Major Principal Stress contours to be plotted on the undeformed shape of the complete model and the second PLØT card will cause the outline of the model to be plotted due to the defaults associated with the CØNTØUR card. Contour stress plots of the Minor Principal Stress will be plotted on the outline of the deformed shape by the third PLØT card.

10. PLØT SET 10 SHRINK .85

The undeformed shape of the elements defined by SET 10 will be drawn, with element sizes reduced to 85 percent of the scaled size. Grid locations will be automatically scaled to fill the image area.

11. SET 10 = ALL
SET 20 = 100 THRU 200
FIND SCALE ORIGIN 1 SET 10
PLØT SET 10
PLØT SET 20 NØFIND
PLØT SET 20

There will be 3 frames of the undeformed structure plotted. The first will display the entire structure, scaled to fill the image area. The second frame will display elements 100 thru 200, using the scale for the previous plot. The third frame will display elements 100 thru 200, scaled to fill the image area.

N85-25865

ABSTRACT

**IMPROVED ACCURACY IN SOLID ISOPARAMETRIC ELEMENTS
USING SELECTIVELY REDUCED INTEGRATION**

by

Dr. W. R. Case
R. S. Mitchell
R. E. Vandegrift

NASA/Goddard Space Flight Center
Greenbelt, Maryland

Currently COSMIC NASTRAN uses the same Gaussian integration order for every term in the stiffness matrix of the solid isoparametric elements. This results in overly stiff elements under some conditions. This paper describes a modification to the CIHEX1, CIHEX2 and CIHEX3 elements which provides the user with the capability of controlling the order of integration for selected terms in the stiffness matrix. A study giving examples of improved accuracy using selectively reduced integration will be provided.

N85-25866

CRACK ELEMENTS FOR COSMIC/NASTRAN

P. J. Woytowitz and R. L. Citerley
Anamet Laboratories, Inc., San Carlos, CA 94070

SUMMARY

A new crack element has been developed and incorporated into COSMIC/NASTRAN. The element is considered linear, isotropic, and homogeneous. Mode I and II stress intensity factors are automatically calculated. Comparisons to theoretical plane strain solutions for several geometries are presented and demonstrate the accuracy of the developed element. Extensions of the element to three dimensions, anisotropic material, and plastic analysis are discussed.

INTRODUCTION

Crack or singular elements have been developed for finite element analysis for almost as long as finite element codes have been available. These elements usually are classified as either hybrid or singular element formulations. Many of the elements developed suffered from either lack of accuracy, generality, or consistency. Barsoum (Ref. 1) points out shortcomings of several different elements. These shortcomings include inability to model rigid body or constant strain modes, inability to include thermal or body force effects, and lack of compatibility with other elements.

The elements developed by Barsoum (Ref. 1) and Henshell (Ref. 2) rectified many of the problems described above; however, these elements were limited to displacement of the form $r^{1/2}$. Consequently, they could only model strain singularities of the form $r^{-1/2}$. Recently, Stern (Ref. 3) and more recently, Hughes and Aikin (Ref. 4) have introduced families of consistent, conforming elements which allow displacements of the form r^γ . While the Stern element appears to have the restriction that $0 < \gamma < 1$, the element of Hughes and Aikin is valid for all $\gamma > 0$. The element described herein is based upon shape functions suggested by Hughes and Aikin (Ref. 4).

The element presented here possesses the required rigid body and constant strain modes. It properly models thermal, body force, and pressure loading conditions. Additionally, it is compatible with standard linear or quadratic isoparametric elements and can possess either 5 or 6 nodes. Finally, it can be used as a nonsingular element with a variable number of nodes.

ELEMENT FORMULATION

The following derivation follows Hughes and Aikin (Ref. 4). Referring to Figure 1, the standard bilinear shape functions are used for nodes 1 through 4:

$$\begin{aligned}
 N_1(r,s) &= (1-r)(1-s) \\
 N_2(r,s) &= r(1-s) \\
 N_3(r,s) &= rs \\
 N_4(r,s) &= (1-r)s
 \end{aligned}
 \tag{1}$$

The shape functions for nodes 5-8 are chosen as:

$$\begin{aligned}
 N_5(r,s) &= (1-s)P(r,\gamma) \\
 N_6(r,s) &= rP(s,2) \\
 N_7(r,s) &= sP(r,\gamma) \\
 N_8(r,s) &= (1-r)P(s,2)
 \end{aligned}
 \tag{2}$$

where

$$P(x,\gamma) = 2 \left(x - \frac{x^\gamma - 2(1/2)^\gamma x}{1 - 2(1/2)^\gamma} \right)
 \tag{3}$$

It can be easily shown that the shape functions for nodes 5-8 reduce to the standard quadratic serendipity element when γ of Equation (3) is set equal to 2. It can also be seen that the shape function for nodes 5-8 satisfies the interpolation property at all nodes of the element. That is:

$$N_i(r_j) = \delta_{ij} \quad \text{and} \quad N_i(s_j) = \delta_{ij}$$

where r_j and s_j are values of r and s at node j and δ_{ij} is the Kronecker delta. However, the shape functions associated with nodes 1-4 do not satisfy the interpolation property at nodes 5-8. Following the standard technique (Ref. 4), the shape functions for nodes 1-4 are modified as follows:

$$\begin{aligned}
N_1 + N_1(r,s) &= [N_8(r,s) + N_5(r,s)]/2 \\
N_2 + N_2(r,s) &= [N_5(r,s) + N_6(r,s)]/2 \\
N_3 + N_3(r,s) &= [N_6(r,s) + N_7(r,s)]/2 \\
N_4 + N_4(r,s) &= [N_7(r,s) + N_8(r,s)]/2
\end{aligned}
\tag{4}$$

where the + reads: "is replaced by."

It can now be seen that the shape functions for all eight nodes satisfy the required interpolation property. Additionally, the shape functions are capable of exactly representing the monomials $1, r, s, r^Y, rs, s^2, r^Y s,$ and $s^2 r$. The presence of $1, r$ and s ensure representation of rigid body and constant strain modes. The presence of r^Y allows exact representation of displacements of the form r^Y . Note that this will result in a line singularity of the form r^{Y-1} upon differentiation.

In order to represent point singularities, the quadrilateral must be degenerated into a triangle. This is done by coalescing nodes 4, 8, and 1 as can be done for standard isoparametric elements (Ref. 5) and as is shown schematically in Figure 2. Thus, finally, for a point singularity, the shape function associated with node 1 is replaced with:

$$N_1(r,s) + N_1(r,s) + N_4(r,s) + N_8(r,s)
\tag{5}$$

This is easily programmed into the element routine. The generality of the above derivation allows use of the same shape functions as the basis of three-dimensional elements which possess line singularities.

In summary, for the 6 node triangle, the shape function associated with node 1 is given by Equation (5), the shape functions associated with nodes 2 and 3 are given by N_2 and N_3 of Equation (4), and the shape functions associated with nodes 5 through 7 are given by N_5 through N_7 of Equation (2).

Given the shape functions for the element, calculation of the stiffness matrix, thermal load vector, and gravity load vector follows the standard procedure as described in Reference 6. These quantities are therefore given as:

$$\begin{aligned}
\tilde{K}^e &= \int_{V^e} \tilde{B}^T \underline{D} \tilde{B} \, dV \\
\tilde{F}_T^e &= \int_{V^e} \tilde{B}^T \underline{D} \underline{\alpha} \Delta T \, dV \\
\tilde{F}_b^e &= \int_{V^e} \tilde{N}^T \underline{b} \, dV
\end{aligned}
\tag{6}$$

where

$$\tilde{B} = \underline{L} \underline{N} \quad , \quad \underline{N} = [N_1 \underline{I}, N_2 \underline{I}, \dots] \quad , \quad \underline{L} = \begin{bmatrix} \frac{\partial}{\partial x} & 0 \\ 0 & \frac{\partial}{\partial y} \\ \frac{\partial}{\partial y} & \frac{\partial}{\partial x} \end{bmatrix} \quad ,$$

and \underline{I} is a 2×2 identity matrix.

See Reference 6 for more details. The actual integration is performed via Gaussian quadrature. That is, the integrals are approximated as:

$$\int f(x) \, dx = \sum_{j=1}^n W_j f(x_j)
\tag{7}$$

Due to the formulation, it can be shown that along the s direction, the integration order needs to be, at most, 4 in order to exactly integrate the element. For an undistorted element, a maximum integration order of 3 is necessary, although often an integration order of 2 yields results just as good. Along the r direction, the method for an exact integration has not been ascertained. Currently, an integration order of 4 or 5 seems to suffice along the r direction. An exact integration formula analogous to the formula presented in Reference 3 or Reference 7 will hopefully be derived in the near future.

Calculation of the stress intensity factors are performed using the equations:

$$K_I = \frac{G}{2(1-\nu)} \lim_{r \rightarrow 0} \left(\frac{2\pi}{r}\right)^{1/2} u_y(\theta = \pi)$$

$$K_{II} = \frac{G}{2(1-\nu)} \lim_{r \rightarrow 0} \left(\frac{2\pi}{r}\right)^{1/2} u_x(\theta = \pi)$$
(8)

where the nomenclature is shown in Figure 3. Alternatively, similar equations in terms of stresses can be used. It has been found here and noted elsewhere (Ref. 8) that Equation (8) yields more accurate results than the similar equations in terms of stresses. The values of the stress intensity factors are calculated at each of the integration points along the r direction and extrapolated to r=0 using Lagrangian interpolation.

Extension of the above formulation to three dimensions is straightforward. As discussed in Reference 4, the three-dimensional shape functions are simply products of the two-dimensional shape functions in r and s with the desired one-dimensional shape function in t. For example, the shape functions for the three-dimensional element of Figure 4 are given by:

$$N_1(r,s,t) = tN_1(r,s)$$

$$\vdots$$

$$N_6(r,s,t) = tN_6(r,s)$$

$$N_7(r,s,t) = (1-t)N_1(r,s)$$

$$\vdots$$

$$N_{12}(r,s,t) = (1-t)N_6(r,s)$$

The above element formulation may be extended to anisotropic materials by using the appropriate anisotropic material matrix D in Equation (6). When appropriate, D could be different at each integration point.

In order to incorporate plasticity effects, it is suggested that standard techniques currently used for plasticity in regular elements could also be applied to the present element. That is, after each load increment, each integration point in the element would be checked to see if it has gone plastic or not. If plasticity has occurred, then an algorithm such as radial-return (Ref. 9) would be used to bring the stress back to the yield surface. The element's internal forces, used to calculate the out-of-balance load vector would be given in standard form as:

$$\underline{R}^e = \int_{V^e} \underline{B}^T \underline{q} dV$$

Additionally, the order of the strain singularity would have to be updated, depending upon the hardening properties of the material (Ref. 10).

IMPLEMENTATION IN NASTRAN

Implementation of the crack element into NASTRAN was performed via the dummy element CDUM1. This procedure is covered in Reference 11. The present element was modeled after the QDMEM1 element routines, due to their similarity.

The first step was to create a subroutine KDUM1 which generates the stiffness and mass matrices. The mass matrix may be either consistent or lumped. When the mass matrix is used for calculation of gravity loads, the consistent mass matrix should be specified. This subroutine is eventually linked to NASTRAN LINK 8.

For computation of thermal loads, the subroutine EDTL must be modified to make a call to SSGETD before calling the routine DUM1. The dummy coding in routine DUM1 is then modified to calculate the thermal load vector based on the connecting grid point temperatures. Optionally, the element centroidal temperature could have been used, although this is generally not recommended since temperature gradients near the crack could not be accurately represented in this way. After modifying EDTL and DUM1, they must be linked to NASTRAN LINK 5.

Finally, the dummy coding for the SDUM11 and SDUM12 routines must be modified so that they perform the required operations. SDUM11 performs the preliminary geometry calculations and creates the S matrix which relates element stresses (including stress intensity factors) to the element's grid point displacements. SDUM12 then uses the S matrix, grid point displacements, and temperatures to compute the centroidal stresses and stress intensity factors and writes them to the output file. After modifying the SDUM11 and SDUM12 coding, it is linked to NASTRAN LINK 13. This completes the implementation into NASTRAN.

NUMERICAL RESULTS

In order to assess the accuracy of the present element, four different crack geometries/loading conditions with known solutions were analyzed. Figure 5 shows the different geometries analyzed. Figure 6 presents four different mesh sizes which were used to analyze the first three crack geometries. Figure 7 shows the boundary conditions used. For the edge crack with a point load, Figure 7 is modified so that the load is applied at the edge of the crack. Table 1 presents the errors associated with both the crack opening displacement (COD) and the mode I stress intensity factor K_I . As can be seen,

the COD is less sensitive to the mesh size, while the K_I values appear to be converging to their exact solutions. However, the edge crack with a point load solution appears to overshoot the exact by about 5%. It should be mentioned that the "exact" solution for the edge crack specimen with a point load is considered to be accurate to within 2%. The other exact solutions were considered to have accuracies better than 1%. These exact solutions were obtained from Reference 12.

Figure 8 presents a model of a central crack in a finite plate. To ascertain the accuracy of the element's mode II stress intensity factor, K_{II} , the model of Figure 8(a) was used. The results for both K_I and K_{II} are presented in Table 2. As can be seen, the K_{II} is within about 4% of the exact solution.

In summary, both COD and stress intensity factors appear to be accurately represented even for relatively coarse meshes. The accuracies obtained are well within the accuracies required by typical engineering calculations. This is due to the fact that the scatter alone, in the K_I values during a typical test, may be 10%.

CONCLUSIONS AND FUTURE RESEARCH

An element formulation has been presented that accurately models singularities. The form of the singularity is general and the two-dimensional element developed may be easily extended to three dimensions. Additionally, the element may be used as a standard, variable number of nodes quadratic element. The element has been incorporated into NASTRAN and compared to several known solutions.

Future research will include more tests of the element against known exact solutions. Additionally, an exact integration rule is desirable, and work to develop this will be performed. The element formulation will then be extended to three dimensions and the code will be incorporated into NASTRAN. Finally, extensions to include anisotropic materials and plasticity are possible and should be studied further.

REFERENCES

1. Barsoum, R. S., "On the Use of Isoparametric Finite Elements in Linear Fracture Mechanics," Int. J. for Numerical Methods in Engineering, Vol. 10, pp. 25-37, 1976.
2. Henshell, R. D. and Shaw, K. G., "Crack Tip Finite Elements are Unnecessary," Int. J. for Numerical Methods in Engineering, Vol. 9, pp. 495-507, 1975.
3. Stern, M., "Families of Consistent Conforming Elements with Singular Derivatives Fields," Int. J. for Numerical Methods in Engineering, Vol. 14, pp. 409-421, 1979.

4. Hughes, J. J. R. and Akin, J. E., "Techniques for Developing Special Finite Element Shape Functions with Particular Reference to Singularities," Int. J. for Numerical Methods in Engineering, Vol. 15, pp. 733-751, 1980.
5. Bathe, K. J. and Wilson, E. L., Numerical Methods in Finite Element Analysis, Prentice-Hall, 1976.
6. Zienkiewicz, O. C., The Finite Element Method, McGraw-Hill, 1977.
7. Dunham, R. S., "A Quadrature Rule for Conforming Quadratic Crack Tip Elements," Int. J. for Numerical Methods in Engineering, Vol. 14, pp. 287-312, 1979.
8. Parker, A. P., The Mechanics of Fracture and Fatigue, E.&F.N. Spon Ltd., London, 1981.
9. Krieg, R. D. and Key, S. W., "Implementation of a Time-Independent Plasticity Theory into Structural Computer Programs," in Constitutive Equations in Viscoplasticity: Computational and Engineering Aspects, J. A. Stricklin and K. J. Saczalski (eds.), ASME, New York, AMD Vol 20, pp. 125-137.
10. Hussain, M. A., Pu, S. L., and Lorensen, W. E., "Singular Plastic Element: NASTRAN Implementation and Application," Sixth NASTRAN Users' Colloquium, NASA Conference Publication 2018, 1977.
11. The NASTRAN Programmer's Manual, NASA SP-223(01), September 1972.
12. Tada, H., Paris, P. C., and Irwin, G. R., The Stress Analysis of Cracks Handbook, Del Research Corporation, Hellertown, Penn., 1973.

TABLE 1 ERRORS IN COD AND K_I AS A FUNCTION OF MESH

		37 Grid Mesh	77 Grid Mesh	86 Grid Mesh	95 Grid Mesh
CENTRAL CRACK	COD Error (%)	- 7.73	- 2.46	- 2.82	- 2.92
	K_I Error (%)	11.63	2.91	1.69	1.22
EDGE CRACK WITH UNIFORM STRESS	COD Error (%)	- 5.24	- 2.51	- 2.60	- 2.64
	K_I Error (%)	- 6.26	- 5.18	- 3.19	- 2.05
EDGE CRACK WITH POINT LOAD	COD Error (%)	-	-	-	-
	K_I Error (%)	-26.11	- 9.38	- 0.40	5.26

40

TABLE 2 ERRORS IN K_I and K_{II} FOR 234 GRID MESH

CENTRAL CRACK IN SHEAR, FINITE PLATE		Error (%)
	K_I	- 1.37
K_{II}	4.23	

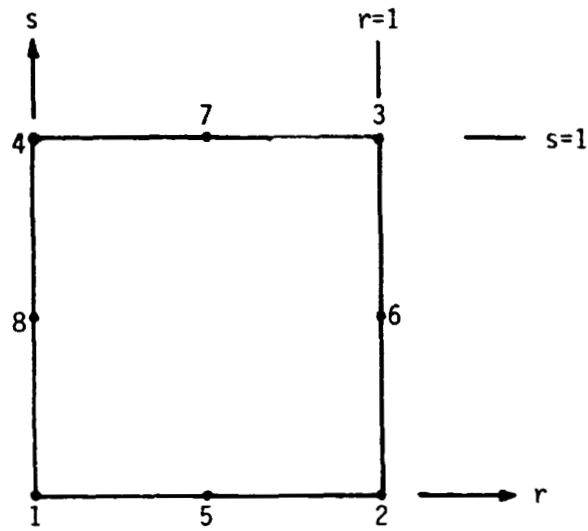


Figure 1 Nomenclature for Eight Node Isoparametric Element

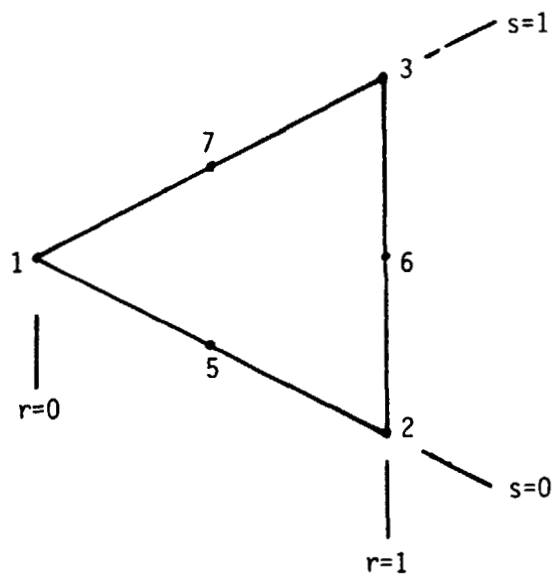


Figure 2 Degeneration of the Eight Node Element to a Six Node Triangular Element

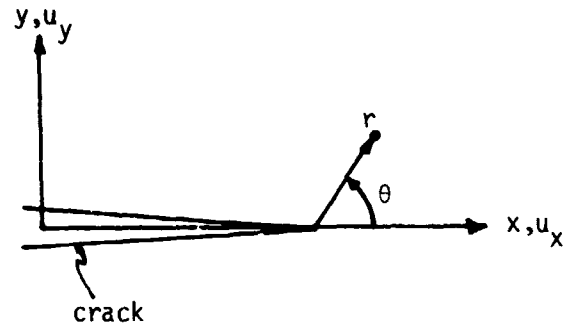


Figure 3 Nomenclature for Crack Geometry

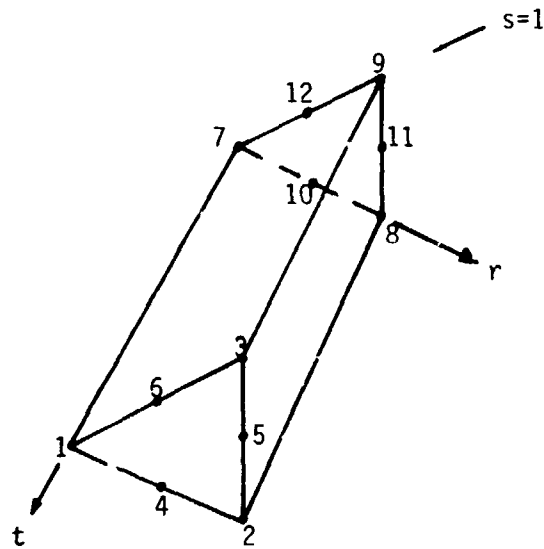


Figure 4 A Possible Three-Dimensional Generalization of the Two-Dimensional Element of Figure 2

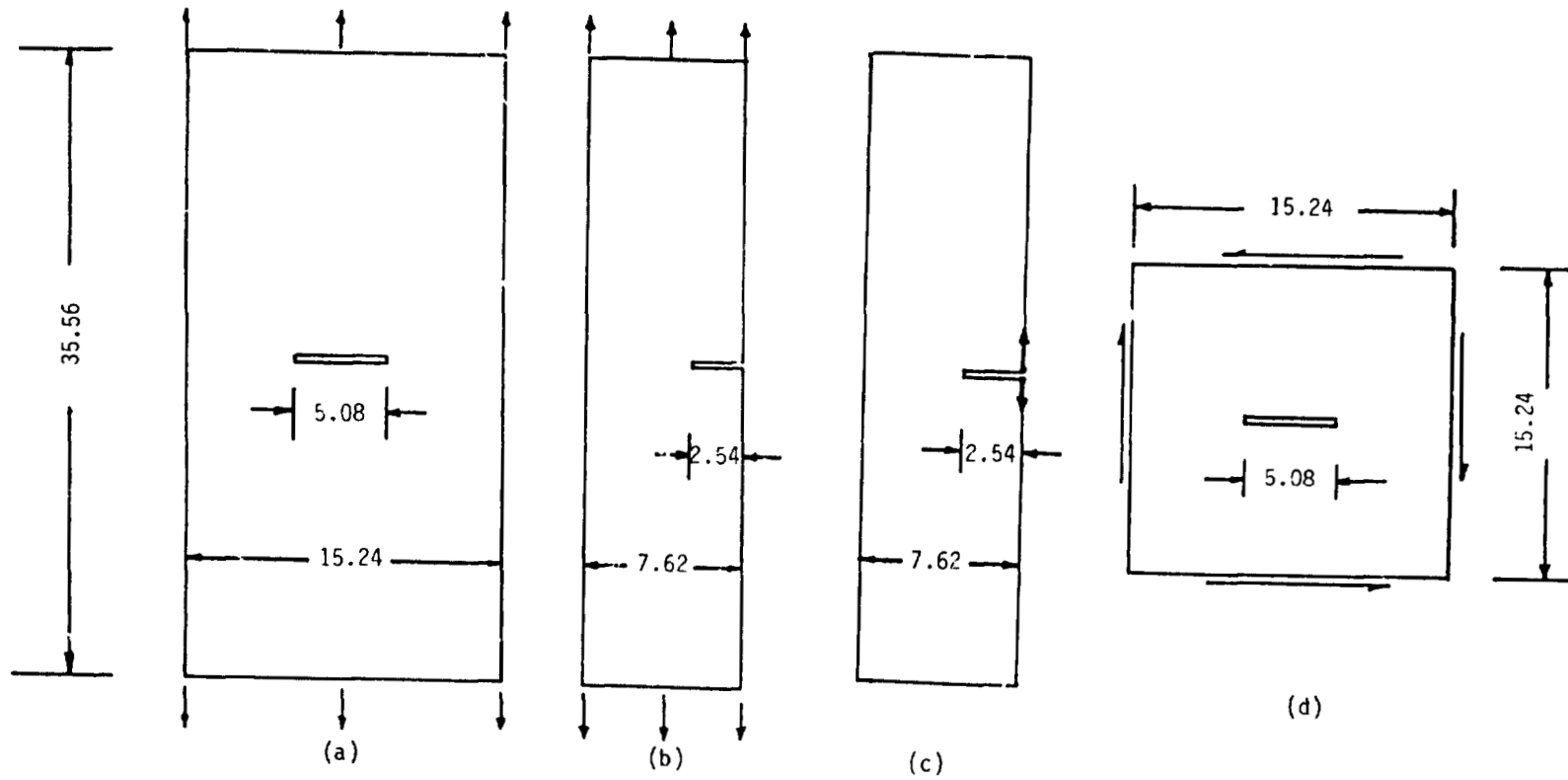
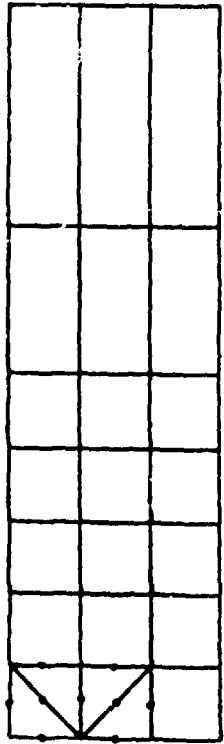
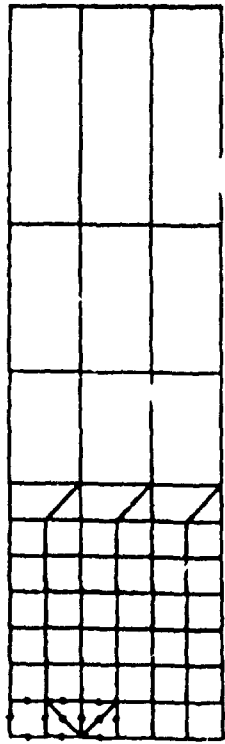


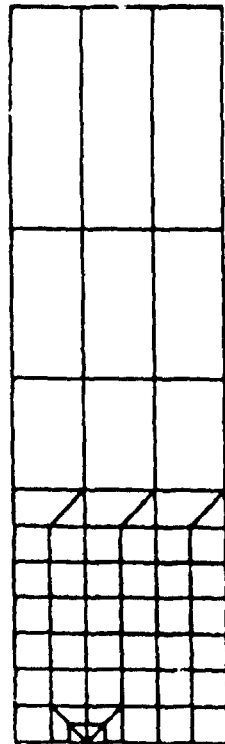
Figure 5 Crack Geometries Modeled (dimensions in cm's)
 (a) central crack
 (b) edge crack, uniform load
 (c) edge crack, point load
 (d) central crack in shear



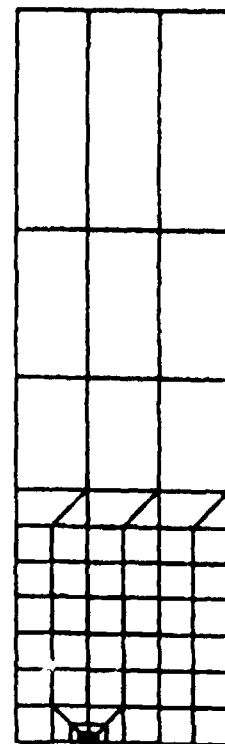
(a)



(b)



(c)



(d)

Figure 6 Different Mesh Sizes Analyzed
(a) 37 grid mesh
(b) 77 grid mesh
(c) 86 grid mesh
(d) 95 grid mesh

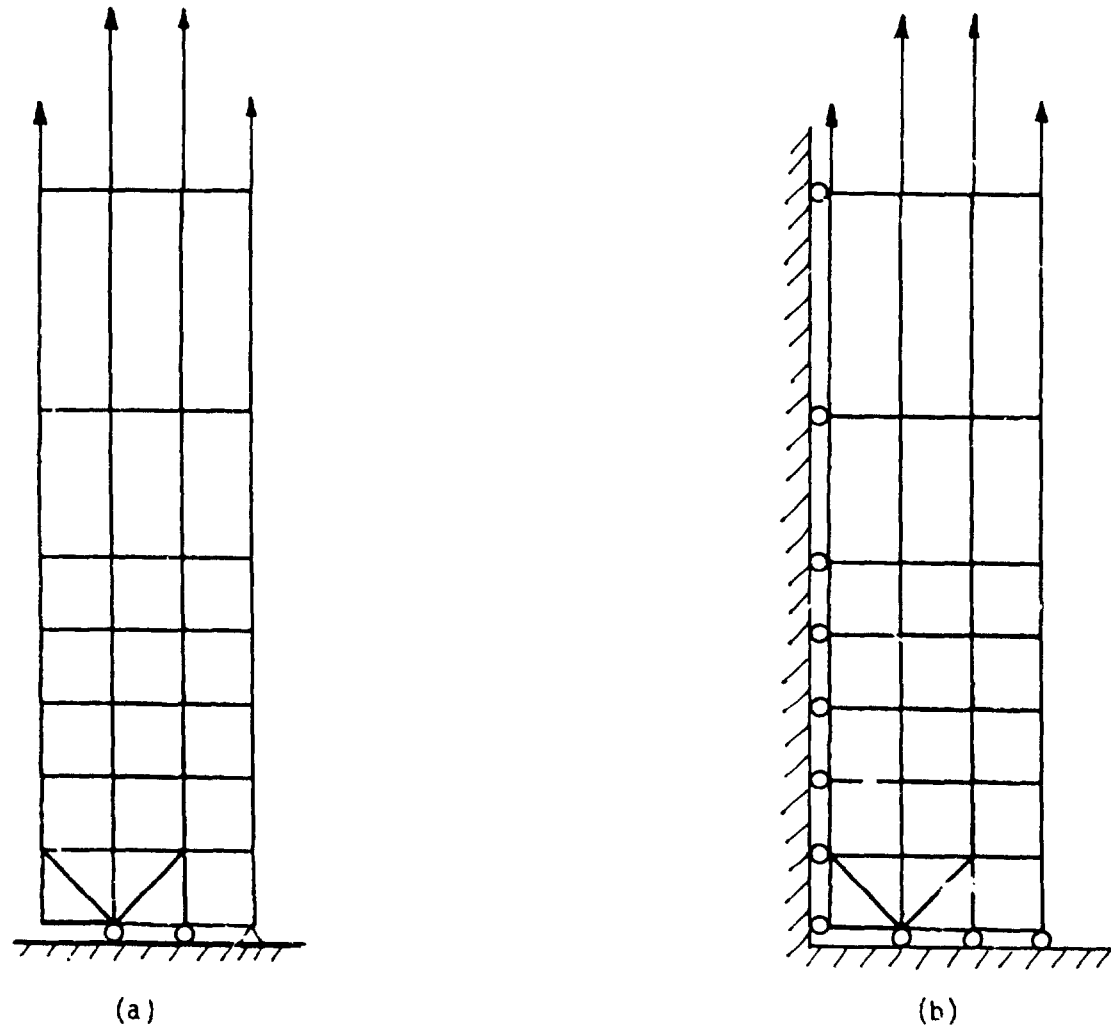
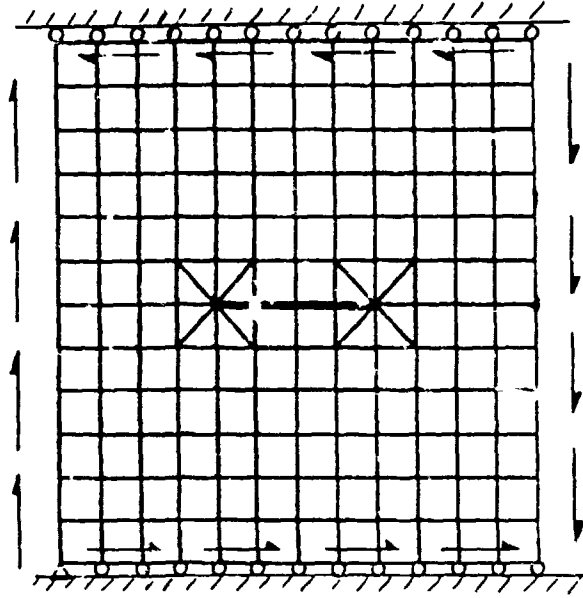
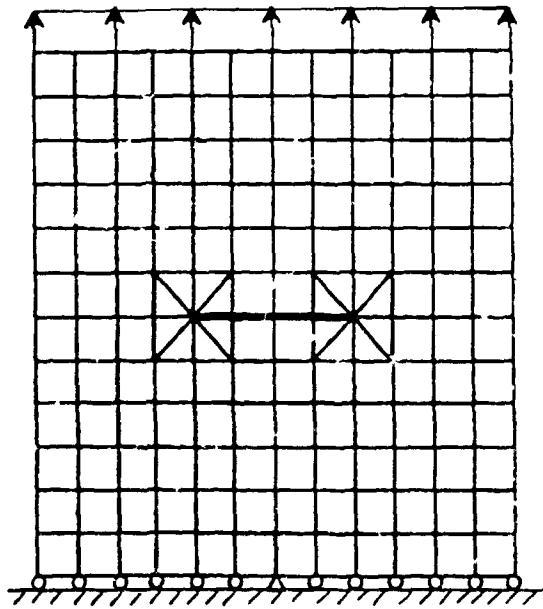


Figure 7 Boundary Conditions for Edge Crack and Central Crack Specimens
(a) edge crack
(b) central crack



(a) loading condition for K_{II} calculation



(b) loading condition for K_I calculation

Figure 8 Model of Central Crack in Finite Plate

N85-25867

**A FOUR-NODE BILINEAR ISOPARAMETRIC ELEMENT
IN ROCKWELL NASTRAN**

C. LIAG and R. E. ALLISON

**ROCKWELL INTERNATIONAL
NORTH AMERICAN AIRCRAFT OPERATIONS
EL SEGUNDO, CALIFORNIA**

SUMMARY

Development and evaluation of the Rockwell NASTRAN four-node quadrilateral (QUAD4) element is presented. The element derivation utilizes bilinear isoparametric techniques both for membrane and bending characteristics. The QUAD4 element coordinate system, membrane properties, lumped mass matrix, and treatment of warping are based upon the COSMIC/NASTRAN QDMEM1 element while the bending characteristics are based upon a paper by T. J. R. Hughes. The effects of warping on the bending stiffness, consistent mass, and geometric stiffness are based upon a paper by R. H. MacNeal. Numerical integration is accomplished by Gaussian quadrature on a 2 x 2 grid. Practical user support features include variable element thickness, thermal analysis and layered composite material definitions.

INTRODUCTION

Rockwell NASTRAN is the NASA/COSMIC released NASTRAN with Rockwell developed technical and efficiency enhancements incorporated. A total of nine Rockwell divisions fund the NASTRAN Group Service activities which include user consultation, development, maintenance, and validation of the production program. Rockwell NASTRAN is installed on IBM and CDC computing systems at three geographical locations. The program is being used by the participating divisions which are located in California, Oklahoma, Ohio, Michigan and Pennsylvania.

The Rockwell QUAD4 has been developed in order to provide our users with a state-of-the-art general quadrilateral element. The improved efficiency and greater accuracy provided by this element eliminate the need of any of the other COSMIC/NASTRAN quadrilateral elements. Practical user support features incorporated in the development include varying element thickness, thermal strains, and laminated composite material inputs. The element derivation utilizes bilinear isoparametric techniques both for membrane and bending characteristics with numerical integration being accomplished by Gaussian quadrature on a 2 x 2 grid.

The QUAD4 element coordinate system, membrane properties, lumped mass matrix and treatment of warping are based upon the COSMIC/NASTRAN QDMEM1 element while the bending properties are based upon a recent paper by T. J. R. Hughes (ref. 1). The effects of warping on the bending stiffness, consistent mass, and geometric stiffness are based upon a paper by R. H. MacNeal (ref. 2). The theory adopted from reference 1 appears to minimize or preclude some of the complications alluded to in reference 2. In particular, no special local Cartesian system or selective integration procedure is required to achieve a reasonably good element behavior.

General theoretical background of the element stiffness matrix is presented in equations 1 through 35 of the theoretical background section. Derivation of the equivalent thermal applied load vector is presented in equations 38 through 41.

The evaluation of element test results as proposed by reference 3 are presented in table 1. The test results for static analysis of various structures, mechanical loadings, and thermal analysis are presented in tables 2 through 8. The results for the real eigenvalue test case are presented in table 9. The transverse central deflection computed for the three composite material test cases using the MSC/QUAD4 and the Rockwell/QUAD4 element is presented in table 10.

THEORETICAL BACKGROUND

The relationship between forces and strains (including thermal terms) is described by the following matrix where the vectors $\{\epsilon^t\}$ and $\{x^t\}$ are thermal generated strains and curvatures, respectively.

$$\begin{Bmatrix} f \\ m \\ q \end{Bmatrix} = \begin{bmatrix} A & B & 0 \\ B & D & 0 \\ 0 & 0 & C \end{bmatrix} \begin{Bmatrix} \epsilon_m - \epsilon^t \\ \chi - \chi^t \\ \gamma \end{Bmatrix} \quad (1)$$

where

$$\{f\} = \begin{Bmatrix} f_x \\ f_y \\ f_{xy} \end{Bmatrix}, \quad \text{membrane forces per unit length} \quad (2)$$

$$\{m\} = \begin{Bmatrix} m_x \\ m_y \\ m_{xy} \end{Bmatrix}, \quad \text{bending moments per unit length} \quad (3)$$

$$\{q\} = \begin{Bmatrix} q_x \\ q_y \end{Bmatrix}, \quad \text{transverse shear forces per unit length} \quad (4)$$

$$\{\epsilon\} = \begin{Bmatrix} \epsilon_x \\ \epsilon_y \\ \epsilon_{xy} \end{Bmatrix}, \quad \text{membrane strains in means plane} \quad (5)$$

$$\{\chi\} = \begin{Bmatrix} \chi_x \\ \chi_y \\ \chi_{xy} \end{Bmatrix}, \quad \text{curvatures} \quad (6)$$

$$\{\gamma\} = \begin{Bmatrix} \gamma_x \\ \gamma_y \end{Bmatrix}, \quad \text{transverse shear strains} \quad (7)$$

The terms A, B and D are defined by the following integrals:

$$A = \int G_e \, dz \quad (8)$$

$$B = \int (-z) G_e \, dz \quad (9)$$

$$D = \int z^2 G_e dz \quad (10)$$

and $C = H_s G_3 \quad (11)$

The limits on the integration are from the bottom surface to the top surface of the plate. The matrix of material moduli, $[G_e]$, has the following form for orthotropic materials:

$$[G_e] = \begin{bmatrix} \frac{E_1}{1-\nu_1\nu_2} & \frac{\nu_1 E_2}{1-\nu_1\nu_2} & 0 \\ \frac{\nu_2 E_1}{1-\nu_1\nu_2} & \frac{E_2}{1-\nu_1\nu_2} & 0 \\ 0 & 0 & G_{12} \end{bmatrix} \quad (12)$$

Here, $\nu_1 E_2 = \nu_2 E_1$, is required that the matrix of elastic moduli be symmetric. The $[G_3]$ is a 2×2 matrix of elastic coefficients for transverse shear. H_s , the effective thickness for transverse shear, has a default value of $H_s / H = 5/6$, which is the correct value for a homogeneous plate with an actual membrane thickness of H .

Figure 1 depicts a plate composed of the eight laminas. For this case, A , B and D are defined as follows:

$$A = \sum_{k=1}^n G_e^k (h_k - h_{k-1}) \quad (13)$$

$$B = -\frac{1}{2} \sum_{k=1}^n G_e^k (h_k^2 - h_{k-1}^2) \quad (14)$$

$$D = -\frac{1}{3} \sum_{k=1}^n G_e^k (h_k^3 - h_{k-1}^3) \quad (15)$$

Let A^c and N_a denote the area and shape functions, respectively, of an element, where n is the number of element nodes. For the case of a homogeneous, isotropic, linearly elastic plate of thickness H , the element stiffness matrix, K^e , may be defined as follows.

$$K^e = K_b^e + K_s^e \quad (16)$$

$$K_b^e = \int_A e^{R^b T} D R^b dA \quad \text{bending stiffness} \quad (17)$$

$$K_s^e = \int_A e^{R^s T} C R^s dA \quad \text{shear stiffness} \quad (18)$$

where

$$R^b = [R_1^b, R_2^b \dots R_n^b] \quad (19)$$

$$R^s = [R_1^s, R_2^s \dots R_n^s] \quad (20)$$

The formulation of the element stiffness matrix follows the procedure defined in reference 4 and 5. Then R^b 's can be written in the following form:

$$R_a^b = \begin{bmatrix} 0 & 0 & N_{a'2} \\ 0 & N_{a'1} & 0 \\ 0 & N_{a'2} & N_{a'1} \end{bmatrix} \quad 1 \leq a \leq n \quad (21)$$

The shear stiffness is obtained by the technique mentioned in reference 1. The detailed procedures are discussed next.

Geometric and kinematic data are defined in figure 2, and the direction vectors have unit length (e.g. $\|e_{11}\| = 1$, etc.). Let w_a and θ_a denote the transverse displacement and rotation vector, respectively, associated with node a. Throughout, a subscript b will equal a+1 modulo 4.

The definition of the element shear strains may be described in the following steps.

- (1) For each element side, define a shear strain component at the midpoint, in a direction parallel to the side.

$$\bar{g}_a = (w_b - w_a) / l_a - \bar{e}_{a1} \cdot (\bar{\theta}_b + \bar{\theta}_a) / 2 \quad (22)$$

- (2) For each node, define a shear strain vector. (See figure 3 geometric interpretation of this process.)

$$\bar{\gamma}_b = \gamma_{b1} \bar{e}_{b1} + \gamma_{b2} \bar{e}_{b2} \quad (23)$$

$$\gamma_{b1} = (1 - \alpha_b^2)^{-1} (g_{b1} - g_{b2} \alpha_b) \quad (24)$$

$$\gamma_{b2} = (1 - \alpha_b^2)^{-1} (g_{b2} - g_{b1} \alpha_b) \quad (25)$$

$$\alpha_b = \bar{e}_{b1} \cdot \bar{e}_{b2} \quad (26)$$

$$g_{b1} = g_b \quad (27)$$

$$g_{b2} = -g_a \quad (28)$$

- (3) Interpolate the nodal values by way of the bilinear shape functions (N_a 's)

$$\boldsymbol{\gamma} = \sum_{a=1}^4 N_a \boldsymbol{\gamma}_a \quad (29)$$

For the transverse shear strain interpolations derived in the previous section, R^S takes on the following form:

$$R_b^S = R_{b1}^S R_{b2}^S R_{b3}^S \quad 1 \leq b \leq 4 \quad (30)$$

$$R_{b1}^S = 1_a^{-1} \bar{G}_a - 1_b^{-1} \bar{G}_b \quad (31)$$

$$R_{b2}^S = (e_{b2}^1 \bar{G}_a - e_{b1}^1 \bar{G}_b) / 2 \quad (32)$$

$$R_{b3}^S = (e_{b2}^2 \bar{G}_a - e_{b1}^2 \bar{G}_b) / 2 \quad (33)$$

$$\bar{G}_a = (1 - \alpha_a^2)^{-1} N_a (\bar{e}_{a1} - \alpha_a \bar{e}_{a2}) - (1 - \alpha_b^2)^{-1} N_b (\bar{e}_{b2} - \alpha_b \bar{e}_{b1}) \quad (34)$$

$$e_{bl} = \begin{pmatrix} e_{bl}^1 \\ e_{bl}^2 \end{pmatrix}, \text{ etc.} \quad (35)$$

The element stress resultants may be obtained from the following relations:

$$\begin{pmatrix} m_x \\ m_y \\ m_{xy} \end{pmatrix} = - D R^b d^e \quad \text{bending moments} \quad (36)$$

$$\begin{pmatrix} q_x \\ q_y \end{pmatrix} = C R^s d^e \quad \text{shear resultants} \quad (37)$$

where

$$d^e = \text{element displacement vector}$$

Finally, thermal expansion is represented by a vector of thermal strains

$$\{\epsilon^t\} = \begin{pmatrix} \alpha_x^t \\ \alpha_y^t \\ \gamma^t \end{pmatrix} = \begin{pmatrix} \cdot \\ \cdot \\ \cdot \end{pmatrix} (T - T_0) = \{t\} (T - T_0) \quad (38)$$

where α^t = thermal expansion coefficients

T = Temperature at any point in the element

T_0 = reference temperature of the material

An equivalent elastic state of stress that will produce the same thermal stress is

$$\{\sigma_t\} = [G] \{\epsilon^t\} \quad (39)$$

An equivalent set of generalized loads P applied to grid points of the element is obtained by

$$P = \int_A \{\epsilon\}^T \{\alpha_t\} h d A \quad (40)$$

The equivalent thermal moment vector is defined as

$$M_t = - \int_z [G] \{\alpha_t\} T' z dz \quad (41)$$

where T' is the thermal gradient at a cross-section of the plate.

NUMERICAL EXAMPLES

The test problems have been selected from reference 3. The elements tested included the COSMIC/QUAD2, the MSC/QUAD4 and the Rockwell/QUAD4. The test runs for QUAD2 and QUAD4 were performed on an IBM 3081 computer at the Rockwell Western Computing Center while the MSC/QUAD4 result were obtained by utilizing version 63 of MSC/NASTRAN on the Rockwell Scientific Computing Center CDC/CYBER equipment.

The grading system for finite elements proposed by reference 3 is:

<u>Grade</u>	<u>Range</u>
A	2% \geq Error
B	10% \geq Error > 2%
C	20% \geq Error > 10%
D	50% \geq Error > 20%
F	Error > 50%

The structures analyzed to evaluate the test elements included a patch test plate (figure 4), a straight cantilever beam (figure 5), a curved cantilever beam (figure 6), a rectangular plate with different aspect ratios (figure 7), a Scordelis-Lo roof (figure 8), and a simply supported plate (figure 9) for normal modes and layered composite analysis.

Table 1 presents the summary of grading results for the tested elements. The result for each of the individual test cases are reported in tables 2 through 10. The patch test results presented in Table 2 are reported in the form of percentage error of the computed stresses. The results reported in tables 3 through 7 are shown in normalized form where the computed displacement data has been divided by the theoretical value. The most disturbing failure of the QUAD2 element is its inability to get a passing grade for the straight beam in-plane shear and twist cases. QUAD2 also failed in the curved beam and Scordelis-Lo roof problems. Neither of the QUAD4's or the QUAD2 could achieve a passing grade for the straight beam in-plane shear with trapezoidal shaped elements. In general, our published results agree, but there are some differences from those reported in reference 3. In particular, the results of the twist case for all element configurations of the straight cantilevered beam problem do not agree with the results presented in reference 3. We believe that this was due to a problem with version 63 of MSC/NASTRAN as installed on our CDC equipment at the time we were making our test case runs.

CONCLUSION

In this paper, we have examined the behavior of the new four-node quadrilateral element implemented in Rockwell NASTRAN. The element has been shown to behave well for a variety of plane problems and has retained simplicity in the formulation. The formulation enabled straightforward generation of a linear triangular bending element, which has also been successfully implemented in Rockwell/NASTRAN.

REFERENCES

1. Hughes, T. J. R. and Tezduyar, T. E.: Finite Element Based on Mindlin Plate Theory with Particular Reference to the Four-Nodes Bilinear Isoparametric Elements. J. Appl. Mech., Sept. 1981, pp. 587-596.
2. MacNeal, R. H.: A Simple Quadrilateral Shell Element. Comp. & Struct., Vol. 8, 1978, pp. 175-183.
3. MacNeal, R. H. and Harder, R. L.: A Proposed Standard Set of Problems to Test Finite Element Accuracy. Proc. AIAA/ASME Struct. Dyn. Conf., Palm Springs, May, 1984.
4. Rockwell NASTRAN Theoretical Manual Level 17.500, NA-79-323, June 29, 1979, pp. 8.19-1-8.19-18.
5. Rockwell NASTRAN Programmer's Manual Level 17.500, NA-79-325, Sept. 10, 1979, pp. 5.8-33-5.8-44.
6. Rockwell NASTRAN Demonstration Manual Level 17.500, NA-79-324, June 29, 1979.

Table 1 Summary of Test Results

Test	Table	Element Shape	RI/ QUAD4	QUAD2	MSC/ QUAD4
1 Patch Test, Membrane	2(a)	Irregular	A	A	A
2 Patch Test, Bending	2(b)	Irregular	A	A	A
3 Straight Beam, Extension	3(a,b,c)	All	A	A	A
4 Straight Beam, In-Plane Shear	3(a)	Regular	B	F	B
5 Straight Beam, In-Plane Shear	3(c)	Irregular	D	F	D
6 Straight Beam, Out-of-Plane Shear	3(b,c)	Regular	A	B	A
7 Straight Beam, Out-of-Plane Shear	3(b,c)	Irregular	B	B	B
8 Straight Beam, Twist	3(a,b,c)	All	B	D	D
9 Curved Beam, In-Plane Shear	4	Regular	C	F	C
10 Curved Beam, Out-of-Plane Shear	4	Regular	B	D	C
11 Rectangular Plate (N=4)	5,6(a)	Regular	A	A	A
12 Scordelis-Lo Roof (N=4)	7	Regular	A	D	A

Failed Test Grade (D's and F's)

Table 2 Patch Test Results (Figure 4)
Max. Errors (%) of Stress

(a) Membrane Plate

	<u>RI/QUAD4</u>	<u>QUAD2</u>	<u>MSC/QUAD4</u>
$\sigma_x = \sigma_y$	4.2	4.2	0.0
τ_{xy}	1.0	1.0	0.0

(b) Bending Plate

	<u>RI/QUAD4</u>	<u>QUAD2</u>	<u>MSC/QUAD4</u>
$m_x = m_y$	4.2	4.2	0.0
m_{xy}	0.9	0.9	0.0
$y = \sigma_y$	4.2	4.2	0.0
τ_{xy}	1.0	1.0	0.0

Table 3. Results for Straight Cantilever Beam (Fig. 5)
Normalized Tip Displacement in Direction of Load

<u>Tip Loading Direction</u>	<u>RI/QUAD4</u>	<u>QUAD2</u>	<u>MSC/QUAD4</u>
(a) <u>Rectangular Elements</u>			
Extension	0.996	0.992	0.996
In-Plane Shear	0.904	0.032	0.904
Out-of-Plane Shear	0.980	0.971	0.986
Twist	0.941	0.567	0.702
(b) <u>Trapezoidal Elements</u>			
Extension	0.996	0.993	0.996
In-Plane Shear	0.071	0.016	0.071
Out-of-Plane Shear	0.964	0.963	0.958
Twist	0.884	0.605	0.705
(c) <u>Parallelogram Elements</u>			
Extension	0.996	0.992	0.996
In-Plane Shear	0.808	0.144	0.795
Out-of-Plane Shear	0.978	0.961	0.977
Twist	0.849	0.615	0.705

Table 4 Results for Curved Beam (Fig. 6)
Normalized Tip Displacement in Direction of Load

<u>Tip Loading Direction</u>	<u>RI/QUAD4</u>	<u>QUAD2</u>	<u>MSC/QUAD4</u>
In-Plane Vertical	0.835	0.025	0.835
Out-of-Plane	0.956	0.597	0.868

Table 5 Results for Rectangular Plate Simple Supports (Fig. 7)
with Concentrated Load

Normalized Transverse Deflection at Center

(a) <u>Aspect Ratio = 1.0</u>			
<u>Mesh Size(N)*</u>	<u>RI/QUAD4</u>	<u>QUAD2</u>	<u>MSC/QUAD4</u>
2	0.992	1.035	0.960
4	0.995	1.011	1.017
8	1.033	1.083	1.045
(b) <u>Aspect Ratio = 5.0</u>			
2	0.844	0.493	0.870
4	0.928	0.685	0.962
8	0.986	0.845	1.005

* only one quadrant is discretized

Table 6 Results for Rectangular Plate Clamped Supports
(Figure 7) With a Uniform Load

Normalized Lateral Deflection at Center

(a) Aspect Ratio = 1.0

<u>Mesh Size (N)</u>	<u>RI/QUAD4</u>	<u>QUAD2</u>	<u>MSC/QUAD4</u>
2	0.961	1.024	1.008
4	0.993	1.019	1.032
8	1.016	1.057	1.040

(b) Aspect Ratio = 5.0

2	1.124	0.873	1.314
4	0.962	1.001	1.016
8	1.002	1.019	1.016

Table 7 Results For Scordelis-Lo Roof (Figure 8)

Normalized Vertical Deflection at Midpoint of Free Edge

<u>Mesh Size (N)</u>	<u>RI/QUAD4</u>	<u>QUAD2</u>	<u>MSC/QUAD4</u>
2	1.309	0.881	1.313
4	1.017	0.690	1.021

Table 8 Comparison of Analytical, QUAD4, and QUAD1
NASTRAN DEMO 1-11-1 (Reference 6)

<u>Category</u>	<u>Max. Analytical</u>	<u>CQUAD1</u>	<u>CQUAD4</u>
Displacement	6.2898×10^{-1}	6.2895×10^{-1}	6.317195×10^{-1}
Moment m_y	1.4770×10^2	1.4888×10^2	1.4832200×10^2
Stress τ_y	7.764618×10^3	7.792977×10^3	7.779586×10^3

Table 9 Natural Frequency Comparison, cps on
 NASTRAN/DEMO 3-1-2 (4x4)

<u>Mode No.</u>	<u>Theoretical</u>	<u>RI/QUAD4</u>	<u>QUAD1</u>
1	0.9069	0.8823	0.9021
2	2.2672	2.3376	2.2837
3	4.5345	4.3515	4.7179

Table 10 Transverse Central Deflection of Simply Supported
 Composite Square Plate Under a Uniform Pressure (Figure 9)

<u>No. of Plies</u>	<u>Type of Laminate</u>	<u>RI/QUAD4(IBM)</u>	<u>MSC/QUAD4(CDC)</u>
2	90°/0°	5.63410x10 ⁻³	5.589612x10 ⁻³
3	0°/90°/0°	5.55896x10 ⁻³	5.423785x10 ⁻³
4	90°/0°/90°/0°	5.58961x10 ⁻³	5.666982x10 ⁻³

ORIGINAL PAGE IS
OF POOR QUALITY

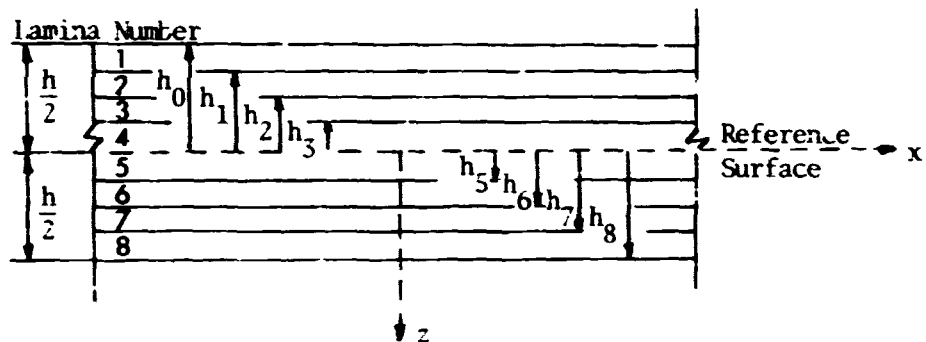


Figure 1. Laminated Plate

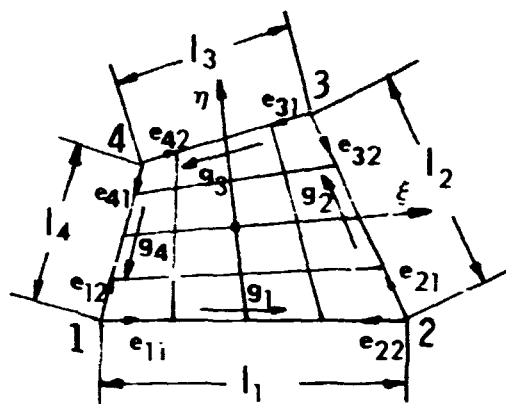


Figure 2. Geometric and Kinematic Data for the Four-Node Quadrilateral Element

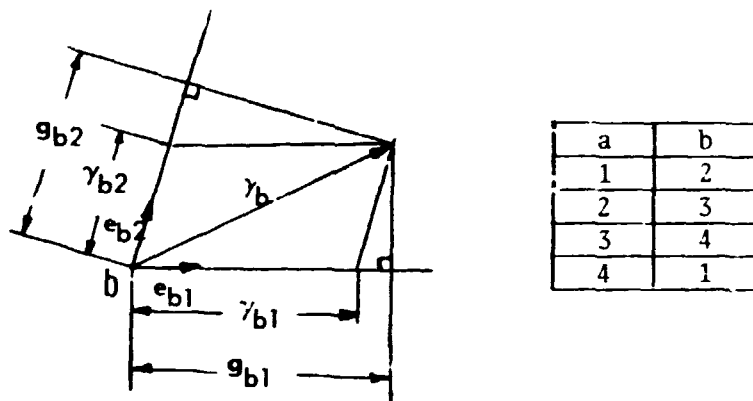
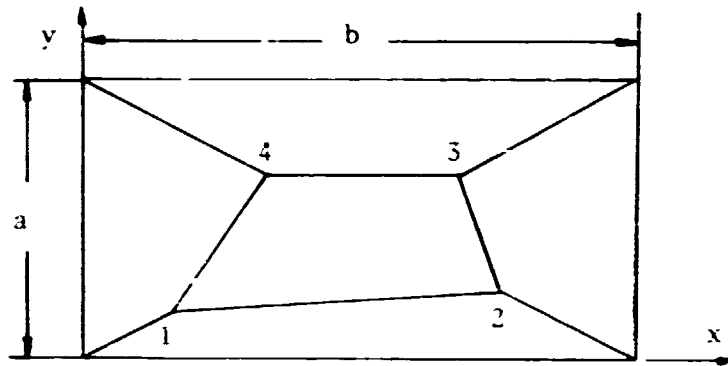


Figure 3. Definition of Nodal Transverse Shear Strain Vector



$$a = .12; \quad b = .24; \quad t = .001$$

$$E = 1.0 \times 10^6; \quad \nu = 0.25$$

Location of Inner Nodes:

	x	y
1	.02	.02
2	.18	.03
3	.16	.08
4	.08	.08

Boundary Conditions:

(a) Membrane

$$u = 10^{-3} (x + y/2)$$

$$v = 10^{-3} (y + x/2)$$

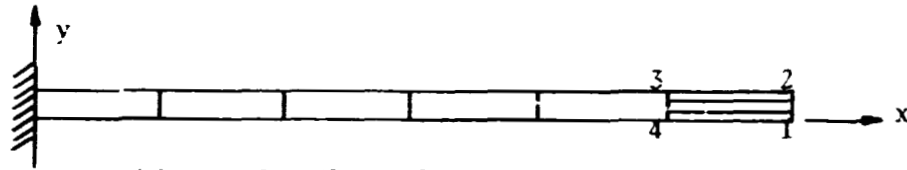
(b) Bending

$$w = 10^{-3} (x^2 + xy + y^2)/2$$

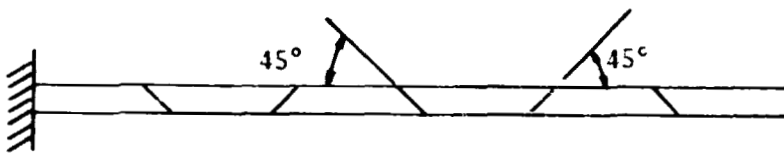
$$\theta_x = 10^{-3} (y + x/2)$$

$$\theta_y = 10^{-3} (-x - y/2)$$

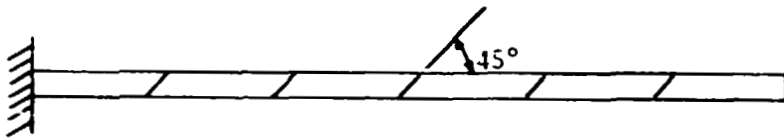
Figure 4. Patch Test for Plates



(a) Regular Shape Elements



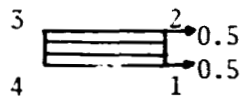
(b) Trapezoidal Shape Elements



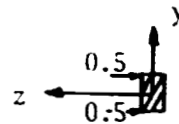
(c) Parallelogram Shape Elements

Length = 6.0; Height = 0.2; Thickness = 0.1
 $E = 1.0 \times 10^7$; $\nu = 0.3$; Mesh = 6 x 1
 Loading: Unit forces at free end

Extension



Out-of-plane shear



In-plane shear



Twist

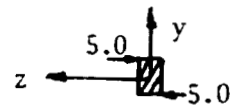
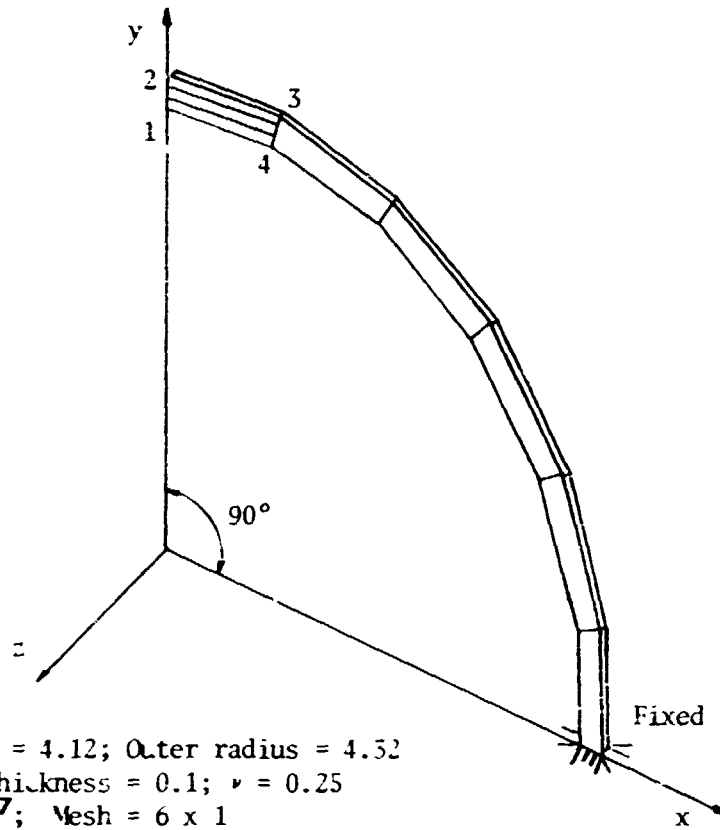


Figure 5. Straight Cantilever Beam



Inner radius = 4.12; Outer radius = 4.52
 Arc = 90°; Thickness = 0.1; $\nu = 0.25$
 $E = 1.0 \times 10^7$; Mesh = 6 x 1
 Loading: Unit forces at tip

In-plane shear

Out-of-plane shear

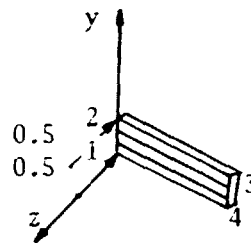
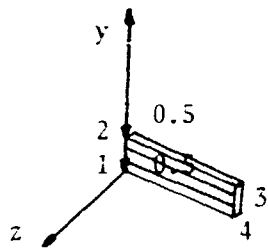
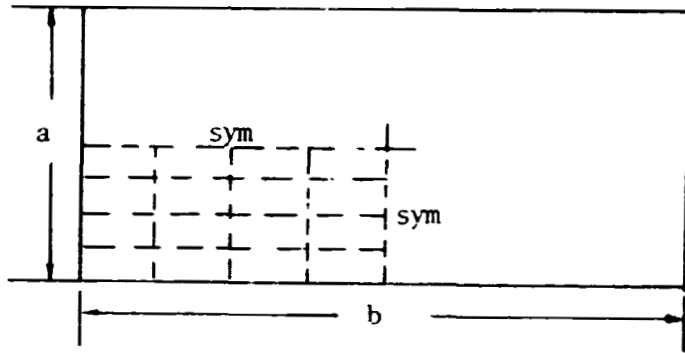
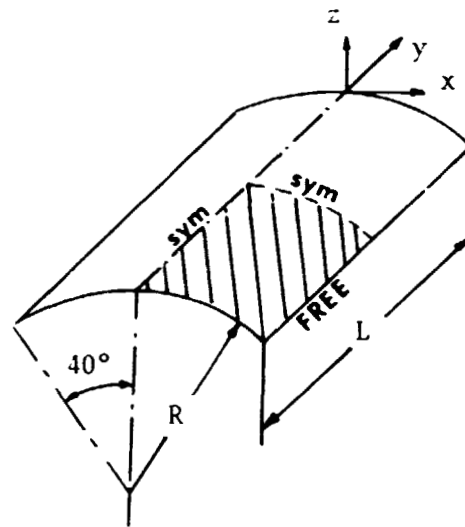


Figure 6. Curved Beam



$a = 2.0$; $b = 2.0$ or 10.0 ; $\nu = 0.3$
 Thickness = 0.001 ; $E = 1.7472 \times 10^7$
 Boundaries = simply supported or clamped
 Mesh = $N \times N$ (on 1/4 of plate)
 Loading: Uniform pressure $q = 10^{-4}$ or
 Central load $p = 4.0 \times 10^{-4}$

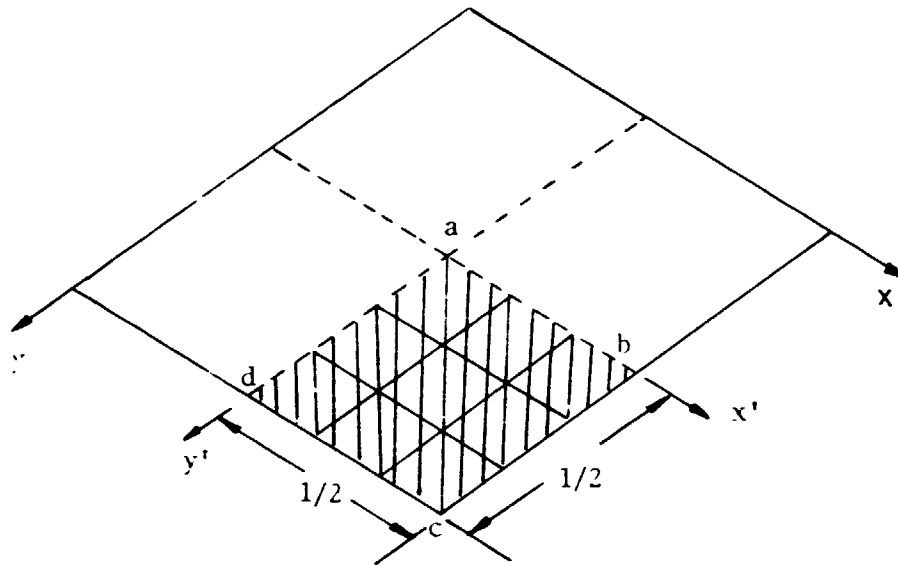
Figure 7. Rectangular Plate



Radius = 25.0 ; Length = 50.0 ; Thickness = 0.25
 $\nu = 0.0$; Loading = 90.0 per unit area in $-z$ direction
 $E = 1.32 \times 10^8$; $U_x = U_z = 0$ on curved edges
 Mesh = $N \times N$ on shaded area

Figure 8. Scordelis-Lo Roof

ORIGINAL PAGE IS
OF POOR QUALITY



$l = 10.0$; $T = 0.2$; $\nu = .25$

$E_1 = 20. \times 10^6$; $E_2 = .5 \times 10^6$; $G = .25 \times 10^6$

Loading Condition: 0.5 psi uniform pressure

Case 1 : 2 piles, material angle of fiber $90^\circ/0^\circ$

Case 2 : 3 piles, " " $0^\circ/90^\circ/0^\circ$

Case 3 : 4 piles, " " $90^\circ/0^\circ/90^\circ/0^\circ$

Figure 9. Simply Supported Square Plate for a Layered Structure

N85-25868

LAYERED COMPOSITE ANALYSIS CAPABILITY

FOR NASTRAN

Dr. R. (Swami) Narayanaswami and Mr. J. G. Cole
Computerized Structural Analysis and Research Corporation

SUMMARY

Laminated composite material construction is gaining popularity within industry as an attractive alternative to metallic designs where high strength at reduced weights is of prime consideration. This has necessitated the development of an effective analysis capability for the static, dynamic and buckling analyses of structural components constructed of layered composites. Theoretical and user aspects of layered composite analysis and its incorporation into C.S.A.R. Corporation's proprietary version of the NASTRAN® program, CSA/NASTRAN*, are discussed. The availability of stress based and strain based failure criteria is described which aids the user in reviewing the voluminous output normally produced in such analyses. Simple strategies to obtain minimum weight designs of composite structures are discussed. Several example problems are presented to demonstrate the accuracy and user convenient features of the capability.

INTRODUCTION

As structural designers turn more often to high strength light weight composite materials to solve critical design problems, the internal loads and stress analysis tasks become more complex. The finite element models generated to describe composite laminates using existing NASTRAN capabilities either require a considerable number of membrane elements "stacked" on top of one another to represent the plies or require some form of lumping/delumping procedure when using a single element to represent the plies. Both methods of modeling are used to overcome the substantial amount of work involved in determining the material properties to be referenced by an element. Neither method is without its drawbacks. The "stacked" membrane model requires a considerable number of elements and neglects bending effects while the single element representation requires pre-processing functions to generate an appropriate set of element and material properties and also requires post-processing to obtain the individual ply stresses and strains. The

*CSA/NASTRAN is an advanced proprietary version of the NASTRAN® general purpose structural analysis program. NASTRAN is a registered trademark of NASA. CSA/NASTRAN is developed, maintained and marketed by the C.S.A.R. Corporation, Northridge, California.

method of composite material construction analysis discussed in this work and incorporated into CSA/NASTRAN employs the single element technique. The user describes the laminate by means of new PCOMP, PCOMP1, PCOMP2 and MAT8 bulk data cards.

The finite elements used to model the composite structure must be capable of representing coupling between the membrane and bending actions to handle the general case of unsymmetrical ply layups and/or element plane offset from the plane of the grid points. Since none of the existing NASTRAN combination membrane/bending plate elements consider coupling, some work on the finite elements available was also required to implement this new layered composite analysis capability. After some review of the current element formulations and implementations, a decision was made to incorporate new general purpose combined membrane/bending plate elements. The two new elements added to the CSA/NASTRAN library are the CQUAD4 and CTRIA3. The CQUAD4 is a 4-node bilinear isoparametric general quadrilateral element. It is capable of membrane/bending coupling, variable thickness over the element surface and considers the effects of transverse shear flexibility. The CTRIA3 is the 3-node triangular shaped companion to the CQUAD4 element.

User convenient features to scan the voluminous output normally produced in such analyses are provided. The evaluation of a "failure index" for each element based on the commonly used failure theories (maximum stress, maximum strain, Hill, Hoffman and Tsai-Wu) allows the user to review at a glance whether any laminate is stressed (or strained) beyond allowable limits. Some simple techniques to obtain minimum weight designs of layered composite structures are also discussed.

THEORETICAL DISCUSSION

Before discussing the theoretical details of the implementation of the layered composite analysis capability, the theory of the CQUAD4 and CTRIA3 elements is discussed briefly.

The CQUAD4 Element

The CQUAD4 element is a four-node bilinear isoparametric element capable of representing membrane, bending (with transverse shear effects) and membrane-bending coupling behavior. Geometric and kinematic data for the element are shown in figure 1.

Shape of the Element

Standard isoparametric theory is used to represent the shape of the element. A set of element parametric co-ordinates (ξ, η) have been selected which vary linearly between zero and one with the extreme values occurring on the sides of the quadrilateral. Lines of constant ξ and lines of constant η are indicated on figure 1.

Element Co-ordinate System

The x-axis is along the line connecting the first two grid points; the y-axis is perpendicular to the x-axis and lies in the "plane" of the element. If all four grid points do not lie in a plane, a mean plane is defined as discussed below. Finally, the z-axis is normal to the plane of the element and forms a right-handed coordinate system with the x- and y-axes.

Mean-Plane

If the four grid points of the CQUAD4 element do not lie in a plane, a mean-plane containing the projections of the four points is defined such that the four points are alternately H units above and H units below the mean-plane as shown in figure 2 and reference 1.

Membrane Behavior

An enhanced formulation of the four noded isoparametric quadrilateral membrane element available in the NASTRAN® program, the CQDMEM1 element, is used to represent the membrane behavior of the CQUAD4 element. The enhancement consists of using reduced integration to the in-plane shear representation (single point integration, at the center of the element, instead of 2x2 integration). All other details of the element formulation are the same as that discussed in reference 2.

If the element is non-planar, mean-plane transformations that produce only forces and not moments at grid points are used to expand the 8x8 stiffness matrix to 12x12 to allow for three displacements per grid point.

Bending Behavior

A simple, inexpensive to formulate and accurate bending behavior is a necessary prerequisite for plate elements that are to be used in a layered composite analysis. The four-node bilinear isoparametric element discussed by Hughes and Tezduyar (ref. 3) possesses these qualities and is therefore used to represent the bending behavior of the CQUAD4 element. Detailed derivation of the element stiffness, load vector calculations and the stress resultants are provided in reference 3; salient points from the derivations are discussed below.

The concept is to have the transverse displacement interpolated via nine-node Lagrange shape functions and the rotations via four-node bilinear shape functions. The transverse shear strains are calculated in a special way independent of the mid side and center node displacement degrees of freedom; hence four-node bilinear shape functions may be used for transverse displacement also. In other words, the use of special calculations for transverse shear strains allows the use of bilinear shape functions for transverse displacement, rotations and transverse shear strains together with the benefit to the element of quadratic accuracy with respect to Kirchoff modes.

The implementation of the element follows standard isoparametric theory. Interested readers may consult references 3 and 4 for additional details.

If the element is non-planar, mean plane transformations are derived to ensure that the element is in equilibrium when the stiffness matrix is transformed from grid points on the mean-plane to the actual grid point locations.

Membrane/Bending Coupling Effects

The membrane and bending actions are decoupled for plate theory. However, practical situations may necessitate use of CQUAD4 elements to model bending of plates about an axis offset from the geometrical neutral axis. Membrane-bending coupling effects have to be included to analyze such models; these effects also occur in unsymmetric laminates. The CQUAD4 element is therefore designed to include membrane-bending coupling behavior.

The CTRIA3 Element

The CTRIA3 element is a three-node linear element capable of representing membrane, bending (with transverse shear effects) and membrane-bending coupling behavior. The element and the element co-ordinate system are shown in figure 3. The membrane behavior is modeled using the TRMEM element formulation (reference 2), the bending and membrane-bending coupling behavior are modeled using a procedure analogous to that used for the CQUAD4. Being a linear element, the CTRIA3 element is not as accurate as the bilinear CQUAD4 element. It must, therefore, be mentioned in this context that the CQUAD4 element is to be used for all plate modeling requirements; the CTRIA3 element is to be used only where geometrical considerations preclude the use of the CQUAD4 element.

The PSHELL Bulk Data Card

The properties for both the CQUAD4 and the CTRIA3 elements are specified using the new PSHELL element property bulk data card. The PSHELL card data input format provides for specification of element thickness, moment of inertia parameter, transverse shear thickness parameter, stress recovery coefficients and material property references. Provisions are made for specifying up to four different material property identification numbers to separately represent membrane, bending, transverse shear and coupled membrane/bending behaviors.

Force-Displacement Relationship

The relationship between forces and strains used for the CQUAD4 and CTRIA3 elements is

$$\begin{Bmatrix} F \\ M \\ Q \end{Bmatrix} = \begin{bmatrix} tG_1 & t^2G_4 & 0 \\ t^2G_4 & IG_2 & 0 \\ 0 & 0 & t_sG_3 \end{bmatrix} \begin{Bmatrix} \epsilon_m - \epsilon^T \\ \chi - \chi^T \\ \gamma \end{Bmatrix}$$

where

$$\begin{Bmatrix} F \end{Bmatrix} = \begin{Bmatrix} F_x \\ F_y \\ F_{xy} \end{Bmatrix},$$

membrane forces per unit length

$$\begin{Bmatrix} M \end{Bmatrix} = \begin{Bmatrix} M_x \\ M_y \\ M_{xy} \end{Bmatrix},$$

bending moments per unit length

$$\begin{Bmatrix} Q \end{Bmatrix} = \begin{Bmatrix} Q_x \\ Q_y \end{Bmatrix},$$

transverse shear force per unit length

$$\begin{Bmatrix} \epsilon_m \end{Bmatrix} = \begin{Bmatrix} \epsilon_x \\ \epsilon_y \\ \epsilon_{xy} \end{Bmatrix},$$

membrane strains in mean plane

$$\begin{Bmatrix} \chi \end{Bmatrix} = \begin{Bmatrix} \chi_x \\ \chi_y \\ \chi_{xy} \end{Bmatrix},$$

curvatures

$$\begin{Bmatrix} \gamma \end{Bmatrix} = \begin{Bmatrix} \gamma_x \\ \gamma_y \end{Bmatrix},$$

transverse shear strains

and

G_1 is the 3x3 elasticity matrix for membrane action
 G_2 is the 3x3 elasticity matrix for bending action
 G_3 is the 2x2 elasticity matrix for transverse shear action.
 G_4 is the 3x3 elasticity matrix for membrane-bending coupling action.
 t is the element thickness
 I is the element moment of inertia
 t_s is the effective thickness for transverse shear

LAYERED COMPOSITE ANALYSIS

Composite laminates have a number of laminae stacked at various orientations (see figure 4 and reference 5). Ideally, a full 3-dimensional analysis using anisotropic material properties is to be performed. However, lamination theory is a good starting point to perform 2-dimensional analysis that gives satisfactory results at a much reduced cost.

Assumptions Used in Lamination Theory

The following assumptions are used in lamination theory:

- (i) Lamina is in a state of plane stress.
- (ii) Perfect bonding exists between layers so that no slippage of one lamina relative to another occurs.
- (iii) There is no z-variation of the transverse displacement; in other words, thin plate theory can be used.

All of the above assumptions are found to be reasonable in practice (especially in cases where the thickness of the laminate is small in comparison with the length and width).

For unidirectional composites, two orthogonal planes of symmetry exist. One plane is parallel to the fibers and the other is transverse to the fibers. Knowing the material properties in this system, the 3x3 elasticity matrix $[G_M]$ can be evaluated for each lamina. Knowing the orientation of each lamina, the elasticity matrix $[G_M]$ can be transformed to $[G_E]$ in a common element system. Knowing the elasticity matrix $[G_E]$ for all laminae in the common element coordinate system, the membrane, bending membrane-bending and transverse shear elasticity matrices for the laminate are calculated as follows:

$$[G_L] = \frac{1}{t} \int [G_E] dz$$

$$[G_2] = \frac{1}{I} \int (-z)^2 [G_E] dz$$

$$[G_4] = \frac{1}{t^2} \int (-z) [G_E] dz$$

The $[G_3]$ matrix is calculated by assuming that the equations of equilibrium similar to the simple beam theory can be developed independently for the X- and Y- directions. It is to be noted that this is an approximation and that the inter-laminar stresses evaluated by lamination theory are only approximate. However, it is felt that this approximate analysis is better than an analysis neglecting the effects of transverse shear matrix $[G_3]$.

USER INPUT

Composite laminate analysis requires input of laminate data and the orthotropic material property information. This is accomplished by designing the following new bulk data cards shown in the Appendix:

MAT8: two-dimensional orthotropic material data

PCOMP, PCOMP1, PCOMP2: Property cards for composites

User specifies the property identification number of a PCOMP (or PCOMP1 or PCOMP2) property card instead of PSHELL property card for the CQUAD4 and CTRIA3 elements for use as a layered composite element. PCOMP, PCOMP1 and PCOMP2 cards refer to the material properties of each lamina using MAT1, MAT2 or MAT8 cards.

OUTPUT FROM LAYERED COMPOSITE ANALYSIS

The stresses and strains output for each lamina for all the elements yield voluminous output. Some of these output items are shown in figure 5(a) and 5(b) (stresses and strains in each lamina). The concept of failure index for each laminate is introduced to review the output easily. Five commonly used failure theories are provided for this purpose. These are (i) maximum stress theory, (ii) maximum strain theory, (iii) Hill's theory, (iv) Hoffman's theory, and (v) Tsai-Wu theory. Based on the user specified failure theory, the state of stress (or strain) in each lamina is used to evaluate a failure index for the

lamina. The highest failure index value among all laminae of the laminate and the interlaminar stress to allowable bonding stress ratio is defined as the failure index of the laminate. By examining the failure index table, the results of the analysis can be easily reviewed to see whether any lamina has failed according to the specified criterion. A sample output of the failure index table is shown in figure 5(c).

NASTRAN MODIFICATIONS

The design of the layered composite analysis capability that has been incorporated into CSA/NASTRAN was driven by two important requirements. The first was that the capability has maximum versatility and convenience in describing the composite laminate with a minimum of user action necessary. The second was that modifications to existing NASTRAN functional capabilities be kept to a minimum. To achieve the first requirement, seven new bulk data card types shown in the Appendix, and a new functional module were designed and added to the program. The second requirement was satisfied without considerable effort when the decision was made to implement new finite element technology, rather than to try and adapt the existing membrane/bending plate elements to the layered composite environment. This decision also reduced the risk of inadvertently disturbing some aspect of the existing finite element implementations. Thus, the modifications made to the NASTRAN program for the layered composite analysis capability can be divided into two parts: (1) those required for the addition of the new general purpose QUAD4 and TRIA3 finite elements, and (2) those required for the specification and data recovery of the composite laminate itself.

The incorporation of the new 4-node quadrilateral shaped plate and 3-node triangular shaped plate finite elements into NASTRAN has been achieved with the addition of only three new bulk data cards. These new cards are the finite element connection cards, CQUAD4 and CTRIA3, and the element property card, PSHELL, which is referenced by both elements. This new general purpose capability required the following modifications to existing areas of the NASTRAN program for Statics and Normal Modes solution sequences:

- ° Preface IFSiP and IFXiBD routines to process the CQUAD4, CTRIA3 and PSHELL bulk data cards
- ° GPTABD block data routine to add the internal descriptions of the new finite elements to the NASTRAN element library and establish various element-dependent pointer data
- ° TAI table processor module routines to process the material property orientation angle definition options available on the CQUAD4 and CTRIA3 element connection cards
- ° EMG module EMGPRO routine to call the new element matrix generation subroutines

- ° SSG1 module TEMPL routine to call the new element thermal load vector generation subroutines
- ° SDR2 module routines to call the new element stress data recovery subroutines
- ° OFP module routines to provide additional output file page headings for the CQUAD4 and CTRIA3 element forces and stresses

Modifications to the DSMG1 module and RANDOM modules are presently underway to extend this capability to differential stiffness/buckling and the dynamics solution sequences.

The incorporation of the composite laminate specification capability has been achieved with the addition of only four new bulk data cards. These new cards are the MAT8 card which describes the material properties of ply layers, and the PCOMP, PCOMP1 and PCOMP2 cards which describe the laminate ply layup with varying degrees of generality and convenience. One new functional module was also required which performs composite element ply stress data recovery operations. A preface processor converts the supplied PCOMP and MAT8 data into equivalent PSHELL and MAT2 data, updates element connection data references to property data and adds the PSHELL data to the element property table (EPT) and the MAT2 data to the material property table (MPT). The preface then also sets a DMAP parameter to control data recovery operations based upon whether composite element properties are referenced. The layered composite analysis capability required the following modifications to the NASTRAN code:

- ° Preface IFSIP and IFXIBD routines to process the PCOMP, PCOMP1, PCOMP2 and MAT8 bulk data cards
- ° A new preface processor, IFP6, which generates equivalent PSHELL and MAT2 bulk data from the PCOMP and MAT8 data supplied; IFP6 also updates the GEOM2 data block to reflect the element references to the newly generated property data and adds the data to the EPT and MPT
- ° XMPLOD routine to establish module properties for the new composite element stress data recovery processor, SDRCOMP
- ° PREMAT/MAT material property processing routine to handle the MAT8 data
- ° SDRCOMP, a new functional module added to generate individual ply stresses and strains for the layered composite elements and to generate a failure index table of ply data based upon several available failure theories
- ° OFP module to process the new composite element Failure Index Table, ply stress data block and ply strain data block

The action required on the part of the user to access this new layered composite analysis capability is considered to be very minimal. The user must insert the

appropriate PCOMP and MAT8 data which describe the composite laminate into the bulk data deck. Then if the user wishes to have ply data recovery operations performed, a STRAIN= case control request must be present and the SDRCOMP and OFP modules must be altered into the rigid format.

Once the initial capability verification testing process was satisfactorily completed, modifications were made to the NASTRAN rigid format data base to provide the necessary CHKPNT/RESTART functions associated with the addition of the new bulk data cards. Quality assurance testing procedures were then completed satisfactorily demonstrating the incorporation of the layered composite analysis capability as a general purpose feature of CSA/NASTRAN.

CAPABILITY VERIFICATION TESTING

When any new capability is added to NASTRAN, a series of tests is performed to ensure that the capability has been incorporated properly. These tests are designed to ensure that the new capability performs according to design specifications and that existing functional capability has not been adversely affected by the new features. The capability verification tests performed to ensure satisfactory implementation of the layered composite analysis feature were divided into two categories. The first series of tests were designed to validate the proper installation of the new CQUAD4 and CTRIA3 finite elements. They demonstrated the accuracy of the elements under various geometry, material property and loading configurations. Several of the test cases were taken from those proposed in reference 6. The remainder of the tests were designed to demonstrate implementation correctness and not necessarily theoretical accuracy. The test problems considered to be most important are now briefly described:

- ° Patch test - measures the ability of the element to represent constant strain states of deformation. The model geometry and results are shown in figure 6.
- ° Twisted beam - measures the effect of warping on the element. The model geometry and results are shown in figure 7.
- ° Equilibrium tests - each column/row of the elemental stiffness matrix was summed about some point (say, node one) of the element to ensure that the matrix represented a set of forces that were in equilibrium. This test was performed on several configurations which included non-rectangular shapes and element warping. In all instances, the resulting summations were computational zeroes. An additional set of tests were also run which extracted the free-free mode shapes of the plate using unit masses at each degree of freedom. This test resulted in extraction of six distinct rigid body modes which further guarantees equilibrium of the stiffness matrix.

Several other elemental tests were performed to ensure that the elements performed according to specifications. These tests are the same as those described in reference 6 and the twisted ribbon problem described in reference 3. The results from these tests are summarized in table 1.

in addition to the tests performed to validate the addition of new finite elements, a series of tests were also performed to validate the installation of the layered composite analysis capability into CSA/NASTRAN. Once again, many sample problems were run to demonstrate that the capability performed up to design specifications. These tests included exercising all of the various options available on the PCOMP, PCOMP1, and PCOMP2 bulk data cards. Two example problems were run to demonstrate the theoretical correctness of the implementation. These problems were taken from reference 7. The geometry for the first problem, a static analysis of a simply supported square plate subjected to sinusoidally varying pressure load, is presented in figure 8. The geometry for the second problem, a modal analysis of a simply supported cylinder, is presented in figure 9. The modal analysis was accomplished using the cyclic symmetry analysis capability within NASTRAN. The results of these example problems are presented in table 2.

EXAMPLE APPLICATION

To illustrate the application of the layered composite capability in CSA/NASTRAN for design of practical composite structures, the example of an optimum design aluminum rectangular plate (ref. 8, 9 and 10) is analyzed using 8-ply laminated composite made of graphite/epoxy (commercially identified by Type T 300/5208). The geometry, loading and finite element modeling is shown in figure 10(a) and 10(b). The material properties and allowable stresses used in the example are those specified in reference 5. Starting from the optimally designed aluminum plate thickness for the various element groupings, the thickness for the composite model is obtained in 2 or 3 iterations using the enhanced fully stressed design algorithm implemented in CSA/NASTRAN. The thickness for the layered composite plate and the aluminum plate are shown in figure 10(c). The mass for the composite model is 0.40275 kg (0.8879 lbs) versus the mass of 1.034 kg (2.28 lbs) reported in reference 8 and 1.0796 kg (2.38 lbs) reported in reference 9 and 0.9487 kg (2.0915 lbs) reported in reference 10. It is to be noted that it is possible to obtain other optimum designs for the layered composite model. The design shown in figure 10(c) is a feasible design (design that satisfies all specified constraints). The objective here was to find the weight savings possible between layered composite construction and aluminum on a practical example problem subjected to stress and displacement constraints. The capabilities provided in CSA/NASTRAN allows the engineers the option of reviewing such "optimum" designs to select the most economical designs for their needs.

WORK IN PROGRESS

Several additions and extensions to the layered composite analysis capability are currently underway. For versatility, two additional plate elements are being formulated and added to the CSA/NASTRAN finite element library. These elements are the 8-node isoparametric general quadrilateral element CQUAD8 and its 6-node triangular companion, the CTRIA6. Both elements will be able to reference com-

posite material properties. An option to model the composite elements for membrane behavior only (without any reference to bending, transverse shear or membrane-bending coupling) to facilitate modeling the upper and lower covers of a wingbox, for example, is now available. This option will be extended to include property optimization methods to consider the thickness or orientation of each individual ply as a design variable. The OPTPR1 and OPTPR2 modules are being enhanced to incorporate evaluation of design sensitivity coefficients so that structural optimization using mathematical programming techniques can be performed in addition to fully stress design resizing.

CONCLUSION

The theoretical formulations of layered composite analysis capability for addition to the NASTRAN program are presented in this paper. The need to have simple, accurate plate elements for layered composite elements is discussed. The addition of two such elements, the CQUAD4 and CTRIA3 elements, and the layered composite capability into the CSA/NASTRAN program, an enhanced proprietary version of the April 1984 release of NASTRAN, developed and maintained by C.S.A.R. Corporation, is described. Verification problems and example application problems to illustrate the useful features available to engineers to analyze and obtain optimum designs of layered composite structures are also presented.

REFERENCES

1. Cook, R. D. Concepts and Applications of Finite Element Analysis. John Wiley and Sons, New York, 1981.
2. The NASTRAN Theoretical Manual. NASA SP-221 (06) January 1981.
3. Hughes, T. J. R. and Tezduyar, T. E.: Finite Elements Based Upon Mindlin Plate Theory with Particular Reference to the Four-Node Bilinear Isoparametric Element. Journal of Applied Mechanics, September 1981.
4. Zienkiewicz, O. C.: The Finite Element Method. McGraw-Hill Book Company (UK) Limited, 1977.
5. Tsai, Stephen W.; and Hahn, H. Thomas: Introduction to Composite Materials. Technomic Publishing Company, Westport, Connecticut, 1980.
6. MSC/NASTRAN Application Manual. March 1984 Application Note; Joseph, J., Editor; The MacNeal-Schwendler Corporation, Los Angeles, CA.
7. MSC/NASTRAN Application Manual. Section 2.12; Joseph, J., Editor; The MacNeal-Schwendler Corporation, Los Angeles, CA.
8. Prasad, B.; and Haftka, R.: Optimal Structural Design with Plane Finite Elements. Proceedings of the ASCE, Journal of the Structural Div., ST 11, Nov. 1979.
9. Fluery, C.; Ramanathan, R. K.; Salema, M.; and Schmit, L. A.: Access Computer Program for the Synthesis of Large Structural Systems. NASA Langley Research Center Optimization Conference, April 1984.
10. CSAR/OPTIM User's Manual. Computerized Structural Analysis and Research Corporation, Northridge, California, July 1984.

Table 1. Summary of Test Results for CSA/NASTRAN QUAD4 Plate Element.

No.	Test	Element Loading		Element Shape*	Displacement		GRADE
		In-Plane	Out-Of-Plane		Theory	QUAD4 Model	
1.	Patch Test	X		Irregular	Figure 6	Figure 6	A
2.	Patch Test		X	Irregular	Figure 6	Figure 6	A
3a.	Straight Beam - Extension	X		Rectangle	3.000-5	2.985-5	
3b.	Straight Beam - Extension	X		Trapezoid	3.000-5	2.976-5	A
3c.	Straight Beam - Extension	X		Parallelogram	3.000-5	2.997-5	
4.	Straight Beam - Bending	X		Rectangle	.10810	.097632	B
5a.	Straight Beam - Bending	X		Trapezoid	.10810	.007668	
5b.	Straight Beam - Bending	X		Parallelogram	.10810	.008734	F
6.	Straight Beam - Bending		X	Rectangle	.43210	.42389	A
7a.	Straight Beam - Bending		X	Trapezoid	.43210	.41611	
7b.	Straight Beam - Bending		X	Parallelogram	.43210	.42216	B
8a.	Straight Beam - Twist			Rectangle	.03208	.03017	
8b.	Straight Beam - Twist			Trapezoid	.03208	.03433	C
8c.	Straight Beam - Twist			Parallelogram	.03208	.02534	
9.	Curved Beam	X		Rectangle	.58734	.04441	D
10.	Curved Beam		X	Rectangle	.50220	.47305	B
11a.	Twisted Beam	X		Regular	.005424	.005373	
11b.	Twisted Beam		X	Regular	.001754	.001721	A
12a.	Rect. Plate (ss-u,N=4,b/a=5)		X	Regular	12.97	12.6976	
12b.	Rect. Plate (ss-c,N=4,b/a=5)		X	Regular	16.96	15.1614	
12c.	Rect. Plate (cc-u,N=4,b/a=5)		X	Regular	2.56	2.4411	B
12d.	Rect. Plate (cc-c,N=4,b/a=5)		X	Regular	7.23	5.6828	
13.	Scordelis-Lo Roof (N=4)		X	Regular	.3024	.31623	B
14.	Spherical Shell (N=8)		X	Regular	.0940	.09288	A
15a.	Thick-Walled Cylinder v=.43	X		Regular	5.0399-3	4.2523-3	
15b.	Thick-Walled Cylinder v=.499	X		Regular	5.0602-3	1.803-3	F
15c.	Thick-Walled Cylinder v=.4999	X		Regular	5.0623-3	2.649E-4	
16a.	Twisted Ribbon (Case A, L=10)		X	Regular	0.0291+	0.02774	
16b.	Twisted Ribbon (Case B, L=10)		X	Regular	0.0291+	0.02774	B
Number of Failed Tests (D's and F's)							3

*Regular means that element shape has not been intentionally distorted

† Theoretical results are taken from a fine mesh finite element solution

Remarks: 1. Letter grades are used to indicate the following error percentages:

A: Error < 2%; B: 2% < Error < 10% C: 10% < Error < 20%
D: 20% < Error < 50%; F: Error > 50%

2. Letter grades show for problem set numbers 3, 5, 7, 8, 11, 12 and 15 have been assigned by averaging the absolute error for each problem in the set.

3. For details of test problem descriptions 1-15, consult the March 1984 MSC/NASTRAN Application Note in the MSC/NASTRAN Application Manual of the MacNeal-Schwendler Corporation, Los Angeles, CA; for problem 16, refer to "Finite Elements Based Upon Mindlin Plate Theory with particular reference to the Four-node Bilinear Isoparametric Element" by T.J.R. Hughes and T.E. Tezduyar, Journal of Applied Mechanics, September 1981.

TABLE 2. Composite Element Accuracy Test Results

SQUARE PLATE ~ Statics

Center point deflection of a simply supported square plate due to a sinusoidally varying pressure load

Number of Plies	Type of Laminate	Center Point Deflection	
		Theory	NASTRAN
2	Unsymmetric	0.010029	0.010056
3	Symmetric	0.00035347	0.00036245
4	Unsymmetric	0.00042175	0.00042622

CYLINDER ~ Cyclic Symmetry Normal Modes

Harmonic Number	Longitudinal Halfwave	FREQUENCY (rad/sec)	
		Theory	NASTRAN
1	1	18.608	18.576
	3	46.605	46.426
	5	61.435	60.810
2	1	9.391	9.377
	3	27.219	27.143
	5	41.842	41.535
3	1	6.274	6.230
	3	18.895	18.864
	5	30.804	30.644
4	1	4.934	4.893
	3	14.578	14.568
	5	24.494	24.404

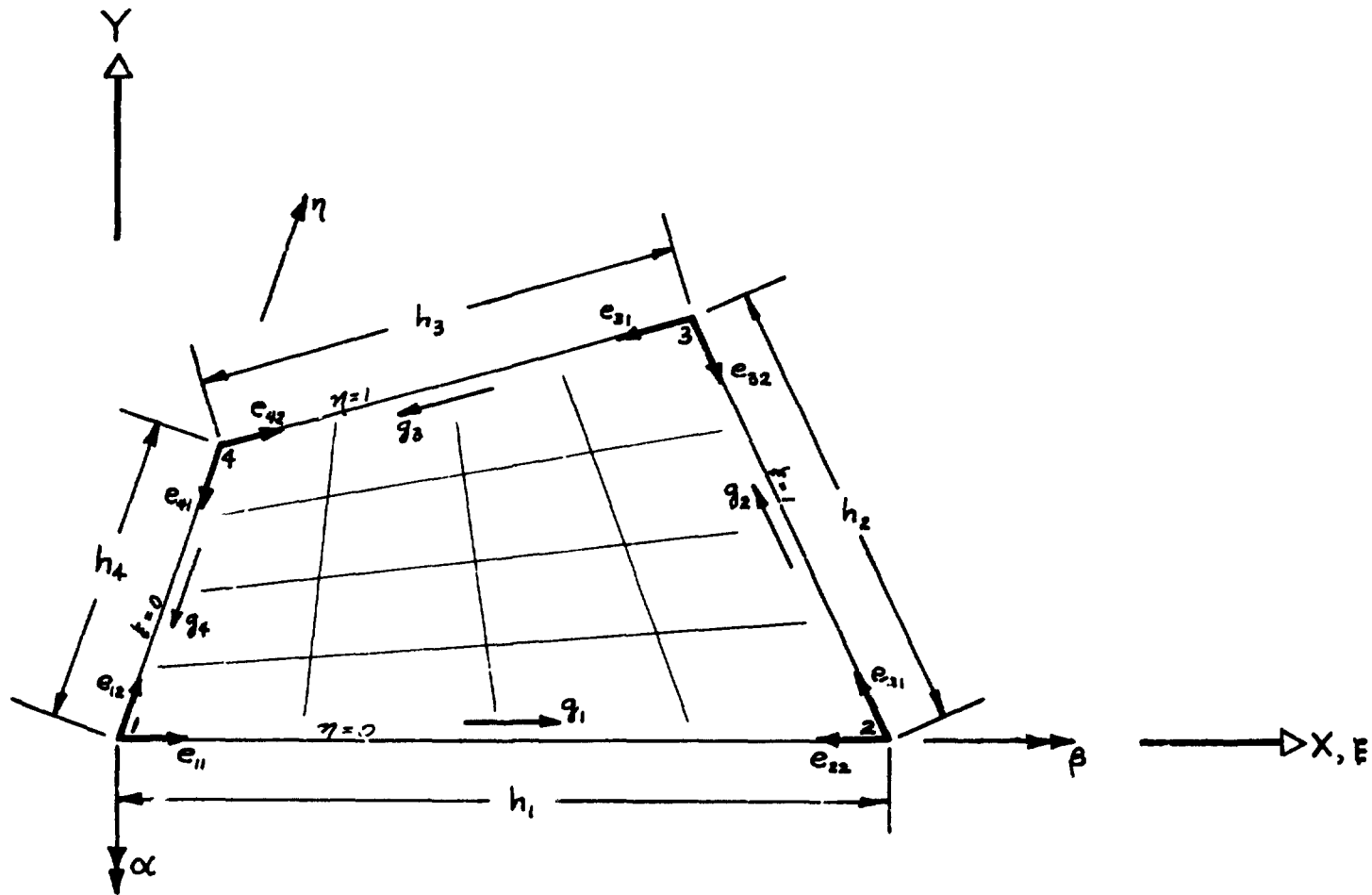


Figure 1. Geometric and Kinematic Data for CQUAD4 Element

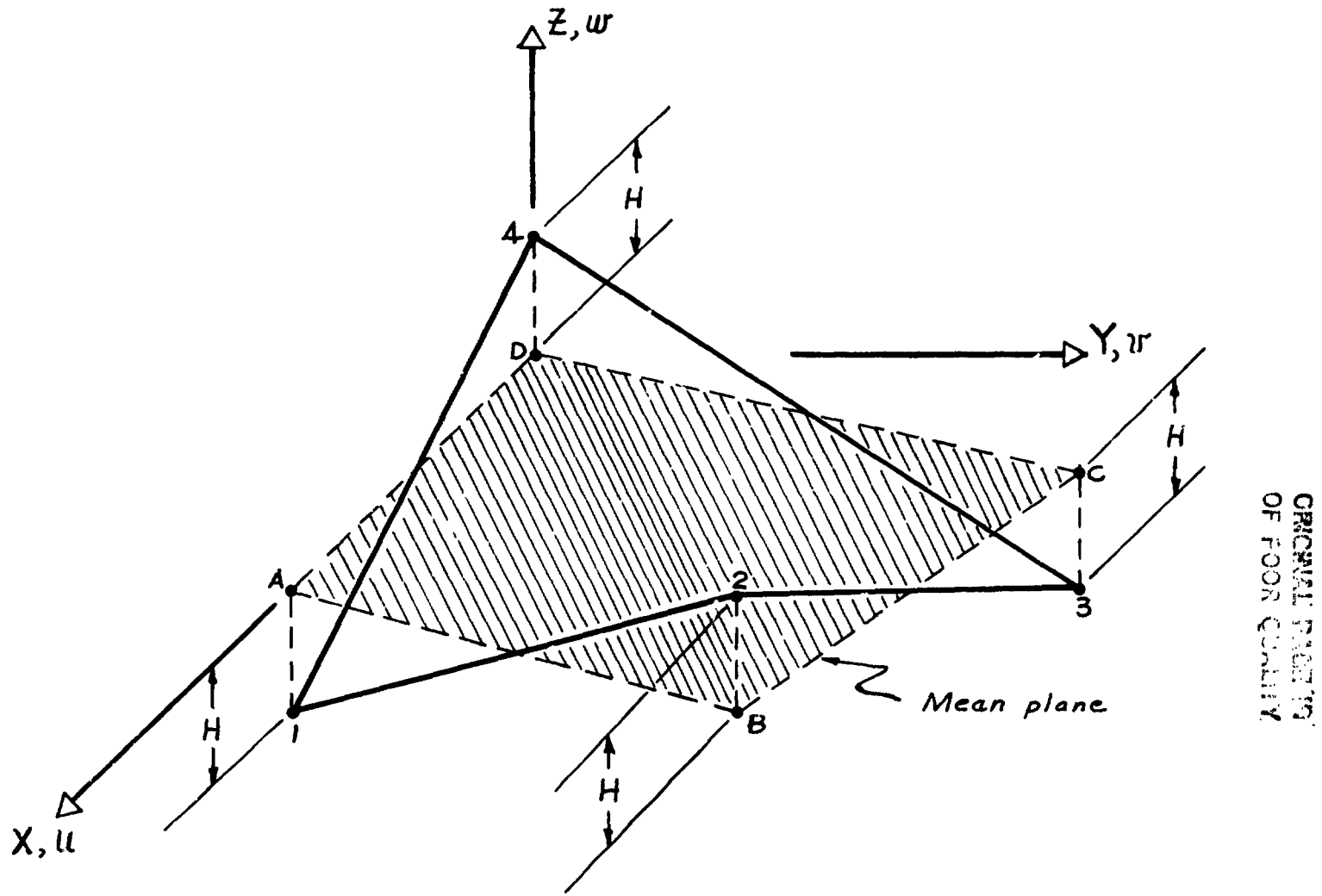


Figure 2. Warped QUAD4 1-2-3-4 in Local coordinates x, y, z

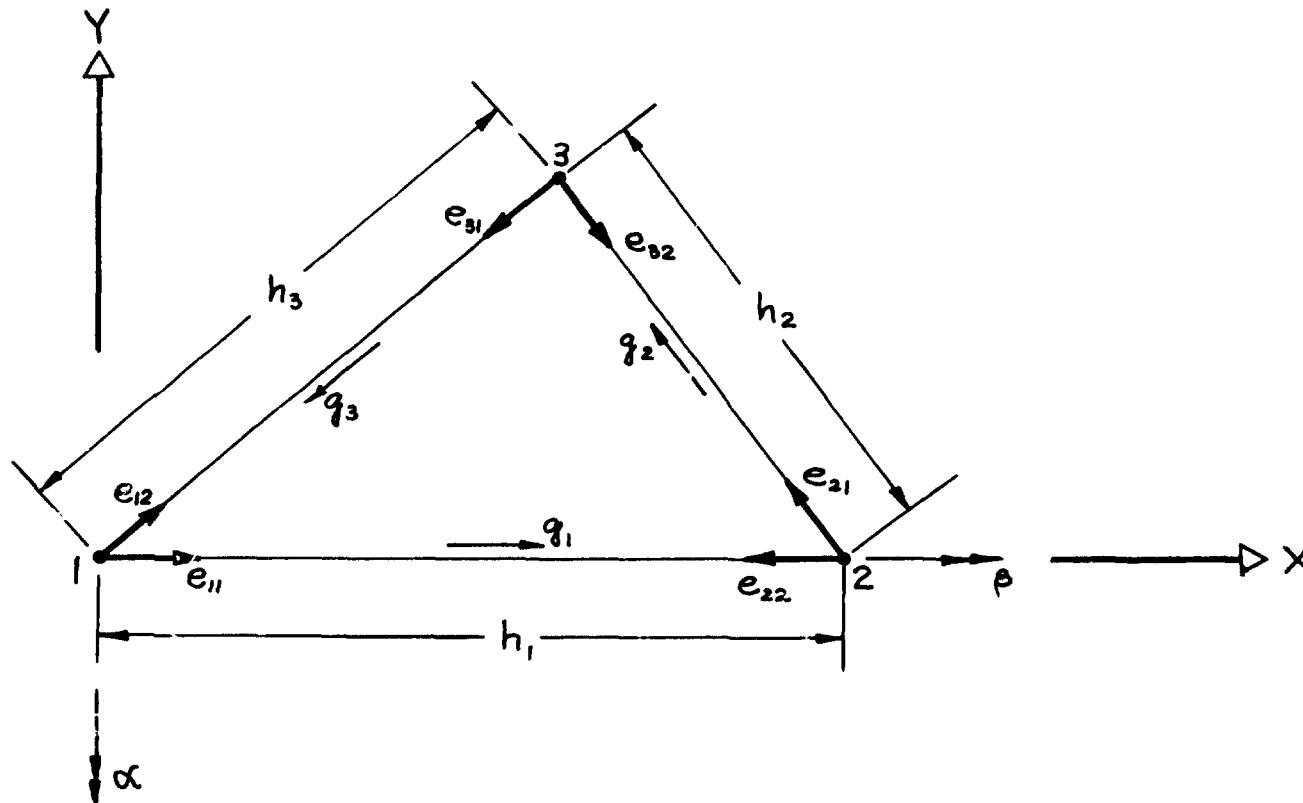


Figure 3. Geometric and Kinematic Data for CTRIA3 Element

ORIGINAL PAGE
OF POOR QUALITY

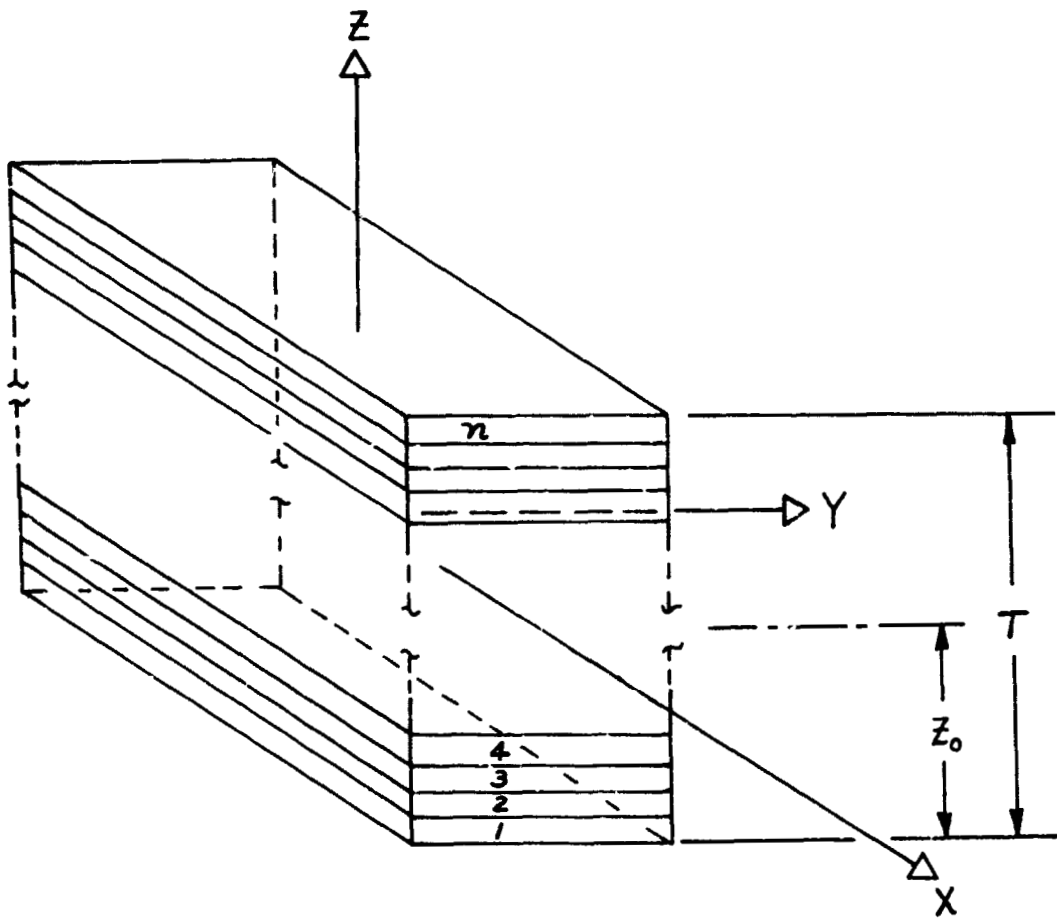


Figure 4. Laminae Identification for n -ply Laminate

USE COMPOSITES INSTEAD OF ALUMINUM

ELEMENT ID	PLY ID	STRESSES IN LAYERED COMPOSITE ELEMENTS (CGUAD4)			INTER-LAMINAR STRESSES		PRINCIPAL STRESSES (ZERO SHEAR) MAJOR	MINOR	MAX SHEAR	
		STRESSES IN FIBRE AND MATRIX DIRECTIONS NORMAL-1	NORMAL-2	SHEAR-12	SHEAR-1Z	SHEAR-2Z				
101	1	-8.94110E+02	-9.83429E+02	1.60752E+02	1.65201E+01	5.08403E+00	37.24	-7.71930E+02	-1.10561E+03	1.66840E+02
101	2	-5.00005E+03	-5.20859E+02	-1.64373E+02	2.01973E+01	2.49705E+01	-84.14	-4.73222E+02	-5.04769E+03	2.28723E+03
101	3	-4.71923E+03	-2.40935E+02	2.78624E+02	2.24036E+01	3.69024E+01	86.45	-2.23667E+02	-4.73650E+03	2.25641E+03
101	4	-2.44536E+03	4.39937E+01	-2.29645E+01	2.25379E+01	4.96653E+01	-89.45	-4.37740E+01	-2.44558E+03	1.20090E+03
101	5	2.44536E+03	4.39937E+01	2.29645E+01	2.24036E+01	3.69024E+01	0.55	2.44558E+03	4.37740E+01	1.20090E+03
101	6	4.71923E+03	2.40935E+02	-2.78624E+02	2.01973E+01	2.49705E+01	-3.55	4.73650E+03	2.23667E+02	2.25641E+03
101	7	5.00006E+03	5.20859E+02	4.64373E+02	1.65201E+01	5.08402E+00	5.86	5.04769E+03	4.73222E+02	2.28723E+03
101	8	8.94110E+02	9.83429E+02	-1.60752E+02	0.0	-3.78227E-06	-52.76	1.10561E+03	7.71930E+02	1.66840E+02
102	1	1.83268E+03	-9.15424E+02	1.35344E+02	7.16597E+00	3.23905E+00	2.81	1.83933E+03	-9.22074E+02	1.38070E+03
102	2	-4.08235E+03	-4.29399E+02	-5.28776E+02	8.76106E+00	1.59088E+01	-81.93	-3.54397E+02	-4.15735E+03	1.90148E+03
102	3	-3.89688E+03	-1.97373E+02	3.17265E+02	9.71811E+00	2.35106E+01	85.13	-1.70362E+02	-3.92369E+03	1.87676E+03
102	4	-2.37724E+03	-2.08959E+01	-1.93348E+01	9.77636E+00	3.16419E+01	-89.53	-2.37371E+01	-2.37740E+03	1.17833E+03
102	5	2.37724E+03	2.08959E+01	1.93348E+01	9.71811E+00	2.35106E+01	0.47	2.37740E+03	2.07371E+01	1.17833E+03
102	6	3.89688E+03	1.97373E+02	-3.17265E+02	8.76106E+00	1.59088E+01	-4.87	3.72389E+03	1.70362E+02	1.87676E+03
102	7	4.08235E+03	4.29399E+02	5.28776E+02	7.16597E+00	3.23905E+00	8.07	4.15735E+03	3.54397E+02	1.90148E+03
102	8	-1.83268E+03	9.15424E+02	-1.35344E+02	0.0	-2.40970E-06	-67.19	9.22074E+02	-1.83933E+03	1.38070E+03

Figure 5(a): Stress Output for Layered Composite Elements

USE COMPOSITES INSTEAD OF ALUMINUM

ELEMENT ID	PLY ID	STRAINS IN LAYERED COMPOSITE			ELEMENTS (CGUAD4)			MAX SHEAR
		STRAINS IN FIBRE AND MATRIX DIRECTIONS			PRINCIPAL	STRAINS (ZERO SHEAR)		
		NORMAL-1	NORMAL-2	SHEAR-12	ANGLE	MAJOR	MINOR	
101	1	-2.357592E-05	-6.489339E-04	1.546283E-04	13.1568	1.256893E-05	-6.850787E-04	3.488238E-04
101	2	-1.849577E-04	-2.954064E-04	-4.466843E-04	-41.4761	2.099030E-04	-6.902672E-04	4.500851E-04
101	3	-1.772439E-04	-1.109746E-04	2.670106E-04	48.5239	1.259418E-04	-4.141603E-04	2.700510E-04
101	4	-9.270482E-05	-3.367991E-06	-2.208976E-05	-76.8432	1.795561E-06	-9.786837E-05	4.983197E-05
101	5	9.270487E-05	3.367984E-06	2.208973E-05	13.1568	9.786840E-05	-1.795554E-06	4.903198E-05
101	6	1.772439E-04	1.109746E-04	-2.670106E-04	-41.4761	4.141603E-04	-1.259418E-04	2.700510E-04
101	7	1.849577E-04	2.954064E-04	4.466843E-04	48.5239	6.902671E-04	-2.099030E-04	4.500851E-04
101	8	2.357592E-05	6.489340E-04	-1.546283E-04	-76.8432	6.850788E-04	-1.256893E-05	3.488239E-04
102	1	7.959603E-05	-6.324911E-04	1.301883E-04	10.0425	1.026514E-04	-6.555465E-04	3.790970E-04
102	2	-1.509667E-04	-2.439583E-04	-5.086337E-04	-42.3885	3.132919E-04	-7.082169E-04	5.107544E-04
102	3	-1.463750E-04	-9.058001E-05	3.051802E-04	47.6115	1.879752E-04	-4.249302E-04	3.064527E-04
102	4	-9.033585E-05	1.137086E-05	-1.859834E-05	-79.9575	1.466449E-05	-9.364948E-05	5.415697E-05
102	5	9.033590E-05	-1.137087E-05	1.859830E-05	10.0425	9.364951E-05	-1.466448E-05	5.415700E-05
102	6	1.463750E-04	9.058004E-05	-3.051802E-04	-42.3885	4.249302E-04	-1.879752E-04	3.064527E-04
102	7	1.509667E-04	2.439583E-04	5.086337E-04	47.6115	7.082170E-04	-3.132919E-04	5.107544E-04
102	8	-7.959604E-05	6.324912E-04	-1.301883E-04	-79.9575	6.555466E-04	-1.026514E-04	3.790970E-04

CHANGE FROM
 OF POOR QUALITY

Figure 5(b): Strain Output for Layered Composite Elements

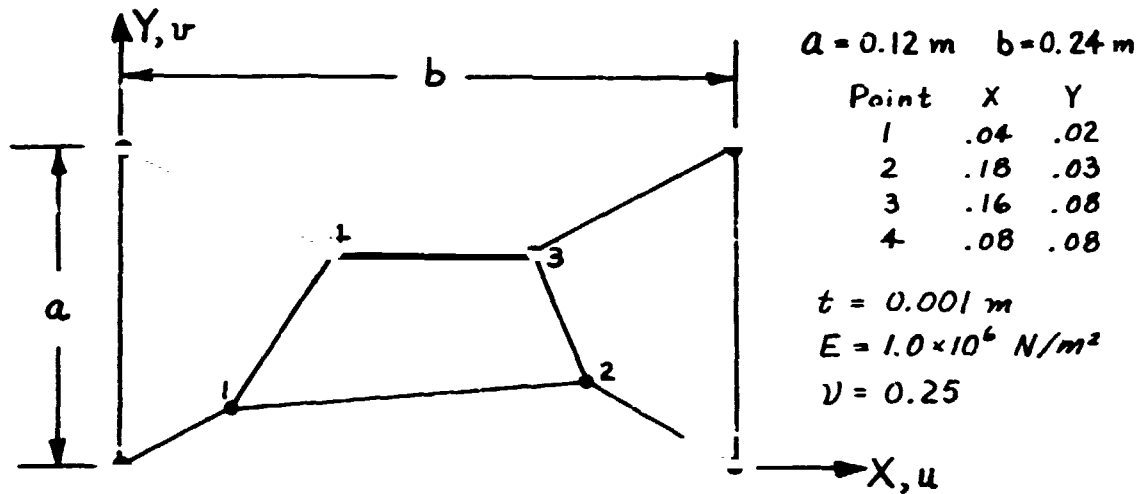
USE COMPOSITES INSTEAD OF ALUMINUM

ELEMENT ID	FAILURE THEORY	PLY ID	FP=FAILURE INDEX FOR PLY (DIRECT STRESSES)	FB=FAILURE INDEX FOR BONDING (INTER-LAMINAR STRESSES)	FAILURE INDEX FOR ELEMENT MAX OF FP,FB FOR ALL PLYS	FLAG
101	HILL	1	0.0013			
		2	0.0025	0.0014		
		3	0.0013	0.0021		
		4	0.0002	0.0031		
		5	0.0002	0.0041		
		6	0.0021	0.0031		
		7	0.0064	0.0021		
		8	0.0153	0.0014		
					0.0153	

88

Figure 5(c): Failure Index Table for Layered Composite Elements

ORIGINAL PAGE IS
OF POOR QUALITY



Membrane Boundary Conditions:

$$u = (x + \frac{1}{2}y) \times 10^{-3} \quad v = (\frac{1}{2}x + y) \times 10^{-3}$$

Bending Boundary Conditions:

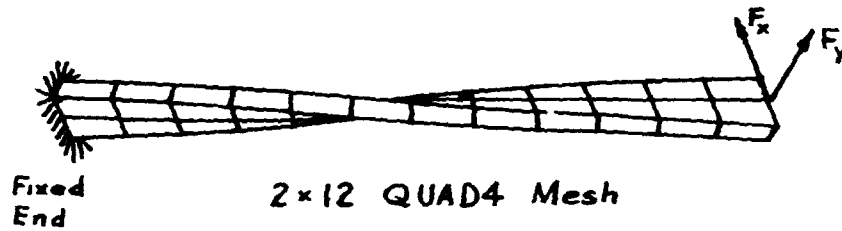
$$w = \frac{1}{2}(x^2 + xy + y^2) \times 10^{-3}$$

$$\theta_x = \frac{\partial w}{\partial y} = (\frac{1}{2}x + y) \times 10^{-3} \quad \theta_y = \frac{\partial w}{\partial x} = (x + \frac{1}{2}y) \times 10^{-3}$$

Test Results:

Element Output Quantity	Theory	NASTRAN
In-Plane Strains $\epsilon_x, \epsilon_y, \gamma$	1.0×10^{-3}	1.0×10^{-3}
Stresses σ_x, σ_y	1333.	1333.
Shear Stress τ_{xy}	400.	400.
Bending Moment per unit length $M_x = M_y$	1.111×10^{-7}	1.111×10^{-7}
Bending Moment per unit length M_{xy}	0.333×10^{-7}	0.333×10^{-7}
Surface Stresses σ_x, σ_y	± 0.667	± 0.667
Surface Shear Stress τ_{xy}	± 0.200	± 0.200

Figure 6. Element Patch Test Results - CQUAD4



Length = 12.0 m

Width = 1.1 m

Depth = 0.32 m

Twist = 90° (root to tip)

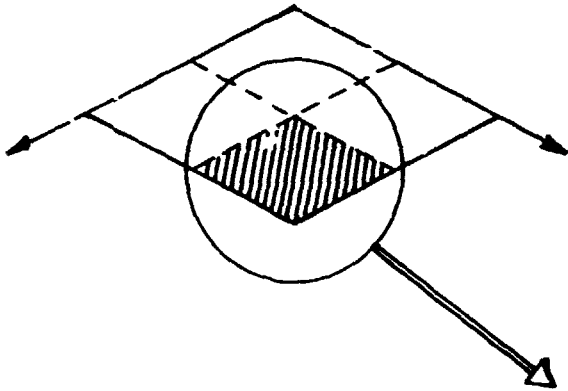
$E = 29.0 \times 10^6 \text{ N/m}^2$ $\nu = 0.22$

Applied Loads: Unit forces at tip

Tip Direction Load	Displacements in Loaded Direction	
	Theoretical	NASTRAN
In-plane Shear	0.005424	0.005373
Out-of-plane Shear	0.001754	0.001721

Figure 7. CQUAD4 Twisted Beam Test Results

ORIGINAL PAGE IS
OF POOR QUALITY



Simply Supported Composite
Square Plate Subjected to
Sinusoidally Varying Pressure
Loading of the form

$$p(x,y) = \frac{1}{2} \sin\left(\frac{\pi x}{l}\right) \sin\left(\frac{\pi y}{l}\right)$$

Finite Element Model

3x3 $\frac{1}{4}$ Symmetric QUAD4 Mesh:

$$E_1 = 20. \times 10^6$$

$$E_2 = .5 \times 10^6$$

$$G_{12} = .25 \times 10^6$$

$$\nu_1 = .25$$

$$\nu_2 = .00625$$

$$t = 0.2$$

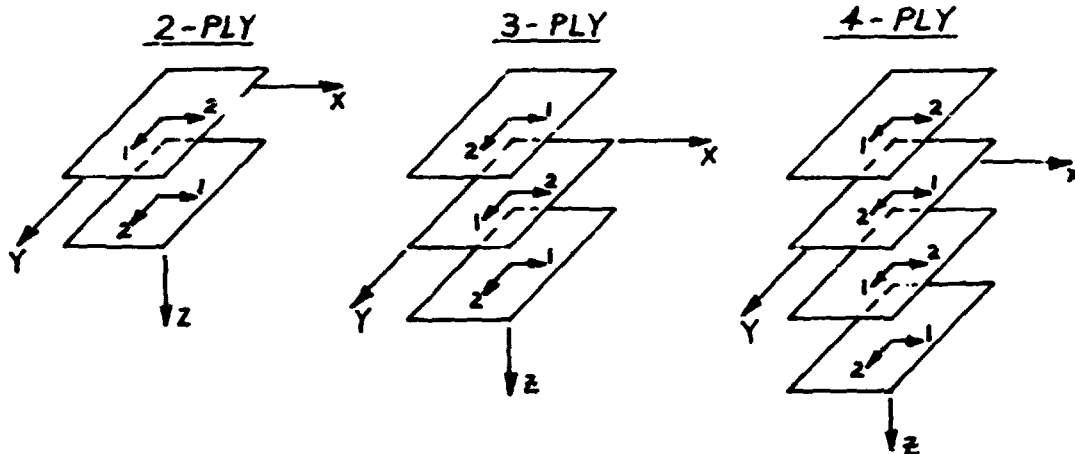
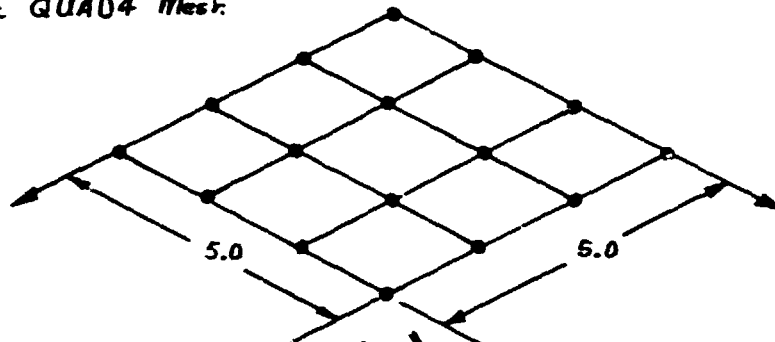
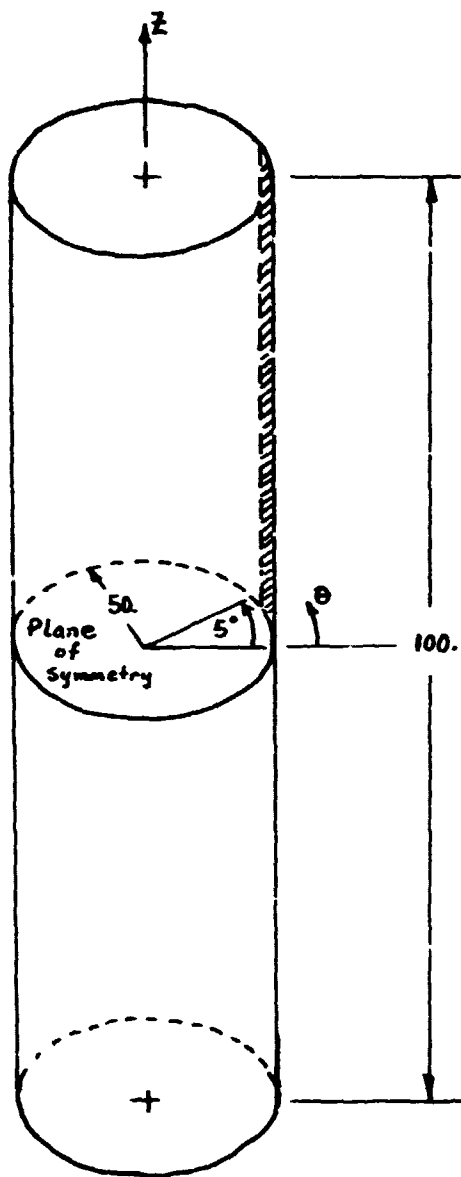
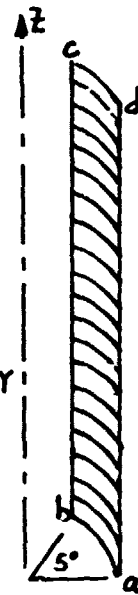


Figure 8. Simply Supported Composite Plate Example

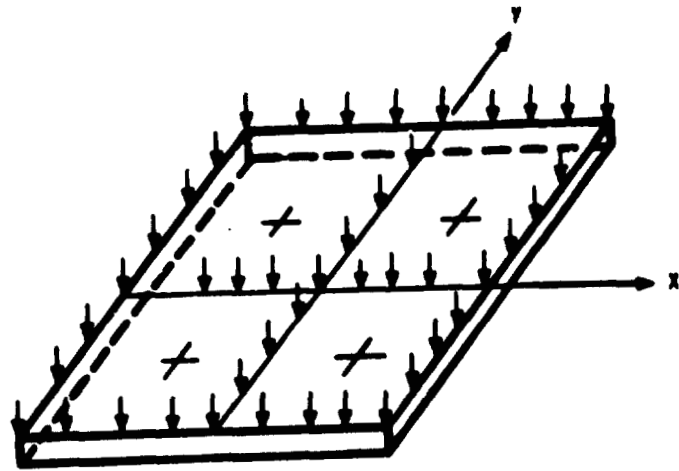


Finite
Element
Model
via
CYCLIC
SYMMETRY



- 20 QUAD4 Elements
Bending, Membrane and
Transverse Shear Effects
- Boundary Conditions
Edge ab:
 $U_z = 0$
 $\theta_r = \theta_z = 0$
 Edge cd: Simply Supported
 $U_r = U_\theta = 0$
 $\theta_z = 0$
- Wall thickness = 0.5
- 12 Segments

Figure 9. Simply Supported Composite Cylinder Example



Composite laminate details:

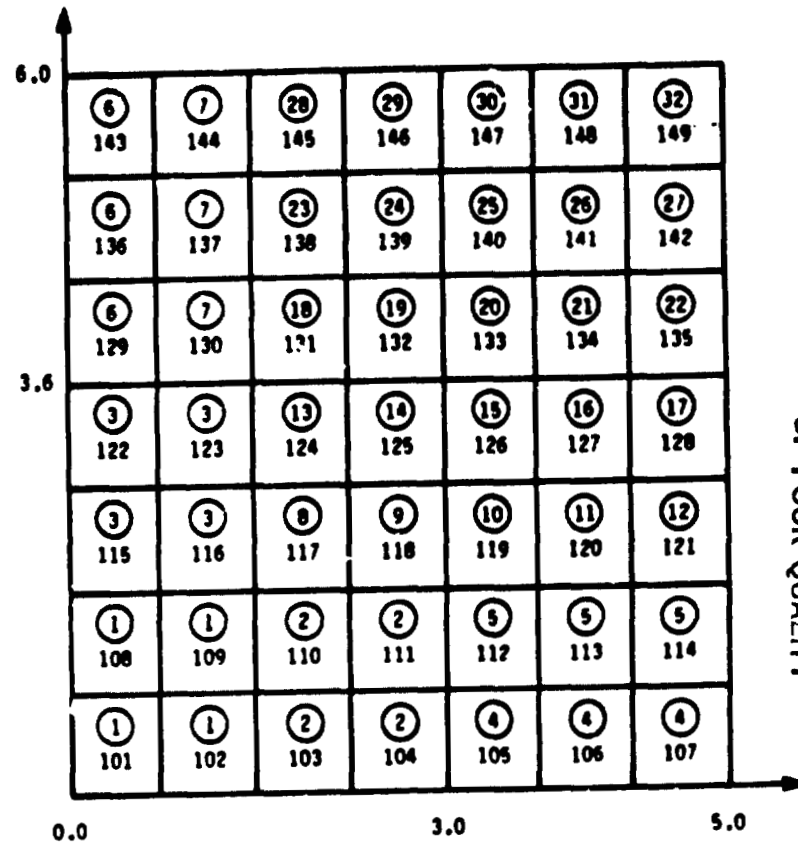
B-ply Graphite/Epoxy (T 300/5208)

(0/+45/-45/90) Symmetric

Constraints:

Element Stress: Hill's Criteria

Displacements: $+.02$ at center and corners
of plate



ORIGINAL PAGE IS
OF POOR QUALITY

(Numbers denote element IDs. Numbers in circles denote element groups by design variable linking.)

(a) Rectangular Plate: Loading and Supports.

(b) Finite Element Model.

Figure 10. Rectangular Plate for Optimum Design

0.199 (0.062)	0.428 (0.268)	0.514 (0.247)	0.251 (0.026)	0.353 (0.181)	0.416 (0.259)	0.246 (0.138)
		0.815 (0.503)	0.847 (0.480)	0.714 (0.365)	0.843 (0.559)	0.317 (0.255)
		0.957 (0.525)	1.005 (0.632)	1.401 (0.829)	0.585 (0.220)	0.235 (0.055)
0.168 (0.028)		0.597 (0.241)	1.260 (0.737)	0.977 (0.576)	1.009 (0.663)	0.302 (0.052)
		0.636 (0.356)	0.659 (0.365)	0.762 (0.347)	0.690 (0.403)	0.524 (0.351)
0.669 (0.406)	0.203 (0.048)	0.143 (0.038)				
		0.624 (0.334)				

(Values denote total thickness of 8-ply graphite/ epoxy laminate (mass = 0.8879 lbs). Values in parentheses denote thickness for aluminum (mass = 2.0135 lbs.))

(c) Plate Thickness for Optimum Design.

Figure 10. Rectangular Plate for Optimum Design with Stress and Displacement Constraints. (Cont.)

APPENDIX

CSA/NASTRAN Bulk Data Card Descriptions

CSA/NASTRAN BULK DATA DECK

Input Data Card CQUAD4 Quadrilateral Element Connection

Description: Defines a quadrilateral plate element (QUAD4) of the structural model. This is an isoparametric membrane-bending element.

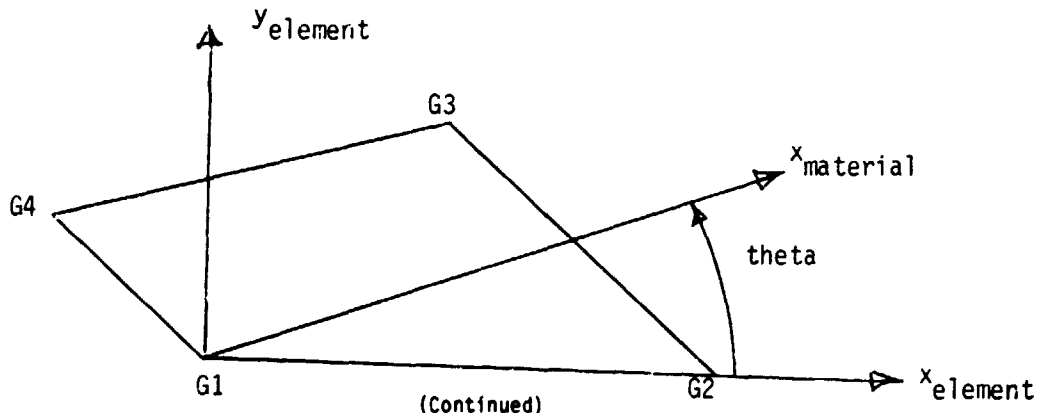
Format and Example:

1	2	3	4	5	6	7	8	9	10
CQUAD4	EID	PID	G1	G2	G3	G4	θ		
CQUAD4	1213	745	92	103	76	1001	32.4		CQ4
			T1	T2	T3	T4			
+Q4			.78	.63	.60	.70			

Field

Contents

- EID Element identification number (unique integer > 0)
- PID Identification number of a PSHELL or PCOMP property card (Integer > 0 or blank, default is EID)
- G1,G2,G3,G4 Grid point identification numbers of connection points (Integers > 0, all unique)
- θ Material property orientation specification (Real or blank; or 0 < Integer < 1,000,000). If Real or blank, specifies the material property orientation angle in degrees. If Integer, the orientation of the material x-axis is along the projection onto the plane of the element of the x-axis of the coordinate system specified by the integer value. The sketch below gives the sign convention for .
- T1,T2,T3,T4 Membrane thickness of element at grid points G1 through G4. (Real ≥ 0, or blank, not all zero. See Remark 4 for default.)



CSA/NASTRAN BULK DATA DECK

CQUAD4 (Continued)

- Remarks:
1. Element identification numbers must be unique with respect to all other element identification numbers.
 2. Grid points G1 through G4 must be ordered consecutively around the perimeter of the element.
 3. All the interior angles must be less than 180°.
 4. The continuation card is optional. If it is not supplied, then T1 through T4 will be set equal to the value of T on the PSHELL data card.
 5. Stresses are output in the element coordinate system.

CSA/NASTRAN BULK DATA DECK

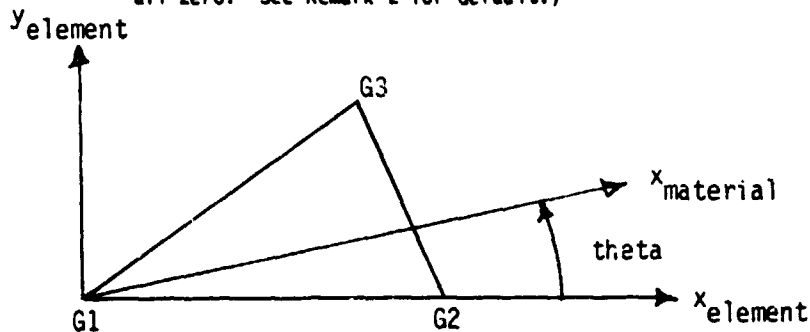
Input Data Card CTRIA3 Triangular Element Connection

Description: Defines a triangular plate element (TRIA3) of the structural model. This is an isoparametric membrane-bending element

Format and Example:

1	2	3	4	5	6	7	8	9	10
CTRIA3	EID	PID	G1	G2	G3	θ			
CTRIA3	401	101	1001	1201	1401	7.5			CTR3
			T1	T2	T3				
+TR3			.83	.81	.74				

<u>Field</u>	<u>Contents</u>
EID	Element identification number (Unique integer > 0)
PID	Identification number of a PSHELL property card (Integer > 0 or blank, default is EID)
G1,G2,G3	Grid point identification numbers of connection points (Integers > 0, all unique)
θ	Material property orientation specification (Real or blank; or 0 < Integer < 1,000,000). If Real or blank, specifies the material property orientation angle in degrees. If Integer, the orientation of the material x-axis is along the projection on to the plane of the element of the x-axis of the coordinate system specified by the integer value. The sketch below gives the sign convention for θ .
T1,T2,T3	Membrane thickness of element at grid points G1, G2, and G3 (Real \geq 0. or blank, not all zero. See Remark 2 for default.)



(Continued)

CSA/NASTRAN BULK DATA DECK

CTRIA3 (Continued)

- Remarks:
1. Element identification numbers must be unique with respect to all other element identification numbers.
 2. The continuation card is optional. If it is not supplied, then T1 through T3 will be set equal to the value of T on the PSHELL data card.

CSA/NASTRAN BULK DATA DECK

Input Data Card MAT8 Material Property Definition, Form 8

Description: Defines the material property for an orthotropic material

Format and Example:

1	2	3	4	5	6	7	8	9	10
MAT8	EID	E1	E2	ν_{12}	G12	G1,Z	G2,Z	RHO	
MAT8	101	28.+6	.5+6	0.25	1.+5	2.+6	1.5+6	0.62	+ABC
	A1	A2	TREF	α_t	α_c	γ_t	γ_c	S	
+ABC	24.-6	1.4-6	70.	1.2+4	1.4+4	1.3+3	1.1+3	1.+3	+DEF
	G_t	F12							
+DEF	1.3-4								

<u>Field</u>	<u>Contents</u>
MID	Material ID (1,000,000 > Integer > 0)
E1	Modulus of elasticity in longitudinal direction (also defined as fibre direction or 1-direction) (Real ≠ 0.0)
E2	Modulus of elasticity in transverse direction (also defined as matrix direction or 2-direction) (Real ≠ 0.0)
ν_{12}	Poisson's ratio (ϵ_2/ϵ_1 for uniaxial loading in 1 - direction). Note that $\nu_{21} = \epsilon_1/\epsilon_2$ uniaxial loading in 2 - direction is related to ν_{12} , E1, E2 by the relation $\nu_{12}E_2 = \nu_{21}E_1$. Real.
G12	Inplane shear modulus (Real > 0.0)
G1,Z	Transverse shear modulus for shear in 1-Z plane (Real > 0.0 or blank)
G2,Z	Transverse shear modulus for shear in 2-Z plane (Real > 0.0 or blank)
RHO	Mass density (Real)
A1	Thermal expansion coefficient in 1-direction (Real)
A2	Thermal expansion coefficient in 2-direction (Real)

(Continued)

CSA/NASTRAN BULK DATA DECK

MAT8 (Continued)

TREF Thermal expansion reference temperature (Real)

X_t, X_c Allowable stresses in tension and compression, respectively, in the longitudinal direction. Required if failure index is desired. (Real > 0.0) (Default value for X_c is X_t)

Y_t, Y_c Allowable stresses in tension and compression, respectively, in the transverse direction. Required if failure index is desired. (Real > 0.0) (Default value for Y_c is Y_t)

S Allowable stress for inplane shear (Real > 0.0)

G_E Structural damping coefficient (Real)

F12 Interaction term in the tensor polynomial theory of Tsai-Mu (Real). Required if failure index by Tsai-Mu theory is desired and if value of F12 is different from 0.0.

Remarks: 1. If $G_{1,z}$ and $G_{2,z}$ values are not supplied, the in-plane shear modulus will be used.

CSA/NASTRAN BULK DATA DECK

Input Data Card PCOMP Layered Composite Element Property

Description: Defines the properties of an n-ply composite material laminate

Format and Example:

1	2	3	4	5	6	7	8	9	10
PCOMP	PID	Z ₀	NSM	S _b	F.T.	TREF	GE	OPT	
PCOMP	991	-1.0	18.7	4.+3	HOFF				+ABC
	MID1	T1	θ ₁	SOUT1	MID2	T2	θ ₂	SOUT2	
+ABC	10	0.25	0.	YES			45.		+DEF
	MID3	T3	θ ₃	SOUT3	MID4	T4	θ ₄	SOUT4	
+DEF			-45.				90.		

<u>Field</u>	<u>Contents</u>
PID	Property ID (1,000,000 > Integer > 0)
Z ₀	Distance from the reference plane to the bottom surface (Real) (Default = -1/2 the thickness of the element)
NSM	Non-structural mass per unit area (Real)
S _b	Allowable shear stress of the bonding material (allowable inter-laminar shear stress). Required if failure index is desired. (Real > 0.0)
F.T.	Failure theory to be used to test whether the element fails or not (BCD). The following theories are presently allowed: HILL for the Hill theory HOFF for the Hoffman theory TSAI for the Tsai-Wu theory STRESS for maximum stress theory STRAIN for maximum strain theory
TREF	Reference temperature (Real)
GE	Damping coefficient (Real)

(Continued)

CSA/NASTRAN BULK DATA DECK

PCOMP (Continued)

OPT Lamination generation option codes (integer ≥ 0)

Code

0 all plies are specified

1 ply layup specified is symmetrical; only the plies on one side of the centerline are specified

2 a "stack" of membrane-only elements will be generated for each element that references this PCOMP card

options may be combined by adding the specific code values

MIDi Material ID of the various plies. MID1 > 0, MID2, ..., MIDn > 0, or blank. The plies are identified by serially numbering them from 1 at the bottom layer. The MIDi must refer to MAT1, MAT2, or MAT8 bulk data cards. (Integer > 0)

Ti Thicknesses of the various plies (Real; T1 > 0.0, T2, T3, ... > 0.0 or blank)

θ_i Orientation angle of the longitudinal direction of each ply with the material axis of the element. (If the material angle on the element connection card is 0.0, the material axis and side 1-2 of the element coincide). The plies are to be numbered serially starting with 1 at the bottom layer (the bottom layer is defined as the surface with the largest -Z value in the element coordinate system). (Real)

SOUTi Stress output required (YES) or not (NO) for the various plies (BCD) (Default = NO)

- Remarks:
1. The default under MID2, MID3, ..., is the last defined MAT card. in this case MID1; so for T2, T3, ..., all these thicknesses will be equal to T1.
 2. At least one of the four values (MIDi, Ti, θ_i , SOUTi) must be present for a ply to exist.
 3. TREF given on the PCOMP card will be used for all plies of the element; it will override values supplied on material cards for individual plies.
 4. CE given on the PCOMP card will be used for the element; it will override values supplied on material cards for individual plies.

CSA/NASTRAN BULK DATA DECK

Input Data Card PCOMP1 Layered Composite Element Property - Alternate Form 1

Description: Defines the properties of an n-ply composite material laminate, all plies being of equal thickness.

Format and Example:

1	2	3	4	5	6	7	8	9	10
PCOMP	PID	Z ₀	NSM	S _b	F.T.	MID	T	OPT	
PCOMP	891	-1.0	18.7	4.+3	STRAIN	10	0.25		+ABC
	θ ₁	θ ₂	θ ₃	θ ₄	θ ₅	θ ₆	θ ₇	θ ₈	
+ABC	0.0	+45.	-45.	+90.	+90.	-45.	+45.	0.0	

Field	Contents
PID	Property ID (1,000,000 > Integer > 0)
Z ₀	Distance from the reference plane to the bottom surface (Real) (Default = -1/2 the thickness of the element)
NSM	Non-structural mass per unit area (Real)
S _b	Allowable shear stress of the bonding material (allowable inter-laminar shear stress). Required if failure index is desired. (Real > 0.0)
F.T.	Failure theory to be used to test whether the element fails or not (BCD). The following theories are presently allowed: HILL for the Hill theory HOFF for the Hoffman theory TSAI for the Tsai-Wu theory STRESS for maximum stress theory STRAIN for maximum strain theory
MID	Material ID of each ply. The plies are identified by serially numbering them from 1 at the bottom layer. The MID must refer to MAT1, MAT2, or MAT8 bulk data cards. (Integer > 0)
T	Thickness of each ply. All plies have the same thickness. (Real > 0.0)

(Continued)

CSA/NASTRAN BULK DATA DECK

PCOMP1 (Continued)

OPT Lamination generation option codes (Integer ≥ 0)

Code

- 0 all plies are specified
- 1 ply layup specified is symmetrical; only the plies on one side of the centerline are specified.
- 2 a "stack" of membrane only elements will be generated for each element that references this PCOMP card

Options may be combined by adding the specific code values

θ_i

Orientation angle of the longitudinal direction of each ply with the material axis of the element. (If the material angle on the element connection card is 0.0, the material axis and side 1-2 of the element coincide). The plies are to be numbered serially starting with 1 at the bottom layer (the bottom layer is defined as the surface with the largest -Z value in the element coordinate system). (Real)

Remarks:

1. Stress and strain output will be generated for all plies if a case control STRESS request is present. See the PCOMP card description for a method of reducing the amount of output generated.

CSA/NASTRAN BULK DATA DECK

Input Data Card PCOMP2 Layered Composite Element Property - Alternate Form 2

Description: Defines the properties of an n-ply composite material laminate

Format and Example:

1	2	3	4	5	6	7	8	9	10
PCOMP2	PID	Z ₀	NSM	S _b	F.T.	MID		OPT	
PCOMP2	891	-1.0	18.7	4.+3	HOFF	10			+ABC
	T1	θ ₁	T2	θ ₂	T3	θ ₃	T4	θ ₄	
+ABC	.25	0.0	.25	45.		-45.		+90.	+DEF
	T5	θ ₅	T6	θ ₆	T7	θ ₇	T8	θ ₈	
+DEF		+90.		-45.		45.		0.0	

<u>Field</u>	<u>Contents</u>
PID	Property ID (1,000,000 > Integer > 0)
Z ₀	Distance from the reference plane to the bottom surface (Real) (Default = -1/2 the thickness of the element)
NSM	Non-structural mass per unit area (Real)
S _b	Allowable shear stress of the bonding material (allowable inter-laminar shear stress). Required if failure index is desired. (Real > 0.0)
F.T.	Failure theory to be used to test whether the element fails or not (BCD). The following theories are presently allowed: HILL for the Hill theory HOFF for the Hoffman theory TSAI for the Tsai-Wu theory STRESS for maximum stress theory STRAIN for maximum strain theory
MID	Material ID of the various plies. The plies are identified by serially numbering them from 1 at the bottom layer. The MID must refer to MAT1, MAT2, or MAT8 bulk data cards. (Integer > 0)

(Continued)

CSA/NASTRAN BULK DATA DECK

PCOMP2 (Continued)

OPT Lamination generation option codes (Integer > 0)

Code

- 0 All plies are specified
- 1 ply layup specified is symmetrical; only the plies on one side of the centerline are specified
- 2 a "stack" of membrane only elements will be generated for each element that references this PCOMP card

Options may be combined by adding the specific code values

Ti Thickness of the various plies (Real; T1 > 0.0, T2, T3...> .0 or blank)

θ_i Orientation angle of the longitudinal direction of each ply with the material axis of the element. (If the material angle on the element connection card is 0.0, the material axis and side 1-2 of the element coincide). The plies are to be numbered serially starting with 1 at the bottom layer (the bottom layer is defined as the surface with the largest -Z value in the element coordinate system). (Real)

- Remarks:
1. At least one of the two values, (Ti, θ_i) must be present for a ply to exist.
 2. Stress and strain output will be generated for all plies if a case control STRESS request is present. See the PCOMP card description for a method of reducing the amount of stress output generated.

CSA/NASTRAN BULK DATA DECK

Input Data Card PSHELL Shell Element Property

Description: Defines the membrane, bending, transverse shear, and coupling properties of thin shell elements

Format and Example:

1	2	3	4	5	6	7	8	9	10
PSHELL	PID	MID1	T	MID2	12I/T ³	MID3	TS/T	NSM	
PSHELL	101	700	0.25	701	1.1	703	.5	7.88	PSHL
	Z1	Z2	MID4						
+SHL	.125	-.125							

<u>Field</u>	<u>Contents</u>
PID	Property identification number (Integer > 0)
MID1	Material identification number for the membrane (Integer > 0 or blank)
T	Default value for the membrane thickness (Real)
MID2	Material identification number for bending (Integer > 0 or blank)
12I/T ³	Bending stiffness parameter (Real or blank, default = 1.0)
MID3	Material identification number for transverse shear (Integer > 0 or blank), must be blank unless MID2 > 0) default = MID2.
TS/T	Transverse shear thickness divided by the membrane thickness (Real or blank, default = .833333)
NSM	Nonstructural mass per unit area (Real)
Z1,Z2	Fiber distances for stress computation. The positive direction is determined by the righthand rule and the order in which the grid points are listed on the connection card. (Real or blank, see Remark 11 for defaults).
MID4	Material identification number for membrane-bending coupling (Integer > 0 or blank, must be blank unless MID1 > 0 and MID2 > 0, may not equal MID1 or MID2)

- Remarks:
1. All PSHELL property cards must have unique identification numbers.
 2. The structural mass is computed from the density using the membrane thickness and membrane material properties.

(Continued)

CSA/NASTRAN BULK DATA DECK

PSHELL (Continued)

3. The results of leaving an MID field blank are:
 - MID1 No membrane or coupling stiffness
 - MID2 No bending, coupling, or transverse shear stiffness
 - MID3 MID2 will be used as default for MID3
 - MID4 No bending-membrane coupling
4. The continuation card is not required.
5. The structural damping (for dynamics rigid formats) uses the values defined for the MID1 material.
6. The MID4 field should be left blank if the material properties are symmetric with respect to the middle surface of the shell. If the element centerline is offset from the plane of the grid points, the MID4 field may be used for modeling the offset but it involves laborious calculations that produce physically unrealistic stiffness matrices ("negative terms on factor diagonal") if done incorrectly.
7. This card is used in connection with the CTRIA3 and CQUAD4 cards.
8. For structural problems, PSHELL cards may reference MAT1, MAT2 or MAT8 material property cards.
9. If the transverse shear material, MID3, references a MAT2 data card, the G1 G12 and G22 values will be used to obtain the symmetric 2x2 $[G_3]$ matrix for the element.
10. For heat transfer problems, PSHELL cards may reference MAT4 or MAT5 material property cards.
11. The default for Z1 is $-T/2$, and for Z2 is $+T/2$, where T is the local plate thickness.

N85-25869

NPLOT: AN INTERACTIVE PLOTTING PROGRAM FOR NASTRAN FINITE ELEMENT MODELS

*Gary K. Jones and Kelly J. McEntire
NASA/Goddard Space Flight Center
Greenbelt, Maryland 20771*

SUMMARY

NPLOT (NASTRAN Plot) is an interactive computer graphics program for plotting undeformed and deformed NASTRAN finite element models. It has been developed at NASA's Goddard Space Flight Center. It provides flexible element selection and grid point, ASET and SPC degree of freedom labelling. It is easy to use and provides a combination menu and command driven user interface. NPLOT also provides very fast hidden line and haloed line algorithms. The hidden line algorithm in NPLOT has proved to be both very accurate and several times faster than other existing hidden line algorithms. It uses a fast spatial bucket sort and horizon edge computation to achieve this high level of performance. The hidden line and the haloed line algorithms are the primary features that make NPLOT unique from other plotting programs.

INTRODUCTION

Structural analysts at the Goddard Space Flight Center, GSFC, have always had the need to be able to graphically display finite element models quickly and accurately. Plots

with depth cues give a much better visual representation and aid the analyst in interpretation and error checking. On a vector type of graphics device (such as Tektronix 4014's or pen plotters) the two best ways to show depth is via hidden line plotting or by haloed line plotting. The problem with the available hidden line algorithms is that they are normally time consuming and interfere with the quick response time desired in interactive graphics. One of the authors, Gary Jones, has developed a hidden line algorithm that satisfies these needs. This algorithm provides fast and accurate hidden line plotting of finite element models. The response time to plot a hidden line view of a model is near that for a normal all lines visible plot and provides linear time performance. A variation of this algorithm was used to produce a fast haloed line plot routine. A haloed line plot shows all aft lines broken to show depth. It is particularly well suited for plotting models composed of many line elements and few surface elements. For this class of models, hidden line plotting is not an effective tool.

This paper describes the current version of NPLOT. First, the development of NPLOT is discussed. Second, a description of NPLOT is

given, describing the many useful features found in NPLOT. Third, a detailed discussion of the hidden/halo line algorithm is presented along with benchmark performance data of NPLOT compared with other hidden line algorithms. Finally, concluding remarks are presented followed by references and figures.

NPLOT DEVELOPMENT / GOALS

The development of NPLOT was informally initiated in 1981 as simply a base for testing haloed and hidden line algorithms. Once these algorithms were developed and had proved to be very effective tools for model display, the main goal became to develop NPLOT into an effective tool for the structural analyst. NPLOT was and is currently being developed to meet specific goals and targets. The prime development target for NPLOT is that it must be an effective state-of-the-art graphics tool for GSFC structural analysts. Some specific requirements are:

1. NPLOT must effectively support the NASTRAN structural analysis code being used at GSFC.
2. NPLOT must run on the Digital Equipment Corporation VAX computers used by the Engineering Directorate at GSFC and support the available graphic hardware; i.e., Tektronix and Raster Technology terminals and Hewlett Packard pen plotters.
3. NPLOT must provide fast interactive performance together with a easy to use human interface.
4. NPLOT must provide effective graphic tools such as haloed and hidden line plotting.

NPLOT used as its starting point the PLOT code developed at GSFC by M. Weiss and M. Johns for the plotting of NASTRAN finite element models; however, at its current state of development, NPLOT contains almost none of that original code. Original algorithms and routines were developed for: haloed line, hidden line, and horizon edge computation. A new executive was developed together with a better and more complete NASTRAN interface. It is expected that NPLOT will continue to evolve to meet new requirements; some of the near term activity will focus on:

1. Develop and add a fast shaded color hidden surface algorithm to NPLOT. The preliminary concept for the algorithm has been developed but it remains to be implemented and debugged. This algorithm would enable NPLOT to provide effective support for displaying model stresses, energy levels, and temperatures.
2. Add mode shape animation capability to NPLOT. This feature would make use of the multiple bit planes on the Raster Technology terminals to provide film strip animation.
3. Interface NPLOT with the Integrated Analysis Capability, IAC, program [1,2] developed by Boeing Aerospace Company for GSFC. This would provide NPLOT with good access to a wide spectrum of useful NASTRAN output data.
4. Investigate the feasibility and effectiveness of running NPLOT on an IBM PC-AT desktop computer system.

DESCRIPTION OF NPLOT

NPLOT has proved to be a very useful and versatile computer graphics program. It meets most of the plotting requirements for those who use NASTRAN at GSFC. It is also in use at NASA/LaRC, NASA/JSC and several GSFC contractors. In this section the NPLOT implementation will be discussed first, followed by a description of NPLOT's features and then a few words on NPLOT's user interface.

Implementation:

NPLOT was developed on a DEC VAX computer running the VMS operating system. The graphics was developed using a Tektronix 40XX storage tube terminal and a Tektronix 4105 raster terminal. NPLOT makes graphics calls to Precision Visual's DI3000 graphics subroutines. This subroutine package follows the Core standard. Making calls to DI3000 allows NPLOT to be device independent and therefore can be run on any terminal that has a DI3000 device driver. For those sites that do not have a license for DI3000, a set of interface routines have been developed that translate the DI3000 calls used in NPLOT into Tektronix PLOT10 calls.

Extensive use of the structured programming constructs and character manipulation functions of FORTRAN 77 are incorporated into the computer code. The character manipulation functions allow NPLOT to efficiently process NASTRAN free field bulk data decks. Non-standard FORTRAN 77 statements were avoided to allow the code to be transportable. The only problem that may occur when compiling NPLOT with a non VAX/VMS FORTRAN 77 compiler may be with a few open statements.

Note however, NPLOT does make use of the virtual memory feature of VAX/VMS to speed operation and simplify implementation; this fact could make transfer of NPLOT to a non-virtual memory computer difficult.

Geometry may be entered in rectangular, cylindrical, and spherical coordinate systems using the CORD2R, CORD2C and CORD2S NASTRAN cards. The CORD1R, CORD1C and CORD1S cards are not supported. The coordinate systems may reference other coordinate systems since it is not a requirement that each reference the basic system. This combination allows a tree structured geometric system to be processed. The NPLOT user may, at his command, output a table to disk containing the grid point ID's and the XYZ coordinates in the basic system.

Features:

Clearly the most important feature of NPLOT is its ability to create hidden line and haloed line views of mathematical models both quickly and accurately. The hidden line algorithm generates views of models with all hidden lines removed, figure 1. The haloed line algorithm displays views with aft lines broken in an effort to show depth while keeping the entire model visible, figure 2. A discussion of these algorithms follows in the next section. NPLOT, of course, also can plot a normal all lines visible view of a model usually referred to as a wire frame view, figure 3.

Another important feature of NPLOT that allows it to perform post processing is its ability to plot deformed shapes, figure 4. NPLOT reads the displacements from a NASTRAN F06 file. It can read either static displacements or eigenvectors.

All subcases or mode shapes can be read in at once. The displacements are written into a unformatted scratch file where they are available for rapid access when the user wishes to display a deformed shape. It is then a simple matter to enable the deformed shape, change subcases or mode shapes and change the scale factor for subsequent plots.

NPLOT allows the user to specify element filters which select specific elements for plotting. Elements can be selected based upon their type, property, and ID. Elements can also be selected by a model segment. This is accomplished by inserting special segment delimiters in the bulk data deck and then specifying the delimiter label during the interactive session. Any or all of these filters can be activated at the same time to allow a great deal of selectivity. The elements can then be labelled with their respective ID's with a simple command once the plot is displayed on the screen, figure 5.

NPLOT also allows the user considerable flexibility in specifying which grid points are to be labeled with their grid point ID's. Specific grid point ID's can be selected and an eight character name tag can be associated with each grid point. The name tag can be useful for distinct identification. The user can also specify SPC sets, ASET and OMIT grid points to be labelled. These grid points will then be labelled with name tags indicating the degrees of freedom involved, figure 6.

NPLOT allows the standard display operations such as rotation and perspective. It also allows different view planes to be selected. These are X-Y, Y-Z and X-Z viewing planes. A zoom function is also allowed on terminals with a locator such as a graphics cursor, tablet, light pen or joy

stick. The center of the area desired for zooming is selected with the locator and then a numeric key is pressed to indicate the zooming scale factor. Another display feature available is the Z-axis cut option which allows the user to cut away a percentage of the fore part of the model, figure 7. This is useful because it can reveal detail on the inside of a model.

The calculation of the model's horizon edges (edges where visibility can change) is normally used just to speed up the hidden line computation. However, missing elements can be clearly located for most models by just plotting the horizon edges. NPLOT lets the user toggle the display set from all edges to just the horizon edges. Illustrated in figure 8 is a wire frame plot of the horizon edges for a model with a missing element.

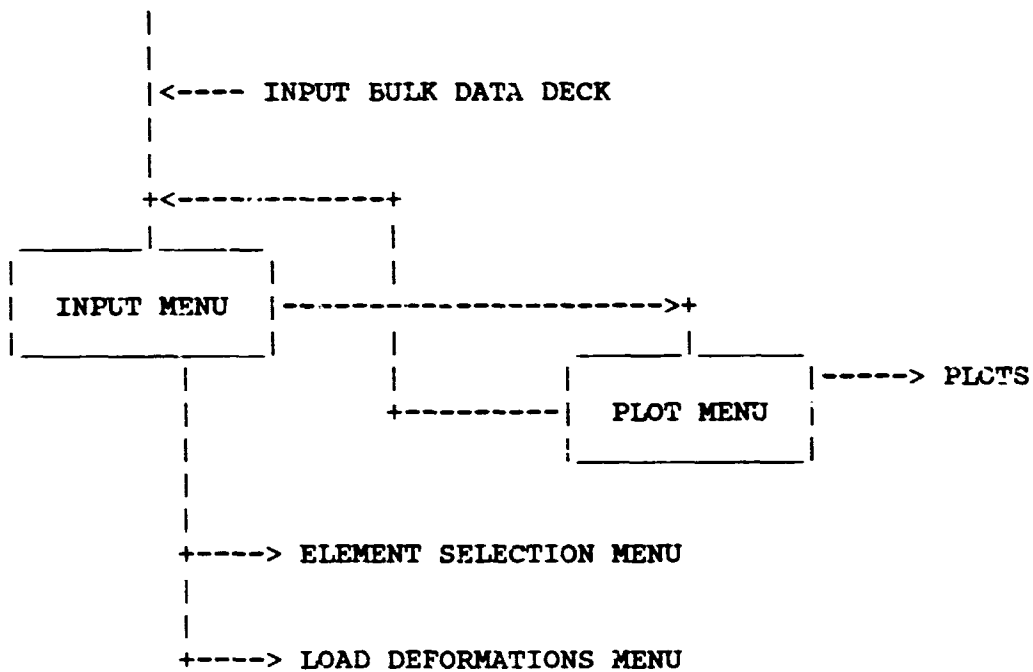
Another feature that aids the user is the plot file generator. Before beginning a plot the user can toggle on the plot file generator which will write all subsequent plot labels and screen vectors into a plot file until the toggle is turned off again. This plot file can then be read by other programs such as a pen plotter program. The HP7580A pen plotter is used by GSFC's Mechanical Engineering Branch when larger and more precise plots are desired.

User Interface:

NPLOT'S user interface is intended to make NPLOT easy and quick to use. It is also intended to allow frequent users to become efficient at using the program. Frequent use will enable users to take short cuts once they are familiar with the instruction set. This aim is accomplished by using a combination of menu and command driven user interface with available help menus for detailed information

concerning each command. NPLOT is controlled via commands from two main menus. The basic command/menu structure is:

Within each of these menus are commands that invoke sub-menus. The input menu is used for selecting element sets, element labels, grid labels and deformation sets. The plot menu is used to select the display operations and then to execute the plot option desired. Once the plot is on the screen the interface becomes command driven. The same commands that were available from the preceding menus are now available for immediate execution. This enables the frequent user to avoid returning to the menu every time he wishes to manipulate the display or execute a command.



COMMAND MENU STRUCTURE

HIDDEN LINE / HALOED LINE ALGORITHMS

Hidden Line:

The development of a new hidden line algorithm was not taken lightly. Techniques to perform hidden line plotting have been much discussed beginning with the advent of computer graphics in the early 1960's and continuing into the present era. Given the bulk of this prior work [3-11], why develop a new method? The answer is that these prior methods, as of 1980, appeared to lack the speed necessary for effective interactive use, lack features necessary to plot NASTRAN models, or the referenced papers provided insufficient implementation details. Except for the Watkins technique [11], coded algorithms were not available. Experience in using the Watkins technique had shown it to be not acceptable for hidden line plotting of NASTRAN models. References 12 through 16 were published after our algorithm had been substantially completed.

Several different variations of the same basic hidden line method have been sequentially developed by G. Jones in the course of this effort. To keep track of the different versions, they were assigned names JONES/A through JONES/E. JONES/D was used in the first production version of NPLOT and was described in reference 17. The fastest and most recent version of the hidden line algorithm, JONES/E, is incorporated into the current version of NPLOT. The basic flow for JONES/E is as follows:

1. INPUT: The main inputs to JONES/E from NPLOT are the global edge list, global surface list, edge/surface adjacency table and

grid point table. It should be noted that NPLOT operates to produce nonredundant global edge and surface lists. The global surface list uses a four node flat surface representation; NPLOT processes triangles through 20 node solid elements to this surface data format.

2. PREPARATION: The edge and surface lists are processed to produce arrays for edge and surface data. For example, the minimum/maximum X, Y, and Z values for each edge and surface are computed. The horizon edges of the object for the viewing transformation are computed. Spatial sorting of the edge and surface data is performed. Illustrated in figure 9 is a simplistic view of the spatial sort cells used by JONES/E. Based on the complexity of the model, N x N mesh X-Y sort cells are imposed on the model and lists of pointers to horizon edge data and surface data are generated for each cell via bucket sorting. Different mesh densities are used for edge and surface sorting. The mesh density used for the horizon edge sort is based on the total number of edges in the model. The mesh density for surface sorting is based on the number of surfaces in the model. The functional relationship between these measures of model complexity and mesh densities are set heuristically by varying the mesh density and observing the resulting performance for a number of models. JONES/E currently uses mesh definitions derived for JONES/D and so may not be optimum. After the cell lists are created, they are depth sorted based on the depth of the horizon edge or surface.

3. **EDGE VISIBILITY:** The global edge list is processed in two passes. On the first pass only the horizon edges are processed and the remaining edges are processed on the second pass. In either case the subsequent loop operations are the same. The edge cell coordinates for the edge are determined via a look-up table. The edge cells associated with the edge are binary searched to find the depth to limit the search for horizon edges that intersect with the edge. Its intersections with all horizon edges, that have not been found to be invisible by a prior calculation, are determined. The edge is broken into segments using its end points and the points of intersection. Each segment is either all visible or all invisible. The mid-point of each segment is computed and checked against the appropriate cell surface list to ascertain visibility. This requires computing the surface cell coordinates for the mid-point and then performing a binary search to find the depth in the surface cell list to limit the search for obscuring surfaces. Containment and depth computations are then performed to ascertain mid-point visibility, and hence, segment visibility.

This algorithm was tailored to support the plotting of NASTRAN models, therefore in the current implementation:

1. A line penetrating a surface usually results in a visible plot error. This is desirable for NASTRAN plotting since this usually indicates a modelling error.
2. Grid points are required where elements meet. This is normally the case in NASTRAN models.

3. Surfaces must be planar for accurate plotting. This is true for commonly used NASTRAN elements.

In operation, the algorithm is remarkably fast for plotting NASTRAN models. There are two chief reasons for this speed. The first being the efficiency of the spatial sort and the horizon edge technique in reducing the number of edge to edge compares in computing the required line intersections. The second being the effectiveness of the spatial sorts in reducing mid-point to surface compares in computing edge segment visibility.

The spatial sort functions as a divide and conquer technique; this is facilitated by the fact that in general NASTRAN models have fairly uniform topological granularity and the relative granule size decreases as model size increases. Thus, the spatial sort serves to linearize the operation of the algorithm. It is worth noting that Writtram [14] in a article published concurrently with the development of NPLOT used a horizontal strip form of spatial sort to achieve a high speed hidden line algorithm. The form of the spatial sort in JONES/E, and in the prior JONES/D, algorithm is somewhat different from Whittram's in that the spatial cells are boxes not strips and the fact that in JONES/E (and JONES/D) the hidden line determination does not make use of the concept of an active edge list or an active polygon list to reduce the computations.

The main difference between the current JONES/E algorithm and the prior JONES/D is the addition of the horizon edge method to the algorithm. A horizon edge is any model edge across which visibility can change. The concept of using horizon edges in hidden line computation was noted by Appel [18] and more recently used by

Hornung [16] to generate a very high speed hidden line algorithm for closed single surface objects. In JONES/E, horizon edges are computed and used to drastically reduce the number of edge compare operations. On a per cell basis, the reduction in operations is from the order of total edges squared to horizon edges times total edges. The net effect of using horizon edges was to speed up the algorithm by about 50 percent.

The authors make no claim to have "solved the hidden line problem". Contrary to what some have claimed, it appears that no existing algorithm is effective for the full spectrum of common topologies, for example curved surfaces. Inadequate research and a lack of understanding of the problem are usually evident when such claims are put forth. JONES/E was simply designed to process NASTRAN models or other similar topologies in an efficient manner.

Haloed Line:

The use of haloed line plotting was first discussed by Appel [5]. In haloed line plotting, the aft edges are broken where they intersect with more forward edges; this produces a well defined depth effect for the viewer, figure 2. The initial haloed line code for NPLOT was written by T. Carnahan, GSFC, based on the techniques defined by Appel [5]. The haloed line algorithm in the current version of NPLOT has been recoded by one of the authors (G. Jones) to incorporate the same spatial sort techniques as in the JONES/E hidden line algorithm and thereby increase its speed of operation.

Haloed line computation requires much more line intersection calculation than hidden line plotting thereby

increasing the cpu time. Whereas hidden line plotting effectively truncates the total edge list, haloed line plotting operates to increase the total edge list by splitting up edges into several segments. Thus, haloed line plotting generates more terminal I/O than wire frame or hidden line plotting. For these reasons, haloed line plotting should be slower than the other plot types.

In haloed line plotting the NPLOT user can specify the size of the gap so as to produce different effects. Haloed line plotting can be very effective in certain situations:

1. For models with few surface elements but many line elements, CBAR's and CROD's, haloed line plotting is very effective at showing depth information. Hidden line plotting is ineffective for this type of model.
2. When the user wants to peer inside a model but retain depth cues, haloed line plotting is an effective technique. This is similar to allowing transparency in hidden surface plotting on raster devices.

Performance:

The basic performance of the three plots type in NPLOT were assessed by measuring their performance with a collection of 20 NASTRAN models. The model sizes ranged from 55 grids/126 edges/67 surfaces up to 3730 grids/7547 edges /3626 surfaces. Wire frame and hidden line plots of the largest model are shown in figures 10 and 11. The performance of the algorithms were measured in terms of a processing rate expressed in terms of edges per cpu second. The cpu times were measured on a normally loaded VAX 11/780

computer and included the time to perform any preparatory work, execute the plot function module (wire frame, haloed, hidden), run the PLOT10 module, and perform the I/O to paint the object on the screen.

Shown in figure 12 is a graph of the measured performance of the three algorithms. All three algorithms show fairly linear performance for the range of models used in the tests. Wire frame plotting yielded an average rate of about 300 edges per cpu second, hidden line plotting was somewhat slower at about 150 edges per cpu second and haloed line plotting was the slowest at around 100 edges per cpu second. Wall clock response time for hidden line plotting was about the same as that for wire frame plotting. This was due to the fact that hidden line plotting involves less terminal I/O than wire frame plotting. Haloed line plotting was the slowest but this was expected. Even so, haloed line plotting was sufficiently fast to meet the demands of the interactive user. Haloed line plotting is the preferred plot type for models with few surfaces and many line elements.

The net effect of the various optimizing techniques employed in the hidden line algorithms can be seen from our experience in plotting one of the test models. The first - cut hidden line algorithm was a basic brute force line intersection technique with little code optimization; its processing rate for the test model was about 2.5 edges per cpu second. A subsequent version with more code optimization and a few simple short cuts worked at a rate of about 18 edges per cpu second. The JONES/D algorithm, which used the X-Y spatial sort, performed at a rate of about 100 edges per cpu second. The JONES/E algorithm in the current version of NLOT uses the X-Y spatial sort together with the horizon edge

technique, and achieves a processing rate of about 175 edges per cpu second for this particular model. Thus in this instance JONES/E performs about 70 times quicker than a brute force method.

How fast can an optimum hidden line algorithm run? A reasonable bounding upper limit might be the speed for wire frame plotting. For the particular hardware / software used at our computer facility (VAX 11/780, FORTRAN 77, Tektronix terminals using 9600 baud) the wire frame process rate was about 300 edges per second, thereby implying that no hidden line algorithm could run more than twice as fast as JONES/E for this particular computing environment.

The Watkins hidden line/surface method [11] and Hedgley's algorithm were compared to the JONES/E algorithm via comparative testing. The MOVIE program uses the Watkins method for hidden line and hidden surface computation. A VAX implementation of MOVIE was used for this study. The MOVIE implementation of Watkins does not support line element types so an all surface model was used to make the comparison. The test model consisted of 857 surfaces and 1242 edges. The cpu time for just the hidden line generation in MOVIE was 41.5 seconds; the corresponding time for NLOT was 6.9 cpu seconds. The SKETCH hidden line routine developed by Hedgley [13] was obtained and converted to the VAX 11/780 computer. The routine as delivered was limited to about 250 polygons; therefore, a relatively small model was used for testing, 183 surfaces/324 edges. The cpu time for SKETCH was 19.3 cpu seconds and the time for the JONES/E algorithm in NLOT was 1.9 cpu seconds. The level of performance for SKETCH, about 9 polygons per cpu second, seems consistent with the data

presented by Hedgley [13]. In reference 13 the processing rate for SKETCH on a CDC 6500 computer, which is about the same speed as a VAX 11/780, was given as about 10 polygons per cpu second.

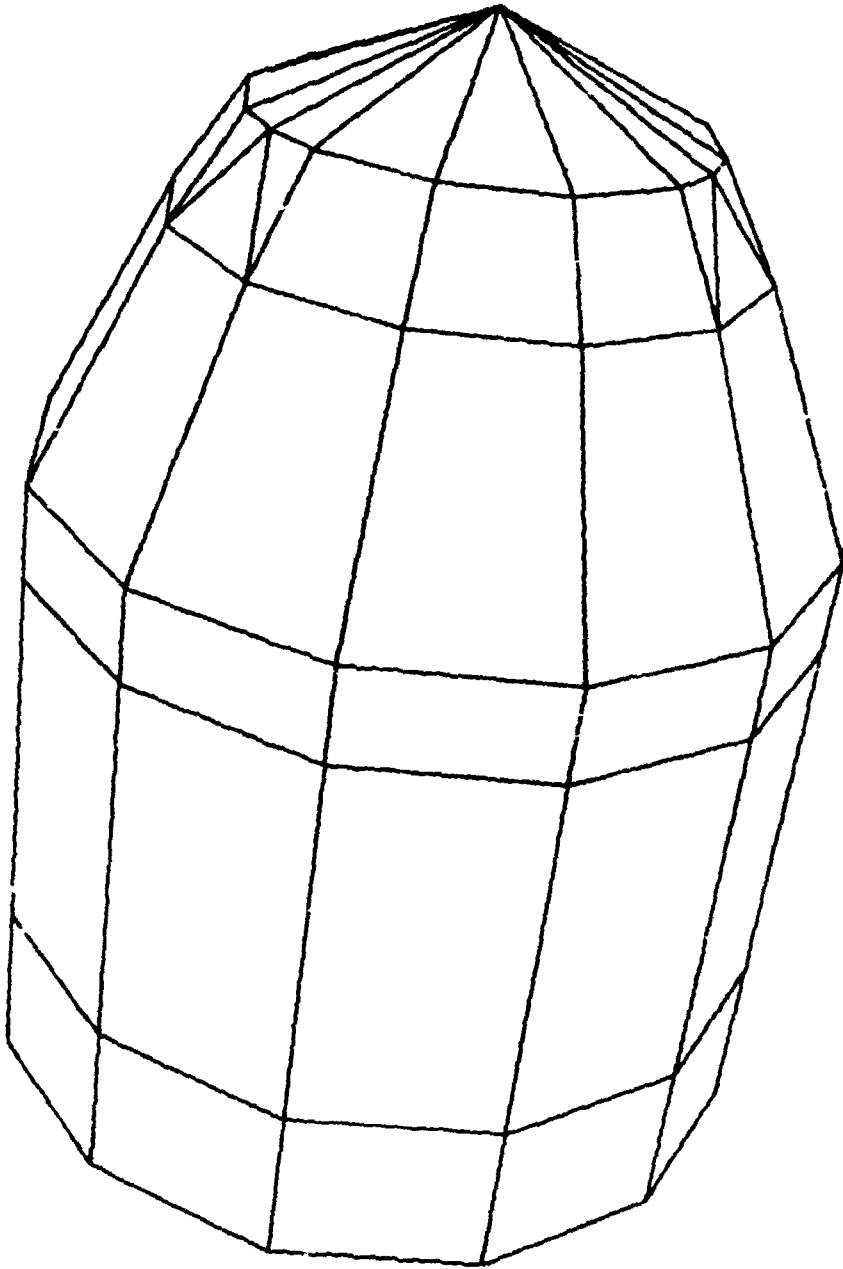
CONCLUDING REMARKS

The NPLOT computer graphics program has been shown to be an effective tool for the interactive display of NASTRAN finite element models. It offers a variety of state of the art tools to aid the analyst. It is easy to use and provides an on line help facility for the inexperienced user. NPLOT's very fast hidden line and haloed line algorithms are unique and effective graphics tools for the analyst. Analysts using NPLOT usually prefer hidden line or haloed line plots in place of wire frame plots due to the more realistic model display. Current activity is focused on increasing the post-processing functionality of NPLOT.

REFERENCES

1. Walker, W., and Vos, R., *IAC Executive Summary*, NASA CR-175196, May 1984.
2. Vos, R.G., Beste, D.L., and Gregg, J., *IAC User Manual*, NASA CR-175300, July 1984.
3. Newman, W.M., and Sproull, R.F., *Principles of Interactive Computer Graphics*, McGraw-Hill Co., 1979.
4. Bateau, H., "Convenient Representation Method For Spatial Finite Element Structures", *Computers & Structures*, 10(5), October 1979, pp. 815-819.
5. Appel, A., Rohlf, F.J., and Stein, A.J., "The Haloed Line Effect for Hidden Line Elimination", *Computer Graphics*, 13(3), August 1979, pp. 151-157.
6. Franklin, W.R., "A Linear Time Exact Hidden Surface Algorithm", *Computer Graphics*, 14(3), August 1980, pp. 117-123.
7. Giloi, W.K., *Interactive Computer Graphics, Data Structures, Algorithms, Languages*, Prentice-Hall Inc., 1978.
8. Griffiths, J.G., "A Surface Display Algorithm", *Computer Aided Design*, 10(1), January 1978, pp. 65-73
9. Griffiths, J.G., "A Bibliography of Hidden-Line and Hidden-Surface Algorithms", *Computer Aided Design*, 10(3), May 1978, pp. 203-206.
10. Griffiths, J.G., "Tape-Oriented Hidden Line Algorithm", *Computer Aided Design*, 13(1), January 1981, pp. 19-26.
11. Watkins, G.S., *A Real Time Visible Surface Algorithm*, University of Utah, UTEC-CSc-70-101, June 1970.
12. Emery, A.F., *VIEW*, University Of Washington, Department of Mechanical Engineering, 1982.
13. Hedgley, D.R., Jr., *A General Solution to the Hidden Line Problem*, NASA RP-1085, March 1982.
14. Writtram, M., "Hidden-Line Algorithm for Scenes of High Complexity", *Computer Aided Design*, 13(4), July 1981, pp. 187-192.
15. Janssen, T.L., "A Simple Efficient Hidden Line Algorithm", *Computers & Structures*, 17(4), 1983, pp. 563-571.

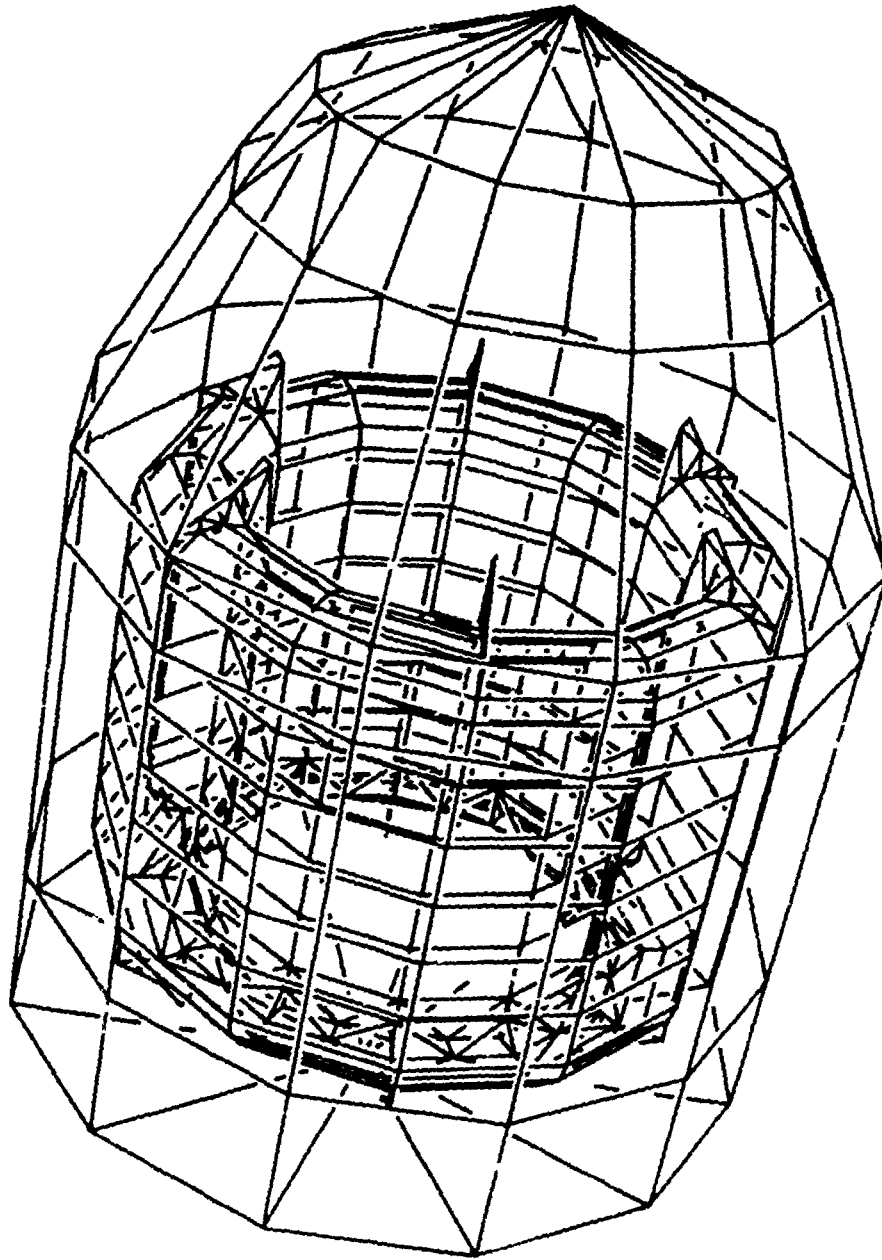
16. Hornung, C., "An Approach To A Calculation-Minimized Hidden Line Algorithm", *Computers & Graphics*, 6(3), 1982, pp. 121-126.
17. Jones, G.K., *A Fast Hidden Line Algorithm For Plotting Finite Element Models*, NASA TM-83981, August 1982.
18. Appel, A., "The Notion of Quantitative Invisibility and the Machine Rendering of Solids", *Proc. ACM National Conference*, 1967, pp. 387-393.



HIDDEN LINE PLOT

FIGURE 1

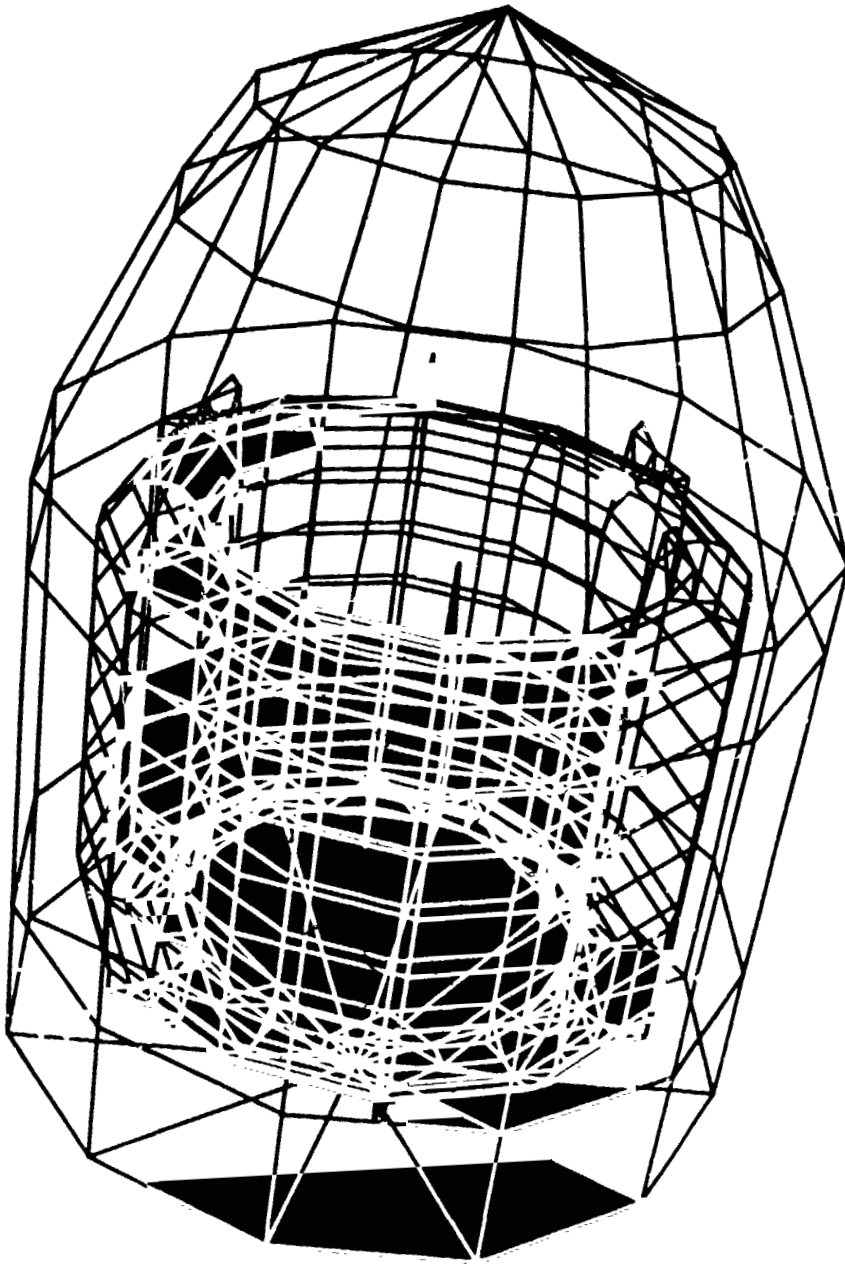
ORIGINAL PAGE IS
OF POOR QUALITY



HALOED LINE PLOT

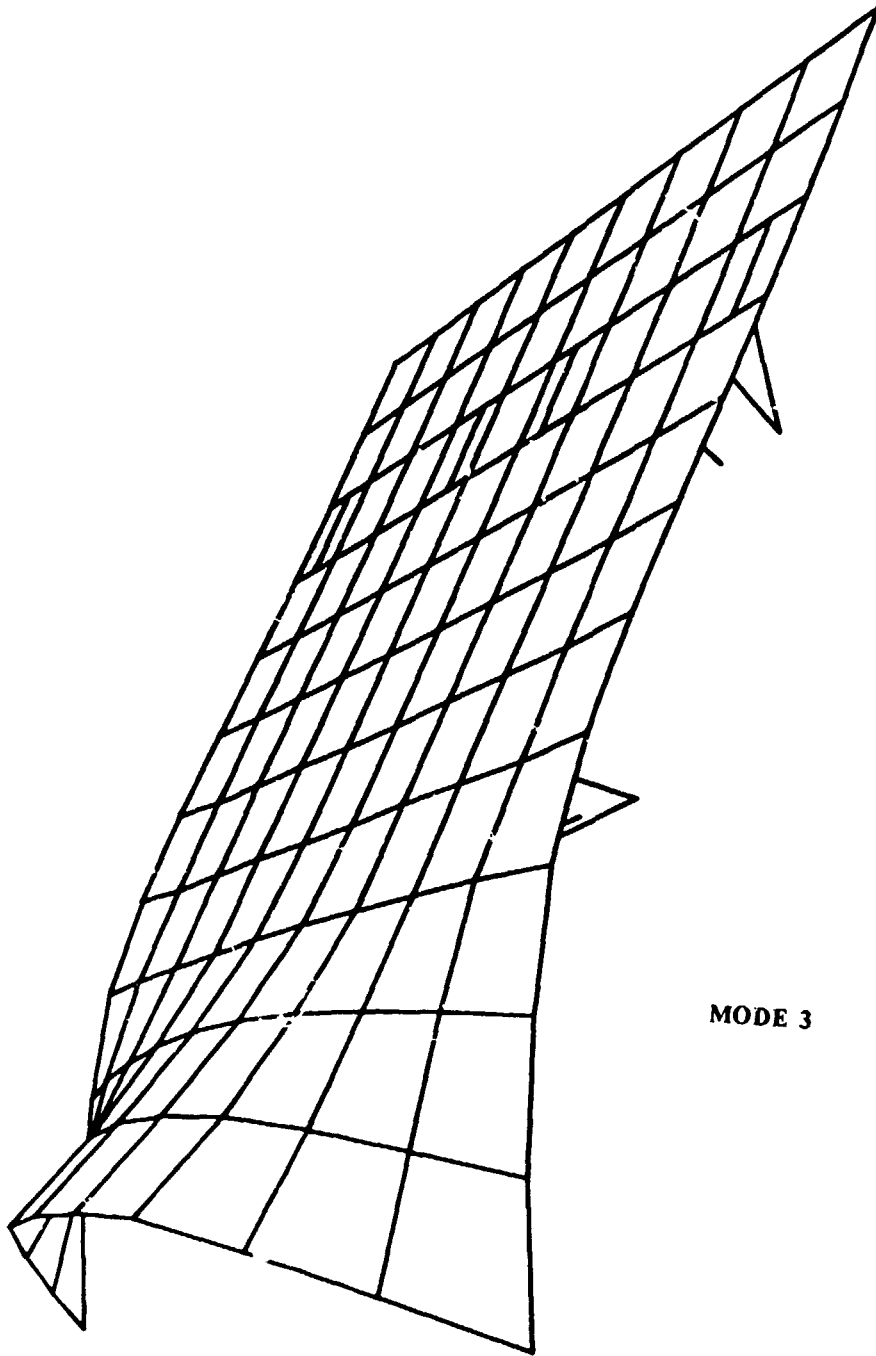
FIGURE 2

ORIGINAL PAGE IS
OF POOR QUALITY.



WIRE FRAME PLOT

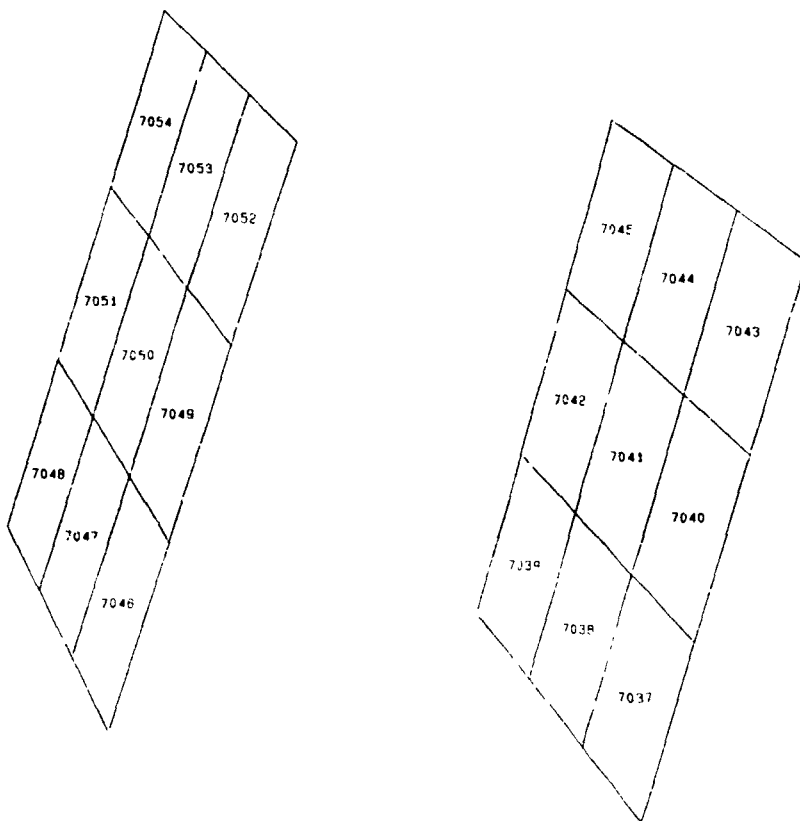
FIGURE 3



PLOT OF DEFORMED SHAPE

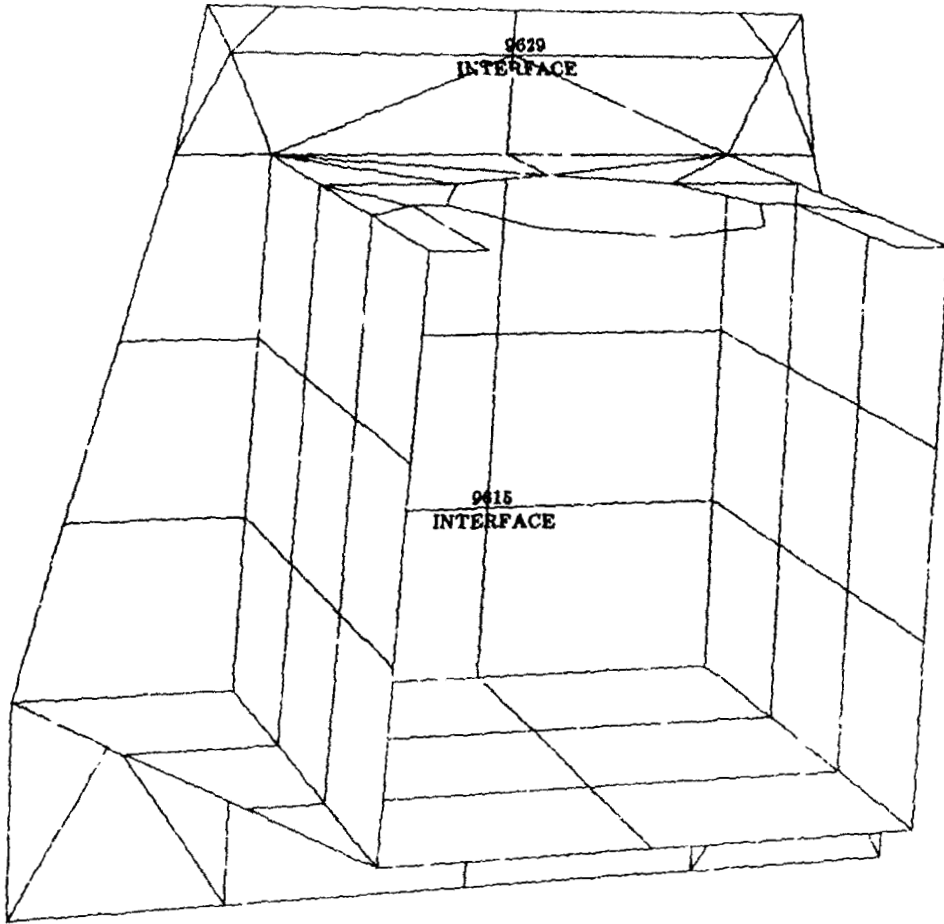
FIGURE 4

ORIGINAL PAGE IS
OF POOR QUALITY



PLOT WITH ELEMENTS LABELLED

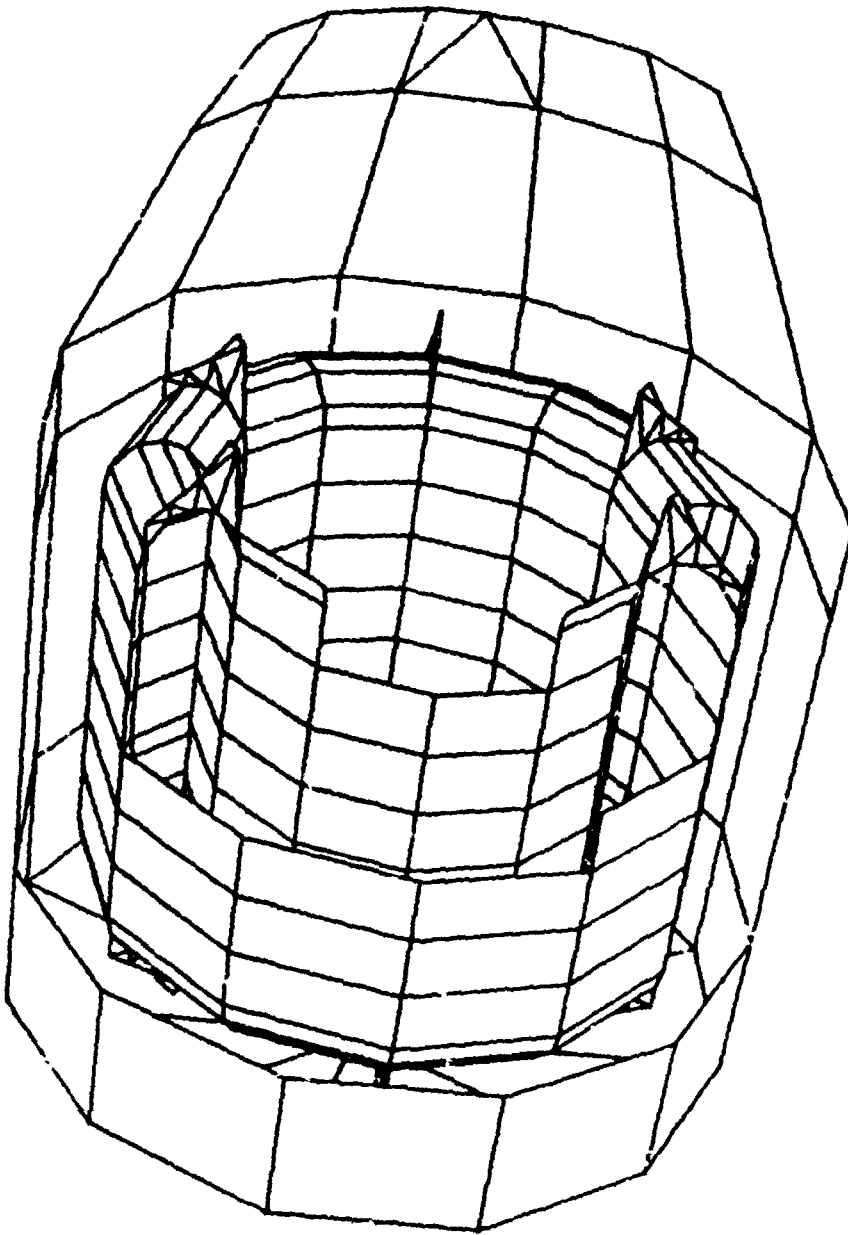
FIGURE 5



PLOT WITH GRIDS LABELLED AND TAGGED

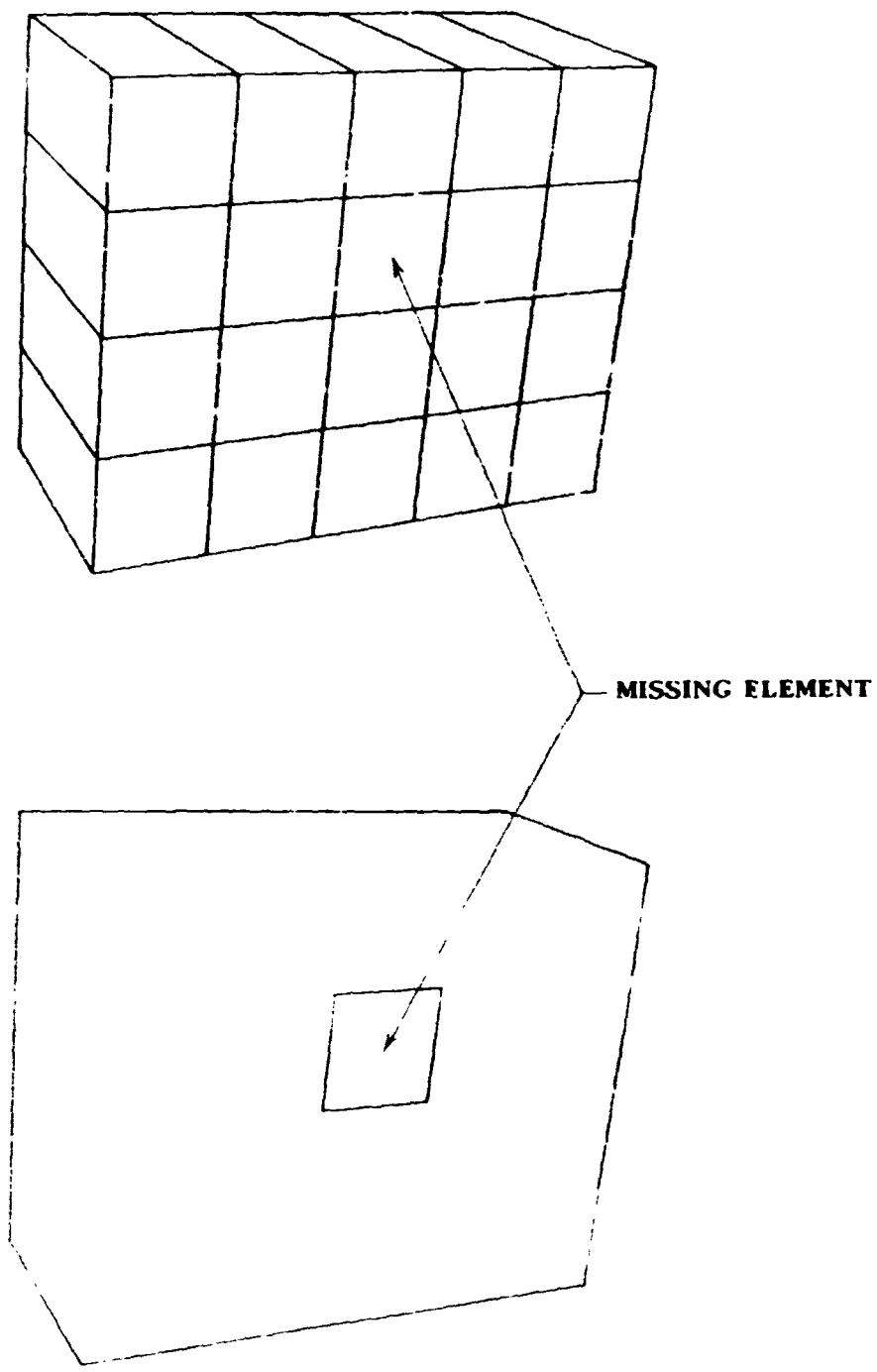
FIGURE 6

ORIGINAL
OF POOR QUALITY



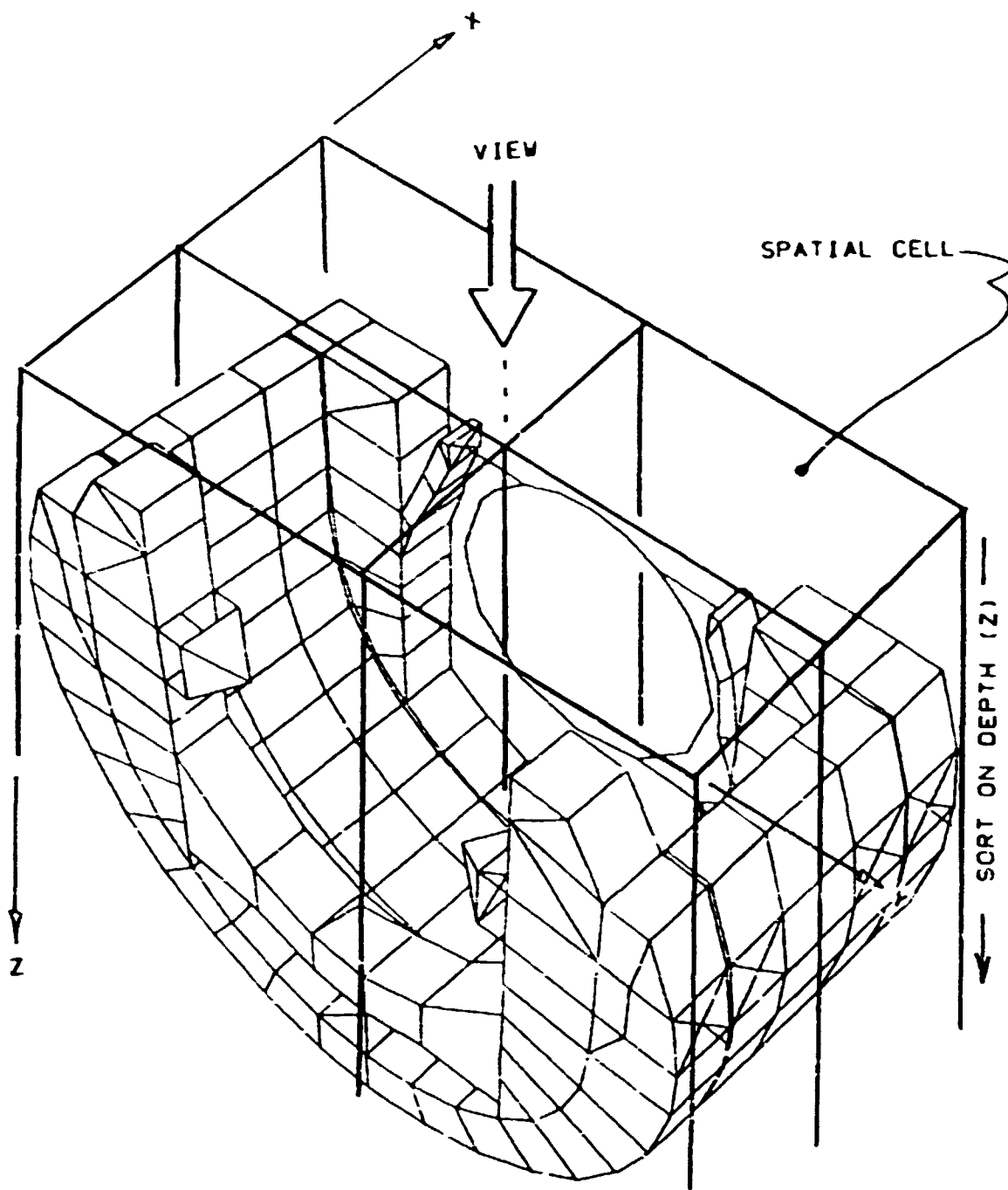
PLOT WITH Z-CUT

FIGURE 7



HORIZON EDGE PLOT

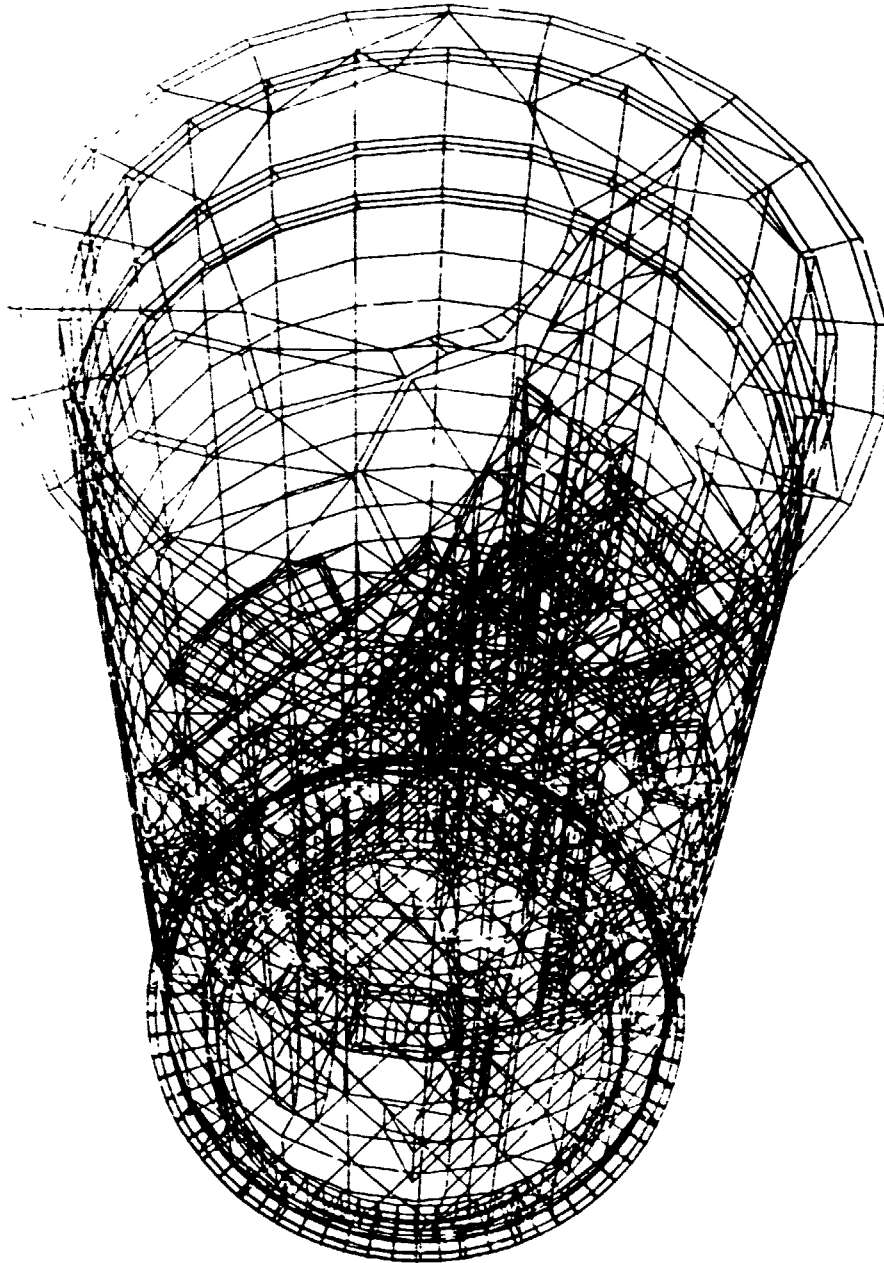
FIGURE 8



SPATIAL CELLS USED IN X-Y BUCKET SORTING

FIGURE 9

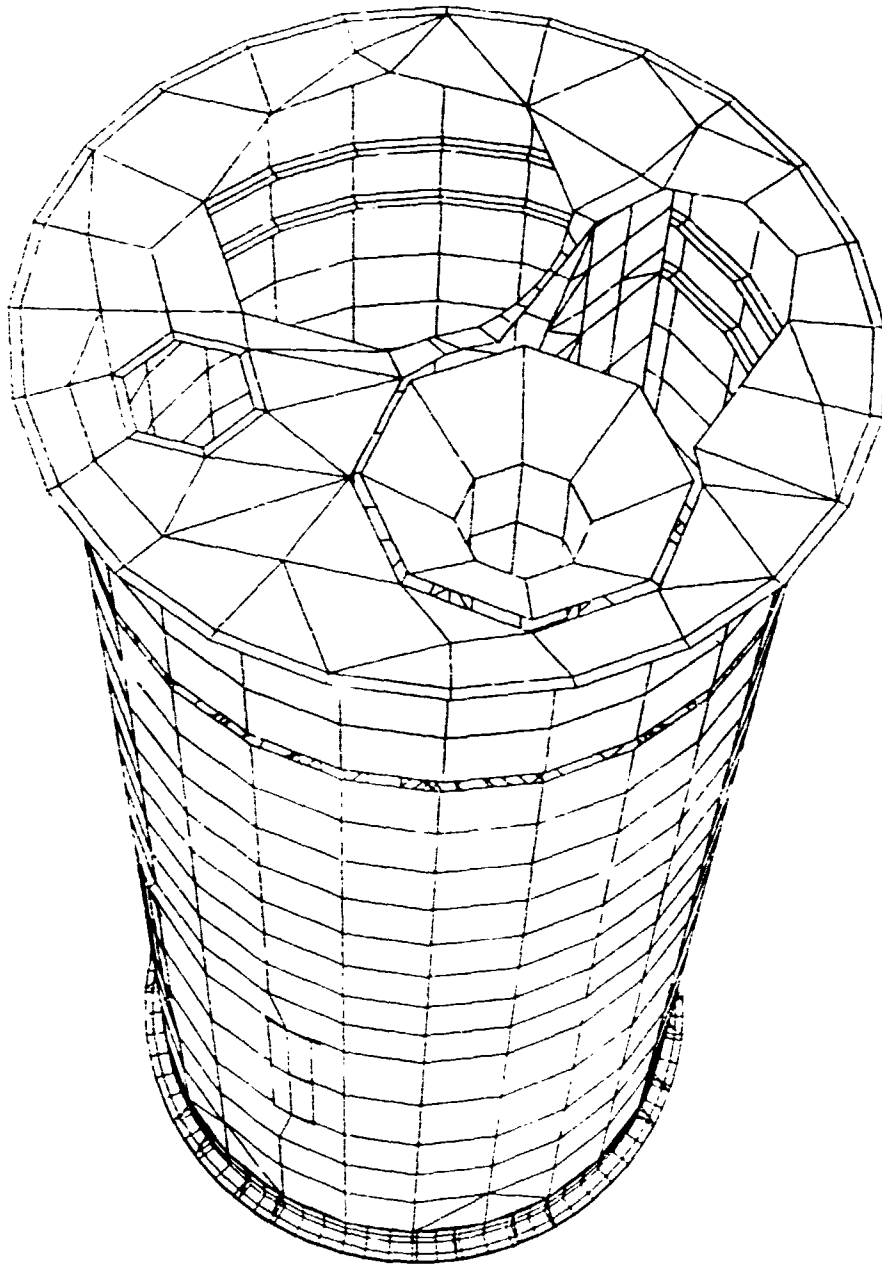
ORIGINAL PAGE IS
OF POOR QUALITY



LARGE TEST MODEL - WIRE FRAME PLOT

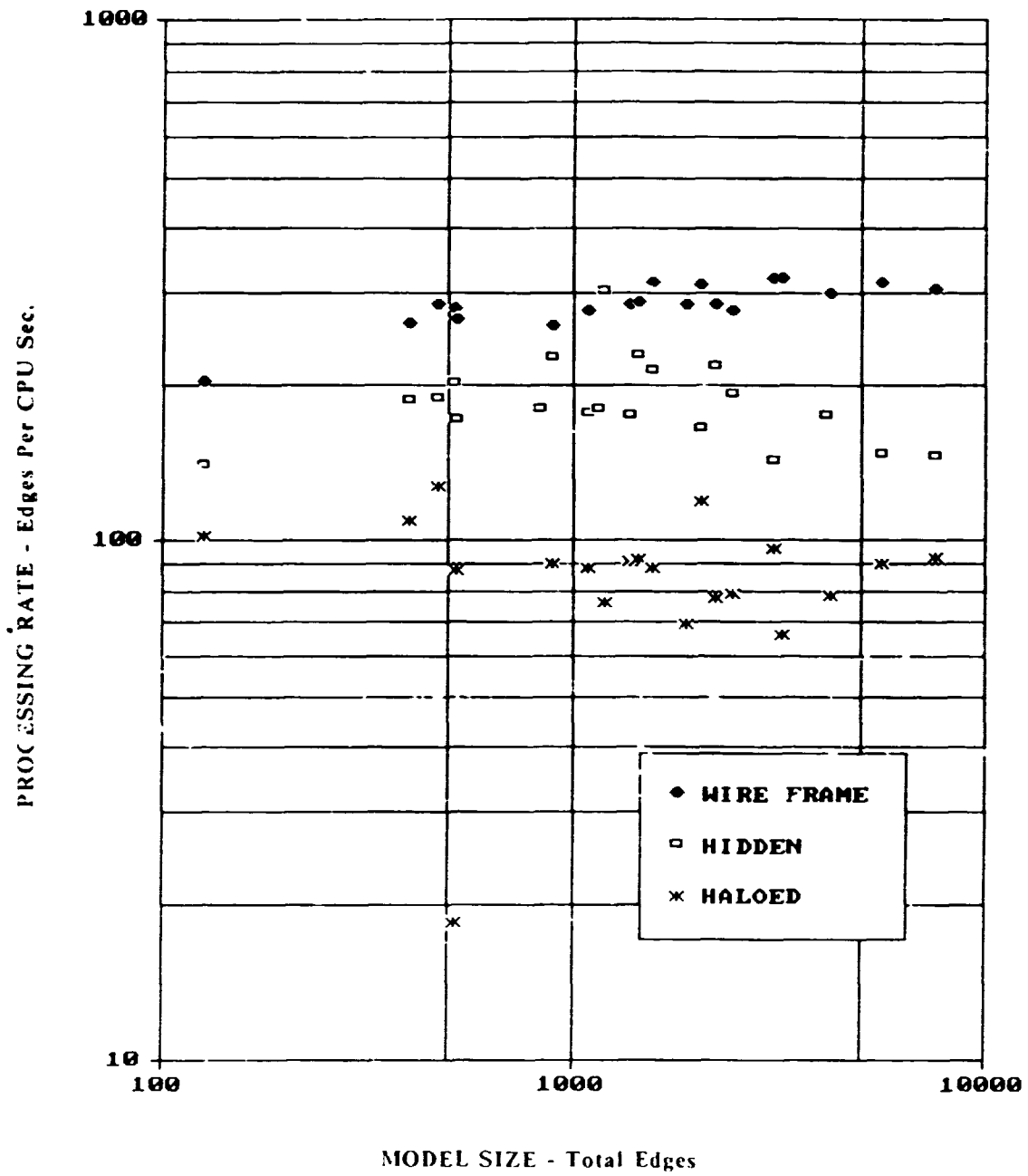
FIGURE 10

ORIGINAL
OF P. 001. 0



LARGE TEST MODEL - HIDDEN LINE PLOT

FIGURE 11



PERFORMANCE OF NPLLOT ALGORITHMS

FIGURE 12

N85-25870

COSMIC/NASTRAN - PATRAN INTERFACE

Daron H. Libby

PDA Engineering
Santa Ana, California
February 1985

ABSTRACT

The capabilities provided by the PATRAN-COSMIC/NASTRAN interface are discussed. While the translator capabilities give some indication of the interface quality between the two programs, certainly there are other attributes to be considered. The ideal interface would be a user-transparent union of the two programs so that the engineer could move from one program to the other fluently and naturally. Hence, a valid assessment of the interface completeness must consider how close the current capabilities are to the idealized case. An example problem is presented to demonstrate how COSMIC/NASTRAN and PATRAN can be used together to meet the requirements of an actual engineering application.

INTRODUCTION

PATRAN [1] is a three-dimensional solid modeling and finite element pre- and postprocessing program developed and marketed by PDA Engineering in Santa Ana, California. Using the latest interactive computer graphics technology, PATRAN provides a visual means to define a finite element model and its environment, and review its resultant model behavior. Although PATRAN offers linear statics and eigenvalue analysis capability as an option, a more detailed analysis is often required. More than 25 translator programs have been developed that move data among PATRAN and external finite element, finite difference, and boundary element analysis programs [2]. It is these interfaces that bring the advanced analysis methods available in general-purpose finite element programs to the PATRAN modeler, and one important interface is to COSMIC/NASTRAN [3].

The COSMIC/NASTRAN interface is comprised of two translators: an analysis translator and a results translator. The analysis translator accepts a PATRAN neutral output file and produces a NASTRAN bulk data file. The forward translator is named PATCOS to indicate the translation from PATRAN to COSMIC/NASTRAN. For postprocessing within the PATRAN system, it is necessary to execute a second program after the analysis. This inverse translator is called COSPAT, because it accepts the COSMIC/NASTRAN results and produces files in a format which PATRAN can read. COSPAT also provides the option of translating an existing analysis input deck into a PATRAN neutral file. Both analysis and results translators are easy to use in that they are menu-driven, execute quickly, and are highly automated. The PATRAN-COSMIC/NASTRAN interface is illustrated in Figure 1.

ANALYSIS MODELING

PATCOS can produce 59 different COSMIC/NASTRAN bulk data card types, including 29 different finite elements. The list of bulk data cards supported is presented in Table 1. The complete analysis model can be defined in PATRAN to include not only the finite element mesh but also element properties, boundary conditions and applied loads. PATRAN also provides visual model verification techniques to check parameters such as element aspect ratio or property assignment.

There are several ways to add the required EXECUTIVE and CASE CONTROL cards to the bulk data deck. The simplest method is to use a text editor and either (1) insert the control cards manually, or (2) copy them in from an existing file.

RESULTS RECOVERY

The results (or inverse) translator, COSPAT, provides the capability to reformat analysis results into PATRAN compatible files. The input file to COSPAT is a binary OUTPUT2 file generated during COSMIC/NASTRAN execution. The output files contain nodal displacements, element centroidal and nodal stress, strain or temperature. To generate an OUTPUT2 file during a COSMIC/NASTRAN execution of a static analysis (SOL 1), the following directives must be added to the COSMIC/NASTRAN input deck. Similar ALTER sequences can be used for other solution approaches: e.g.

```
ALTER      143 $
OUTPUT2    OUGV1,OES1//C,N,-1/C,N,11/V,N,Z $
ENDALTER
CEND
DISP      = ALL
STRESS    = ALL
```

PATRAN can then be used to combine the results information with the finite element model to evaluate model behavior. Using graphical methods such as animation and color bring unparalleled insight into understanding the voluminous output data often generated from a complex analysis. The engineer can interactively view any piece of the model from any perspective and see color variations of results. Hence one simple exercise for PATRAN might be to crack open an egg and display the variation in circumferential stress on the inside of the shell.

MODEL TRANSLATION

COSPAT also provides the capability to reformat COSMIC/NASTRAN analysis input data into PATRAN neutral format. This method not only brings all PATRAN postprocessing capabilities to bear on existing COSMIC/NASTRAN models (generated by other means or by hand), but also suggests a medium in which to convert a COSMIC/NASTRAN input deck to that of another analysis program format. The COSPAT model translator currently recognizes the 58 different card types as listed in Table 2.

AN APPLICATION

While the translator capabilities give some indication of the interface quality between the two programs, it is clear that there are other attributes to be considered. The ideal interface would be a user-transparent union of the two programs so that the engineer could move from one program to the other fluently and naturally. Hence, a valid assessment of the interface completeness must consider how close the current capabilities are to the idealized case. This can be explored through the use of an example problem.

One common step in the analysis of a part or structure is to determine the structural response to an imposed thermal environment. This involves creating a thermal model subjected to various thermal conditions, solving for a resultant temperature distribution, and then calculating the stresses induced by the applied thermal loads. Both a thermal and a structural analysis must be performed, very often using a structural analytical model of a different mesh density than that of the thermal analysis. The following example demonstrates how PATRAN and COSMIC/NASTRAN can be used together to model, analyze, and evaluate a thermal stress problem.

Problem Definition

The example chosen is a pipe with stepped cooling fins subjected to an internal fluid temperature of 500°F and an outside ambient temperature of 70°F (Figure 2). The structure consists of a 6-inch (0.5 ft) stainless steel pipe with 14.4-inch (1.2 ft) cooling fins. The emphasis here is not on the actual dimensions and properties of the model but rather the technique applied. The objective is to use axisymmetric elements with heat boundary elements to solve for a linear steady-state temperature distribution. Then, determine the stress induced by the resulting temperatures on two different structural models: (1) a finite element mesh matching the thermal mesh, and (2) a non-uniform structural mesh with higher element density.

Thermal Model

The thermal model is represented with axisymmetric trapezoidal ring elements (CTRAPRG). The only material property required for this element is a thermal conductivity equal to 15 Btu/hr-ft-°F. The convection surfaces are defined by heat boundary line elements (CHBDY). The material property for this element is the convective film coefficient equal to 12 Btu/hr-ft-°F on the inside of the pipe and 3 Btu/hr-ft-°F on the outside of the fin. The appropriate PATRAN directives are used to define these data (Table 3), namely element connectivity (CFEG), element geometric properties (PFEG), and material properties (PMAT). The only other value to be defined is the ambient temperatures referenced by the convection surfaces. Because PATRAN originated from structural analysis, there is currently no straightforward way to define this relationship. Hence, a special technique must be used. This technique consists of first constraining scalar points to the appropriate fixed temperatures and then referencing these scalar points in the element associate data field as the convection surface elements are created. The complete list of PATRAN directives required to generate the thermal model is listed in Table 3. The final model is illustrated in Figure 3.

PATCOS is then executed to translate the PATRAN neutral output file into COSMIC/NASTRAN bulk data. A minor coding modification translated the element data associated with the heat boundary elements as the ambient reference points. The EXECUTIVE and CASE CONTROL cards were added and included two important directives: (1) THERMAL(PUNCH) = ALL to write the resultant nodal temperatures to a punch file and (2) OUTPUT2 to save the temperatures for PATRAN postprocessing displays. A sampling of the COSMIC/NASTRAN input file is shown in Table 4.

COSPAT can be executed to read the OUTPUT2 file and generate PATRAN postprocessing files. Figure 4 illustrates the temperature distribution that resulted from the linear steady-state heat transfer analysis.

Structural Model (Mesh 1)

The first structural model is created by slightly modifying the thermal model using PATRAN. The heat boundary elements are deleted, the structural properties for the CTRAPRG elements are defined, and axisymmetric boundary conditions are added. For this case, Young's modulus is given as 194,400 lb/ft, Poisson's ratio is 0.3, and the coefficient of thermal expansion is 0.00009 ft/ft- F.

PATCOS is then used to generate the corresponding COSMIC/NASTRAN bulk data. This time the appropriate EXECUTIVE and CASE CONTROL cards are added, as well as a single point constraint card to eliminate all degrees of freedom except the in-plane axisymmetric motion. Also, because the structural mesh corresponds identically to the preceding thermal mesh, the punch file generated during the thermal analysis can be appended directly to the structural COSMIC/NASTRAN input file. Clearly, this is a most desirable situation and, for this reason, many thermal models are commonly over-modeled such that a structural analysis can be performed easily at a later time.

The OUTPUT2 file generated during the COSMIC/NASTRAN run is processed by COSPAT and PATRAN is used to plot the deformed shape (Figure 5) and stress contours (Figure 6).

Structural Model (Mesh 2)

The next step is perhaps the most difficult, in that a new structural mesh is to be defined but subjected to the temperature distribution calculated in the initial thermal analysis. Many schemes have been devised to interpolate resultant temperature fields onto new structural meshes. The inherent capability to the PATRAN approach of defining a model's environment in terms of the model geometry and not the finite element mesh shows great potential to solving this problem. However, direct methods have not yet been developed.

The approach taken here is to define PATRAN data patches (surfaces) that lie in the thermal distribution field. PATRAN data entities (lines, surfaces, and volumes) can be created to represent a parametric cubic variation of any scalar function [4]. These data surfaces can then be applied to the geometry independent of the finite element mesh density. This is made possible by taking advantage of the axisymmetric nature of the problem. It is noted that the spatial orientation of the model is completely defined by X- and Z-coordinates and that the Y-coordinate is always zero. Hence, a 100-line FORTRAN program, developed in two hours, combines the spatial model coordinates with the nodal temperatures to define PATRAN geometric points (grids) in a PATRAN neutral file. The three coordinates of these grid points are specified as X, TEMP, Z so that they actually lie in the temperature field.

The next step is to delete all finite elements and nodes in the PATRAN axisymmetric model, leaving only the model geometry. The temperature neutral file is then combined with the PATRAN model and these new grid points are used to define PATRAN data patches. The cubic data patches are defined by specifying scalar values that lie in the distribution field. Hence, it is an easy task to have PATRAN extract the r-coordinates of selected grid points to define the desired data patch (scalar function).

A new structural mesh is defined with a non-uniform element density (Figure 7). Then, each patch is loaded with its corresponding data patch and each finite element node is assigned automatically a temperature depending on its location in the data patch function (Figure 8). Geometric patches were constructed to show the temperature distribution.

PATCOS then translates this new model and loading combination into COSMIC/NASTRAN bulk data. The EXECUTIVE and CASE CONTROL cards are added and the analysis is run. COSPAT is used to generate the postprocessing files that lead to the final Z-X shear stress plots for the critical area shown in Figure 9.

CONCLUDING REMARKS

An overview of the current capabilities provided by the PATRAN-COSMIC/NASTRAN interface is described. While the extent of these capabilities is important in assessing the interface quality, the example problem illustrates the wide range of flexibility provided. PDA Engineering, in its short history of interface development, has made major strides in linking up the unique analysis tools found in many different programs. Improvements have been made which were primarily due to a close working relationship with the engineering community. We were thus able to define, and meet, the rising needs and expectations of the analysts.

The future holds a great promise for more efficient, complete, and sophisticated methods in software and hardware networks, to solve a growing diversity of engineering problems. PDA's interface developments already are considering new approaches to thermal modeling, substructuring, and composite material modeling. It is clear that PDA is committed to providing the engineering community with the highest quality modeling and analysis software through more efficient, complete, and accurate data definition and transfer -- very often based on user recommendations.

REFERENCES

1. PDA/PATRAN User's Guide Vol. I-II (Rev 1.5), 1984, PDA Engineering, Santa Ana, California.
2. Fong, Henry H., "Interactive Graphics and Commercial Finite Element Codes", Mechanical Engineering, June 1984, pp. 18-25 (published by The American Society of Mechanical Engineers, New York, New York).
3. Field, E. I., D. N. Herting, and M. J. Morgan, NASTRAN User's Guide (Level 17.5), Prepared by Universal Analytics, Inc. (Playa Del Rey, California) for Langley Research Center, NASA CR-3146, June 1979.
4. Casale, Malcolm S. and Edward L. Stanton, "An Overview of Analytic Solid Modeling", IEEE Computer Graphics and Applications, February 1985 (published by The Computer Society of The Institute of Electrical and Electronics Engineers, Los Alamitos, California), pp. 45-56.

Table 1
 COSMIC/NASTRAN Card Types Supported By PATCOS (5°)

<u>Coordinate Frames</u>	<u>Element Properties</u>	<u>Node Forces</u>
CORD2C	PBAR	FORCE
CORD2R	PHBDY	MOMENT
CORD2S	PIHEX	<u>Specified Node Displacements</u>
	PQDMEM1	
	PQDMEM2	
	PQDPLT	
	PQUAD1	
<u>Node Coordinates</u>	PQUAD2	SPC
GRID	PSHEAR	<u>Constraints</u>
	PTRBSC	
	PRTIA1	
<u>Element Definitions</u>	PRTIA2	SPC1
	PTRIM6	
CBAR	PTRMEM	<u>Temperatures</u>
CELAS2	PTRPLT	
CHBDY	PTRSHL	
CHEXA1		
CHEXA2		TEMP
CIHEX1		
CIHEX2		
CIHEX3	<u>Material Properties</u>	
CONM2		
CQDMEM1	MAT1	<u>Bar Deformation</u>
CQDMEM2	MAT2	
CQDPLT	MAT3	
CQUAD1	MAT4	
CQUAD2	MAT5	
CROD		DEFORM
CSHEAR		
CTETRA		
CTRAPRG		
CTRBSC		
CTRIA1		
CTRIA2		
CTRIARG		
CTRIM6		
CTRMEM		
CTRPLT		
CTRSHL		
CWEDGE		
CNGRNT		
	<u>Pressure Loads</u>	
	PLOAD	
	PLOAD2	
	PLOAD3	

Table 2
 COSMIC/NASTRAN Cards Supported By COSPAT (58)

- A. Coordinate frames
 CORD2C, CORD2R, CORD2S
- B. Grid points
 GRID ,GRDSET
- C. Elements
 BAROR , TRIA1, CBAR , CTRIA3, CROD , CQDMEM1
 CTBSC, CTRIA2, CTRIA2, CTRMEM, CQUAD1, CQDMEM2
 CSHEAR, CTRAPRG, CQDMEM, CQUAD2, CHEXA2, CWEDGE
 CIHEX2, CTRPLT , CTETRA, CQDPLT, CTRIM6,
 CTRSHL, CTRPLT1, CHEXA1, CIHEX1,
- D. Properties
 PBAR , PBEAM , PROD , PTRIA1, PTRMEM
 PQUAD1, PQUAD2, PQDMEM, PTRIA2, PHEX
 PSOLID, PHBDY , PSHEAR, PSHELL
- E. Materials
 MAT1 , MAT2 , MAT3 , MAT4 , MAT5 , MAT9
- F. Forces and Constraints
 SPC , SPC1 , FORCE , MOMENT, TEMP , DEFORM

Table 3
PATRAN Input Directives To Create Thermal Model

```

GO                                ! Initialize PATRAN
1
1
2
VI                                ! Change view to X - Z plane
1
.90
GR,1,,.45                          ! Begin geometry creation
GR,2,,.55
GR,3,,.85
GR,4,,1.75
LI,3#,26,,1T3,2T4
LI,4#,TR,/.3,1
LI,5#,TR,/.15,2
LI,6#,TR,/.05,3
PA,7#,2L,,1T3,4T6                  ! Finish geometry creation
GF,P1,,4/7                          ! Define thermal mesh
GF,P2,,4/4
GF,P3,,13/2
CF,PIT#,QUAD/4/7                    ! Define axisymmetric quad. elements
LI,4#,26,,6/8/10/5,7/9/4/1         ! Create geometry for convection boundary
GF,10L,,7                            ! Mesh boundary
GF,4L/7/5,,4
GF,8L,,3
GF,6L,,13
GF,9L,,2
COLOR,BAR,BLUE
GRID,100,,100                       ! Define scalar points
GRID,200,,200
CF,10L,BAR/2/5                      ! Define convection elements
1
G
100                                 ! Reference ambient source
4
CF,4LT9,BAR/2/5
1
G
200
4
E                                    ! Use menu sytem to optimize bandwidth
2
3

```

Table 3 (Continued)

```

N
2
1
Y
7
3
3
1
NODE,100,ADD           ! Define scalar points for ambient temperature
1
1
100.0
5
NODE,200,ADD
1
1
200.0
5
DISP,N100,ADD,1       ! Specify ambient temperatures
500.C
DISP,N200,ADD,1
70.0
PF,P1T3,QUAD/4/7,,M1  ! Assign material types
PF,10L,BAR/2/5,2,2
PF,4LT9,BAR/2/5,3,3
PMAT,1,TIS,15         ! Specify material properties
PMAT,2,TIS,12
PMAT,3,TIS,3
E
5                       ! Create PATRAN neutral file
1
1
AXISYMMETRIC COOLING FIN (THERMAL MODEL)
N
STOP

```

Table 4
Sampling Of NASTRAN Thermal Analysis Input

```

ID DHL,NASTRAN
APP HEAT
SOL 1
TIME 90
DIAG 14
ALTER 109 $
PARAM /,C,N,NOP/V,N,TRUE=-1
EQUIV HOUGV1,OUGV1,/TRUE $
OUTPUT2 ,,,,//C,N,-1/C,N,92/V,N,Z $
OUTPUT2 OUGV1,,,,//C,N,0/C,N,92/V,N,Z $
OUTPUT2 ,,,,//C,N,-9/C,N,92/V,N,Z $
ENDALTER
CEND
TITLE = LINEAR STEADY STATE CONDITION THROUGH A COOLING FIN
SUBTITLE = AXISYMMETRIC RING ELEMENTS, FILM HEAT TRANSFER
OUTPUT
THERMAL(PRINT,PUNCH) =ALL
OLOAD = ALL
SPC = 1
BEGIN BULK
$AXISYMMETRIC COOLING FIN (THERMAL MODEL)
$--BULK DATA CARDS PRODUCED BY "PATCOS" VERSION 1.6A: 09-JAN-85 15.54:40
SPC 1 100 1 500.000
SPC 1 200 1 70.0000
GRID 1 0.45000 0. 0.
GRID 2 0.48333 0. 0.
GRID 3 0.48333 0. 0.05000
GRID 4 0.45000 0. 0.05000
GRID 100 100.0000 0. 0.
GRID 200 200.0000 0. 0.
CTRAPRG 1 1 2 3 4 0.000 1
CTRAPRG 2 2 5 6 3 0.000 1
CTRAPRG 3 5 7 8 6 0.000 1
CTRAPRG 4 4 3 9 10 0.000 1
CHBDY 40 2REV 26 22 E 40
+E 40 100 100
CHBDY 41 2REV 22 18 E 41
+E 41 100 100
CHBDY 42 2REV 18 14 E 42
+E 42 100 100
CHBDY 43 2REV 14 10 E 43
+E 43 100 100
CHBDY 69 3REV 64 63 E 69
+E 69 200 200
PHBDY 2 2
PHBDY 3 3
MAT4 1 15.0000
MAT4 2 12.0000
MAT4 3 3.00000
ENDDATA

```


Figure 1
PATRAN - To - COSMIC/NASTRAN Interface
(August 1984)

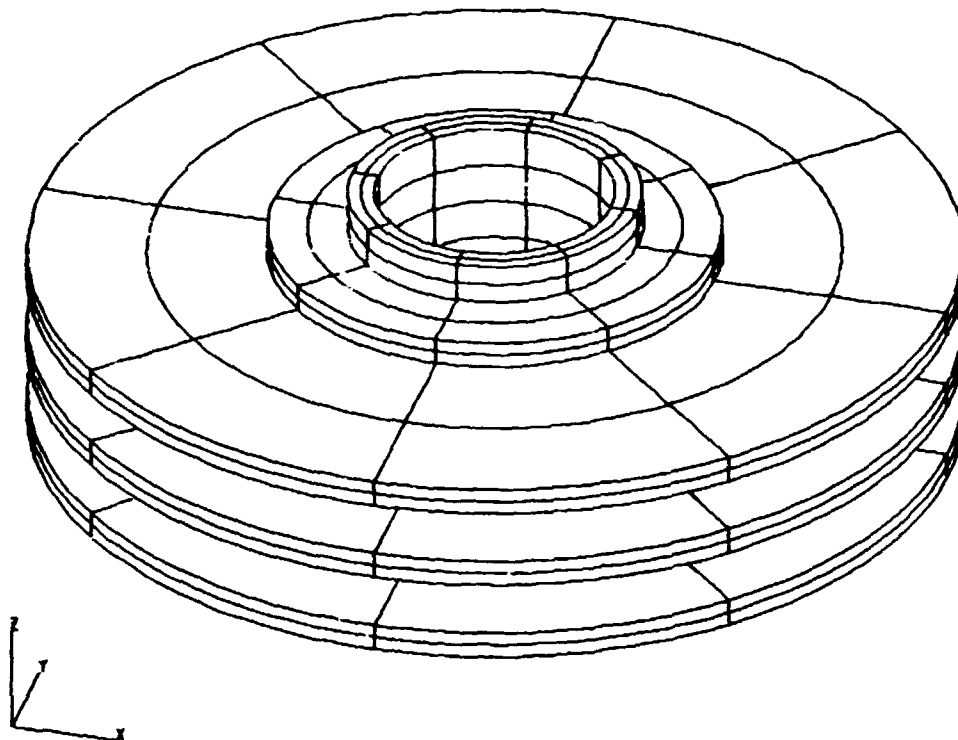
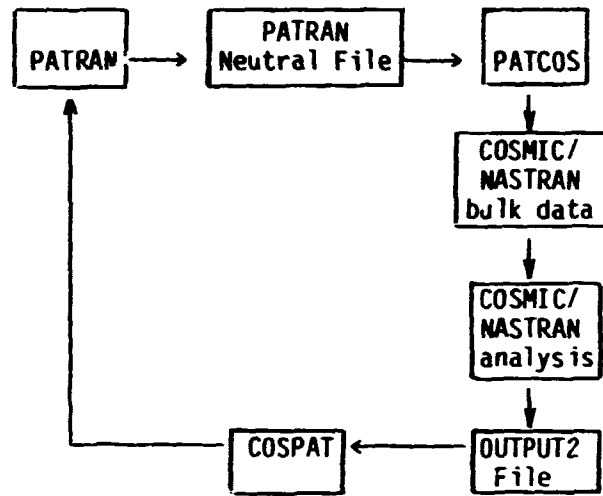


Figure 2 - Pipe With Cooling Fins

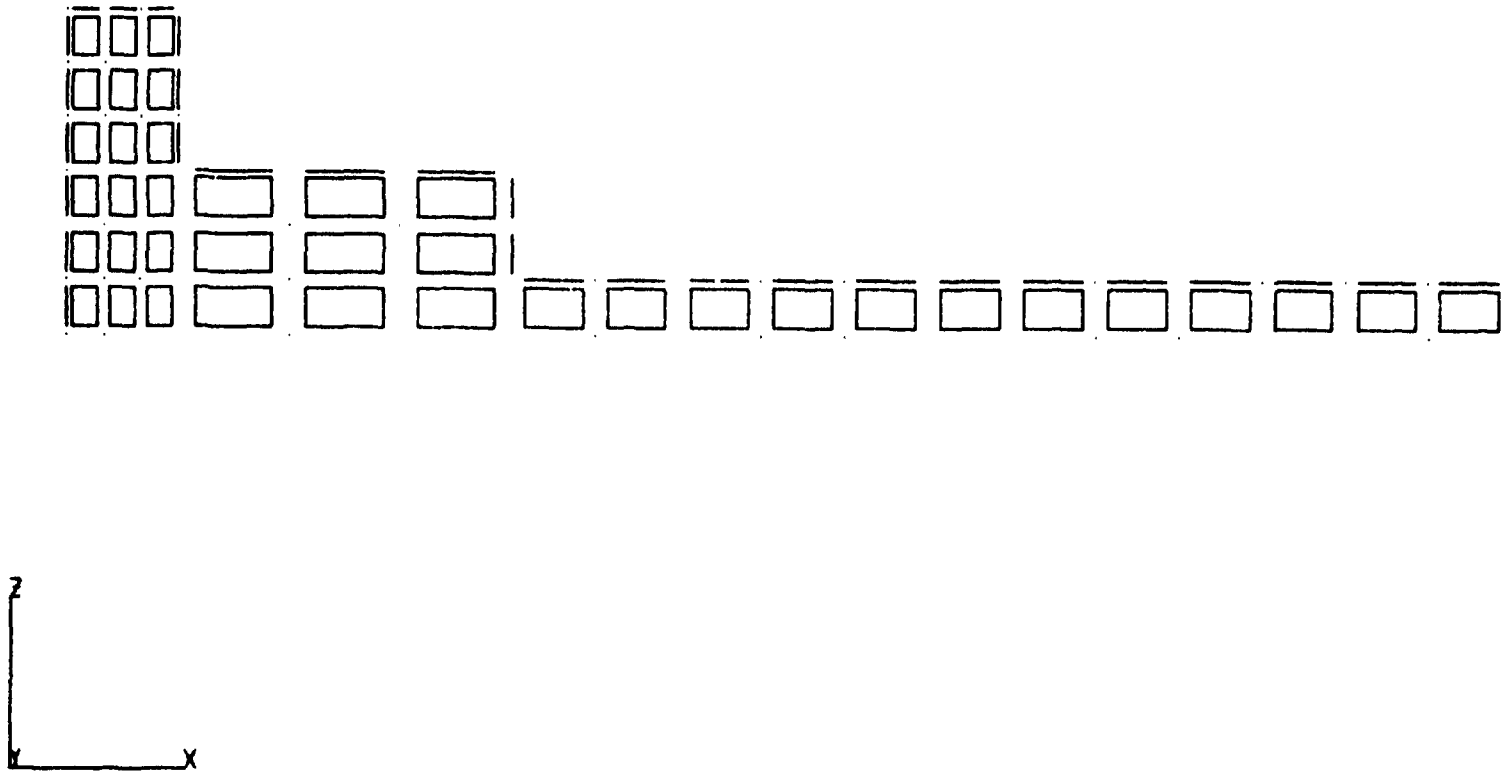


Figure 3 - The Thermal Model (also Structural Mesh 1)

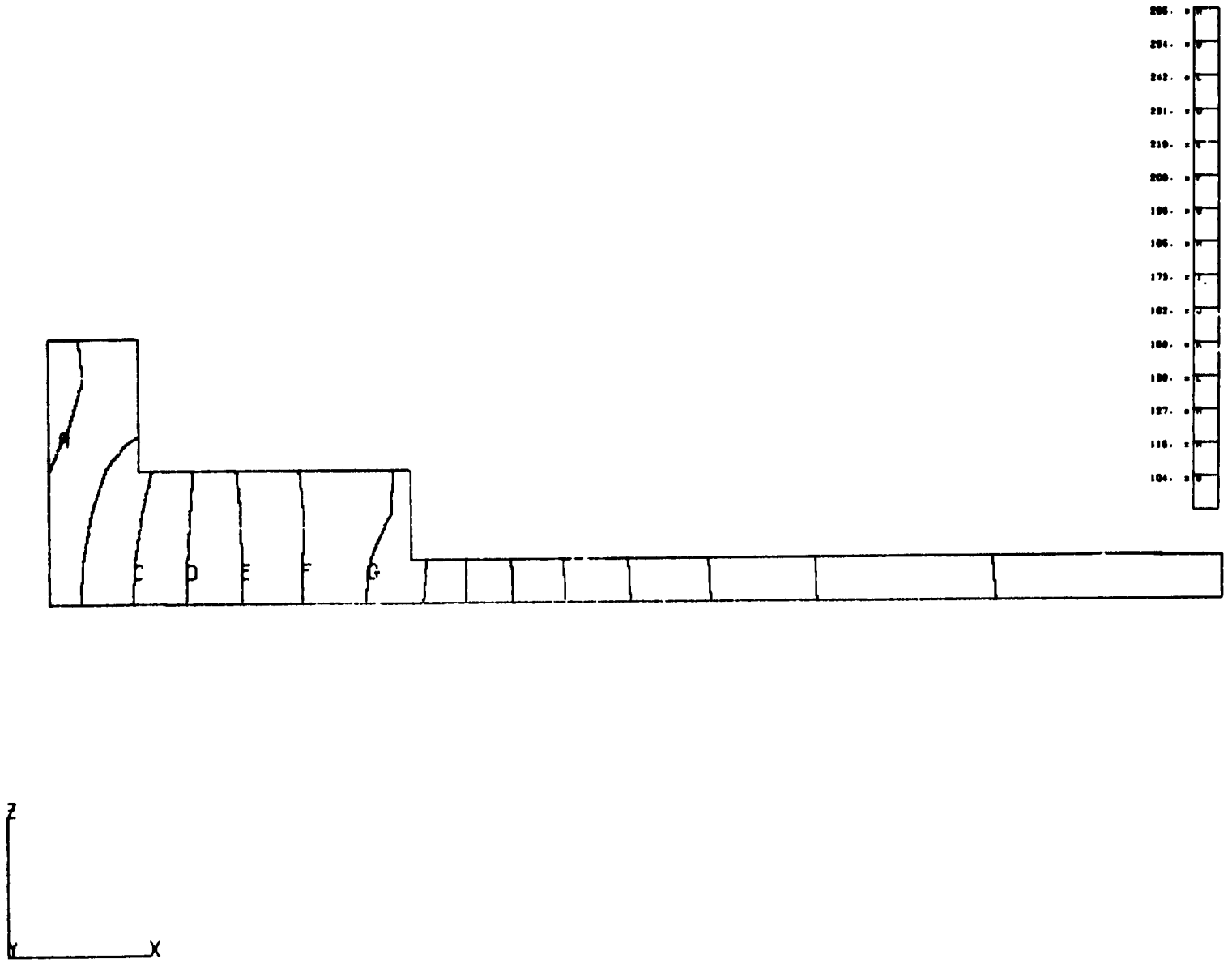


Figure 4 - Resultant Temperature Distribution

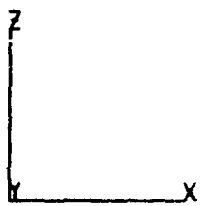
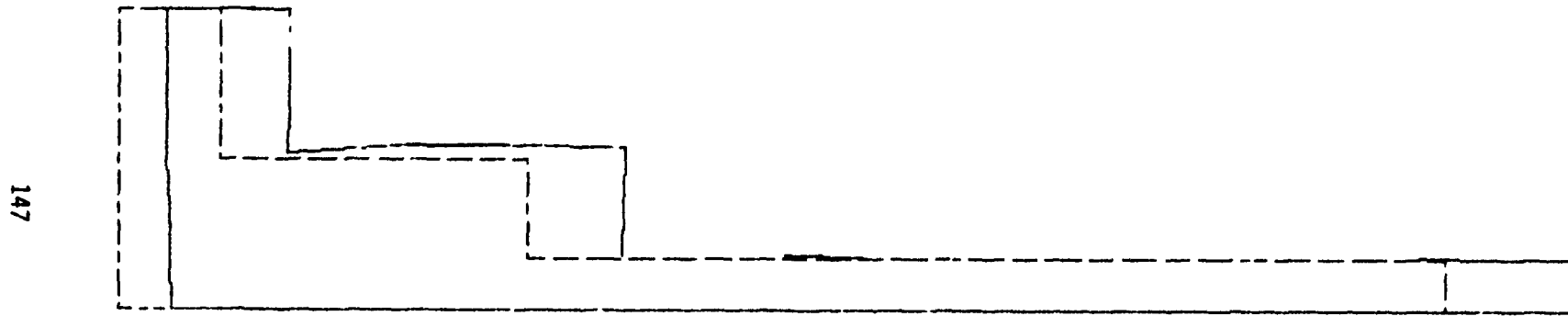


Figure 5 - Deformed Shape (Mesh 1)

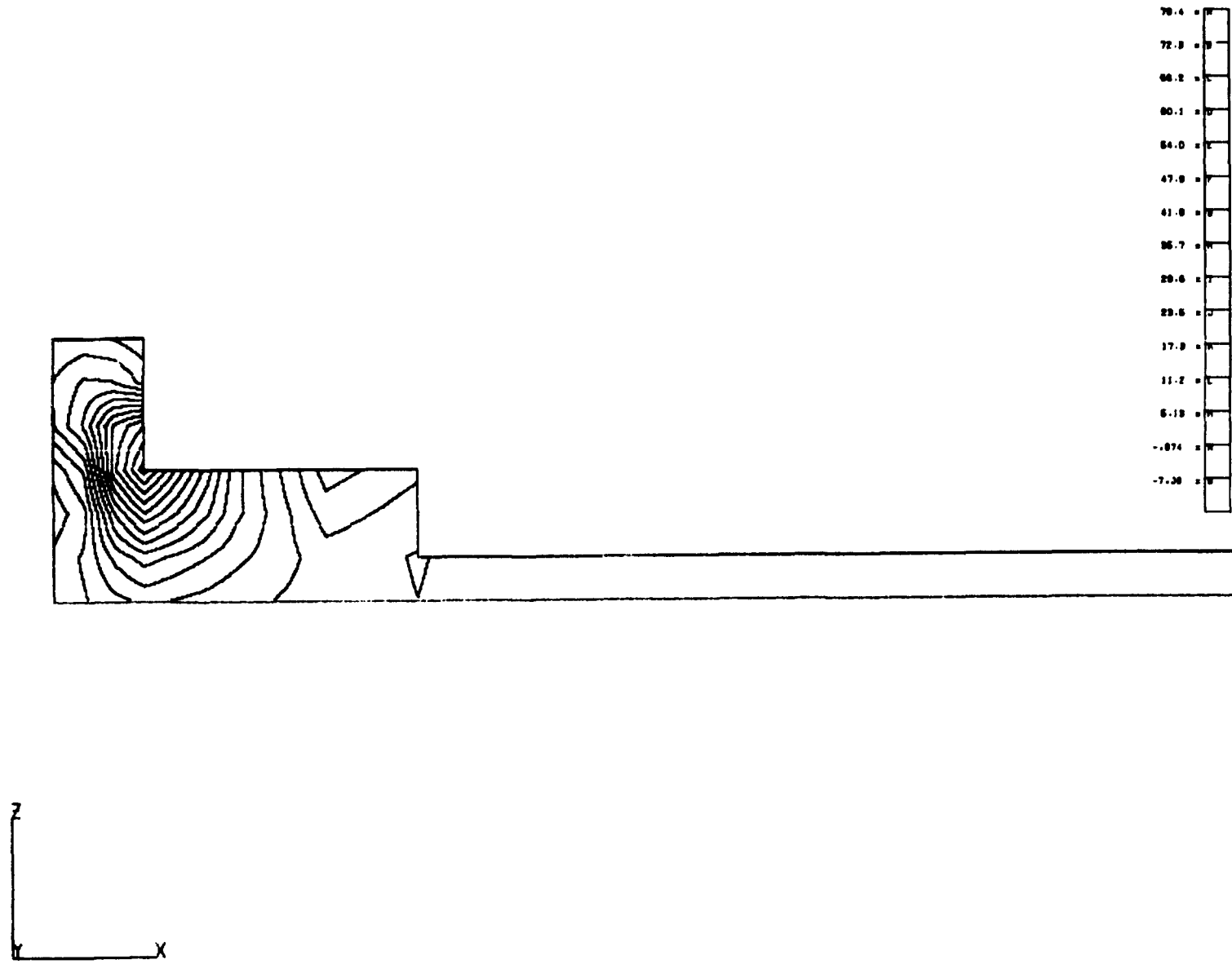


Figure 6 - Z-X Shear Stress (Mesh 1)

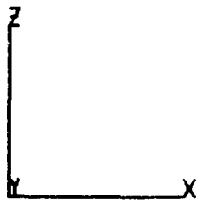
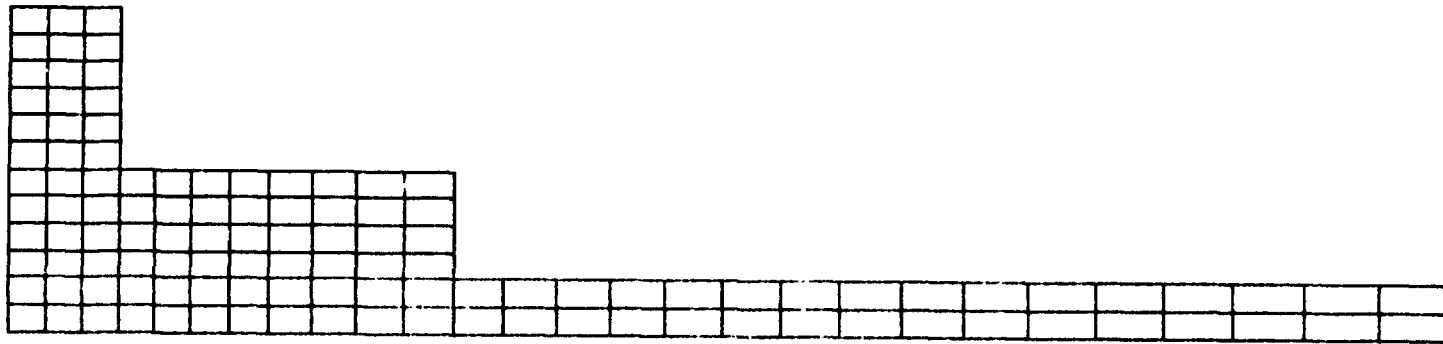


Figure 7 - Structural Model (Mesh 2)

150

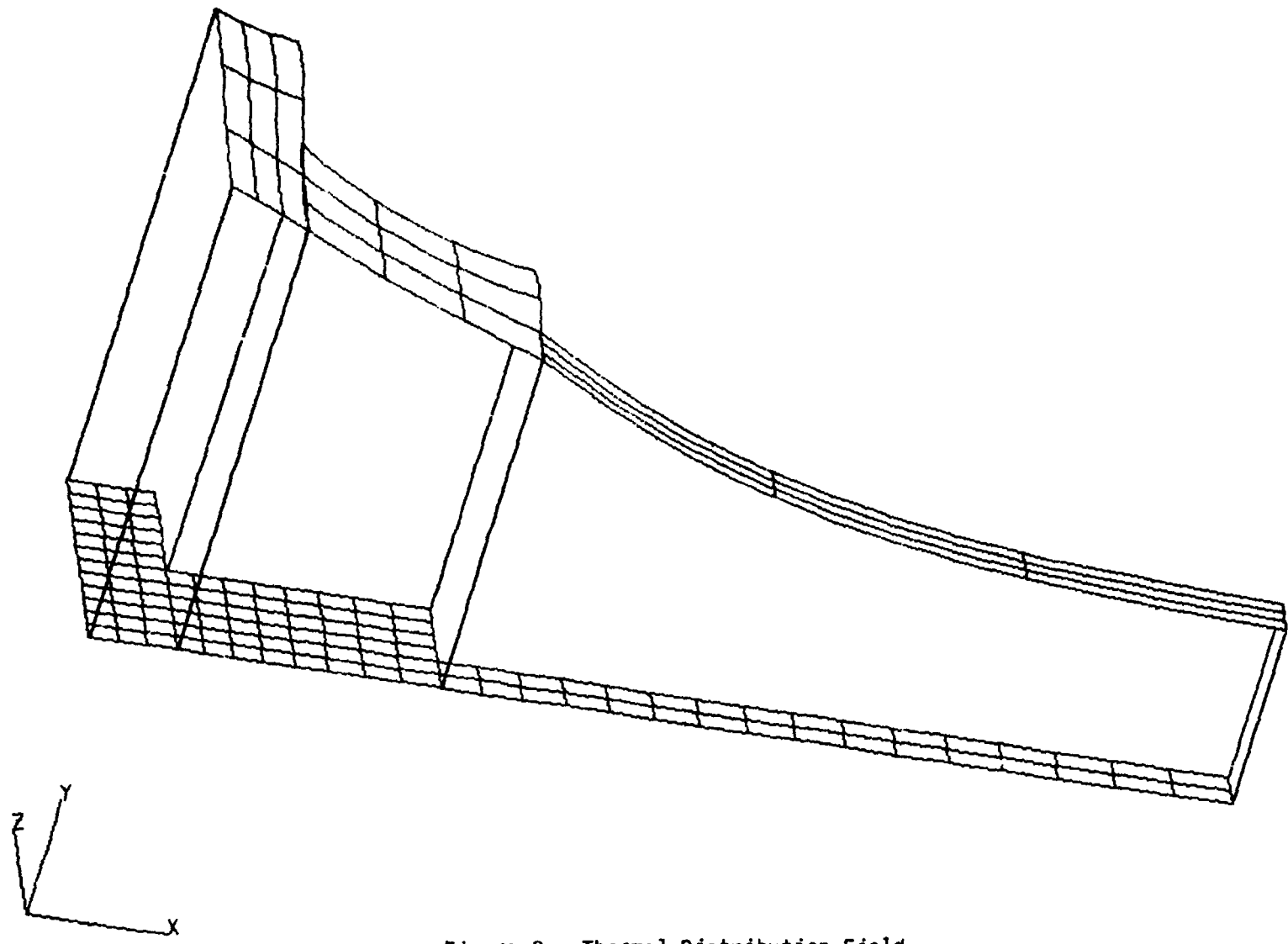


Figure 8 - Thermal Distribution Field

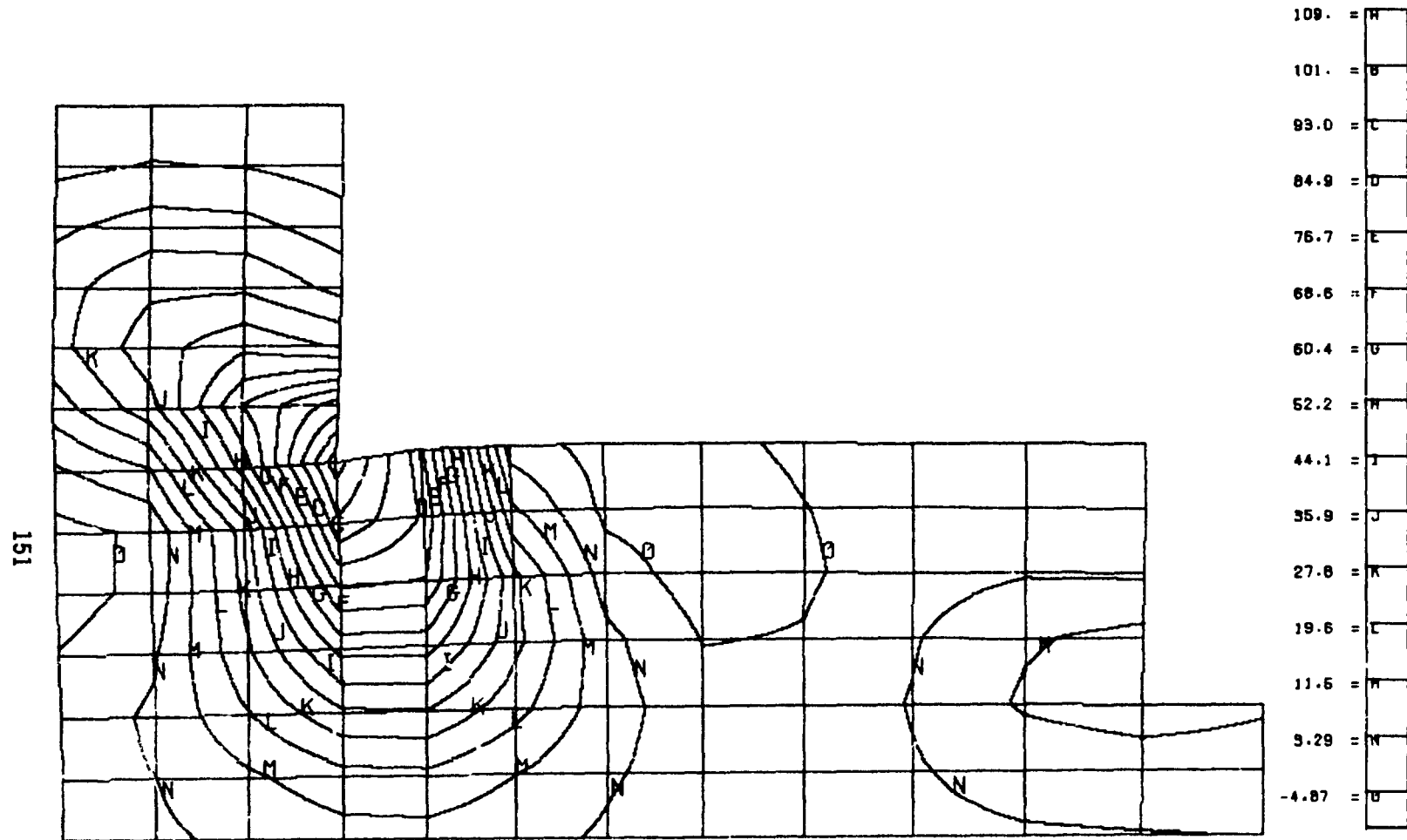


Figure 9 - Z-X Shear Stress On Deformed Shape (Mesh 2)

N85-25871

TWO INTERACTIVE GRAPHICS POSTPROCESSORS FOR NASTRAN

Robert R. Lipman

David W. Taylor Naval Ship Research and Development Center
Numerical Structural Mechanics Branch
Bethesda, Maryland 20884-5000

SUMMARY

Two new interactive computer graphics postprocessors, MAGGRAF and NASTEK, used for displaying NASTRAN-generated results are described. MAGGRAF is capable of displaying magnetic potentials or fields computed from results generated by a NASTRAN magnetostatic analysis. NASTEK is capable of displaying NASTRAN-generated PLT2 files on most Tektronix terminals. Examples of the plotting capabilities for each of the programs will be presented. Sample plots of the magnetic field around a ferromagnetic sphere and a rectangular plate are drawn with solid and dotted lines.

MAGGRAF

Introduction

MAGGRAF is an interactive computer graphics postprocessor used to display magnetic potentials, total fields, or field components computed from results generated by a NASTRAN magnetostatics analysis. This type of analysis computes magnetic potentials about ferromagnetic bodies due to source magnetic fields. MAGGRAF computes the magnetic fields or potentials from the prolate spheroidal harmonic expansion coefficients generated by NASTRAN. Magnetic fields or potentials can be displayed outside the prolate spheroidal surface at single points, along lines, or on planes in the form of X-Y graphs, two-dimensional (2D) contour plots, or three-dimensional (3D) surface plots.

Solving for the Magnetic Potential

The theory behind the governing equations for determining the magnetic potential around a ferromagnetic body is described in reference 1. Solving for the magnetic potential in MAGGRAF requires the solution of Laplace's equation in prolate spheroidal coordinates. The solution is given by

$$\phi(\xi, \eta, \theta) = \sum_{n=0}^{\infty} \sum_{m=0}^n \left[A_{mn} \cos(m\theta) + B_{mn} \sin(m\theta) \right] P_n^m(\eta) \left[\frac{Q_n^m(\xi)}{Q_n^m(\xi_0)} \right] \quad (1)$$

where

- ϕ = reduced magnetic scalar potential
- ξ, η, θ = prolate spheroidal coordinates
- ξ_0 = coordinate of the interior prolate spheroidal surface
- P_n^m, Q_n^m = Legendre functions of the first and second kind, respectively
- A_{mn}, B_{mn} = prolate spheroidal harmonic expansion coefficients

$$\left. \begin{matrix} A_{mn} \\ B_{mn} \end{matrix} \right\} = \frac{\epsilon_m}{4\pi} (2n+1) \frac{(n-m)!}{(n+m)!} \int_0^{2\pi} \frac{\cos(m\theta)}{\sin(m\theta)} d\theta \int_{-1}^{+1} \phi_0(\eta, \theta) P_n^m(\eta) d\eta$$

$$\epsilon_m = \begin{cases} 1, & m = 0 \\ 2, & m > 0 \end{cases}$$

$\phi_0(\eta, \theta)$ = distribution of potential ϕ on prolate spheroidal surface $\xi = \xi_0$

If the user has included in the finite element model a prolate spheroidal surface which encompasses all of the ferromagnetic material, then NASTRAN can compute the prolate spheroidal harmonic expansion coefficients and store them on a Fortran-readable file. MAGGRAF accesses these coefficients and solves equation (1) for any point outside the surface.

Input

Several quantities must be input to MAGGRAF before the program can compute the magnetic potential or field including the name of the file containing the prolate spheroidal harmonic expansion coefficients, a user-defined title, the type of graphic output to be generated, the component of the magnetic field strength or induction to be computed, and the output units. The type of graphic output selected determines the input, i.e., the coordinates of the points which define the X,Y,Z locations at which the magnetic field or potential is to be computed. For example, to define a set of points on a line, the Y and Z coordinates, the beginning and ending X coordinates, and the number of increments in X are input. To define a rectangular grid of points on a plane, the Y coordinate, the bounding X and Z coordinates of the plane, and the number of increments in X and Z are input. Linear combination factors are also input. These factors multiply the value of the source magnetic fields specified in subcases in the NASTRAN data deck to produce a total source magnetic field from various combinations of individual sources.

Output

All of the examples of output generated by MAGGRAF shown in figures 1-4 are of a component of the magnetic field strength or induction around a ferromagnetic sphere. An X-Y graph is shown in figure 1. A 2D contour plot is

shown in figure 2. A 3D perspective surface plot is shown in figure 3. A 3D orthogonal surface plot with hidden lines removed is shown in figure 4.

To generate a 2D contour plot, contour lines are drawn in rectangular regions formed by four adjacent points at which the magnetic field or potential was calculated. For each rectangle, a fifth point is interpolated in the center. The five points define four triangular subregions. Given the values of a contour line and of the magnetic field or potential at the five points, the coordinates of the points at which a contour line will cross the sides of the triangular subregions can be determined.

The elevation of a 3D surface corresponds to the values of the magnetic field or potential. To remove the hidden lines in the 3D surface plot, the surface is rotated such that points along a diagonal of the grid of points at which the magnetic field or potential was computed will appear along a vertical line on the plot (ref. 2). Then MAGGRAF can compute the points that are visible along any vertical line on the plot.

NASTEK

Introduction

NASTEK plots NASTRAN-generated PLT2 files on Tektronix 4010, 4050, 4100, and 4110 series terminals (ref. 3). Many options are available in NASTEK. Any frame in the PLT2 file can be plotted, or the entire file can be plotted automatically with a hardcopy made of each frame. Frames can be reduced or enlarged by setting a scale factor. Plots can be drawn with solid, dotted, dashed, or colored lines by using the PEN option on the PLOT card. Four styles of dotted or dashed lines are available. Eight different colored solid lines are available on the color Tektronix terminals.

Output

Figures 5-8 are examples of plots generated by NASTEK. Figure 5 is a plot of displacement contours. Figure 6 is an enlarged plot of the frequency deformation of a structure. Figure 7 is an enlarged plot of the undeformed shape of a structure. Figure 8 is an enlarged plot of the same structure as in figure 7, plotted with different types of dotted lines to differentiate parts of the structure. Colored lines could have been used instead of the dotted lines.

COMPUTER CODE

Both MAGGRAF and NASTEK are written in Fortran 77. MAGGRAF and NASTEK are approximately 4000 and 600 lines long, respectively. Currently, both programs are written with subroutines from the Tektronix TCS and Advanced Graphing II library of graphics subroutines. The future version of MAGGRAF will be rewritten with Metagek's TEMPLATE graphics software and will produce plots in color. The future version of NASTEK will be software independent.

REFERENCES

1. The NASTRAN User's Manual, NASA SP-222(06), September 1983.
2. Coleman, H. P.: A Fortran IV Plot Routine with Hidden Line Suppression for use with Small Computer Systems. Naval Research Laboratory Report NRL 4776, March 1982.
3. Lipman, R. R.: NASTEK - Interactive Display of NASTRAN-Generated Plots. David W. Taylor Naval Ship Research and Development Center Report DTNSRDC/CMLD-84/01, January 1984.

FERROMAGNETIC SPHERE
Z COMPONENT OF MAGNETIC FIELD INDUCTION VERSUS X COORDINATE POSITION

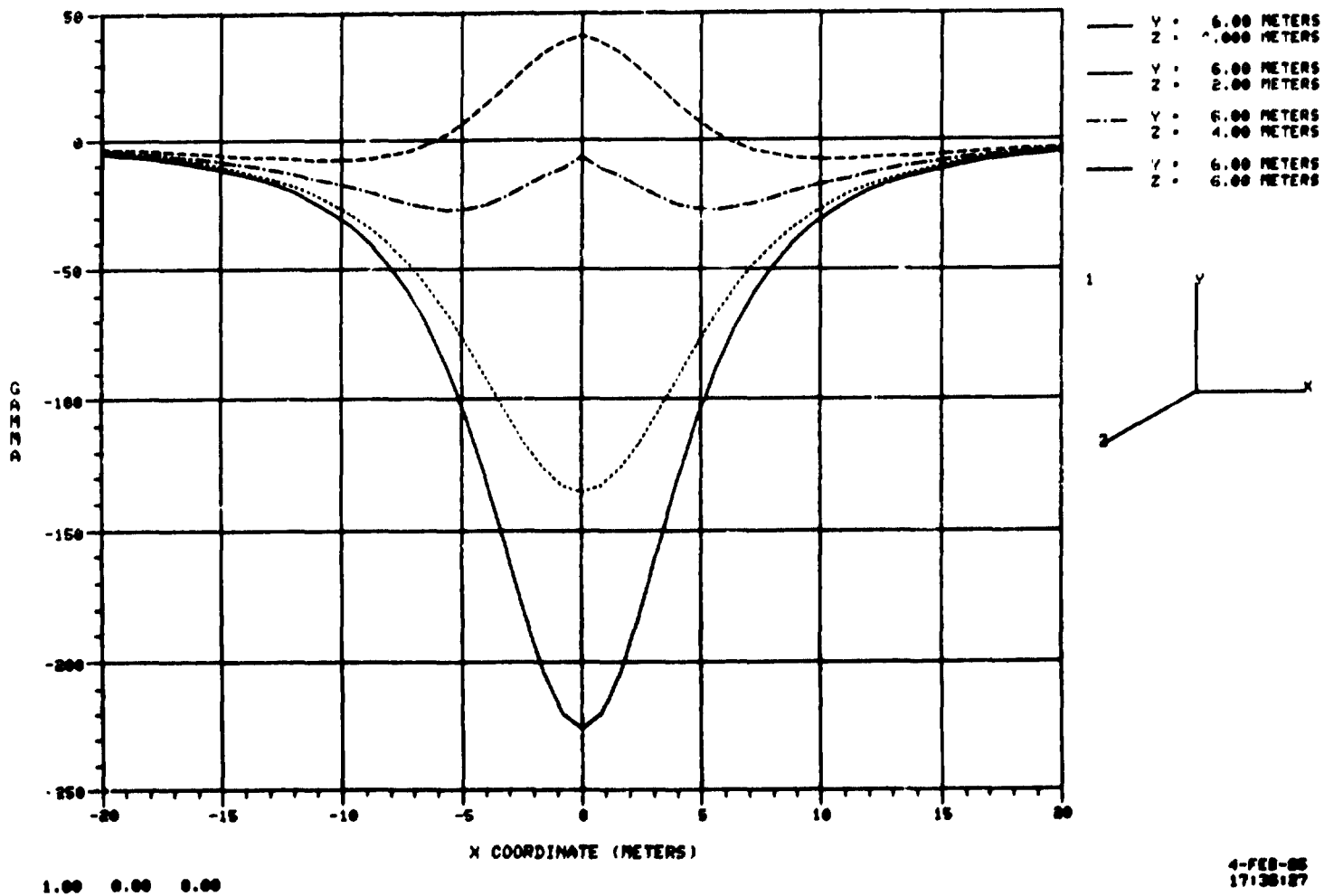
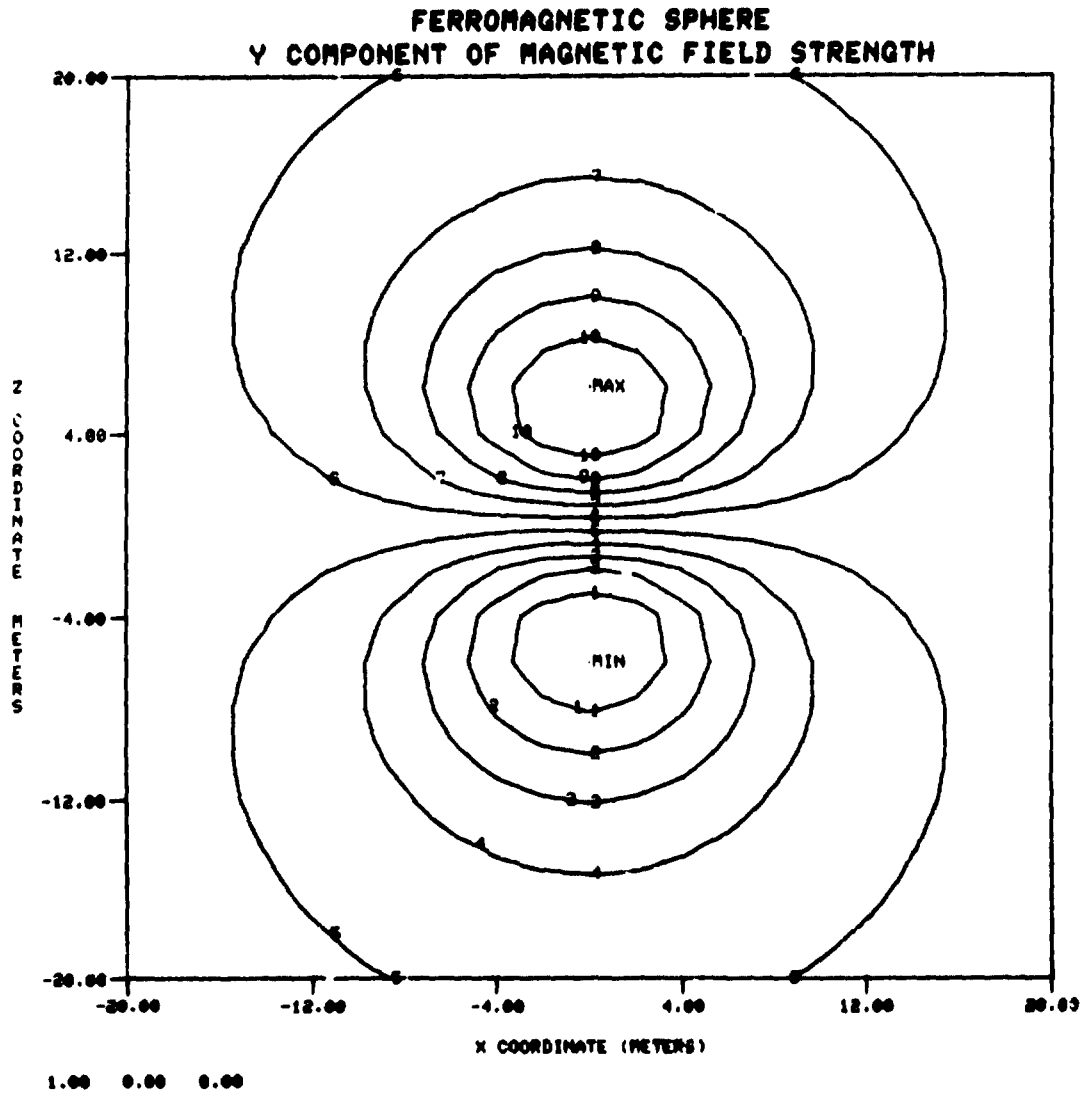
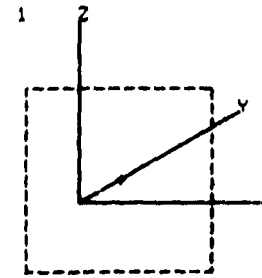


Figure 1 - X-Y graph



	AMPS/METER
MIN	-0.32458E-01
1	-0.26556E-01
2	-0.20655E-01
3	-0.14754E-01
4	-0.88521E-02
5	-0.29507E-02
6	0.29507E-02
7	0.88521E-02
8	0.14754E-01
9	0.20655E-01
10	0.26556E-01
MAX	0.32458E-01

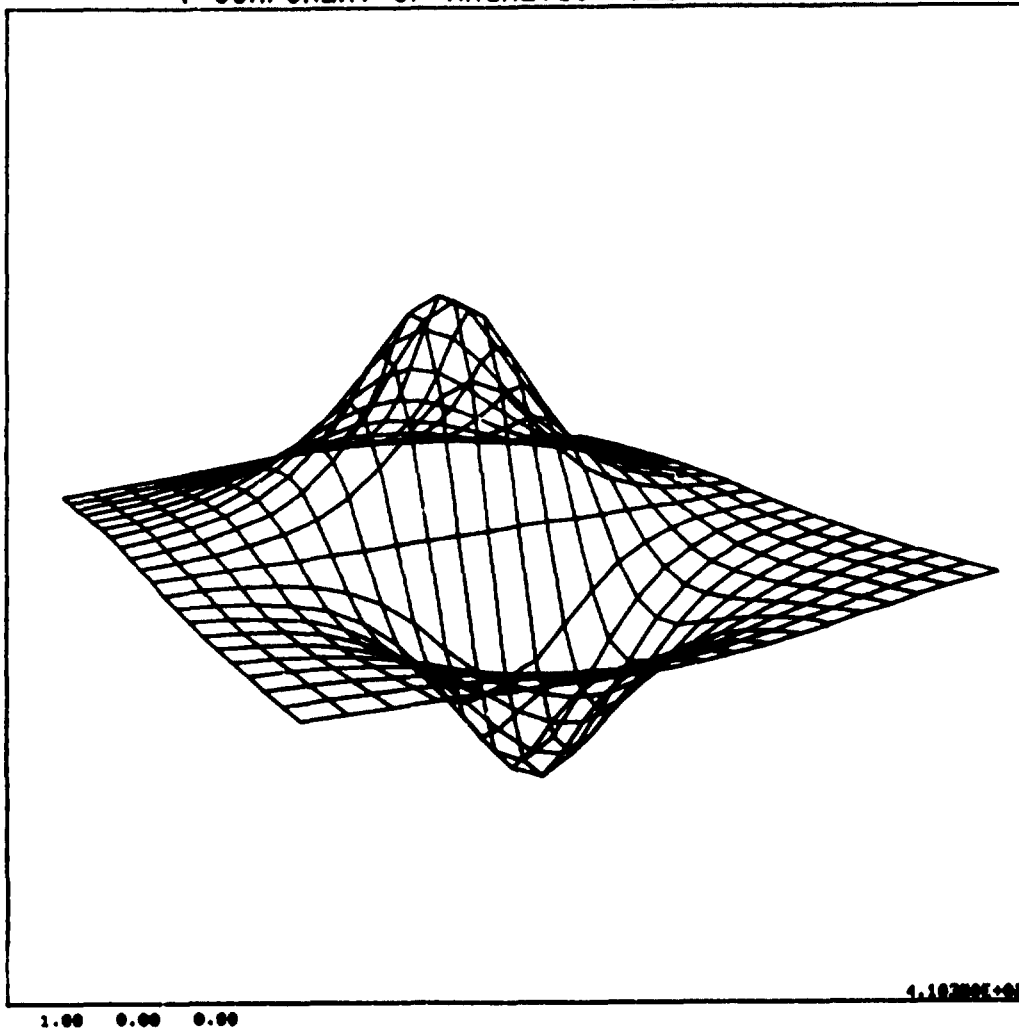
Y = 10.0 METERS



4-FEB-85
17:20:18

Figure 2 - 2D contour plot

**FERROMAGNETIC SPHERE
Y COMPONENT OF MAGNETIC FIELD STRENGTH**



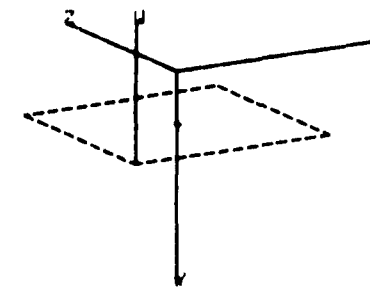
UMIN = -0.32456E-01 AMPS/METER
UMAX = 0.32458E-01 AMPS/METER

XMIN = -20.0 METERS
XMAX = 20.0 METERS

ZMIN = -20.0 METERS
ZMAX = 20.0 METERS

Y = 10.0 METERS

1

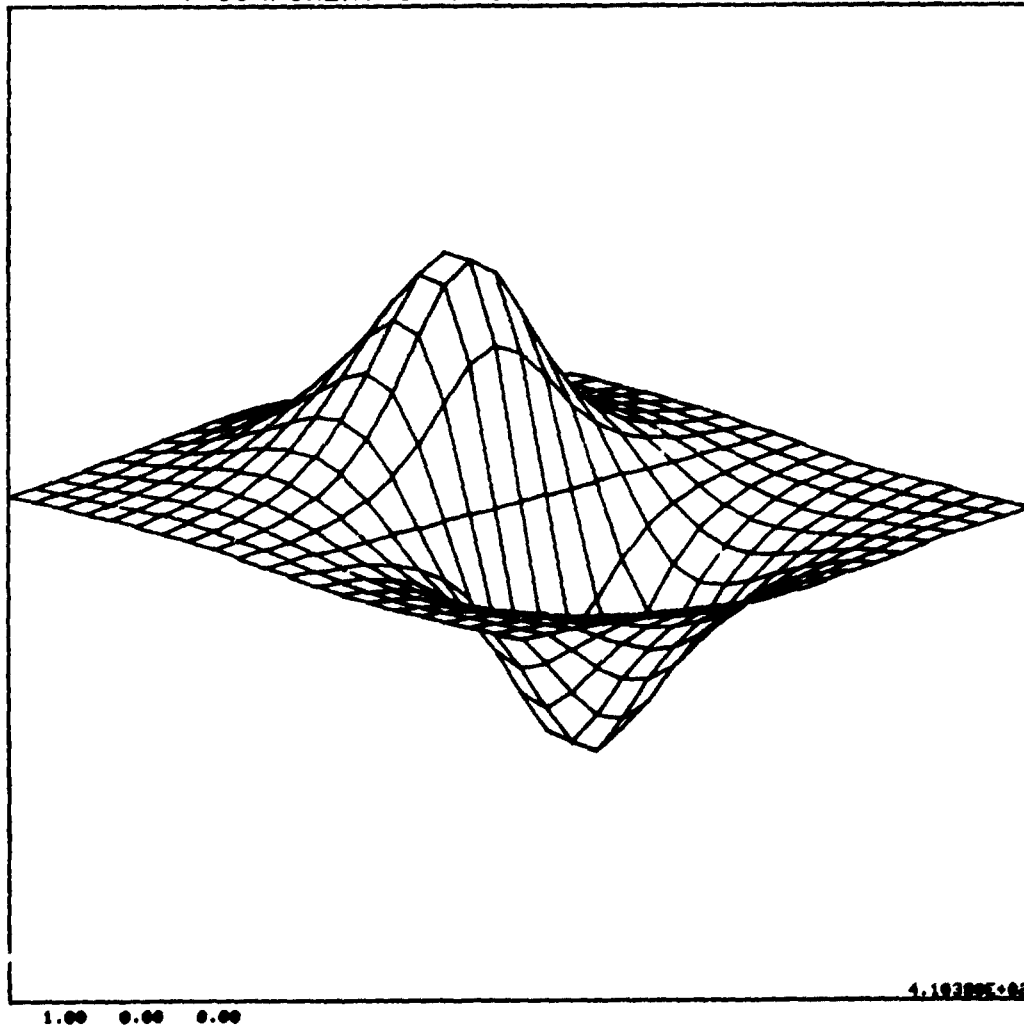


THETA X = 15.00
THETA Y = 30.00
THETA Z = 0.00

4-FEB-85
17140138

Figure 3 - 3D surface plot

**FERROMAGNETIC SPHERE
Y COMPONENT OF MAGNETIC FIELD STRENGTH**

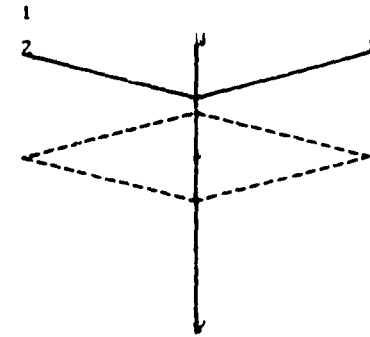


U_{MIN} = -0.32452E-01 AMPS/METER
U_{MAX} = 0.32452E-01 AMPS/METER

X_{MIN} = -20.0 METERS
X_{MAX} = 20.0 METERS

Z_{MIN} = -20.0 METERS
Z_{MAX} = 20.0 METERS

Y = 10.0 METERS



THETA_X = 15.00
THETA_Y = 45.00
THETA_Z = 0.00

ORIGINAL
OF POOR COPY

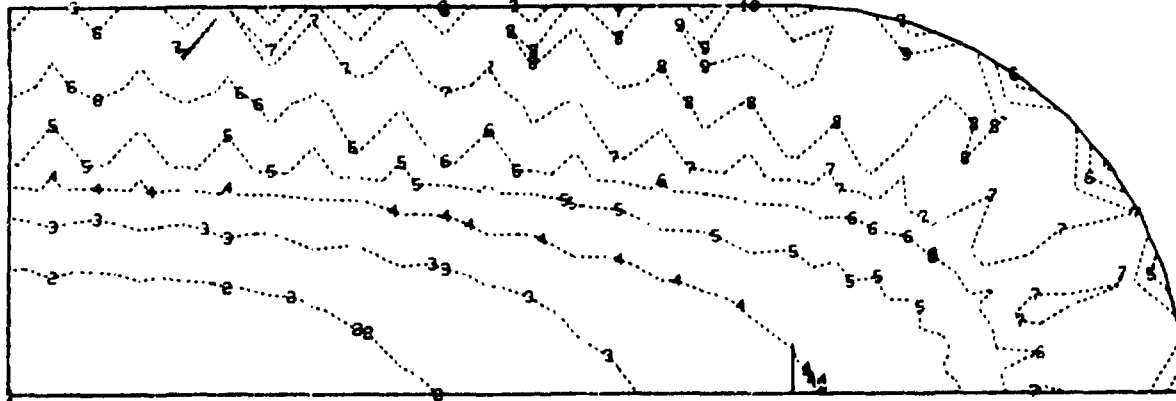
4-FEB-86
17:41:54

Figure 4 - 3D surface plot with hidden lines removed

PLOT FRAME NUMBER 2

3 11-27-84 MAX-DEF. = 0.00162548

3



L1=2. U1=1. U2=.55 T1=1.25 T2=.1 / LP=20.

TOP SURFACE, Z=1.36

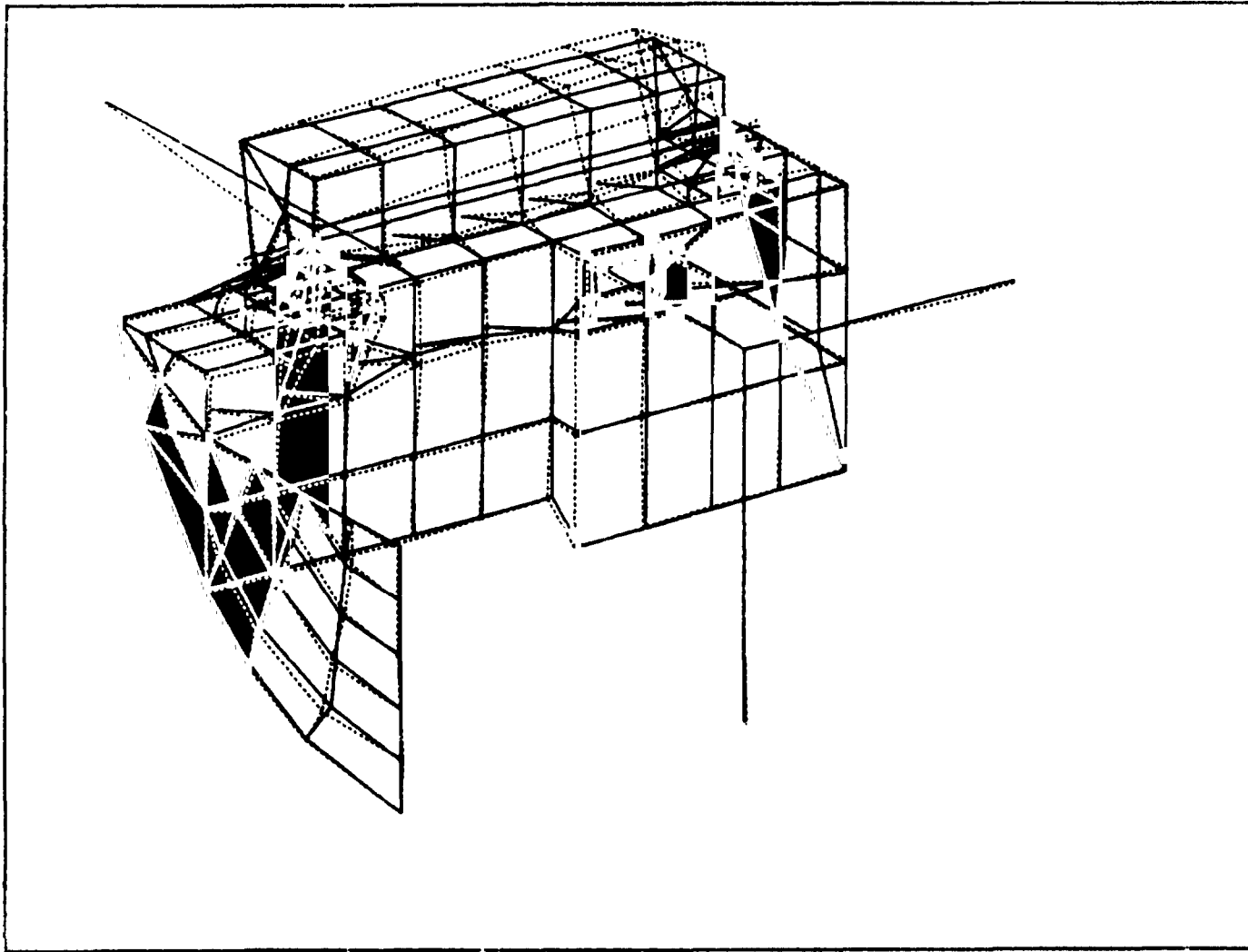
STATIC DEFOR. SUBCASE 1 LOAD 41

1.03

160

Figure 5 - Displacement contours

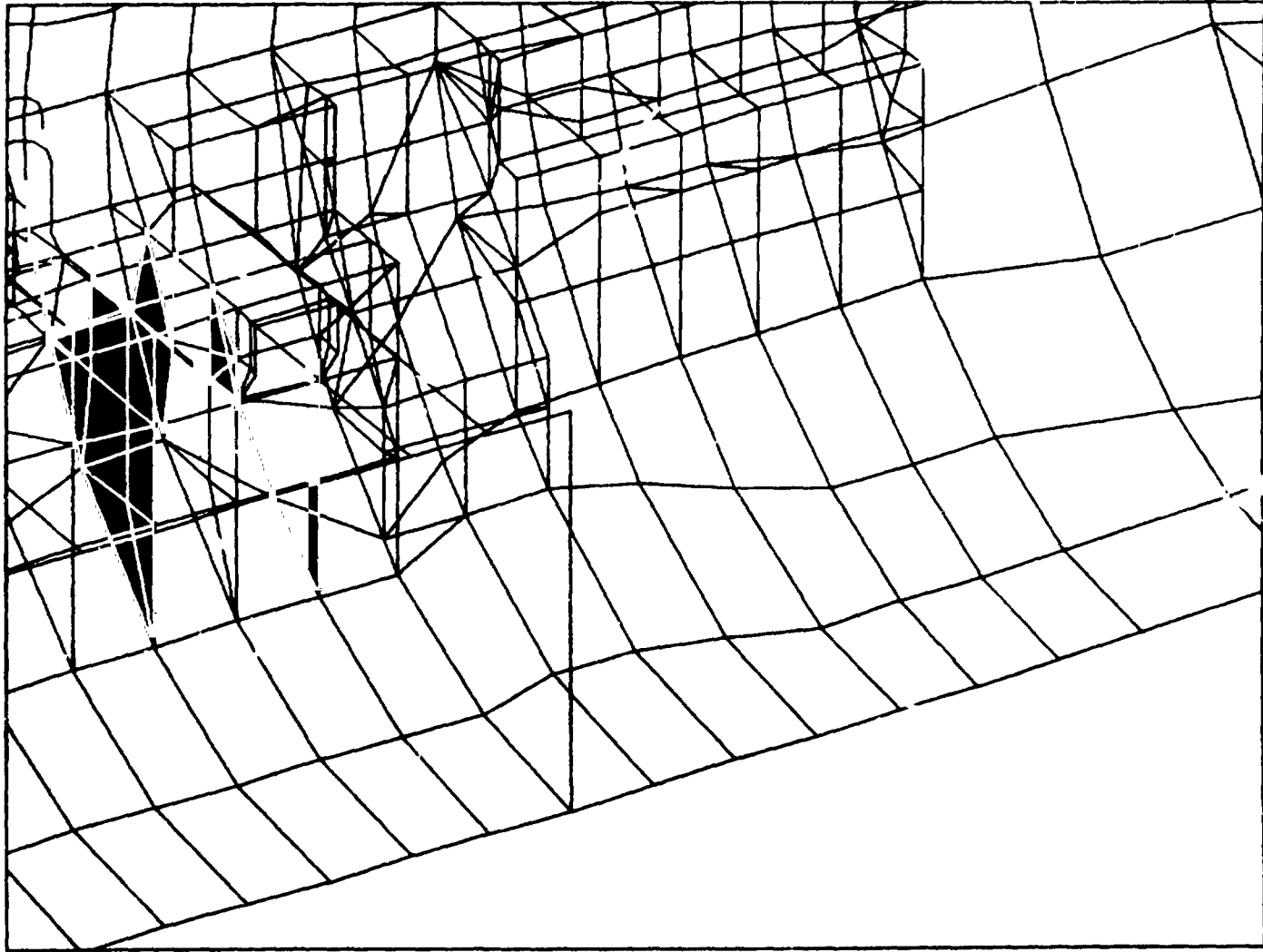
PLOT FRAME NUMBER 7



ORIGINAL PAGE IS
OF POOR QUALITY

Figure 6 - Plot of frequency deformation

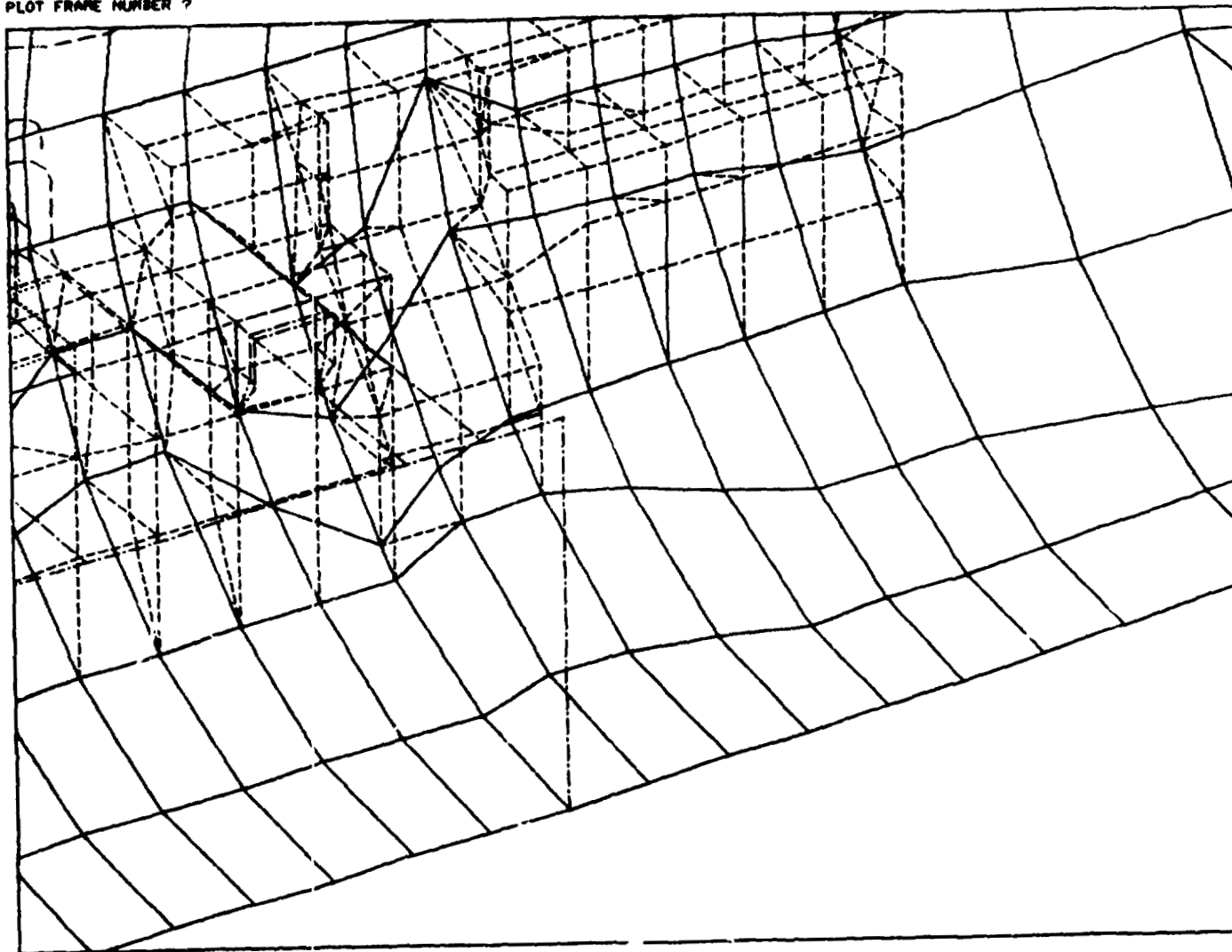
PLOT FRAME NUMBER 7



162

Figure 7 - Undeformed shape of a structure

PLOT FRAME NUMBER ?



ORIGINAL PLOT
OF POOR QUALITY

163

Figure 8 - Undeformed shape of structure plotted with dotted lines

N85-25872

AN UNUSUAL APPLICATION OF NASTRAN CONTOUR

PLOTTING CAPABILITY

S. Mittal, M. Gallo and T. Wang
BELL AEROSPACE TEXTRON

SUMMARY

A simple procedure to obtain contour plots of any physical quantity defined on a number of points of the surface of a structure is presented. Rigid Format 1 of HEAT approach in Cosmic NASTRAN is ALTERED to enable use of contour plotting capability for scalar quantities. ALTERED DMAP sequence and examples are included.

INTRODUCTION

In many engineering situations either a user has the need for visual verification of the input data for structural analysis, e.g., temperature distribution for thermal stress analysis in heat exchangers or might wish to obtain contour plots of a nonstructural engineering quantity like flux or angles of incidence, etc. Most often, a detailed structural analysis of the same piece of the hardware is also required, for which a NASTRAN finite element model is already available. In such situations, the contour plotting capability in NASTRAN can be very conveniently used to generate desired plots. In NASTRAN contour plots can only be obtained for surfaces that have 2-dimensional elements. However, for models with solid elements only, dummy layers of very thin plate elements have been used to successfully draw contour plots even in the interior of the structure.

Heat approach, solution 1 in COSMIC NASTRAN is preferred for this application because it permits defining a scalar quantity at a grid point and makes the data preparation easier. Procedure is inexpensive because almost all the solution steps in the Rigid Format are skipped and only the plotting capability is made use of.

The application of the presented technique requires, for large problems, some additional computer programming effort where grid point definition data is read from a NASTRAN deck, the physical quantity is computed on the coordinates of grid points and the results are written out on NASTRAN formatted SPC cards. Alternatively, for small problems, this data can be manually input on NASTRAN cards.

CONTOUR PLOTTING PROCEDURE

To obtain contour plots, a regular NASTRAN run with DMAP alters, presented in Appendix A as part of a sample executive deck, is required to be submitted. Normal input data processing for geometry definition in terms of GRID and element connection cards and plot set definitions is done as usual.

The physical quantity must be defined as enforced displacement SPC cards for each grid point. The entire solution sequence is skipped and an equivalence is made between the single point constraint set (U_g) and the structural set (U_g) (Reference 1). This step redefines the input as output so that the output vector can now be processed to generate plots. Once the user defines the SPC cards the rest of the procedure is automatic.

The case control deck consists of the selection of SPC set and printing out, if desired, of the physical quantity as temperature. The plotting itself is requested via regular NASTRAN cards. A sample case control deck is shown in Appendix B.

Bulk data must include GRID cards, element connection cards to define two dimensional surfaces and dummy property and material cards. In addition the SPC cards contain the information required to generate the contour plots. Appendix C shows a sample Bulk Data deck.

EXAMPLES

The first need at Bell Aerospace Textron for this uncommon application arose during thermal stress analysis of cooled laser mirrors. The temperature distribution on the mirror surface and the interior was used as one of the loading conditions for the stress analysis. The temperature had been computed using a finite difference heat transfer program. An intermediate FORTRAN program generated NASTRAN input data cards. As a verification of input data it was decided to obtain contour plots of the input temperature distribution. Typical temperature contour plot obtained is shown in Figure 1. This represents the temperature distribution on the mirror face. This process helped detect and correct errors in the input data for subsequent structural analysis.

A second example of the successful application of this technique relates to the angle of incidence plots for airborne radar applications. Structural analysis of a typical radome housing was required and a NASTRAN finite element model was already available. The current technique helped obtain contour plots of the angle of incidence on the radome surface. This provided useful information at relatively little cost. A short FORTRAN program was written to compute angles of incidence at a given point by reading the coordinates of grid points and computing normals to the neighboring elements. Typical contour plot is shown in Figure 2.

CONCLUDING REMARKS

1. A simple and inexpensive method of obtaining contour plots of any nonstructural quantity has been presented.
2. This method is most efficient when a structural finite element model of the surface on which contour plots are desired, is already available.
3. The physical quantity is defined on SPC cards. Usually, an intermediate computer program is helpful in generating input data for large problems.
4. DMAP ALTERS to be used in HEAT approach, Rigid Format 1 are provided.

5. Applications at Bell Aerospace Textron have been varied and have provided useful quick-look information.

REFERENCE

1. The NASTRAN User's Manual, NASA SP-222(06), Section 1.4.5, September 1983.

APPENDIX A

SAMPLE EXECUTIVE CONTROL DECK

```
NASTRAN BANDIT=-1
ID      SECOND EXAMPLE
APF     HEAT
SOL     1
TIME    3
ALTER 33,80
PARAM // *NOF*/P1=-1 $
EQUIV YS,HUGV/P1 $
SDR2 CASECC,CSTM,MPT,DIT,HEQEXIN,HSIL,GPTT,FDT,BGPDF,,,HUGV,HEST,,/
      ,,HOUGV1,,,HPUGV1/*STATICS* $
OFF HOUGV1,,,,,/S,N,CARDNO $
ENDALTER
CEND
```


APPENDIX B

SAMPLE CASE CONTROL DECK

```
TITLE      = NASTRAN USER'S COLLOQUIUM # 13
SUBTITLE   = CONTOUR PLOTS OF INCIDENT ANGLES
LABEL      = RADOME SURFACE
SFC        = 1
THERMAL(PRINT) = ALL
OUTPUT(PLOT)
PLOTTER NASTFLT, MODEL D, 0
PAPER SIZE 10.5 BY 8.0
VIEW 0.0,0.0,0.0
AXES Z,X,Y
SET 1      = QUAD2,TRIA2
FIND SCALE,SET 1,ORIGIN 1
PTITLE = FRONT VIEW
CONTOUR MAGNITUDE,LIST 0.0,10.0,20.0,30.0,40.0,50.0,52.5,55.0,
                    57.5,60.0,62.5,65.0,67.5,70.0,72.5,75.0,77.5,80.0,90.0
PLOT CONTOUR, SET 1, ORIGIN 1, OUTLINE
BEGIN BULK
```

APPENDIX C

SAMPLE BULK DATA DECK

GRID	420		9.816	8.633	2.439	
CRUAD2	420	101	420	520	521	421
CTRIA2	217	201	215	317	318	
FQUAD2	101	1001	.001			
PTRIA2	201	1001	.001			
MAT4	1001	1.0				
SPC	1	420	1	60.231		
ENDDATA						

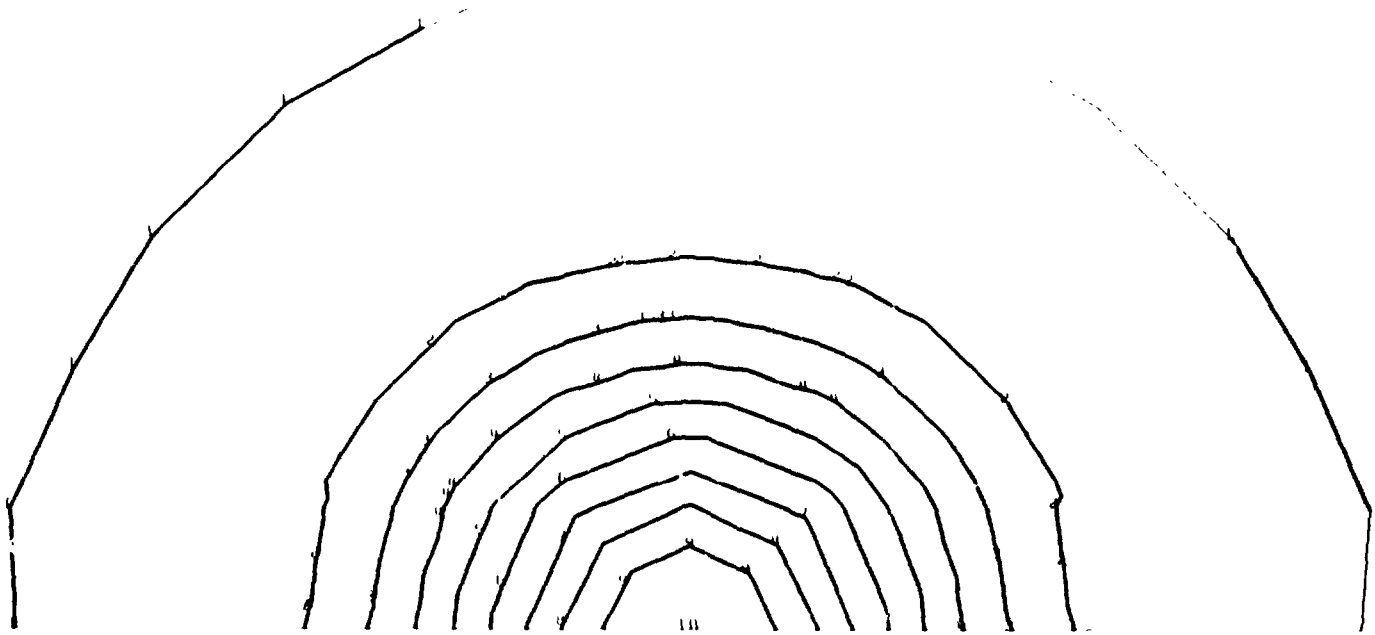


FIGURE 1. TEMPERATURE CONTOURS ON THE SURFACE OF LASER MIRROR

ORIGINAL PAGE IS
OF POOR QUALITY

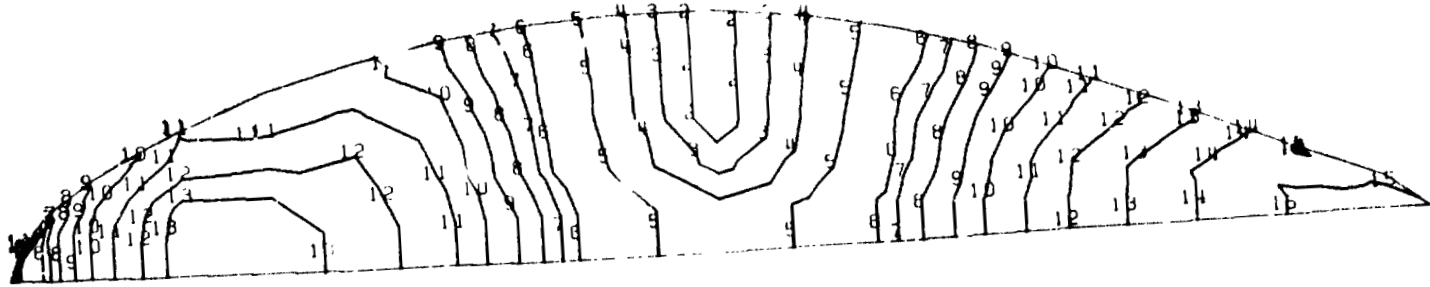


FIGURE 2. ANGLE OF INCIDENCE CONTOURS ON A RADOME SURFACE

ORIGINAL PAGE IS
OF POOR QUALITY

N85-25873

ISOPARAMETRIC 3-D FINITE ELEMENT MESH GENERATION USING INTERACTIVE COMPUTER GRAPHICS

Cuneyd Kayrak and Dr. Tulga Ozsoy
Department of Mechanical Engineering and Mechanics
Lehigh University

SUMMARY

An isoparametric 3-D finite element mesh generator was developed with direct interface to Lehigh developed interactive geometric modeler program called POLYGON. POLYGON defines the model geometry in terms of boundaries and mesh regions for the mesh generator. The mesh generator controls the mesh flow through the 2-dimensional "spans of regions" by using the topological data defines the connectivity between regions. The program is menu driven and the user has a control of element density and biasing through the spans and can also apply boundary conditions, loads interactively.

INTRODUCTION

The POLYGON (1) package developed at the CAD Laboratory of Lehigh University has been quite successful in providing the user with tools for 3-D wire frames to B-REP type solid model representations conversion process. POLYGON can accept 3-D wire frame data from other CAD systems either directly or through formatted files. POLYGON also provides some geometry generation and manipulation capabilities. Furthermore, different files can be written from POLYGON to be input for other solid modelers use B-REP type representations. The finite element modeling package was developed as a sub module within POLYGON, thus it has a direct access to the wire frame data as well as to the bounded surfaces, "regions" created by POLYGON. The main purpose of this integrated approach is to reach a high degree of automation during the mesh generation by reducing the model preparation time with less required user input. Mesh flow is automatically directed through the number of spans which can be defined using the topological data for regions. Currently only four and/or three-sided regions are allowed. In each region nodes are created using curvi-linear coordinate system and quadratic shape functions (2). Supported element types are linear or parabolic triangular and quadrilateral elements. Loads and restraints can also be applied interactively to the model. Finally, files can be written for input to COSMIC NASTRAN and SDRC's SUPERB finite element analysis programs. Full color visualization of the finite element model is possible at any stage with extensive view control capabilities such as dynamic rotation, scaling, translation, zooming, etc. Interactive menus linked in a tree-like structure allows users a natural way of communication with the system. The program currently has been implemented on DEC's VS11 raster terminals with 16 colors attached to a VAX 11/780, and is supported by Lehigh developed VS11-3D Graphics Package (3).

CURRENT CAPABILITIES OF THE FEM SYSTEM

Finite element model creation consists of six basic steps:

1. Geometry creation: POLYGON provides user with some geometry creation and manipulation capabilities. Points, lines, arcs, conics and cubic splines are currently supported wire frame entity types. Thus, 3-D wire frame geometry can be either created from scratch within POLYGON or on another CAD system and then can be transferred to the POLYGON program. Figure 1 is an example of part-geometry using 3-D wire frame representation.
2. Region creation: Bounded surfaces of planar, ruled and surface of revolution type can be defined automatically and/or manually at this step. The same geometry given in Figure 1 is shown in Figure 2 with all regions defined. These bounded surfaced (polygons), "regions" must be either four or three-sided because of the mesh generation scheme used. Once regions are defined they can be ordered either clockwise or counter-clockwise automatically. The edges of the regions are converted into parabolic type and the region data is formatted in a way so it can be used directly by the FEM module.
3. Span generation: Span defines the flow of mesh generation through the regions connected by opposite edges. Using the edge and region data the program can create spans automatically. Spans can be highlighted for user checking (Figure 3 and Figure 4). Spans can also be created and/or extended manually to include more regions (Figure 5). Number of elements across the span and biasing can be entered by selecting individual spans or system provided default values can be used.

Search for the spans is basically defining the opposite edge of the current region and the other region shares the same edge. Region data contains the edge loop and the edge data contains the region numbers attached to it. A span ends when there is no more region attached to the current edge (free edge) or if the first edge of the span is reached. Each region will be crossed by two spans. After the first span has been defined, search continues to define all other spans crossing all the regions inside the first span. Automatic search ends when all the regions in the model are crossed by two different spans.

4. Mesh generation: Once the spans are defined, mesh is generated throughout the structure at once (Figure 6). First nodes are generated using the number of divisions and biasing information given across the spans. Node generation is performed in parametric space using curvi-linear coordinate system and quadratic shape functions with mid-side nodes placed half-way between corner-nodes, then they are mapped into the current coordinate system. After all the nodes have been defined the elements are generated. Since the nodes are generated in an ordered manner the generation of elements is a trivial process. Nodes and elements are labeled automatically during their generation (Figure 7 and Figure 8). Currently only linear or parabolic triangular and quadrilateral isoparametric element types are supported.

5. Finite element model preparation: For each region different material type numbers can be assigned to the elements. Material property values can be input by the user and stored in material tables which then can be accessed by material type numbers. Default restraint and load definitions can be edited and they can be applied to the selected nodes or along the edges of the region. Different color codings and arrow heads are used for different load types and restraints to enhance the user's visualization.
6. Creating input data for finite element analysis: Once the finite element model information is generated, input files can be written for either COSMIC NASTRAN or SDRC's SUPERB finite element analysis packages.

CONCLUDING REMARKS

The current approach uses the extended concept of regions with span definition. Region refers to a bounded area inside a span and its position is topologically defined. Spans can be referenced as other type of finite element entities but at higher level than regions. Thus a data set assigned to a span can be applied to all the other lower level related entities, i.e. regions, elements, nodes, etc., such as grouping for application of boundary conditions, or blanking for better visualization. By using span definition remarkable savings can be reached easily by reducing the number of user interactions required at model preparation stage. Traditionally all the regions are defined one by one, then the mesh is generated in each of them individually. In Figure 2 the part contains 47 regions but there are only 15 spans. Since the information related to the number of divisions and biasing across the span is entered at span level but not at region level considerable time savings can be reached at this stage of the model preparation process.

REFERENCES

1. Ozsoy, T. and Ochs, J.B., "An Interactive Modeling Program for the generation of Planar Polygons for Boundary Type solids Representations of Wire Frame Models", Proceedings from the Symposium of Computer-Aided Geometry Modeling, NASA Langley, Hampton, VA, April 21, 1983.
2. Zienkiewicz, O.C. and Phillips, D.V., "An Automatic Mesh Generation Scheme for Plane and Curved Surfaces by Isoparametric Co-ordinates," International Journal for Numerical Methods in Engineering, Vol. 3, No. 4, 1971, pp. 519-528.
3. Ozsoy, T. and Ochs, J.B., "Lehigh University's VS11-3D Graphics Package", Proceedings from 1983 DECUS Meeting, St. Louis, MO, May 23, 1983.

ORIGINAL PAGE
COLOR PHOTOGRAPH

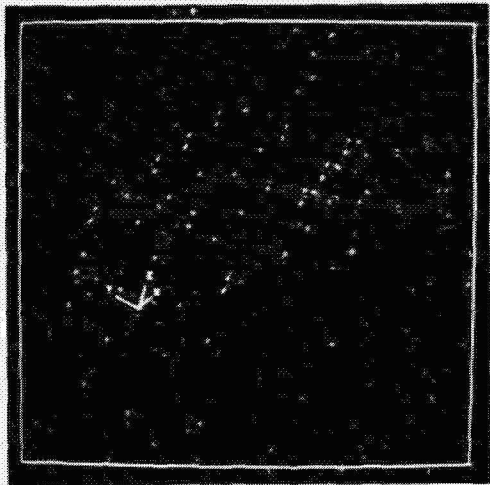


Figure 1. 3-D Wire frame representation of a robot arm with region boundaries

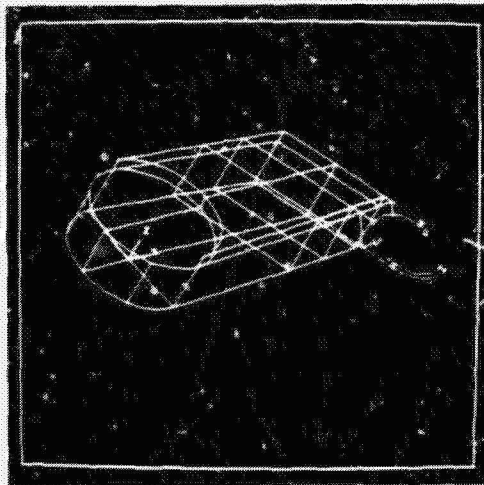


Figure 2. Regions are automatically defined and ordered in clockwise direction.

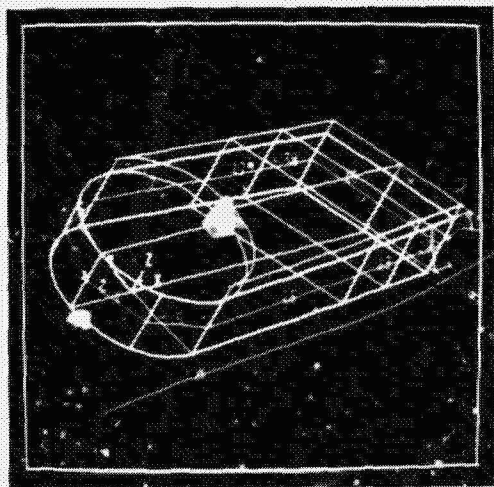


Figure 3. A span is displayed in different color with span direction arrow and region labels on.

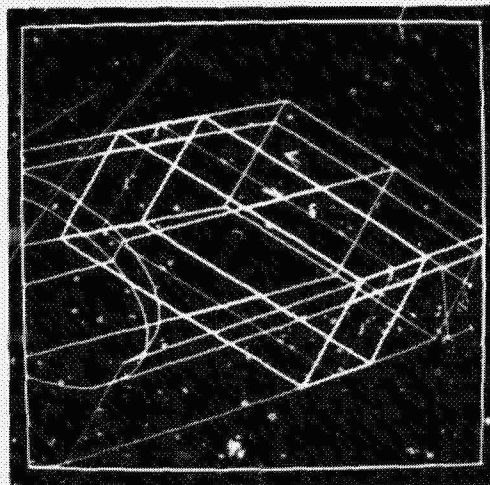


Figure 4. A crossing span is displayed after zoomed in.

ORIGINAL PAGE
COLOR PHOTOGRAPH

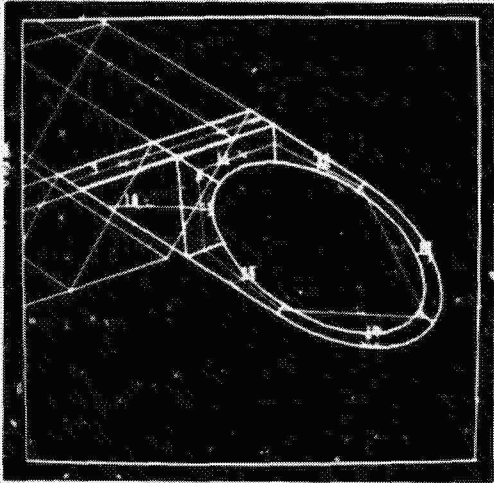


Figure 5. A span is extended manually to include more regions.

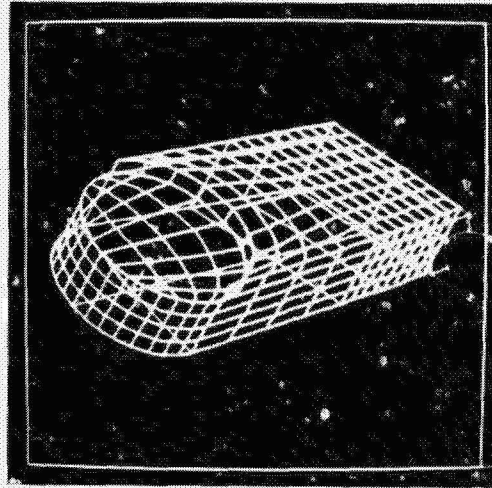


Figure 6. Mesh is displayed in selected regions.

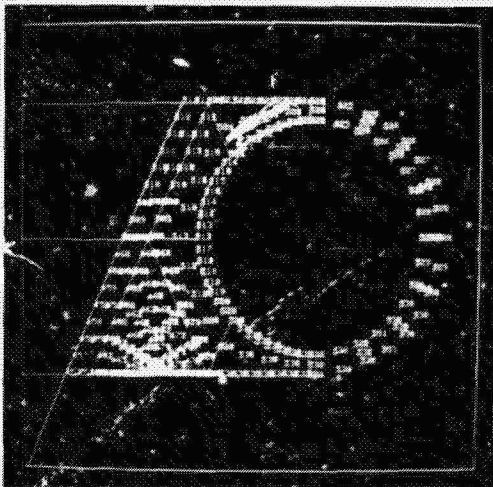


Figure 7. All the nodes in a span are displayed with their labels on.

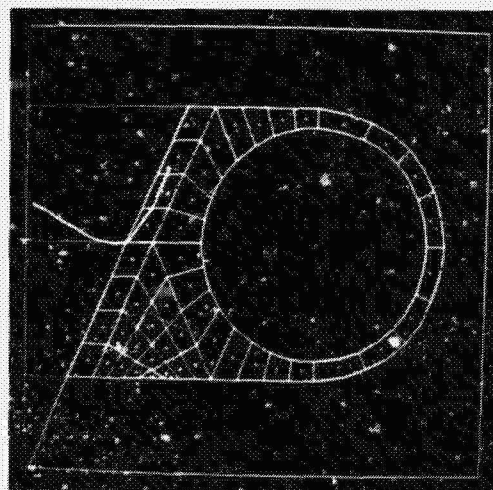


Figure 8. All the elements in a span are displayed with their labels on.

85-25874

A NEW NASTRAN CAPABILITY FOR DATA REDUCTION

Michael Gallo and S. Mittal
Bell Aerospace Textron

SUMMARY

A new module, MODB, for the data reduction of NASTRAN results is described. NASTRAN analysis results can be filtered and sorted for minimum/maximum values and the printed output resulting from large NASTRAN runs can be limited based on a number of available user options. The sorting is done on stresses, forces and vector quantities like displacements, velocity, and acceleration. The module can be accessed via DMAP alters to existing rigid formats, and has been used on a large number of statics and dynamics problems at Bell Aerospace resulting in considerable savings in cost, time, and the amount of printing.

INTRODUCTION

The high computational speed and large storage capacity of modern computers have enabled the analysis of large and complex structures. As a consequence, the structural engineer devotes much of his time to visually scanning, processing, and interpreting a large amount of finite element analysis results. This process is both time-consuming and error-prone. The way to alleviate the problem is to automate, whenever possible, the scanning and interpretation of the results, and to give the analyst the option to reduce the amount of computer output according to his engineering requirements.

The need for these capabilities has been felt for some time and a number of proprietary post-processors have been developed by various NASTRAN users. However, none have been integrated into COSMIC/NASTRAN for general use. Bell Aerospace has, therefore, developed an engineering-oriented module for data reduction which has been integrated into and offered to COSMIC/NASTRAN. MODB is currently in COSMIC/NASTRAN release April, 1984, at Bell Aerospace Textron. No new Case Control or Bulk Data cards are required for input definition, only existing PARAM and DTI cards are used.

This paper describes the data reduction module and its capabilities and demonstrates its application on an actual analysis.

DESCRIPTION OF MODB

MODB can process any real or complex OFF data block in SORT1 format. This includes element stresses, element forces, loads, displacements, forces of SPC, eigenvectors, velocities, and accelerations. MODB currently contains coding for the 75 elements that existed in NASTRAN release April, 1982. The code is easily modifiable to include new OFF data blocks and elements as the need arises.

User requests are processed to update program controls used to suppress elements and to identify vector or element type components to be used for filtering and/or sorting. For complex vectors, stresses, or forces, the user can specify a real component number. The vector component specified for either real or complex vectors must be in the range of 1 to 6. For both real and complex stresses and forces, the user input component number is checked to determine if it is in the range of valid component numbers for that particular element. The input data block undergoes a number of checks to insure it is valid for the current version of MODB.

The stress, force, or vector quantities in the OFP data block are filtered and stored in compact form in memory for subsequent use. The packed data is sorted and efficient data reduction is performed in accordance with the user's requirements. The filtered/sorted data block is output in standard OFP format with appropriate labels and printed by the existing OFP module.

MODB may be run either in conjunction with NASTRAN as a single job or as a separate run following a regular NASTRAN analysis for which the necessary OFP data blocks to be filtered/sorted have been saved via CHECKPT or by using NASTRAN's OUTPUTT1 or OUTPUTT2 modules.

MODB CAPABILITIES

The following is a brief description of the different capabilities presently available in MODB:

A) Output Selection

NASTRAN Case Control Set cards are used to define lists of node point numbers, element numbers or frequencies for use in output requests in the normal manner. The MODB user can then limit the data reduction process to selective element types and components through Direct Table Input (DTI) if he so desires.

B) Component Selection

The user has the option to filter/sort element stresses and forces on any selected stress or force component. Vectors can also be filtered and/or sorted on a user specified component. In all cases, a default component will automatically be selected by the program depending on the value of other filter/sort parameters input by the user.

C) Sorting: Output in a Preferred Sequence

Sorting on maximum magnitude, minimum magnitude, maximum algebraic value, or minimum algebraic value is possible, as well as no sorting in cases where only filtering is desired. Multiple sorts in the same run may be requested.

D) Filtering: Envelopes of Stresses, Forces, and Vector Quantities

The user may define a value which defines a lower bound beyond which the search for sorting is to begin. Stresses and forces are filtered on a

specified stress or force component. Vectors are initially filtered using all six components and then on the user selected component. All line items falling below the filter value are not printed.

E) Reduced Output

The user can control the number of lines of printed output. A maximum of N lines will be output after filtering and/or sorting has been performed.

MODB INPUT

The main input to MODB comes from NASTRAN OFP type data blocks generated by the regular analysis. The Case Control deck SET cards define the actual element identification numbers and node numbers to be output for each subcase in the usual manner. The Bulk Data deck contains the main information required for data reduction by MODB. This information is input through the use of existing PARAM and DTI cards unless defaults are used.

In order to use MODB, the following DMAP statements must be included in the Executive Control deck either as a replacement for or an addition to the existing OFP module in any rigid format that uses SORT1 type OFP data blocks.

```
MODB OFPD, INDTI/OFPDX/C,Y,NUMOUT = 0/C,Y,BIGER = 0./C,Y,SRTOPT=0/C,N,STRELYP=0 $  
OFP OFPDX,,,, // S,N,CAFDNO $
```

The data block and parameter names used in the above DMAP statements must be changed depending on the particular rigid format used and OFP data block to be processed by MODB. The Appendix contains a description of the input and output data blocks, and parameters used by MODB.

SAMPLE APPLICATION

A listing of the complete input and a sample of the output generated by MODB are given in figures 1 and 2.

CONCLUSION

Scanning of analysis results and data reduction may be performed with the aid of MODB in an automated fashion, thereby eliminating possible errors and waste of valuable man hours, both of which occur when performing data reduction in a manual and/or visual manner. As a result, the analyst is free to devote a larger portion of his time to engineering-oriented decision making based upon results obtained in an organized and comprehensive form.

The use of MODB provides the analyst with an efficient and convenient tool for the study of NASTRAN analysis results and their presentation for project documentation.

REFERENCES

1. Wall, S. E. (Ed): MSC/NASTRAN Programmers' Manual. MSR-50, September, 1976.
2. Raibstein, A. I.; and Pipano, A.: RINA - An Interactive System for the Rapid Interpretation of NASTRAN Results. Sixth NASTRAN Users' Colloquium, NASA CP-2018, October, 1976.

APPENDIX

ENTRY POINT: MODB

PURPOSE

To filter and/or sort SORT1 OFP formatted data blocks.

DMAP CALLING SEQUENCE

MODB OFPD,INDTI/OFPDX/C,Y,NUMOUT=+0/C,Y,BIGER=0.0/C,Y,SRTOPT=0 C,N,STRELTYP=0 \$

INPUT DATA BLOCKS

OFPD--- Any of the following OFP SORT1 data blocks.

- a. Element forces (Major ID = 4 or 1004)
- b. Element stresses (Major ID = 5 or 1005)
- c. Displacements (Major ID = 1,1001,15 or 1015)
- d. Loads (Major ID = 2 or 1002)
- e. Force of SPC (Major ID = 3 or 1003)
- f. Eigenvectors (Major ID = 7,1007,14 or 1014)
- g. Velocities (Major ID = 10,1010,16 or 1016)
- h. Accelerations (Major ID = 11,1011,17 or 1017)

INDTI--- User input DTI which can control the elements and components to be sorted. INDTI may be purged.

The DTI table consists of pairs of values B_i and C_i .

B_i - Element type identification number (Integer). If the B_i value is 0, then the corresponding C_i value is assumed to be a vector component.

C_i - Stress/Force component identification number on which sorting is to be performed (Integer).

If the C_i value is -1, the element type will be suppressed on the output file. An example of this feature could be as follows: If an element type is to be sorted on two different values and output twice, this can be accomplished by two calls to MODB with two unique DTI tables.

NOTES:

- a. Data block OFPD must be SORT1, real or complex.
- b. If OFPD is purged or not recognized by MODB, then a non-fatal error will be generated and MODB will return.
- c. If INDTI is purged, the default sorting code will be determined by the value that satisfies the condition defined by parameter SRTOPT.
- d. INDTI can be used to modify the SORT codes as follows:

APPENDIX, con't.

DTI	INDTI	0						
DTI	INDTI	1	(entry ₁)	(entry ₂)				+A
+A		etc.	etc.					+B
+B			etc.					
								+Z
+Z	etc.		ENDREC					

- e. Each entry is one of the following:
 - 1) For element types with existing data, two (2) words are used:
 - a) Element type code (vectors use a zero).
 - b) Stress item code.
- f. The data item "ENDREC" must appear following the last word of the last entry input.
- g. A limit of 100 stress items may be handled. New element types having more than 100 items of stress data per element entry cannot be handled. The TRPLT1 elements have 65 items per element entry.

OUTPUT DATA BLOCKS

OFPDX--- Filtered and sorted OFP data block.

Note: OFPDX may not be purged.

PARAMETERS

NUMOUT--- Integer-input-default=0, NUMOUT controls the number of output lines.

NUMOUT=0 implies that all items will be output after filtering and/or sorting has been done as controlled by parameters SRTOPT and BIGER.

NUMOUT=+N implies that only a maximum of N lines will be output after filtering and/or sorting has been done as controlled by parameters SRTOPT and BIGER.

BIGER--- Real-input-default=0.0, BIGER is the filter value below which items will not be output.

Since magnitudes are compared against BIGER, the default value of BIGER results in no filtering.

Stresses and Forces are filtered versus a specific stress or force component.

Vectors are filtered initially only if all six (real) degrees of freedom are less than BIGER and later, on only the component determined by default or DTI input.

APPENDIX, con't.

SRTOPT--- Integer input-default=0. Controls the sorting option to be performed.

<u>Value</u>	<u>Description</u>
-1	No sorting.
0	Sort on maximum magnitude.
1	Sort on minimum magnitude.
2	Sort on maximum algebraic value.
3	Sort on minimum algebraic value.

STRELTYP--- Integer input-default=0. Controls the element type to be processed for stresses and forces.

<u>Value</u>	<u>Description</u>
C	All element types will be processed.
.GT.0	Only element type STRELTYP will be processed.

NASTRAN EXECUTIVE CONTROL DECK ECHO

```

ID      DEM102,NASTRAN
APP     DISPLACEMENT
SOL     1,0
TIME    5
ALTER  104
MOBB   OES1,/OES1X/C,N,-1/C,N,0.0/C,N,0/C,N,0 $
OFF    OES1X,,,,, // $
MOBB   OES1,/OES2X/C,N,-1/C,N,1.0E2/C,N,0/C,N,0 $
OFF    OES2X,,,,, // $
ENDALTER
CEND

```

SPHERICAL SHELL WITH PRESSURE LOADING, NO MOMENTS ON BOUNDARY FEBRUARY 11, 1985 RELEASE APR. 1984 PAGE 2
 NASTRAN DEMONSTRATION PROBLEM NO. 1-2

MIKE GALLO

CASE CONTROL DECK ECHO

```

CARD
COUNT
1      TITLE = SPHERICAL SHELL WITH PRESSURE LOADING, NO MOMENTS ON BOUNDARY
2      SUBTITLE = NASTRAN DEMONSTRATION PROBLEM NO. 1-2
3      LABEL = MIKE GALLO
4      LOAD = 1
5      SPC = 2
6      OUTPUT
7      DISP = ALL
8      STRESS = ALL
9      BEGIN BULK

```

*** USER INFORMATION MESSAGE 297. BULK DATA NOT SORTED,XSORT WILL RE-ORDER DECK.

FIGURE 1 - EXECUTIVE & CASE CONTROL INPUT

DESIX SORTED ON MAXIMUM MAGNITUDE VALUE, COMPONENT 7, BIGER = 0.0, NUMOUT = -1

STRESSES IN GENERAL TRIANGULAR ELEMENTS (CIRIA2)
 (IN ELEMENT COORDINATE SYSTEM)

ELEMENT ID.	FIBRE DISTANCE	STRESSES IN ELEMENT COORD SYSTEM			ANGLE	PRINCIPAL STRESSES (ZERO SHEAR)		MAX SHEAR
		NORMAL-X	NORMAL-Y	SHEAR-XY		MAJOR	MINOR	
26	-1.500000E+00	3.141028E+02	-1.750751E+01	-1.670134E+01	-2.8753	3.149414E+02	-1.842635E+01	1.666839E+02
	1.500000E+00	6.417648E+00	2.761341E+00	2.570280E+01	42.9658	3.033722E+01	-2.117822E+01	2.576773E+01
24	-1.500000E+00	1.660572E+02	2.337326E+00	8.909364E+01	23.7115	2.051079E+02	-3.679332E+01	1.209906E+02
	1.500000E+00	9.283432E+01	-8.445576E+01	-4.453304E+01	-13.3369	1.033917E+02	-9.501318E+01	9.920247E+01
27	-1.500000E+00	1.279637E+02	4.444475E+01	-5.398787E+01	-26.4774	1.548545E+02	1.957396E+01	6.764027E+01
	1.500000E+00	-8.388870E+01	8.175385E+00	-1.615448E-01	-89.8995	8.175659E+00	-8.388870E+01	4.603232E+01
28	-1.500000E+00	1.420986E+02	1.210494E+01	-3.205495E+01	-13.4080	1.499306E+02	4.273010E+00	7.282878E+01
	1.500000E+00	3.415269E+01	-1.555220E+01	2.665134E+01	23.5002	4.574112E+01	-2.714064E+01	3.644009E+01
25	-1.500000E+00	1.253143E+02	-3.037149E+01	5.800562E+01	18.3460	1.445495E+02	-4.960672E+01	9.707811E+01
	1.500000E+00	-8.102733E+01	1.733096E+01	-8.331900E+01	-60.2757	4.490224E+01	-1.285906E+02	9.675041E+01
17	-1.500000E+00	1.213877E+02	-1.523353E+01	-1.404747E+01	-5.8102	1.228170E+02	-1.666290E+01	6.973997E+01
	1.500000E+00	-8.811514E+01	5.029917E+00	3.820423E+00	87.6552	5.186356E+00	-8.027156E+01	4.672896E+01
29	-1.500000E+00	6.585297E+01	5.392976E+01	-2.982939E+01	-39.3490	9.031054E+01	2.947208E+01	3.041928E+01
	1.500000E+00	-4.921719E+01	-1.217244E+01	1.360869E+01	71.8473	-7.710587E+00	-5.367903E+01	2.298422E+01
16	-1.500000E+00	6.537312E+01	-2.607967E+01	5.061255E+01	23.9517	8.785620E+01	-4.856274E+01	6.820947E+01
	1.500000E+00	-7.554433E+01	1.585683E+01	-8.271609E+01	-59.4603	6.465752E+01	-1.243450E+02	9.450127E+01
30	-1.500000E+00	8.359991E+01	1.434454E+01	-1.594507E+01	-12.3624	8.709468E+01	1.084978E+01	3.812245E+01
	1.500000E+00	2.538086E+01	-2.007843E+01	8.715087E+00	10.4390	2.699437E+01	-2.169194E+01	2.434315E+01
18	-1.500000E+00	6.914362E+01	1.741324E+01	-2.151494E+01	-19.8716	7.693983E+01	9.637009E+00	3.365141E+01
	1.500000E+00	-1.019585E+02	-5.160648E+00	6.021778E+00	86.4538	-4.787476E+00	-1.023316E+02	4.877200E+01
9	-1.500000E+00	4.464894E+01	-4.239378E+01	5.921770E+01	26.8432	7.461801E+01	-7.236285E+01	7.349043E+01
	1.500000E+00	-5.381195E+01	2.738875E+01	-7.078654E+01	-59.9185	6.839183E+01	-9.481503E+01	8.160344E+01
19	-1.500000E+00	6.176284E+01	1.501022E+01	-2.140913E+01	-21.2424	7.008516E+01	6.687912E+00	3.169862E+01
	1.500000E+00	-5.359483E+01	-2.408005E+01	2.391499E+01	60.8389	-1.073570E+01	-6.693916E+01	2.810173E+01
4	-1.500000E+00	4.138046E+01	-6.584657E+01	5.593094E+01	23.1059	6.524388E+01	-8.970999E+01	7.747694E+01
	1.500000E+00	-3.934612E+01	4.803261E+01	-5.221292E+01	-64.9605	7.242371E+01	-6.373721E+01	6.808046E+01
15	-1.500000E+00	3.577985E+01	-3.537155E+00	4.471141E+01	33.1330	6.496359E+01	-3.272092E+01	4.884225E+01
	1.500000E+00	6.429749E-01	-5.670753E+01	-7.477538E+01	-34.5094	5.205284E+01	-1.081174E+02	8.008511E+01
6	-1.500000E+00	3.484444E+01	-4.621033E+01	-5.478094E+01	-26.7525	6.246129E+01	-7.382518E+01	6.814323E+01
	1.500000E+00	-3.348335E+01	4.244910E+01	5.737177E+01	61.7475	7.327936E+01	-6.431355E+01	6.879643E+01

ORIGINAL PAGE IS
 OF POOR QUALITY

185

FIGURE 2 - SAMPLE OUTPUT

DES2X , SORTED ON MAXIMUM MAGNITUDE VALUE , COMPONENT 7 , BIGER = 100.000, NUMOUT = -1

STRESSES IN GENERAL TRIANGULAR ELEMENTS (CTRIA2)
 (IN ELEMENT COORDINATE SYSTEM)

ELEMENT ID.	FIBRE DISTANCE	STRESSES IN ELEMENT COORD SYSTEM			ANGLE	PRINCIPAL STRESSES (ZERO SHEAR)		MAX SHEAR
		NORMAL-X	NORMAL-Y	SHEAR-XY		MAJOR	MINOR	
26	-1.500000E+00	3.141028E+02	-1.758751E+01	-1.670134E+01	-2.8753	3.149414E+02	-1.842435E+01	1.666839E+02
	1.500000E+00	6.417648E+00	2.761341E+00	2.570200E+01	42.9658	3.035722E+01	-2.117022E+01	2.576773E+01
24	-1.500000E+00	1.660572E+02	2.337326E+00	8.909364E+01	23.7115	2.051079E+02	-3.679332E+01	1.209906E+02
	1.500000E+00	9.283432E+01	-8.445576E+01	-4.453304E+01	-13.3369	1.033917E+02	-9.501318E+01	9.920247E+01
27	-1.500000E+00	1.279637E+02	4.646475E+01	-5.398707E+01	-26.4774	1.548545E+02	1.957396E+01	6.764027E+01
	1.500000E+00	-8.388870E+01	8.175385E+00	-1.615448E-01	-89.8995	8.175659E+00	-8.388898E+01	4.603232E+01
28	-1.500000E+00	1.420986E+02	1.210494E+01	-3.285495E+01	-13.4080	1.499306E+02	4.273010E+00	7.202078E+01
	1.500000E+00	3.415269E+01	-1.555220E+01	2.665134E+01	23.5002	4.574112E+01	-2.714064E+01	3.644089E+01
25	-1.500000E+00	1.253143E+02	-3.037149E+01	5.800562E+01	18.3460	1.445495E+02	-4.960672E+01	9.707011E+01
	1.500000E+00	-8.102733E+01	1.733096E+01	-8.331900E+01	-60.2757	6.490224E+01	-1.285906E+02	9.675041E+01
17	-1.500000E+00	1.213877E+02	-1.523353E+01	-1.404747E+01	-5.8102	1.220170E+02	-1.666290E+01	6.973997E+01
	1.500000E+00	-8.811514E+01	5.029917E+00	3.820423E+00	87.6552	5.186356E+00	-8.827156E+01	4.672896E+01

MIKE GALLO

STRESSES IN GENERAL TRIANGULAR ELEMENTS (CTRJA2)
 (IN ELEMENT COORDINATE SYSTEM)

ELEMENT ID.	FIBRE DISTANCE	STRESSES IN ELEMENT COORD SYSTEM			PRINCIPAL STRESSES (ZERO SHEAR) ANGLE	PRINCIPAL STRESSES (ZERO SHEAR) MAJOR MINOR		MAX SHEAR
		NORMAL-X	NORMAL-Y	SHEAR-XY				
1	-1.500000E+00	-9.680287E+00	-6.203754E+01	4.088985E+01	28.6858	1.269313E+01	-8.441093E+01	4.855203E+01
	1.500000E+00	5.144141E+00	4.704821E+00	-6.393283E+01	-44.9195	6.889757E+01	-5.896860E+01	6.393309E+01
2	-1.500000E+00	-9.912994E+00	-3.837282E+01	-6.326425E+00	-38.6617	4.070197E+01	-8.898776E+01	6.484486E+01
	1.500000E+00	1.066493E+01	3.094138E+01	3.609038E+01	52.8454	5.829045E+01	-1.668416E+01	3.748730E+01
3	-1.500000E+00	-1.715546E+01	-3.093681E+01	5.419623E+01	41.3770	3.058640E+01	-7.867865E+01	5.463252E+01
	1.500000E+00	4.598263E+00	-4.491492E+00	-6.051071E+01	-42.8542	6.073022E+01	-6.063145E+01	6.048085E+01
4	-1.500000E+00	4.138046E+01	-6.584657E+01	5.593094E+01	23.1059	6.524388E+01	-8.970999E+01	7.747694E+01
	1.500000E+00	-3.934612E+01	4.803261E+01	-5.221292E+01	-64.9605	7.272371E+01	-6.373721E+01	6.808046E+01
5	-1.500000E+00	4.430872E+01	-6.295383E+01	-1.043111E+01	-5.5032	4.531371E+01	-6.395882E+01	5.463626E+01
	1.500000E+00	-6.509410E+01	5.121202E+01	4.214071E+00	87.9276	5.136450E+01	-6.524658E+01	5.830554E+01
6	-1.500000E+00	3.484644E+01	-4.621033E+01	-5.478094E+01	-26.7525	6.246129E+01	-7.382518E+01	6.814323E+01
	1.500000E+00	-3.348335E+01	4.244910E+01	5.737177E+01	61.7475	7.327930E+01	-6.431355E+01	6.879643E+01
7	-1.500000E+00	-2.855817E+01	-1.985600E+00	-5.398062E+01	-51.9137	4.031970E+01	-7.086354E+01	5.559166E+01
	1.500000E+00	2.370406E+01	2.549191E+01	4.416751E+01	45.5798	6.877454E+01	-1.957858E+01	4.417656E+01
8	-1.500000E+00	-8.938426E+00	-1.011365E+01	4.800084E+01	44.6493	3.847841E+01	-5.753047E+01	4.800444E+01
	1.500000E+00	-5.091117E+00	-2.327359E+01	-6.755052E+01	-41.1674	5.397716E+01	-8.234186E+01	6.815952E+01
9	-1.500000E+00	4.464894E+01	-4.239378E+01	5.921770E+01	26.8432	7.461801E+01	-7.236285E+01	7.349043E+01
	1.500000E+00	-5.381195E+01	2.738875E+01	-7.078654E+01	-59.7185	6.839183E+01	-9.481503E+01	8.160344E+01
10	-1.500000E+00	5.715228E+01	-3.838950E+01	-2.978342E+00	-1.7838	5.724504E+01	-3.848225E+01	4.786365E+01
	1.500000E+00	-9.398026E+01	2.643570E+01	-3.388356E+00	-88.3894	2.653098E+01	-9.407553E+01	6.030325E+01
11	-1.500000E+00	5.413382E+01	-2.574419E+01	-1.229937E+01	-8.5582	5.598473E+01	-2.759509E+01	4.178992E+01
	1.500000E+00	-7.413164E+01	1.872682E+01	1.496099E+01	81.0697	2.107776E+01	7.640757E+01	4.878017E+01
12	-1.500000E+00	2.539616E+01	-1.386382E+01	-2.269194E+01	-24.5690	3.577051E+01	-2.423817E+01	3.000435E+01
	1.500000E+00	-6.009029E+01	1.216897E+01	2.753471E+01	71.3443	2.146523E+01	-6.938652E+01	4.542587E+01
13	-1.500000E+00	2.639954E+01	-3.406783E+00	-4.850990E+01	-36.4610	6.224393E+01	-3.925117E+01	5.074756E+01
	1.500000E+00	-3.595285E+01	-1.293504E+00	6.218715E+01	52.7858	4.593346E+01	-8.317979E+01	6.455663E+01
14	-1.500000E+00	-3.669026E+01	1.343955E+01	-2.656743E+01	-66.6666	2.489967E+01	-4.815038E+01	3.652502E+01
	1.500000E+00	2.541075E+01	5.992762E+00	3.208257E+01	36.5814	4.922122E+01	-1.781772E+01	3.351947E+01
15	-1.500000E+00	3.577985E+01	-3.537155E+00	4.471141E+01	33.1330	6.496359E+01	-3.272092E+01	4.884225E+01
	1.500000E+00	6.429749E+01	-5.670753E+01	-7.477538E+01	-34.5094	5.205284E+01	-1.081174E+02	8.008511E+01

187

ORIGINAL PAGE IS
 OF POOR QUALITY

N85-25875

AUTOMATIC DYNAMIC AIRCRAFT MODELER (ADAM) FOR THE COMPUTER PROGRAM NASTRAN

Hugh Griffis
Nuclear Survivability Group
System Survivability Branch
ASD/ENSSS
Wright-Patterson AFB OH 45433-6503

SUMMARY

Large general purpose finite element programs require users to develop large quantities of input data. General purpose pre-processors are used to decrease the effort required to develop structural models. Further reduction of effort can be achieved by specific application pre-processors. Automatic Dynamic Aircraft Modeler (ADAM) is one such application specific pre-processor.

INTRODUCTION

General purpose pre-processors use points, lines and surfaces to describe geometric shapes. Specifying that ADAM is used only for aircraft structures allows generic structural sections, wing boxes and bodies, to be pre-defined. Hence with only gross dimensions, thicknesses, material properties and pre-defined boundary conditions a complete model of an aircraft can be created.

NASTRAN models generated by ADAM include the executive, case control and the bulk data sets for normal modes analysis. The bulk data cards generated by ADAM are: GRID, CQDMEM2, CSHEAR, CROD, PQDMEM2, PSHEAR, PROD, MAT1, MAT2, CONM2, SPC1, ASET1, EIGR and PARAM (REF1). Additionally, the case control deck is setup to plot the first ten eigenvectors.

WING BOXES

Geometric Modeling

Geometric modeling is completed by using simple quadrilateral surfaces. Surfaces are easily defined, meshed and connected to other surfaces. The upper wing surface coordinates must be defined, then the lower surface coordinates may be defined or automatically generated. The surfaces use CQDMEM2 elements to represent the aircraft skin. Once the upper and lower surfaces are defined, they are automatically connected by CSHEAR and CROD elements. CSHEAR elements represent spars and ribs, while CROD elements represent spar and rib caps. Figure 1 shows the type of data required for each quadrilateral surface.

The software's logic allows multiple quadrilateral wing sections to be created separately and then later connected to generate a complete wing. When multiple wing sections are connected, the duplicate grid points are deleted and the element connectivity list along with the grid identification (GID) for constraints and active degrees of freedom (DOF) are altered accordingly. Grid points which are

within ERROR distance apart are treated as duplicate grid points. The ERROR distance is a user input value.

Surface element thickness is automatically tapered inboard (maximum thickness) to outboard (minimum thickness), while element thickness from the leading edge to the trailing edge remains constant. Figure 2 shows how the actual structure varies from the finite element model. The skin tapering routine is available for homogenous and composite materials. In-plane composite materials are simulated by stacking elements. Each layer has its own fiber orientation description which is defined from a reference orientation.

Mass Modeling

Structural and nonstructural mass (NSM) modeling is available in ADAM. Structural mass includes skin, spars, ribs, spar and rib caps. Nonstructural mass includes fuel, avionics, crew and all other nonstructural materials. ADAM's structural mass modeling only requires the material density, then NASTRAN distributes the mass to grid points by using the element thickness and area

$$\text{Mass} = \text{Thickness} \times \text{Area} \times \text{Density.}$$

Nonstructural mass is applied to the element area. NASTRAN requires the user to input the NSM as

$$\text{NSM} = \text{NSM Thickness} \times \text{Density.}$$

NASTRAN distributes the mass to grid points by using the element area

$$\text{Mass} = \text{NSM} \times \text{Area.}$$

Calculation of NSM thickness for each element in the wing box is a tedious job. Hence ADAM calculates the NSM thickness of the wing by using the corner points of each element

$$Z \text{ thick} = \frac{\sum(Z \text{ upper} - Z \text{ lower})}{3}$$

$$Y \text{ thick} = \frac{\sum(Y \text{ upper} - Y \text{ lower})}{8}$$

$$\text{Thickness} = \sin(\text{wing dihedral}) \times Y \text{ thick} + \cos(\text{wing dihedral}) \times Z \text{ thick.}$$

Half of the thickness, hence the NSM is applied to the upper element and the other half of the NSM is applied to the lower element. Since ADAM calculates the thickness, the user is only required to input nonstructural mass density. Typically, nonstructural mass density for a wing section is not known, thus this value is changed until the gross weight is correct.

Boundary Conditions

ADAM has six wing sections with default boundary conditions: vertical wing with free boundary conditions, horizontal wing with free boundary conditions, horizontal wing carry through, vertical centerline wing carry through, vertical centerline wing with symmetric boundary conditions and vertical centerline wing with anti-symmetric boundary conditions. Figure 3 shows the cross sectional view of the above wing sections.

Horizontal and vertical wing carry through sections are designed for uncoupled wing-body motion, with the inboard part of the wing fixed. However, coupled wing-body motion can be correctly modeled by manually changing the inboard constraints. Geometric modeling for wing-body coupling is more difficult, hence is not used unless strong coupling is expected.

Centerline wing sections only model half of the structure and the skin on the centerline is not generated. Grid points on the centerline are constrained for symmetric or anti-symmetric analysis. Symmetric boundary conditions allow motion in the Z direction along the centerline

SPC1 GID 12456,

while anti-symmetric boundary conditions allow motion in the Y direction along the centerline

SPC1 GID 13456.

Active Degrees of Freedom

ASET1 cards are automatically generated for each wing surface. An optional switch generates ASET1 cards for upper and lower surfaces or for the upper surface only. Little error is introduced by using ASET1 cards on the upper surface only and the active degrees of freedom are cut in half. Another option allows the user to spatially distribute the ASET1 cards in the chord and span directions. This option gives the user an automatic method of assigning ASET1 cards to selected grid points for each wing surface.

Reducing six degrees of freedom to one for each grid point can introduce large error. However, by assigning the active degree of freedom in the dominant direction of motion the error can be reduced to the engineering accuracy of the original model. Once the desired accuracy has been reached, further reduction of the analysis set can be achieved by selecting a smaller set of grid points with the same active degrees of freedom. Since each wing section is uniform in terms of mass and stiffness, spatical distribution of ASET1 card causes no loss of accuracy. However, high frequency modes may be lost if too many grid points are skipped. A convenient rule of thumb to determine the maximum number of modes that are calculated for a given direction is

$$\text{number of modes} = \text{number ASET1 cards} - 1$$

Additional care must be used when large concentrated masses are used. The user must ensure that each grid point with large mass has the appropriate active degree of freedom since ADAM only distributes ASET1 cards spatially.

BODIES

Geometric Modeling

Geometric modeling is completed by defining an X station with several radial vectors, angles and magnitudes. The outer radius defines the skin location. CQDMEM2 elements represent the skin. The inner and outer radii define the height of the

frames and longerons. CSHEAR elements represents frames and longerons, while CROD elements represent frame and longeron caps. Figure 4 shows the type of data required for each body.

Complex body shapes can easily be created, hence the volume of input data is large when compared to the wing input data. Geometric modeling of bodies does not support skin tapering and composite materials, however automatic renumbering for duplicate grid points is available.

Mass Modeling

Structural and nonstructural mass modeling is available for bodies. This section is identical to the wing mass modeling except for the thickness calculation. ADAM calculates the cross sectional thickness of the body for each element

$$\text{Thickness} = \left[\left(\frac{\sum(Z - \text{camber})}{4} \right)^2 + \left(\frac{\sum(Y \text{ inner} - Y \text{ outer})}{2} \right)^2 \right]^{1/2}$$

The mass is only applied to the grid points defined by the outer radius.

Boundary Conditions

ADAM has four body sections with default boundary conditions: user defined active degree of freedom, all points fixed, centerline body with symmetric boundary conditions and centerline body with anti-symmetric boundary conditions. Figure 5 shows the above body sections.

Only half of the structure is modeled if the centerline body option is chosen. Grid points on the centerline are constrained for symmetric or anti-symmetric analysis. Symmetric boundary conditions allow motion in the Z direction along the centerline

SPC1 GID 12456,

while anti-symmetric boundary conditions allow motion in the Y direction along the centerline

SPC1 GID 13456.

Active Degree of Freedom

ASET1 cards are automatically generated for each body section. This section is identical to wing modeling except that ASET1 cards are only assigned to grid points defined by the outer radius.

MASS

Structural and nonstructural mass can automatically be distributed for wings

and bodies. Additionally, concentrated masses can automatically be assigned to the nearest grid point. ADAM determines the nearest grid point then calculates the offset distance. This routine requires relatively large amount of computer time, hence is turned off until the final structural model is completed.

SUMMARY TABLE

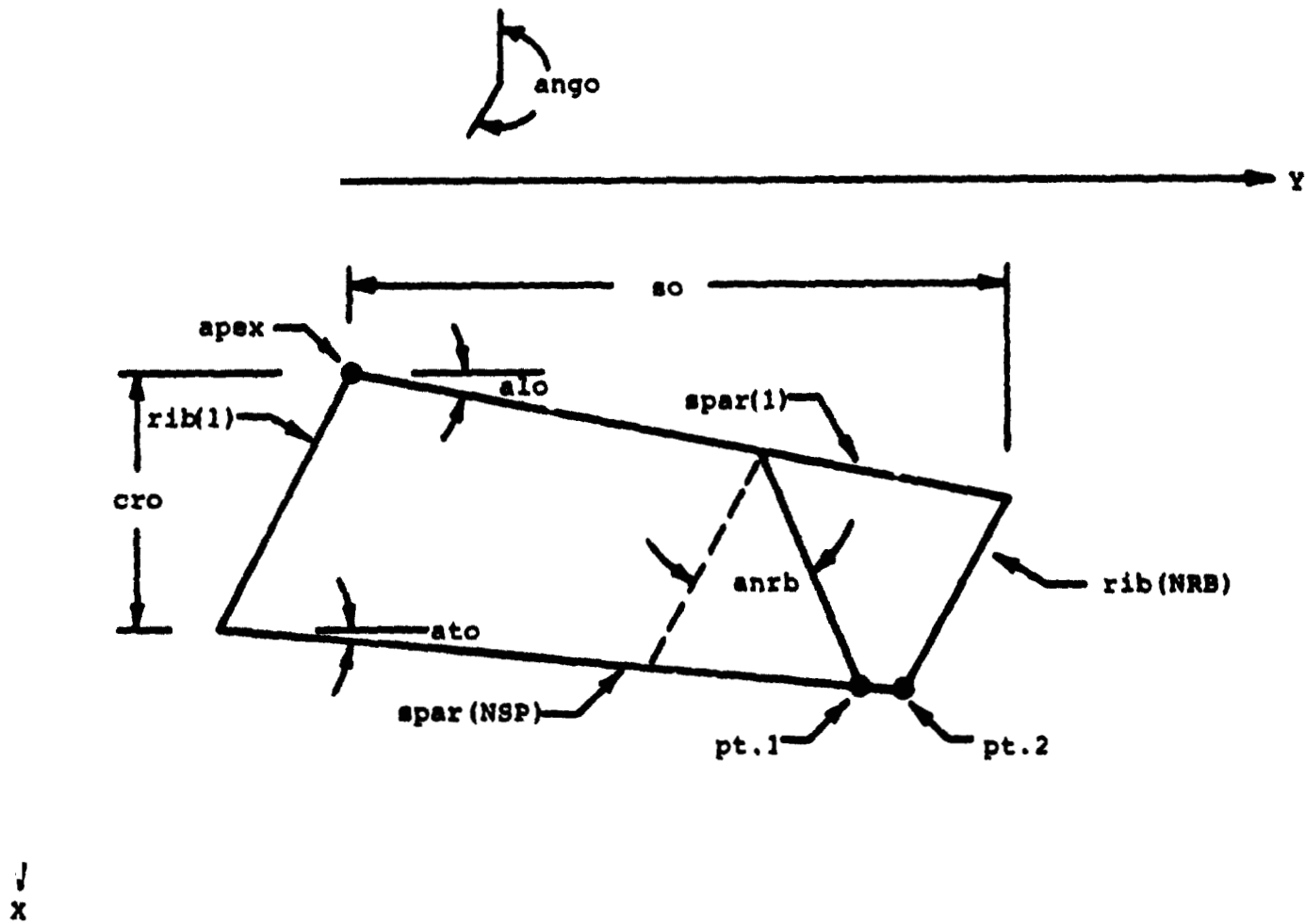
In addition to the NASTRAN model, ADAM also generates a summary table. The summary table is mainly the input data with appropriate labels. Other labels denote which input values are used for geometric, constraint, material and mass modeling. These labels provide convenient guidelines when debugging ADAM's input data. The summary table is written immediately after the input data is read, hence the data on the summary table is conveniently in the same order.

Coordinates of the corner grid points of each wing section are calculated from the input angle data. The coordinates and the GID's for the corner points of each wing section are written on the summary table after all duplicate grid points have been deleted. This data aids the user when multiple wing sections are being connected.

Warning messages are written on the summary table when CQDNEM2 and CSHEAR elements have three or less unique grid points. Typically, the routine which deletes duplicate grid points triggers this warning message and can be corrected by decreasing the ERNOR distance.

CONCLUSION

The logic built into ADAM reduces the effort and knowledge required to build complex aircraft structural models. ADAM's pre-defined wing boxes and bodies gives even novice NASTRAN users advanced modeling skills. Advanced NASTRAN users will find that the tedium of data generation for parametric and design studies is greatly reduced. In general, anyone who builds structural models with ADAM will be more productive and adaptable to design changes.



↓
x

Top view of wing planform. If pt.1 is rotated such that pt.1 equals pt.2, the quadrilaterals degenerate into triangles.

FIGURE 1 WING GEOMETRIC DEFINITIONS

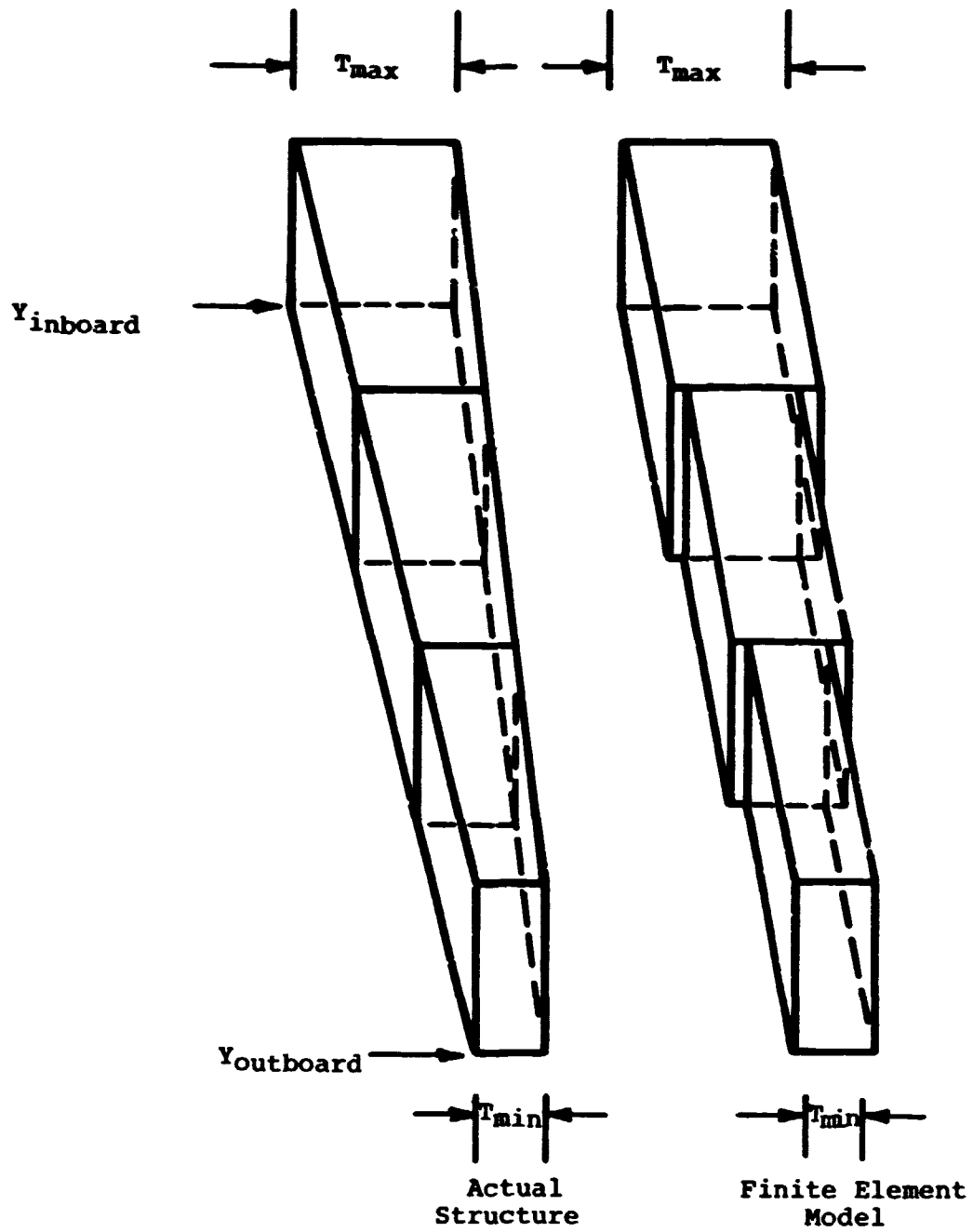
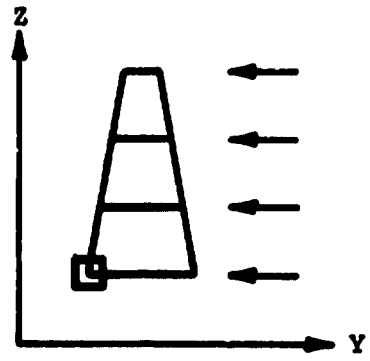
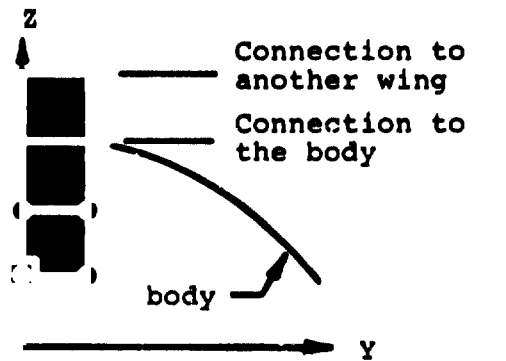


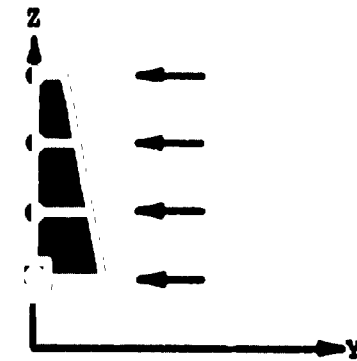
FIGURE 2 SKIN TAPERING



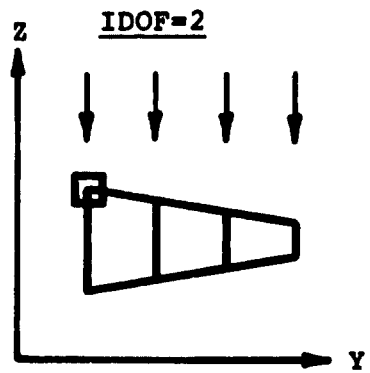
Vertical wing with free boundary conditions



Vertical wing carry through

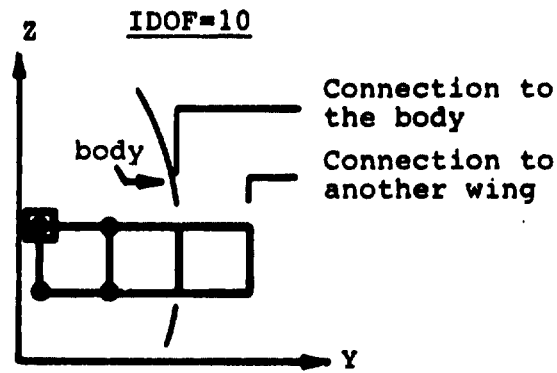


Wing with anti-symmetric boundary conditions



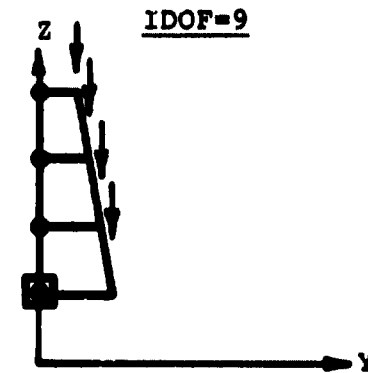
Horizontal wing with free boundary conditions

IDOF=3



Horizontal wing carry through

IDOF=7



Wing with symmetric boundary conditions

IDOF=8

Cross section view looking from leading to trailing edge of wing section. The arrows, \downarrow , denote the direction of the active degree of freedom. The squares, \square , denote the apex. The dots, \bullet , denote the point is fixed. If IDOF is equal to 8, 9 or 10, the apex must be on the centerline.

FIGURE 3 WING BOUNDARY CONDITIONS

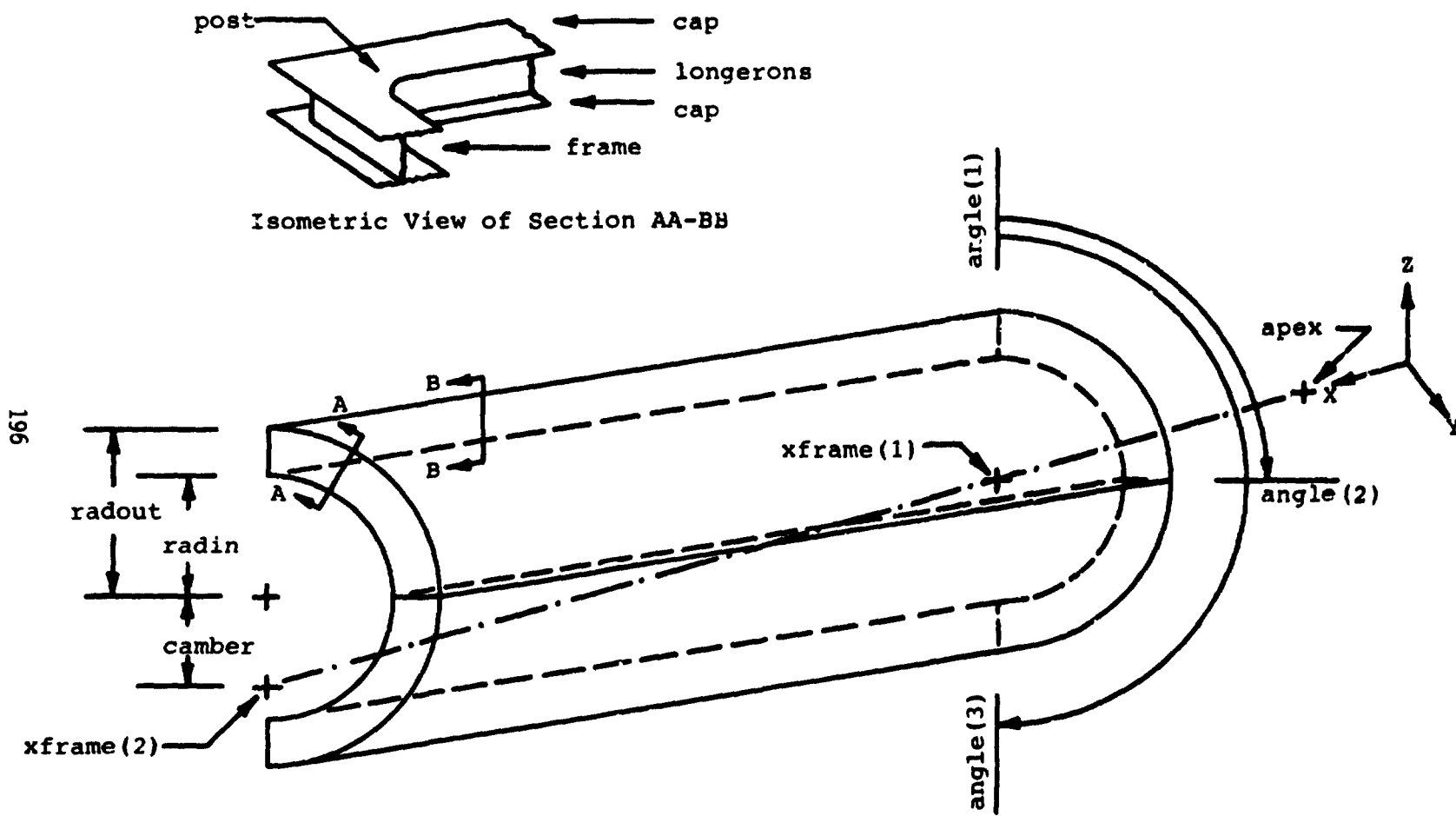
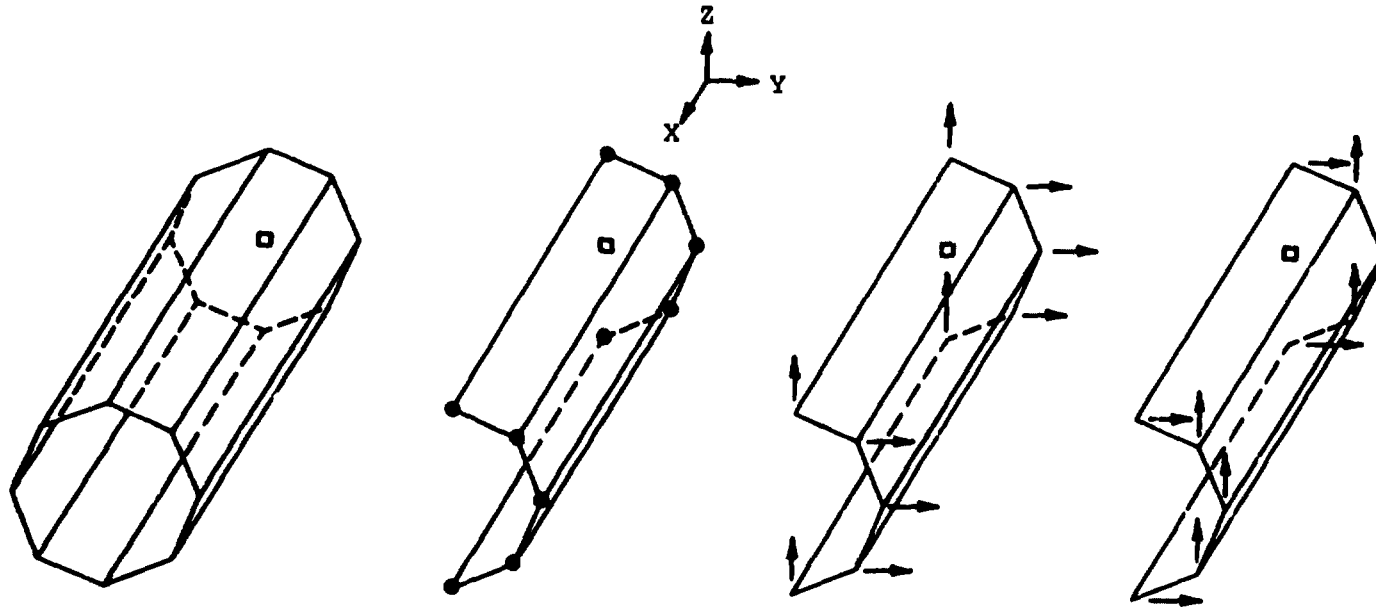


FIGURE 4 BODY GEOMETRIC DEFINITIONS



User defined active
degree of freedom:

- 1 for X direction
- 2 for Y direction
- 3 for Z direction

All points are fixed

The centerline is
fixed in the X
and Y direction.
Centerline has
active degree of
freedom in Z
direction. All
other points have
an active degree
of freedom in the
Y direction.

The centerline is
fixed in the X
and Z direction.
Centerline has
active degree of
freedom in Y
direction. All
other points have
an active degree
of freedom in the
Z direction.

IDOF = 1, 2, 3

IDOF = 7

IDOF = 8

IDOF = 9

The arrows, \downarrow , denote the direction of the active degree of freedom. The squares, \square , denote APEX. The dots, \bullet , denote the point is fixed.

FIGURE 5 BODY BOUNDARY CONDITIONS

REFERENCES

1. NASTRAN Users Manual
2. Automatic Dynamic Aircraft Modeler (ADAM) Volume I. January 1985, ASD/TR
3. Flexible Airframe Design Loads (FLEXLOADS) Volume II. March 1984,
AFWAL-TR-80-3036
4. MSC/NASTRAN Primer, Static and Normal Modes Analysis. January 1982.

85-25876

CADS

A COMPUTER AIDED DESIGN SYSTEM

Victoria A. Tischler and Elizabeth M. Copenhaver
Air Force Wright Aeronautical Laboratories (AFWAL/FIBRA)
Wright-Patterson Air Force Base, Ohio 45433

Michael C. Less and Susan Manuel
Rockwell International, North American Aircraft Operations
Los Angeles, California 90009

SUMMARY

CADS, a Computer Aided Design System, runs on the DEC VAX 11/780 minicomputer. The system supports six functional modules controlled by an Executive Monitor. All of these modules communicate with a data base through a data manager. The data base consists of 2 data files, one for model geometry and one for program output. CADS can be interfaced with relative ease with any given finite element program. The CADS modular organization and its capabilities are examined in detail. Several examples are used to illustrate its broad band of capabilities.

INTRODUCTION

The widespread use of a large variety of finite element based structural analysis and optimization programs both in industry and the Air Force has focused attention on a common problem: the relatively large amount of time and effort required to perform data preparation, data validation, and interpretation of results. To reduce this time and effort a unique, interactive graphics, minicomputer based, command driven, Computer Aided Design System (CADS) has been developed. This system is modular in nature with various functional modules accessed through a common Executive Monitor and makes use of common data base routines. CADS includes mesh generation and data validation capabilities as preprocessing functions as well as graphically postprocessing analysis or optimization code's output data.

The system is designed for a 32-bit minicomputer and is written in Fortran 77. CADS graphics is accomplished through DI-3000 (Ref. 1), a device independent graphics package. As a result CADS can be executed on a variety of graphics terminals. CADS is compiled once. At execution time the user chooses a graphics device to be run with the system. At the present time the CADS software is implemented on a DEC VAX 11/780 with secondary testing for transportability having been performed on an IBM 4341 and a PRIME 850.

To date CADS has been interfaced with three finite element programs: NASTRAN, ANALYZE (Ref. 2) and OPTSTAT (Ref. 3). ANALYZE is an Air Force developed static analysis program for in-house studies in structural analysis, and OPTSTAT is an Air Force developed optimization code for the optimal design of structures subjected to static loads. The triangular and quadrilateral membrane elements in OPTSTAT can be used with isotropic, orthotropic or layered composite materials. CADS was especially designed to provide for composite material property input and output. A key feature is the ease with which the experienced user may interface CADS to any given finite

element based program.

This paper will present an in-depth look at the CAD3 organization and its capabilities and will illustrate these capabilities with several examples.

OVERVIEW

CAD3 is a command-driven program which interprets and executes individual user commands. Commands are entered in free format using commas, blanks or equal signs as delimiters. In general all commands can be executed using a two character abbreviation, the first two letters of the command. The CAD3 program is modular in nature with processors acting under the modules. Figure 1 shows the CAD3 program design. The program is controlled through an Executive Monitor which calls in the READ, OUTPUT, SET, DISPLAY, EDIT and END functional modules. The READ module reads in bulk data or model generation steering files. The OUTPUT module outputs data base information in a specified bulk data format. The SET module defines sets of nodes and/or elements for plotting and other functions. The DISPLAY module displays information at a graphics terminal through the SET module. The EDIT module edits the GEOM data base file and saves it as a permanent file. The END module terminates the CAD3 program and returns control to the host processor. All of these functional modules communicate with the CAD3 data base through a data manager, which is a common set of input and output subroutines. The data base consists of two data files, identified as GEOM and POST. The GEOM data base file will contain all model geometric data, element connectivities, and the attributes associated with each type of data. The POST data base file is generated using the CAD3 Post Processor, CAD3PP, and will contain selected output of the finite element program. The role of the Executive Monitor, all the modules, and CAD3PP will be discussed in detail in subsequent paragraphs.

EXECUTIVE MONITOR

The Executive Monitor controls all program activities. It initializes the user session, maintains communications between the various functional modules and the user during the session, and terminates the session. The Executive Monitor invokes the functional modules in response to user commands. The user may request the READ module, the DISPLAY and EDIT modules and the OUTPUT module in a typical session to generate, display, validate, and output a new model. In another session only CAD3PP and the DISPLAY module may be invoked to interpret the finite element analysis results quickly and accurately. Modularity of the Executive Monitor is a necessary requirement for a multifunctional program such as CAD3.

In the initialization of CAD3 the user must specify the format of the input data, i.e. either NASTRAN, ANALYZE, OPTSTAT or NATURAL. The NATURAL format implies a model generation steering file. The contents of this steering file will be discussed in detail in the discussion of the READ module. The Executive Monitor prompts for each command with the prompt string ?CAD3. At this point any of the functional modules may be specified.

READ MODULE

The READ module is used to read a finite element model's data and to translate it to the CADs GEOM data base file. Basically, this involves the development of translator interfaces which are capable of decoding input bulk data information so that it can be stored in the data base through the data manager. The prompt string for this module is ?READ. At the present time the READ module supports four processors where a processor defines the type of translation to be performed. The four processors are NASTRAN, ANALYZE, OPTSTAT, and NATURAL.

The NATURAL processor provides the user with the capability to generate nodes, elements and element attributes for finite element models. Three submodules are available in the NATURAL processor: NODE, ELEMENT and PROPERTY. The NODE submodule is used for node data generation, the ELEMENT submodule is used for element connectivity data generation, and the PROPERTY submodule is used for element attribute generation. Each of these submodules will be examined in greater detail. A schematic representation of the NATURAL processor and its submodules and subprocessors is given in Figure 2.

NATURAL PROCESSOR - NODE SUBMODULE

The NODE submodule controls five subprocessors: DIRECT, SHAPES, FREEDOM, TRANSFORM and LOAD. Together these subprocessors allow the user to generate coordinates, apply boundary conditions, and develop external load data. Each of the subprocessors provides the user with a specific set of possible commands.

The DIRECT subprocessor provides commands for coordinate definitions on a point-by-point, a linear interpolation, a biased line, and a repetition factor basis. An AXIS command allows the user to specify the order of the coordinate data input with respect to the axes. A MIRROR command mirrors the generated nodes about a specified axis or axes incrementing the node numbers by a user specified value. A PERCENT command can be used to bias the default, equally spaced, interpolation process, to a user defined percent process. An EQUATE command allows the user to change previously defined node numbers to new numbers. A NODE command can be used to specify the node numbers and the coordinates of the nodes to be generated along a line in space. Equal increments are used to space the generated nodes. If a PERCENT command had been specified, the nodes would be biased by those percent values. A REPEAT command allows the user to repeat the previous NODE command to generate repetitively located nodes. In general, commands in CADs have several parameters. When these are chosen judiciously, a particular command's capability can be considerably expanded.

The SHAPES subprocessor provides commands for generating nodes along circles, ellipses, and arcs of parabolas. In each case the user basically provides the information to determine the correct equation for the command. A PERCENT command can be used to specify the spacing of the nodes along the circle, ellipse or parabola.

The FREEDOM subprocessor provides commands for changing the constraints of the model. The nodes created by the DIRECT and SHAPES subprocessors are without constraints and are free to both translate and rotate. A SUPPRESS command can be used to define the motions to be suppressed and the nodes to be constrained. An SFREE command frees a previously defined suppression from a given node.

The TRANSFORM subprocessor provides commands for transforming the coordinates of a user defined local system to the model's global system. An OFFSET command followed by X, Y and Z values can be used to move the local system origin to the global system coordinates. A ROTATE command followed by X, Y, and Z rotational angles can be used to rotate a local system in order to align it to the global system. A NODES or POINTS command can be used to have the necessary translations and/or rotations computed.

The LOADS subprocessor provides the user with the means to apply external forces to a set of nodes. The CASE command identifies the case or load condition number for the load or moment commands which follow it. The FL and FM commands define the scale factors for the applied LOAD or MOMENT commands. The CID command specifies the coordinate system reference number for the applied loads or moments. The LOAD and MOMENT commands define the translational force or rotational moment vector directions to be applied to a given list of nodes.

NATURAL PROCESSOR - ELEMENT SUBMODULE

The ELEMENT submodule provides the means for generating element types, groups, and connectivities for a wide variety of different elements. All of the ANALYZE and OPTSTAT elements are supported, while twenty-two of the most commonly used NASTRAN elements are supported. The ANALYZE and OPTSTAT elements include the rod, the membrane triangle and quadrilateral, and the shear panel. The NASIRAN elements include: the simple beam, the rod, shear panels and twist panels, plates and membranes, axisymmetric solids, solid polyhedrons and isoparametric solid hexahedrons. Each of the elements has a separate, unique name as part of the NATURAL processor. For example a membrane triangle, CTRMEM in NASTRAN or a 3 in ANALYZE and OPTSTAT, is called TM, a shear panel, CSHEAR, is called QS4, and a simple beam, CBAR, is called B2. All elements are referred to by their natural element type name in the NATURAL processor. There are no subprocessors in this submodule. One of the ways CAD5 splits a structural model into smaller and more easily displayed parts is to define a group of elements where each element in the group is of the same type. A GROUP command specifies the group number to be used for those new elements which are to be generated. The TYPE command specifies the element type or name and its connectivities. This command allows the generation of a string of elements. The REPEAT command permits the user to repeat on the previously defined element type and its node connectivity a given number of times by a specified increment. The DUPE command duplicates a previously defined group. The connectivities of the first group are incremented by a specified value to define the connectivities of the new group.

NATURAL PROCESSOR - PROPERTY SUBMODULE

The PROPERTY submodule controls two subprocessors: DIRECT and ANISOTROPIC. Together these subprocessors allow the user to specify element sizes and materials.

The DIRECT subprocessor provides commands for generating material and element properties. At the present time CAD5 supports material properties defined in material tables MAT1 and MAT2 for structural analysis and MAT4 and MAT5 for heat transfer. The commands are MAT1, MAT2, MAT4, and MAT5. Corresponding to each unique element name in the NATURAL processor is a corresponding property command. For

example corresponding to the TM and QS4 elements is property command PID and corresponding to the B2 element is property command PB2. These property commands specify the element properties defined in PTRMEM, PSHEAR, PBAR, etc. The element sizes and materials are applied to previously defined element groups through the use of the following four commands. The GROUP command defines the default sizes and material properties to be applied to the entire group of elements. The PLIST, MLIST, and CHANGE commands selectively change the sizes or properties of particular elements in the group defined by the GROUP command. Any number of PLIST, MLIST and CHANGE commands may follow a GROUP command.

The ANISOTROPIC subprocessor provides commands for generating sizes and material property inputs for either orthotropic or anisotropic membrane elements using basic lamina characteristics. The BASIS command defines the zero-degree direction for the composite lamina. The angle between this direction and the individual element axes forms the material orientation angle associated with each individual element. The CID command identifies a table of lamina material properties for the definition of composite laminates using the PLIES command. Typical information specified by each CID command includes the longitudinal, transverse and shear moduli, Poisson's ratio, the thickness of an individual ply, thermal and moisture expansion coefficients and allowable stress data. The GROUP command defines a group of elements against which the PLIES commands will be processed. The PLIES command defines the number and the orientation of the individual lamina which make up the element laminates.

A typical session in the NATURAL processor to generate a small composite plate would produce the following steering file:

```

BEGIN          NATURAL
BEGIN          NODE
BEGIN          DIRECT
AXIS           X Y Z
NODE           1  0.0  0.0  0.0  TO  10  9.0  4.0  2.0
REPEAT 3      10  0.0  3.0  0.0      10  0.0  2.0  0.0
NODE           41  0.0  12.0  0.0  TO  50  9.0  12.0  2.0
END
BEGIN          FREEDOM
SUPPRESS      TX TY TZ  NODE 1  TO  41  BY  10
END
BEGIN          LOAD
CASE           1
FI            500.0
LOAD          X=1.0 Y=1.0 Z=0.0  NODE 10  TO  50  BY  10
LOAD          Z=1.0  NODE 10  50
END
END
BEGIN!!       ELEMENT
GROUP         1
QM1           1  2  12  11  TO  9  10  20  19
REPEAT 3      8*10
END
BEGIN          PROPERTY
BEGIN          DIRECT
PID           1  T=.50
GROUP         1  PID  1
END
BEGIN          ANISOTROPIC

```

```

CID          1  EL=20.0E+6  ET=10.0E+6  GL=5.0E+6  UL=.3  T=.0125
CID          2  EL=20.0E+6  ET=10.0E+6  GL=5.0E+6  UL=.3  T=.00625
BASIS       :NODE 1 12
GROUP       1
PLIES       10  CID=1  LA = 0.0  ELEMENTS 1 TO 18
PLIES       10  CID=1  LA = 90.0 ELEMENTS 1 TO 18
PLIES       10  CID=1  LA = 45.0 ELEMENTS 1 TO 18
PLIES       10  CID=1  LA = -45.0 ELEMENTS 1 TO 18
PLIES       20  CID=2  LA = 0.0  ELEMENTS 19 TO 36
PLIES       20  CID=2  LA = 90.0 ELEMENTS 19 TO 36
PLIES       20  CID=2  LA = 45.0 ELEMENTS 19 TO 36
PLIES       20  CID=2  LA = -45.0 ELEMENTS 19 TO 36
END
END
END

```

The finite element model of the composite plate has 50 nodes and 36 composite elements. Nodes 1, 11, 21, 31 and 41 are constrained in the X, Y and Z directions. There is only one loading condition. A 500 lb. load is applied to nodes 10, 20, 30, 40 and 50 in the X and Y directions and to nodes 10 and 50 in the Z direction. All the elements are in group 1, and the total laminate thickness is .50. The zero degree direction for the laminate is defined by nodes 1 and 12. The material properties defined for the laminate are the longitudinal, transverse, and shear moduli, Poisson's ratio, and the layer thickness. All the elements are standard $0^\circ/+45^\circ/90^\circ$ laminates with elements 1 to 18 having 40 lamina, 10 lamina in each direction, and elements 19 to 36 having 80 lamina, 20 lamina in each direction. A plot of the composite plate is shown in Figure 3. At the user's request CADS will display the model as it is being generated at the terminal.

OUTPUT MODULE

The OUTPUT module is used to output the model in a specific data format. This module will translate information from the GEOM data base file to a specified data format through the use of a separate translator interface for each program. The prompt string for this module is ?OUTPUT. The OUTPUT module supports three processors: NASTRAN, ANALYZE and OPTSTAT.

SET MODULE

The SET module is used to define node or element sets for plotting. There are three kinds of commands in the SET module: general, node and element set definition, and set algebra. The prompt string for this module is ?SET.

There are four general commands: CLEAR, PRINT, LIST and DISPLAY. The CLEAR command erases all sets currently defined. The PRINT command lists all the members of a given set. The LIST command lists the nodes of the model or the element group tables. The DISPLAY command sends a node or element set to the DISPLAY module and begins execution of that module.

All set names are assigned by the user. Node set names must begin with the letter N. All node set definition commands begin with the node set name followed by

an equals sign and command keywords. The ALL keyword places all of the model's nodes into a node set. A specified list of nodes or a generated list of nodes may be placed into a node set. The SPHERE, CYLINDER and BOX keywords place all nodes inside the given shape into a node set. The SLAB keyword places all nodes on or within a defined slab into the node set. A command keyword can also be the name of a previously defined element set in which case all the nodes referenced in the element set would be placed in the node set.

Element sets are generally used for most displays, since they contain the connectivities between the nodes. The element set name must begin with the letter E. The format of the element set definition commands is the same as that given for a node set. The ALL keyword defines an element set containing all of the elements in the given model. In the NATURAL processor, Element submodule, the concept of a group was defined as a way of splitting a structural model into smaller and more easily displayed parts. The NASTRAN, ANALYZE and OPTSTAT processors in the READ module automatically separate the various element types into individual groups. The GROUP keyword places all the elements in a specified group into an element set. Selected elements from a specific group or several groups may be placed in an element set. A specified list of elements may define an element set. A keyword can be an element name from the Element submodule of the NATURAL processor or a NASTRAN element type. For example, ESET=TM or ESET=CTRMEM. Element sets can also be defined from previously generated node sets using a combination of operator and/or type parameters. The valid operators are OPEN and CLOSE. OPEN requires that at least one of the element's nodes be in the given node set before the element is placed in the element set. CLOSE requires that all of the element's nodes be in the node set before it is added to the element set. An element type can also be used to define a new element set from a node set. For example E1=OPEN CROD N5 will generate an element set E1 containing all CROD elements which have at least one node in node set N5.

The set algebra commands allow the user to perform set algebra on previously defined sets in order to generate a new set. In using these commands all sets must be of the same type, i.e. either node sets or all element sets. The intersection command, I, defines a new set by the intersection of two old, previously defined sets. The union command, U, defines a new set by the union of two old sets. The exclusion command, E, defines a new set by excluding the first set from the second set on the command line.

DISPLAY MODULE

The DISPLAY module is used to interactively display the finite element model at the terminal. A variety of commands are available to obtain a particular display or plot format. The prompt string for this module is ?DISPLAY. In addition to supporting its own set of commands, the DISPLAY module supports the following three sub-modules: ATTRIBUTE, PLOT, and GRAPH. Details of the DISPLAY commands and each sub-module will be examined further in the following paragraphs.

The DISPLAY module commands are: MARGIN/NOMARGIN, TITLE, ROTATE, DISTORT, DEFINE, LIST, CASE, MODE and DEFORM/NODEFORM. The MARGIN/NOMARGIN command allows the user to have square labeled or rectangular non-labeled displays. The margin information consists of rotation angles, distortion factors, sight distance, model reference, date and time. The TITLE command can be used to define a title of up to 72 characters which is printed at the top of each display. The ROTATE command defines

the amount of rotation about an axis in degrees. The keyword SCALE is available on the ROTATE command where the value of SCALE is used to factor or scale the deformations. The DISTORT command allows the user to distort the horizontal and/or vertical axis of the plot in order to take full advantage of the display window. The DEFINE command is used to directly define a new set for plotting instead of returning to the SET module. The LIST command lists the nodes of the model or the element group tables. The CASE command is used to specify the load case number or mode shape number for output displays. For NASTRAN this number is the subcase number called out in the NASTRAN case control deck. The MODE command is used to define or redefine the type of output to be processed. This command is also available in the ATTRIBUTE submodule and will be discussed there in more detail. The DEFORM/NODEFORM command allows the user to request deformation plots. DEFORM can also be used as a keyword on the ROTATE command.

ATTRIBUTE SUBMODULE

The ATTRIBUTE submodule is used to define the output data components to be displayed. This output data resides in the POST data base file. Its prompt string is ?ATTRIB and the valid commands are PROG, MODE, NAME, and CLEAR. The PROG command is used to specify the type of output data to be retrieved. The valid types are NASTRAN, ANALYZE or OPTSTAT. The MODE command is as defined above. The types of output which can be processed include element stresses (STRESS), element forces (FORCE), node point displacements (DISPLACE), and mode shapes (EIGEN). For each element in the element libraries supported by CAD5, available component types are tabulated for both element forces and element stresses if applicable. For example, for the CBAR element available element force output includes: the bending moment at A1, A2, B1, and B2, the shear at points 1 and 2, the axial force, and the torque. Also for the CBAR element, available element stress output includes: the stress at A1, A2, A3 and A4, the axial stress, the minimum and maximum stress at A, the margin of safety in tension and compression, the stress at B1, B2, B3 and B4, and the minimum and maximum stress at B. For the 3 element in OPTSTAT, i.e. the membrane triangle, available stress output includes: the X, Y and XY local element stresses, the effective stress ratio, the total strain energy and the margin of safety. DISPLACE and EIGEN output includes node point translations and rotations in the X, Y and Z directions. The NAME command references either an element name from the Element submodule of the NATURAL processor or the word NODE. The keyword on the NAME command is COMPONENT which references one of the available tabulated component types. For example, the following commands will request axial stresses to be displayed for all CROD elements and stresses in the X, Y and XY direction to be displayed for all CQDMEM1 elements.

```
MODE STRESS
CROD A
CQDMEM1 SX SY SXY
```

The CLEAR command erases or clears the internal switches for either a specified element name, all previously defined components, or the word NODE.

PLOT SUBMODULE

The PLOT submodule executes the plot requests to be displayed on the screen. The PLOT command is the only command. Keywords on the plot command provide all the display options, and multiple keywords may be specified for a given plot. These keywords apply only to the current display and must be entered each time information is requested. Each keyword is listed and described. DASH - The membrane elements are displayed with dashed lines instead of solid lines. NODE - The node numbers are displayed. ELEMENT - The element numbers are displayed. AXIS - The element local axis is displayed on all planar elements. LABEL - The element type (e.g. CROD, CBAR) is displayed on the elements. COORDINATE - The X, Y and Z coordinates of the nodes are displayed. TYPE - An element type is specified and output values are displayed for that element type only. BREAK - Elements are displayed shrunken about their centroids and disconnected from their nodes. SHRINK - The user specifies a factor between 0.0 and 1.0 which is used to scale the elements. This keyword must be used along with BREAK. SCALE - A scale factor is specified and used to scale the output element stress and force displays.

SIZE - The major size value of the elements is displayed (e.g. rod area, membrane thickness). MATERIAL - An element material table component specified by the user is displayed. The available components are a subset of those given on the MAT1 and MAT2 cards. SUPPRESS - The user specifies one or more suppressed degrees of freedom, then only nodes with those suppressions are numbered in the display. A small set of axis arrows on each node in the direction of the suppressed degrees of freedom can also be displayed. HIDE - The model is displayed with all hidden lines removed. CADS uses the hidden-line routine developed by David R. Hedgley, Jr. at NASA/DRYDEN (Ref. 4). A plot of a composite wing with hidden lines removed is shown in Figure 4.

CONTOUR - Surface contours of stresses, forces, and selected material properties can be displayed. The stress and force contours will display the first component type defined for each of the element types. The command PLOT CONTOUR STRESS as applied to the example given in the description of the ATTRIBUTE submodule will contour ϵ , the axial stress, for the CROD element and SX, the stress in the X-direction, for the CQDMEM1 element. Only laminate material properties A11 through A33 as defined on the MAT2 card can be contoured. LEVELS - The number of contour levels to be used on a contour plot is specified. The user also defines the values for the contour levels on the contour display. If LEVELS is not specified, CADS will establish between 10 and 15 levels at even spacing by default. A contour plot of SX, the stress in the X-direction, for the top skin of a metallic wing is shown in Figure 5.

STRESS - The element stress values are displayed on the individual elements. The component types requested in the ATTRIBUTE submodule are displayed for the given load case. A plot of AVRS, the average shear stress, along the spars of a metallic wing is shown in Figure 6. FORCE - The element force values are displayed on the individual elements. DISPLACE - The grid point displacements are displayed at the nodes. BOTH - The deformed shape is displayed on top of the undeformed shape for a given deformation set. The deformed shape is displayed in dashed lines while the undeformed shape is displayed in solid lines. EIGEN - A specified mode shape is displayed either alone or on top of the undeformed shape. A plot of the first mode of a metallic wing is shown in Figure 7.

After a plot is completed, one of five characters can be entered to continue processing. A W character will initiate the window definition process for blowing up

displays. After the W is entered, the cross-hairs will appear on the screen. They are then positioned to the center of the area to be blown up and an integer number, 1 through 9 is entered to define the window. A window represents ten percent of the original plot centered about the cross-hairs. As each window is defined, a 24 character title can be input. Up to nine windows can be defined. To display a specific window, the keyword WINDOW followed by an integer number is used. The window is blown-up to occupy the entire screen. Several of the previously defined keywords can also be specified, e.g. NODE or ELEMENT. Plots of a window defined on a composite wing are shown in Figures 8a and 8b.

A P character will initiate window definitions through a port or box. Again the cross-hairs will appear and a box will be defined by positioning the cross-hairs on the diagonal end points and entering an integer number. Up to nine ports can be defined, and a title can be entered for each port. To display a specific port, the keyword PORT followed by an integer number is used. The port is blown-up to occupy the entire screen. As with the WINDOW several of the previously defined keywords can also be specified. Plots of a port defined on a composite wing are shown in Figures 9a and 9b.

A V character, for view, will allow the expansion of a boxed area of the current display to another area of the same display without erasing the screen. After the cross-hairs appear the first box is defined as for the port. Another box is defined in a clear section of the display in the same manner. If the first character used to define the first box is a D, then the first box is distorted into the second box. If any character besides a D is used to define the first box, then a square box is plotted into a square box with no distortion. A plot of a view defined on a composite wing is shown in Figure 10.

An L character will request detailed composite layer information for composite layered elements. The cross-hairs are used to pick up to nine different elements. A plot of composite lamina information is shown for selected elements on the top skin of a composite wing in Figure 11.

A K character keeps the current display, but allows the user to add more information to the display. A subsequent E character adds the element numbers to the display, and an N character adds the node numbers to the display.

GRAPH SUBMODULE

The GRAPH submodule provides commands for displaying sets of values as an X-Y graph. The user specifies up to five sets of values, titles, and legends which are then used to build the actual X-Y display. In addition to accessing values from the CADS data base, the user may also enter lists of real values from the terminal for display. The prompt string for the GRAPH submodule is ?GRAPH. The TITLE command allows the user to define a title for the X-Y graph. The title will be printed at the top of the graph and can be as long as two lines where each line is 72 characters. The XTITLE command is used to specify the X-axis title, while the YTITLE command specifies the Y-axis title. Both are one-line titles of at most 48 characters. The CURVES command is used to specify the number of sets of values to be plotted as separate curves. The CASE command is used to define those load cases from which the data will be taken. The XVALUE and YVALUE commands are used to specify the sets of values to be plotted as X-Y curves. Keywords for the XVALUE and YVALUE commands include AXIS, DISPLACE, TIME, EIGEN, and NODE. The AXIS keyword implies that

CADSPP

The CADS Post Processor (CADSPP) is a stand-alone program on the VAX 11/780 which reads an 80 column card image output file generated by the finite element program, translates the information, and stores it in the POST data base file. It stores element stresses and forces, grid displacements and mode shapes. As referenced in the ATTRIBUTE submodule the stress and force components supported for each element are tabulated in Reference 5. Since CADSPP establishes the POST data base file, it must be run separately before trying to obtain deformation or stress and force value plots in CADS.

CONCLUSIONS

Not all the commands available in CADS were described and those commands that were referenced were not all described in their entirety. Emphasis was placed on the modular nature of the CADS organization and its basic capabilities. A detailed description of CADS is available in References 5 and 6. Assistance in maintaining and upgrading the CADS software is available in Reference 7.

REFERENCES

1. DI-3000 User's Guide, Precision Visuals, Incorporated, Boulder, Colorado, Apr. 1981.
2. Venkayya, V. B.; and Tischler, V. A.: ANALYZE - Analysis of Aerospace Structures with Membrane Elements, AFFDL-TR-78-170, Dec. 1978.
3. Venkayya, V. B.; and Tischler, V. A.: OPTSTAT - A Computer Program for the Optimal Design of Structures Subjected to Static Loads, TM-FBR-79-67, June 1979.
4. Hedgley, David R., Jr.: A General Solution to the Hidden-Line Problem, NASA Reference 1085, COSMIC No. ARC-11446, 1982.
5. Less, M.; and Manuel, S.: CADS User's Guide, AFWAL-TR-85- , Rockwell International, North American Aircraft Operations, Apr. 1985.
6. Less, M.; and Manuel, S.: CADS - Final Summary Report, AFWAL-TR-85- , Rockwell International, North American Aircraft Operations, Apr. 1985.
7. Less, M.; and Manuel, S.: CADS - Program Maintenance Manual, AFWAL-TR-85- , Rockwell International, North American Aircraft Operations, Apr. 1985.

either the X, Y or Z coordinate values of the nodes will be plotted along the X or Y axis. The DISPLACE keyword implies that a specified displacement component will be plotted along the X or Y axis. TIME implies that a time step interval will be specified for the X or Y values. The EIGEN keyword implies that a specified mode shape component will be plotted along the X or Y axis. The NODE keyword defines the nodes to be used in the given X-Y plot. The LEGEND command permits the user to define a short, 12 character legend for each curve. The TERMINAL command is used to start the interactive input of values for X-Y plotting from the terminal. A plot of the Z displacements along the trailing edge of a metallic wing is shown in Figure 12.

EDIT MODULE

The EDIT module is used to edit the GEOM data base file by adding, deleting and changing nodal, element, material and property data. The prompt string for this module is ?EDIT. The EDIT module supports four processors: NODE, ELEMENT, PROPERTY, and MATERIAL.

The NODE processor provides commands for modifying the current nodal data. The LIST command allows the user to list part or all of the node numbers, coordinates and constraint information stored on the GEOM data base file. The DELETE command deletes specified nodes from the data base. The CHANGE command is used to change the coordinate locations or suppressions of specified nodes. The ADD command uses the NODE command in the NODE submodule of the READ module for adding new nodes and their coordinates.

The ELEMENT processor provides commands for modifying the current element connectivity data. The LIST command lists all element data via the element group. Group numbers, the number of elements in each group, and all or part of the element data in a specific group can be listed. The DELETE command deletes specified elements from the data base. The CHANGE command is used to change the element connectivity of specified elements. The ADD command adds elements to a specified group.

The PROPERTY processor provides commands for modifying element property data. The LIST command is the same as the LIST command described for the ELEMENT processor. The CHANGE command allows the user to change element sizes for specified elements. All changes must be made by reference to the group in which the element resides.

The MATERIAL processor provides commands for modifying material property data. The LIST command either lists the material data associated with a specific group or lists all the material values in the MATI tables where I is 1, 2, 4 or 5. The ADD command is used to add new material property values to MAT1 and MAT2 material tables. The CHANGE command is used to change the material properties of specific lists of elements within a given group.

The ELEMENT, PROPERTY, and MATERIAL processors provide a HELP command. The HELP command gives information on the valid material and property types for the different element types or groups. The HELP ELEM lists all of the elements supported by CAD5 and the property type name for each element. The HELP command followed by a property type name lists all the element names which reference that property type. The HELP MAT TYPE lists all the keywords for the specified material property table type, i.e. MAT1, MAT2, MAT4, or MAT5.

• EXECUTIVE MONITOR

• USER MODULES

• PROGRAM DATABASE

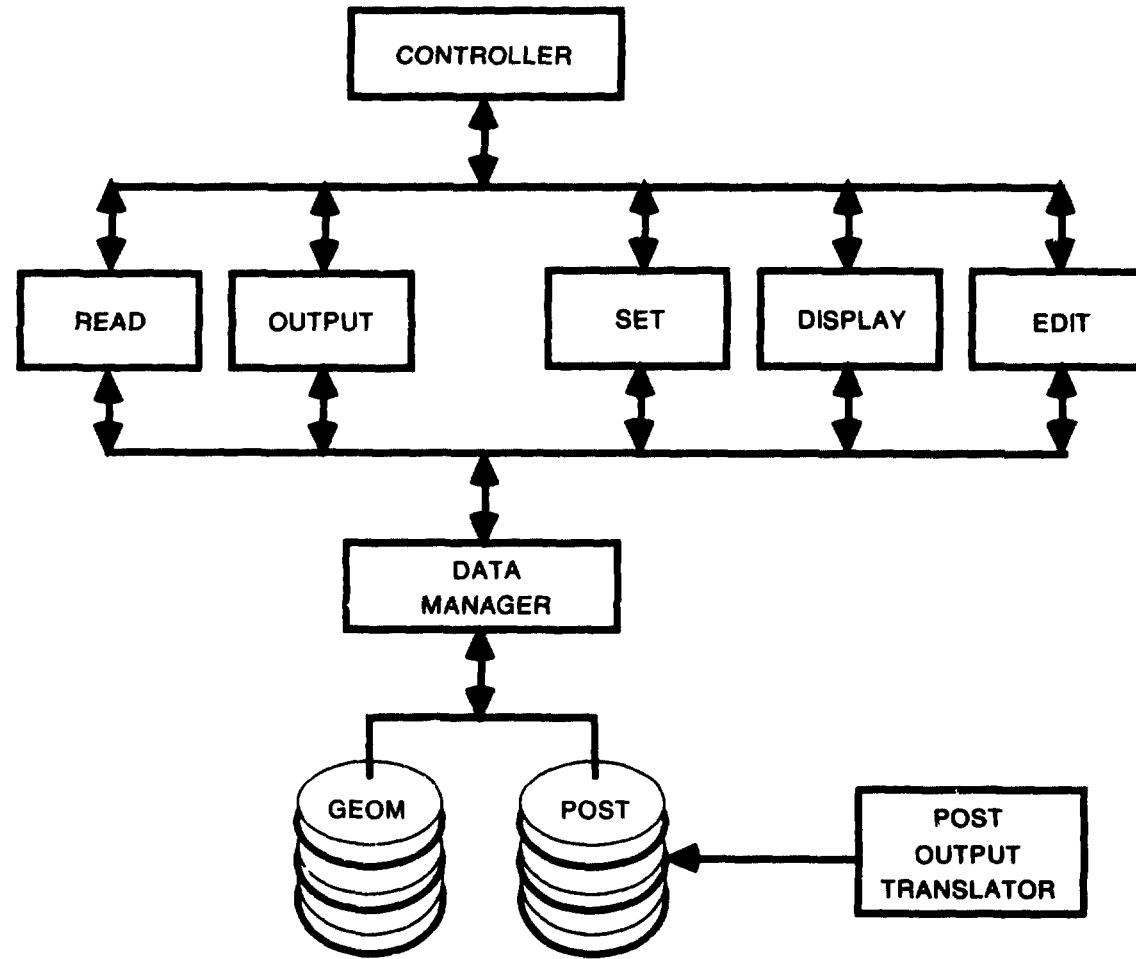


FIGURE 1. CADS PROGRAM DESIGN

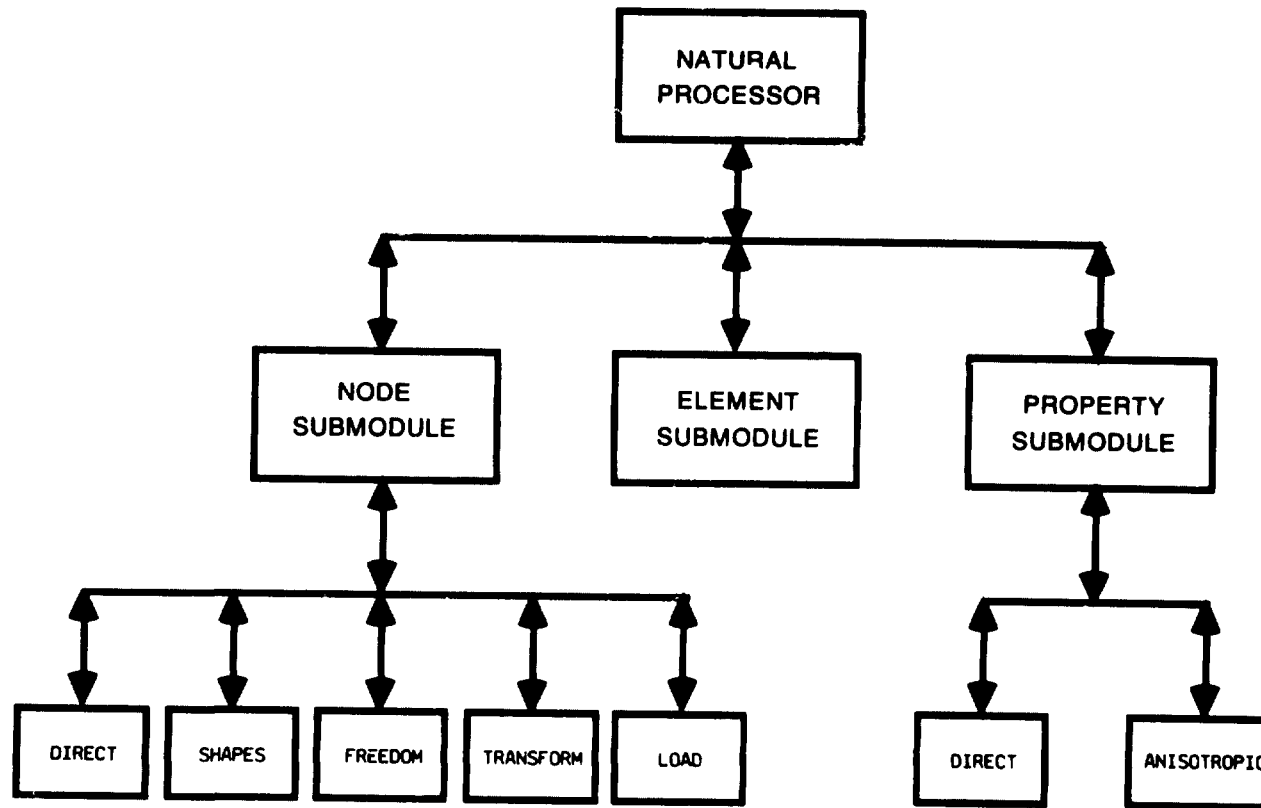


FIGURE 2. A SCHEMATIC OF THE NATURAL PROCESSOR

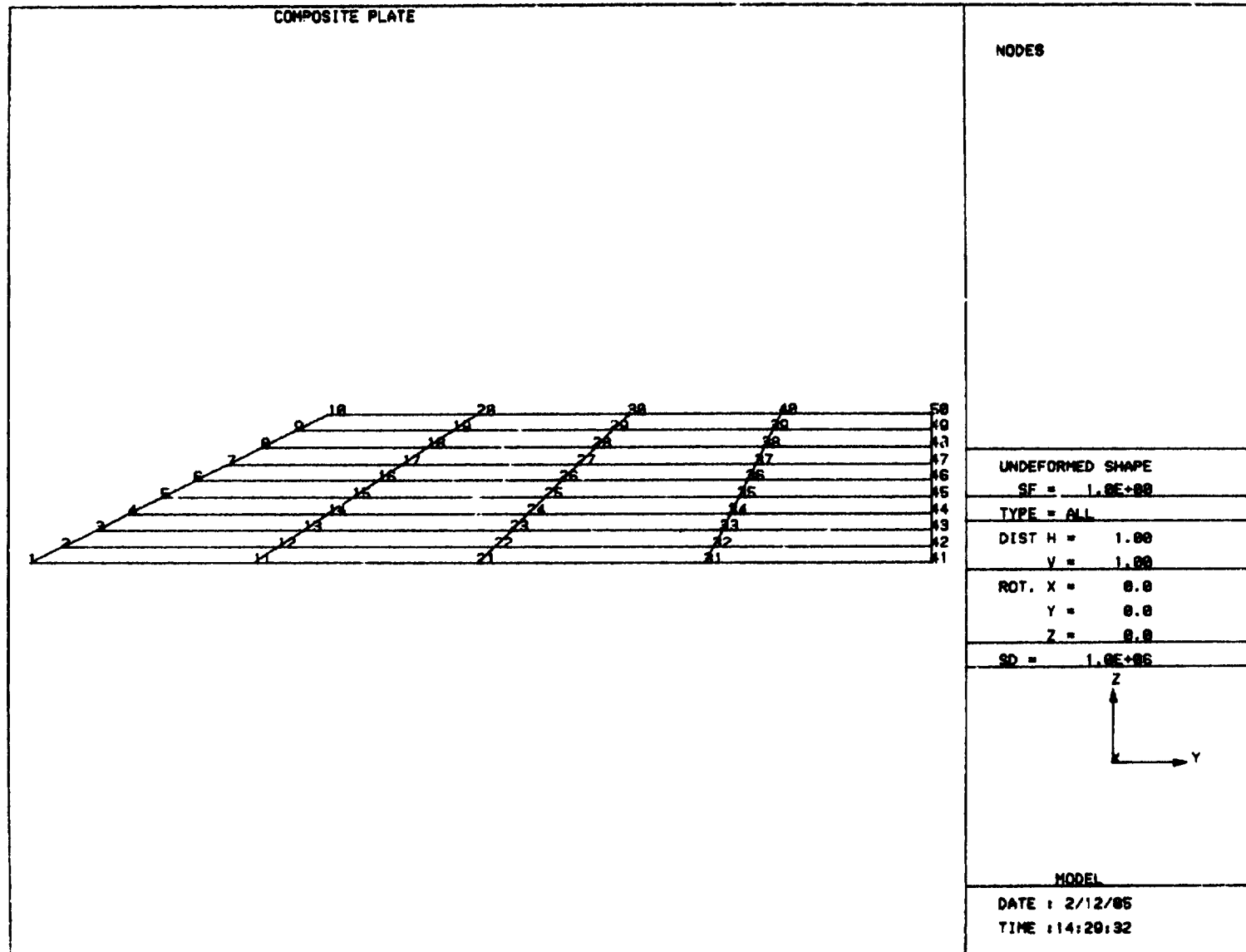


Figure 3. Finite Element Model of a Composite Plate

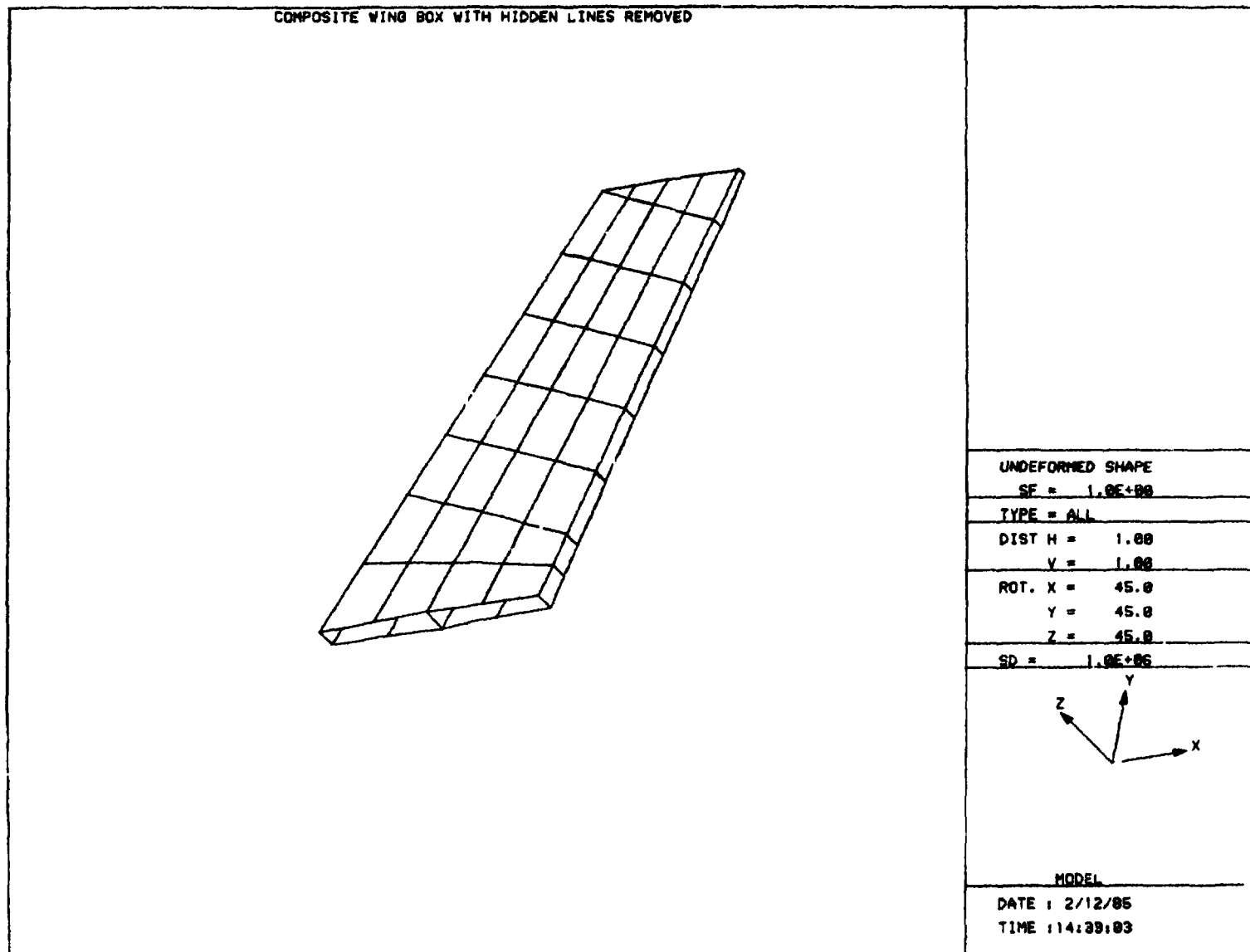


Figure 4. Composite Wing with Hidden Lines Removed

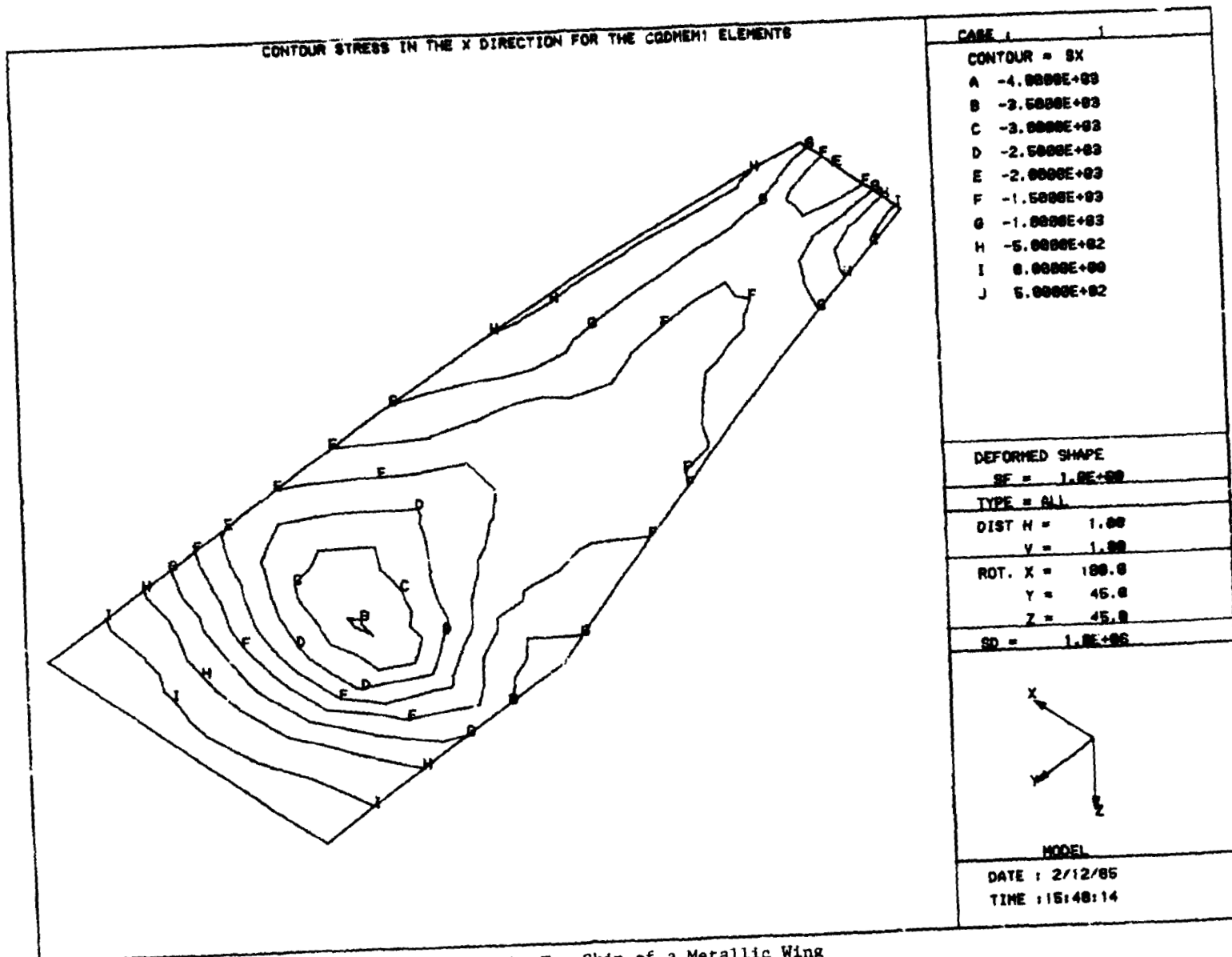


Figure 5. Contour Plot of SX for the Top Skin of a Metallic Wing

ORIGINAL PAGE IS
OF POOR QUALITY

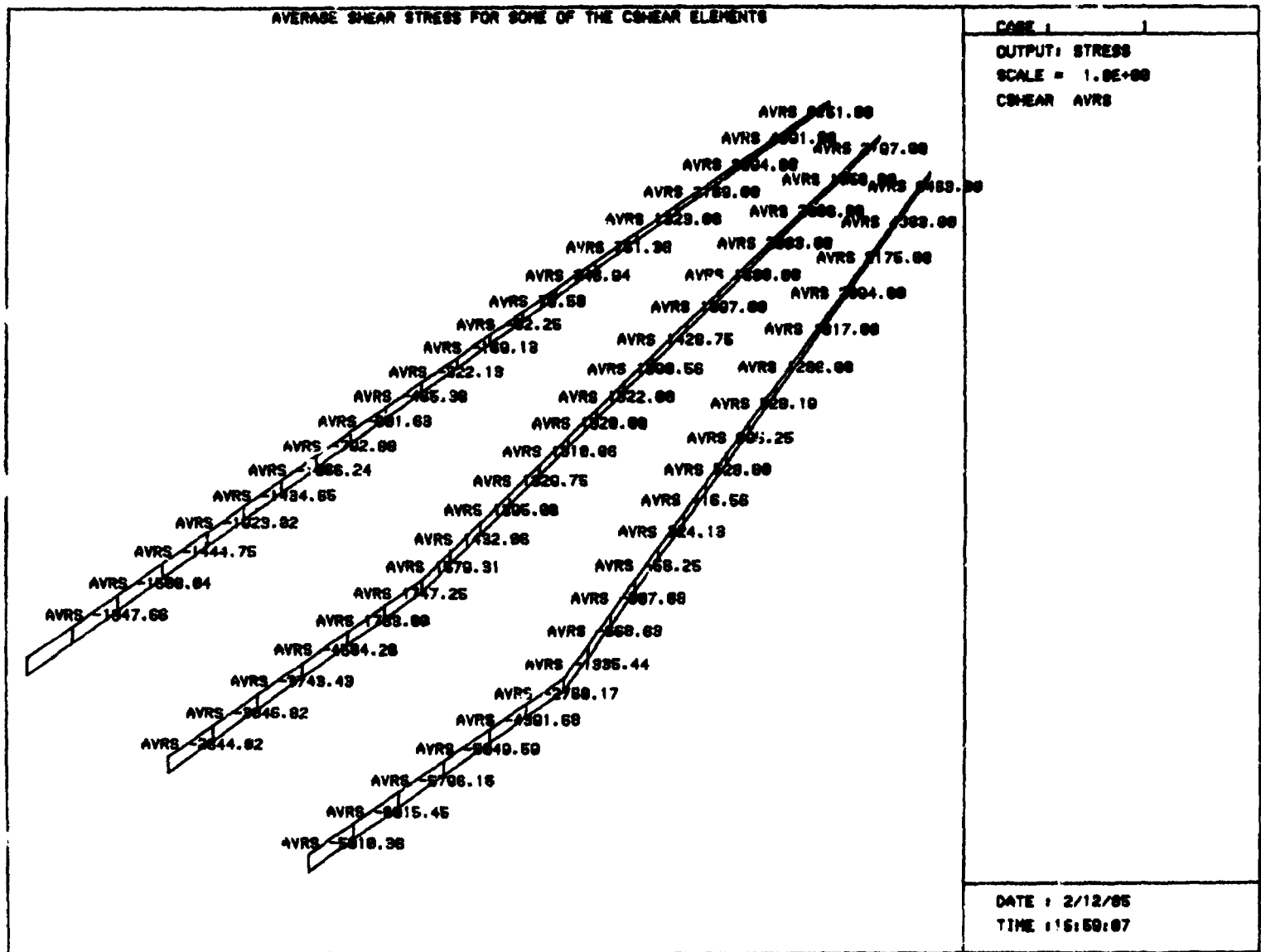


Figure 6. Average Shear Stress along the Spars of a Metallic Wing

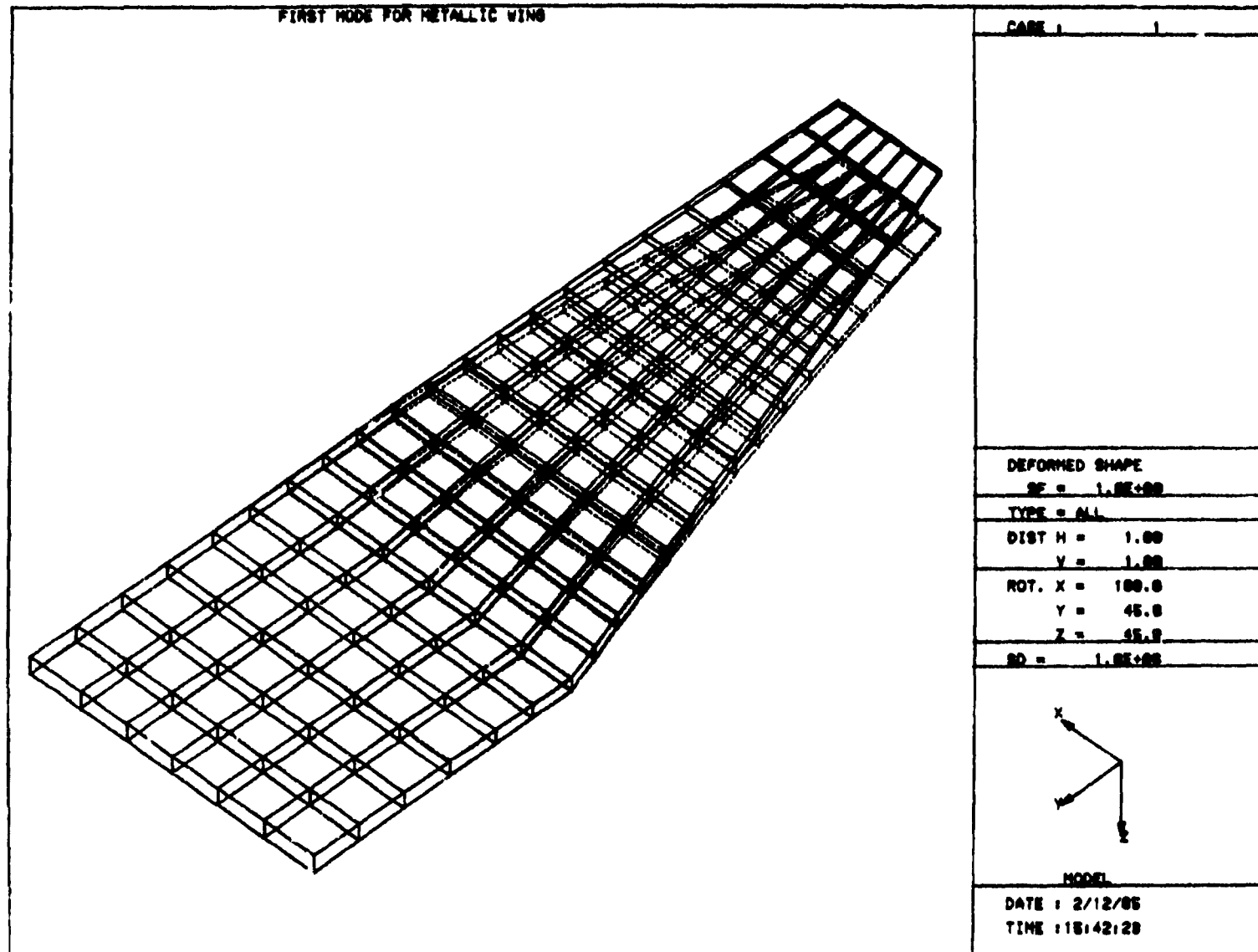


Figure 7. First Mode of a Metallic Wing

 ORIGINAL PAGE IS
 OF POOR QUALITY

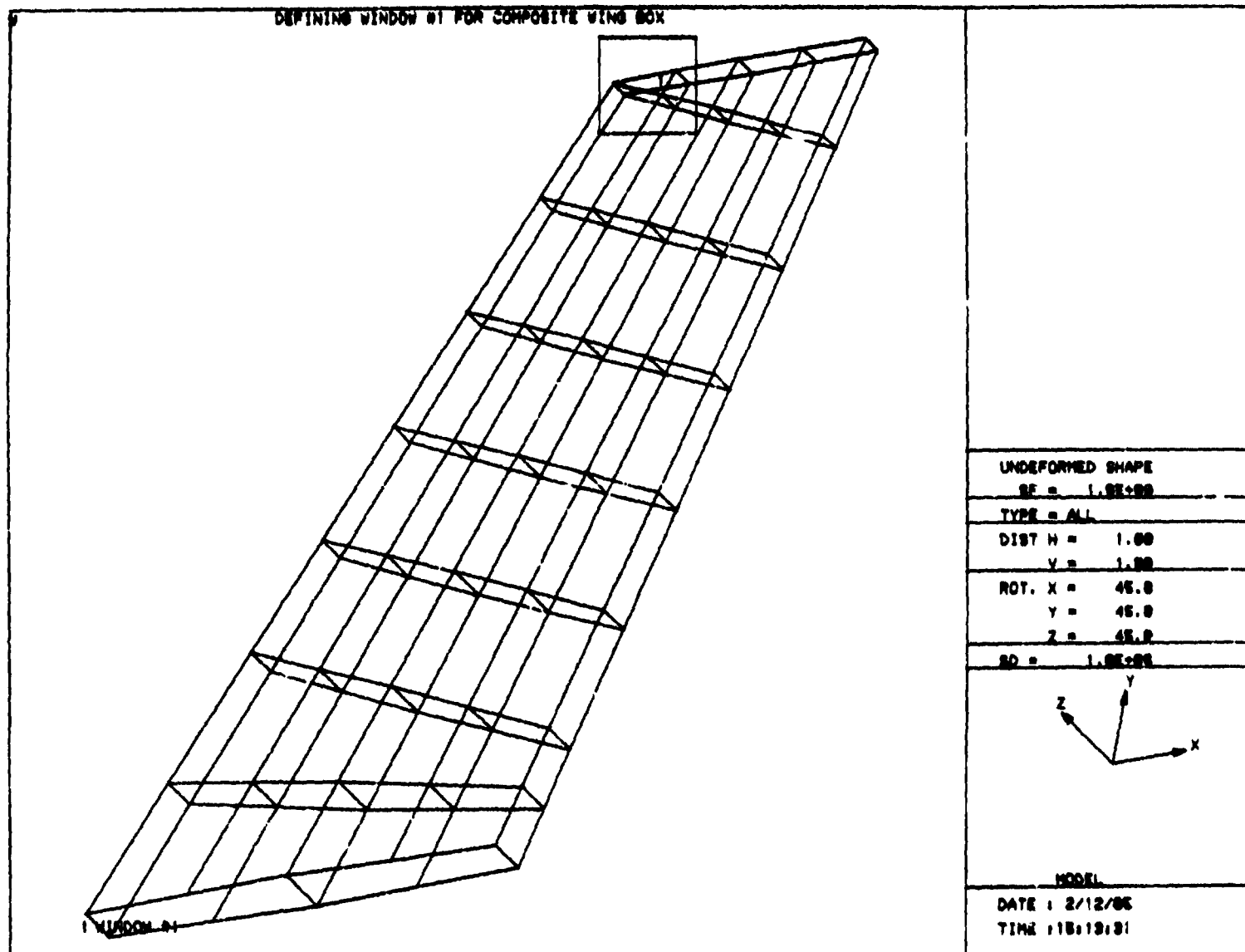


Figure 8a. Defining Window #1 on the Composite Wing

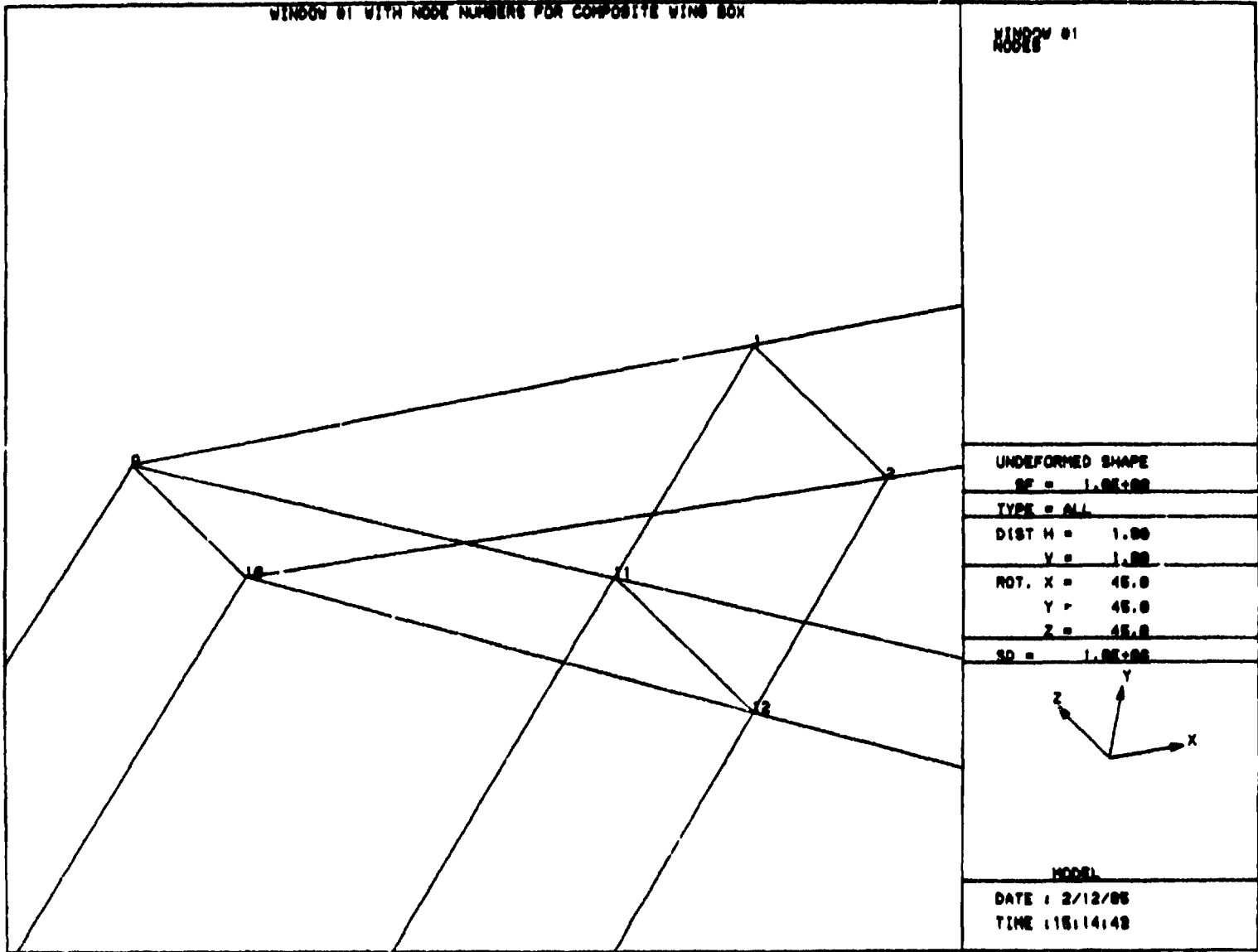


Figure 8b. Window #1 with Node Numbers

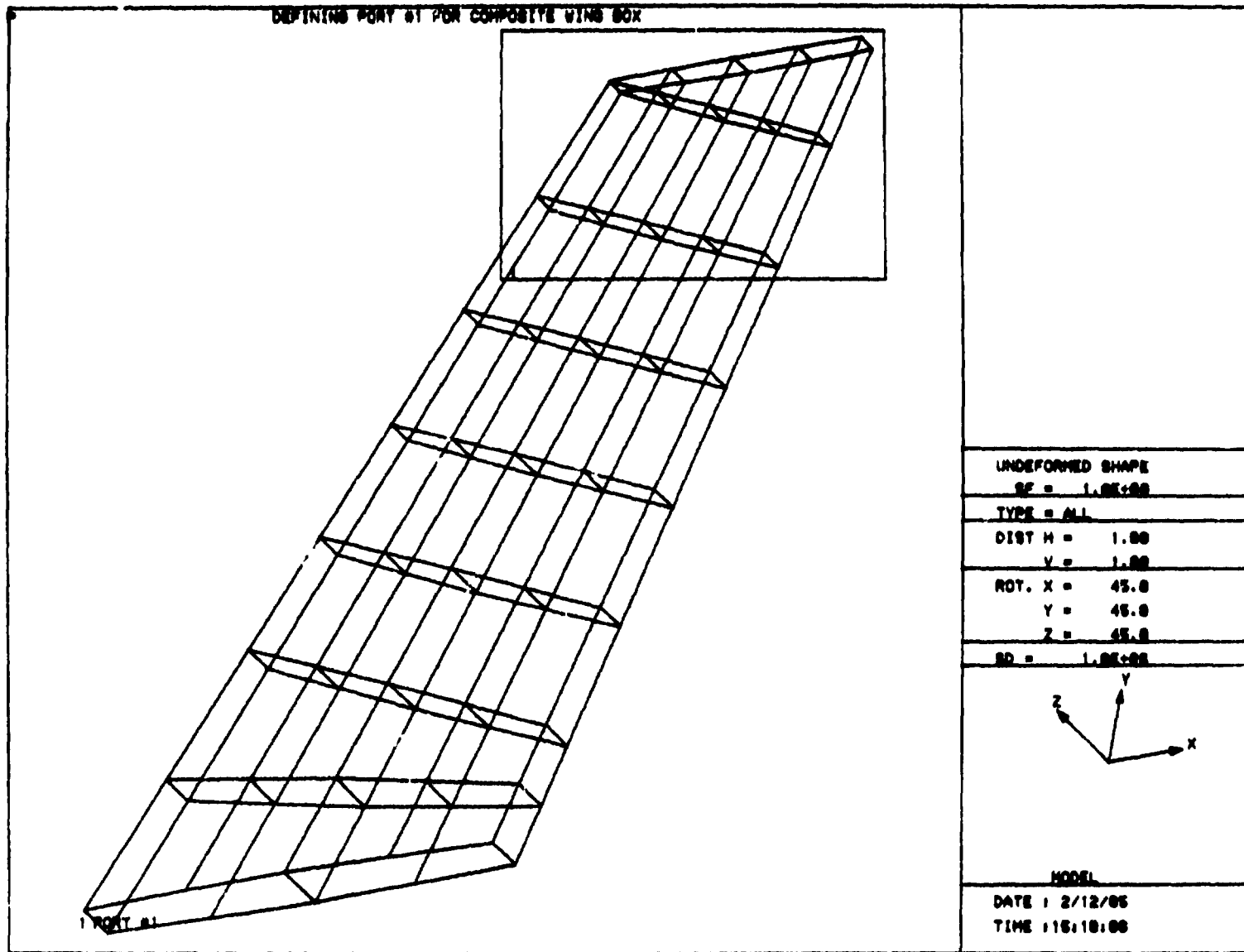


Figure 9a. Defining Port #1 on the Composite Wing

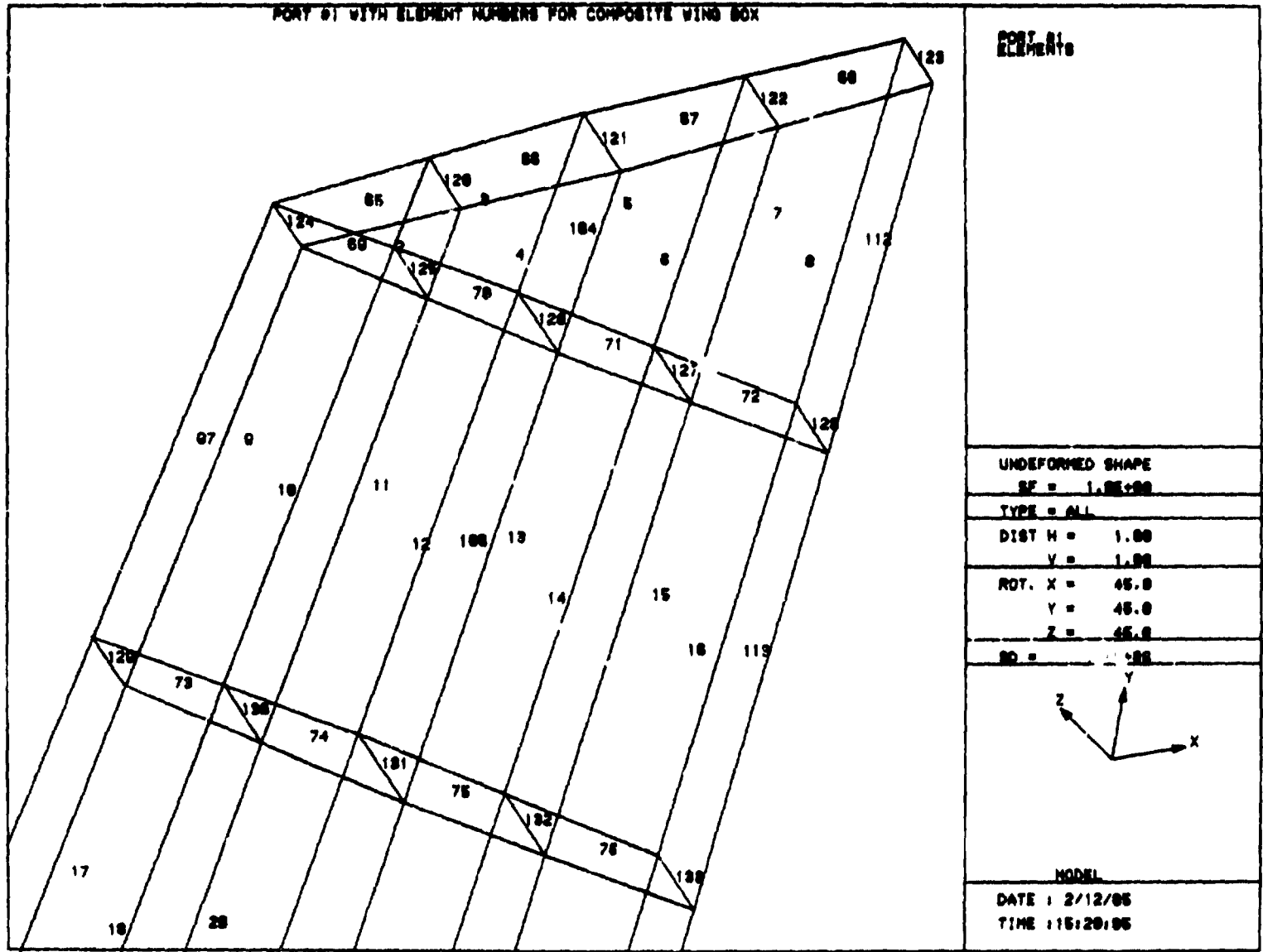


Figure 9o. Port #1 with Element Numbers

ORIGINAL PAGE IS
OF POOR QUALITY

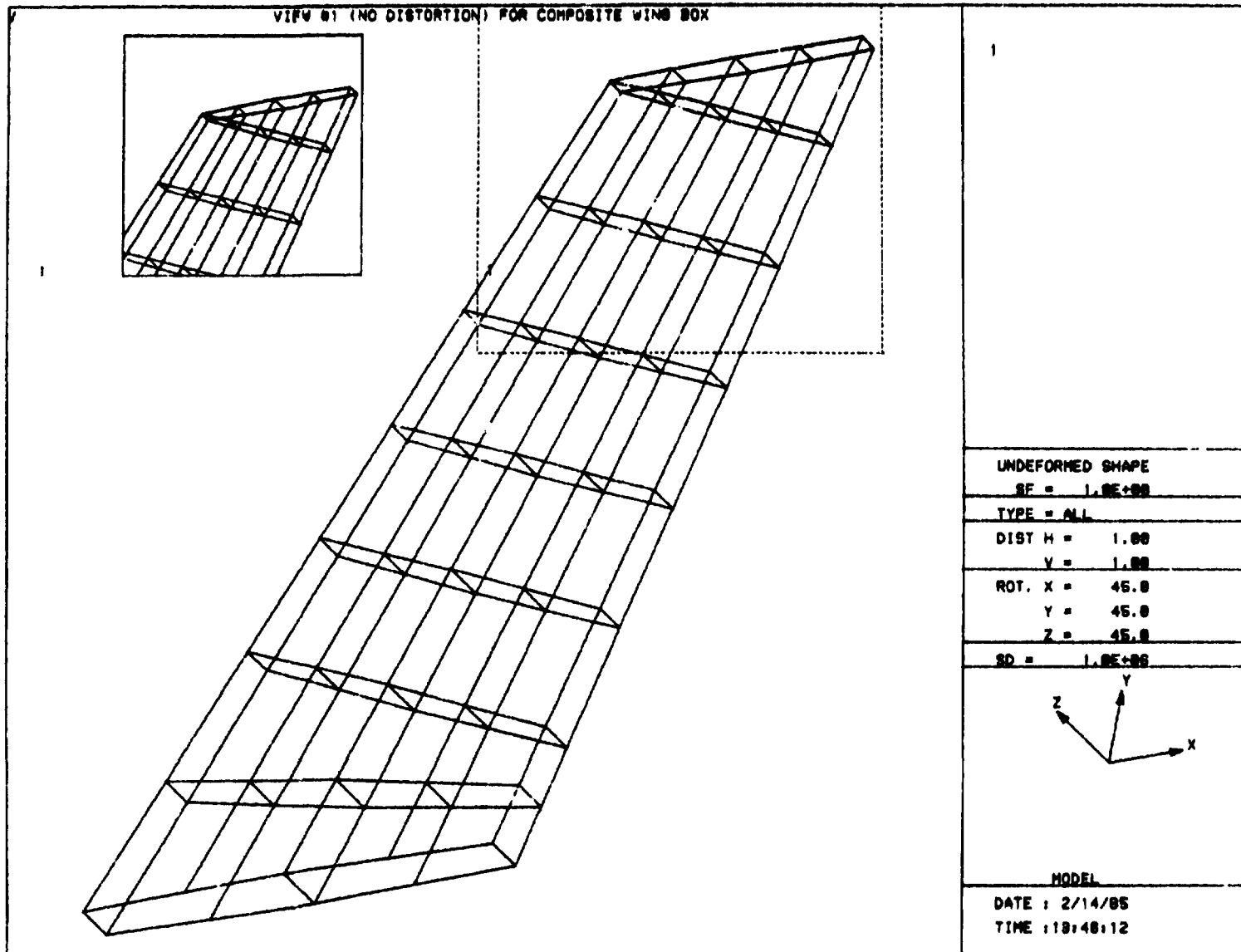


Figure 10. View Defined on a Composite Wing

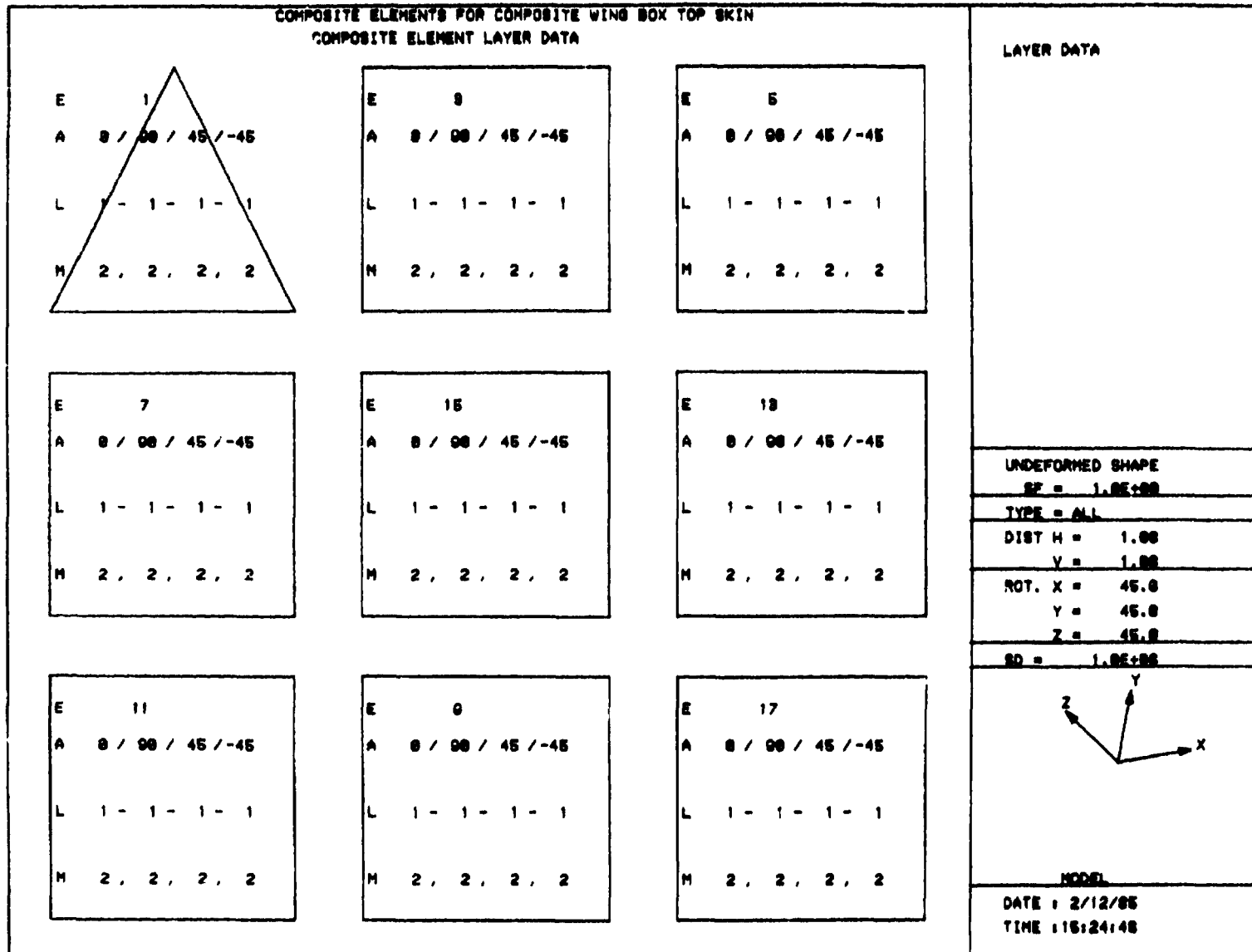


Figure 11. Composite Lamina Data for Selected Elements on the Top Skin of a Composite Wing

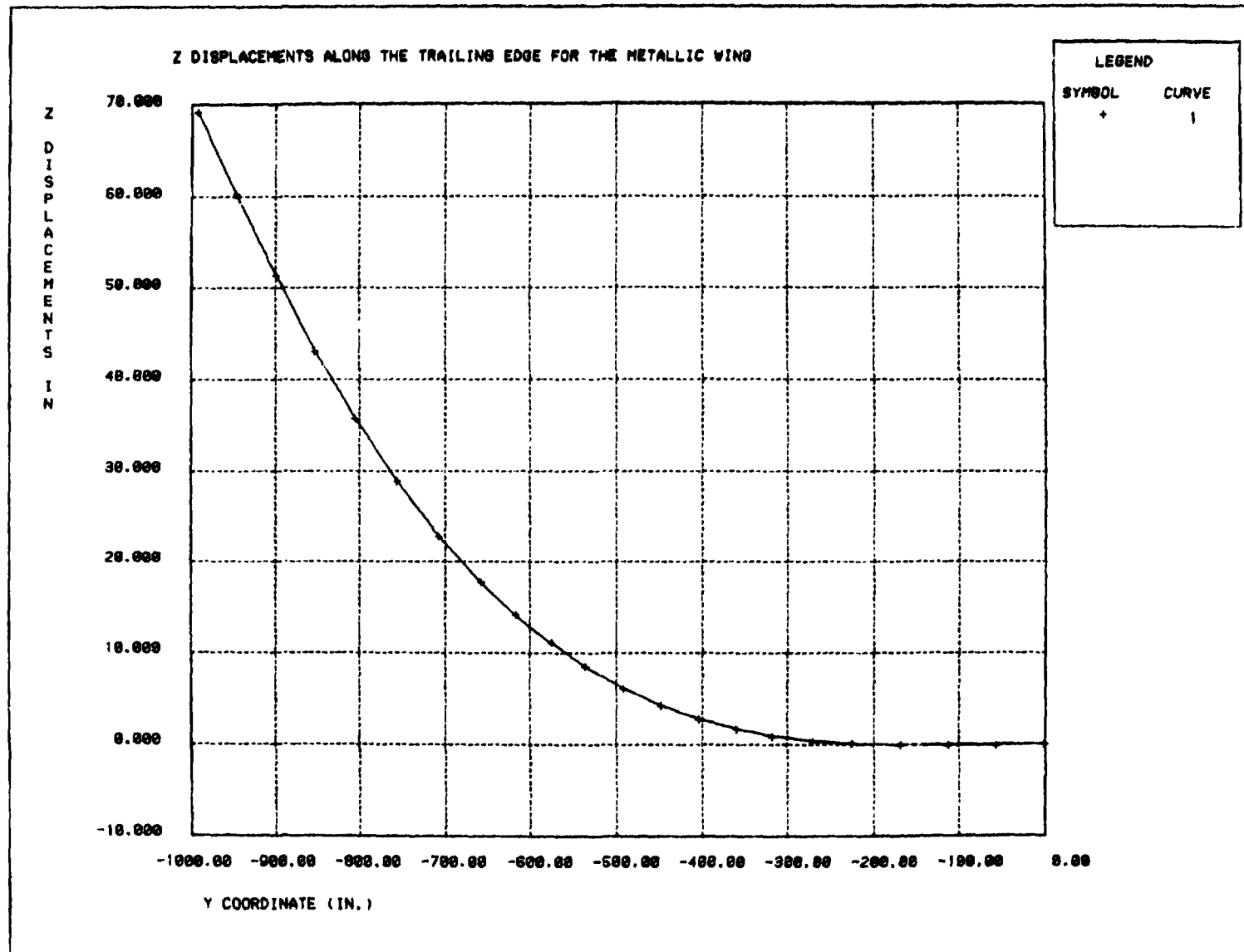


Figure 12. A Plot of the Z Displacements along the Trailing Edge of a Metallic Wing

N85-25877

RITZ PROCEDURE FOR COSMIC/NASTRAN

R. L. Citerley and P. J. Woytowicz
Anamet Laboratories, Inc., San Carlos, CA 94070

SUMMARY

An analysis procedure has been developed and incorporated into COSMIC/NASTRAN that permits large dynamic degree of freedom models to be processed accurately with little or no extra effort required by the user. The method employs existing capabilities without the need for approximate Guyan reduction techniques. Comparisons to existing solution procedures presently within NASTRAN are discussed.

INTRODUCTION

The search for an effective method for performing a dynamic analysis of complex structures has been under continuing study for many decades. In order to reduce the number of governing equations, the usual approach was to use modal coordinates. These modal coordinates are developed by employing classical eigenvalue extraction procedures. With this approach as the accepted analysis procedure, a concerted effort starting in the 1950's was made in developing various eigenvalue extraction methods. Several of these options presently exist in NASTRAN to develop these dynamic properties.

In pursuit of efficient and accurate eigenvalue methods, Jennings (Ref. 1) gives a rather brief but complete review of methods for solving dynamic equations to determine characteristic responses. The Lanczos method was reported as one of the more efficient methods for the solution of structural eigenvalue problems. Further investigation by Nour-Omid et al. (Ref. 2), illustrated that the Lanczos method had tremendous advantages over other classical eigenvalue extraction methods. With all the various eigenvalue procedures available, the choice of which numerical procedure should be used for solving a dynamic response problem depends upon the problem characteristics and solution requirements.

The solution process for the dynamic analysis developed in NASTRAN is separated into three phases: assembly, solution, and response recovery. As pointed out in Section 4.0 of the NASTRAN Theoretical Manual, as problem size increases, the cost of the first and third phases increases linearly; whereas the second increases cubically with the number of degrees of freedom. The eigenvalue solution phase is usually considered the most costly.

Wilson (Ref. 3) demonstrated how the eigenvalue procedure could be circumvented. He classified it as the "Ritz" method. Arnold et al. (Ref. 4), demonstrated how the Ritz procedure could be incorporated into MSC/NASTRAN and showed that it would be less costly and more efficient than previous techniques. Reference 4 also discusses the relationship between Lanczos and Ritz.

Other methods using the basic concept of Lanczos have been suggested by Gupta (Ref. 5) using a Lanczos-Householder algorithm, Newman and Flanagan (Ref. 6) using FEER, and by Newman and Mann (Ref. 7) using complex FEER methods for COSMIC/NASTRAN. These methods differ from the present case in the selection process of the starting vectors. Also, the method of obtaining the additional vectors is different.

TECHNICAL DISCUSSION

Although the use of Ritz vectors can be applied to the dynamic analysis of any linear system, it is particularly well suited to application in the field of dynamic structural analysis. The nature of certain dynamic loadings, or rather the analytical representation of the loadings, allows the Ritz approach to almost assuredly use fewer modes for the same accuracy as a conventional analysis using natural frequencies and mode shapes. The use of a static load vector in the dynamic excitation direction in deriving the starting Ritz vector eliminates the need for a static correction due to higher order modes.

As mentioned earlier, the solution of the eigenvalue problem for large systems is the major computational task involved in dynamic analysis. For very large systems, this task is often not even practical, and instead is supplemented with an additional step of static condensation and Guyan reduction, or by use of substructuring techniques. All these techniques are acceptable and are in standard practice with COSMIC/NASTRAN today; however, all involve the solution of large eigenvalue problems even if the total problem has been reduced into workable substructures. The Ritz algorithm, to be defined in detail later, allows the analyst to bypass the solution of a large eigenvalue problem, and instead solve a smaller eigenvalue problem involving only the Ritz modes of significance to the analysis. Nour-Omid and Clough (Ref. 8) have shown how even this step could be eliminated. Also presented here is a method of using an error norm to define the number of Ritz vectors required to obtain accurate dynamic analysis results.

Derivation of Ritz Vectors

Given a physical system whose mass and stiffness properties have been discretized to N degrees of freedom given by the structure mass matrix, M , and structure stiffness matrix, K , the initial step in the algorithm is to factor K such that

$$K = LDL^T \quad (1)$$

The starting vector x_1^* can then be obtained by solving

$$Kx_1^* = f \quad (2)$$

where f is a static load vector which represents the spatial distribution of the dynamic loading.

Once the first Ritz vector x_1^* is obtained, an iterative process is begun for the solution of a full L set of Ritz vectors. This process can be divided into three steps which are given below.

Step 1: Solution for x_i^* is made using the factored stiffness matrix from Equation (1)

$$Kx_i^* = Mx_{i-1} \quad (3)$$

Step 2: $i = i + 1$, if $i \leq L$ go to 1, otherwise proceed

Step 3: Orthogonalize x_i^* with respect to previous $i - 1$ vectors

$$c_j = x_j^T Mx_i^*, \quad j = 1, \dots, i - 1 \quad (4)$$

$$x_i^{**} = x_i^* - \sum_{j=1}^{i-1} c_j x_j \quad (5)$$

and normalize with respect to M to find x_i

$$x_i^T Mx_i = 1 \quad (6)$$

The result of this iterative process is an N by L matrix of vectors, X , which is mass orthogonal, but still must be orthogonalized with respect to the stiffness matrix. The final set of Ritz vectors must be mass and stiffness orthogonal to uncouple the equations of motion, and this orthogonalization can be accomplished by solving the following eigenvalue problem for z_i ,

$$[K^* - \omega_i^2 M^*]z_i = 0 \quad (7)$$

where $K^* = X^T K X$ (8)

$$M^* = X^T M X = I \quad (9)$$

The final matrix of Ritz vectors, 0X , is then obtained using the matrix of z_i vectors, Z , as a transformation for X ,

$${}^0X = XZ \quad (10)$$

Error Norm Definition

The definition of an error norm is a key element in application of the Ritz algorithm. Wilson originally devised an error norm defined as

$$e = \frac{f^T (f - \sum_j p_j M {}^0x_j)}{f^T f} \quad (11)$$

where

$$p_j = {}^0x_j^T f = \text{participation factor} \quad (12)$$

and the vectors 0x_j are the final mass and stiffness orthogonal Ritz vectors obtained from Equation (10). This error norm varies from $e = 1.0$ if no vectors are used, to $e = 0.0$ if all vectors are used. Arnold, Citerley, et al., used this same definition of error, but applied it using the non-stiffness-orthogonalized Ritz vectors x_j , rather than 0x_j . This definition then permits error estimation prior to eigenvalue extraction performed on Equation (7). In addition, they established another error norm to quantify the influence of the input excitation frequency content on the adequacy of the selected Ritz vectors. Examination of this type of error norm will be required for high frequency input excitation.

IMPLEMENTATION INTO NASTRAN AND NUMERICAL RESULTS

The Ritz procedure was implemented into NASTRAN using the DMAP capabilities. A flow chart of a typical DMAP alter is shown in Figure 1. The procedure has been incorporated into SOL 3, 11, and 12. Although details of the DMAP alter are slightly different for each rigid format, the flow chart of Figure 1 outlines the general procedure.

Block 1 of Figure 1 processes the static loads. As many subcases as necessary are input by the user to generate the static loads which are to represent the spatial distribution of the dynamic loads. Modules SSG1, SSG2, and SSG3 are used for the processing and subsequent set reduction.

Block 2 of Figure 1 uses the lower triangular factor of the stiffness matrix (L of Equation (1)) to solve for the first set of vectors. Block 3 is a loop, which calculates additional vectors described previously.

Block 4 uses a dummy module, MODB, to orthonormalize the generated vectors (see Equations (4-6)). Block 5 then calculates the generalized mass and stiffness matrices of Equations (8) and (9). Block 6 uses the READ module to perform the eigenvalue/eigenvector analysis of Equation (7) and form the Ritz vectors using Equation (10). Finally, Block 7 equivalences the Ritz vectors to the regular A set eigenvectors (PHIA) for subsequent use in the DMAP rigid format.

A dummy module, MODB, was written to perform several tasks depending upon the input parameters. It is used in Block 3 to append the newly calculated vectors to the previous vectors. Additionally, although not shown, it was found necessary to normalize the newly computed vectors in Block 3 after each pass through the loop in order to prevent numerical round-off problems. This was also performed by the dummy module. The dummy module's final job was to orthonormalize the vectors in Block 4, using the Gram-Schmidt orthonormalization procedure.

The Ritz procedure was previously implemented into the MacNeal-Schwendler version of NASTRAN. Comparisons of the Ritz procedure to MSC/NASTRAN's Generalized Dynamic Procedure have been reported (Ref. 3). The Ritz procedure was also compared to COSMIC/NASTRAN's FEER method. Table 1 presents frequency comparisons and total CPU time using the FEER method and the Ritz method on a relatively small problem. As can be seen, both methods yield similar results, the Ritz method being slightly faster.

However, it is not proper to directly compare the FEER method with Ritz, since they are intended to serve different purposes. The FEER (or any other eigen-extraction) routine is designed to find all the eigenvalues and associated eigenvectors below a certain user specified number. These modes may or may not be good representations for use in a forced dynamic response. Often it is found that only certain modes participate due to the nature of the forcing function. The Ritz method uses static representations of the dynamic

forces applied as a basis for its "eigenvectors". The only "modes" calculated correspond to those excited by the forcing function. Therefore, fewer unnecessary modes are used; additionally, as pointed out previously, static corrections (such as Modal Acceleration) techniques are not necessary, since the Ritz vectors necessarily accurately represent the total force applied to the structure.

CONCLUSIONS

The Ritz procedure for dynamic analysis has been presented. The procedure is related to other popular methods of eigenvalue/eigenvector analysis; however, it does not attempt to obtain all the modes of the system. Instead, only those "modes" which are excited by the dynamic loading are obtained.

A flow chart of the DMAP implementation has been presented. NASTRAN's DMAP capability, along with the use of a dummy module, made this implementation fairly simple. The method was compared to the FEER method for one problem. The predicted frequencies compared well, while the cost of the Ritz method was less. The same conclusions were shown by Arnold, Citerley, et al. with more dramatic cost savings for very large analysis problems. These results clearly demonstrate the impact that the Ritz algorithm can have on reducing analysis cost.

The benefits of the Ritz algorithm in dynamic analysis can therefore be summarized as:

1. Order of magnitude reduction in deriving eigenvalues and eigenvectors for mode superposition analysis.
2. Better accuracy for fewer vectors.
3. No static correction needed for higher order modes.
4. No static condensation or Guyan reduction required for large systems.
5. Error estimation can be made to determine the adequacy of selected Ritz vectors.

REFERENCES

1. Jennings, A., "Eigenvalue Methods for Vibration Analysis II," Shock & Vibration Digest, Vol. 16, No. 1, Jan. 1984.
2. Nour-Omid, B., Parlett, B. N., and Taylor, R. L., "Lanczos versus Subspace Iteration for Solution of Eigenvalue Problems," Int. J. for Numerical Methods in Engineering, Vol. 19, pp. 859-871, 1983.

3. Wilson, E. L., Yuan, M., and Dickens, J., "Dynamic Analysis by Direct Superposition of Ritz Vectors," Earthquake Engineering and Structural dynamics, Vol. 10, 1982.
4. Arnold, R. R., Citerley, R. L., Chargin, M., and Galant, D., "Application of Ritz Vectors for Dynamic Analysis of Large Structures," presented at the Symposium on Advances and Trends in Structures and Dynamics, sponsored by NASA, Washington, DC, Oct. 1984, to be published in Computers and Structures.
5. Gupta, V., Cole, J., and Mock, W., "A Cost-Effective Eigensolution Method for Large Systems with Rockwell NASTRAN," Twelfth NASTRAN User's Colloquium, 1984.
6. Newman, M. and Flanagan, P. F., "Eigenvalue Extraction in NASTRAN by the Tridiagonal Reduction (FEER) Method - Real Eigenvalue Analysis," NASA CR-2731, Aug. 1976.
7. Newman, M. and Mann F., "Complex Eigenvalue Extraction in NASTRAN by the Tridiagonal Reduction (FEER) Method," NASA CR-145258, Sept. 1977.
8. Nur-Omid, B. and Clough, R. W., "Dynamic Analysis of Structures Using Lanczos Coordinates," Earthquake Engineering and Structural Dynamics, Vol. 12, pp. 565-577, 1984.

TABLE 1
 FREQUENCY AND TIME RESULTS FOR A SMALL MODEL,
 RITZ VERSUS FEER METHODS

MODE	CYCLIC FREQUENCY	
	RITZ (HZ)	FEER (HZ)
1	2.836471E+02	2.836471E+02
2	5.015972E+02	5.015972E+02
3	7.418652E+02	7.401528E+02
4	8.908441E+02	8.792196E+02
5	9.876880E+02	9.876871E+02
6	1.189213E+03	1.189210E+03
7	1.902981E+03	1.691335E+03
8	2.178580E+03	2.165648E+03
9	2.852047E+03	2.467984E+03
10	3.239252E+03	2.906139E+03
Total Run Time (cpu-sec)	218	270

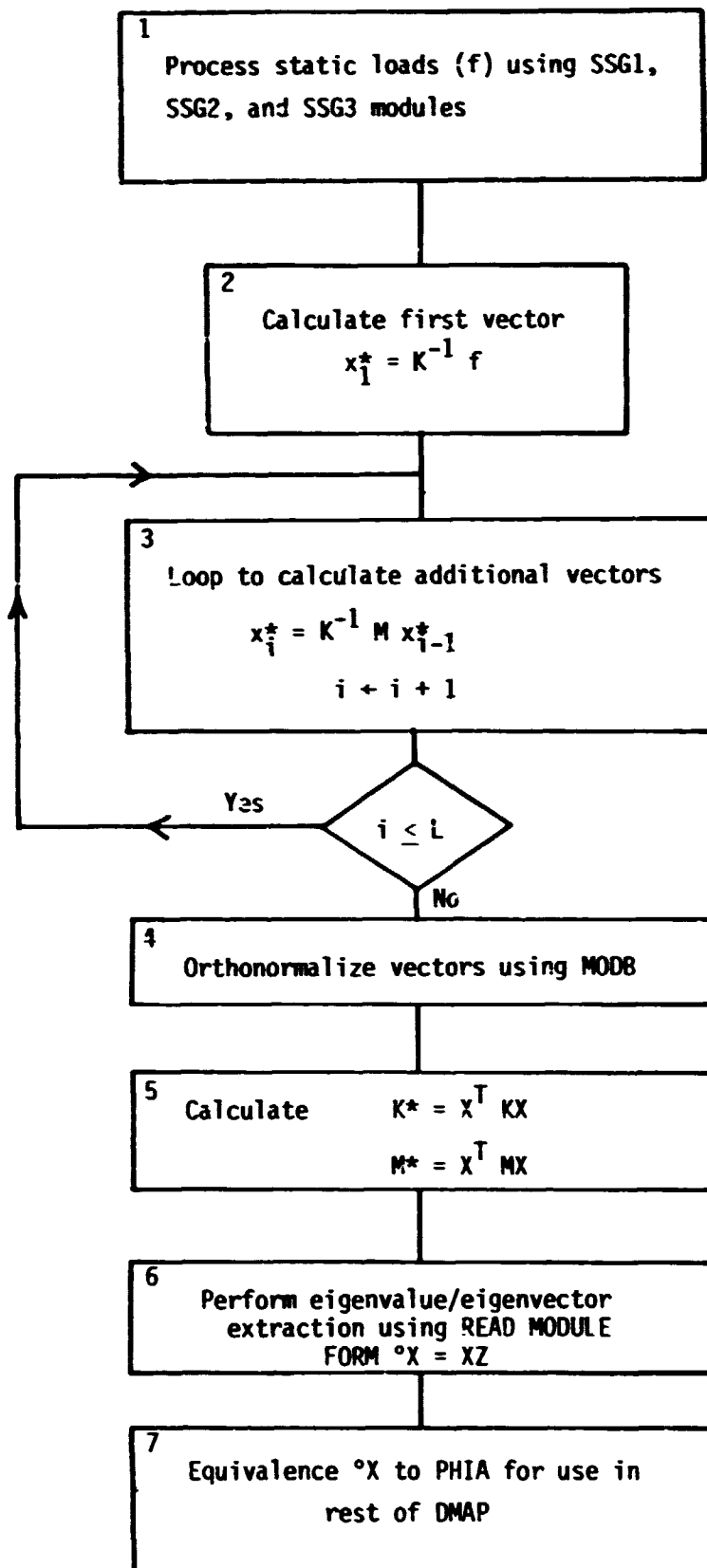


Figure 1 Flow Chart for Implementing Ritz Procedure into NASTRAN

N85-25878

SYMMETRIC COMPOSITE LAMINATE STRESS ANALYSIS

T. Wang, K. F. Smolinski, and S. Gellin
Bell Aerospace Textron, Buffalo, New York

SUMMARY

In this paper it is demonstrated that COSMIC/NASTRAN may be used to analyze plate and shell structures made of symmetric composite laminates. Although general composite laminates cannot be analyzed using NASTRAN, the theoretical development presented herein indicates that the integrated constitutive laws of a symmetric composite laminate resemble those of a homogeneous anisotropic plate, which can be analyzed using NASTRAN. A detailed analysis procedure is presented, as well as an illustrative example.

INTRODUCTION

Composite laminates have been used in many engineering structures recently, and researchers in this field have developed many finite element programs [1]. To date, the composite laminate theory has not been incorporated into any NASTRAN plate element formulation [2].

The governing equilibrium equations for symmetric laminates resemble those for anisotropic plates [3]. Since NASTRAN possesses the capability to analyze anisotropic plates, symmetric laminates can be analyzed using NASTRAN if the equivalent anisotropic plate material properties can be obtained.

The purpose of this study is to obtain equivalent anisotropic plate material properties for symmetric laminates consistent with the governing plate theory, and thus extend the capability of NASTRAN to include analysis of symmetric laminates. This theoretical formulation is given in the next section. Subsequently, a step-by-step analysis procedure and an illustrative example problem are presented.

THEORY

The classical laminate theory [4] will be used. A Cartesian coordinate system is assumed with the x-y plane located at the midplane of the laminate. The normal coordinate is z, and the total laminate thickness is h. The laminate consists of perfectly bonded laminae. If h is considered small compared to the x and y dimensions of the laminate, the Kirchoff hypothesis may be assumed to be applicable. The displacements can then be written as

$$\left. \begin{aligned} u &= U_0 - z \frac{\partial W_0}{\partial x} \\ v &= V_0 - z \frac{\partial W_0}{\partial y} \\ w &= W_0 \end{aligned} \right\} \quad (1)$$

where U_0 , V_0 , and W_0 are the midplane displacements in the x , y , and z directions, respectively. The strains at distance z from the midplane can be written as

$$\begin{Bmatrix} \epsilon_x \\ \epsilon_y \\ \gamma_{xy} \end{Bmatrix} = \begin{Bmatrix} \epsilon_x^0 \\ \epsilon_y^0 \\ \epsilon_{xy}^0 \end{Bmatrix} + z \begin{Bmatrix} \kappa_x \\ \kappa_y \\ \kappa_{xy} \end{Bmatrix} \quad (2)$$

where

$$\left. \begin{aligned} \epsilon_x^0 &= \frac{\partial U_0}{\partial x}; \quad \epsilon_y^0 = \frac{\partial V_0}{\partial y}; \quad \epsilon_{xy}^0 = \frac{\partial U_0}{\partial y} + \frac{\partial V_0}{\partial x}; \\ \kappa_x &= -\frac{\partial^2 W_0}{\partial x^2}; \quad \kappa_y = \frac{\partial^2 W_0}{\partial y^2}; \quad \kappa_{xy} = -\frac{\partial^2 W_0}{\partial x \partial y} \end{aligned} \right\} \quad (3)$$

The constitutive law at any point in the laminate may be written in the form

$$\begin{Bmatrix} \sigma_x \\ \sigma_y \\ \tau_{xy} \end{Bmatrix} = \begin{bmatrix} \bar{Q}_{11} & \bar{Q}_{12} & \bar{Q}_{16} \\ \bar{Q}_{12} & \bar{Q}_{22} & \bar{Q}_{26} \\ \bar{Q}_{16} & \bar{Q}_{26} & \bar{Q}_{66} \end{bmatrix} \begin{Bmatrix} \epsilon_x \\ \epsilon_y \\ \gamma_{xy} \end{Bmatrix} \quad (4)$$

where $(\sigma_x, \sigma_y, \tau_{xy})$ are the stresses and the \bar{Q}_{ij} are the reduced moduli.

Relations between the stress and moment resultants and the stretching and curvature strains are obtained by integrating Equation (4) through the thickness; specifically,

$$\begin{Bmatrix} N_x \\ N_y \\ N_{xy} \\ M_x \\ M_y \\ M_{xy} \end{Bmatrix} = \begin{bmatrix} A_{11} & A_{12} & A_{16} & B_{11} & B_{12} & B_{16} \\ A_{12} & A_{22} & A_{26} & B_{12} & B_{22} & B_{26} \\ A_{16} & A_{26} & A_{66} & B_{16} & B_{26} & B_{66} \\ B_{11} & B_{12} & B_{16} & D_{11} & D_{12} & D_{16} \\ B_{12} & B_{22} & B_{26} & D_{12} & D_{22} & D_{26} \\ B_{16} & B_{26} & B_{66} & D_{16} & D_{26} & D_{66} \end{bmatrix} \begin{Bmatrix} \epsilon_x^0 \\ \epsilon_y^0 \\ \gamma_{xy}^0 \\ \kappa_x \\ \kappa_y \\ \kappa_{xy} \end{Bmatrix} \quad (5)$$

where

$$(A_{ij}, B_{ij}, D_{ij}) = \int_{-h/2}^{h/2} \bar{Q}_{ij} (1, z, z^2) dz \quad (6)$$

Presently, the general form Equation (5) is not used for any plate element in NASTRAN; however, if the laminate is symmetric, then $B_{ij}=0$, and thus the inplane extension and out of plane bending effects decouple. Equivalent anisotropic constitutive laws can be written for each effect. For in plane extension, the equivalent stress-strain law is

$$\begin{Bmatrix} \sigma_x \\ \sigma_y \\ \tau_{xy} \end{Bmatrix} = \frac{1}{h} \begin{bmatrix} A_{11} & A_{12} & A_{16} \\ A_{12} & A_{22} & A_{26} \\ A_{16} & A_{26} & A_{66} \end{bmatrix} \begin{Bmatrix} \epsilon_x \\ \epsilon_y \\ \gamma_{xy} \end{Bmatrix} \quad (7)$$

and for bending it is

$$\begin{Bmatrix} \sigma_x \\ \sigma_y \\ \tau_{xy} \end{Bmatrix} = \frac{12}{h^3} \begin{bmatrix} D_{11} & D_{12} & D_{16} \\ D_{12} & D_{22} & D_{26} \\ D_{16} & D_{26} & D_{66} \end{bmatrix} \begin{Bmatrix} \epsilon_x \\ \epsilon_y \\ \gamma_{xy} \end{Bmatrix} \quad (8)$$

The coefficients in Equations (7) and (8) are denoted as the equivalent anisotropic material properties. Since NASTRAN can be used for the stress analysis of a homogeneous anisotropic plate, it can thus be used for symmetric laminate stress analysis.

THE ANALYSIS PROCEDURE

Incorporating the aforementioned theory into NASTRAN for symmetric laminate stress analysis is not a straightforward task. The analysis procedure may be outlined as follows:

- (1) The theoretical development presented above is used to calculate the coefficients of Equations (7) and (8). The results are inputted to NASTRAN by using MAT2 cards.
- (2) To analyze plate or shallow shell structures, plate elements CTRIA1 and/or CQUAD1 are used, with associated MAT2 cards. Output will include grid point displacements and the midplane stretching and curvature strains of each element.
- (3) The strains in each layer of the element are calculated using Equation (2) and the stresses in the layer are calculated using Equation (4).
- (4) The stresses in each layer are transformed to the principal material directions and the failure criterion [5]

$$\left(\frac{\sigma_1}{S_1}\right)^2 + \left(\frac{\sigma_2}{S_2}\right)^2 - \left(\frac{\sigma_1 \sigma_2}{S_1 S_1}\right) + \left(\frac{\sigma_{12}}{S_{12}}\right)^2 = F \quad (9)$$

is used for ply failure evaluation. If the value of F exceeds unity, that layer is failed.

EXAMPLE PROBLEM

A Kevlar 49*/Epoxy cylindrical shell with $[-60/0/60]_{3s}$ layup is used to illustrate the analysis procedure. The geometry and finite element mesh are shown in Figure 1. The mechanical properties in principal material directions 1 and 2 of a unidirectionally reinforced lamina are

$$E_{11} = 7.6 \times 10^{10} \text{ Pa}$$

$$E_{22} = 5.5 \times 10^9 \text{ Pa}$$

$$G_{12} = 2.1 \times 10^9 \text{ Pa}$$

$$\nu_{12} = 0.34$$

where the 1 and 2 directions are parallel and normal to the fiber direction, respectively. The ultimate strengths of the lamina are

$$(S_1)_T = 1.38 \times 10^9 \text{ Pa}$$

$$(S_1)_C = -2.76 \times 10^8 \text{ Pa}$$

$$(S_2)_T = 2.96 \times 10^7 \text{ Pa}$$

$$(S_2)_C = -1.38 \times 10^8 \text{ Pa}$$

$$S_{12} = 6.00 \times 10^7 \text{ Pa}$$

where T and C denote tension and compression, respectively. The shell was subjected to 6895 Pa (1 psi) uniform pressure and its periphery was pinned.

The equivalent homogeneous anisotropic plate constitutive law for in plane calculation was calculated as

$$\begin{Bmatrix} \sigma_x \\ \sigma_y \\ \tau_{xy} \end{Bmatrix} = \begin{bmatrix} 3.225 \times 10^{10} & 1.071 \times 10^{10} & 0 \\ 1.071 \times 10^{10} & 3.225 \times 10^{10} & 0 \\ 0 & 0 & 1.080 \times 10^{10} \end{bmatrix} \begin{Bmatrix} \epsilon_x \\ \epsilon_y \\ \gamma_{xy} \end{Bmatrix}$$

while for bending it was

$$\begin{Bmatrix} \sigma_x \\ \sigma_y \\ \tau_{xy} \end{Bmatrix} = \begin{bmatrix} 3.178 \times 10^{10} & 1.075 \times 10^{10} & -17.25 \times 10^9 \\ 1.075 \times 10^{10} & 3.178 \times 10^{10} & -5.096 \times 10^9 \\ -1.725 \times 10^9 & -5.096 \times 10^9 & 1.093 \times 10^{10} \end{bmatrix} \begin{Bmatrix} \epsilon_x \\ \epsilon_y \\ \gamma_{xy} \end{Bmatrix}$$

The input to NASTRAN was made according to Step (2) of the procedure given above.

The output displacement contours in the x, y, and z directions are shown in Figures 2, 3, and 4, respectively. Note that these deformations are not symmetric with respect to the centerlines of the shell. This is due to the presence of the D_{16} and D_{26} terms.

Table 1 summarizes the layer stresses in principal material directions for a typical element. The small values of F indicate that no ply failures occur.

*Kevlar 49 aramid fibers, manufactured by E. I. duPont de Nemours & Co., Inc.

CONCLUSIONS AND SUGGESTIONS

NASTRAN has been demonstrated to be a feasible tool for the stress analysis of symmetric composite laminates, though equivalent anisotropic material properties and layer stress calculations must be performed outside the NASTRAN framework. To increase the NASTRAN analysis capability to unsymmetric laminate and to simplify the analysis procedure, it would be worthwhile to incorporate the newly developed composite laminate finite element programs into NASTRAN in order to analyze the ever-increasing number of composite laminate structures.

REFERENCES

1. J. N. Reddy, "A Penalty Plate-Bending Element for the Analysis of Laminated Anisotropic Composite Plates", *Int. J. Num. Meth. Engng.*, Vol. 15, p. 1187, 1980.
2. The NASTRAN Theoretical Manual.
3. J. E. Ashton, J. C. Halpin, P. H. Petit, "Primer on Composite Materials", Technomic Publishing Co., 1969, p. 63.
4. R. M. Jones, "Mechanics of Composite Materials", Scripta Book Company, Washington, D.C., 1975.
5. S. W. Tsai, "Strength Theories of Filamentary Structures", in R. T. Schwartz and H. S. Schwartz (eds.), *Fundamental Aspects of Fiber Reinforced Plastic Composites*, Wiley Interscience, New York, 1968, p. 3.

TABLE 1. LAMINATE STRESSES IN PRINCIPAL MATERIAL DIRECTIONS AND FAILURE PARAMETER (F) OF ELEMENT 85

PLY NO.	σ_1 (Pa)	σ_2 (Pa)	τ_{12} (Pa)	F
1	8.136×10^6	-2.275×10^6	-2.048×10^5	0.000
2	-2.779×10^7	-6.102×10^5	-8.963×10^5	0.010
3	-2.055×10^7	-1.027×10^6	1.144×10^6	0.006
4	6.405×10^6	-2.427×10^6	-2.930×10^5	0.000
5	-3.075×10^7	-6.798×10^5	-8.481×10^5	0.012
6	-2.075×10^7	-1.248×10^6	1.186×10^6	0.006
7	4.675×10^6	-2.579×10^6	-3.820×10^5	0.000
8	-3.372×10^7	-7.722×10^5	-7.998×10^5	0.015
9	-2.096×10^7	-1.475×10^6	1.227×10^6	0.006
10	-2.103×10^7	-1.551×10^6	1.234×10^6	0.006
11	-3.668×10^7	-8.618×10^5	-7.515×10^5	0.017
12	1.793×10^6	-2.834×10^6	-5.288×10^5	0.001
13	-2.124×10^7	-1.779×10^6	1.276×10^6	0.006
14	-3.964×10^7	-9.515×10^5	-7.033×10^5	0.020
15	6.143×10^6	-2.985×10^6	-6.178×10^5	0.001
16	-2.144×10^7	-2.006×10^6	1.317×10^6	0.006
17	-4.261×10^7	-1.041×10^6	-6.536×10^5	0.023
18	-1.668×10^6	-3.137×10^6	-7.033×10^5	0.001

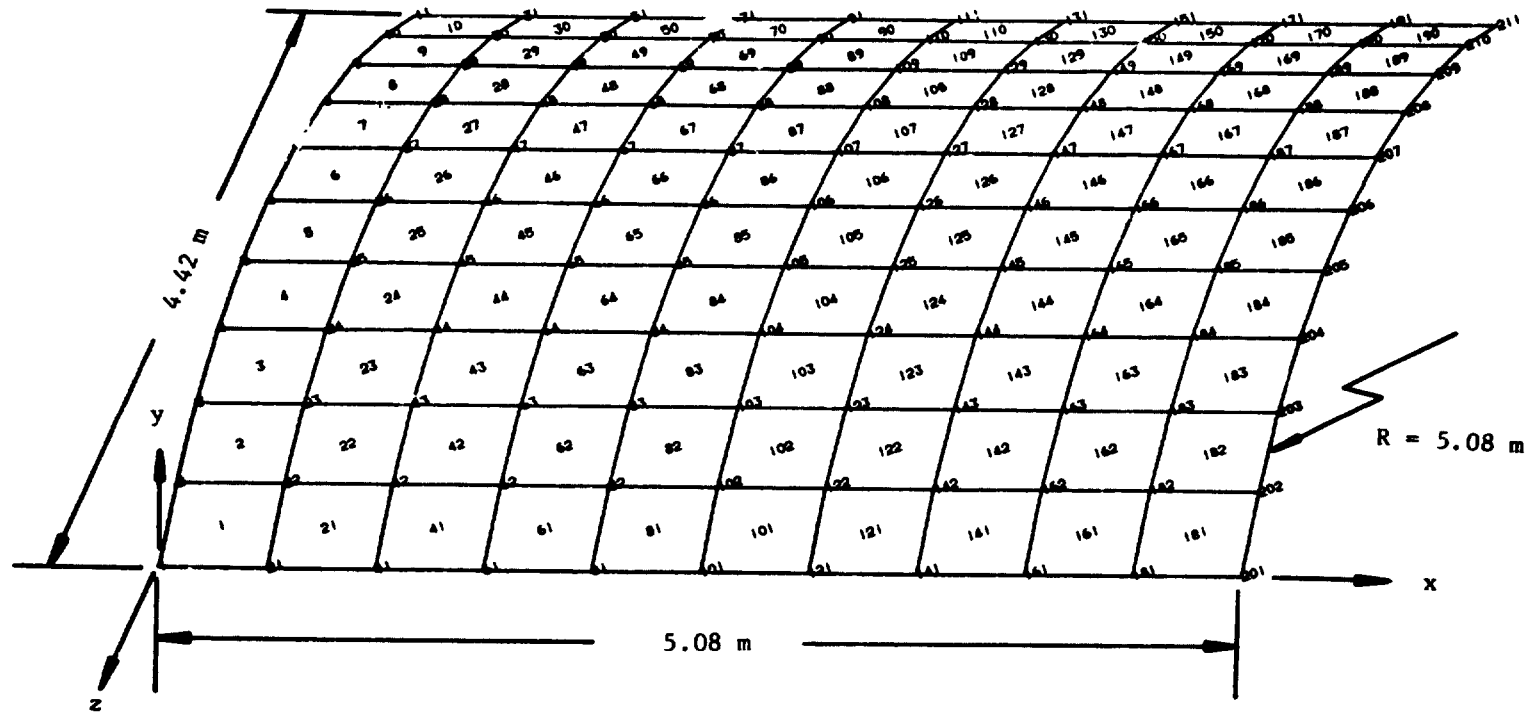
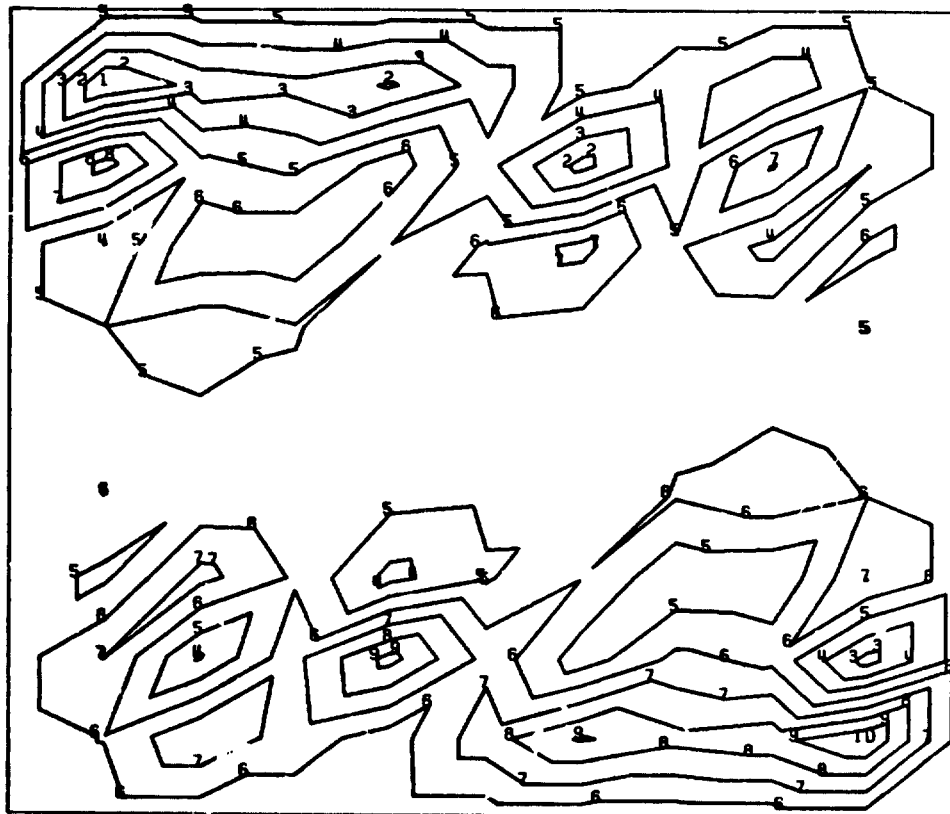
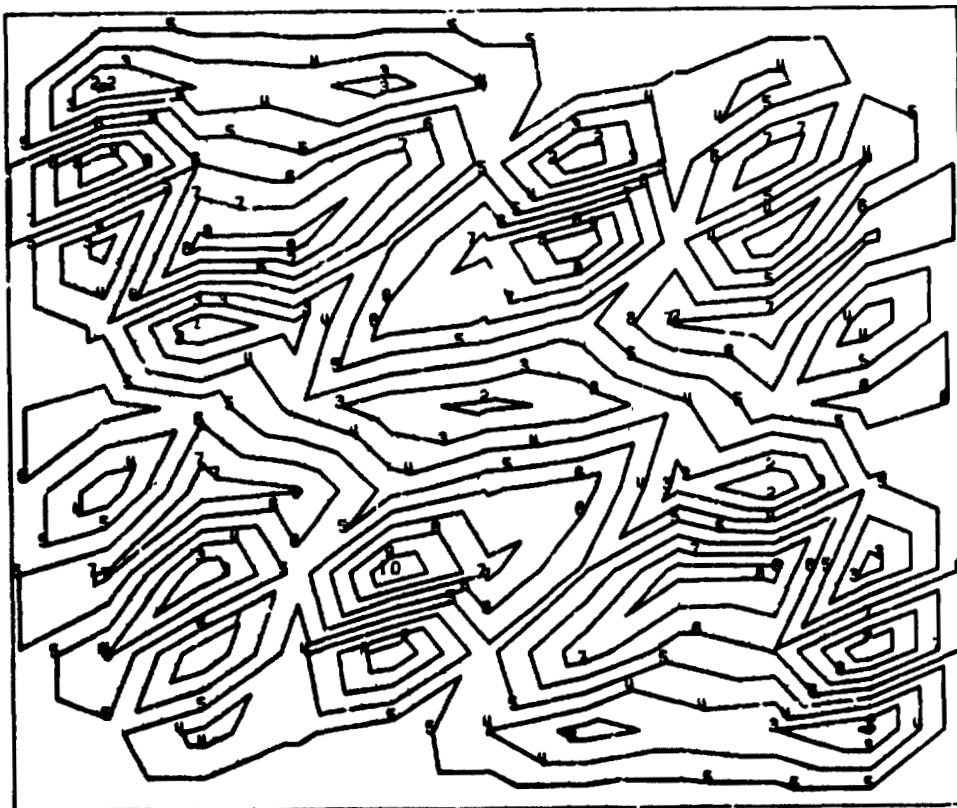


FIGURE 1 - SYMMETRIC LAMINATED COMPOSITE SHELL WITH $[-60/0/60]_{3S}$ LAY-UP AND 0 DEGREE IS ALONG THE X-AXIS



CONTOUR NO.	DISPLACEMENT (mm)
1	-4.857
2	-3.778
3	-2.699
4	-1.619
5	-0.540
6	0.540
7	1.619
8	2.699
9	3.778
10	4.857

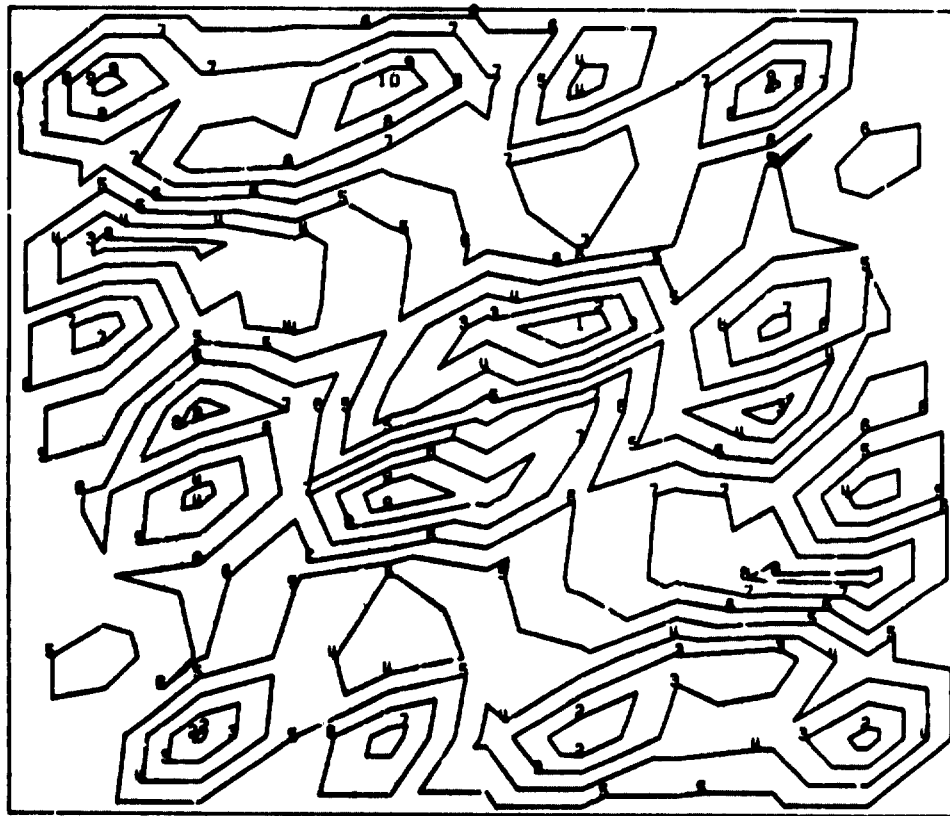
FIGURE 2 - X-DISPLACEMENT CONT' PLOT



CONTOUR NO.	DISPLACEMENT (mm)
1	-14.248
2	-11.348
3	-8.449
4	-5.549
5	-2.649
6	0.250
7	3.150
8	6.050
9	8.949
10	11.849

ORIGINAL PAGE IS
OF POOR QUALITY

FIGURE 3 - Y-DISPLACEMENT CONTOUR PLOT



CONTOUR NO.	DISPLACEMENT (mm)
1	-0.100
2	-0.080
3	-0.056
4	-0.029
5	-0.011
6	0.011
7	0.029
8	0.056
9	0.080
10	0.100

ORIGINAL PAGE IS
OF POOR QUALITY

FIGURE 4 - Z-DISPLACEMENT CONTOUR PLOT

N85-25879

ON THE INTERCONNECTION OF INCOMPATIBLE
SOLID FINITE ELEMENT MESHES USING MULTIPOINT CONSTRAINTS

Gary L. Fox
Hughes Drilling Equipment
Division of Hughes Tool Corporation
Torrance, California

SUMMARY

Incompatible meshes, i.e. meshes that physically must have a common boundary, but do not necessarily have coincident grid points, can arise in the course of a finite element analysis. For example, two substructures may have been developed at different times for different purposes and it becomes necessary to interconnect the two models. A technique that uses only multipoint constraints, i.e. MPC cards (or MPCs cards in substructuring), is presented. Since the method uses only MPC's, the procedure may apply at any stage in an analysis; no prior planning or special data is necessary.

INTRODUCTION

When two separate finite element solid meshes are combined with a common boundary, the degrees of freedom on the common surface of one of the models must be eliminated. The elimination process must preserve the compatibility of the joined surface when the model is subjected to external loads which cause the interface surface to deform. The use of MPC's can provide this capability to first order, i.e. linear in terms of grid point displacements.

The MPC equations presented are based on a linear surface spline. A three dimensional surface spline is a mathematical tool used to find a function, $f(u,v,w)$ for all points (x,y,z) when $(u(x,y,z), v(x,y,z), w(x,y,z))$ is known for a discrete set of points, (x_i, y_i, z_i) and (u, v, w) are displacements in the (x, y, z) directions. The three dimensional surface spline given here is based on the shape function of the linear displacement tetrahedra. This shape function will produce compatible surface deformations for models using linear elements.

The example presented implements this method by assuming that one surface is composed of a set of imaginary triangles formed by grid points on one of the mating surfaces. The vertices of a triangle form a unique surface described by (x_i, y_i, z_i) , where $i = 1, 2, 3$. Grid points of the surface to be interconnected that lie within the boundary of the triangle are MPC'ed to the displacement of the vertices, (u_i, v_i, w_i) , based on the spline functions $f(u(x_i, y_i, z_i), v(x_i, y_i, z_i), w(x_i, y_i, z_i))$. Results of a practical example in substructure analysis are presented. A computer program that automatically writes the MPC cards is included in the Appendix.

DEFINITION OF THE PROBLEM

Consider a planar triangle in space defined by three points; A, B and C, as shown in Figure 1.

The vector [A] represents the distance from the origin to point A; similarly for points B, C and O. The subject of this paper is the determination of the

relationship between displacements of points A, B, C and O when

$$\begin{aligned} \{dA\} &= \{A' - A\} = (u^a, v^a, w^a) \\ \{dB\} &= \{B' - B\} = (u^b, v^b, w^b) \\ \{dC\} &= \{C' - C\} = (u^c, v^c, w^c) \\ \{dO\} &= \{O' - O\} = (u^o, v^o, w^o) \end{aligned} \quad (1)$$

such that the point O' lies in the plane described by the triangle in space defined by the three points A', B' and C'.

In the application described, the points A, B and C lie on the surface of a region described by a group of finite elements; the point "O" is a grid (or node) in the same or in a different group of finite elements defining a region that has a physically congruent undeformed boundary that the points A, B, C and O lie on.

In the notation used here, { } is a row vector and () is a scalar quantity. A matrix multiplication, { } [] [] results in a scalar, as indicated by the left and right elements; similarly, [] { } would indicate a matrix result. In the text a scalar will often be written without the braces.

SELECTION OF THE SPLINE FUNCTION

Some rule must be selected that relates the displacement of any point in the plane of the triangle with the motion of the three reference points A, B and C, i.e. a spline function. The shape function of a linear displacement tetrahedra is used for this purpose. However, in order to use this shape function, a tetrahedra must be constructed from the reference triangle. This is easily accomplished by forming a cross product of the vectors {vab} and {vac};

$$\{vap\} = \{vab\} \times \{vac\} \quad (2)$$

where

$$\{v^{ij}\} = \{v^j\} - \{v^i\}$$

The result of equation (2) is the formation of a reference point, P, which forms the fourth vertex of the reference tetrahedra. Clearly, if {vab} and {vac} are unique, then point P will be unique.

The shape function for a linear displacement tetrahedra is [Reference 1, Section 5.12]

$$\begin{Bmatrix} u^a \\ u^b \\ u^c \\ u^p \end{Bmatrix} = \begin{bmatrix} 1 & x^a & y^a & z^a \\ 1 & x^b & y^b & z^b \\ 1 & x^c & y^c & z^c \\ 1 & x^p & y^p & z^p \end{bmatrix} \begin{Bmatrix} D_1 \\ D_2 \\ D_3 \\ D_4 \end{Bmatrix} \quad (3)$$

or

$$\{u^i\} = [T]\{D\}$$

where

u^i = the displacement of the i^{th} vertex in the x coordinate direction

Two additional sets of equations, similar to equation (3), relate v and w, the y and z displacement, to the undetermined coefficients, {D}. The displacement of a point "O" is, in the x direction

$$\{u^o\} = D_1 + D_2X^o + D_3Y^o + D_4Z^o \quad (4)$$

or from the solution of equation (3)

$$\{u^o\} = \{i \ x^o \ y^o \ z^o\} [S] \{u\}$$

where

$$[S] = [T]^{-1}$$

Similar equations exist for v and w.

It is useful to write equation (4) in the following form for the displacements in the three coordinate directions:

$$\begin{aligned} u^o(x^o, y^o, z^o) &= A u^a + B v^b + C w^c + P u^p \\ v^o(x^o, y^o, z^o) &= A v^a + B v^b + C v^c + P v^p \\ w^o(x^o, y^o, z^o) &= A w^a + B w^b + C w^c + P w^p \end{aligned} \quad (5)$$

where

$$\begin{aligned} A &= S_{11} + S_{21}x^o + S_{31}y^o + S_{41}z^o \\ B &= S_{12} + S_{22}x^o + S_{32}y^o + S_{42}z^o \\ C &= S_{13} + S_{23}x^o + S_{33}y^o + S_{43}z^o \\ P &= S_{14} + S_{24}x^o + S_{34}y^o + S_{44}z^o \end{aligned}$$

and

$$\begin{aligned} u^i &= \text{displacement of point } (x^i, y^i, z^i) \text{ in X direction} \\ v^i &= \text{displacement of point } (x^i, y^i, z^i) \text{ in Y direction} \\ w^i &= \text{displacement of point } (x^i, y^i, z^i) \text{ in Z direction} \end{aligned}$$

Now equation (5) is in the form of a multipoint constraint (MPC) relationship [Reference 1, Section 3.5]. The coefficients A, B, C and P are constants that depend only on the constrained geometry. Equation (5) cannot be used directly, however, since point P does not actually exist. Point P must be removed from the set of equations.

The motion of point P, in terms of the motion of point A and the rotation vector, $\{\alpha, \beta, \gamma\}$, of the triangle is [Reference 1, Section 3.5]:

$$\begin{Bmatrix} u^p \\ v^p \\ w^p \end{Bmatrix} = \begin{Bmatrix} u^a \\ v^a \\ w^a \end{Bmatrix} + \begin{bmatrix} 0 & z^{ap} & -y^{ap} \\ -z^{ap} & 0 & x^{ap} \\ y^{ap} & -x^{ap} & 0 \end{bmatrix} \begin{Bmatrix} \alpha \\ \beta \\ \gamma \end{Bmatrix} \quad (6)$$

or

$$\{u^p\} = \{u^a\} + [H]\{\alpha\}$$

where

$$\alpha, \beta, \text{ and } \gamma = \text{rotation about } x, y, z \text{ axes.}$$

CALCULATION OF THE ROTATION VECTOR

It is necessary to determine the relative angular displacement of the unstrained and strained triangles in terms of the displacements of points A, B and C. Equation (6) can be written in matrix form for the three points A, B and C and the rotation vector $\{\alpha, \beta, \gamma\}$ as:

$$\begin{bmatrix} 0 & z^{ab} & -v^{ab} \\ -z^{ab} & 0 & x^{ab} \\ y^{ab} & -x^{ab} & 0 \end{bmatrix} \begin{Bmatrix} \alpha \\ \beta \\ \gamma \end{Bmatrix} = \begin{Bmatrix} u^{ab} \\ v^{ab} \\ w^{ab} \end{Bmatrix} \\
 \begin{bmatrix} 0 & z^{bc} & -y^{bc} \\ -z^{bc} & 0 & x^{bc} \\ y^{bc} & -x^{bc} & 0 \end{bmatrix} \begin{Bmatrix} \alpha \\ \beta \\ \gamma \end{Bmatrix} = \begin{Bmatrix} u^{bc} \\ v^{bc} \\ w^{bc} \end{Bmatrix} \\
 \begin{bmatrix} 0 & z^{ca} & -y^{ca} \\ -z^{ca} & 0 & x^{ca} \\ y^{ca} & -x^{ca} & 0 \end{bmatrix} \begin{Bmatrix} \alpha \\ \beta \\ \gamma \end{Bmatrix} = \begin{Bmatrix} u^{ca} \\ v^{ca} \\ w^{ca} \end{Bmatrix} \tag{7}$$

or, symbolically

$$[R]\{\alpha\} = [\Delta u]$$

where

$$\begin{Bmatrix} u^{ar} \\ v^{ar} \\ w^{ar} \end{Bmatrix} = \begin{Bmatrix} u^r - u^a \\ v^r - v^a \\ w^r - w^a \end{Bmatrix}$$

Now a unique solution to equation (7) exists so long as the triangles (A, B, C) and (A', B', C') are unique. Physically this must be the case, otherwise a zero strain would result. The solution is [Reference 2]:

$$\{\alpha\} = ([R]^T [R])^{-1} [R]^T [\Delta u] \tag{8}$$

Equation (8) gives the rotation vector, for small angles, when the displacements are known at the triangle vertices.

Equation (6), when $\{\alpha\}$ is determined from equation (8) becomes:

$$[u^P] = [u^a] + [Q][\Delta u] \tag{9}$$

where

$$[Q] = [H](R^T R)^{-1} [R]^T$$

Equation (9), when combined with equation (5) provides the MPC relationship that is a function of the displacements of the original four points of the tetrahedra, A, B, C and P.

Equation (9) written in detail is:

$$\begin{Bmatrix} u^P \\ v^P \\ w^P \end{Bmatrix} = \begin{Bmatrix} u^a \\ v^a \\ w^a \end{Bmatrix} + \begin{bmatrix} Q_{11} & Q_{12} & \dots & Q_{19} \\ \vdots & \vdots & \vdots & \vdots \\ Q_{31} & Q_{32} & \dots & Q_{39} \end{bmatrix} \begin{Bmatrix} u^b - u^a \\ v^b - v^a \\ w^b - w^a \\ u^c - u^b \\ v^c - v^b \\ w^c - w^b \\ u^a - u^c \\ v^a - v^c \\ w^a - w^c \end{Bmatrix}$$

The displacement of point P can be determined from the displacements u^a , u^b and u^c in accordance with equation (9), i.e.

$$\begin{aligned}
u^p &= (1 + Q_{17} - Q_{11})u^a + (Q_{11} - Q_{14})u^b + (Q_{14} - Q_{17})u^c \\
&+ (Q_{18} - Q_{12})v^a + (Q_{12} - Q_{15})v^b + (Q_{15} - Q_{18})v^c \\
&+ (Q_{19} - Q_{13})w^a + (Q_{13} - Q_{16})w^b + (Q_{16} - Q_{19})w^c
\end{aligned} \tag{10}$$

and similarly for v^p and w^p .

SPLINE EQUATION FINAL FORM

Substituting equation (10) into the MPC equation (5) gives the final form of the spline equations:

$$u(x^0, y^0, z^0) =$$

$$\begin{aligned}
&[A + P(1+Q_{17} - Q_{11})]u^a + [B+P(Q_{11} - Q_{14})] u^b + [C+P(Q_{14} - Q_{17})] u^c \\
&+ P(Q_{18} - Q_{12}) v^a + P(Q_{12} - Q_{15}) v^b + P(Q_{15} - Q_{18}) v^c \\
&+ P(Q_{19} - Q_{13}) w^a + P(Q_{13} - Q_{16}) w^b + P(Q_{16} - Q_{19}) w^c
\end{aligned}$$

$$v(x^0, y^0, z^0) =$$

$$\begin{aligned}
&P(Q_{27} - Q_{21}) u^a + P(Q_{21} - Q_{24}) u^b + P(Q_{24} - Q_{27}) u^c \\
&+[A + P(1+Q_{28} - Q_{22})]v^a + [B+P(Q_{22} - Q_{25})] v^b + [C+P(Q_{25} - Q_{28})] v^c \\
&P(Q_{29} - Q_{23}) w^a + P(Q_{23} - Q_{26}) w^b + P(Q_{26} - Q_{29}) w^c
\end{aligned}$$

$$w(x^0, y^0, z^0) =$$

$$\begin{aligned}
&P(Q_{37} - Q_{31}) u^a + P(Q_{31} - Q_{34}) u^b + P(Q_{34} - Q_{37}) u^c \\
&+ P(Q_{38} - Q_{32}) v^a + P(Q_{32} - Q_{35}) v^b + P(Q_{35} - Q_{38}) v^c \\
&+[A + P(1+Q_{39} - Q_{33})]w^a + [B+P(Q_{33} - Q_{36})] w^b + [C+P(Q_{36} - Q_{39})] w^c
\end{aligned}$$

A SIMPLE NUMERICAL EXAMPLE

Consider a triangle with vertices at $A=(1,0,0)$, $B=(0,1,0)$ and $C=(0,0,1)$. The point, O , to be removed is at $O=(1/3, 1/3, 1/3)$. This point lies in the plane of the triangle ABC with the distance to the origin of $1/\sqrt{3}$. Values of the various scalars, vectors, and matrices used in calculating the MPC coefficients are given below.

$$[v^aP] = (1.0, 1.0, 1.0)$$

$$[T] = \begin{bmatrix} 1.0 & 1.0 & 0.0 & 0.0 \\ 1.0 & 0.0 & 1.0 & 0.0 \\ 1.0 & 0.0 & 0.0 & 1.0 \\ 1.0 & 2.0 & 1.0 & 1.0 \end{bmatrix}$$

$$[S] = \begin{bmatrix} .6667 & .3333 & .3333 & -.3333 \\ .3333 & -.3333 & -.3333 & .3333 \\ -.6667 & .6667 & -.3333 & .3333 \\ -.6667 & -.3333 & .6667 & .3333 \end{bmatrix}$$

$$\begin{aligned} \mathbf{A} &= 1/3 \\ \mathbf{B} &= 1/3 \\ \mathbf{C} &= 1/3 \\ \mathbf{P} &= 0 \end{aligned}$$

$$[R] = \begin{bmatrix} 0 & 0 & -1 \\ 0 & 0 & -1 \\ 1 & 1 & 0 \\ \hline 0 & 1 & 1 \\ -1 & 0 & 0 \\ -1 & 0 & 0 \\ \hline 0 & -1 & 0 \\ 1 & 0 & 0 \\ 0 & 0 & 0 \end{bmatrix}$$

$$[R]^T[R] = \begin{bmatrix} 4 & 1 & 1 \\ 1 & 4 & 1 \\ 1 & 1 & 4 \end{bmatrix}$$

$$([R]^T[R])^{-1} = \begin{bmatrix} .2778 & -.0556 & -.0556 \\ -.0556 & .2778 & -.0556 \\ -.0556 & -.0556 & .2778 \end{bmatrix}$$

$$([R]^T[R])^{-1} [R]^T =$$

$$\begin{bmatrix} .0556 & .0556 & .222 & -.111 & -.2778 & -.2778 & .0556 & .2222 & .0556 \\ .0556 & .0556 & .222 & .222 & .0556 & .0556 & -.2778 & -.1111 & -.2778 \\ -.2778 & -.2778 & -.111 & .222 & .0556 & .0556 & .0556 & .2222 & .0556 \end{bmatrix}$$

$$[Q] =$$

$$\begin{bmatrix} .3333 & .3333 & .3333 & .0000 & .0000 & .0000 & -.3333 & -.3333 & -.3333 \\ -.3333 & -.3333 & -.3333 & .3333 & .3333 & .3333 & .0000 & .0000 & .0000 \\ .0000 & .0000 & .0000 & -.3333 & -.3333 & -.3333 & .3333 & .3333 & .3333 \end{bmatrix}$$

and finally,

$$\begin{aligned}
 u(1/3, 1/3, 1/3) = & \\
 & .3333u^a + .3333u^b + .3333u^c \\
 & + .0 v^a + .0 v^b + .0 v^c \\
 & + .0 w^a + .0 w^b + .0 w^c
 \end{aligned}$$

$$\begin{aligned}
 v(1/3, 1/3, 1/3) = & \\
 & .0 u^a + .0 u^b + .0 u^c \\
 & + .3333v^a + .3333v^b + .3333v^c \\
 & + .0 w^a + .0 w^b + .0 w^c
 \end{aligned}$$

$$\begin{aligned}
 w(1/3, 1/3, 1/3) = & \\
 & .0 u^a + .0 u^b + .0 u^c \\
 & + .0 v^a + .0 v^b + .0 v^c \\
 & + .3333w^a + .3333w^b + .3333w^c
 \end{aligned}$$

If the displacements of points **A**, **B**, and **C** each move along the x, y and z axes, respectively, as shown in Figure 2, then

$$u^0 = .3333, \quad v^0 = .3333, \quad w^0 = .3333$$

and point $0' = (.6667, .6667, .6667)$. It is useful to note that since $P = 0$ the MPC equations (11) reduce to:

$$\begin{aligned}
 u(x^0, y^0, z^0) &= \mathbf{A} u^a + \mathbf{B} u^b + \mathbf{C} u^c \\
 v(x^0, y^0, z^0) &= \mathbf{A} v^a + \mathbf{B} v^b + \mathbf{C} v^c
 \end{aligned}$$

This situation apparently results when the point to be removed, 0, lies in the plane of the triangle formed by points **A**, **B** and **C**. The equations derived are such that the strain perpendicular to the triangle **ABC** are null. Points lying in the plane of the triangle have non-null strains only in the plane of the triangle.

A PRACTICAL APPLICATION

The technique presented in this paper was developed during the course of a finite element analysis of a bolted, flange-type coupling used in marine risers [3,4]. Figure 3 shows the coupling components in the bolt-up condition. The coupling is modeled as three separate substructures; the Pin, Box, and Bolt, as shown in Figures 4, 5, and 6. Advantage is taken of the cyclic symmetry of the coupling, hence a 22.5° pie section is modeled with the appropriate boundary conditions. The finite element mesh of the Pin in the area of the countersink used very small elements in order to properly calculate stress concentrations. The corresponding area of the Bolt, at the Pin-Bolt interface, need not be modeled with a mesh this fine.

A considerable savings in computer run time is achieved if the interface of the Pin and Bolt can be made consistent with the boundary conditions but allow a lower density mesh on the Bolt. Grid points on the Pin that were not coincident with grid points on the Bolt were removed. The results of a stress analysis of the Pin are shown in Figure 7. These results show that, in the region of the grids that were removed by MPCS cards, a smooth and consistent stress pattern results.

REFERENCES

1. The NASTRAN® Theoretical Manual, NASA SP-221(06), January, 1981.
2. Mood, A.M. and Graybill, F.A., Introduction to the Theory of Statistics, McGraw-Hill, 1963, pp 343-346.
3. Fox, Gary L. and Geminder, Robert, "Analysis of the HMF Riser Connector", Proceedings of Oceans '84, September, 1984, IEEE.
4. Fox, Gary L., "Nonlinear Analysis of a Bolted Marine Riser Coupling Using NASTRAN® Substructuring", Twelfth NASTRAN® Users' Colloquium, May, 1984, NASA Conference Publication 2328.

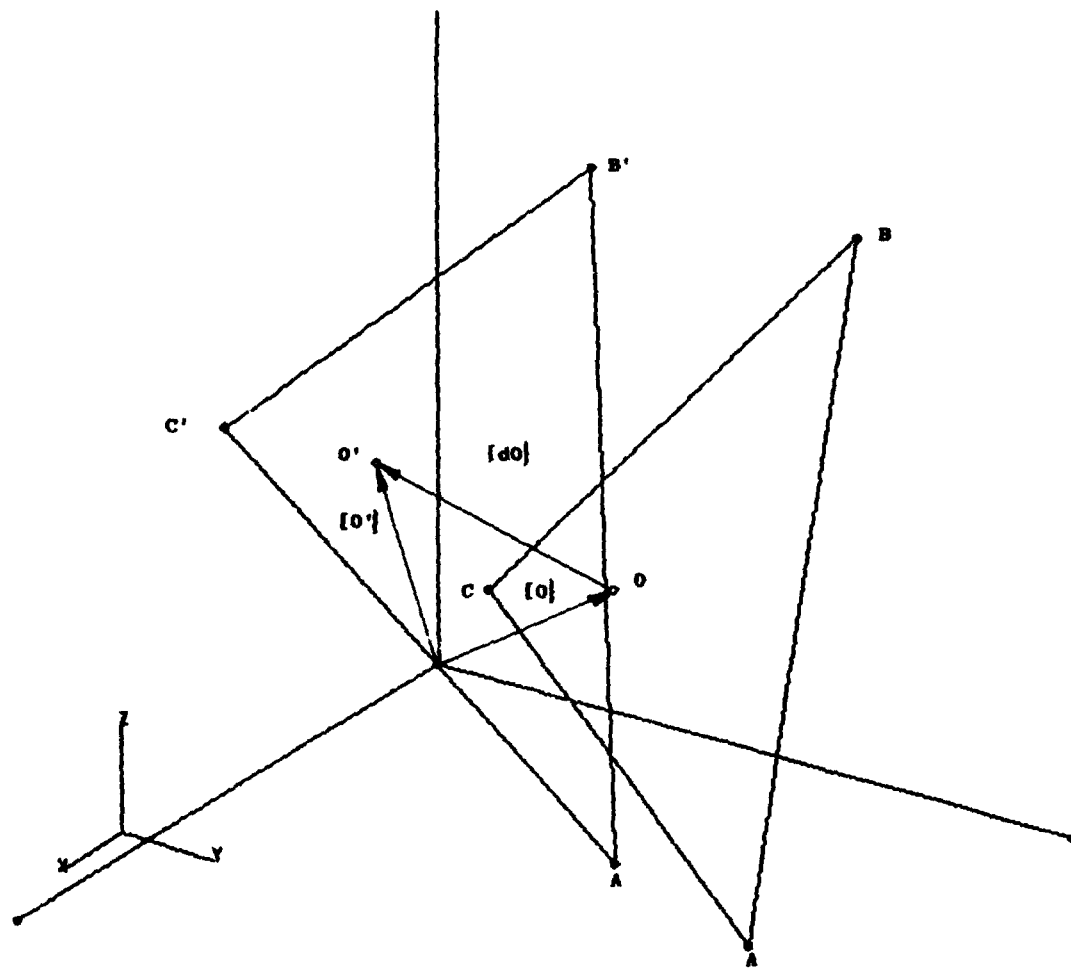


FIGURE 1 - SCHEMATIC REPRESENTATION OF AN UNSTRAINED TRIANGLE (A,B,C) AND A STRAINED TRIANGLE (A',B',C')

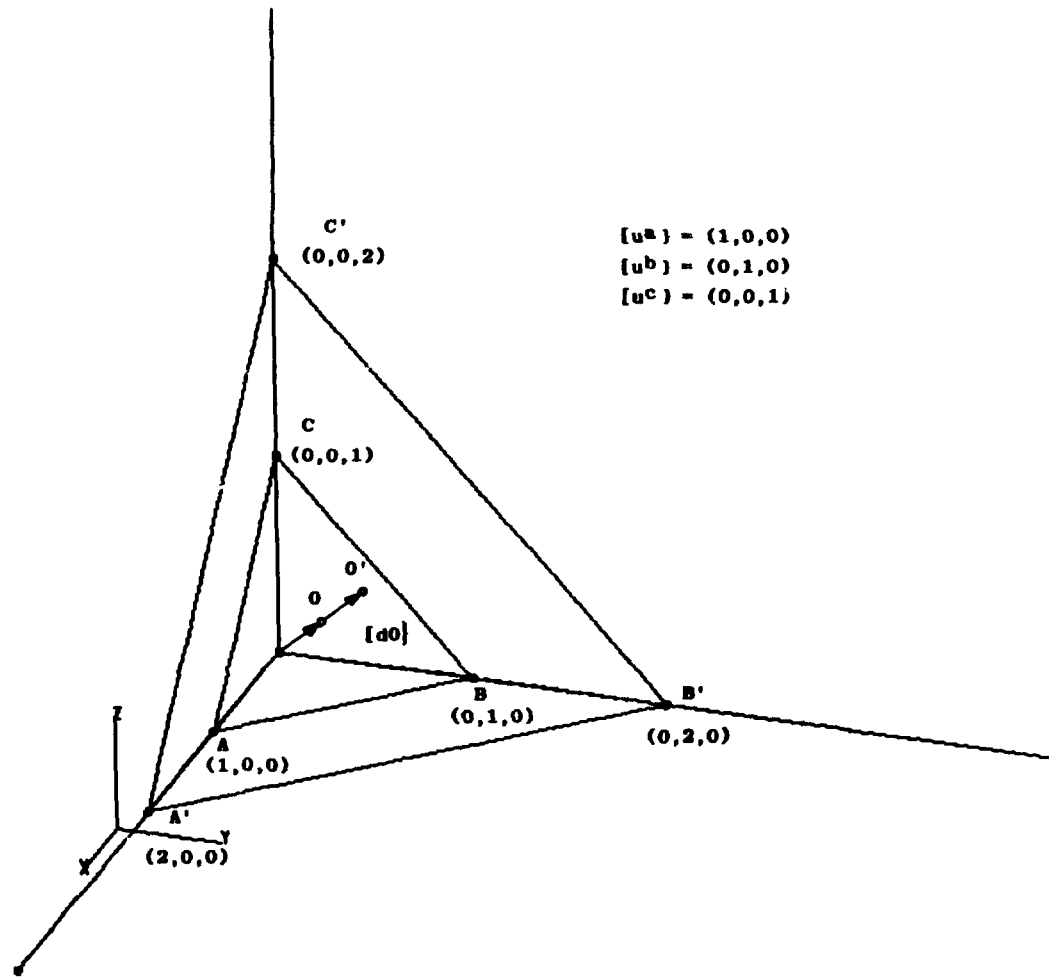


FIGURE 2 - EXAMPLE PROBLEM

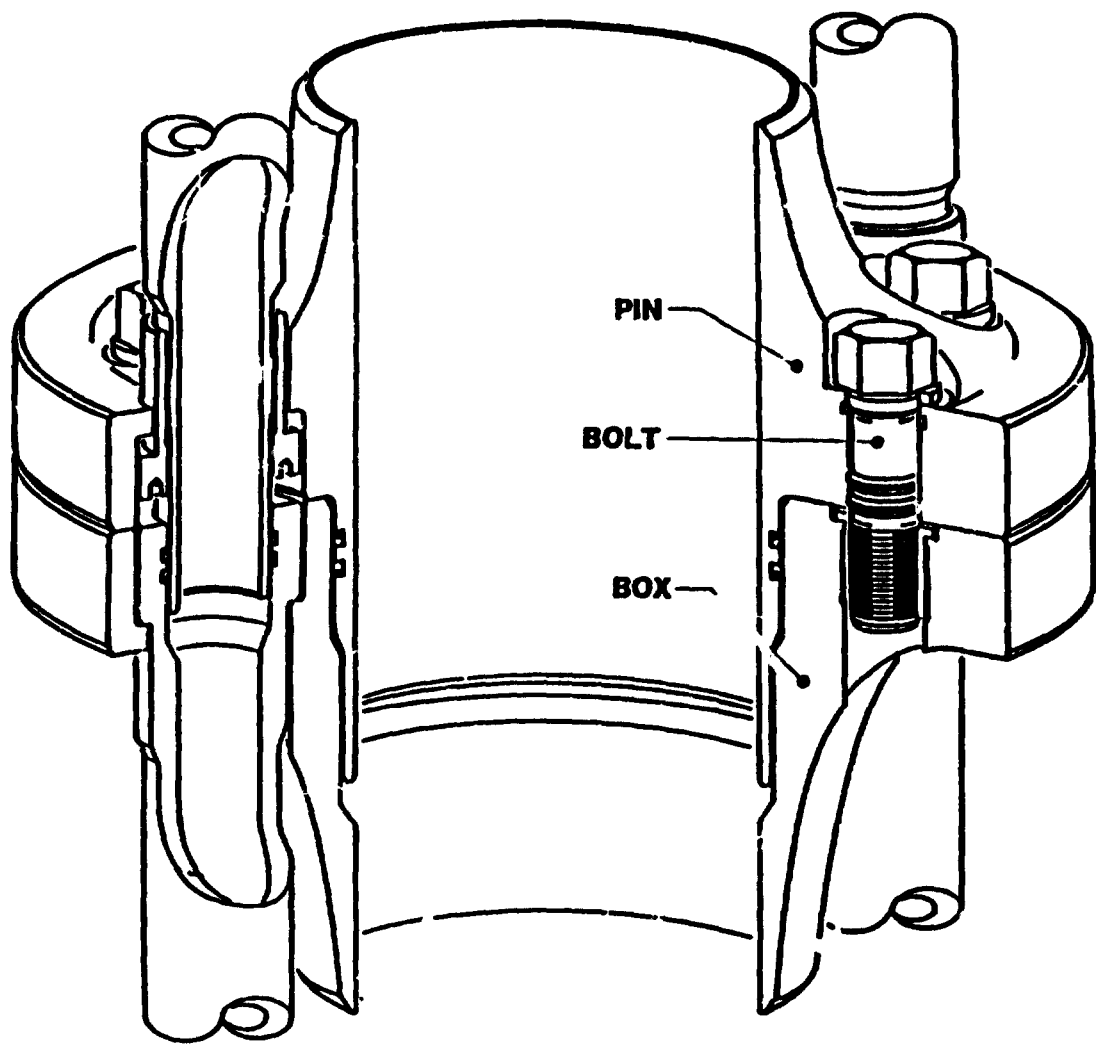


FIGURE 3 - HMF RISER CONNECTOR

ORIGINAL OF POC

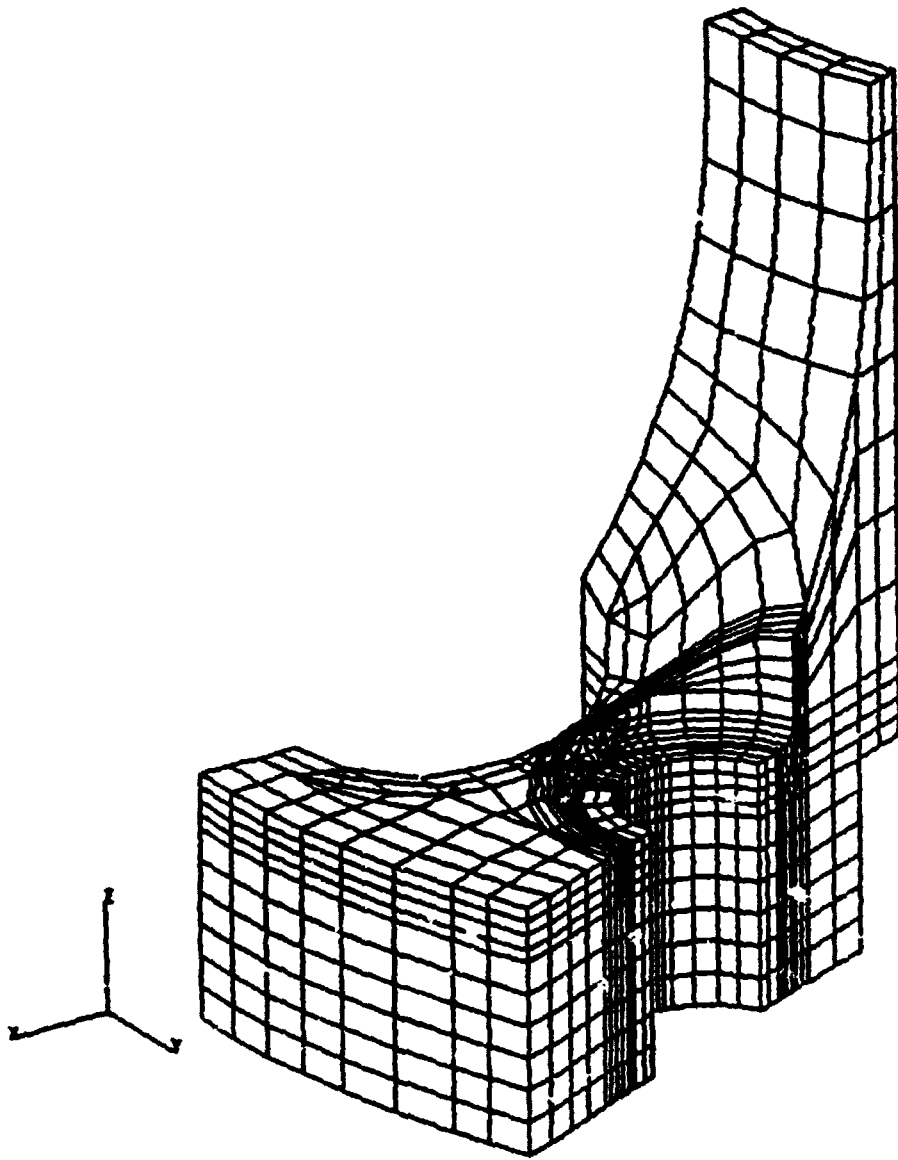


FIGURE 4 - HIDDEN LINE VIEW OF HPF PIN, 22.5° PIE SECTION

ORIGINAL PAGES
OF POOR QUALITY

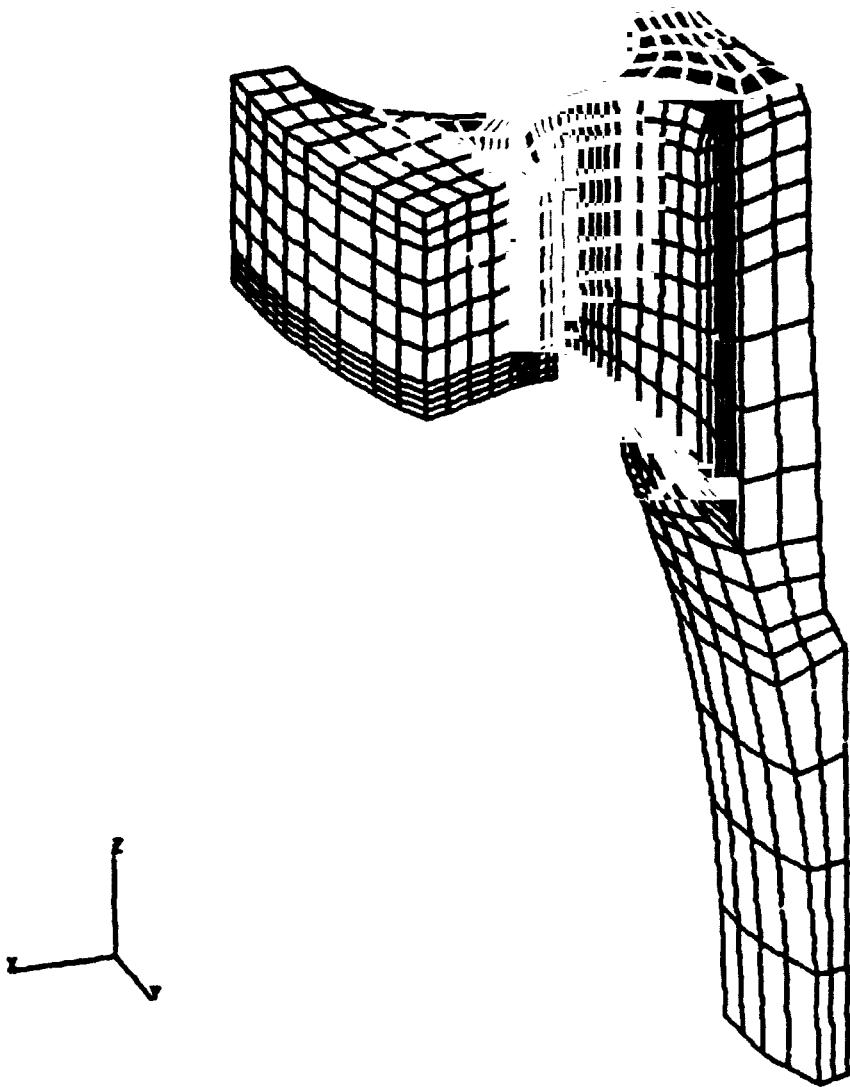


FIGURE 5 - HIDDEN LINE VIEW OF HPF BOX, 22.5° PIE SECTION

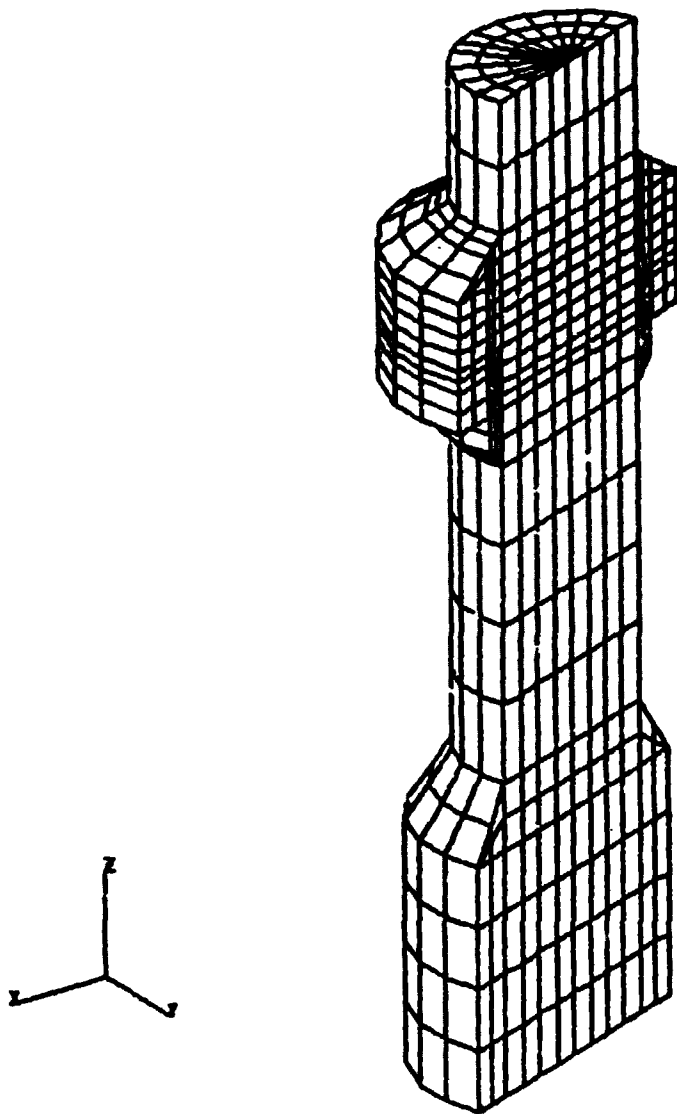


FIGURE 6 - HIDDEN LINE VIEW OF HMF BOLT, 22.5° PIE SECTION

ORIGINAL PAGE
OF POOR QUALITY



FIGURE 7 - VON MISES EQUIVALENT STRESS
CONTOURS MAPPED ONTO A HIDDEN LINE PLOT
OF HMF PIN

APPENDIX

This Appendix gives the source code of a FORTRAN computer program that reads a control file (BDY MPC.INP), the NASTRAN grid card file (BDY MPC.BDF), and produces MPC cards for inclusion to the NASTRAN Bulk Data File. Figure A-1 shows the control file for the sample problem. The first line gives the number of points, NG, to be MPC'ed and the three GRID ID's. The next NG lines contain the GRID ID's. The group may be repeated as many times as necessary. Figure A-2 shows the GRID cards and Figure A-3 shows a listing of MPC cards generated for the sample problem. The source listing is given in Figure A-4.

1
25

21

22

23

FIGURE A-1 SAMPLE PROBLEM CONTROL FILE

GRID	21	0	1.0	0.0	0.0
GRID	22	0	0.0	1.0	0.0
GRID	23	0	0.0	0.0	1.0
GRID	25	0	.33333	.33333	.33333

FIGURE A-2 SAMPLE PROBLEM GRID CARD INPUT

MPC		312	25	1	-1.000	21	1	.333	+M	1
+M	1		22	1	.333	23	1	.333	+M	2
+M	2		21	2	.000	22	2	.000	+M	3
+M	3		23	2	.000	21	3	.000	+M	4
+M	4		22	3	.000	23	3	.000		
MPC		312	25	2	-1.000	21	1	.000	+M	5
+M	5		22	1	.000	23	1	.000	+M	6
+M	6		21	2	.333	22	2	.333	+M	7
+M	7		23	2	.333	21	3	.000	+M	8
+M	8		22	3	.000	23	3	.000		
MPC		312	25	3	-1.000	21	1	.000	+M	9
+M	9		22	1	.000	23	1	.000	+M	10
+M	10		21	2	.000	22	2	.000	+M	11
+M	11		23	2	.000	21	3	.333	+M	12
+M	12		22	3	.333	23	3	.333		

FIGURE A 3 SAMPLE PROBLEM MPC CARD OUTPUT

```

C
C
C   FORM CROSS PRODUCT  $\overline{AB}$  X  $\overline{AC}$  FOR VECTOR  $\overline{AP}$ 
C
XAB=T(2,2)-T(1,2)
XAC=T(3,2)-T(1,2)
XBC=T(3,2)-T(2,2)
YAB=T(2,3)-T(1,3)
YAC=T(3,3)-T(1,3)
YBC=T(3,3)-T(2,3)
ZAB=T(2,4)-T(1,4)
ZAC=T(3,4)-T(1,4)
ZBC=T(3,4)-T(2,4)
C
AP(1)=YAB*ZAC-ZAB*YAC
AP(2)=ZAB*XAC-XAB*ZAC
AP(3)=XAB*YAC-YAB*XAC
C
C   POINT P ADDED TO T MATRIX
C
T(4,2)=T(1,2)+AP(1)
T(4,3)=T(1,3)+AP(2)
T(4,4)=T(1,4)+AP(3)
CALL MINV4(T,S)
C
C   FORM R AND H MATRICES
C   NOTE THAT ZCA=-ZAC, ETC.
C
R(1,1)= 0.0
R(1,2)=+ZAB
R(1,3)=-YAB
R(2,1)=-ZAB
R(2,2)= 0.0
R(2,3)=+XAB
R(3,1)=+YAB
R(3,2)=-XAB
R(3,3)= 0.0
R(4,1)= 0.0
R(4,2)=+ZBC
R(4,3)=-YBC
R(5,1)=-ZBC
R(5,2)= 0.0
R(5,3)=+XBC
R(6,1)=+YBC
R(6,2)=-XBC
R(6,3)= 0.0
R(7,1)= 0.0
R(7,2)=-ZAC
R(7,3)=+YAC
R(8,1)=+ZAC
R(8,2)= 0.0
R(8,3)=-XAC
R(9,1)=-YAC
R(9,2)=+XAC
R(9,3)= 0.0
C

```

```

C
H(1,1)= 0.0
H(2,2)= 0.0
H(3,3)= 0.0
H(1,2)= AP(3)
H(1,3)=-AP(2)
H(2,3)= AP(1)
H(2,1)=-H(1,2)
H(3,1)=-H(1,3)
H(3,2)=-H(2,3)

C
DO 135 I1=1,3
DO 135 J1=1,9
RT(I1,J1)=R(J1,I1)
135 CONTINUE

C
C      T
C      FORM R * R = RTR
C
DO 136 I1=1,3
DO 136 J1=1,3
RTR(I1,J1)=0.0
DO 136 K1=1,9
RTR(I1,J1)=RTR(I1,J1)+RT(I1,K1)*R(K1,J1)
136 CONTINUE
CALL MINV3(RTR,RTRI)

C
C      FORM RTRI*RT
C
DO 137 I1=1,3
DO 137 J1=1,9
RTRI(I1,J1)=0.0
DO 137 K1=1,3
137 RTRI(I1,J1)=RTRI(I1,J1)+RTRI(I1,K1)*RT(K1,J1)

C
DO 138 I1=1,3
DO 138 J1=1,9
Q(I1,J1)=0.0
DO 138 K1=1,3
138 Q(I1,J1)=Q(I1,J1)+H(I1,K1)*RTRI(K1,J1)

C
WRITE(14,3) ((R(IL,JL),JL=1,3),IL=1,9)
-,( ( T(IL,JL),JL=1,4),IL=1,4)
&,( ( RTR(IL,JL),JL=1,3),IL=1,3)
&,( ( RTRI(IL,JL),JL=1,3),IL=1,3)
&,AP
&,( (RTRI(I1,JL),JL=1,9),IL=1,3)
&,( ( Q(IL,JL),JL=1,9),IL=1,3)
3 FORMAT(1X,' MATRIX R ',/9(/3F8.4)
&,//1X,' MATRIX T ',/4(/4F8.4)
&,//1X,' MATRIX RTR ',/3(/3F8.4)
&,//1X,' MATRIX RTRI ',/3(/3F8.4)
&,//1X,' VECTOR AP ',/3F8.4
&,//1X,' MATRIX RTRI(I1,J1) ',/3(/9F8.4)
&,//1X,' MATRIX Q ',/3(/9F8.4) )

```

```

C
C
C   START LOOP FOR EACH GRID TO BE MPC'ED - GRID ID IS THE KEY
C
DO 200 IMG=1,NG
READ(11,5,END=3000) IDR
NCR=NCR+1
REWIND 12
140 READ(12,2,END=2000)DUM, ID, IDUM, X
IF(ID.NE.IDR) GOTO 140
C
C   CALC OF A,B,C,P
C   ALL ARE FUNCTIONS OF GRID COORDINATE TO BE REMOVED, X(1),X(2),X(3)
C
A=S(1,1)
B=S(1,2)
C=S(1,3)
P=S(1,4)
DO 150 I=1,3
A=A+S(I+1,1)*X(I)
B=B+S(I+1,2)*X(I)
C=C+S(I+1,3)*X(I)
P=P+S(I+1,4)*X(I)
150 CONTINUE
WRITE(14,6) A,B,C,P
6  FORMAT(1X,/1X,'A= ',F10.4,' B= ',F10.4,' C= ',F10.4
&,' P= ',F10.4,/1X )
C
C   CALC COEF FOR DIRECTION 1 AND WRITE MPC CARDS ON UNIT 13
C
XMPC(2)= P*(1+Q(1,7)-Q(1,1) )+A
XMPC(3)= P*( Q(1,1)-Q(1,4) )+B
XMPC(4)= P*( Q(1,4)-Q(1,7) )+C
XMPC(5)= P*( Q(1,8)-Q(1,2) )
XMPC(6)= P*( Q(1,2)-Q(1,5) )
XMPC(7)= P*( Q(1,5)-Q(1,8) )
XMPC(8)= P*( Q(1,9)-Q(1,3) )
XMPC(9)= P*( Q(1,3)-Q(1,6) )
XMPC(10)=P*( Q(1,6)-Q(1,9) )
CALL MPCR(1, IDR)
LINE=LINE+4
C
C   CALC COEF FOR DIRECTION 2 AND WRITE MPC CARDS ON UNIT 13
C
XMPC(2)= P*( Q(2,7)-Q(2,1) )
XMPC(3)= P*( Q(2,1)-Q(2,4) )
XMPC(4)= P*( Q(2,4)-Q(2,7) )
XMPC(5)= P*(1+Q(2,8)-Q(2,2) )+A
XMPC(6)= P*( Q(2,2)-Q(2,5) )+B
XMPC(7)= P*( Q(2,5)-Q(2,8) )+C
XMPC(8)= P*( Q(2,9)-Q(2,3) )
XMPC(9)= P*( Q(2,3)-Q(2,6) )
XMPC(10)=P*( Q(2,6)-Q(2,9) )
CALL MPCR(2, IDR)
LINE=LINE+4
C

```

```

C      CALC COEF FOR DIRECTION 3 AND WRITE MPC CARDS ON UNIT 13
C
XMPC(2)= P*( Q(3,7)-Q(3,1) )
XMPC(3)= P*( Q(3,1)-Q(3,4) )
XMPC(4)= P*( Q(3,4)-Q(3,7) )
XMPC(5)= P*( Q(3,8)-Q(3,2) )
XMPC(6)= P*( Q(3,2)-Q(3,5) )
XMPC(7)= P*( Q(3,5)-Q(3,8) )
XMPC(8)= P*(1+Q(3,9)-Q(3,3) )+A
XMPC(9)= P*( Q(3,3)-Q(3,6) )+B
XMPC(10)=P*( Q(3,6)-Q(3,9) )+C
CALL MPCR(3, IDR)
LINE=LINE+4
C
2000 CONTINUE
      GOTO 105
1000 STOP
2000 WRITE(14,*) ' ERROR NO. 2000 '
      STOP
3000 WRITE(14,*) ' ERROR NO. 3000 '
      STOP
      END
C
C
C
C
SUBROUTINE MINV4(C,A)
C
C      A=INV(C)  C IS NOT DESTROYED. ONE=A*C FOR CHECK
C
      IMPLICIT REAL*8 (A-H,O-Z)
      DIMENSION ONE(4,4)
      DIMENSION A(4,4),C(4,4),B(4,4),IPVOT(4),INDEX(4,2),PIVOT(4)
      N=4
      M=0
      DO 999 I=1,N
      DO 999 J=1,N
999  A(I,J)=C(I,J)
      WRITE(14,1) ((A(I,J),J=1,4),I=1,4)
1  FORMAT(1X,'INPUT MATRIX TO MINV4',/1X,4(/1X,4F12.4),/1X )
57  DET=1.0D0
      DO 17 J=1,N
17  IPVOT(J)=0.0D0
      DO 135 I=1,N
C
C      FOLLOWING 12 STMTS SEARCH FOR PIVOT ELEMENT
C
      T=0.0D0
      DO 9 J=1,N
      IF(IPVOT(J)-1) 13,9,13
13  DO 23 K=1,N
      IF(IPVOT(K)-1) 43,23,81
43  IF(ABS(T)-ABS(A(J,K))) 83,23,23
83  IROW=J
      ICOL=K

```

```

T=A(J,K)
23 CONTINUE
9 CONTINUE
IPVOT(ICOL)=IPVOT(ICOL)+1
C
C FOLLOWING 15 STMTS TO PUT PIVOT ELEMENT ON THE DIAGONAL
C
IF(IROW-ICOL) 73,109,73
73 DET=-DET
DO 12 L=1,N
T=A(IROW,L)
A(IROW,L)=A(ICOL,L)
12 A(ICOL,L)=T
IF(M) 109,109,33
33 DO 2 L=1,M
T=B(IROW,L)
B(IROW,L)=B(ICOL,L)
2 B(ICOL,L)=T
109 INDEX(I,1)=IROW
INDEX(I,2)=ICOL
PIVOT(I)=A(ICOL,ICOL)
DET=DET*PIVOT(I)
C
C NEXT 6 STMTS TO DIVIDE PIVOT ROW BY PIVOT ELEMENT
C
A(ICOL,ICOL)=1.0D0
DO 205 L=1,N
A(ICOL,L)=A(ICOL,L)/PIVOT(I)
205 CONTINUE
IF(M) 347,347,66
66 DO 52 L=1,M
52 B(ICOL,L)=B(ICOL,L)/PIVOT(I)
C
C NEXT 10 STMTS REDUCE NON PIVOT ROWS
C
347 DO 135 LI=1,N
IF(LI-ICOL) 21,135,21
21 T=A(LI,ICOL)
A(LI,ICOL)=0.0D0
DO 89 L=1,N
89 A(LI,L)=A(LI,L)-A(ICOL,L)*T
IF(M) 135,135,18
18 DO 68 L=1,M
68 B(LI,L)=B(LI,L)-B(ICOL,L)*T
135 CONTINUE
C
C NEXT 11 INTERCHANGE COLUMNS
C
222 DO 3 I=1,N
L=N-I+1
IF(INDEX(L,1)-INDEX(L,2)) 19,3,19
19 JROW=INDEX(L,1)
JCOL=INDEX(L,2)
DO 549 K=1,N
T=A(K,JROW)

```

```

      A(K,JROW)=A(K,JCOL)
      A(K,JCOL)=T
549  CONTINUE
3    CONTINUE
81   CONTINUE
      WRITE(14,992) ((A(L,M),M=1,N),L=1,N),DET
992  FORMAT(/1X,' INVERSE OF MATRIX IN MINV4 ',/1X,4(/1X,4F8.4)
&,/1X,' DET T = ',1PE12.4)
C
C    CHECK INVERSE AND WRITE TO UNIT 14
C
      DO 120 I=1,N
      DO 120 J=1,N
      ONE(I,J)=0.000
      DO 120 K=1,N
      ONE(I,J)=ONE(I,J)+A(I,K)*C(K,J)
120  CONTINUE
      WRITE(14,991) N,ONE
991  FORMAT(1X,//1X,' CHECK INV ORDER OF MATRIX = ',14,//1X
&,4(/1X,4F8.4))
      RETURN
      END
C
C
C
C    SUBROUTINE MINV3(T,S)
C
C    S=INV(T)  T IS NOT DESTROYED. ONE=S*T FOR CHECK
C
      IMPLICIT REAL*8 (A-H,O-Z)
      DIMENSION T(3,3),S(3,3),ONE(3,3),B(3),C(3),A(4,4)
      DATA ONE/9*0.0/,B/3*0.0/,C/3*0.0/,A/16*0.0/
C
C    MAKE SURE FIRST PIVOT ELEMENT IS NOT ZERO
C
      N=4
      NN=N-1
      WRITE(14,3) ((T(L,M),M=1,NN),L=1,NN)
3    FORMAT(1X,//1X,' MATRIX T ',/1X,3(/1X,3F8.4) )
      A(1,1)=1.000
      DO 10 I=1,NN
      DO 10 J=1,NN
10   A(I+1,J+1)=T(I,J)
      A(1,1)=1.000/A(1,1)
      DO 110 M=1,NN
      K=M+1
50   DO 60 I=1,M
      B(I)=0.000
      DO 60 J=1,M
60   B(I)=B(I)+A(I,J)*A(J,K)
      D=0.000
      DO 70 I=1,M
70   D=D+A(K,I)*B(I)
      D=-D+A(K,K)
      A(K,K)=1.0/D

```

```

      DO 88 I=1,M
29  A(I,K)=-B(I)*A(K,K)
      DO 98 J=1,M
      C(J)=0.000
      DO 98 I=1,M
98  C(J)=C(J)+A(K,I)*A(I,J)
      DO 108 J=1,M
108 A(K,J)=-C(J)*A(K,K)
      DO 118 I=1,M
      DO 118 J=1,M
118 A(I,J)=A(I,J)-B(I)*A(K,J)
      DO 111 I=1,MM
      DO 111 J=1,MM
111 S(I,J)=A(I+1,J+1)
      WRITE(14,2) ((A(L,M),M=1,MM),L=1,MM),D
2  FORMAT(/1X,' INVERSE OF AUGMENTED T ',/1X,4(/1X,4F8.4)
&,/1X,' DET T = '.1PE12.4)
C
C  CHECK INVERSE AND WRITE TO UNIT 14
C
      DO 128 I=1,MM
      DO 128 J=1,MM
      ONE(I,J)=0.000
      DO 128 K=1,MM
      ONE(I,J)=ONE(I,J)+S(I,K)*T(K,J)
128 CONTINUE
      WRITE(14,1) MM,ONE
1  FORMAT(1X,//1X, ' CHECK INV ORDER OF MATRIX = ',I4,//1X
&,3(/1X,3F8.4))
      RETURN
      END
C
C
C  SUBROUTINE MPCR(ICOR,IIDR)
      IMPLICIT REAL*8 (A-H,O-Z)
      CHARACTER MPC*8,SPACE*8,PM*2
      COMMON /XMPCR/ XMPC(18),IDG(3),LINE,X(3)
      DATA MPC,SPACE,PM/'MPC ',' ','+M'/
      ISID=312
      I1=1
      I2=2
      I3=3
      WRITE(14,1) IIDR, ICOR, X, XMPC
1  FORMAT(1X,' MPC EQUATIONS: GRID REMOVED ',
&I8,' DIRECTION ',I4,4X,/1X,4F12.4,
1/1X,F9.4,' UA ',F9.4,' UB ',F9.4,' UC ',
2/1X,F9.4,' VA ',F9.4,' VB ',F9.4,' VC ',
3/1X,F9.4,' WA ',F9.4,' WB ',F9.4,' WC ')
      L1=LINE
      L2=LINE+1
      L3=LINE+2
      L4=LINE+3
      WRITE(13,2) MPC, ISID, IIDR, ICOR, XMPC(1)
1, IDG(1), I1, XMPC(2), SPACE, PM, L1, PM, L1, SPACE, IDG(2), I1, XMPC(3)

```



```
2, IDG (3), I1, XMFC (4), SPACE, PM, L2, PM, L2, SPACE, IDG (1), I2, XMFC (5)
3, IDG (2), I2, XMFC (6), SPACE, PM, L3, PM, L3, SPACE, IDG (3), I2, XMFC (7)
4, IDG (1), I3, XMFC (8), SPACE, PM, L4, PM, L4, SPACE, IDG (2), I3, XMFC (9)
5, IDG (3), I3, XMFC (10)
2  FORMAT (1X, A8, 3I8, F8.3
1, 2I8, F8.3, A8, A2, I6, /1X, A2, I6, A8, 2I8, F8.3
2, 2I8, F8.3, A8, A2, I6, /1X, A2, I6, A8, 2I8, F8.3
3, 2I8, F8.3, A8, A2, I6, /1X, A2, I6, A8, 2I8, F8.3
4, 2I8, F8.3, A8, A2, I6, /1X, A2, I6, A8, 2I8, F8.3
5, 2I8, F8.3)
END
```

1 N85-25880

NASTRAN'S APPLICATION IN AGRICULTURAL ENGINEERING

TEACHING AND RESEARCH

Garrett L. Van Wicklen
Agricultural Engineering Department
University of Georgia

SUMMARY

Finite element analysis has been recognized as a valuable solution method by agricultural engineers. NASTRAN has been obtained by the Agricultural Engineering Department at the University of Georgia. The NASTRAN Thermal Analyzer has been used in the teaching program for an undergraduate course in heat transfer and will be used for a new graduate course in finite element analysis. The NASTRAN Thermal Analyzer has also been applied to several research problems in the Agricultural Engineering Department.

INTRODUCTION

Twenty years ago as engineers and computer scientists were initiating work on NASTRAN, I am certain that they never thought that their finite element analysis program would be applied to the solution of engineering problems in agriculture. In fact, many people are likely unaware of the existence of agricultural engineering. The most popular misconception of an agricultural engineer is that of a grease-covered farmhand tinkering with a sputtering tractor. While agricultural engineers deal with the design, production, and testing of farm machinery, they are involved with a wide range of engineering problems. Agricultural engineers also work in the areas of farm structures and their environments; soil, water, and plant relationships; food production and processing; the application of microelectronics to agriculture; and the management of agricultural wastes. Agricultural engineers face a wide realm of problems and must utilize the latest technology and techniques to solve them. It is little wonder that agricultural engineers have become involved with the finite element method as a solution method for problems in all the previously mentioned areas.

The use of finite element analysis by agricultural engineers began in 1974. An instructional workshop on the use of the finite element method was presented at the 1974 Winter Meeting of the American Society of Agricultural Engineers. The workshop was organized by Drs. Larry Segerland and Robert Gustafson. Segerland and Gustafson have each published numerous research papers which apply the finite element method to agricultural problems; organized courses at Michigan State University and the University of Minnesota, respectively; and have written software to encourage the use of finite elements. Segerland has written an excellent text for a first course in finite element analysis entitled, Applied Finite Element Analysis (1). Several research papers have been published since 1974 by agricultural engineers utilizing the finite element method for such problems as determining the shrinkage stresses of soybeans during drying (2); modeling stomatal guard cells in

plant leaves (3); measuring the mechanical and thermal strength of avian eggs (4); the freezing rates of food products (5); and the thermal analysis of livestock housing (6).

Agricultural engineers, like engineers of other disciplines, have employed the finite element package programs such as NASTRAN, STRUDL, and ANSYS. NASTRAN was obtained by the Agricultural Engineering Department at the University of Georgia in July, 1983. It has since been incorporated into an undergraduate course in heat transfer, and will soon become part of a graduate course in finite element analysis. The NASTRAN Thermal Analyzer (NTA) has been useful for analysis in several projects in areas such as structural environments, post-harvest handling of vegetables, and biomass fuels. The purpose of this paper is to describe the application of NASTRAN to the teaching and research program of the Agricultural Engineering Department at the University of Georgia.

INSTRUCTIONAL APPLICATION

A basic course in heat transfer is required of all students majoring in Agricultural Engineering at Georgia. This course, taught during the junior year, is designed to introduce the students to conduction, convection, and radiation heat transfer. Approximately 25 percent of the course is devoted to an introduction to numerical methods for solution of heat transfer problems. The finite difference method is introduced initially, followed by an introduction to finite element analysis. Usually three, simple, one dimensional transient conduction problems are assigned for solution using finite differences on a microcomputer. These same problems are later solved using NASTRAN to illustrate the benefits of a packaged program. The students are also exposed to several example NASTRAN programs during their laboratory period to show how easy it is to use finite element analysis to solve "complicated" problems. Students are encouraged to use NASTRAN to attempt to solve larger, applied problems. To illustrate the effectiveness of the finite element analysis, actual data from a simple class demonstration is compared to data generated by a NASTRAN model. The demonstration usually consists of monitoring the transient cooling of a piece of fruit instrumented with thermocouples. Using NASTRAN has allowed students to be exposed to finite element analysis without discouraging them by lengthy discussions of its theory and computing methods. The students gain an instant appreciation for numerical methods as a solution technique.

A graduate course in finite element analysis has recently been approved by the faculty of the University of Georgia College of Agriculture. The course will likely be taught during the Summer Quarter, 1985. Since the Agricultural Engineering Department is the only engineering discipline offered at the University of Georgia, the expected enrollment is five to ten students per quarter. The course is designed with the assumption that this is a first course in numerical methods for the student and that their background will consist of only a brief introduction to finite element analysis at the undergraduate level. The course will consist of the basic concepts of the finite element method including the various elements and domain discretization, the methods of equation formulation, solution procedures, computer implementation, and a sampling of software packages. Before utilizing software packages, students will be required to develop their own computer solution for a number of small problems using a microcomputer. The small class size will offer the opportunity for students to develop individual term projects. These projects will require a student to choose a particular problem, hopefully related

to their thesis area, to which a finite element analysis may be applied. The numerical results will be compared to experimental and analytical data taken by the student. NASTRAN will be used as an example of a software package available on the mainframe computer, and should be an important tool which students use for the term project. Anticipated projects will involve thermal modeling of animal housing and greenhouses, fruit and vegetable processing, irrotational flow of groundwater, and the structural integrity of agricultural structures and machinery. A similar course taught since 1979 at Auburn University (7) resulted in the following interesting array of student projects: the structural analysis of a bow string truss for a center pivot irrigation system; vibration analysis of a rotary mower cutter blade; steady state water seepage in porous media; and an evaluation of the strain distribution in a proposed load transducer for use in a tillage implement force system measurement. As was the case with its use in the undergraduate course, NASTRAN will allow the graduate students to use finite element analysis for solution of more rigorous problems without drowning with involved computer programming and development.

RESEARCH APPLICATIONS

The NASTRAN Thermal Analyzer (NTA) has been applied to several problems under study in the Agricultural Engineering Department at the University of Georgia. A short discussion of each project will be given to illustrate the application of the NTA to agricultural research.

Passive Solar Wall for Poultry Brooding

The poultry industry is very important to the agricultural economy of Georgia. Broiler chickens, which are slaughtered at seven weeks of age, accounted for over \$610 million in sales at the farm level in Georgia during 1982. Birds less than 2 weeks old require supplemental heat, usually provided by LP gas burners, to maintain their body temperature. Although Georgia has a relatively mild winter climate, the primary factor in poultry house design is the summer heat. Only recently have enclosed, insulated, fan ventilated poultry houses been built in Georgia. A tremendous amount of brooding heat is necessary during the winter months regardless of the type of house construction because of ventilation air flow necessary to limit heat and moisture, and because of brooding temperatures between 29 and 35 C.

One method to reduce the heat consumption is to use partial house brooding where birds are contained in only a portion of the house to reduce the air volume heated. The use of solar heat has also been studied, primarily using active systems. Instead of an active system, the Agricultural Engineering Department explored the feasibility of using a south facing, passive solar wall. The wall could be constructed of poured concrete and tilted into place as a retrofit on existing houses with a southern exposure, or easily included in new construction. A project was initiated to investigate the feasibility of a concrete passive solar wall in a Georgia broiler house using partial house brooding. The design process could be most efficiently handled by a thermal model using the NTA for finite element analysis. This project consisted of (a) a wall thickness and conductivity test, (b) a verification of the finite element application, and (c) the simulation of the entire broiler house. The wall thickness and thermal conductivity were examined by using a model consisting of one dimensional elements (Fig. 1). The outside wall

surface was exposed to the same set of boundary conditions as the wall thickness and conductivity were varied. The thermal lag time for the inside surface to reach a given temperature was the criteria used to select wall characteristics for the larger simulation. Concrete wall thicknesses of 0.1, 0.2, and 0.25 m having a thermal conductivity of 0.42 W/mC were found to deliver the majority of the solar heat to the brooding area beginning at 8 p.m., and were chosen for use in the simulation of the entire house.

This application of the finite element method was verified by comparing data from a vacant, instrumented warehouse to the simulated results. The actual and simulated data were quite close (Figure 2).

The broiler house simulated was 11 x 91.5 m, containing 13,000 chickens. Heat and moisture production data for birds at ages 1, 2.5, and 4 weeks of age were used (8). Temperature and solar data were chosen for a clear, December 21 day at Athens, GA. The passive solar wall occupied the south wall in the partial house brooding area. Half and one-third house brooding were simulated. Radiation and convective boundary conditions were used in the finite element model consisting of one dimensional elements (Figs. 3 and 4).

Results of the simulation indicated that the wall produced 1321 kW-hr of heat for a clear, December 21 day using half house brooding. The benefit of the solar wall was determined by comparison to the temperature within a similar broiler house without the wall. The solar wall raised air temperatures within the house 3 C above the conventional house for broilers 1 week old. This temperature difference between house types decreased as the birds became older because it became necessary to increase the ventilation rate (Figs. 5, 6, and 7). The outer wall surface was found to re-radiate heat after dark to the outdoors. It was necessary to use an insulated curtain ($R=1.06 \text{ m}^2\text{C/W}$) to cover the solar wall at night. This curtain might also reflect solar radiation from the wall during warm weather. It was concluded that the passive solar wall constructed of concrete and used in this manner was unfeasible without using additional heat sources. The cost and management of an insulated curtain are an added burden.

Insulation Requirements for Buried Thermal Storage

Georgia is among the nation's leaders in biomass production, primarily wood. There has been interest by the poultry industry in providing brooding heat birds by burning biomass furnaces. While some studies involving forced air systems have not proven feasible (9), circulating heated water through heat exchangers in the brooding area has been more promising. Concrete septic tanks are inexpensive and can be used to store the heated water. To improve the thermal efficiency of a system, the storage tank can be buried and insulated. The NTA was used to model the heat loss from a 3785 liter tank during typical winter conditions at various locations. A two dimensional finite element model was used (Figure 8). The finite element model was verified by monitoring the heat loss from a 3785 liter septic tank buried 0.3 m below grade and comparing it to data generated by the simulation. The heat loss simulated by the finite element analysis exceeded the actual heat loss by 13.1 percent over a 12 hour period.

Results of this study indicated that during a 12 hour night heat storage period in January, an uninsulated 3785 liter concrete tank buried 0.3 m below grade and filled with water heated to 60 C will lose 15 percent more heat than the same tank

insulated with a material having a thermal resistance of $0.87 \text{ m}^2\text{C/W}$ (one inch of smooth skin polystyrene). Addition of an identical second layer of insulation would only reduce the heat loss from the tank an additional 2 percent. Based on reported burning efficiencies and system losses (10), addition of an insulation material with a thermal resistance of $0.87 \text{ m}^2\text{C/W}$ will require approximately 18 percent less cord wood than a system with an uninsulated tank.

Thermal Analysis of Nursery Containers

Commercial plant nurseries commonly grow plants in black and green nursery containers. The growth media in the containers can reach temperatures of 50 C or greater as a result of solar radiation. Plant root growth retardation generally occurs above 30 C, while growth cessation occurs above 28 C. Root damage may occur at media temperatures greater than 45 C (11). Several attempts have been made to alleviate the thermal stress suffered by plant roots including using perforated containers, white plastic containers, and evaporative cooling (12). Most studies of container soil temperatures have been empirical (11). A finite element analysis using the NTA is currently in progress to quantify the thermal environment of a nursery container exposed to summer solar radiation. A three dimensional model comprised of wedge elements is being used (Figure 9). In hopes of reducing high media temperatures, the following parameters are being investigated: a) container surface color, b) media composition, c) container geometry, and d) the container dimensions.

Post-Harvest Cooling of Southern Peas

The development and use of pea harvesting combines has resulted in more efficient and economical harvesting and allowed for an increase in planted acreage (13). An indirect problem resulting from this improvement in mechanization and larger pea harvest is post-harvest quality deterioration due to excessive temperatures of the peas before they can be cooled at the processing plant. Quality loss begins when the pea temperature reaches 25-30 C. Temperatures of peas harvested during summer when the air temperature is 32 C frequently rise to approximately 45 C as the peas are loaded in bins for transport from the field. Agricultural engineers are investigating the use of convective and evaporative cooling of the post-harvest peas while enroute to the processing plant. An initial finite element model using the NTA is being used to investigate the required air velocity to produce sufficient convective cooling to maintain pea quality. A two dimensional finite element model of an individual pea is being evaluated (Figure 10). Modeling of several peas in a bin with void spaces filled with air is currently being developed.

CONCLUSION

The finite element method has been applied to a wide array of agricultural problems. NASTRAN has been very beneficial in applying the finite element analysis in research projects, and in developing a positive attitude for numerical solution methods in the students who are in the instructional program. Engineers are able to use the finite element analysis as a solution technique without becoming mired in computer programming and the theoretical background of the method. Use of NASTRAN will expand in the Agricultural Engineering Department at the University

of Georgia beyond the current use of only the NTA. Student and faculty interest, already evident, will apply NASTRAN to several new applications.

REFERENCES

1. Segerlind, L.J.: Applied Finite Element Analysis. John Wiley and Sons, New York. 1976. pp.422.
2. Misra, R.N.; Young, J.H.: Finite Element Analysis of Simultaneous Moisture Diffusion and Shrinkage of Soybeans During Drying. ASAE Paper 78-3056, ASAE, St. Joseph, MI 1978.
3. Cooke, J.R.; Rand, R.H.; Mang, H.A.; DeBaerdemaeker: A Nonlinear Finite Element Analysis of Stomatal Guard Cells. ASAE Paper 77-5511, ASAE, St. Joseph, MI 1977.
4. Upadhyaya, S.V.; Cooke, J.R.; Rand, R.H.: Finite Element Analysis of the Mechanical and Thermal Strength of Avian Eggs. ASAE Paper 81-3042, ASAE, St. Joseph, MI 1981.
5. Purwadaria, H.K.; Heldman, D.R.: Finite Element Model for Prediction of Freezing Rates in Food Products With Anomalous Shapes. ASAE Paper 80-6015, ASAE, St. Joseph, MI 1980.
6. Timmons, M.B.; Bottcher, R.W.: Finite Element Analysis of Livestock Housing. ASAE Paper 81-4025, ASAE, St. Joseph, MI 1981.
7. Turner, J.; Young, S.; Grisso, R.; Anderson, C.; Grant, T.; Evans, D.; Nichols, T.: Teaching Finite Elements in Agricultural Engineering. ASAE Paper 83-5535, ASAE, St. Joseph, MI 1983.
8. Reece, F.N.; Lott, B.D.: Heat and Moisture Production of Broiler Chickens During Brooding. Poultry Science, Vol. 61, pp. 661-666, 1982.
9. Ross, C.C.; Smith, M.S.: Wood Heating for a Commercial Broiler House. ASAE Paper 83-4011, ASAE, St. Joseph, MI 1983.
10. Thompson, S.A.; Stuckey, T.A.; McLendon, B.D.: Predictive Algorithm for Heating Broiler Houses With Cord Wood. ASAE Paper 83-3074, ASAE, St. Joseph, MI 1983.
11. Tollner, E. W.; Verma, B.P.; Vandergrift, S.: Thermal Conductivity of Artificial Potting Soils. ASAE Paper 84-1086, ASAE, St. Joseph, MI 1984.
12. Verma, B.P.: Container Design for Reducing Root Zone Temperature. Proc. SNA Res. Conf. pp. 179-182, 1979.
13. Smittle, D.A.; Hurst, W.C.; Ghatge, R.R.: Maintaining Quality of Southern Peas for Processing. Research Report 363, The University of Georgia College of Agriculture Experiment Station, Jan., 1981.

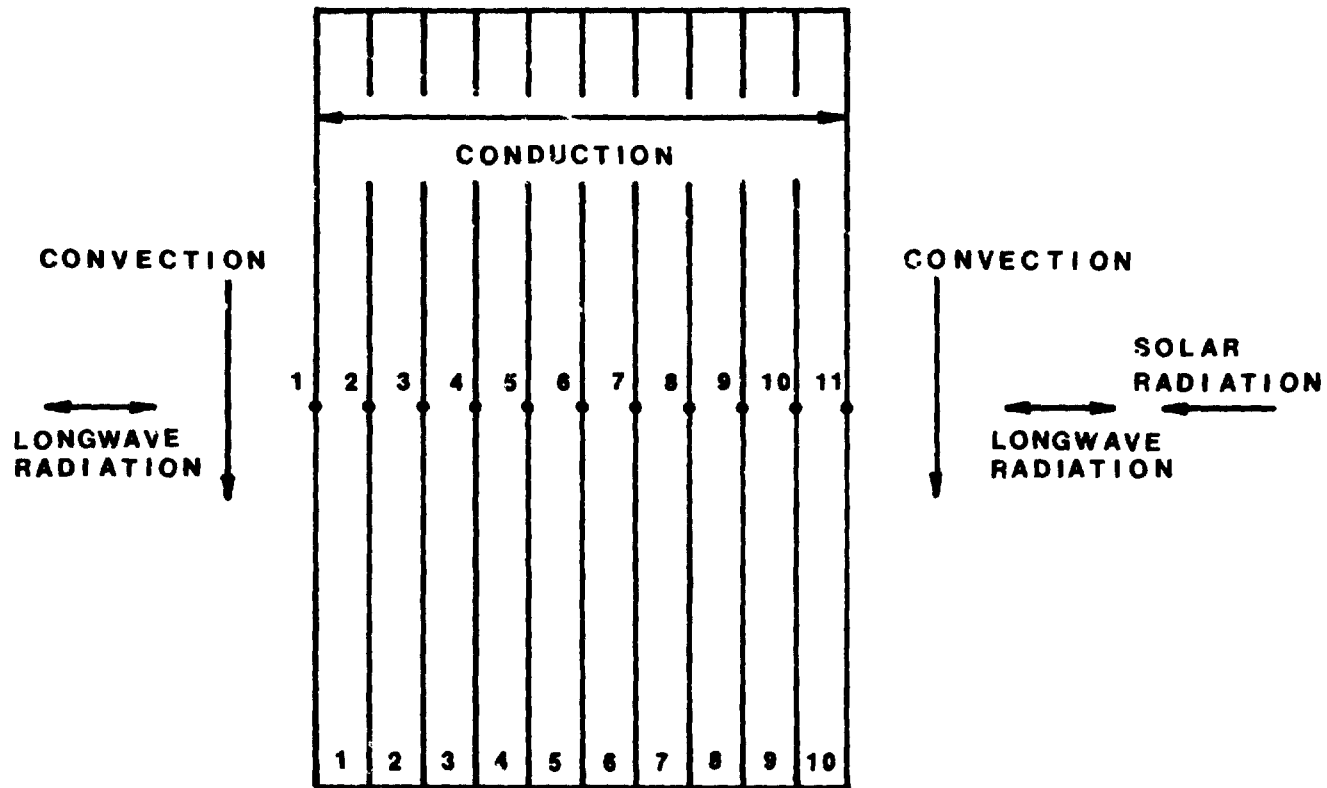


Figure 1. Finite element grid for the passive solar wall simulation.

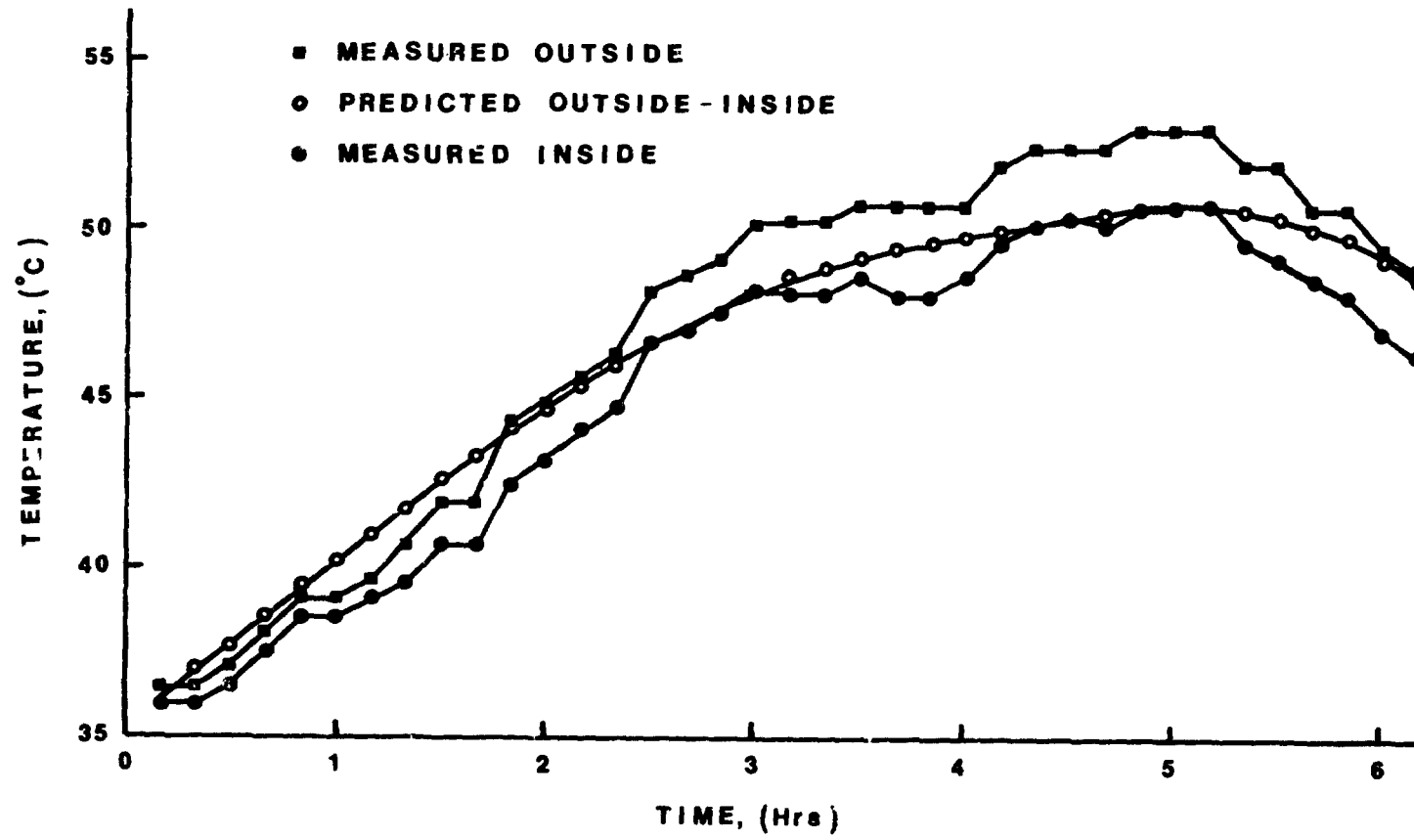


Figure 2. Wall temperature versus time of measured and predicted thermal analysis.

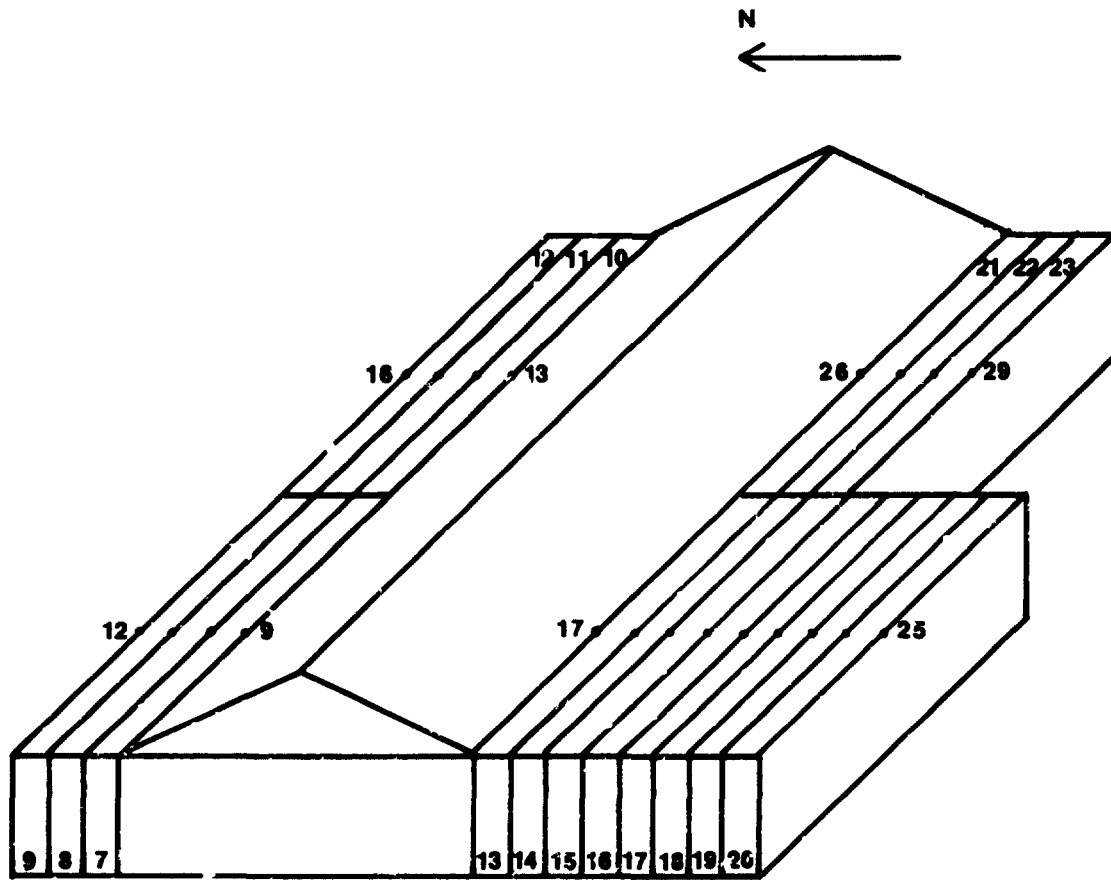


Figure 3. Finite element grid for sidewalls of the simulated poultry house using half house brooding.

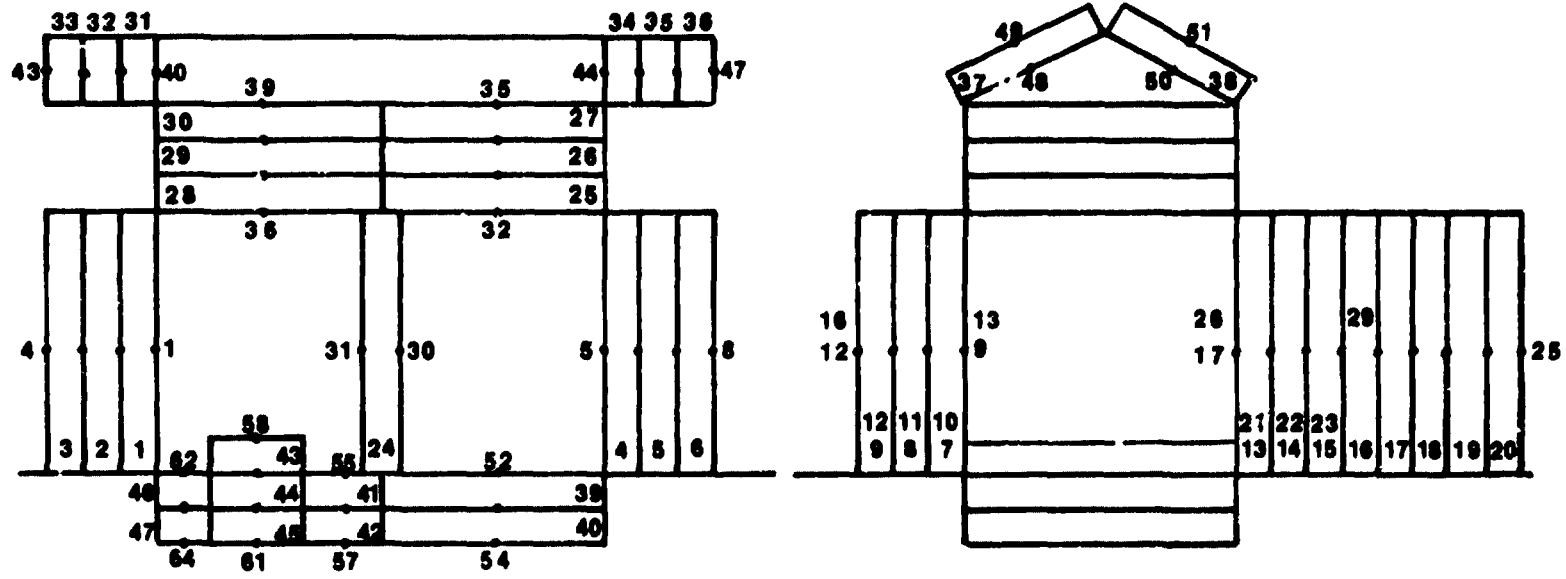


Figure 4. Finite element grid of the simulated poultry house (side and west views).

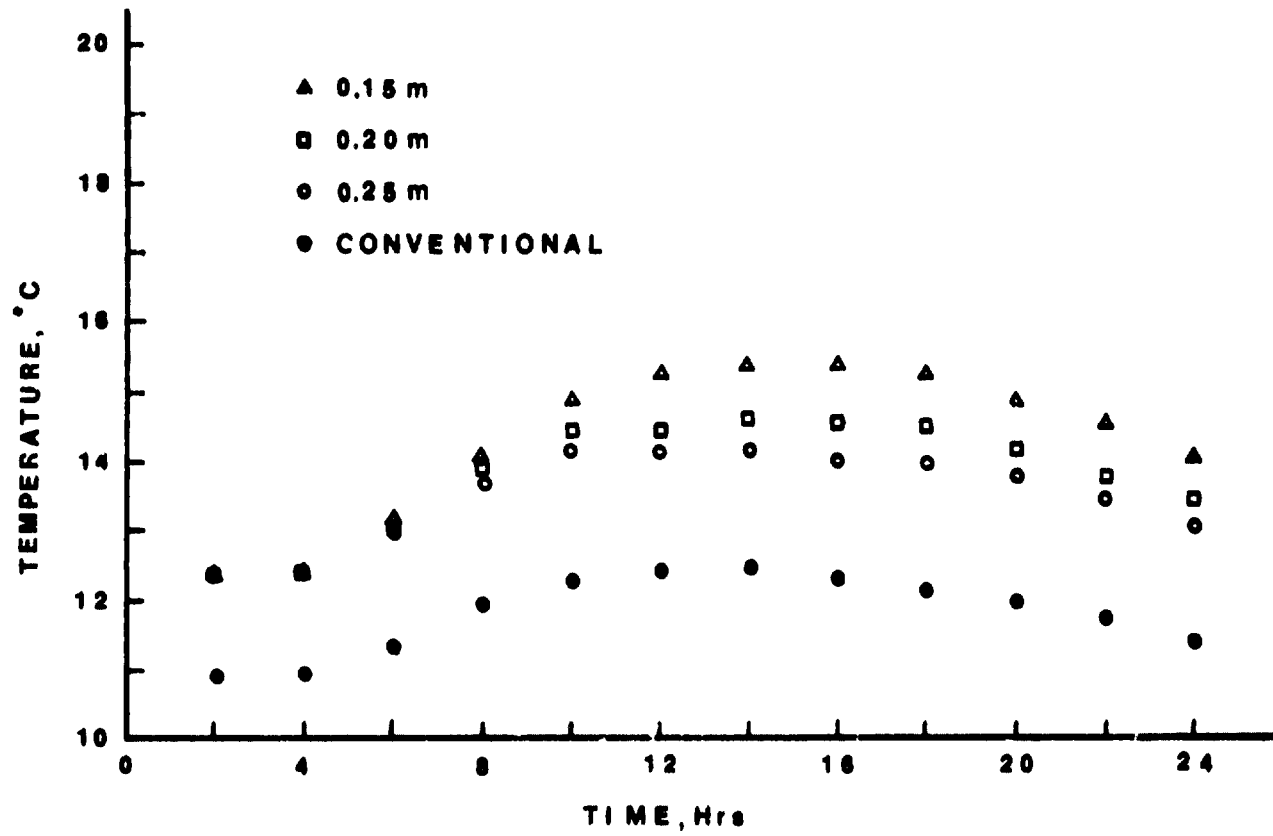


Figure 5. Brooding area temperature versus time for half house brooding for 1 week old birds.

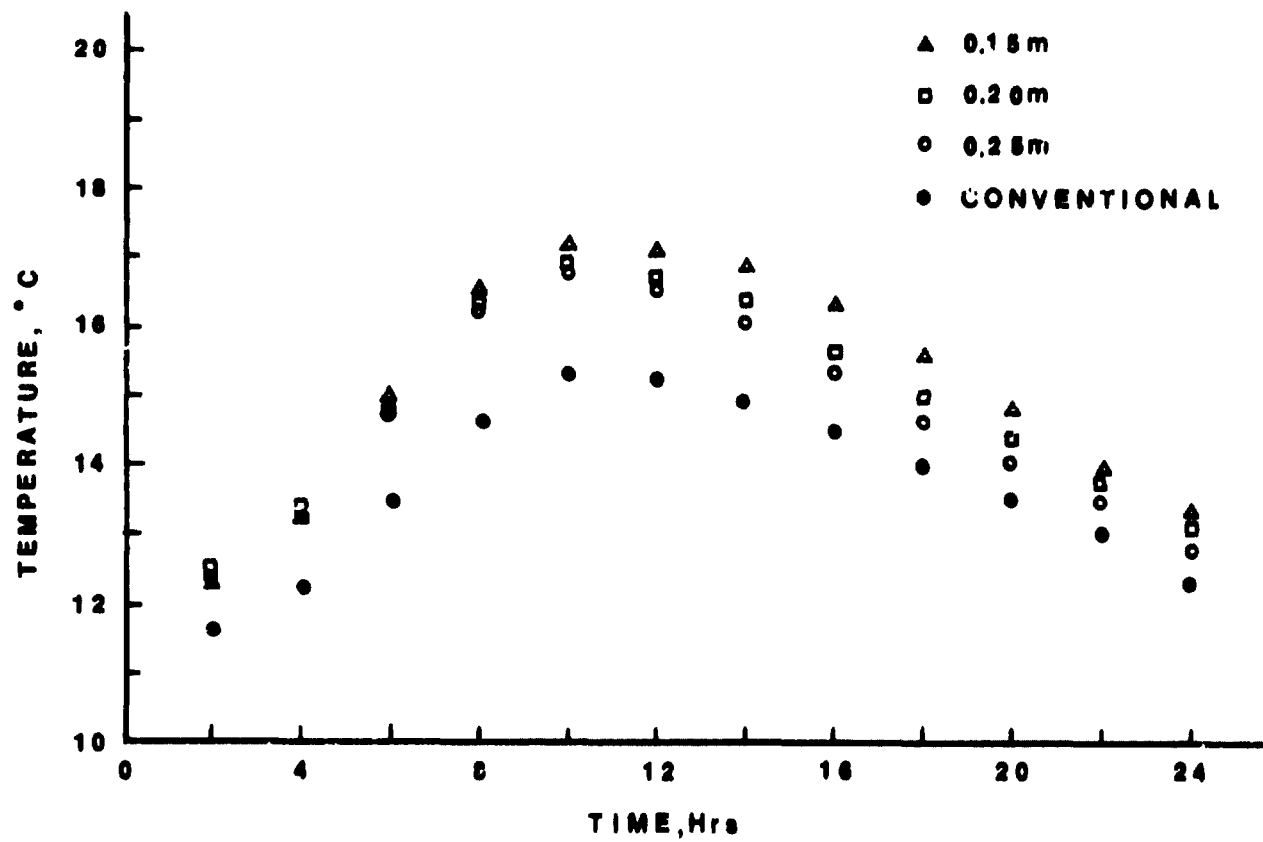


Figure 6. Brooding area temperature versus time for half house brooding for 2.5 week old birds.

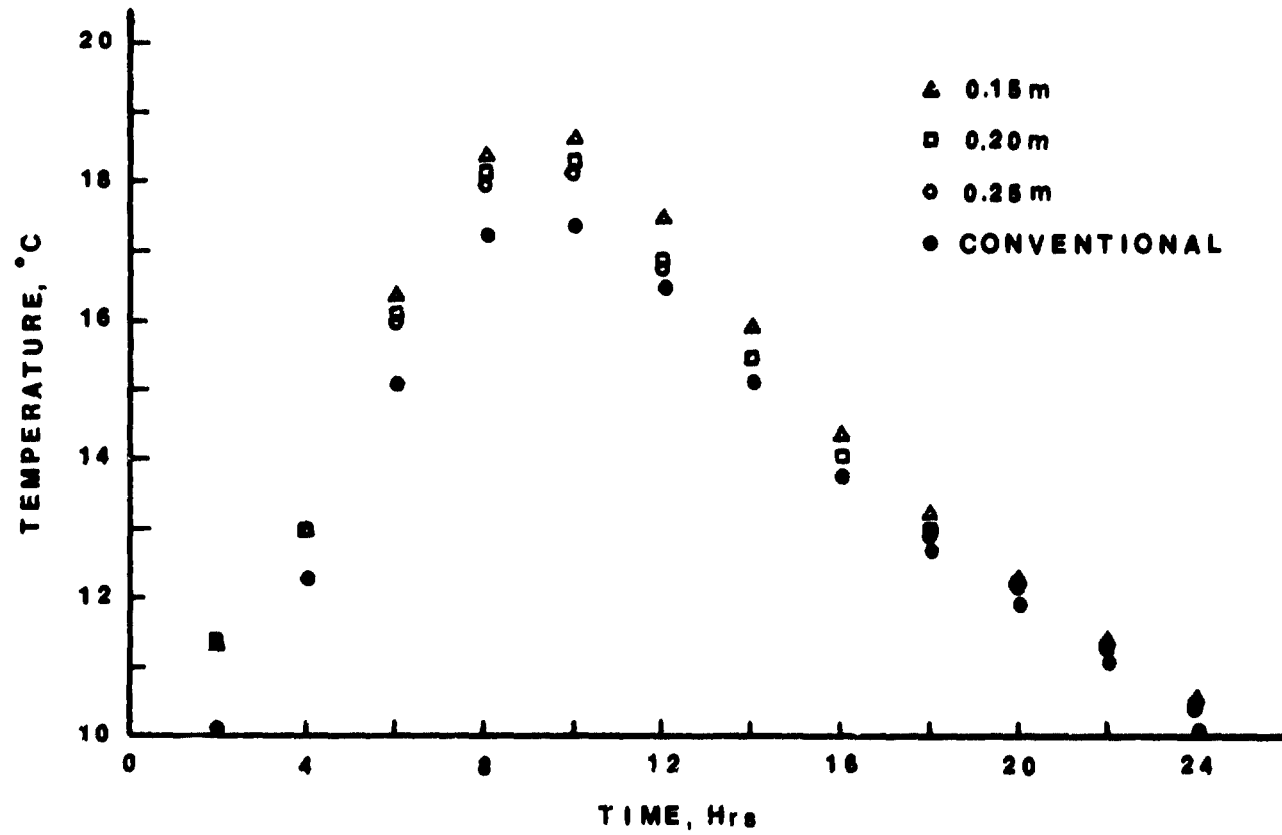


Figure 7. Brooding area temperature versus time for half house brooding for 4 week old birds.

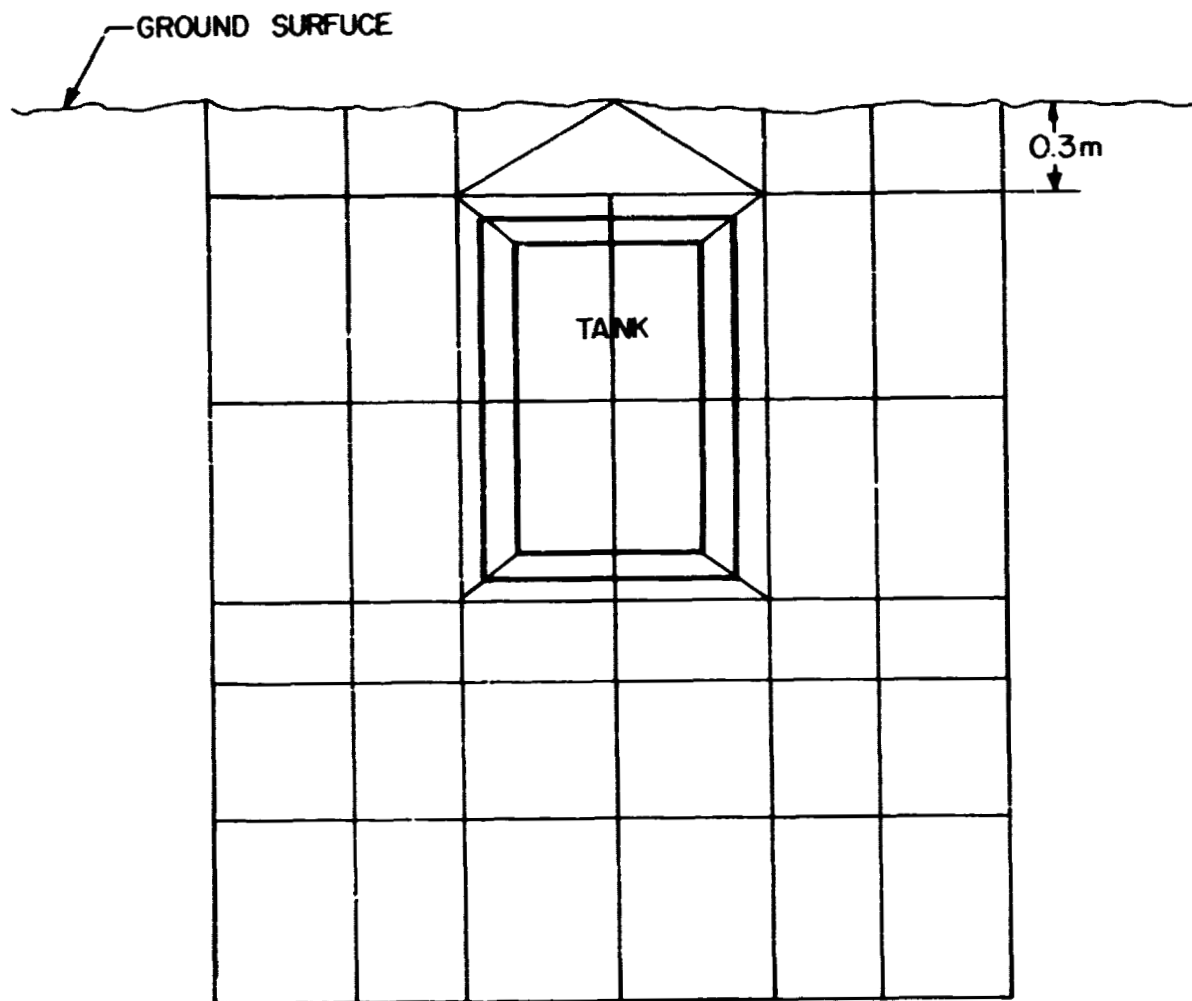


Figure 8. Finite element model of a buried thermal storage tank.

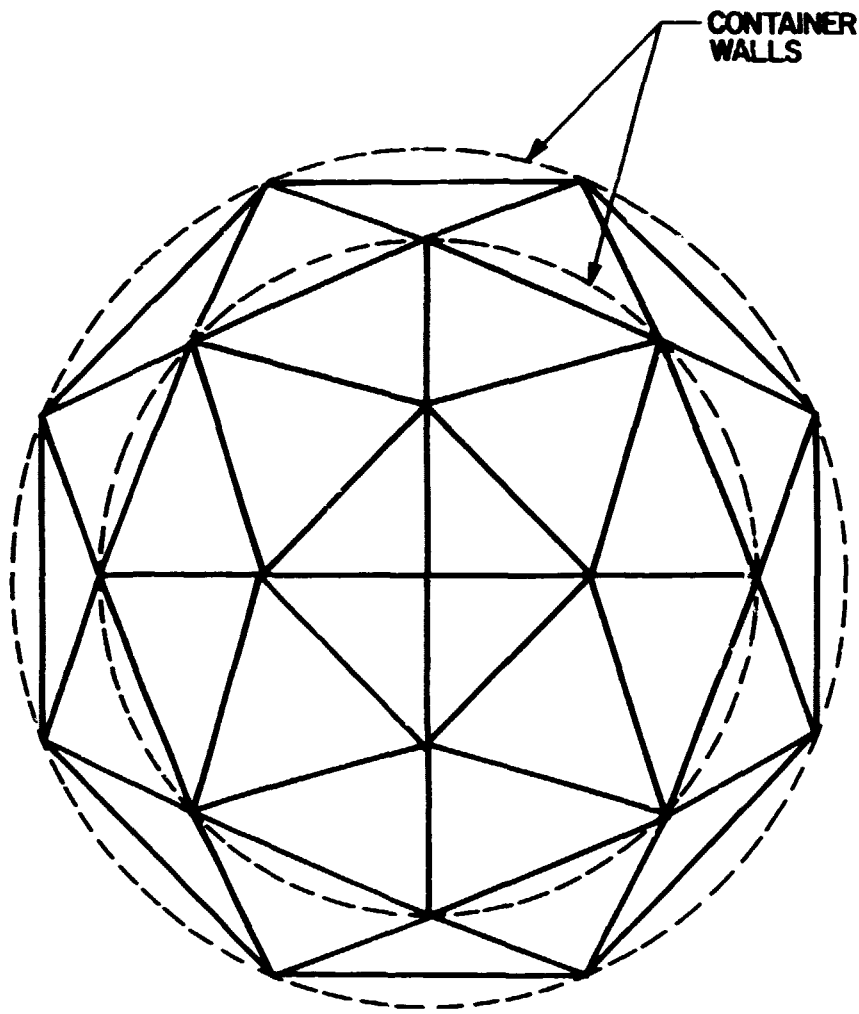


Figure 9. Finite element model of a nursery plant container.

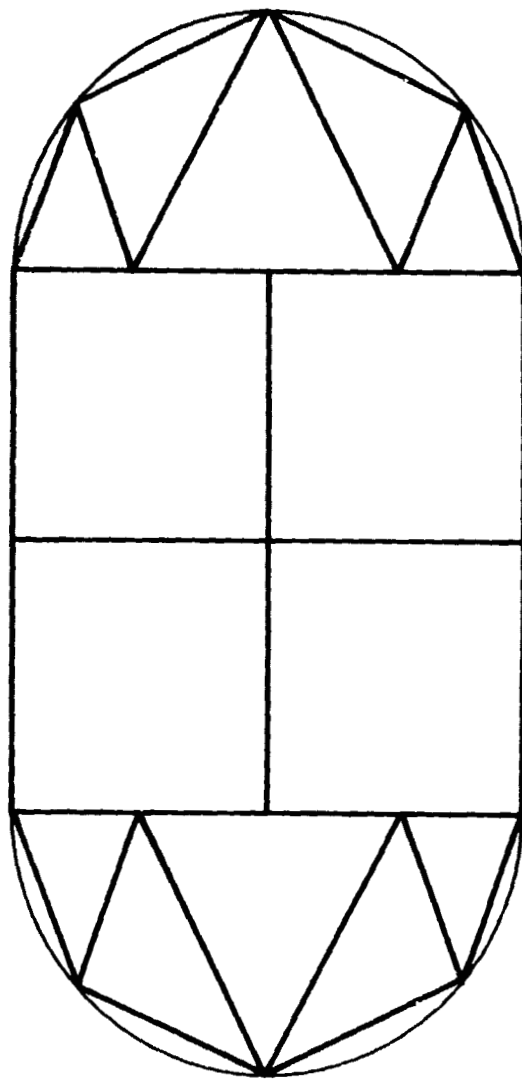


Figure 10. Finite element model of a southern pea.

7 N85-25881

USE OF COSMIC NASTRAN IN A DESIGN DEPARTMENT

Richard C. Coddington and Jose O. Nazario
John Deere Dubuque Works
Dubuque, Iowa 52001

SUMMARY

Application of COSMIC NASTRAN to product development in a design department requires low cost, rapid model construction and interactive evaluation of results. The NASTRAN processor developed by Jose O. Nazario meets these requirements by automating many of the modeling activities.

INTRODUCTION

The proliferation of finite element codes in today's competitive environment complicates the choice, "Which code is best for me?". Generally the user prefers to use one general purpose code that covers most of his or her applications.

NASTRAN is an ideal candidate for several reasons. It is thoroughly tested with thousands of practical applications in diverse situations. It handles large scale problems. It is well documented and well supported.

In the past, lack of automation of model construction, of model checking and of display of results hindered efficient use of NASTRAN. This was especially true in a product engineering environment. Jose Nazario's NASTRAN INTERFACE PROGRAM (NASTI) overcomes these objections by fully automating these needed functions.

PURPOSE

The main purpose of this paper is to highlight the manner in which NASTI automates model preparation, model checking and display of results. The writers will emphasize the features that make NASTI a cost effective tool for structural analysis in a product engineering department.

We will create a simple model of a bucket (Figure 1) to illustrate the many automation features in NASTI. Later, we will include applications of finite element models to three frames. These applications illustrate the level of detail included and the size of models run to date.

FEATURES OF NASTRAN INTERFACE PACKAGE

NASTI contains four main parts.

- * Digitize the model
- * Plot and check the model
- * Create the bulk data and submit job
- * Display the results

On line documentation in each of the main parts assists the user in executing the variety of options available.

Digitize the Model

While in DIGITIZE MODEL the user can create regions using the tablet, the screen or the keyboard (this geometry is three-dimensional), can generate the finite element mesh and can save either the regions, the mesh or both.

Plot and Check the Model

While in PLOT AND CHECK MODEL the user has a myriad of options that automate model construction and data checks.

Create the Bulk Data

CREATE BULK DATA formats the bulk data. It creates the executive and case control statements and automatically generates SPC's and MPC's. Elements currently supported include CBAR, CTRIA, CQUAD, CWEDGE, CTETRA, CTRSHL and CHEXA.

Display the Results

Is not a picture worth a thousand words? NASTI permits the user to plot the results of the analysis. Options include:

- * Plot deformed geometry
- * Plot stress or strain contours
- * Plot stress vectors
- * Plot Von Mises stresses

The more important display features include:

- * Automatic location and display of maximum displacement
- * Automatic location and display of maximum and minimum stresses or strains
- * Interactive zoom and window of plots

DIGITIZING THE MODEL USING NASTI

NASTI provides a four step process to create a finite element mesh. Suggested steps include create regions, generate the mesh, save the mesh and save the regions. Editing and graphical options permit the user to change and view the regions and/or mesh at any convenient intermediate step.

Creating regions

To start the user divides the structure into a collection of four sided regions. The sides of the regions may be straight, curved, or a combination of the two. Figure 2 shows the seven regions we picked to form the side of the bucket.

Regions can be created thru the digitizing tablet, the keyboard, the screen or by copying regions from a file. In many applications to new designs use of the digitizing tablet is most convenient. We will describe mesh creation using the tablet.

The user defines regions created to be in three-dimensional space. The surfaces created may be flat or curved. The user simply inputs three points (x_i, y_i, z_i) , $i=1,2,3$ to define a flat plane. As each region is created, it is automatically connected to neighboring regions to form a "patchwork" that makes up the planar part.

Frequently frame structures consist of intersecting flat plates. In this case, each flat plate is created individually. NASTI automatically ties contiguous plates together along their common edge.

For a curved surface the user creates points along the curved sides of the region. Later he can form the regions using the cursor or keyboard.

Copy feature automates creation of regions

The copy feature in NASTI simplifies construction of regions for both flat and curved surfaces. To construct regions with curved sides, the user simply copies the "key" nodes along the curved boundaries to the desired location and then uses the cursor or keyboard to form regions.

The user may also choose to copy regions to the desired location (See Figure 3) and later delete unwanted regions (regions 8 thru 14). The user then uses the cursors to form the back of the bucket (regions 16 thru 20). Figure 4 shows the final "patchwork" of regions forming one-half of the total bucket. The plane $z = 0$ is a plane of symmetry. Later, the symmetry generator can be used to automatically form the "other half" of the bucket.

Regions, key nodes or both may be copied as desired to form new regions. The flexibility and ease of this feature greatly reduces model construction time.

Generating the finite element mesh

Once the user has his regions it is easy to automatically generate the elements. The user simply selects the generate option to specify the number of elements along the first two sides for each region. He can do this individually for each region or for all regions if they are to be the same. Figure 5 shows the mesh generated for one-half of the bucket.

Interactive documentation aids casual users

On-line documentation guides the user in selecting each option. The experienced user can enter options without this aid whereas the inexperienced user can press the RETURN key for help. The interactive documentation also helps jog the memory of the occasional user who may not recall which option to use next.

Saving the regions and mesh

Once the user is satisfied with the mesh, then he can save both the mesh and the regions for later recall should the design be modified at a later date. He is then ready to go on to plotting and checking the model.

PLOTTING AND CHECKING THE MODEL

The user needs to check the finite element mesh for accuracy. Potential errors cover a broad spectrum of possibilities. Some of these include wrong direction for connectivity, incorrect connectivity, holes and overlaps with the mesh, errors in geometry, wrong material specifications and many others.

In addition to checking the model, this part of NASTI permits the user to efficiently alter the geometry of the part to reflect a design change. Constraints on material, manufacturing process, part fitup, cost of the part, use of existing parts and many other reasons may dictate the need for a design change. For whatever reason, this change must be easy and fast to accomplish. Otherwise, results of the analysis may arrive too late to aid in final design decisions.

NASTI has four main parts to facilitate model checking and modification. These parts include preset options, graphic options, edit options and input of loading and boundary conditions. Once again, as the user selects an option, interactive help is available to assist the user in proper use of the option.

Stringing together commands saves time

Many of the available options are not necessary but are extremely handy in automating model checking and changes. It is also very helpful to be able to string options together. This capability saves considerable time for the experienced user while not hindering the casual user. The casual user simply enters one option at a time. With experience the user gains confidence and starts to string options together. The following two examples illustrate the idea.

EXAMPLE 1

R A 30 150 0 O N T N G N P

The meaning of this string of commands is as follows:

COMMAND	MEANING
R A 30 150 0	Rotate the view using angles 30,150,0 degrees
O N	Turn off the outline (Let's user see elements)
T N	Turn the element tag off
G N	Turn grid number tag off
P	Plot the structure

The options selected by the user remain active until turned off. Thus the user need not repeat the options each time. Figure 6 shows the outline of the part prior to execution of the options shown. Figure 7 shows the result. The user can magnify the view, tag the elements and plot the result with the following string of options:

EXAMPLE 2

Z Y T Y P

COMMAND	MEANING
Z Y	Turn the zoom option on
T Y	Tag the elements
P	Plot the results

Figure 8 shows the part prior to execution of these options. Figure 9 shows the result.

Part Identification with structure

Frequently the total structure consists of many distinct parts. It is convenient to identify the individual parts to facilitate the checking process. It's usually easier to check each part individually than collectively. In addition, it is convenient to display the results as contour plots for individual parts of the total structure. Thus identification of individual parts by physical property type serves a dual purpose.

The writers changed the material specification for the leading edge of the back of the bucket from 4 to 5. This change permits flexibility to specify a stronger material for the cutting edge of the bucket.

Checking the Model for Cracks and/or Connectivity

Figure 10 shows the outline of the bucket. The top right portion represents the side of the bucket and the bottom left portion the back of the bucket. The outline on the bottom right portion of the bucket is its cutting edge.

The line between the back and side of the bucket could indicate either different materials, a crack exists between the back and the side, double elements (one on top of another) exist, elements are disconnected or elements are missing. Let's determine which of these alternatives apply.

Select the edit option thru the cursors by entering U C .
These options include:

- * Change element connectivity
- * List grid points and element properties
- * Form or delete elements
- * Align grid points along a line or in a plane
- * Measure distances between grid points
- * Copy or interpolate grid points
- * Show relative element connectivity

Use the V option to show differences (if they exist) in the connect'vity of each element. A plus sign in each element indicates that no elements are missing. By turning the outline option off and the element tag option on, the user can verify that no double elements exist. Next the user can plot the elements associated with material 2 by using the preset option for material groups in the main menu. The result is a plot of the side of the bucket only. This result indicates that differences in material cause the line shown between the side and the back of the blade.

Automating Design Change to include a hole in the bucket

Suppose the designer decides to include a circular hole in the back of the bucket after completion of the model. This modification is easily done by deleting elements in the area where the hole is to go, by using a local coordinate system to create grid points on the edge of the hole and by forming elements using the cursors. Figures 11 thru 16 show the sequence of options to rapidly modify the initial design to include this circular hole. The steps include:

Action	Figure(s)
* Delete elements in region where hole is to occur	11
* Use copy option to create nodes on radius of hole about a local x-axis	12
* Use the align option to place the nodes in the surface of the blade	13
* Use the interpolate and copy options to create additional nodes for mesh near the hole	14
* Fill in elements around the hole and display the back of the bucket	15
* Rotate the view to check that all elements in the back of the bucket are in the surface of this part	16

Automated Mesh Generation

After the analyst completes checking the model he is ready to generate the other half of the bucket. To do so the user merely specifies the plane of symmetry, the grid point increment (for numbering the new nodes) and the element increment (for numbering the new elements). For flexibility the user can save grid points, elements or both. Further, the user can choose to translate the "master set" of elements and/or grid points if desired.

Interactive application of Constraints and Loads

Once the model geometry is complete (See Figure 17) the user is ready to apply loads and to restrain the structure where it attaches to other components or to the ground. The user first selects the material number that identifies the part where he will apply constraints. Next he rotates this part to a convenient view. He can either automatically generate constraints in user specified directions or manually apply them using the cursors.

Figure 18 shows the fore-aft constraints on the back of the bucket. They might represent the the restraining action of a hydraulic cylinder on the back of the bucket.

Application of point loads is easily and quickly done by specifying the part, picking a good view, stating the force components and by using the cursors to show where they apply. The final step is to check the accuracy of the information by plotting the parts where the constraints and loads occur and selecting the display option for this information.

Figure 18 displays the pry load acting on the cutting edge of the bucket.

CREATION OF THE BULK DATA

NASTI fully automates the creation of the bulk data prior to job submission. Even on a large problem (over 10 000 degrees of freedom), the time to create the bulk data is under five minutes.

Removal of Singularities and Selecting Material Properties

The first step in creating the bulk data in NASTI is to

apply the single and multipoint constraints to remove the singularities from the stiffness matrix. Nazario developed an algorithm to automate the calculation and application of these constraints. The actual calculation is transparent to the user and normally takes less than one minute to complete.

The remaining steps to complete the bulk data include the following specifications:

- * Number of load cases
- * Thickness for each material
- * Material properties

After this input is complete, NASTI informs the user that the bulk data is complete and lists totals for the number of elements and grid points.

Submitting the Job for Batch Processing

NASTI fully automates the clerical work involved in preparing the executive control, the case control and file manipulation. Input includes:

- * Job Name and Project Number
- * Destination for Output
- * Time estimate for solution
- * Job Priority
- * Name for Output Data Set
- * Checks for creation of checkpoint tape
- * Checks to see if Restart Dictionary is to be used
- * Number of subcases
- * OK to submit job for batch execution

If the user wants to use non-standard options, then he elects not to submit for execution. He can then interactively edit the executive control, the case control or any feature in the bulk data to suit his needs.

DISPLAY OF RESULTS

Rapid data reduction is essential to effective use of finite element technology in today's modern design department. The design engineer must get the reduced data at a time where he can use it to make timely design decisions.

NASTI shrinks the time for data reduction by automatically sorting the output for maximum principal stresses, minimum principal stresses, maximum shearing stresses and maximum Von Mises stresses. The user can exploit this data to quickly zero in on regions of high stress and by using the interactive plotting features to display these regions.

Displacement Plots give Clue to Overall Structural Response

Figure 20 shows the deformation of the bucket due to pry loads on the cutting edge. Relative movement of the sides and back of the bucket give a qualitative "feel" of response of the bucket to pry loading. The printed maximum displacement quantifies this movement of material.

Contour Plots of Stress and Strain

Eighteen standard contour plots are available to display the distribution of stress or strain in the structure. The options include:

- * Principal Stress Contours
- * Principal Strain Contours
- * Shearing Stress Contours
- * Shearing Strain Contours
- * Von Mises Stress Contours
- * Von Mises Strain Contours

The usual procedure is to select the material to plot, rotate to a convenient view and pick the desired contour plots. Rotate, window and zoom features permit the user to focus on areas with large stress or strain gradients.

Figure 21 shows the distribution of strain on the front surface of the back side of the bucket. Figure 22 shows the detailed maximum principal strain distribution where the hydraulic cylinder attaches to the back of the bucket.

PRODUCT EVALUATION USING COSMIC NASTRAN

Engineers at the Dubuque Works use COSMIC NASTRAN to evaluate structural response of new and current products. The application to the design of frames, booms, buckets, castings and weldments has been particularly fruitful.

The level of complexity and model size used for the simulations depends on the particular application, the time frame for the analysis and the cost limits for the evaluation. The three examples included below illustrate the larger models used for evaluation of frames on our motor graders, our four wheel drive loaders and our two wheel drive loader-backhoes.

Figure 23 shows a schematic of the motor grader main frame. The model of this frame contains quadrilateral plate elements, triangular plate elements and bar elements. It has about 5000 elements, 4700 grid points and 24 000 degrees of freedom. As the design progressed the analyst used this model to try various plate thicknesses, reinforcements, and geometry changes to "tune the design" for improved performance.

Figure 24 shows a schematic of the engine frame on a four wheel drive loader. The model of this frame contains quadrilateral plate elements, triangular plate elements, solid elements and bar elements. It has about 7200 elements, 5300 grid points and 20 000 degrees of freedom. The analyst used this model to conduct "numerical tests" of the structure to evaluate its performance for different types of loading.

Figure 25 shows a schematic of the main frame of a two wheel drive loader-backhoe. The model of this frame contains quadrilateral plate elements, triangular plate elements, solid elements and bar elements. It has about 18 000 elements, 10 000 grid points and 50 000 degrees of freedom. The analyst used this model to evaluate design options for the mast and for its interaction with the main channel of the frame.

CONCLUSIONS

The NASTRAN INTERFACE PROGRAM (NASTI) fully automates construction, checking and data reduction in finite element models using COSMIC NASTRAN for structural analysis. This automation is essential to the fast paced environment that exists in new product design.

Design changes "on the fly" mandate the need for rapid and accurate data to support decisions on the proposed changes. The NASTI program meets this need by shrinking the time to "test" more proposed changes. The significant impact on our business is a better performing product at lower cost.

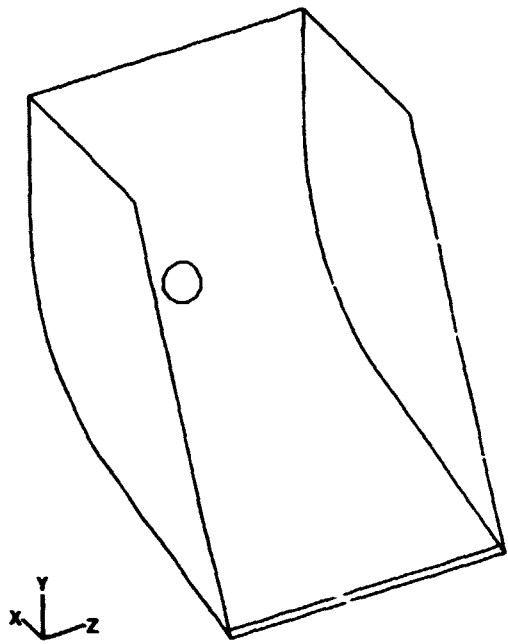


FIGURE 1 BUCKET

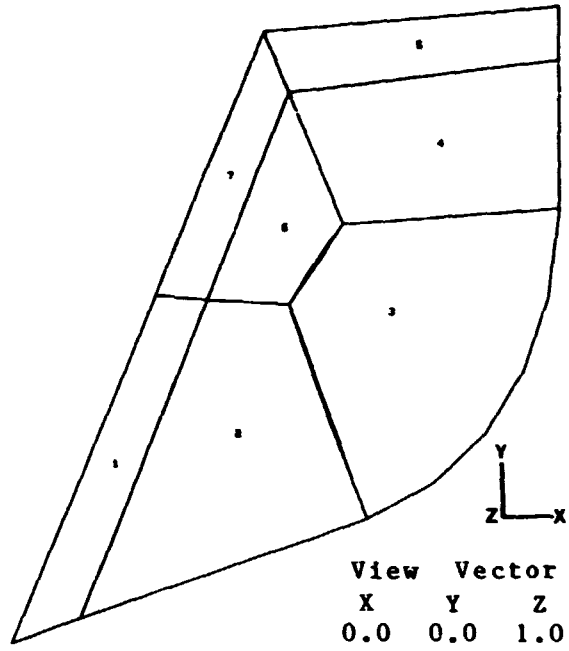


FIGURE 2 REGIONS

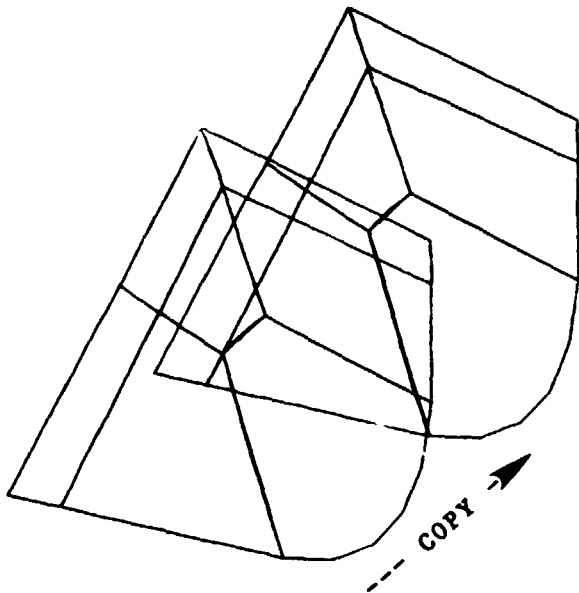


FIGURE 3 REGION COPY

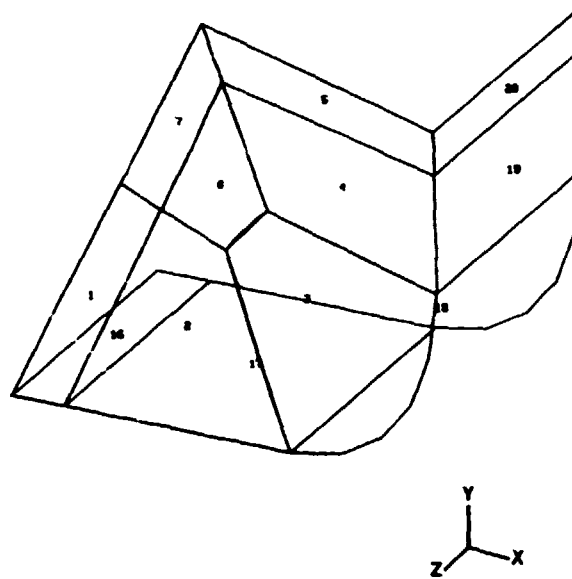


FIGURE 4 REGIONS FOR ONE-HALF OF THE BUCKET

ORIGINAL PAGE IS
OF POOR QUALITY.

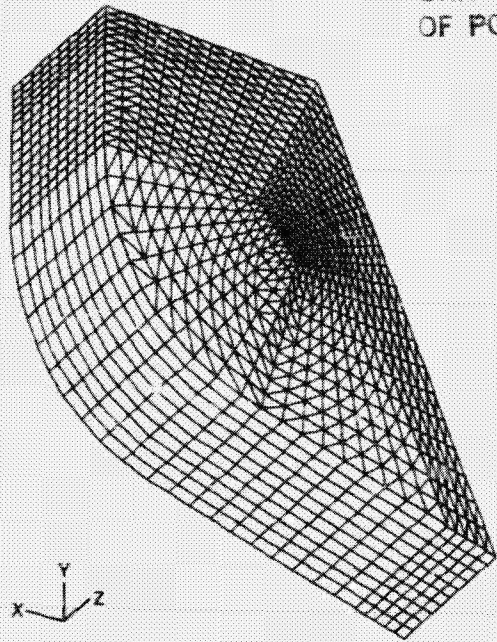
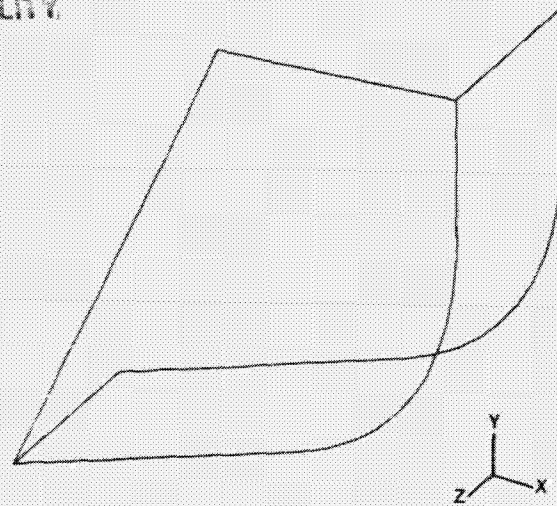
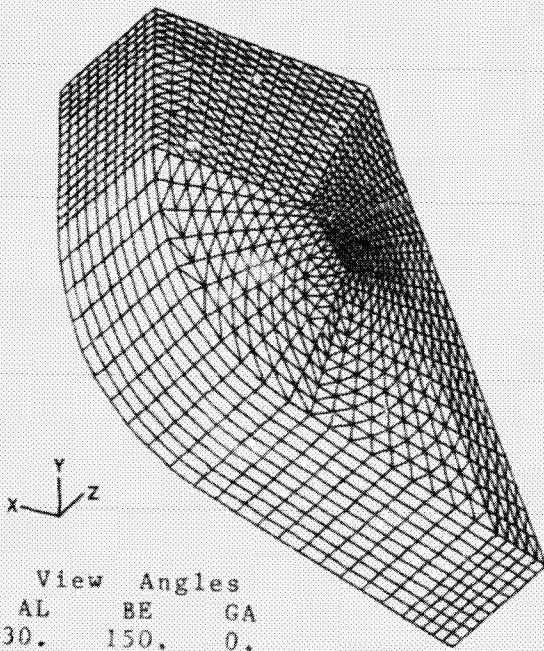


FIGURE 5 FINITE ELEMENT MESH
FOR ONE-HALF OF BUCKET



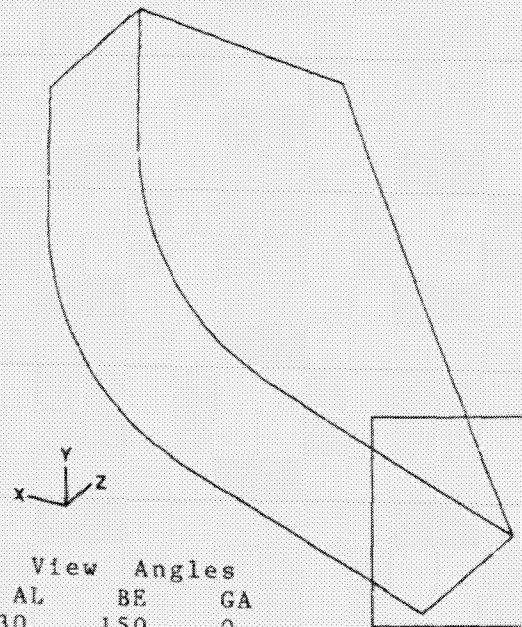
View Angles		
AL	BE	GA
30.	-30.	0.

FIGURE 6 OUTLINE OF BUCKET



View Angles		
AL	BE	GA
30.	150.	0.

FIGURE 7 ROTATED VIEW
SHOWING ELEMENTS



View Angles		
AL	BE	GA
30.	150.	0.

FIGURE 8 ZOOM AND TAG
ELEMENTS

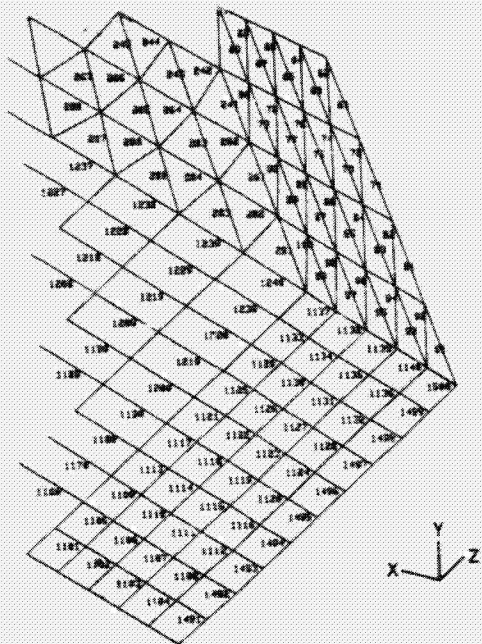


FIGURE 9
ELEMENT IDENTIFICATION

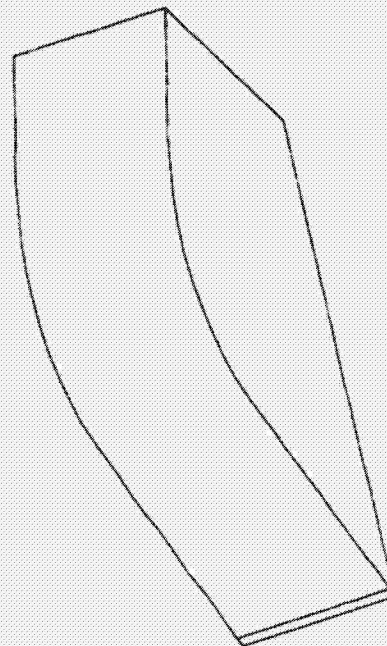


FIGURE 10 BUCKET OUTLINE

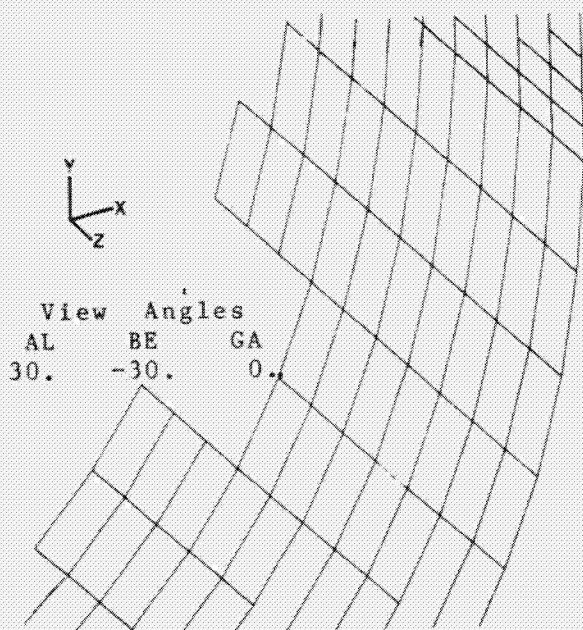


FIGURE 11 DELETION OF ELEMENTS
FOR CIRCULAR HOLE

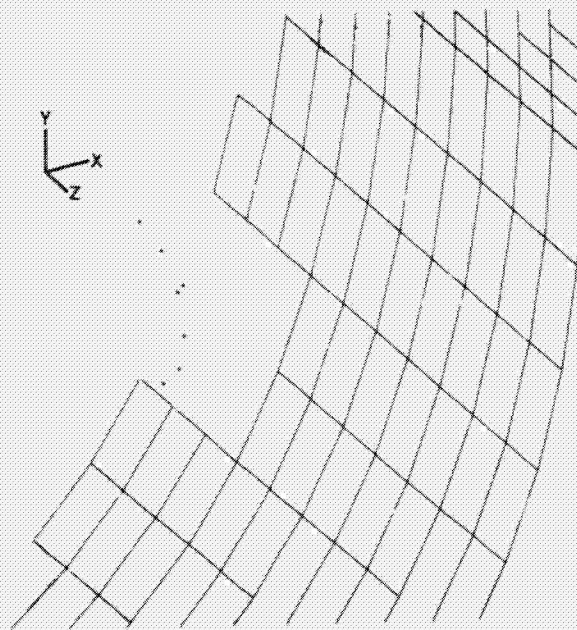


FIGURE 12 GENERATE GRID POINTS
USING COPY FEATURE

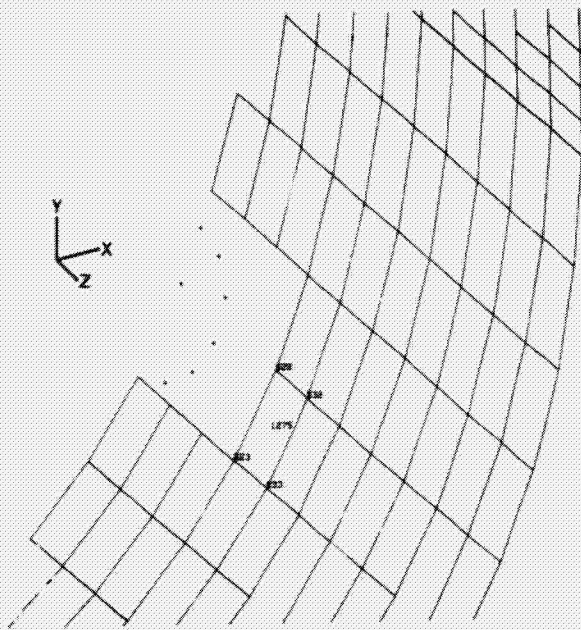


FIGURE 13 USE OF ALIGN OPTION

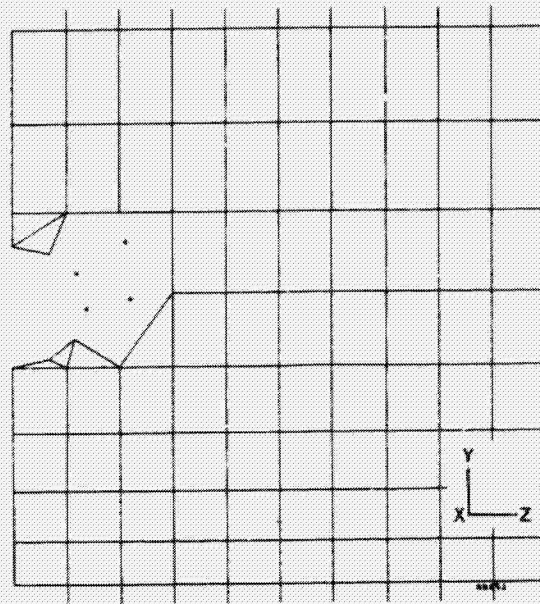


FIGURE 14
INTERPOLATE AND COPY
TO CREATE NEW GRID POINTS

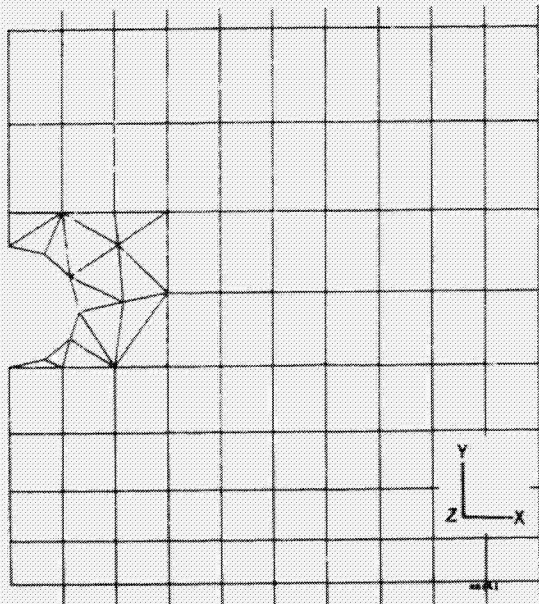


FIGURE 15
MESH AROUND CIRCULAR HOLE

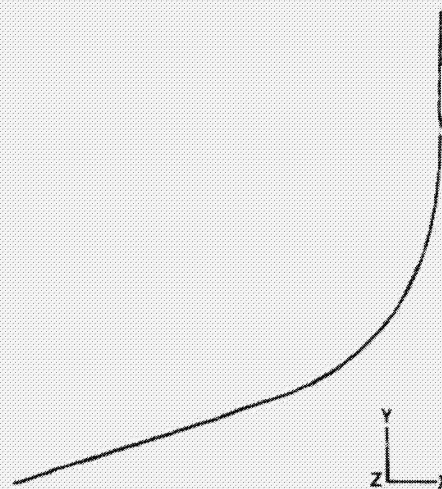


FIGURE 16
SIDE VIEW OF BACK
OF BUCKET

ORIGINAL PAGE IS
OF POOR QUALITY

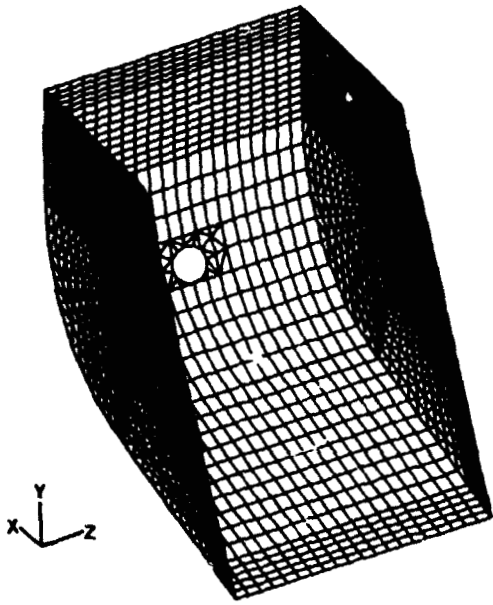


FIGURE 17 MODEL OF BUCKET

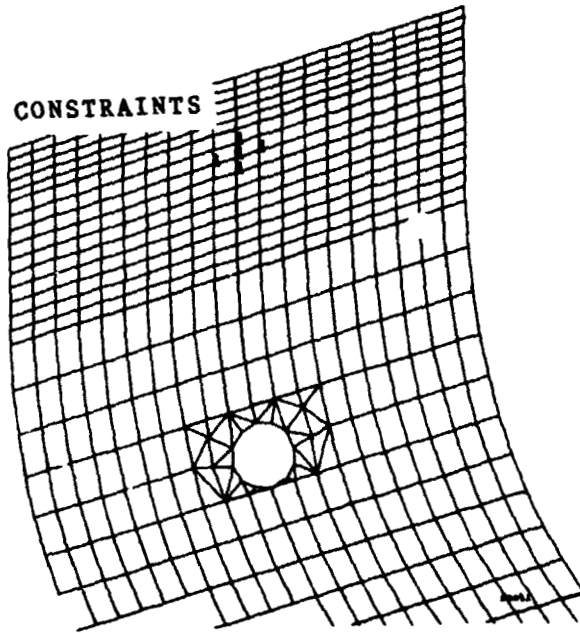


FIGURE 18 FORE-AFT CONSTRAINTS

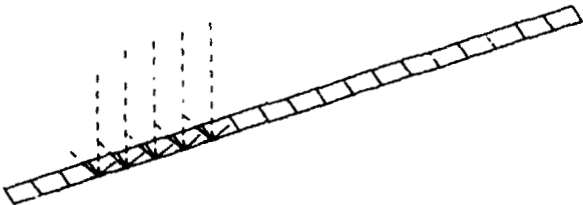
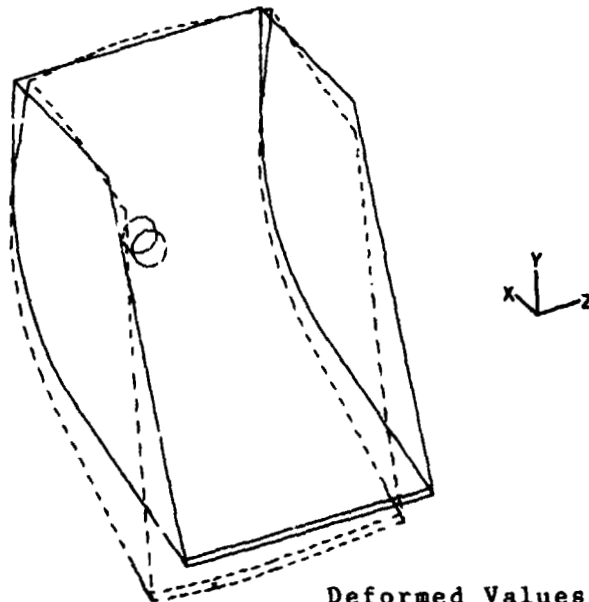


FIGURE 19
PRY LOAD ON CUTTING EDGE
OF BUCKET



Deformed Values:
Max-Resultant Disp = 5.95
... At Gridpoint = 2622

FIGURE 20 DEFORMATION OF BUCKET

ORIGINAL PAGE IS
OF POOR QUALITY

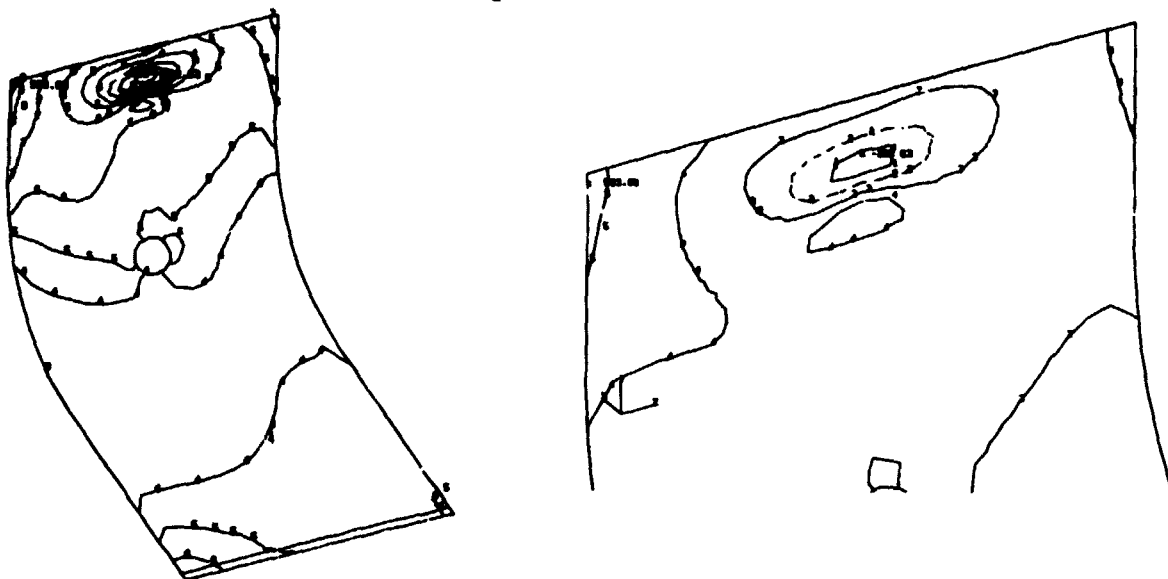


FIGURE 21 DISTRIBUTION OF STRAIN
IN BACK PLATE

FIGURE 22
STRAIN DISTRIBUTION
NEAR HYDRAULIC CYLINDER

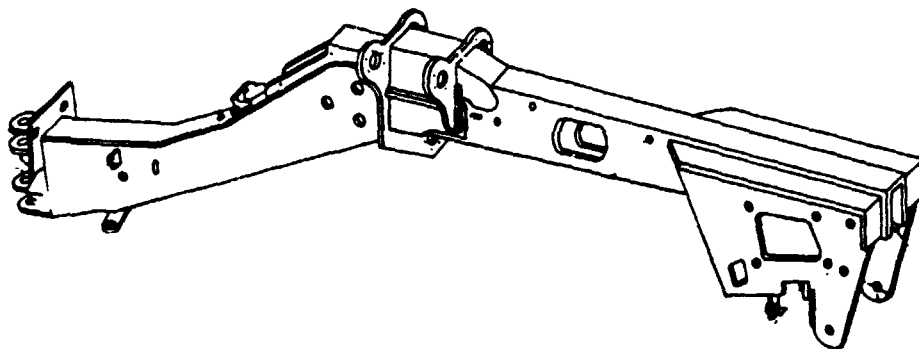


FIGURE 23 SCHEMATIC OF MOTOR GRADER
MAIN FRAME

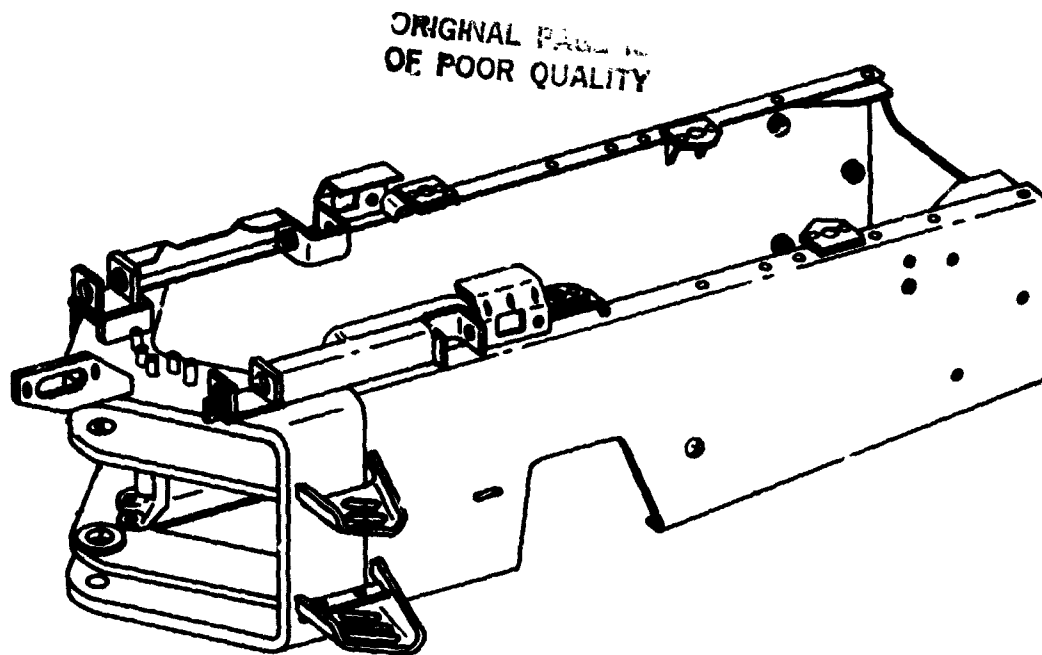


FIGURE 24 SCHEMATIC OF ENGINE FRAME
ON FOUR WHEEL DRIVE LOADER

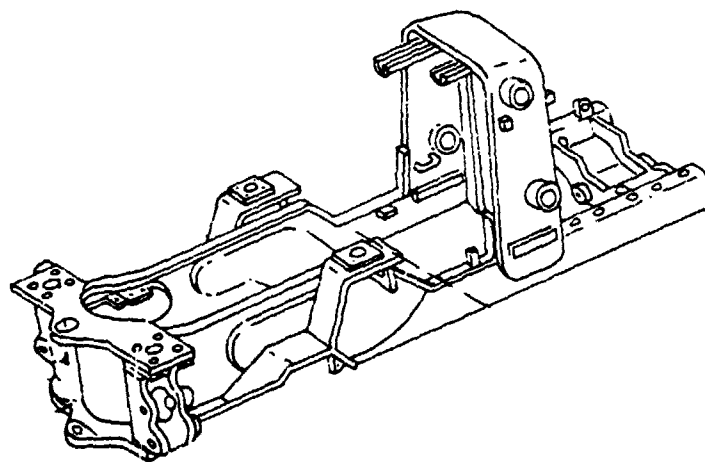


FIGURE 25 SCHEMATIC OF FRAME ON
TWO WHEEL DRIVE LOADER-BACKHOE

N85-25882

AN ELASTIC ANALYSIS OF A PLATED BONE TO
DETERMINE FRACTURE GAP MOTION

Francis W. Cooke and William M. Vannah
Bioengineering Department, Clemson University

SUMMARY

An elastic analysis to determine fracture gap motions occurring in the osteotomized and plated canine femur was performed using the finite element program NASTRAN. The femur was idealized as a hollow right cylinder, and transverse anisotropy was assumed for the elastic properties of the bone. A 3-D 360 degree model consisting of 224 isoparametric quadrilateral hexahedral and 11 beam elements was created. A range of plate stiffnesses was tested by varying the modulus of elasticity of the plate from 207 GPa to 1 GPa. Moments were applied in the plane of the plate, about the axis of the plate, and in the plane of the screws.

Results showed that, for plates of typical geometry and elastic modulus under 10 GPa, the contribution to fracture gap motion occurring due to deformation in the bone was negligible compared to that contribution from deformation in the plate. Fracture gap motion for bone-plate systems using plates in this modulus range could therefore be estimated using beam theory. Deformations occurring in the bone were relatively unaffected by plate stiffness. The relationship of gap motion to plate stiffness was non-linear above 10 GPa due to the decreasing contribution of the plate's deformation.

INTRODUCTION

The use of a compression plate as a method of treating severe bone fractures is a currently accepted practice in orthopedics. In this design (Figure 1), the plate is applied in such a manner that it locks in a small amount of press-fit between the fragments; the applied force and close fit of the fragments induces the bone to grow faster. However, the demand for this close, solid fit means the compression plate must be stiff - so stiff, in fact, that the plate continues to carry much of the load on the bone even after the fracture has healed. Most bones need strains imposed on them to maintain their size and strength; in the absence of these strains, they atrophy in a manner similar to unused muscles. It has been shown experimentally (8,9,10,11) that the application of a stiff bone plate to an intact bone will generally lead to a long-term

loss in the volume of bone under the center of the plate. The resulting decreased wall thickness under the plate midspan makes the bone prone to refracture after plate removal.

To solve the problem of stress shielding, a number of researchers have experimented with an increasingly more flexible series of plates. The most obvious lower bound to plate flexibility occurs when the plate permits so much motion of the fragments that it is no longer possible for the fracture gap to be bridged. As the plate stiffness approaches the non-union point, the time required for the fracture to heal increases to infinity. In much of this research, the osteotomized canine femur has been used as a model. Selected results of these tests, in terms of elapsed time before union of the fracture versus plate stiffness, are shown in Table I.

We were interested in the possibility of a resorbable plate but, since the resorbable material we were working with was fairly flexible, we were unsure whether we could make a plate stiff enough to be above the non-union bound. While estimates of the value of this bound could be made from the data of other researchers, we wished to define it as accurately as possible before making our own plates. Before starting a series of implantation studies in dogs to define this bound, we performed a mechanics analysis to determine the characteristics of the bone-plate system. This analysis is the subject of this report.

METHODS

It was assumed that motion at the fracture gap was the governing variable determining whether or not a fixed fracture would go to union. To determine the total deflection at the gap, it was necessary to determine how much of the total deflection was due to plate deformation and how much was due to bone deformation. While it was easy to estimate the plate bending using beam theory, defining the bone deformation required a complex mechanics analysis easiest done, and perhaps only possible, with the finite element method. It was expected that the application of loads from the relatively narrow plate to the bone might cause the bone to deflect significantly in the area of the plate. This was especially true because our plate design created a line contact between the plate and bone. Since this effect could not be simulated with a two dimensional (2D) model, it was decided to create a three dimensional (3D) model with the bone composed of solid quadrilateral elements, and the plate and screws of one dimensional (1D) beam elements.

The dog femur was modelled as a hollow right cylinder. The outer radius of 9.5 mm and the inner radius of 6.9 mm were determined from inspection of available femurs and the published data of other investigators, and are intended to represent dogs in the 18 to 27 kg range. The length of bone modelled was chosen to be the length covered by the plate plus one bone diameter more past

the end of the plate to allow point loads applied at the end to spread out.

The geometry of the plate (Figure 2) had been previously fixed as a preliminary to the manufacture of prototype plates. It was intended that factors such as orientation of the composite layers and percentages of resin would be varied to produce the desired stiffnesses. This effect was simulated in the model by simply varying the modulus of elasticity of the beam elements. The high stiffness plate used the elastic modulus of 316L stainless steel. The geometry and size of our plate was approximately what would be chosen to fix a bone this size in clinical practice. The results for the high stiffness plate could therefore be considered to represent a typical case where stress shielding might be a problem. The modulus used for the medium stiffness plate was chosen to produce a stiffness slightly above the estimated non-union bound. The modulus used for the low stiffness plate produced a stiffness below the non-union bound.

Values for the elastic modulus of canine bone were available in the literature, but were taken under conditions inappropriate for the loadings anticipated in this study. The material properties used were those determined for human cortical bone by Reilly and Burstein (7); these properties assume transverse anisotropy. The bone was idealized as being composed of purely cortical bone, no attempt was made to model cancellous bone.

With these dimensions settled, a model was then created using the NASTRAN finite element program. The input deck to NASTRAN was generated using the PATRAN graphics pre- and post-processor. The model was made to be roughly the maximum size that would allow reasonable execution times on the DEC VAX-11/780 computer. The model consisted of 224 solid isoparametric quadratic CIHEX2 elements and 11 CBAR beam elements, and executed in eight hours cpu time. A smaller, faster executing 180 degree model was also constructed for use in those cases where it was possible to assume symmetry about the plane of the screws (Figure 3). It was not possible to run a more finely divided model to test for convergence. The results shown in this report will be checked against a similar physical model in an experimental program currently underway. Additionally, a model similar to the 180 degree model with nearly identical mesh but isotropic material properties was tested against a strain-gauged test model by Cheal et al. (5) and shown to be accurate.

In order to most efficiently utilize the available computer time, only those cases which would produce the most significant deflections were run. Axial compression was not applied since it was felt that, because loads were applied to the axis of the plate, this load case would result in only minor deflection in the plate and a small shear deflection in the bone. A force causing a moment in the plane of the screws, directed so as to open the osteotomy, was applied on the axis of the plate at the far end of the bone. This is referred to here as the bending open or BO load case. A

moment was applied about the axis of the plate; this axial torque is referred to as the TA load case. A force causing a moment in the plane normal to the axis of the screws was applied on the axis of the plate at the far end of the bone. This moment, which produced a bending against the plate's stiffest direction, is referred to here as the BA load case.

In the final "load case", an axial torque was again applied, and also a configuration change was made. The plate-bone contact was changed from a line contact at the axis of the plate to a two line contact. These lines were at the axis of the plate and the outer edge of the plate which would be driven into contact with the bone by an axial torque. This load/configuration case, which modelled a "wide-wheelbase" plate, is referred to as the WW load case.

RESULTS

The fracture gap motions resulting from the various load cases are presented in Table II. The deformed shapes are presented in Figures 4a-d.

DISCUSSION

The highest deflections were produced by the BO and TA load cases. The BA load case produced deflections which were almost negligibly small in comparison.

For the BO load case, the deflection took place primarily in the plate. This was especially true for the lower stiffness plates. With the high stiffness plate, significant deflection (accounting for 34% of the motion at the gap) occurred in the bone. This was not a whole-scale bending of the bone, but instead appeared to be a local deformation under the plate. This was especially visible as a raised dimple under the screw closest to the fracture. A shallow depression under the far end of the plate was also visible. This would seem to indicate that the area under the screws (where load transfer occurs) was highly stressed, consistent with the proliferation of bone seen in this area on X-rays. A possible hypothesis is that what really affects fracture gap motion is not the bone's moment of inertia as a cylinder, but the stiffness of the wall under the plate. However, this is not a critical point since, for the low stiffness plates, the motion at the gap was almost entirely a function of the plate stiffness.

Deformation under axial torsion (TA) also took place primarily in two modes. The first mode, responsible for the great majority of the motion at the gap, was twist of the plate in the span between the fracture gap and the closest screw. The second mode was twist of the bone cylinder itself. This was less visible on the plots

with flexible plates because the twist of the plate was greatly increased, making the bone twist appear relatively small (the deflections for plots were scaled by the computer for readability). The torsional twist of the bone appears to be an action of the whole bone, rather than a local action as was the case under the BO load.

The BO and TA load cases produced roughly the same amount of deflection at the fracture gap for equivalent applied moments.

Bending in the plane of the plate took place mainly as a bending of the plate. The beam element bent against their stiffest direction. The fracture gap motion produced was more than an order of magnitude less than the deflections produced by either the BO or TA load cases, on an equivalent applied moment basis.

Changing the plate bone contact to the wide wheelbase configuration and applying an axial torsional load produced a noticeable flattening of the bone cylinder under the outer plate edge. The bone appeared to be more distorted in this case than in any other, yet fracture gap motion was only decreased by one-third. This leads to the conclusion that the wide wheelbase plate design may not be necessary if the screw/plate fit can be relied upon to provide rotational stiffness.

The fracture gap motions predicted are quite high compared to what might be expected to be the maximum movement allowable for healing. Carter et al. (4), implanted strain gauges on the femur of a 35 kg dog and studied the strains under normal gait. From these strains, they calculated the loads at the instant of maximum net loading of the mid-femoral diaphysis as a 250 N axial compression, a 2.5 N-m bending moment directed to produce tension anteriorly, a 1.4 N-m bending moment producing tension laterally, and a torsional moment of 0.56 N-m where the vector points proximally. These loads produce hypothetical fracture gap motions of 5.2 to 0.33 mm due to bending moments, and 9.0 to 0.44 mm due to torsional moments, depending on the stiffness of the plate used. With the medium stiffness plate, the predicted fracture gap deflections are 5.0 and 1.1 mm, for bending and torsional loads respectively. A possible hypothesis is that these magnitudes are realistic, but that the deflections in bending stay low because the plate is positioned so that it is usually in tension (i.e., bending to open the osteotomy doesn't occur), and that the torsional displacements do occur and are the relevant concern in the design of fixation plates. In cases of fractures, the interdigitation of the ragged fracture edges could be expected to lend support and there may be some stiffening due to the surrounding tissues; neither of which was considered in this model. The main conclusion from this result though is that unusual care probably would have to be taken of a fracture stabilized with a flexible plate.

The total deflection of the system was a product of the deflections of the plate, the screws in the bone, and the bone itself. In this analysis, only the plate stiffness was varied, and

therefore the deflection in the bone and screws was relatively constant (although affected somewhat by the bracing action of the plate). The two ends of the deflection-stiffness curve, that is the response at very high and very low plate stiffnesses, could then be estimated. In the case of very flexible plates, the plate would deform so much that the deformation of the bone and screws would be negligible by comparison. In this case, the deflection would vary with the inverse of the stiffness and have a constant slope which could be calculated by beam theory. In the case of an infinitely stiff plate, the deflections present would all occur in the bone and screws. Therefore, in this case the deflection would be constant; that is, it would not vary (or would vary only a negligible amount) as the beam stiffness was varied. Using this reasoning to predict the shape of the tails, the general shape of the deflection curve can be predicted (Figure 5).

The calculated results show that the deflections varied in nearly exact proportion with the plate flexibility across the range of the two lower stiffness plates tested. Even as the plate stiffness greatly increased to the stiffness of a typical solid stainless steel plate, the bending in the bone contributed only a small portion of the fracture gap motion. This implies that, for flexible plates, the fracture gap motion is a function solely of the plate stiffness and can be directly calculated from beam theory.

TABLE I. Materials evaluated using the canine femur model

Investigator	Material	EI (Nm ²)	Results (weeks)
Bradley (1)	SS	16.80	U
	GEC	5.48	U
	GPC	1.45	U
Brown (2)	PA	0.49	4
	PBT	0.41	4-5
	PBT	0.23	6
	PBT	0.49	12-13
Brown (3)	PA	0.265	4-12
	PBT	0.221	4-6
	PP	0.239	22
	UHMWPE	0.161	>40
Zenker (11)	GFMM	3.01	U
Kusenose (6)	M90	0.040	9-30
	CR20	0.067	38->40
NASTRAN model	high	6.02	-
	medium	0.29	-
	low	0.029	-

Legend:

- GFMM - graphite fiber reinforced methyl methacrylate
- SS - stainless steel
- GEC - glass-epoxy resin composite
- GPC - graphite reinforced polysulfone
- PA - polyacetal
- PBT - polybutyleneteraphtalate
- PP - polypropylene
- UHMWPE - ultrahigh molecular weight polyethylene
- U - proceeded to union, no exact time given

TABLE II. Calculated fracture gap motions

Load case	Plate stiffness	Slope (1/Nm)	Fracture gap (mm/Nm)
BO	high	0.00304	0.116
BO	medium	0.0458	1.74
BO	low	0.474	18.0
TA	high	0.00659	0.25
TA	medium	0.0506	1.92
TA	low	0.424	16.1
WW	high	0.00440	0.167
BA	low	0.0489	0.929

BO - bending to open the osteotomy
 TA - axial torsion
 WW - axial torsion, wide wheelbase plate
 BA - bending in the plane of the plate

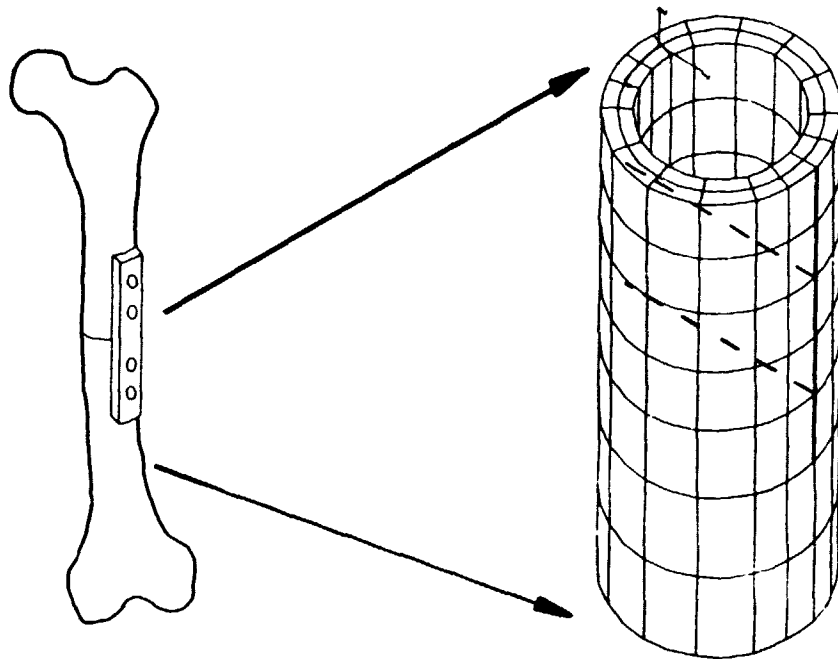
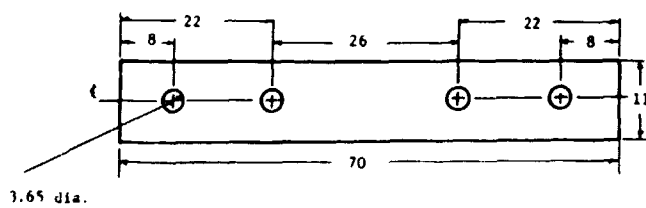
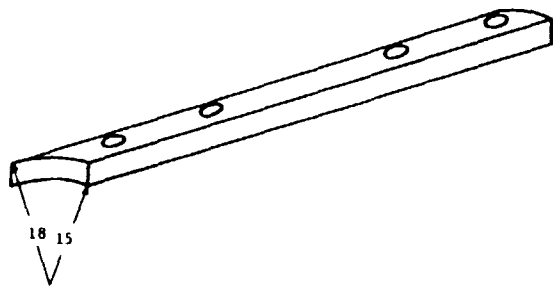


Figure 1. Derivation of model

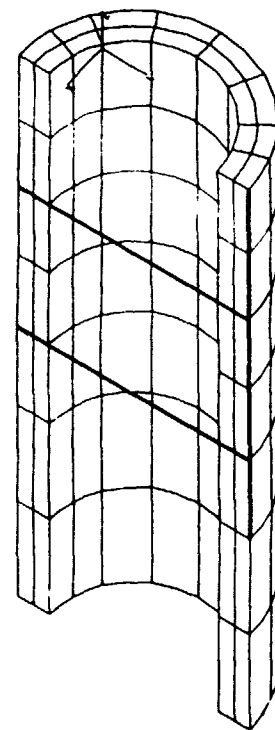
Figure 3. 180 degree model

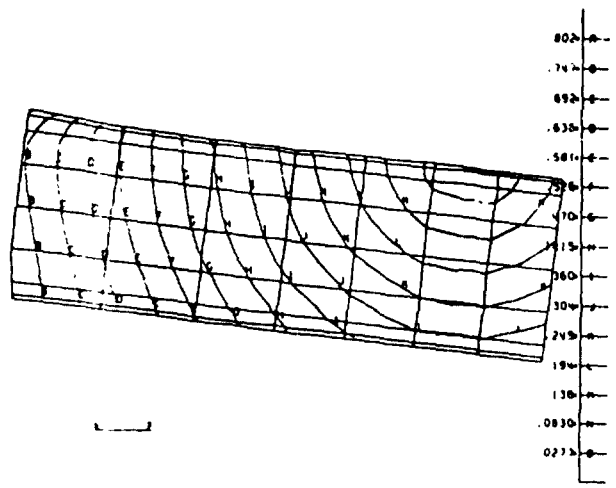


3.65 dia.

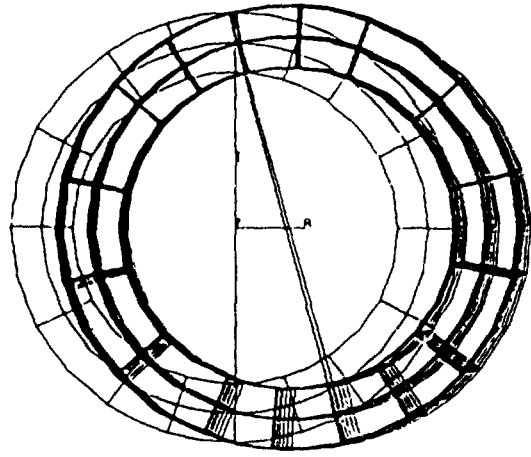
All dimensions in millimeters.

Figure 2. Plate geometry

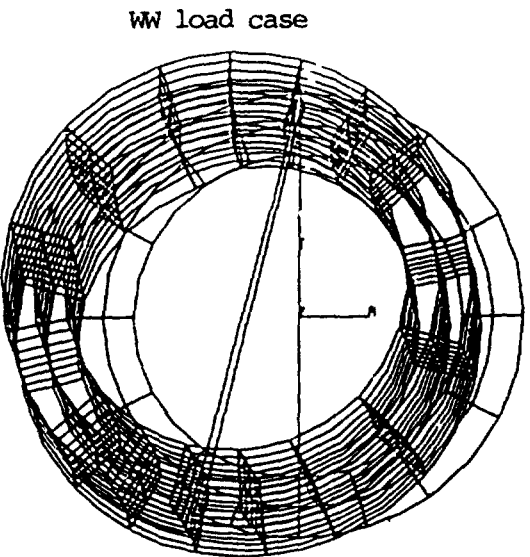




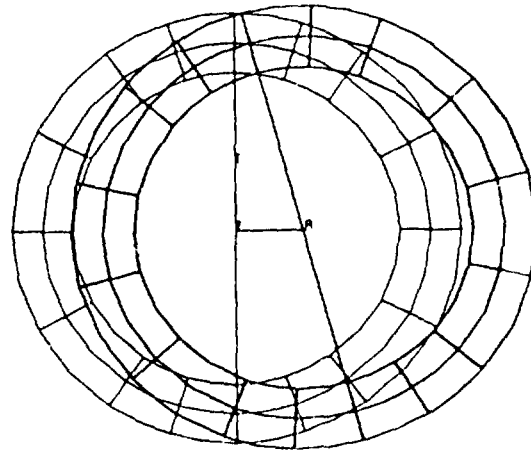
BO load case



TA load case, high stiffness



WW load case



TA load case, low stiffness

Figures 4a-d. Deformed shapes

OPTIMIZATION OF POOR QUALITY

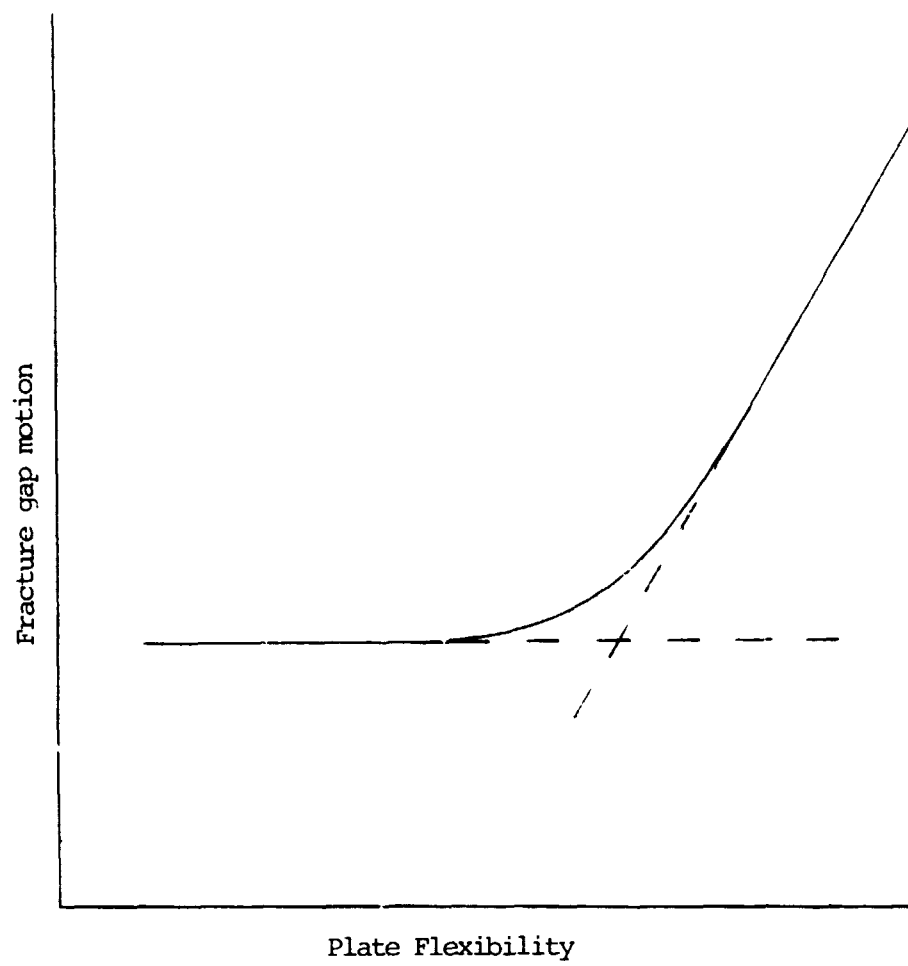


Figure 5. Predicted fracture gap motion

REFERENCES

1. Bradley, G. W., McKenna, G. B., Dunn, H. K., Daniels, A. U. and Statton, W. O. "Effects of Flexural Rigidity of Plates on Bone Healing." *J. Bone and Joint Surgery*, 61A:866-872. 1979.
2. Brown, S. A., Merritt, K. and Mayor, M. B. "Internal Fixation with Metal and Thermoplastic Plates." In: *Current Concepts of Internal Fixation of Fractures* Uhthoff, H. K., ed., Berlin: Springer Verlag 1980. pg. 334-341.
3. Brown, S. A. and Vandergrift, J. "Healing of Femoral Osteotomies with Plastic Plate Fixation." *Biomat., Med. Dev., Art. Org.*, 9:27-35. 1981.
4. Carter, D. R., Vasu, R., Spengler, D. M. and Dueland, R. T. "Stress Fields in the Unplated and Plated Canine Femur Calculated from In Vivo Strain Measurements." *J. Biomechanics*, 14:63-70. 1980.
5. Cheal, E. J., Hayes, W. C. and White A. A. "Stress Analysis of a Simplified Compression Plate Fixation System for Fractured Bones." *Computers and Structures*, 17:845-855. 1983.
6. Kusenose, J. "Experimental Studies on Less Rigid Polyacetal Plates for Fracture Fixation." *J. Japan Orthop. Assn.*, 56:8. 1982.
7. Reilly, D. T. and Burstein, A. H. "The Elastic and Ultimate Properties of Compact Bone Tissue." *J. Biomechanics* pg. 393-405. 1975.
8. Tonino, A. J., Davidson, C. L., Klopper, P. J. and Linclau, L. A. "Protection from Stress in Bone and it's Effects: Experiments with Stainless Steel and Plastic Plates in Dogs. *J. Bone and Joint Surgery*, 58B:107-113. 1976.
9. Uhthoff, H. K. and Dubuc, F. L. "Bone Structure Changes in the Dog Under Rigid Internal Fixation." *Clin. Ortho.*, 81:165-170. 1971.
10. Woo, S. L., Akeson, W. H., Coutts, R. D., Rutherford, L., Doty, D., Jermott, G. F. and Amiel, D. "A Comparison of Cortical Bone Atrophy Secondary to Fixation with Plates with Large Differences in Bending Stiffness." *J. Bone and Joint Surgery*, 58A:190-105. 1976.
11. Zenker, H., Bruns, H., Hepp, W. and Nerlich, M. "Long Term Results of Animal Investigations with Elastic Fixation Plates for Osteosynthesis." In: *Current Concepts of Internal Fixation of Fractures* pg. 363-374.

N85-25883

LEARJET MODEL 55 WING ANALYSTS

WITH LANDING LOADS

Robert R. Boroughs
Gates Learjet Corporation

SUMMARY

NASTRAN analysis has been used to determine the impact of new landing loads on the Learjet Model 55 wing. These new landing loads were the result of a performance improvement effort to increase the landing weight of the aircraft to 18,000 lbs. from 17,000 lbs. and extend the life of the tires and brakes by incorporating larger tires and heavy duty brakes. Landing loads for the original 17,000 lb. airplane landing configuration were applied to the full airplane NASTRAN model. These analytical results were correlated with the strain gage data from the original landing load static tests. Then, the landing loads for the 18,000 lb. airplane were applied to the full airplane NASTRAN model, and a comparison was made with the original Model 55 data. The results of this comparison enabled Learjet to determine the difference in stress distribution in the wing due to these two different sets of landing loads, and consequently, this comparison helped Learjet to reduce the number of tests that would have otherwise been necessary.

INTRODUCTION

The Learjet Model 55 wing has evolved from the Learjet 28/29 wing (see ref. 1). Both the Model 55 and 28/29 wings are similar to the Learjet 35/36 wing geometrically (see ref. 2) except that the two foot wing extension and tip tank on the Model 35/36 wing is replaced by a six foot extension and a winglet on the Model 28/29 and Model 55 wing. The Model 55 wing is fabricated using eight spars and eight ribs per side. This network of spars and ribs is covered with a machined aluminum skin on both the top and bottom surfaces. However, the skin thicknesses and spar section properties are very different from the previous Model 35/36 wing (see ref. 1).

Attachment of the wing to the fuselage is accomplished through eight fittings. The fitting locations are distributed equally between the right and left with four attachment points on each side of the fuselage. These four points in the wing are located at spars two, five, seven and eight. A centerline splice plate provides the carry-through capability to connect the right hand and the left hand halves of the wing, thus allowing the wing to be continuous through the fuselage.

The main landing gear is supported in the wing at the forward end of the trunnion arm by a fitting integral with spar five and at the aft end of the trunnion arm by a fitting integral with spar seven. These two support fittings also serve as the pivot points for landing gear extension and retraction. Actuation of the main landing gear is achieved by a hydraulic cylinder which attaches to the landing gear cylinder at the outboard end and at spar seven on the inboard end. The main landing gear is a dual wheel air-oil type gear with an aluminum cylinder and a steel piston.

BACKGROUND

The Learjet Model 55 aircraft was originally certified by the Federal Aviation Administration in March of 1981. In 1984 a performance improvement package was made available for the Model 55 aircraft as an option to the basic configuration. This option permitted an increase in takeoff and landing weight with the incorporation of a larger set of tires and brakes on the main landing gear. The takeoff weight was increased to 21,500 lbs. from 21,000 lbs., and the landing weight was increased to 18,000 lbs. from 17,000 lbs.

This increase in takeoff and landing weight necessitated the development of a new set of loads for these conditions. The results of these new load calculations revealed that the increase in landing weight had more of an impact on the wing structure than the increase in takeoff weight. Consequently, most of the analytical effort was directed toward resolving the differences between the original Model 55 landing loads and the new landing loads. The original landing loads for the Model 55 were developed using conventional static aeroelastic methods, but since the time when these data were generated, Learjet has developed the analytical capability to generate flexible body dynamic landing loads. These flexible body dynamic loads have been demonstrated to be more realistic than the more conservative static aeroelastic landing loads for many applications. Dynamic flexible body loads are also almost always lower than the static aeroelastic landing loads. Consequently, there was good reason to believe that the landing loads developed with the flexible body dynamic methods for an 18,000 lb. airplane could be less than or equal to the landing loads developed with static aeroelastic methods for a 17,000 lb. airplane.

Since the landing loads on the wing consisted of one "G" airloads as well as main landing gear loads, a method was needed to verify that the net effect of the new 18,000 lb. aircraft landing loads on the wing was less severe than that of the older 17,000 lb. aircraft landing loads. NASTRAN analysis was proposed as a method to help determine the impact of the new 18,000 lb. landing weight loads on the Model 55 wing structure. A finite element model was available of the complete Learjet Model 55 aircraft, and these types of load conditions had been run earlier for the 17,000 lb. landing weight condition.

MODELING CRITERIA

The NASTRAN model for the Learjet 55 aircraft included the full fuselage, vertical tail and complete wing and consisted of over 16,000 elements and 26,000 degrees of freedom. The original model used substructuring techniques (see ref. 3) in the finite element analysis mainly due to the limitations and restrictions on computer resources that were available during that time period. However, since then, Learjet has acquired and installed an IBM 3033 and an IBM 3081. Both of these main frames are much faster and have more memory and disk space than was available on the previous in-house IBM 370-158. These new computers allowed Learjet to run the full aircraft model without using substructure techniques on a regular overnight turn-around basis.

Geometry in the finite element model is defined extensively through the use of local coordinate systems. Almost all installations in the aircraft model are defined in a local coordinate system which is more oriented to the geometry of that installation as opposed to the basic coordinate system definition. Another reason for using local coordinate systems is to provide flexibility for future modifications

and additions such as a fuselage plug. These changes could then easily be accommodated by simply changing the origin of the appropriate local coordinate systems. Sufficient intervals in node and element numbering were also established to facilitate this type of model revision. A total of 102 local coordinate systems are used in the model with this number being almost equally divided between rectangular and cylindrical coordinate system.

The wing and main landing gear are modeled using five local rectangular coordinate systems. The right hand half of the wing is modeled in one local rectangular system and the left hand half of the wing is modeled in a second local rectangular system. A third rectangular system is used to model the wing centerline rib which is in a plane parallel to the centerline plane of the airplane. Each main landing gear is defined in a local rectangular system with the positive "z" axis directed aft from the forward pivot point to the aft pivot point and with the positive "x" axis pointing down (see fig. 1). Since the landing gear elements are to simulate the static test conditions with the main concern being the wing and wing support structure, the hydraulic characteristics of the gear are not included in the NASTRAN model. The landing gear was modeled with the intent of representing the geometry and stiffness of the gear so that the landing loads would be transferred accurately into the wing structure.

Attachment of the wing to the fuselage is accomplished through four fittings on each side of the fuselage. These eight fittings are represented in the model with the appropriate stiffness and degrees of freedom to reflect the load paths from the wing to the fuselage. The wing is bolted to the fuselage at these fitting points with a single bolt, and each joint is modeled to simulate a pinned connection. However, the fitting at spar five in the wing in addition to being pinned also transfers drag load, and this degree of freedom had to be included at that joint.

FUSELAGE

A complete representation of the fuselage structure is included in the NASTRAN analysis basically because the model was already in this format, and this version could easily be run overnight. Another reason for using this configuration was that an accurate definition was desired of the wing to fuselage internal loads and the wing internal loads and stresses in the members adjacent to the attachment points. The fuselage geometry is generally defined with grid points on the outside contour being located at frame and stringer intersections. Almost all of these grid points were defined in local cylindrical coordinate systems which were established at each frame location. Interior grid points such as those on bulkheads were usually located at the intersections of beams and intercostals. These interior grid points were defined in local rectangular coordinate systems which were also created at each frame location (see ref. 3).

The outer surface of the fuselage, or skin covering, is modeled using the QDMEM2 membrane element (see ref. 4). Simulation of the frame members bending capability is accomplished using BAR elements. Stringers are represented using the axial load capability in the CONROD element, and intercostals and beams are modeled using BAR elements. QUAD1 elements are used to simulate the aluminum honeycomb aft pressure bulkhead and the baggage floor over the wing. A significant feature simulated in the fuselage model is the cabin door and the escape/baggage door. These members are modeled with a double row of nodes along the door boundary. One row of nodes defines the cutout in the fuselage, and the second row of nodes defines the

edge of the door. The cabin door is split at the mid-line into an upper and lower door with the upper half being hinged on the upper edge and the lower half being hinged at the lower edge. In the closed position the door is secured by shear pins and tension lugs along the forward and aft edges. The escape/baggage door is of similar type construction except that this member is a one-piece type construction and is hinged only on the upper edge, and tension lugs are not used.

Another major feature simulated in the fuselage section with considerable detail is the cutout to allow the wing to pass through the fuselage. The lower portion of the fuselage at the wing intersection is essentially designed around the wing. Structure in this region had to have the capability of transferring fuselage bending and pressure loads around the wing. The forward portion of the cutout is sealed by a partial bulkhead at frame 24, while the aft portion of the cutout is sealed by another partial bulkhead at frame 31. An aluminum honeycomb floor panel is installed just above the wing to seal the upper portion of this cutout in the cabin pressure vessel. Once the wing is attached to the fuselage, a removable keel beam is installed across the lower portion of this cutout connecting frame 24 and frame 31. The keel beam basically extends from the forward pressure bulkhead almost all the way to the vertical tail attachment structure in one form or another. In the forward fuselage this structure is of dual "I" beam construction and extends from the forward pressure bulkhead to the forward edge of the wing cutout in the fuselage at frame 24. Beneath the wing the keel beam is fabricated as a closed box section (see fig. 2 & 3). This type of construction is also used aft of the wing cutout in the fuselage, although in this portion of the fuselage the keel beam is integrated with the frame and stringer construction.

Elements used to represent the structure in the partial bulkhead at frame 24 are BAR members for the beams and stiffeners and QDMEM2 membranes for the webs. Modeling of the partial bulkhead at frame 31 is accomplished using BAR elements for the beams and stiffeners and QUAD2 plates for the bulkhead webs. The keel beam is basically modeled using CONRODS for the caps and SHEAR elements for the vertical webs. Beneath the wing, where the keel beam is a closed box section, QDMEM2 panels are used to simulate the skin covers. Additional details on the fuselage model can be found in ref. 3.

WING

The entire wing is simulated in the finite element model by duplicating the right hand half from the left hand half. Each half of the wing is modeled in a separate local rectangular coordinate system. The local coordinate system for the left wing had the X axis positive aft, the Y axis positive left hand outboard, and the Z axis positive down. The local rectangular system for the right hand wing is oriented with the X axis positive forward, the Y axis positive right hand outboard, and the Z axis positive down. Since the centerline rib is not really oriented in either one of these coordinate systems, this member is modeled in a third local rectangular coordinate system. This local system is established with the X axis positive aft, the Y axis positive left hand outboard, and the Z axis positive down.

Grid points for the wing are located at the outer contour along the spar mold lines. Since the Learjet 55 wing is basically an eight spar wing in the inboard section and a ten spar wing in the outboard section no more grid points were added in between the spars. The spacing between ribs is much greater than the spacing between the spars, and consequently the distance between ribs is divided into four

or five bays in order to obtain square panels as best as possible.

The Learjet 55 wing is an all aluminum type fabrication. Spar members are basically designed to be continuous while most of the ribs are designed as segmented elements with the exception of the centerline rib and the landing gear rib at the outboard end of the wheel well. Wing skins are generally fabricated in two pieces with a wing skin splice in the outboard section at W.S. 181. Centerline skin splices on the top and bottom are used to join the right hand and left hand halves of the wing. ROD elements are used to model the spar caps and rib caps while SHEAR elements are used to represent the spar and rib webs. The skin and skin splices are simulated using QDMEM2 membrane elements. Fittings and other attachment members are generally modeled using BAR elements. Additional details on the wing model can be found in ref. 1.

WING TO FUSELAGE ATTACHMENT

Attachment of the wing to the fuselage is accomplished with four fittings on each side of the fuselage. These fittings are symmetrically located from the right hand side to the left hand side and are positioned in the wing at the intersection of the fuselage attachment rib at spars two, five, seven and eight. All ribs in the wing are located on constant wing station lines except the fuselage attachment rib which follows the outer contour of the fuselage. The attachment at spar two is a linkage type joint with a strap pinned at both the fuselage and wing ends. The fitting at spar five has the capability to transfer vertical, side, and drag loads, while the fittings at spars seven and eight can only transfer vertical and side loads (single pinned joint).

Four frame locations were created in the fuselage to match the four fitting points on the wing. These support points are frame 25 which matches the wing fitting at spar two, frame 27 which corresponds to the spar five wing fitting, frame 29 which is located over the spar seven wing fitting, and frame 30 which is positioned above the wing fitting at spar eight. These frames are actually double frames with a plate connecting the inner flanges to form a closed box cross section. This reinforcement is necessary to provide sufficient stiffness and an adequate load path and redistribution system for transferring wing reactions into the fuselage.

Each of the double frames over the wing attach fittings are modeled using BAR elements. The use of BAR elements helps to reduce the number of degrees of freedom that would have otherwise been required to simulate this structure. BAR elements are also used to represent the fuselage attach fittings at the bottom of the double frames at all four locations on each side of the airplane. The lower end of these fittings is pin flagged in the third rotational degree of freedom, and the fittings at frames 29 and 30 are also pin flagged in the fore and aft translational degree of freedom.

Attachment fittings on the wing are generally separated into that portion of the fitting that is internal to the wing and that portion which extends outside the wing contour. The portion of the wing fitting that is inside the wing contour is generally designed to reinforce the local internal structure to carry large concentrated loads. These loads are transferred to the fitting from the adjacent spars, ribs, and wing skin. BAR elements are used to simulate these internal fitting members in the NASTRAN finite element model. The portion of the wing fitting which extends above the wing contour is also modeled using BAR elements. These members

provide load transfer capability in all six degrees of freedom at the lower end, but at the upper end of the BAR element the rotation about the fore and aft axis is pin flagged at all four fittings per side, and the drag translational degree of freedom is pin flagged at spars one, seven, and eight. The drag load capability is not released at spar five since this fitting is designed as the main drag load reaction path. Arrangement of these fittings in the finite element model can be seen in figures 3 and 4.

LANDING GEAR

Each main landing gear is modeled in a separate local rectangular coordinate system. These local rectangular systems are defined with respect to the wing local rectangular system with the landing gear local Z axis oriented along the gear retraction pivot axis and pointing aft. The landing gear cylinder is defined in the X-Z plane so that when the main landing gear is extended the X axis positive direction is pointing down toward the wheels. Consequently, the positive Y axis is always oriented toward the right for both the left hand and right hand gears in the down position.

Since the main landing gear simulation was to be a part of a much larger finite element model, a simplified representation of the gear was established for this project. The geometry of the gear is defined with the piston in the 25 percent compressed position. This geometry was incorporated to facilitate the application of the critical landing loads which were defined with the landing gear in this position. This position of the gear was used on the previous Model 55 static tests, and the main concern in this analysis was to be able to correlate the NASTRAN results with the strain gage data on the wing rather than simulating the functional characteristics of the main landing gear. The effect of the piston sliding inside the cylinder and the compressibility of the air-oil mixture in the piston and the cylinder are not simulated in this model. Using these guidelines, grid points are located along the center of the cylinder, piston, and axle to represent not only the center line geometry, but also the major points where section property changes occur in these members. BAR elements are used to model all parts of the cylinder, piston and axle.

Extension and retraction of the gear is achieved by means of a hydraulic actuator which attaches to a lug on the landing gear cylinder on the outboard end and to a fitting on spar seven on the inboard end (see fig. 5). This actuator is basically pinned at each end, and when the gear is extended the actuator has a locking mechanism which locks the gear into the down position. Since this system is pinned at each end, a ROD element is used to represent the actuator system stiffness (see fig. 6).

Attachment of the main landing gear to the wing is achieved at three support points (see fig. 5). Two of these points are at the upper end of the landing gear assembly. The first point, or forward support, is located at spar five, while the second point, or aft support, is located at spar seven. A group of four BAR elements is used to simulate each of the trunnion fittings. All four BAR elements are connected at one end to the grid point which defines the intersection of the trunnion pivot axis and the mid-plane of the support fitting lug. Two of these BAR elements are connected to two separate points on the upper spar cap while the other two BAR elements are connected to two separate points on the lower spar cap. This connectivity arrangement is very similar for both the forward and aft trunnion support fittings. The third attachment point for the main landing gear is the actuator

support fitting located on spar seven at the inboard end of the wheel well. This fitting is also modeled with BAR elements using the same concept as the other two fittings (see fig. 6). The grid point which represents the inboard actuator support point is defined at the location where the actuator is pinned to the support fitting.

CONSTRAINTS

Since the loads to be applied to the aircraft model consist of landing gear and air loads on the wing and balancing loads on the fuselage, only a minimal number of constraints are required to maintain equilibrium. The constraints on the model are established mainly to neutralize any unbalanced rotations rather than serving as major reaction points. Consequently, constraints are established at two points on the forward pressure bulkhead and at two points on the top of the vertical tail. The two points on the forward pressure bulkhead are located on the maximum breadth line of that fuselage cross section at the outside contour on the left hand and right hand sides. These grid points are constrained in the three translational degrees of freedom. Constraints on the vertical tail are located at the two outboard points of the horizontal tail pivot fitting where the horizontal tail attaches to the vertical tail. The horizontal tail is not included in this analysis, since this structure is not necessary for this load case, and the removal of this assembly from the finite element model reduces the size of the problem. All three translational degrees of freedom are constrained at these grid points on the top of the vertical tail as was done on the two grid points on the forward pressure bulkhead.

LOADS

Landing loads applied to the wing consist of the main landing gear spin up and spring back conditions with one "G" wing air loads. Generally speaking, the main gear spin up condition is the most critical for this analysis. The loads applied to the main gear are distributed on a 60% and 40% basis between the outboard wheel and inboard wheel respectively. This distribution is applied to both the vertical and drag load components. Wheel loads are applied to the main gear axle at the centerline of the wheel with the vertical and drag components being normal and parallel to the ground, and in the NASTRAN model these loads are defined in the basic coordinate system (fuselage reference system). The one "G" wing air loads are applied to simulate the air loads experienced by the wing at the moment of touchdown by the aircraft. These loads are distributed over the outboard portion of the wing and are located toward the aft chord of the wing, since this is a maximum nose down torque condition.

The loads for the increased landing weight cases were generated using a dynamic landing computer program which was not available during the original Model 55 certification effort. Original Model 55 landing loads were developed using a conventional static aeroelastic program. These loads are conservative, since the static aeroelastic theory did not account for the aircraft flexibility and response. Landing loads calculated using the new dynamic landing program normally gave lower loads for the same conditions as opposed to the static aeroelastic program. Consequently, there was good reason to expect that the impact of the new landing loads on the wing would be less than or equal to the old landing loads. The one "G" wing air loads are distributed so as to produce the correct shear moment and torque defined about the elastic axis of the wing. Both the landing gear loads and the one "G" wing air loads are applied to the NASTRAN model using FORCE cards. The balancing fuselage

loads are applied symmetrically between the right hand side and left hand side of the fuselage at the maximum breadth point of the frames and at the engine support points, and these loads are also defined using FORCE cards.

ANALYTICAL RESULTS

NASTRAN runs were made for the critical landing conditions. Since the wing skin stresses were below the buckling allowable, a wing skin buckling simulation was not performed on this project as has been done on previous maximum wing bending conditions. The first series of NASTRAN runs were made for the original Model 55 landing conditions with a 17,000 lb. landing weight. A correlation analysis was performed with these data and the strain gage data from the Model 55 landing condition static test. Plots were made of the upper and lower spar cap NASTRAN stresses and the strain gage data for spars five, seven and eight. Spar five was the gear forward support point and the forward boundary of the wheel well, and spar seven served as the gear aft support point and the aft boundary of the wheel well. These data have been plotted in figures 7 through 12. A comparison of the NASTRAN analytical results with the static test strain gage data shown in these figures indicated that the NASTRAN data agreed very well with the experimental data in almost all areas. Consequently, the NASTRAN analysis was considered a justifiable approach for comparing the original Model 55 landing conditions at the 17,000 lb. landing weight with the new Model 55 landing conditions using an 18,000 lb. landing weight.

The second series of NASTRAN runs were made with the new Model 55 landing conditions at the 18,000 lb. landing weight. Loads applied in these conditions were developed using the dynamic landing methods while the original Model 55 loads were generated using the static aeroelastic techniques. The results of these runs were also plotted along with the original Model 55 analytical results and test data and can be seen in figures 7 through 12. Stresses in the spar caps for the new landing conditions were generally less than the stresses in the spar caps for the original Model 55 landing conditions. In those areas where the stresses due to the new 18,000 lb. landing weight loads were not less than the stresses due to the old 17,000 lb. landing weight loads, the margins of safety were normally quite high. A comparison of the stresses resulting from these two load conditions can be seen in these six figures.

Since the highest stresses in almost all areas of the wing were lower for the new loading conditions, or the margins of safety were quite high in those areas where the stresses for the new load conditions were greater than the stresses due to the older load conditions, Learjet was able to reduce the number of static test conditions that were required for this program. The need for a full schedule of wing tests using the new landing load conditions was eliminated from the certification program as well as many of the individual landing gear static tests.

CONCLUDING REMARKS

A series of NASTRAN finite element analyses have been performed on the Learjet Model 55 aircraft to help determine the structural impact of increasing the aircraft landing weight to 18,000 lbs. from 17,000 lbs. The correlation of the NASTRAN analysis for the 17,000 lb. aircraft landing condition with the strain gage data from the corresponding static test demonstrated that the NASTRAN results simulated this condition very closely. Therefore, the NASTRAN model was considered to be an accurate

representation of the wing and wing support structure. A comparison of the NASTRAN results using the landing loads for an 18,000 lb. airplane with the NASTRAN results using the landing loads for a 17,000 lb. airplane revealed that the highest stresses in almost all areas of the wing were less due to the new load condition. In those areas of the wing where the stresses due to the new loads exceeded the stresses due to the original Model 55 loads, margin of safety calculations indicated that the structure was more than adequate. Consequently, the results of this NASTRAN analysis helped Learjet to significantly reduce the number of static test conditions that had to be conducted during the development of this performance improvement capability for the Learjet Model 55 aircraft.

REFERENCES

1. Boroughs, Robert R., "Development of the Learjet 28/29 Wing Using NASTRAN Analysis", pp 11-32, Eighth NASTRAN User's Colloquium, NASA CP 2131, October 1979.
2. Abia, Mike H., Boroughs, Robert R., and Cook, Everett L., "Analysis of the Learjet 35/36 Wing and Correlation With Experimental Results", NASTRAN User's Experiences, NASA TMX-3428, October 1976, pp 331-352.
3. Boroughs, Robert R., Paramasivam, Sivam, and Werner, Joanna K., "Development and Analysis of the Learjet 54/55 Fuselage NASTRAN Model Using Substructure Techniques", Ninth NASTRAN User's Colloquium, NASA CP 2151, October 1980.
4. The NASTRAN User's Manual, NASA SP-222(06), Washington, D.C., September 1983.

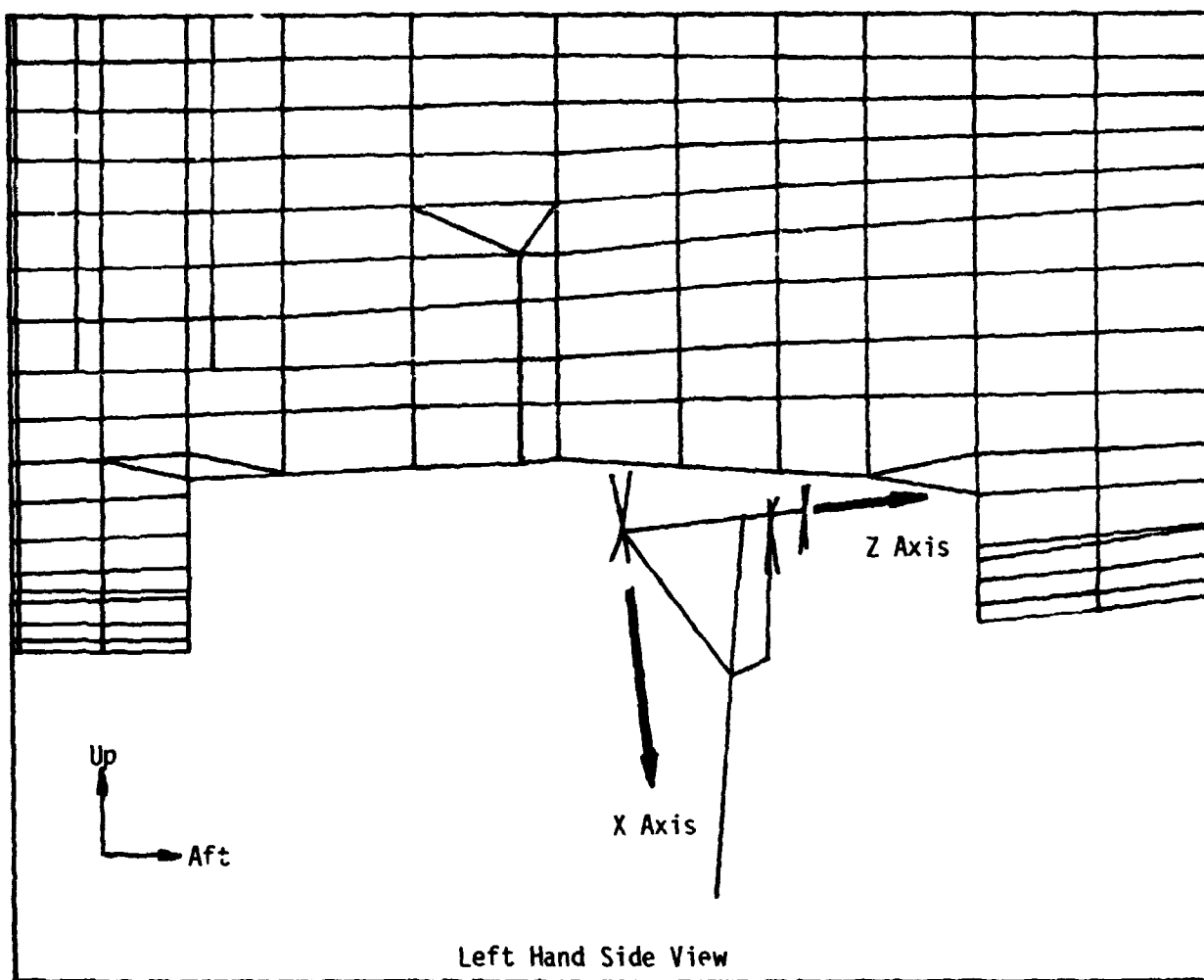


Figure 1 - Landing Gear Coordinate System

ORIGINAL PAGE IS
OF POOR QUALITY

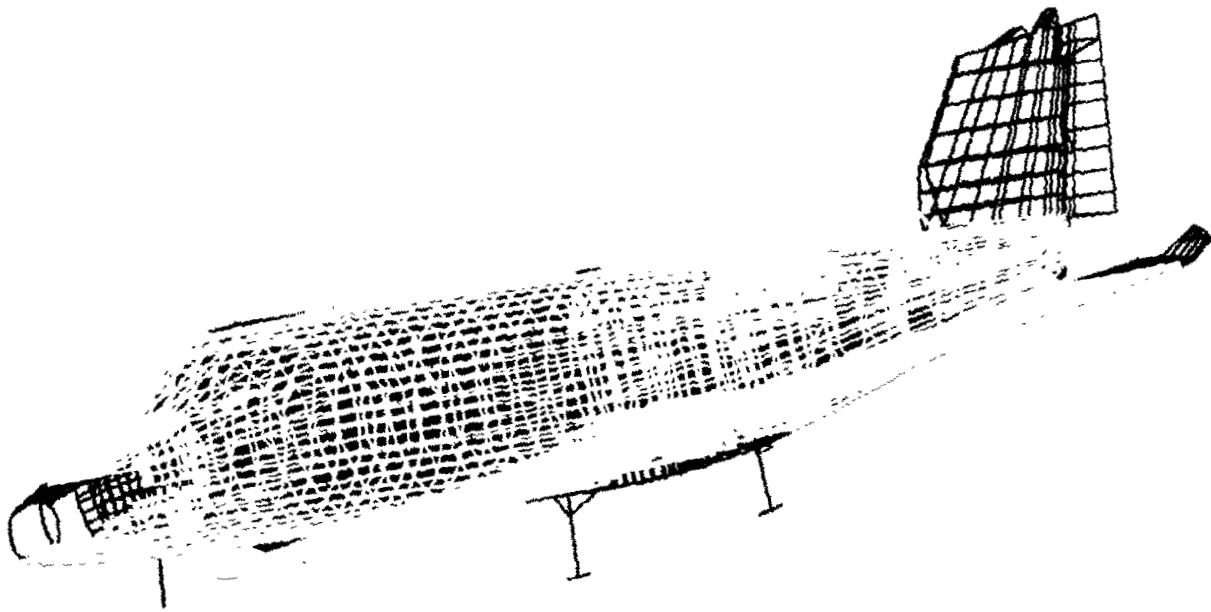


Figure 2 - Learjet 55 NASTRAN model

ORIGINAL PAGE 10
OF POOR QUALITY

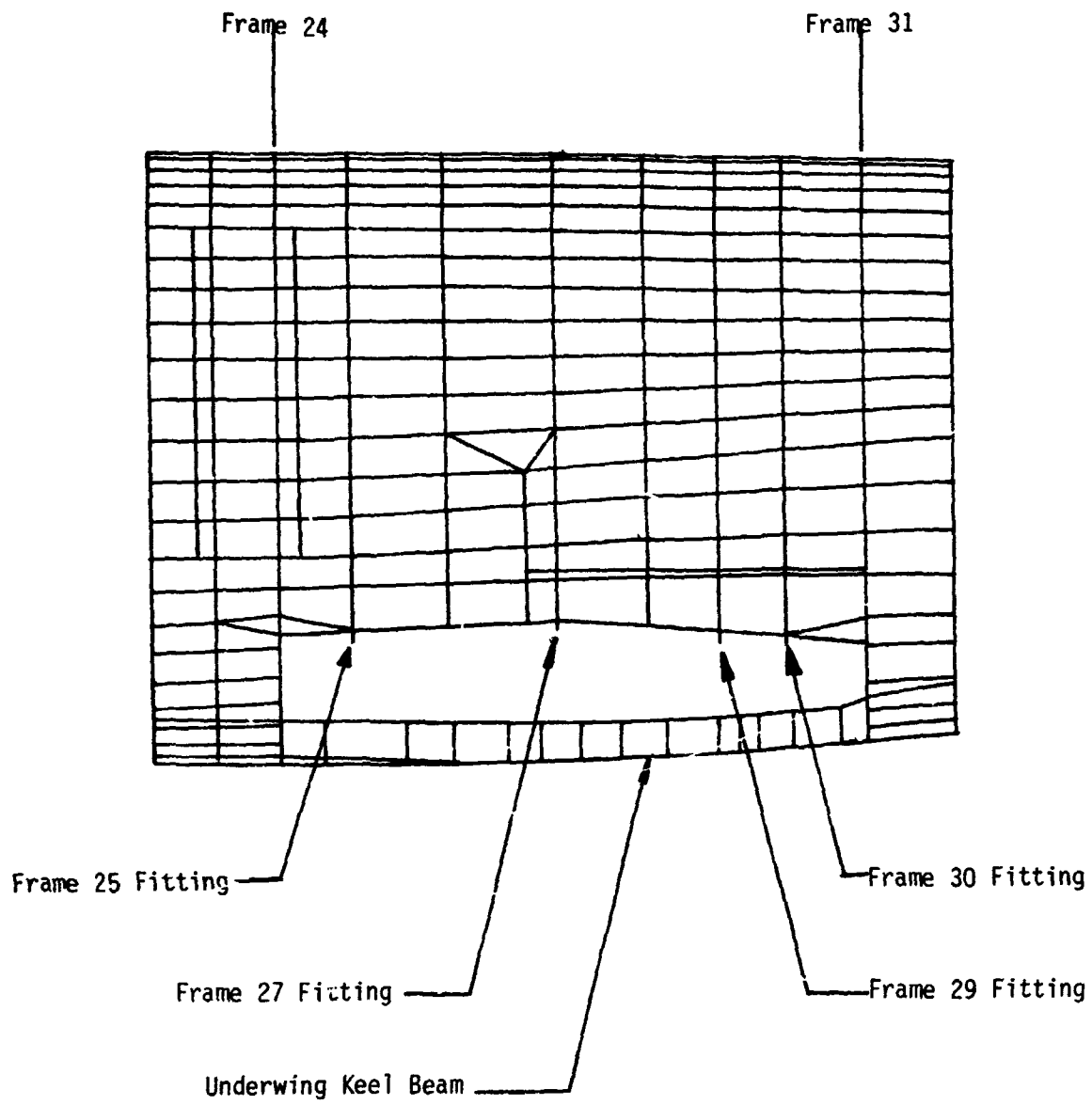


Figure 3 - Fuselage Attach Fittings

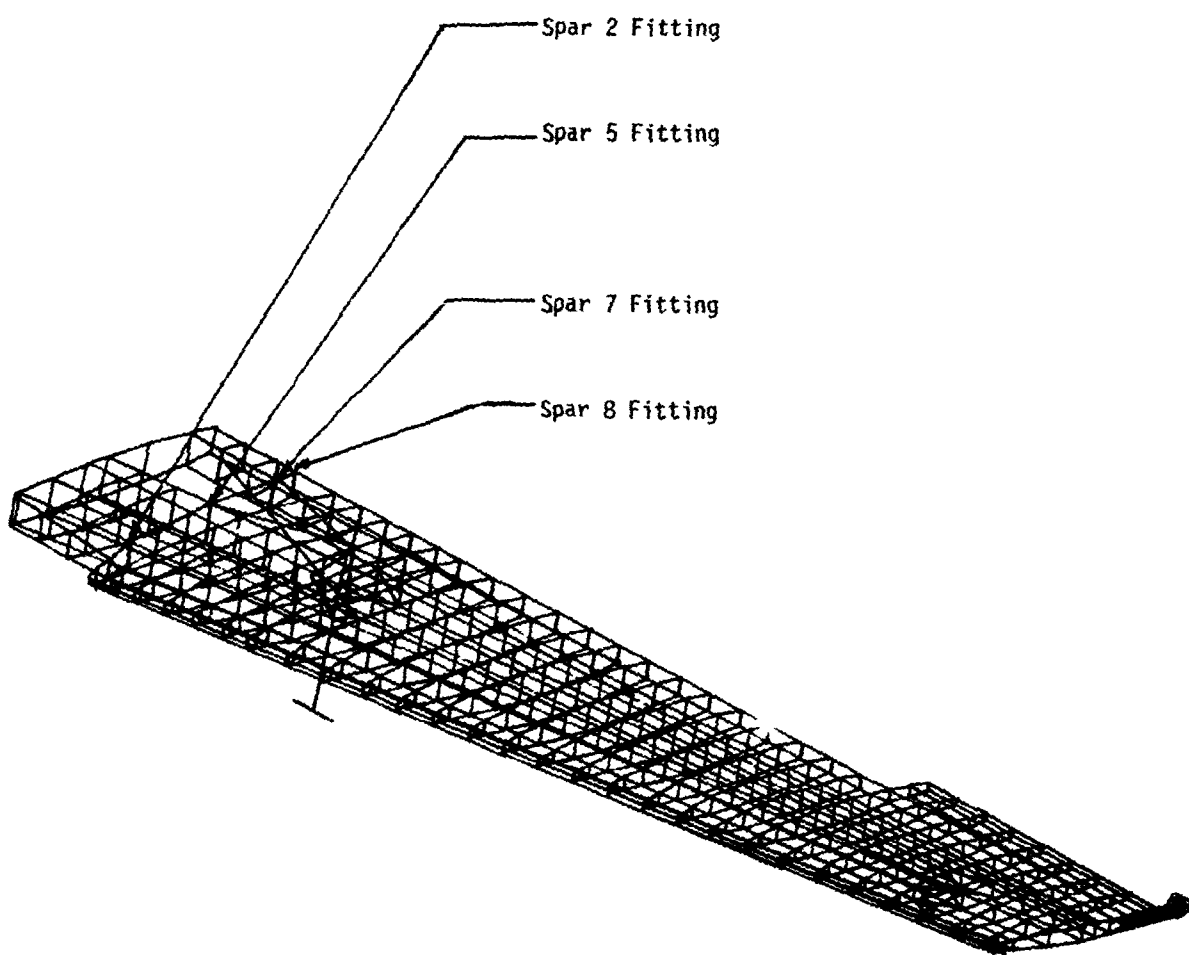


Figure 4 - Wing Attachment Fittings

ORIGINAL PARTS
OF POOR QUALITY

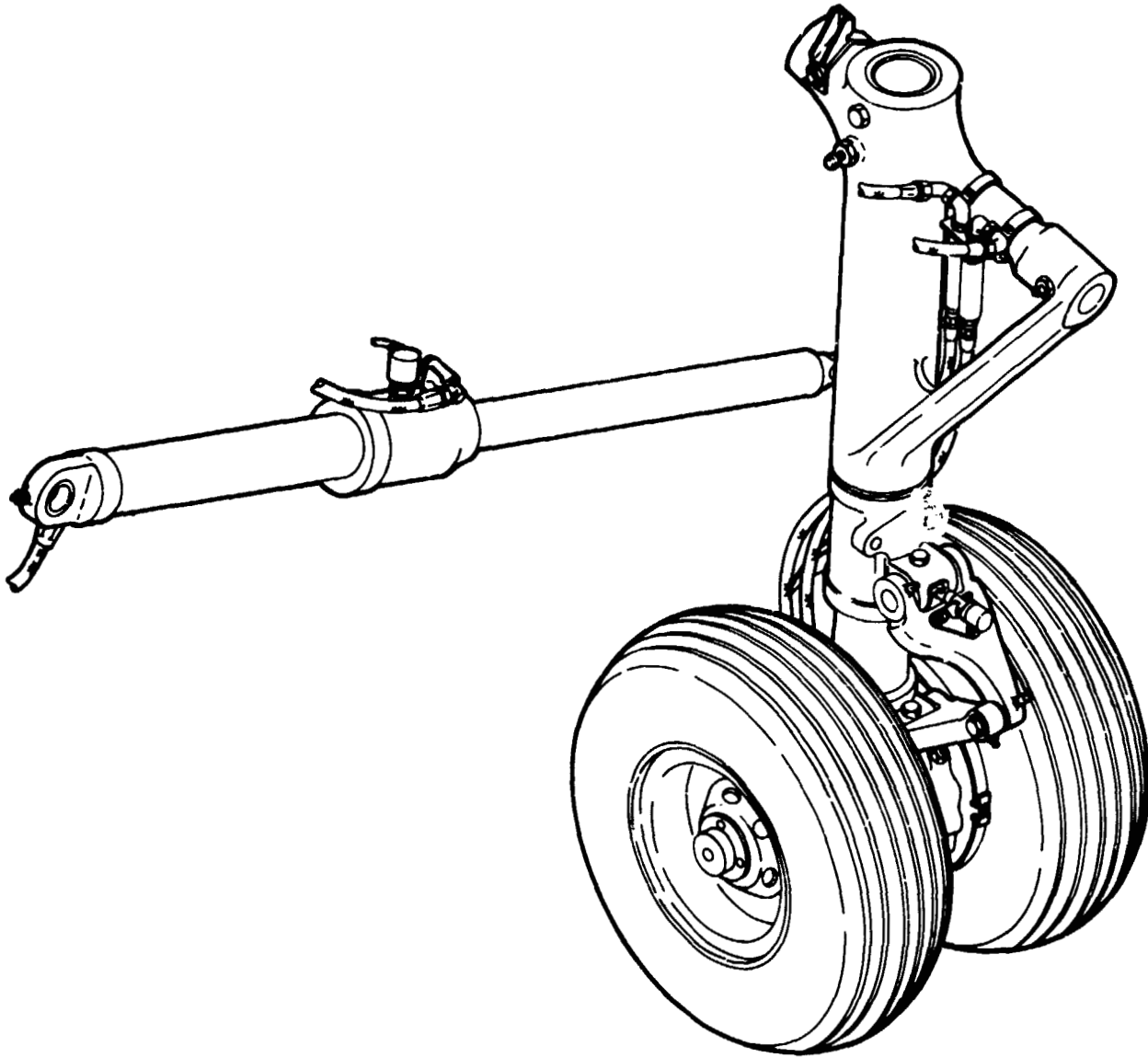


Figure 5 - Main Landing Gear

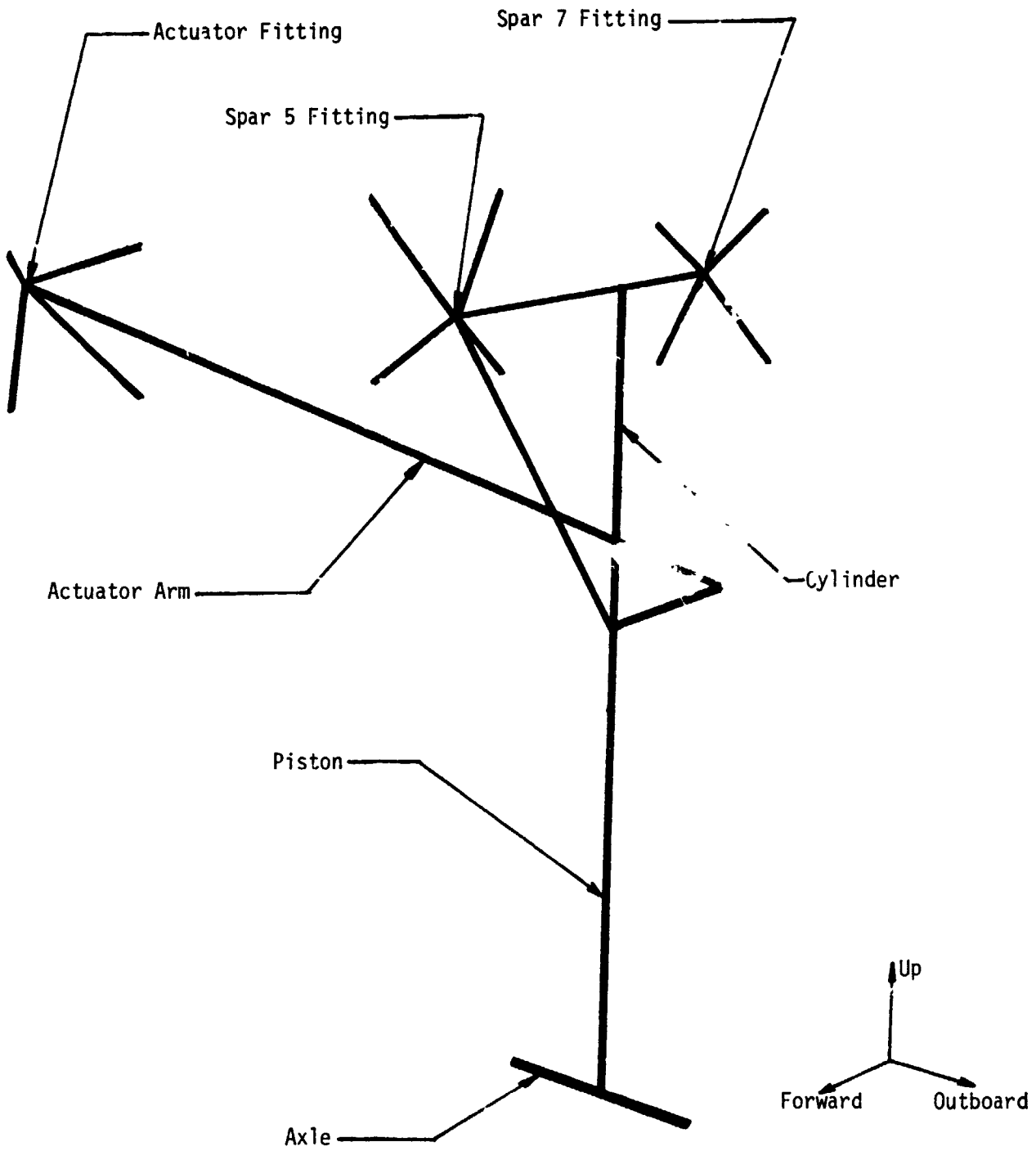


Figure 6 - Landing Gear Finite Element Model

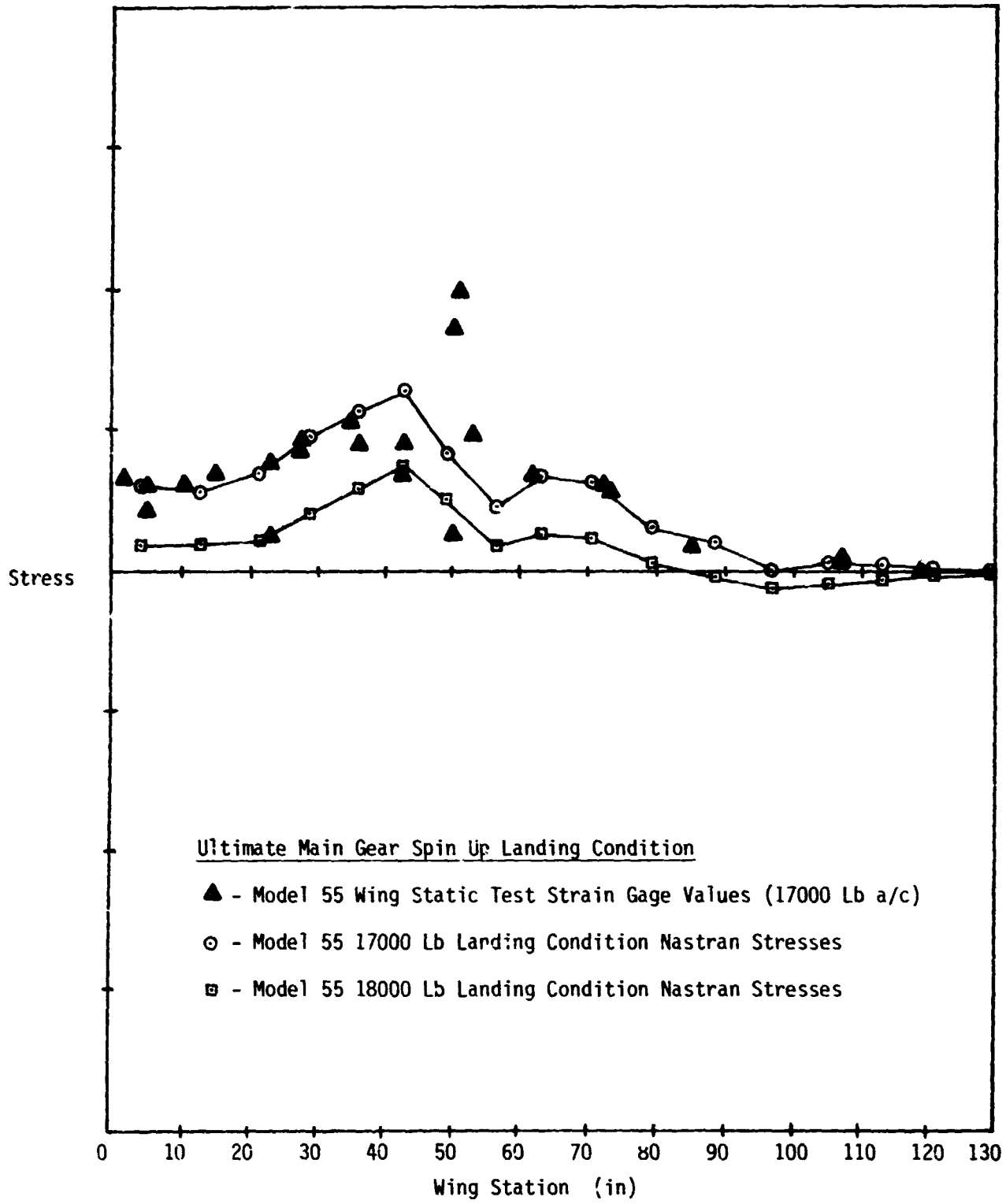


Figure 7 - Stresses In Spar 5 Lower Cap

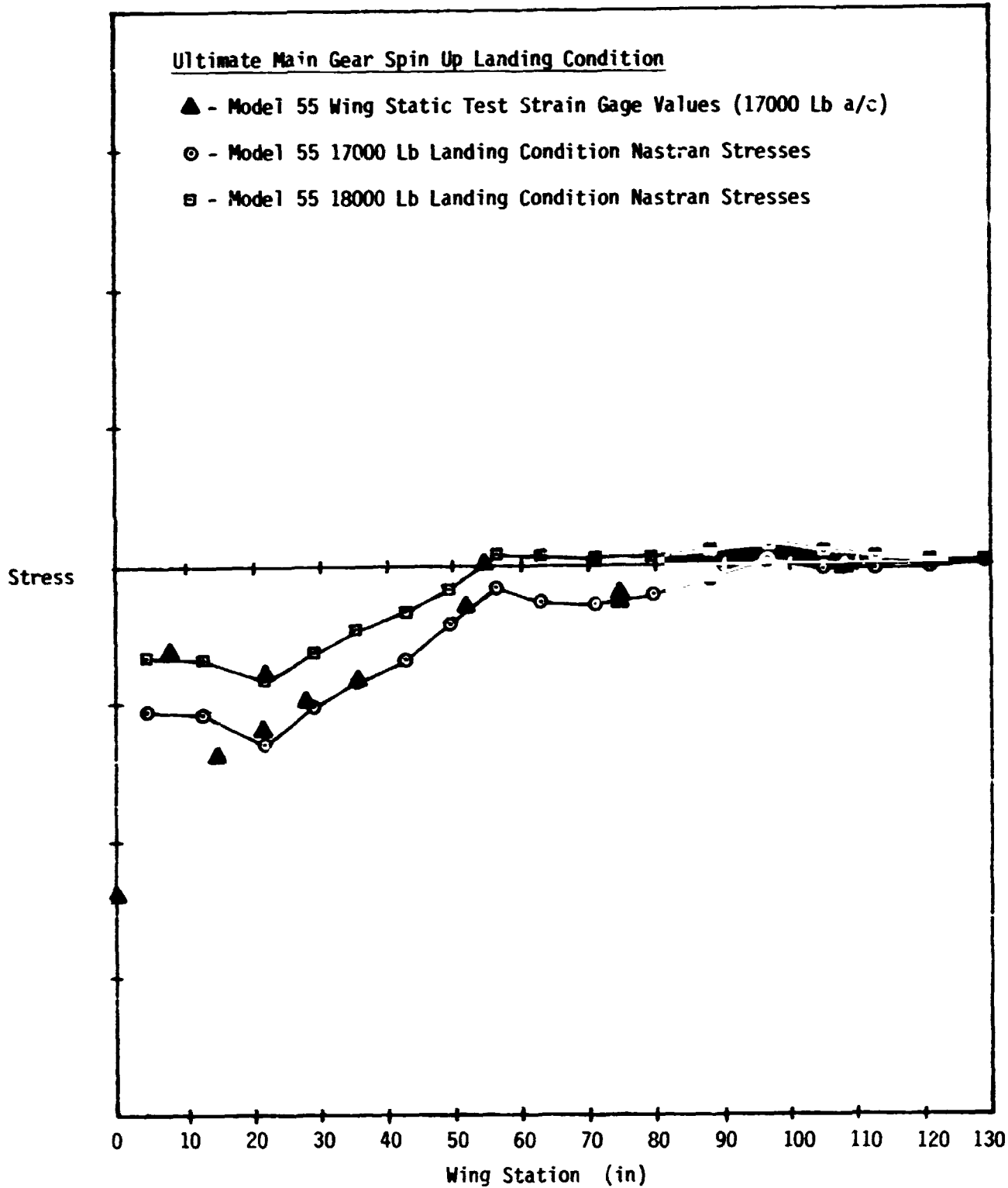


Figure 2 - Stresses In Spar 5 Upper Cap

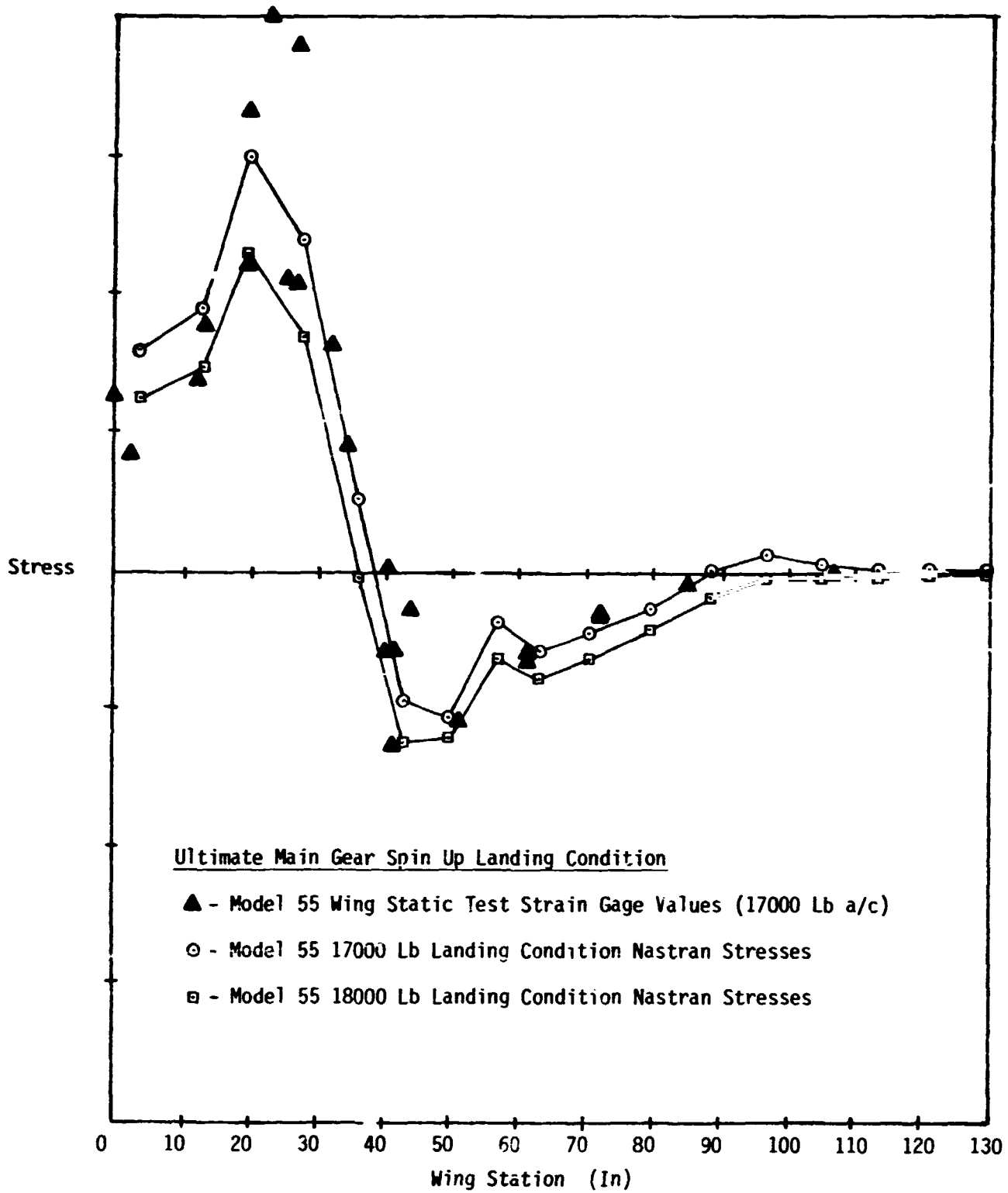


Figure 9 - Stresses In Spar 7 Lower Cap

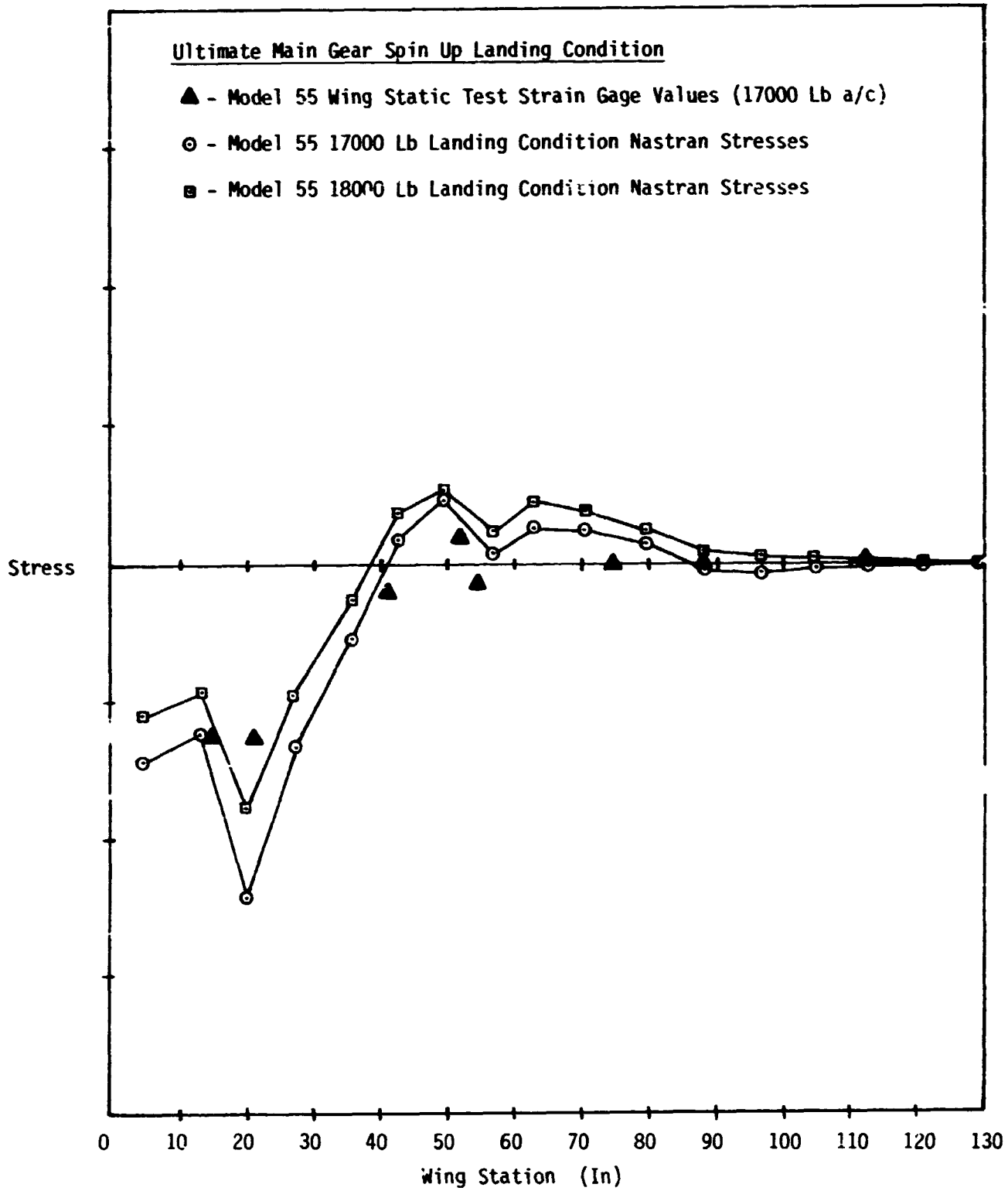


Figure 10 - Stresses In Spar 7 Upper Cap

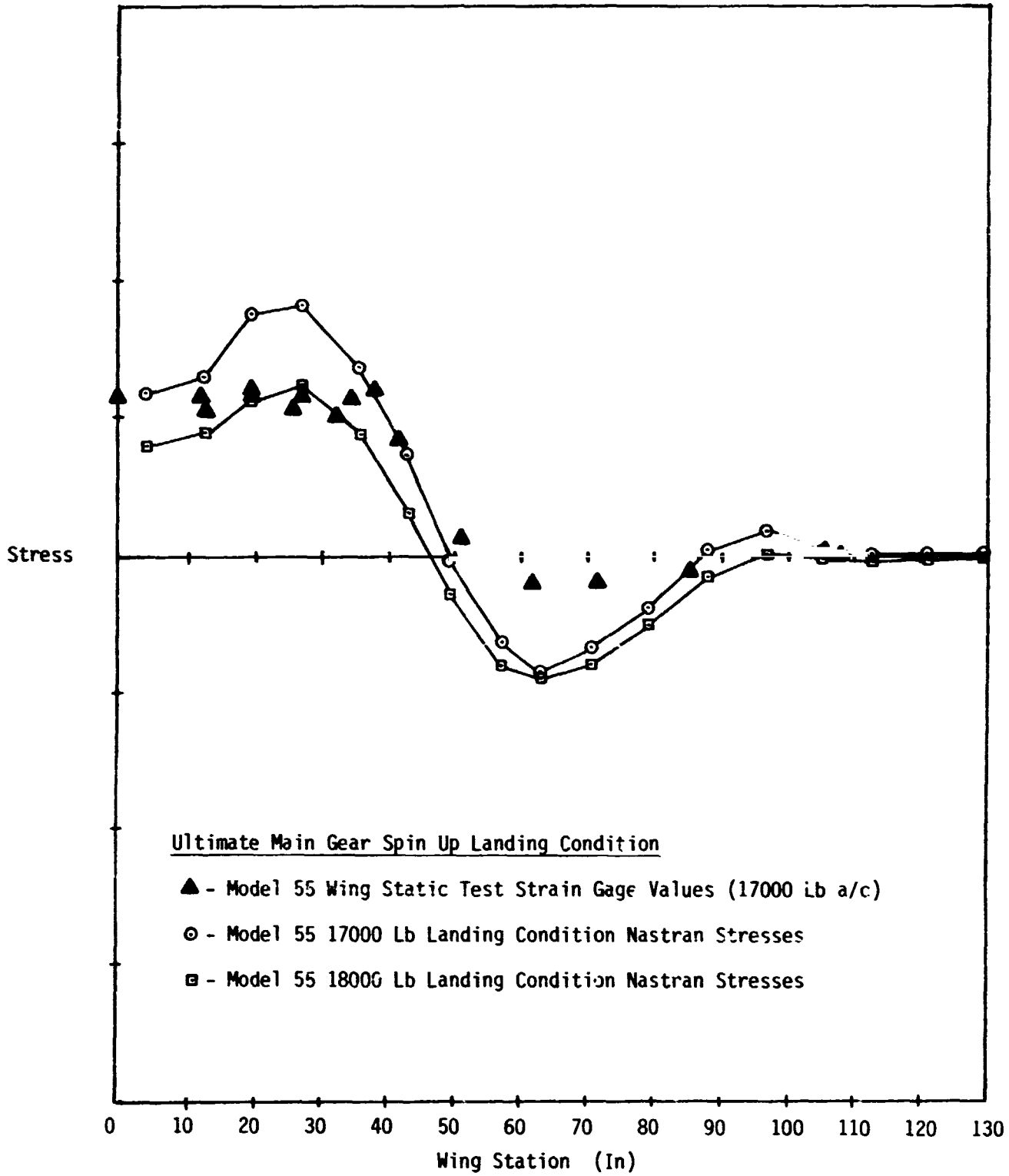


Figure 11 - Stresses In Spar 8 Lower Cap

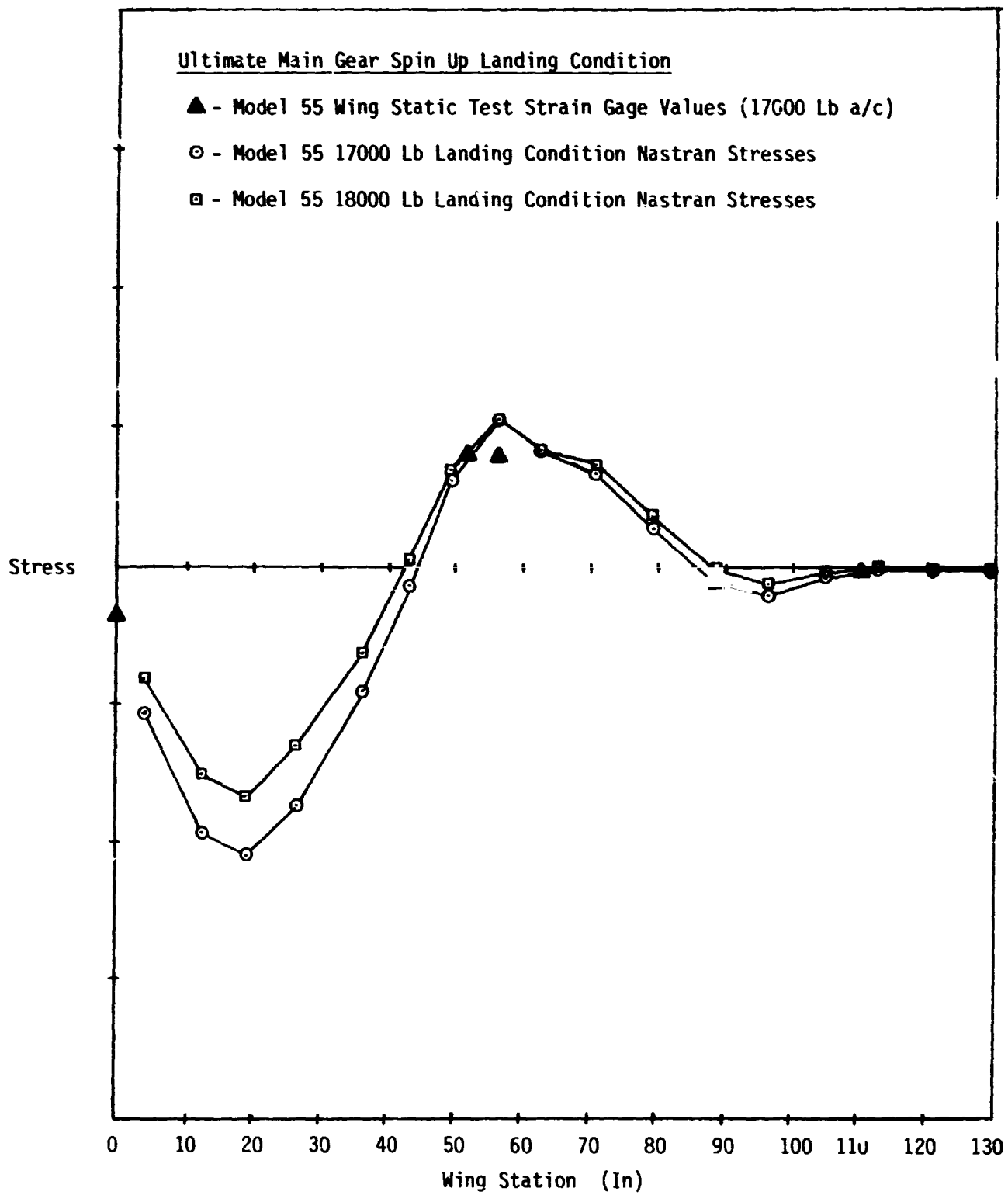


Figure 12 - Stresses In Spar 8 Upper Cap

N85-25884

FILLET WELD STRESS USING FINITE ELEMENT METHODS

Terry F. Lehnhoff
University of Missouri-Rolla

Gerald W. Green
University of Missouri-Rolla

SUMMARY

Average elastic Von Mises equivalent stresses were calculated along the throat of a single lap fillet weld. The average elastic stresses were compared to initial yield as well as to plastic instability conditions to modify conventional design formulas so that they can be used to predict either extreme of failure by yielding. A new multiplying factor for the conventional design formulas is presented. The factor is a linear function of the thicknesses of the parent plates attached by the fillet weld.

INTRODUCTION

In theoretical analyses of stresses in welds, approximations have not only been traditionally accepted but have been considered appropriate. Much of the justification for this has been based on the presumption that analytical means for accurate solutions are not available. Furthermore, the limited quality control that is possible with many welding processes has supported this viewpoint. Welding technology is, however, steadily improving along with the quality control that is necessary to ensure consistency as well as reliably welded joints. This improvement will continue as welding becomes an even more significant part of future manufacturing processes.

The purpose of the present investigation was to establish more precise design formulas for single lap fillet welds subjected to tensile loading. The study has revealed a complexity in what appears to be a relatively simply geometry (fig. 1). In addition, it indicated that variations in the thicknesses of the welded plates have an influence on such welds. Different plate thicknesses affect the geometry as well as the load paths. The change in geometry is rather obvious, but the additional bending load, which is a natural consequence of the change in geometry, has not been considered in the conventional theory.

BASIC THEORY

Because the throat area of a weld as indicated by line BD in figure 1 is the minimum area through which loads must be transferred, it is the most probable area of failure. Leg BC is loaded predominantly in shear, whereas leg BE is primarily in tension. The throat must then be subjected to a combination of tension and shear. Shigley and Mitchell (ref. 1) showed that the largest principal stress on a throat area is defined as

$$\sigma_1 = 1.618(F/hl) , \quad (1)$$

and the maximum shear stress as

$$\tau_{\max} = 1.118(F/h\ell) \quad (2)$$

in which F is the applied load, ℓ the length of the weld in a direction normal to the page, and h the leg length. These stresses are calculated as averages for the entire throat. Norris (ref. 2), Salakian and Claussen (ref. 3), and Bagci (ref. 4) showed that the stresses vary significantly along both legs and that the throat has a large stress concentration at point B. Thus, although equations (1) and (2) are known to give average results, Shigley and Mitchell (ref. 1) noted that for design purposes, it is customary to base the shear stress on the throat area and to neglect the normal stress altogether. On this basis, the equation for average shear stress becomes

$$\tau = 1.414(F/h\ell) \quad (3)$$

and τ from equation (3) is 1.27 times greater than from equation (2). Obviously, an unknown safety factor has been incorporated in equation (3).

The present study brought out the fact that there is a logical rationale for a multiplying factor somewhat different than the one used in equation (3). Because the failure of mechanical components from either static or fatigue loading was shown by Shigley and Mitchell (ref. 1) to be related to the Von Mises-Hencky equivalent stress, it is used extensively in the discussion which follows.

If it is assumed as in equation (3) that the throat is subjected to pure shear, then the equivalent Von Mises stress can be shown to be

$$\sigma = \sqrt{3} 1.414(F/h\ell) = 2.449(F/h\ell). \quad (4)$$

In the present investigation, the finite element method was used to determine the actual distribution of the Von Mises stresses along the throat for several weld configurations. Averages of the results from elastic analyses were obtained, and these were compared with the results from some plastic analyses.

MODELS

Models were prepared, and analyses were performed by senior mechanical engineering students at the University of Missouri-Rolla. The finite element method was used to develop the models shown in figures 1 and 2. Several types and refinements of meshes were used at various stages of the work. Four-node quadrilateral and three-node triangular elements as well as eight-node quadrilateral and six-node triangular elements were used in the models. In each model, elastic analyses were performed with the element dimensions varying from 0.0635 (0.025) in most of the weld to 0.254 mm (0.010 in.) in the area of the most significant stress concentration (point B in fig. 1). For the elastic analyses, the maximum number of nodes was 2121, and the maximum number of elements was 806. For the plastic analyses, the maximum number of nodes was 411, and the maximum number of elements was 160. The maximum computer time on an IBM 4341 for the elastic analyses was 92 min, and the maximum for the plastic analyses was 10 min. Plastic analyses for which a refined mesh was used required almost four hours and were deemed impractical for multiple analyses.

The grid size was selected so that after sufficient refinement in the area of point B the nodal stresses from all elements surrounding a given node were the same to at least one significant figure. Point B was an exception because of the steep stress gradients.

ELASTIC ANALYSIS

Elastic studies were performed for plate thicknesses varying from 6.35 (0.25) to 22.22 mm (0.875 in.) in 3.18 mm (0.125 in.) increments. The weld leg length was kept constant at 6.35 mm (0.25 in.) for all plate thicknesses. Only the data for models 1 (Green), 2 (Morlock), and 3 (O'Brian) as defined in figure 1 have been shown in subsequent figures. Similar results were obtained for the other models.

Three load and constraint configurations were selected. The first one, which is shown in figure 2a (Case 1), was an attempt to subject the weld as nearly as possible to a direct load without a moment. Complete elimination of any moment would have been desirable but was impossible for the unsymmetrical geometry of the configuration. The loading and restraining conditions for practical applications are shown in figures 2b (Case 2) and 2c (Case 3). These are considered more realistic, because the loads in most physical components would be uniformly transferred through the thickness.

Because the results in Case 3 for symmetric geometry and loading were not significantly different from Case 1, they are not discussed in detail here.

Figure 3 shows a deformed plot of a simplified version of Case 1. It illustrates that although the loading and restraints were aligned, the unsymmetrical geometry caused the weld to rotate somewhat.

Figures 4a-4c show the general trends of the stress contours for maximum principal stress, minimum principal stress and maximum shear stress for the same model and load case as shown in figure 3. These are representative of the stress distribution throughout the weld.

Figure 5 shows the distribution of the Von Mises equivalent stress along the weld throat (BD in fig. 1) for Case 1. Figure 6 shows the same Von Mises equivalent stress as figure 5. The large stress at point B has been omitted to show more clearly the variations occasioned by the plate thicknesses in the various models.

Figure 7 shows the distribution of the Von Mises equivalent stress along the throat for Case 2. Figure 8 shows the same Von Mises stress as figure 7, and, again, the large stress at point B has been omitted to show the variations occasioned by the plate thicknesses in the various models.

Figures 5 and 7 are of different scales because of the large stresses at point B. However, figures 6 and 8 are of the same scale and can be overlaid for the purpose of comparing the effects of the loads of Cases 1 and 2.

PLASTIC ANALYSIS

Elastic perfectly plastic analyses were conducted for an AWS E80XX electrode with a tensile strength of 552 MPa (80 kpsi), a yield strength of 462 MPa (67 kpsi) and an assumed identical parent plate material. In general, the calculations were performed with increasing load increments until the strength became unstable.

The less refined models with nominal element dimensions of 0.635 mm (0.025 in.) were used in the plastic studies. This was necessary, because the iterative solution procedure was more demanding of computer resources. Figures 9, 10 and 11 show the development of the plastic zones as the load on a weld of unit length was increased to the point of instability. The results in figure 9 are for model 1 (Green) with Case 2 loading. The results in figure 10 are for model 2 (Morlock) with Case 2 loading, whereas the results in figure 11 are for model 3 (O'Brian) with Case 2 loading. Similar results were also obtained for the other models defined in figure 1.

DISCUSSION

The average elastic Von Mises stresses along the throat shown in figures 5 through 8 are suggested as being more indicative of failure than the traditional relationship given by equation (3). Failure in the static sense can be either the initiation of yielding or the point of plastic instability where a weld has essentially yielded along the entire length of its throat.

For the models defined in figure 1 in each of the elastic analyses, the load was taken as 4.448 N (1.0 lb) acting on a weld of leg length 6.35 mm (0.25 in.) and length 25.4 mm (1.0 in.). For these conditions, the conventional theory as expressed by equation (4) indicates an average Von Mises stress of 67538 Pa (9.796 psi). Furthermore, the conventional theory does not include plate thickness as a variable.

With Case 1 (fig. 2) and 4.448 N (1.0 lb) loading, figures 5 and 6 show that the stress does not vary significantly with plate thickness. The average stress was determined to be 58086 Pa (8.425 psi). With Case 2 (fig. 2) and 4.448 N (1.0 lb) loading, the average Von Mises stress was determined to be 105699 Pa (15.331 psi) for model 1, 178470 Pa (25.886 psi) for model 2 and 248207 Pa (36.001 psi) for model 3. Case 2 loading thus shows a definite deviation from conventional theory.

If it is assumed that the finite element results indicate a correct average Von Mises stress, then the conventional equation should be multiplied by $58086/67538 = 0.86$ for Case 1 type loading. If, instead of assuming pure shear as in the conventional approach, it is assumed that the Von Mises stress corresponding to equations (1) and (2) is appropriate, then a multiplier of 0.82 for equation (4) should be the result. The most accurate conventional theory, therefore, deviates by only 4 percent from the finite element method. However, by expressing equations (3) and (4) as they should be applied for Case 1 (fig. 2) loading, one has

$$\tau = 0.86(1.414)(F/hl) = 1.22(F/hl) \quad (5)$$

and

$$\sigma = 0.86(2.449)(F/hl) = 2.11(F/hl). \quad (6)$$

Now the multipliers in equations (3) and (4) for Case 2 (fig. 2) loading should be 1.57 for model 1, 2.64 for model 2 and 3.68 for model 3. Thus, conventional theory is inadequate when the plates are thicker and the load is distributed.

The comparison given above in equations (5) and (6) shows what is necessary to make the conventional formulas for the average shear stress on a plastic weld throat and the corresponding Von Mises equivalent normal stress agree with more accurate calculations of those stresses. However, the objective of the design engineer is to

be able to predict not only the beginning of yielding but the fully plastic instability condition as well. Consequently, one must relate equations (5) and (6) to these yield conditions.

Plastic analyses allow one to adjust the conventional formulas (eqs. (3) through (6)) so that either initial yielding or plastic instability can be predicted. To determine the constant for the initiation of yielding, it is assumed that the load at which yielding first occurs corresponds to the load when an element in the parent material immediately to the left of the corner at point B (fig. 1) has experienced general yielding, and the corner element in the weld has just started to yield. It was noted during the numerical experiments that at this load the weld also begins to yield in the region of point D. For each of the models, this load was divided by the load at which plastic instability occurred. The average of these ratios was approximately 2/3 for all of the models for both Case 1 and Case 2 loading. None of the models varied significantly from the 2/3 value. Thus, the ratio of the load for initial yielding to the load for plastic instability is relatively constant for the models and for the material illustrated in figures 9 through 11 as well as for the others noted in the table of figure 1 for both Case 1 and Case 2 loading.

It remains to show how the average elastic Von Mises equivalent stress relates to either initial yielding or plastic instability. Figures 9 through 11 show the progression of the plastic deformation zones for three of the models. As noted earlier, the parent material and weld were assumed to be identical with a yield strength of 462 MPa (67 kpsi). For this material and an elastic perfectly plastic assumption, the various models became unstable at the next load increment. That is in figure 9 for model 1, the instability is shown to have occurred between 17.8 (4.0) and 18.7 kN (4.2 kips), and in figure 10 for model 2 the instability is shown to have occurred between 10.7 (2.4) and 11.6 kN (2.6 kips), whereas in figure 11, the instability is shown to have occurred between 8.0 (1.8) and 8.9 kN (2.0 kips). Furthermore, for Case 1 loading, the instability is shown to have occurred at approximately the same load for all models and was between 33.8 (7.6) and 35.5 kN (8.0 kips).

The loads at which the average elastic Von Mises stress equals the yield strength of the material were determined. This was done on the presumption that general plastic yielding and instability occur when the average elastic Von Mises equivalent stress is equal to the yield strength of the material. To determine these loads, the yield strength was divided by the average elastic Von Mises stresses as indicated in figures 5 through 8. For Case 2 loading for model 1, the ratio is 19.4 kN (4.37 kips), and for model 2, the ratio is 11.4 kN (2.59 kips), whereas for model 3, the ratio is 8.3 kN (1.86 kips). For Case 1 loading, the load when the average Von Mises stress equaled the material yield strength was 35.4 kN (7.95 kips), and it was approximately the same for all models. The loads are compared in Table 1 where it is evident that the average elastic Von Mises stress along the throat is an excellent indicator of plastic instability.

Because equation (6) permits a more accurate calculation of the average Von Mises equivalent stress along the throat of the weld, it also predicts the fully plastic instability condition when the calculated Von Mises stress equals the yield strength of the material. Furthermore, equation (6) can be used to predict the onset of yielding when the calculated stress equals 2/3 of the material yield strength.

To obtain a design equation for the onset of yielding, equation (6) can be multiplied by 3/2 as follows:

$$\sigma = (3/2)(0.86)(2.449)(F/h\ell) = 3.16(F/h\ell). \quad (7)$$

When the applied load F is such that σ equals the material yield strength, then for Case 1 loading, the weld will experience the initiation of yielding. For Case 2 loading, the 0.86 factor must be replaced by 1.57, 2.64, and 3.68 for models 1, 2, and 3 respectively. All of the constants are listed in Table 2. The data for load Case 2 from Table 2 are plotted in figure 12. Because the constants are related linearly, one can write equation (7) as follows:

$$\sigma = f(F/hl) \quad (8)$$

in which

$$f = 3.88(A/h) + 1.90 \quad (9)$$

for Case 2, and A/h , the plate thickness to weld leg length ratio, must be greater than or equal to one. Equations (7) and (8) provide the basis for the design of single lap fillet joints for the initiation of yielding of the weld throat. Equation (6) allows for fully plastic design. However, the influence of strain hardening will usually make equation (6) somewhat conservative.

REFERENCES

1. Shigley, J. E.; and Mitchell, L. D.: Mechanical Engineering Design. Fourth Edition, McGraw Hill 1983, p. 417.
2. Norris, C. H.: Photoelastic Investigation of Stress Distribution in Transverse Fillet Welds. Welding Journal, vol. 24, 1945, p. 557.
3. Salakian, A. G.; and Claussen, G. E.: Stress Distribution in Fillet Welds; A Review of the Literature. Welding Journal, vol. 16, May 1973, pp. 1-24.
4. Bagci, C.: Finite Stress Elements and Applications in Machine Design. OSU Applied Mechanisms Conference, Denver, October 1979.

TABLE 1.-RELATION OF AVERAGE ELASTIC VON MISES AND PLASTIC LOADS

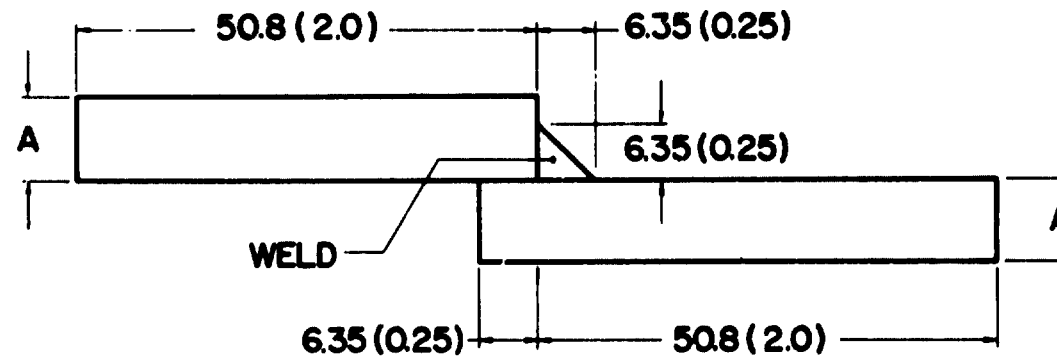
LOAD CASE	PLATE THICKNESS mm (in.)	Load for Average Von Mises Stress Equal to Material Yield Strength kN (kips)	Load Range for Plastic Instability kN (kips)
1	All	35.4 (7.95)	33.8 (7.6) - 35.6 (8.0)
2	6.35 (0.25)	19.4 (4.37)	17.8 (4.0) - 18.7 (4.2)
2	12.70 (0.50)	11.5 (2.59)	10.7 (2.4) - 11.6 (2.6)
2	19.05 (0.75)	8.3 (1.86)	8.0 (1.8) - 8.9 (2.0)

TABLE 2.-CONSTANTS FOR EQUATION 7

LOAD CASE	PLATE THICKNESS mm (in.)	CONSTANTS FOR EQUATION 7
1	All	3.16
2	6.35 (0.25)	5.76
2	12.70 (0.50)	9.70
2	19.05 (0.75)	13.52

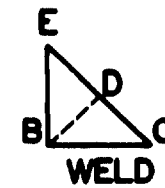
LIST OF FIGURES

- FIGURE 1. Fillet Weld Model Dimensions
- FIGURE 2. Load and Restraint Cases
- FIGURE 3. Deformed Geometry, Case 1
- FIGURE 4a. Typical Maximum Principal Stress, Case 1
- FIGURE 4b. Typical Minimum Principal Stress, Case 1
- FIGURE 4c. Typical Maximum Shear Stress, Case 1
- FIGURE 5. Von Mises Stress Along Throat, Case 1
- FIGURE 6. Von Mises Stress Along Throat, Case 1 (Expanded Scale)
- FIGURE 7. Von Mises Stress Along Throat, Case 2
- FIGURE 8. Von Mises Stress Along Throat, Case 2 (Expanded Scale)
- FIGURE 9. Development of Plastic Instability, Model 1, Case 2
- FIGURE 10. Development of Plastic Instability, Model 2, Case 2
- FIGURE 11. Development of Plastic Instability, Model 3, Case 2
- FIGURE 12. Factor for Equation 8



NOTE ALL DIMENSIONS IN mm (in.)

MODEL	A
1 (GREEN)	6.35 (0.250)
(ILISEVIC)	9.52 (0.375)
2 (MORLOCK)	12.70 (0.500)
(ROGAN)	15.88 (0.625)
3 (O'BRIAN)	19.05 (0.750)
(BOHR)	22.22 (0.875)



BC - SHEAR LEG
 BD - THROAT
 BE - TENSION LEG

FIGURE 1 FILLET WELD MODEL DIMENSIONS

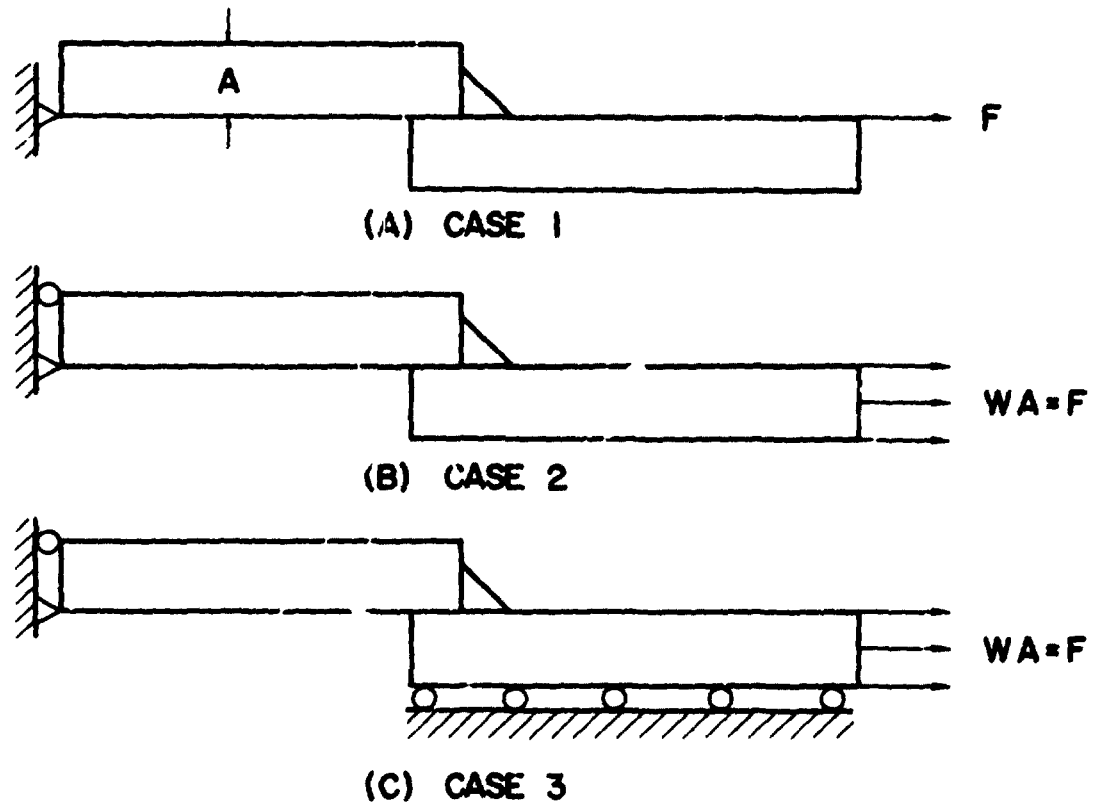


FIGURE 2 LOAD AND RESTRAINT CASES

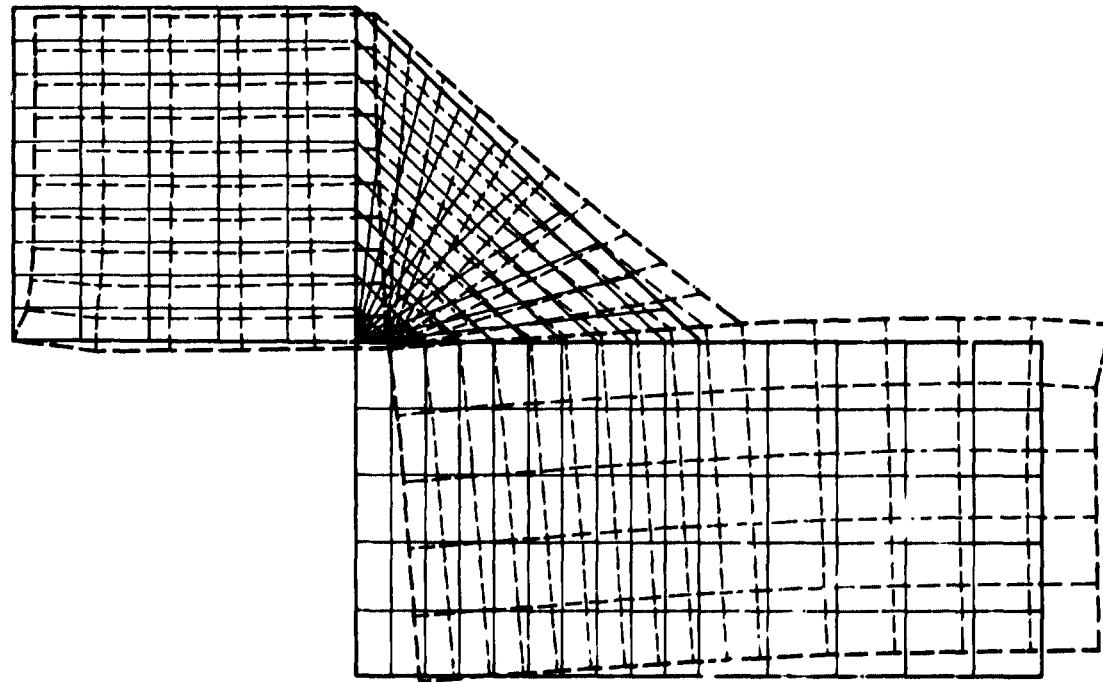


FIGURE 3 DEFORMED GEOMETRY, CASE I

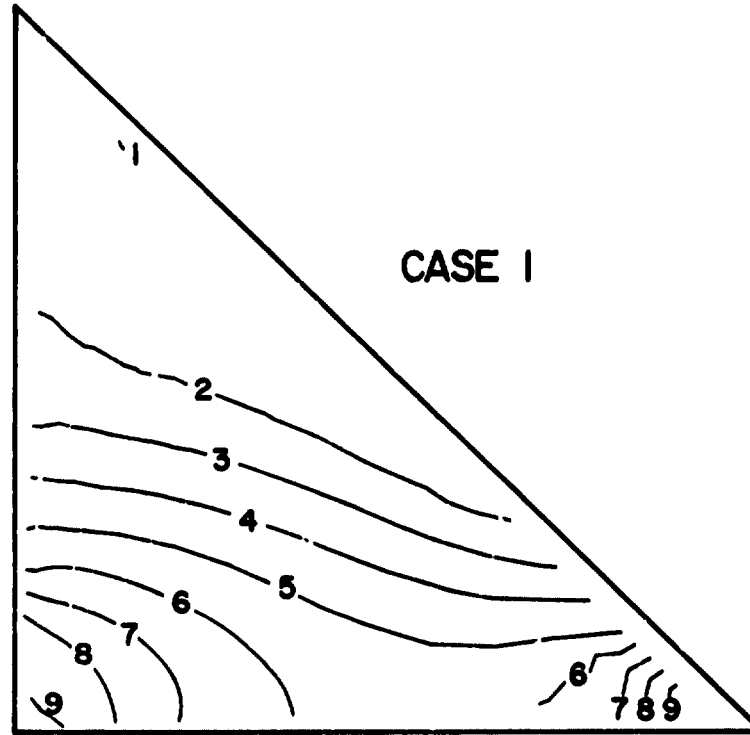


FIGURE 4a TYPICAL MAXIMUM PRINCIPAL STRESS

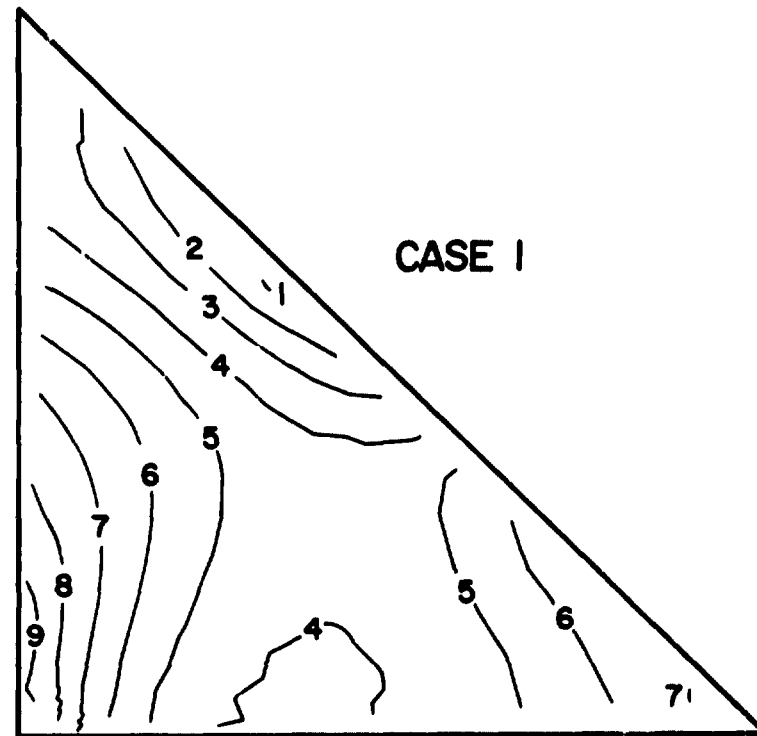


FIGURE 4b TYPICAL MINIMUM PRINCIPAL STRESS

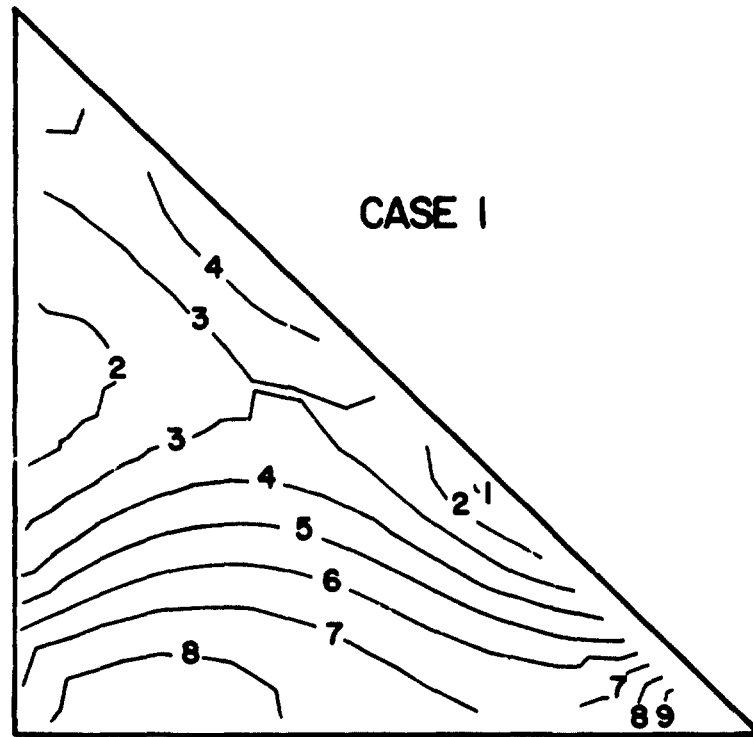


FIGURE 4c TYPICAL MAXIMUM SHEAR STRESS

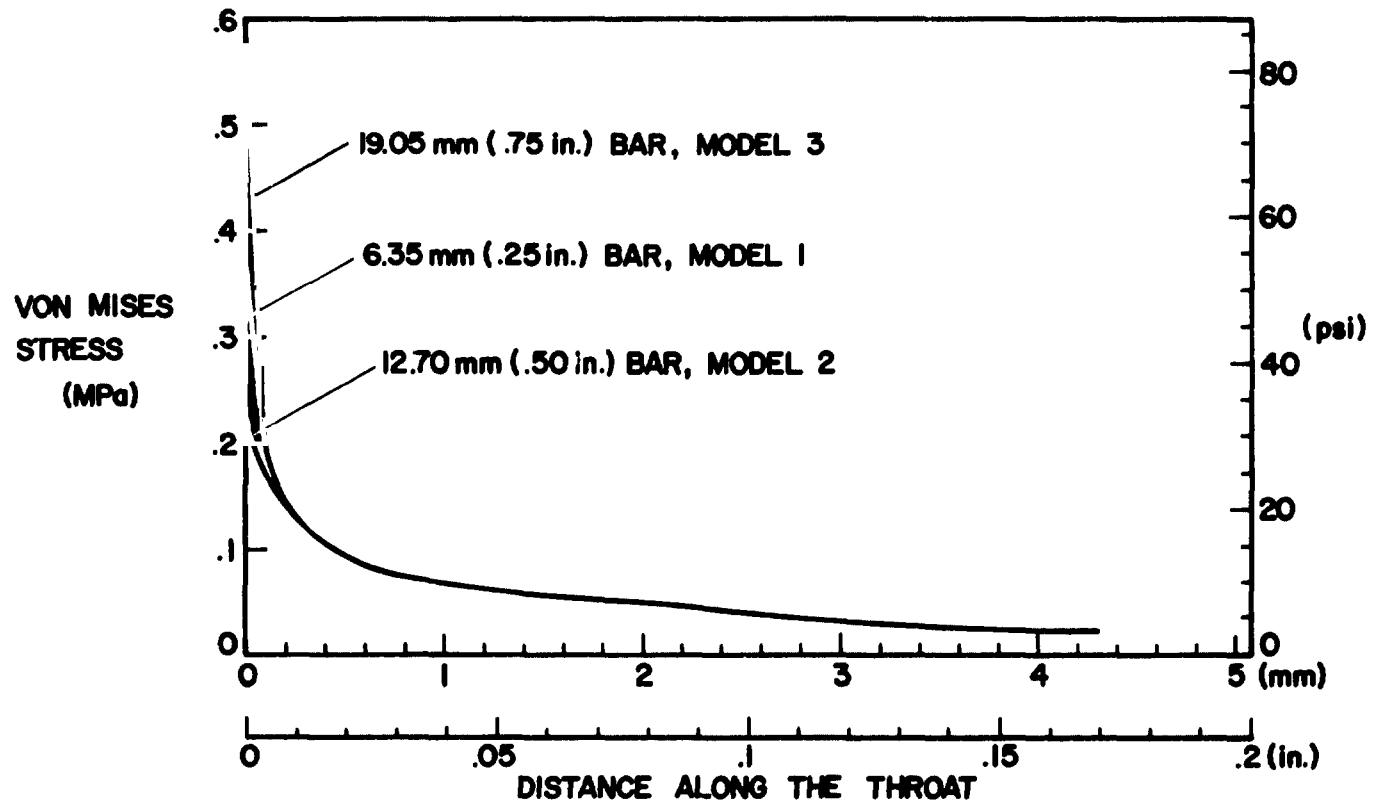


FIGURE 5 VON MISES STRESS ALONG THROAT, CASE I

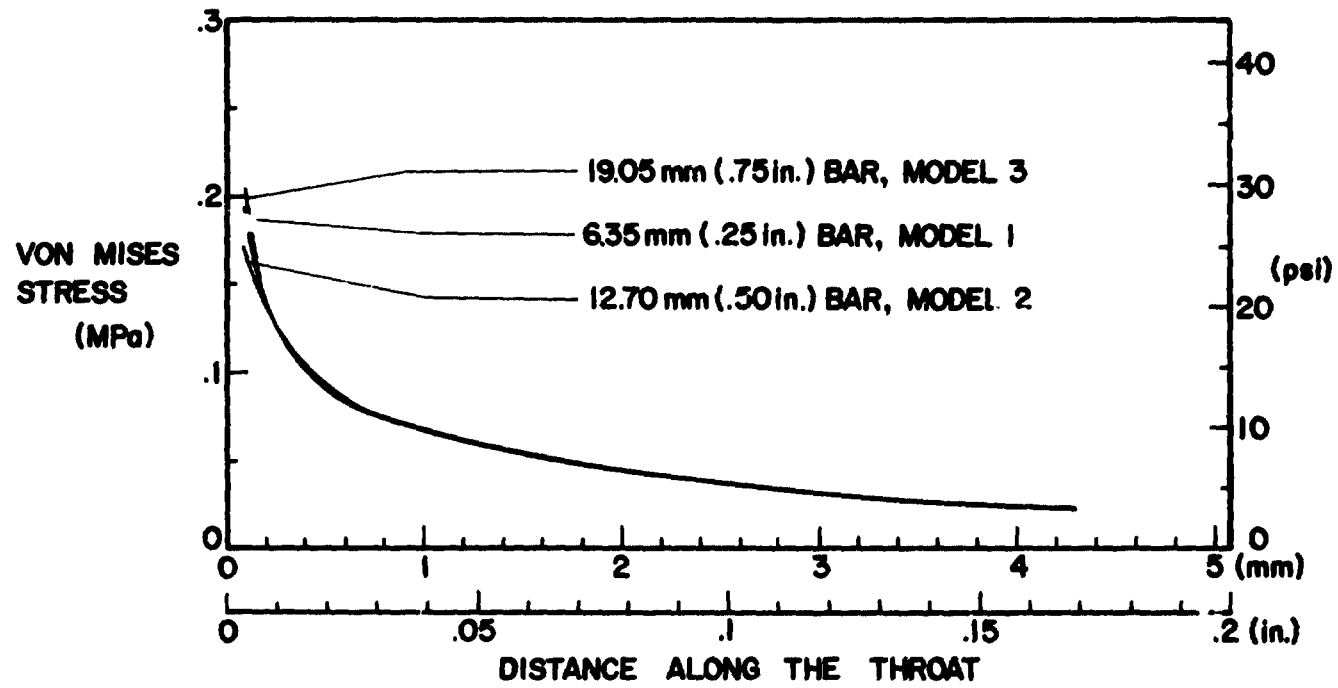


FIGURE 6 VON MISES STRESS ALONG THROAT, CASE I
(EXPANDED SCALE)

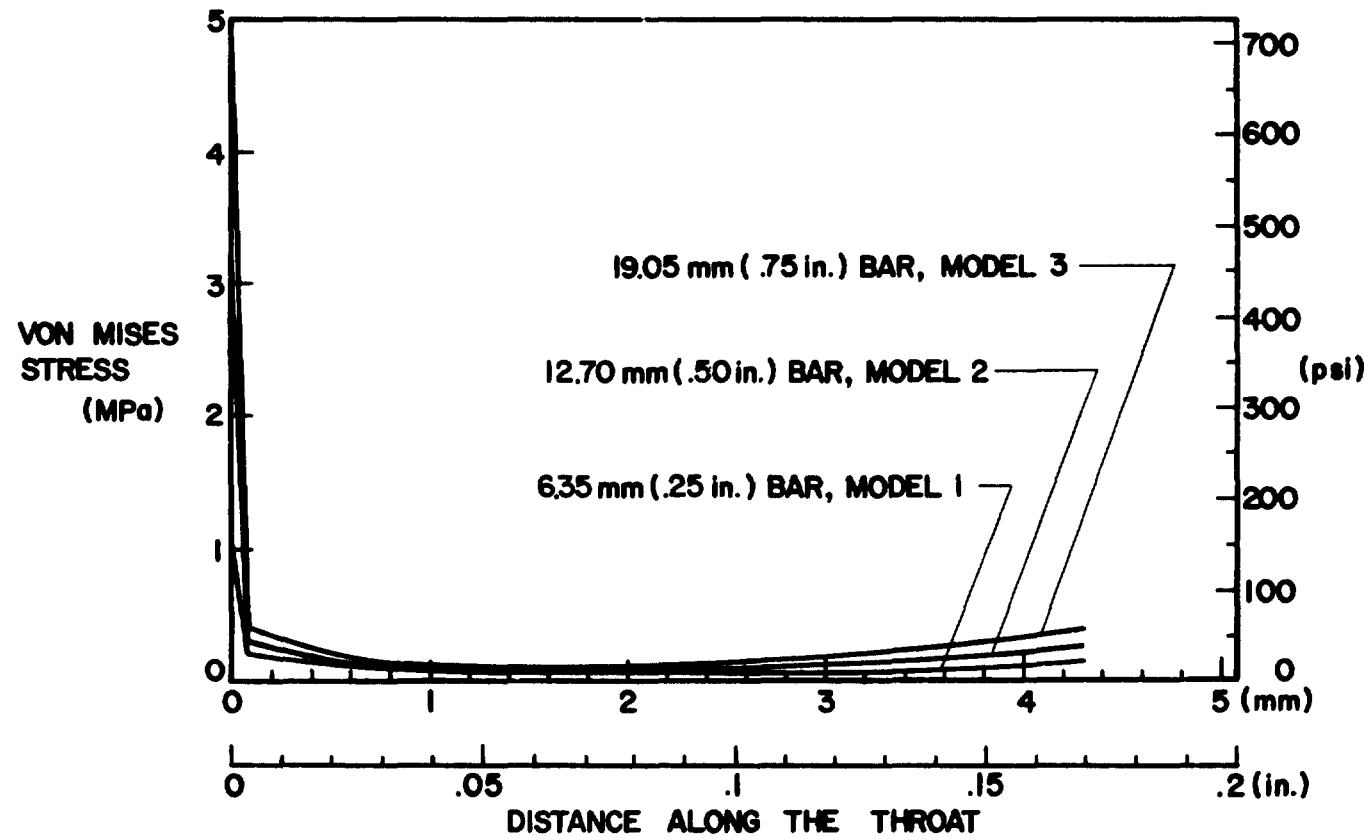


FIGURE 7 VON MISES STRESS ALONG THROAT, CASE 2

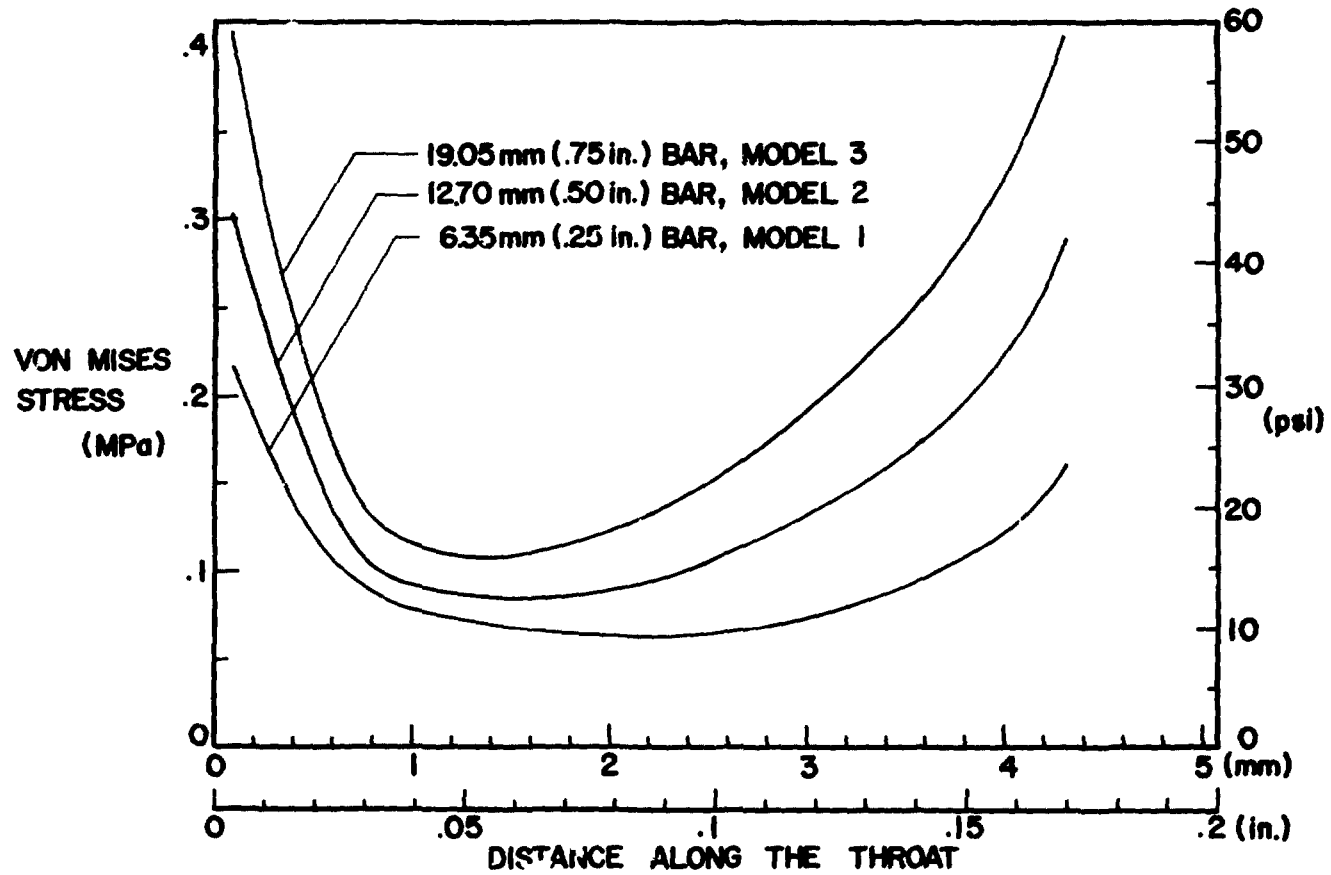
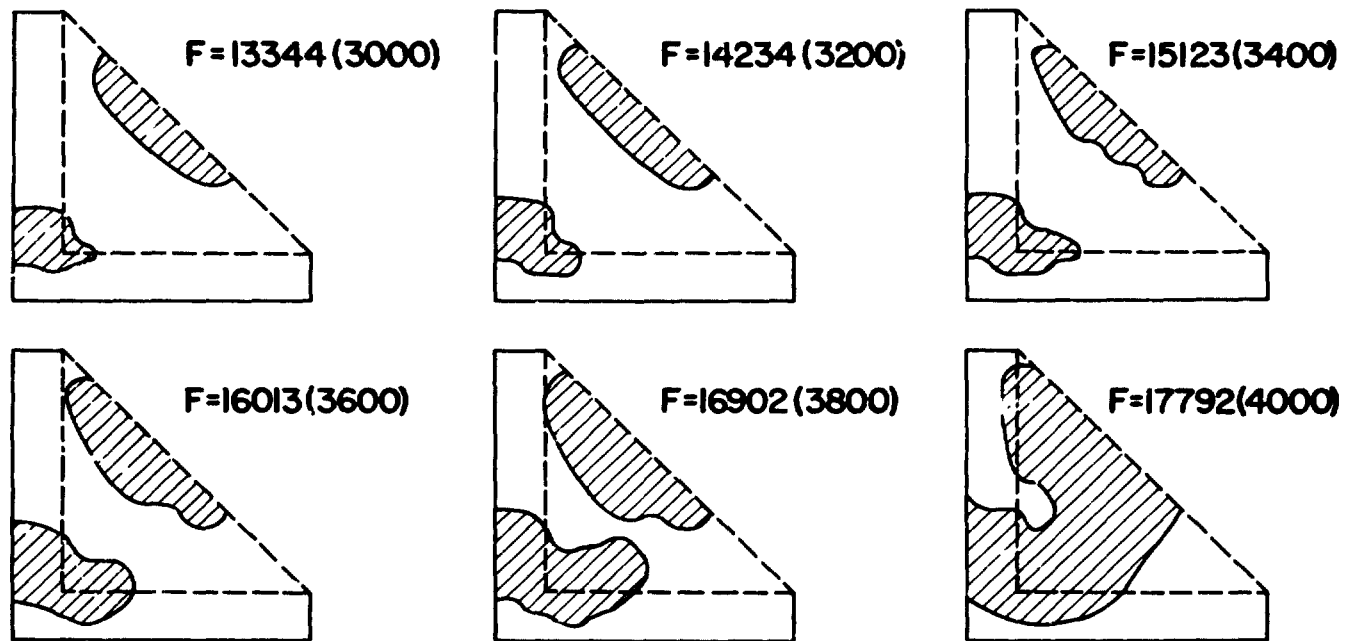
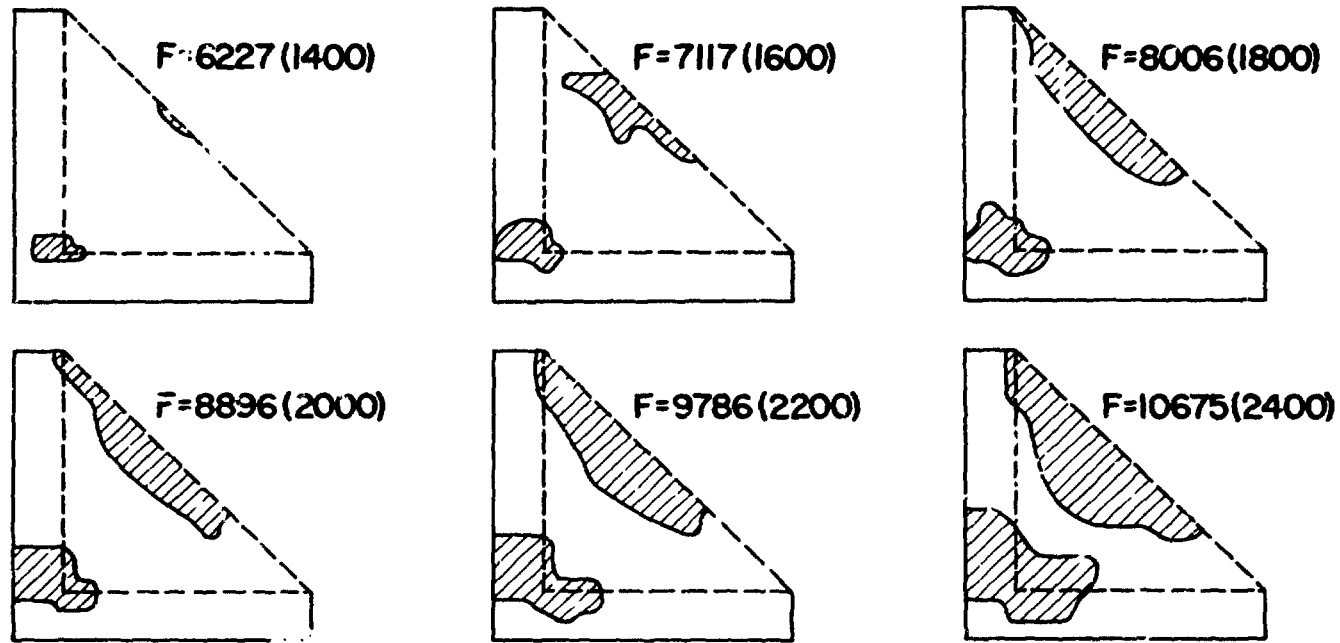


FIGURE 8 VON MISES STRESS ALONG THROAT, CASE 2 (EXPANDED SCALE)



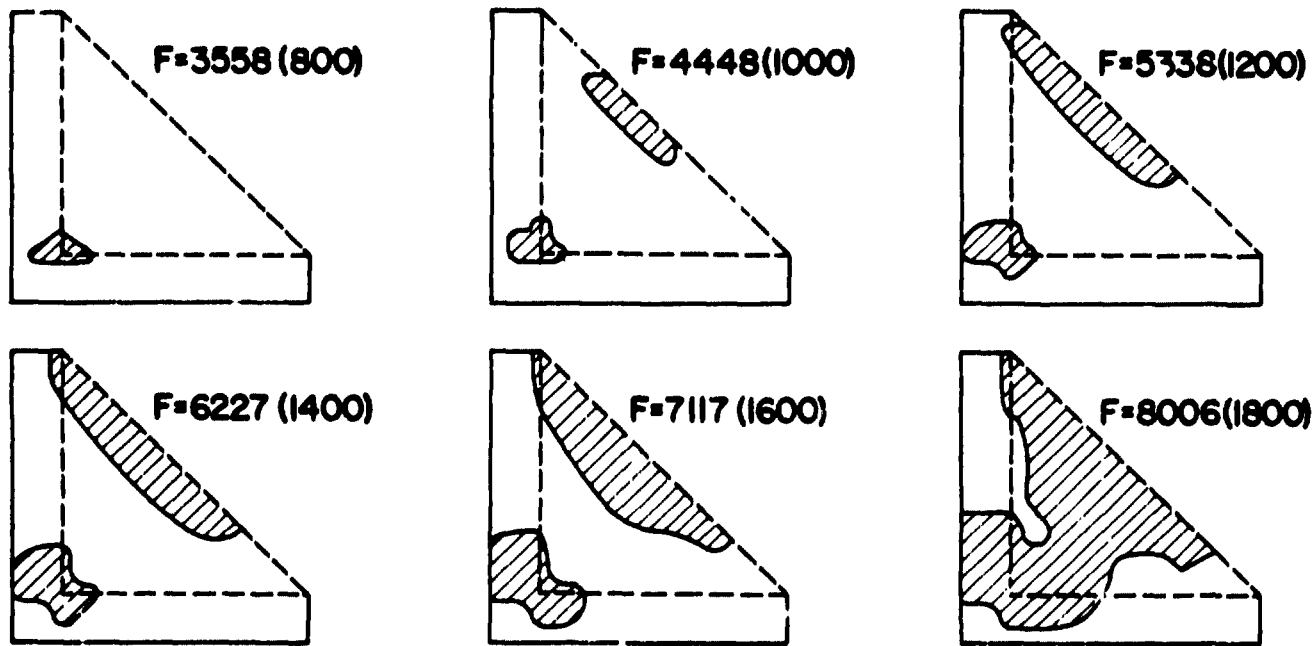
NOTE ALL DIMENSIONS IN N (lbs)

FIGURE 9 DEVELOPMENT OF PLASTIC INSTABILITY, MODEL 1, CASE 2



NOTE ALL DIMENSIONS IN N (lbs)

FIGURE 10 DEVELOPMENT OF PLASTIC INSTABILITY, MODEL 2, CASE 2



NOTE ALL DIMENSIONS IN N (lbs)

FIGURE 11 DEVELOPMENT OF PLASTIC INSTABILITY, MODEL 3, CASE 2

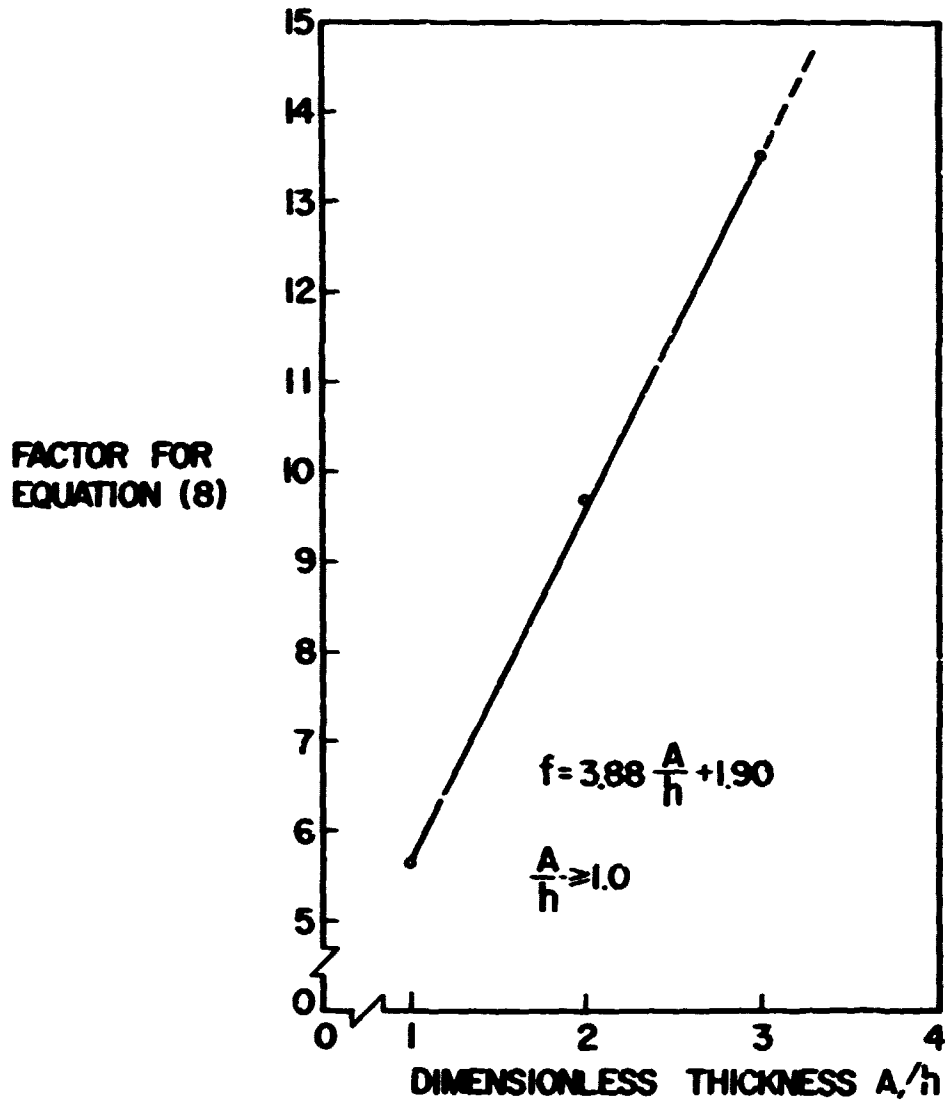


FIGURE 12 FACTOR FOR EQUATION 8

N85-25885

THE STRUCTURAL FINITE ELEMENT MODEL OF THE C-5A

Gisela W. McClellan
Lockheed-Georgia Company

SUMMARY

A substructured NASTRAN model of the C-5A was analyzed for several different load conditions. The size of the model as well as the number of load cases used presented special problems in computer file and space management. This also resulted in revisions to the in-house NASTRAN code. Despite the problems encountered the analyses were completed with excellent results.

INTRODUCTION

The C-5A is a very large transport aircraft. The primary structure of the aircraft is composed of frames connected by stringers and covered by skin panels in the fuselage and of ribs and spars covered by integrally stiffened skin panels in the wing. The C-5A contains a cargo floor and a second floor to carry troops. It has a hinged visor at the forward end which opens upward and a large cargo door at the aft end. Hinged ramps and removeable ramp extensions on either end permit drive-through loading of this unique aircraft.

During the late 1960's the C-5A was modeled using a Lockheed-developed finite element analysis program called FAMAS. The analysis used a force method. The FAMAS program limited the size of a model more severely than NASTRAN does. Thus the original model was substructured into relatively small modules. The forward fuselage was idealized as a full model (left and right sides) as was the aft fuselage. The center fuselage and wing were represented as a half model since that portion of the aircraft is essentially symmetric about the center line. Since FAMAS uses a left handed coordinate system, only the left side was actually modelled. The center fuselage substructures and the wing were also coupled. However, a complete coupling of forward, aft and center sections was never carried out. To reduce the size of individual substructures, the FAMAS model contained much lumping, both for frames and stringers.

In order to provide an improved quality of the predicted stresses and stress distributions for damage tolerance and durability analyses, to provide compatibility with detail structural models of the C-5A, and to ensure a modern, state-of-the-art analysis tool, the FAMAS C-5A model was converted to a NASTRAN model. The basic substructure configurations of the FAMAS model were retained with the exception of a 360-inch-long section of the forward fuselage. This section had previously been represented by repeated couplings of a 40-inch barrel section and was converted into two completely new substructures. Further changes include geometry alterations where structural modifications had been incorporated, a switch to a Lockheed-developed semi-monocoque element to represent skin-stringer combinations, and flexibility changes where errors were detected or material or structural changes had occurred.

NASTRAN Model Geometry

The NASTRAN C-5A model has two levels of substructures. The model is divided into 27 basic substructures which are grouped into 3 sections. Section 1, the forward fuselage, contains substructures one through twelve; Section 2, the aft fuselage, contains substructures 18 through 27; and the center fuselage, Section 3, contains substructures 13 through 17 including substructure 14 which represents the entire outer wing. The reason for grouping the substructures into sections will be explained later.

The model is composed of rod, beam, shear, triangular membrane, and rigid elements all of which are standard NASTRAN elements, and the previously mentioned Lockheed-developed semi-monocoque element for skin-stringer combination representation. Rods and beams are used primarily to represent fuselage frames, longitudinal beams, wing spars and ribs, and intercostals. Shear elements represent beam webs, bulkhead webs, spar webs, and in a few instances, skin panels. Rigid elements represent extremely stiff structural members usually found in fittings. Triangular membrane elements occur both as isotropic and anisotropic elements - the anisotropic elements represent stringers and overlay isotropic elements representing the skin panels in the same location. Finally, the semi monocoque elements represent skin-stringer combinations and specify stringer size, spacing and orientation and percentage of skin effectivity.

The C-5A NASTRAN model retains one of the FAMAS model idiosyncracies - the pseudoframe. Normally, if a substructure boundary falls at a frame location, in a substructured model, the frame would appear in both substructures with half of the area represented for that frame in each substructure. In this instance, the full frame is contained in one substructure while only the skin-stringer connecting grid points appear in the adjoining substructure, creating a phantom - or pseudoframe. This method creates some problems in specifying the degrees of freedom which are coupled between substructures since, for example, the substructure containing the frame could react bending forces while the substructure containing the pseudoframe could not. It was deemed simpler to keep the FAMAS configuration, however, than to create a new frame for the pseudoframe substructure and change the appropriate properties and connectivities in the two affected substructures.

A further legacy from the FAMAS model are the half models in the center fuselage section. Since the FAMAS model was never completely coupled through from nose to tail, the existence of half models only in the center fuselage presented no problems in the FAMAS analysis and served to reduce the model size significantly. In the NASTRAN analysis the half models result in an extra step in the Phase 2 analysis. The half models must be equivalenced and mirror imaged, then coupled to each other before the coupled center fuselage section can be combined with the full model aft and forward sections.

The complete C-5A model is reacted externally in six degrees of freedom on three points in substructure 13 in the center fuselage. Since all the points lie on coupling boundaries, and since substructure 13 is a half model, the reaction points are actually located in 6 equivalenced and coupled substructures. In checking the external reaction forces against internal loads this distribution caused a problem in retrieving all the data since so many numbers were involved.

APPLIED LOADS

The C-5A NASTRAN model was analyzed with three different systems of applied loads. During the first iteration a system of loads referred to as SRS loads was applied. SRS loads are single reference station unit loads which are applied at 6 locations on the airplane. Six components of a load are applied at each location. An additional load case consists of a unit internal pressure applied to all elements within the pressure boundary of the airplane. SRS loads were, until recently, used to determine stress/load ratios for use in fracture analysis. The disadvantage to SRS loads is that answers can be considered accurate for a given load only at a point relatively far removed from the point of load application.

During the second iteration of the analysis, two design loads which had previously been applied to the FAMAS model and had also been used in actual specimen testing were applied to the C-5A NASTRAN model. The results were compared to previous answers to assess the NASTRAN model accuracy and locate possible problem areas or errors.

During the third and most important iteration of the analysis a system of loads called MRS (multiple reference station) loads were applied to the C-5A NASTRAN model. This system of loads was recently developed at Lockheed and involves both a new loading approach and a new computer program for calculating load distributions. Previous repeated loads analyses utilized a very limited definition of external (SRS) loads. Stress spectra for use in fracture analyses were generated using, at most, six load components near the analysis area of interest. This approach is adequate for simple loading conditions and in situations where all external loads are remote from the area of interest. However, in a complicated structure such as the center fuselage of an aircraft where complex load sources (aerodynamic, landing gear, cargo, etc.) affect the structure this approach may be inaccurate. Furthermore, historical repeated loads analyses were limited to six load components by load phasing constraints. This problem has been solved in the MRS system by allowing the combination of many external loads in a repeated loads system and resulting in more accurate internal loads. No new technology was required in the FEM analysis. However a much larger number of unit load conditions applied to the FEM model are required to generate stress/load ratios for all external load sources. A total of 733 separate load cases are applied during the MRS NASTRAN analysis of the C-5A model. This unusual number of load cases (at least at Lockheed) caused problems with the NASTRAN code - the limits on the number of load cases that could be applied had to be extended. Furthermore, checking the output for that many load cases for possible errors became a monumental task for the 27 substructures involved. To check external reaction forces against internal loads a special DMAP (direct matrix abstraction program) was written to sum the reaction loads contained in the various substructures for all load cases. In order to streamline the recovery of stress/load ratios by future users the output was also written to tape and then stored in a separate Relational Information Management (RIM) database for user access.

DATA MANAGEMENT

A model with 27 substructures, each of which contains from 150 to 1400 grid points, requires quite a bit of data management. Automated substructuring analysis

requires access to geometry and property data, load data, SOF (Substructure Operating File) files, output files and restart tapes. In order to simplify the bookkeeping, a separate file for geometry and property data was assigned to each substructure. Since several engineers were involved in the analysis, another file was established to contain the runstreams for all analysis stages for all substructures. This was done so that any one engineer could easily locate the appropriate information for making any NASTRAN run. A separate loads file was also established for each substructure.

SOF files presented a challenge. Because the SOF files needed to be manipulated separately we tried to keep them relatively small. This was not a problem for the first two iterations. With the initiation of the MRS iteration the problem of establishing a size which could accommodate the 733 load cases surfaced. Largely by trial and error we eventually ended up with SOF files which required 317,000 kilobytes (kb) of mass storage.

Because we wanted to take advantage of graphic display capabilities for both geometry and output such as deflections and stresses, the output for the first two iterations was stored in another set of files. Because of space limitations this was not possible for the MRS iteration.

Along with some intermediate files required for the Phase SOLVE step the total amount of computer mass storage for all the required files for the MRS iteration came to 421,000 kb! In addition, 27 restart tapes and 36 output tapes were required for the MRS analysis.

ANALYSIS FLOW

The analysis of the model followed the normal NASTRAN automated substructuring analysis with a few twists. The first step consisted of the checkout of each individual substructure. The checkout procedure included both computer program checks which search the geometry and property data for format errors as well as graphic display checks. Visual display of geometry allows checking connectivity data and locating missing or duplicate elements. Visual display of properties allows checking of property data accuracy, property trends and continuities between substructures. Possibly the most time consuming check concerns the A-Sets for the boundaries, particularly for substructures which connect to four or five other substructures. Once each substructure has been checked, the Phase 1 runs can begin.

As mentioned earlier, the model was not only substructured but divided into three primary sections. One of the reasons for this further subdivision was the allocation of SOF files. Since we wished to keep the size of the SOF files small and since NASTRAN allows a maximum of 10 physical SOF files, the SOF files used in Phase 1 were assigned to the primary sections. One set of SOF files was used for substructures in the forward fuselage, one set for substructures in the aft fuselage, and one set for substructures in the center fuselage. Because the load cases applied differed from substructure to substructure, the PG (static applied loads) matrix for each substructure in Phase 1 was written out onto a PG loads file. Beyond these changes, the Phase 1 runs were normal for an automated substructuring static analysis.

The Phase 2 runs, again, followed normal Phase 2 procedure for the substructures in Sections 1 and 2. In Section 3, the individual substructures required equivalencing and mirror imaging first, then coupling with the mirror images before they could be coupled to other substructures. Once all substructures in each Section were combined and reduced an intermediate step was taken before the SOLVE could be accomplished. All matrices for the last pseudo structure in each Section were read into an intermediate SOF file. Using this intermediate file the SOLVE was then accomplished along with the BRECOVER for the three last pseudo structures. The matrices for these pseudo structures were then copied back into their respective Section SOF files.

Phase 3 could then be accomplished. Since a different set of load cases was applied to each substructure originally, the PG matrix written out during Phase 1 was read back in during Phase 3. This was our solution to the NASTRAN logic problem which prohibits load case number incompatibility between Phases 1 and 3. Although we had a total number of applied load cases of 733, not every case was applied to every substructure during Phase 1. However, during the SOLVE operation in Phase 2, all the load cases were combined with LOAD C cards. During Phase 3, the load case number compatibility once again had to be restored and thus the Phase 1 PG matrix was read in externally. A Restart RECOVER was then performed for each individual substructure. In the case of the first two iterations the OCQ1, OES1 and OUGV1 matrices were output on a file for later graphic display. During the MRS iteration, the EST and OES1 matrices were written out to tape for storage in the stress/load ratio database.

SPECIAL PROBLEMS

The first two analysis iterations presented few special problems except for the intermediate Phase 2 steps described above. The major problems arose with the MRS analysis and its 733 load cases. As mentioned before, changes had to be made in the code to accommodate this many load cases. A small problem, but an annoying one, was the huge volume of the output. Although only an average of 50 load cases was actually recovered for each substructure, the volume of paper that this generated for the 27 substructures was enormous. Keeping all the output separated and properly bound and labeled became a chore especially since several errors detected after completed runs necessitated reruns. Our work areas soon became labyrinths made up of stacks of computer output.

A new problem surfaced when we tried to limit output size by including sets for certain substructures. We discovered a limit on the number of elements which could be included in a set and this limit had to be eliminated in the code.

When the MRS iteration began we tried to determine how much space would be required for the SOF files and found no accurate method of determining SOF file sizes. It became a matter of trial and error to find the required size and also brought to light the fact that once a size for a SOF file has been used, the physical file cannot be reduced in size without creating havoc.

Our most aggravating problem, however, was the space requirement that this model had for the MRS iteration. Our NASTRAN analyses are run using a UNIVAC 1100 main frame computer. Our FEM group is allocated approximately 1,000,000 kb mass storage.

As mentioned above, the model required 412,000 kb of storage space. Moreover, several substructures required 120,000 kb HICORE allocation to run which severely cramped the space available to other users of the system. The amount of mass storage used also created space binds for other models concurrently in the works. This space bind caused a very close monitoring of file sizes all during the analysis.

CONCLUDING REMARKS

The NASTRAN automated substructuring analysis of the C-5A was successfully completed for three different loading systems. Correlation of stresses between the original FAMAS model and the converted NASTRAN model was very good where direct comparison was possible. The NASTRAN analysis resulted in better correlation with actual test data and provided better and more complete results. For example, stresses in triangular elements are now available and stringer stresses are output directly - no complicated delumping process is required. Grid point loads for use as load input for detail models are now available and the NASTRAN model now reflects all major structural changes incorporated since the FAMAS analysis was completed.

The analysis process in its third iteration uncovered several problems in the NASTRAN code of which anyone attempting a substructured model of this scale should be aware. For a model requiring a large number of load cases, the code must be altered to accommodate the load cases. If output for a large model is to be limited with a set definition card, the set number limitation in the NASTRAN code must first be removed.

A further consideration in constructing very large models is the availability of mass storage space. Space requirements dictate that a very large model must be analyzed using a large main frame computer. In addition, a good data management system is essential for a successful analysis of a large substructured model.

The system of grouping the substructures of a large model into larger sections is very efficient since it allows several engineers to work on a single model independently of each other while totally maintaining the integrity of the model. Finally, mechanizing the modeling process, from geometry generation to geometry and property plots to force summation to deflection, load and stress plots, is an invaluable asset to completing an analysis of a large substructured model with many applied load cases in an efficient and timely manner.

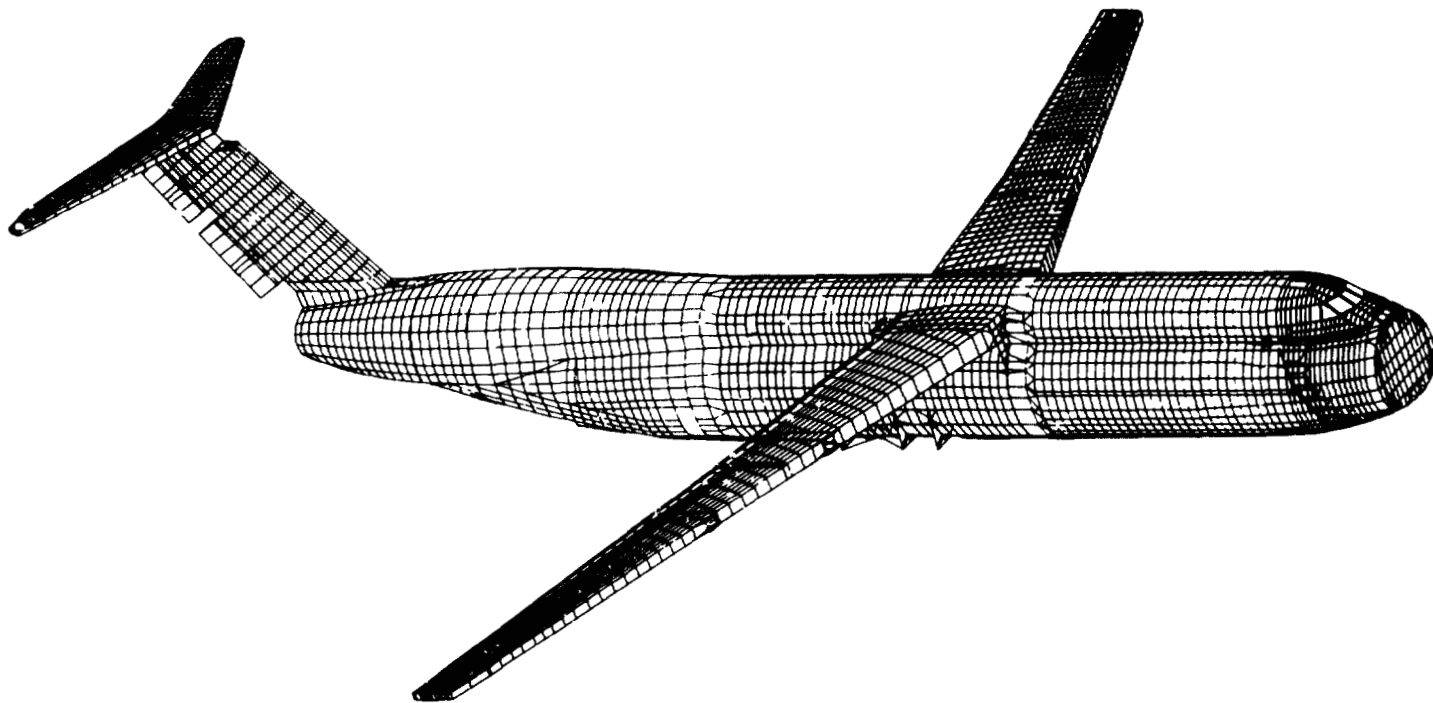
TABLE 1 - C-5A MODEL STATISTICS

Substruct.	Grid Points	Elements	DOF	A-set G.P.	A-set DOF
01	352	1160	1070	63	173
02	627	2033	2065	145	389
03	597	2093	1909	115	304
04	152	658	595	8	18
05	557	2100	1360	21	44
06	647	2205	1747	41	97
07	468	1330	1408	99	263
08	362	957	1042	117	337
09	292	750	794	136	399
10	296	838	721	135	398
11	738	1808	1573	128	397
12	578	1369	1296	112	342
13*	399	1229	982	114	364
14*	1380	4216	4184	32	96
15*	497	1382	1423	160	499
16*	562	1590	1504	147	467
17*	143	368	337	65	217
18	232	574	689	107	336
19	416	1085	1178	101	290
20	479	1339	1283	97	292
21	326	975	759	107	273
22	247	610	779	74	210
23	301	797	929	63	175
24	588	1790	2362	52	148
25	600	1897	1581	26	78
26	401	1271	1286	41	59
27	243	784	773	18	20

12,580 37,208 35,626
 (15,561)** (45,993)** (44,056)**

* Half Model Only

**Full Model



ORIGINAL PAGE IS
OF POOR QUALITY

FIGURE 1: COMPOSITE PLOT OF SUBSTRUCTURED C-5A MODEL

ORIGINAL PAGE IS
OF POOR QUALITY

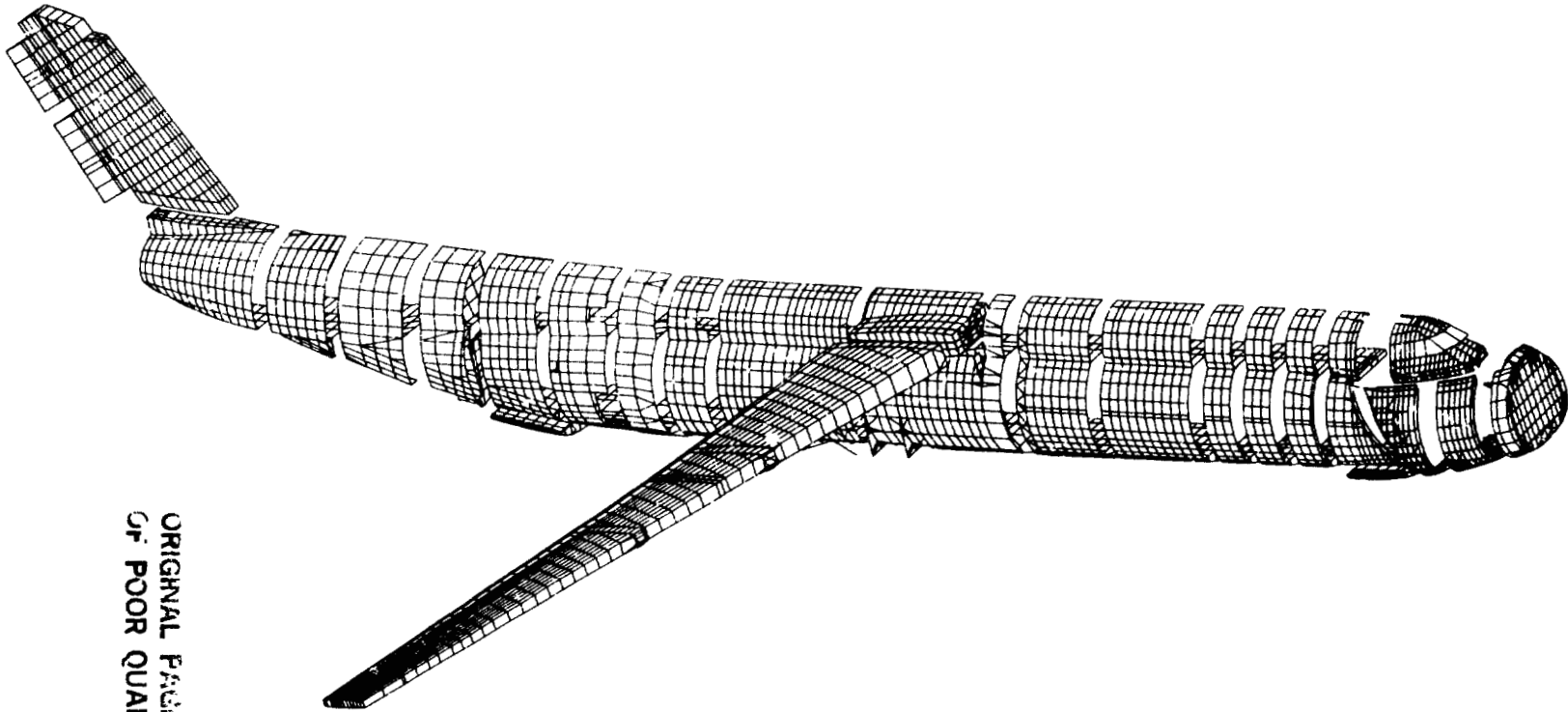


FIGURE 2: EXPLODED VIEW OF SUBSTRUCTURED C-5A MODEL, RIGHT SIDE

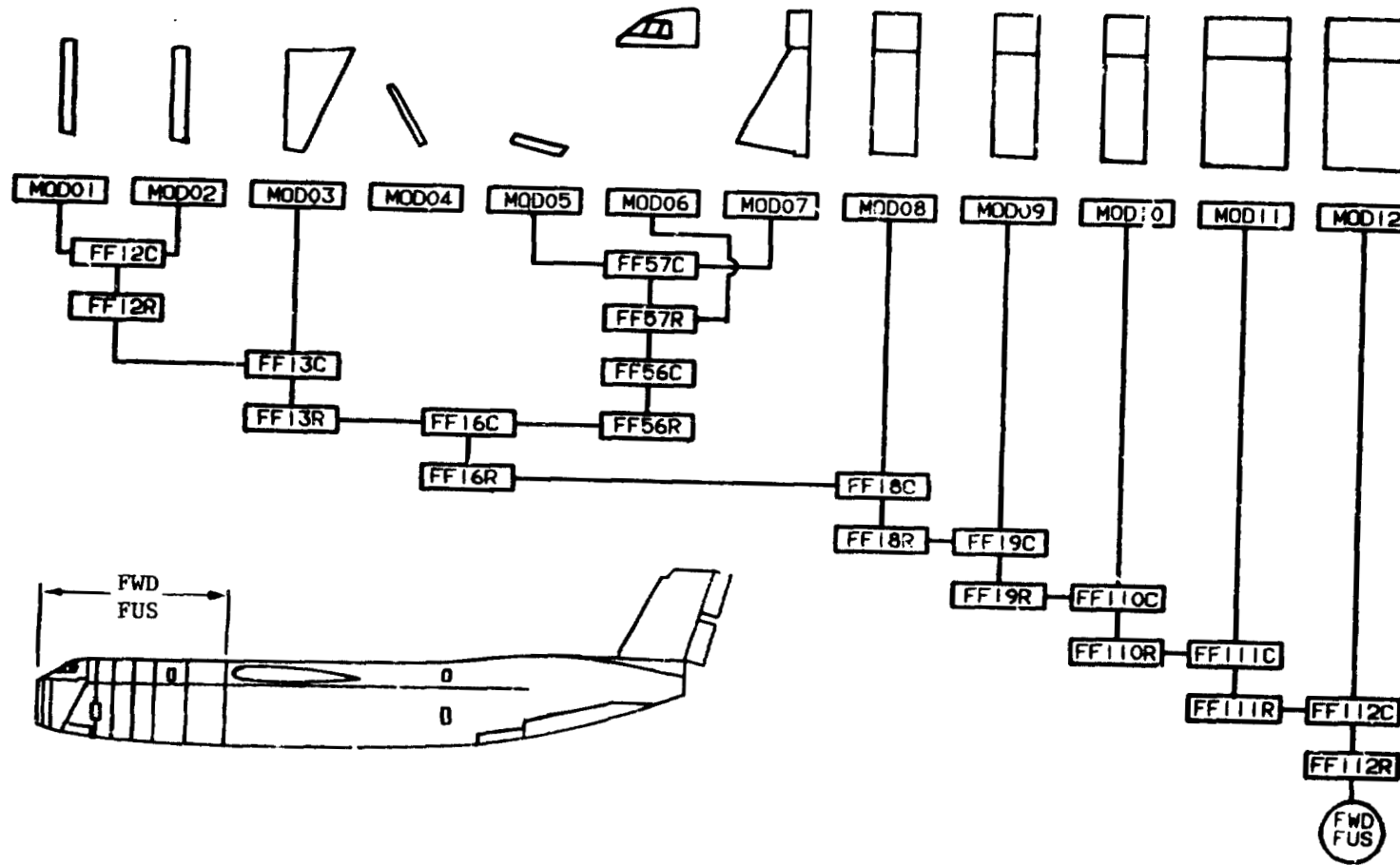


FIGURE 3: FORWARD FUSELAGE COUPLING TREE

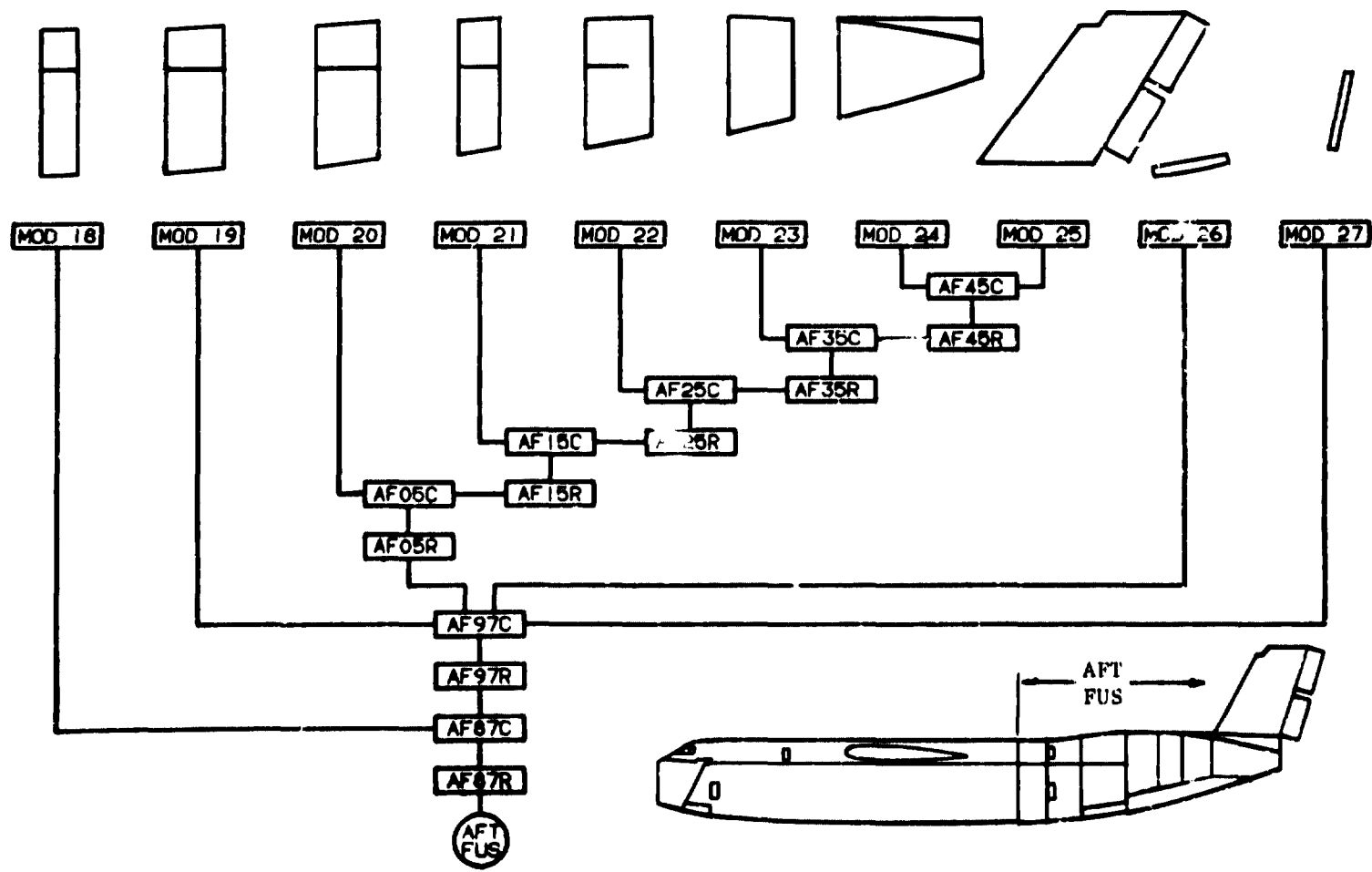
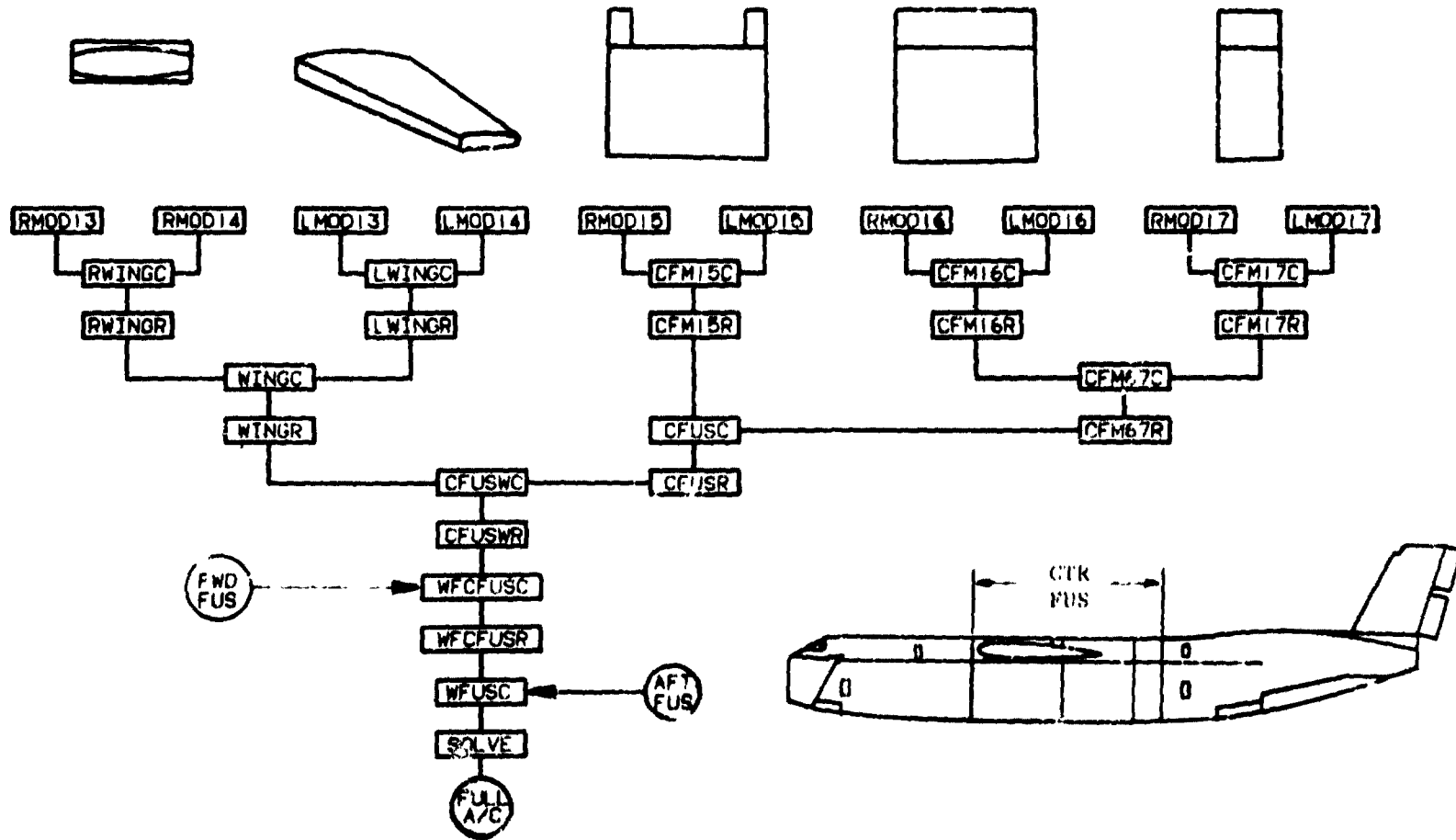


FIGURE 4: AFT FUSELAGE COUPLING TREE



ORIGINAL PAGE IS
OF POOR QUALITY

FIGURE 5: CENTER FUSELAGE/AIRCRAFT COUPLING TREE

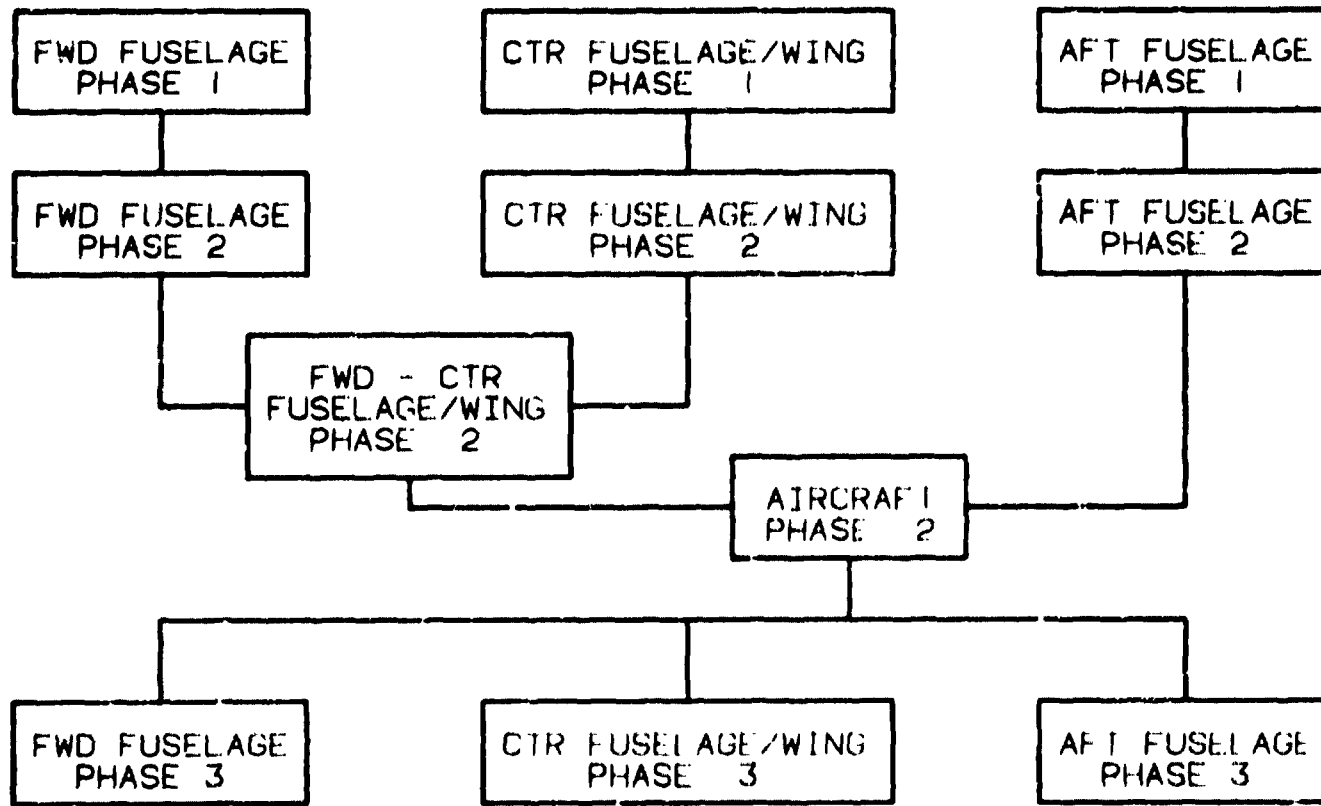


FIGURE 6: ANALYSIS FLOW FOR SUBSTRUCTURED C-5A MODEL

N85-25886

ABSTRACT

USING NASTRAN TO MODEL MISSILE INERTIA LOADS

by

Ron Marvin
Craig Porter

Naval Weapons Center
China Lake, California

An important use of NASTRAN at the Naval Weapons Center is in the area of structural loads analysis on weapon systems carried aboard aircraft. Specifically, the center uses the program to predict bending moments and shears in missile bodies, when subjected to aircraft induced accelerations. The missile, launcher and aircraft wing are idealized, using rod and beam type elements for solution economy. Using the inertia relief capability of NASTRAN, the model is subjected to various acceleration combinations. Difficulty modeling the launcher sway braces and hooks has occurred. These transmit compression only or tension only type forces respectively. A simple, but time consuming, iterative process has been developed to overcome this modeling difficulty. A proposed code modification would help model compression or tension only contact type problems.

N85-25887

EXPERIENCE WITH FREE BODIES

T.G. BUTLER

BUTLER ANALYSES

It is encouraging to see that analysis and test activities are moving away from competitive postures and toward mutually beneficial cooperation. When some structure is examined for its vibration characteristics by both analysis and test, and the results are to be compared; the matching of boundary conditions becomes a problem. Free bodies can be simulated easily by both disciplines, so it is often the condition to be prescribed by a project. In order for a free body analysis to be valid it must exhibit six clean rigid body (zero frequency) modes. Free body analyses are some of the easiest kinds of analysis to perform if one does everything right. They can be real headaches if one goofs too much. This paper deals with some of the problems that confront an analyst in modeling, if he is to satisfy rigid body conditions; and with some remedies for these problems. It also deals with the problems of detecting these culprits at various levels within the analysis. The paper concludes with the publication of a new method within NASTRAN for checking the model for defects very early in the analysis without requiring the analyst to bear the expense of an eigenvalue analysis before discovering these defects.

MECHANISMS-SPC

Single point constraints (SPC's), multipoint constraints (MPC's), and springs to ground are candidates for interfering with free body motion. The ways that they interfere are obvious in some cases, but for others are fairly subtle. These topics will be elaborated in order; first SPC's. There is a need to constrain the rotational degree of freedom, of grid points to which only plates connect, about the normal to the plate. NASTRAN reports a singularity for any failure to apply such constraints. These constraints are usually invoked on the GRID card and, after initial debugging, usually end up with the necessary --and only-- the necessary rotational constraints applied. Overconstraints inevitably arise when changes to a design occur and modifications are made to its analytical model. Any new constraints always get added, but many of the old constraints, which now need to be purged, are often overlooked, resulting in overconstraints. Thus when the analysis for rigid body eigenvectors is run, some of the six rigid body modes don't appear and elastic modes erupt in their place. The only remedy for points overconstrained by SPC's is to ferret them out. Various ways to detect them will be explored later.

Another more subtle case arises when the normal to a plate is not aligned with one of the displacement coordinate axes. NASTRAN's "GPSP" module is satisfied if a rotational freedom about any one of the coordinate directions is constrained, just so the constrained coordinate provides a component in the direction of the normal to the plate. Satisfying GPSP is not enough for purposes of free motion. There remains a

connection to ground in the constrained rotational degree of freedom, such that a component of elastic action still feeds to ground, so it sabotages the rigid body mode. See figure 1.

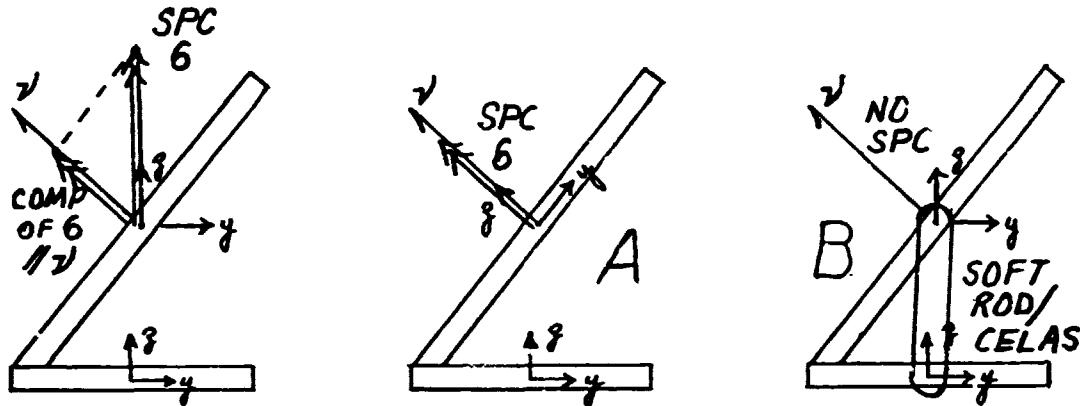


Figure 1

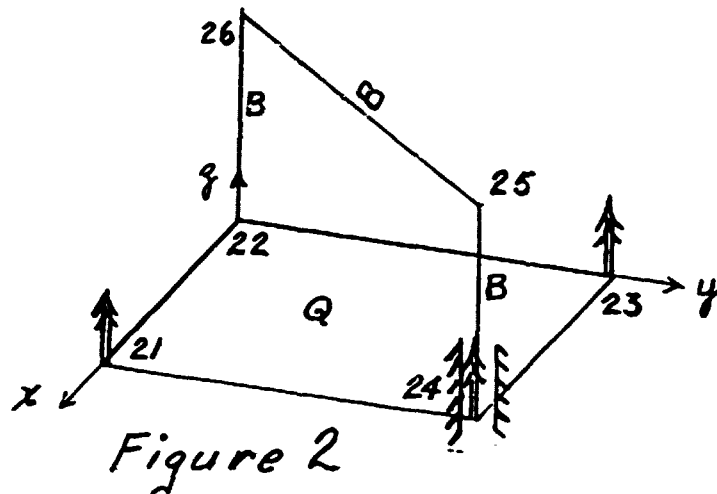
There are at least 3 ways to remedy this intolerable situation, and still satisfy GPSP.

- A. Change the displacement coordinate system at the offending grid point so that one coordinate axis is aligned with the normal; then constrain that rotational dof.
- B. Opt not to constrain the normal rotation, but provide instead an alternate elastic path many orders of magnitude softer than the neighboring elements. Two simple devices can be employed:
 - B1. Use a CONROD between the point in question and some neighbor, or
 - B2. Use a CELAS2 between the point in question and (a) some neighbor or (b) to ground.

The reason that the grounded elastic scalar works is that the amount of force developed in a soft scalar, from its connection to ground is so small that the rigid body motion is effectively not interfered with. The value of the stiffness should be soft enough that it does not cause a disruption to the elastic behavior, but not so small that it causes matrix ill-conditioning.

There is a very special set of conditions in which this analyst got trapped. The situation involves a BAR element, aligned with a coordinate axis, making a perpendicular connection with a plate. See figure 2. The BAR rides in a sleeve bearing at the connection to the plate which makes it impossible for the BAR to transmit torsion to the GP. One sets a pin flag in element dof 4 of the BAR. Now comes the trap. Since the plate doesn't involve moments about the normal and since the moment from the BAR about that same axis is pinned, the situation seems ripe for producing a singularity. Constraining the rotational dof about the normal to the plate seems logical to avoid a singularity. This situation was a part of a much larger model which failed to produce a rigid body mode in rotation about the vertical when the constraint was

applied, but did exhibit the rigid body mode when the constraint was removed. It forces one to rethink the situation. What's wrong? What does the grid point see? What does the constraint do? What is happening internally in the BAR? A small pilot problem, depicted in figure 2, was run to test the condition.



The grid point sees elastic paths in 5 dof coming from the plates. But, does it also see only 5 elastic paths coming from the BAR? Yes. This is confirmed by glancing at the stiffness matrix of the sample problem above, which was modeled as intended, for dof 6 of GP 24. This is column 24 of KGG. Note: col 24 of the matrix is null.

COLUMN	23	ROWS	3 THRU	29	(GP 24 DOF 5)
5.44896E+00	-4.84359E+03	1.60435E+03	0.00000E+00	0.00000E+00	0.00000E+00
0.00000E+00	1.20968E+03	1.33302E+04	4.45448E+03	0.00000E+00	0.00000E+00
0.00000E+00	0.00000E+00	-7.76474E+03	4.84359E+03	2.10148E+04	2.10148E+04
0.00000E+00	6.00000E+05	0.00000E+00	6.54961E+03	-1.17895E+03	-1.17895E+03
4.03848E+06	0.00000E+00	-6.00000E+05	0.00000E+00	0.00000E+00	0.00000E+00
0.00000E+00	2.00000E+06				

COLUMNS	24 THRU	24 ARE NULL.	(GP 24 DOF 6)	(No contributions) (from plate or) (bar)
COLUMN	25	ROWS	19 THRU	36 (GP 25 DOF 1)
-1.20000E+05	0.00000E+00	0.00000E+00	0.00000E+00	-6.00000E+05
0.00000E+00	4.94767E+05	3.32340E+05	0.00000E+00	0.00000E+00
-6.00000E+05	2.12132E+05	-3.74767E+05	-3.32340E+05	0.00000E+00
0.00000E+00	0.00000E+00	2.12132E+05		

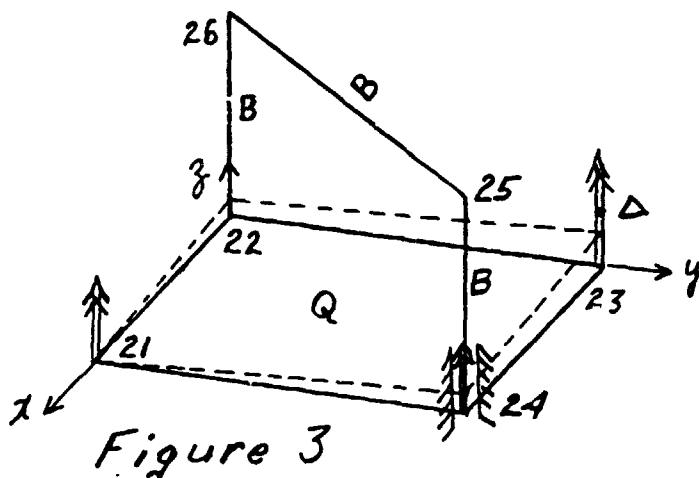
For a similar orientation, but with a full 6 dof connection, the stiffness matrix shows that for column 12 corresponding to dof 6 @ GP 22 the matrix is non-null.

COLUMN	11	ROWS	3 THRU	35	(GP 22 DOF 5)
7.76474E+03	4.84359E+03	2.10148E+04	0.00000E+00	6.00000E+05	
0.00000E+00	-6.54961E+03	-1.17895E+03	4.03848E+06	0.00000E+00	
0.00000E+00	0.00000E+00	-5.44896E+00	-4.84359E+03	1.60435E+03	
0.00000E+00	0.00000E+00	0.00000E+00	-1.20968E+03	1.33302E+04	
4.45448E+03	0.00000E+00	0.00000E+00	0.00000E+00	0.00000E+00	
0.00000E+00	0.00000E+00	0.00000E+00	-6.00000E+05	0.00000E+00	
0.00000E+00	0.00000E+00	2.00000E+06			

COLUMN	12	ROWS	12 THRU	36	(GP 22 DOF 6) == Non null.
3.75940E+05	0.00000E+00	0.00000E+00	0.00000E+00	0.00000E+00	
0.00000E+00	0.00000E+00	0.00000E+00	0.00000E+00	0.00000E+00	
0.00000E+00	0.00000E+00	0.00000E+00	0.00000E+00	0.00000E+00	
0.00000E+00	0.00000E+00	0.00000E+00	0.00000E+00	0.00000E+00	
0.00000E+00	0.00000E+00	0.00000E+00	0.00000E+00	-3.75940E+05	

COLUMN	13	ROWS	2 THRU	20	(GP 23 DOF 1)
4.66418E+05	0.00000E+00	0.00000E+00	0.00000E+00	0.00000E+00	
-4.69925E+05	-3.50688E+03	0.00000E+00	0.00000E+00	0.00000E+00	
0.00000E+00	1.87269E+06	-4.66418E+05	0.00000E+00	0.00000E+00	
0.00000E+00	0.00000E+00	-1.40276E+06	3.50688E+03		

If this pilot model is run without dof 6 of GP 24 being constrained, it aborts in the decomposition of K00. This shows that there is a singularity and that a constraint in dof 6 is needed. The original suspicion is confirmed; the model is run through eigenvalues with the constraint in dof 6 of GP 24 in place. All 6 rigid body modes appear so one can say that this is a model of correct behavior. The question still remains, what happened to the large model to cause the rigid body modes to be interfered with? To investigate this problem, modifications were made to the pilot model. If there is a mistake in the model such that the z coordinate of one of its points, say GP 23 is above the plane of the other three points by a small amount, say $\Delta = .08''$, the mean plane of the quad is not perpendicular to the z-axis. This anomaly was run with and without the constraint on dof 6 of GP 24 in place. Figure 3 shows the position of the mean quad in dotted lines.



The results of the three runs are tabulated.

MODEL	EIGENVALUE RESULTS	SPCF COMPARISONS						
		MODE 1	MODE 2	MODE 3	MODE 4	MODE 5	MODE 6	MODE 7
AS INTENDED	6 FN = 0	-----	NO ---	SPCF ---	IN ---	ANY ---	MODE ---	-----
23(6) WARPED	4 FN = 0	21(6)=0	==	==	==	==	==	==
24(6) SPC	#5 = .02	23(6)=0	==	==	==	==	==	==
	#6 = .14	24(6)	=2.-6	=3.-6	=3.-6	=.028	=7.25	=21.39
	#7 = 106.	=.004						
23(6) WARPED	4 FN = 0	21(6)=0	==	==	==	==	==	==
24(6) NO-SPC	#5 = .014	23(6)=0	==	==	==	==	==	==
	#6 = .036	24(6)=0	==	==	==	==	==	==
	#7 = 2.67							

FREQUENCIES OF NEXT SIX ELASTIC MODES		
AS INTENDED	23(6) WARPED & 24(6) SPC	23(6) WARPED & 24(6) NOT SPC
1.068969E+02	1.064876E+02	1.066318E+02
1.892820E+02	1.893139E+02	1.893587E+02
2.989922E+02	2.866197E+02	3.050661E+02
3.107471E+02	3.076186E+02	3.719919E+02
3.214566E+02	6.107463E+02	2.653362E+03
3.018417E+03	3.073824E+03	3.209373E+03

The constraints @ GP's 21, 23, & 24 provide interference with components of the elastic action coming from the plate and sabotage the rigid body mode. Note that the two first elastic modes are almost independent of the mistake in modeling, but after that differences separate their behavior. This turns out to be a particular case of the problem in figure 1 above with the canted plate, except that it appears to shift the blame to the BAR instead of pointing to the mislocated grid point. The BAR acted as a decoy. This is a classic case of the analyst swearing that "he knows that everything is correct, but the computer..", or "but NASTRAN....." is giving these crazy results." In the data that follows it is remarkable that a small glitch can cause g-r-e-a-t disruption. We can call this case the "out-of-plane" type of SPC difficulty.

MECHANISMS-MPC

Multipoint constraints (MPC's) are less conspicuous offenders. One's intuition seems comforted by the idea that if two dof's are required to move together, this is a kind of a rigid body motion and should be compatible with the execution of general rigid motion. The answer is sometimes yes and sometimes no. An example, figure 4, that is easy to visualize, is a pair of points that are constrained so that motion transverse to the line between the points is always to be the same.

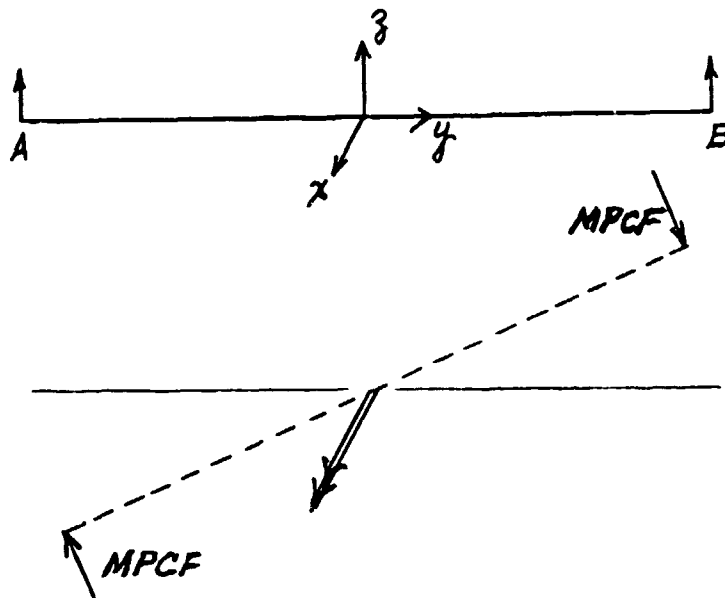


Figure 4

NASTRAN is a faithful servant in carrying out such an assignment. If the analyst says that these two points shall always move up and down together no matter what, NASTRAN will see to it. Thus, any attempt by the body to perform a rotation about an axis perpendicular to the paper is sternly opposed. External forces are set up to create couples to balance the elastic moments produced by neighboring elements tending to rotate the line between A & B. These are called MPC forces, and they interfere with free rigid body movement. In this case the MPC would interfere with the rotation about X. Does this rule out the use of MPC's? Not at all. Does this mean that all rigid elements are off limits? Not at all. If the analyst refers to eqn (56) in section 3.5.6.3 of the theoretical manual, he will see that the formulation of the rigid elements includes rotations so that the relative distance from A to B is maintained invariant for all small displacements, and causes no interference with rigid body motion. If the analyst writes his own MPC'S for two points, he must also ensure that there is no resistance to rigid body motion.

$$\begin{Bmatrix} u_{A1} \\ u_{A2} \\ u_{A3} \\ u_{A4} \\ u_{A5} \\ u_{A6} \end{Bmatrix} = \begin{bmatrix} 1 & 0 & 0 & 0 & (z_B - z_A) & -(y_B - y_A) \\ 0 & 1 & 0 & -(z_B - z_A) & 0 & (x_B - x_A) \\ 0 & 0 & 1 & (y_B - y_A) & -(x_B - x_A) & 0 \\ 0 & 0 & 0 & 1 & 0 & 0 \\ 0 & 0 & 0 & 0 & 1 & 0 \\ 0 & 0 & 0 & 0 & 0 & 1 \end{bmatrix} \begin{Bmatrix} u_{B1} \\ u_{B2} \\ u_{B3} \\ u_{B4} \\ u_{B5} \\ u_{B6} \end{Bmatrix} \quad (56)$$

MECHANISMS-SPRINGS

Non-small scalar spring elements are also less conspicuous agents for opposing free body motion if they are connected to ground. Since any grounding opposes free body motion, forces develop in the elements when displacements are imposed in the freedoms which are contained in the scalar springs. These scalar springs to ground must be removed, because they operate contrary to a model of a free body. The purpose for the springs being there in the first place has to be re-examined.

DETECTION

If a point is overconstrained with GRID SPC's that were unintended, NASTRAN doesn't give a fatal message. It assumes that the analyst knows what he is doing and dutifully puts the SPC's into operation. The unwanted behavior is ultimately seen in the eigenvalue results. Even these could be overlooked, if the analyst bravely presumes nothing would go wrong and specifies a frequency range over the elastic spectrum of interest only without including the zero part of the spectrum. This would be foolhardy. When doing a free body analysis it is prudent to check to see that the body is truly free by ensuring that all rigid body modes are present. As a minimum the analyst should (1) use 0.0 as the specification for the lower frequency bound on the EIGR card so that he will get a report on how many modes were zero frequency modes. (2) The EIGR request for eigenvectors should embrace 6 in addition to the expected number in the elastic range in order to recover all calculated rigid body mode shapes. If fewer than 6 natural frequencies are zero, there is something in the model opposing some free motion. Inspecting the eigenvectors (both plotted and printed) for the missing actions will give a hint as to the kind of unintended constraints that are inhibiting the free movement. In addition to these two minimum requirements the analyst is advised to request (3) SPCFORCES = ALL and (4) MPCFORCES = ALL. He will not get page after page of zeroes for having specified all, he will get a report of only those points where single point constraints are applied via an elastic path to ground in each mode. SPCF should be zero for every rigid body mode and for every non-zero frequency mode. If some of the 6 rigid body modes are not present, the low frequency modes should be examined for single point constraint forces; these modes could be candidates to be repaired and for converting into rigid body modes. The associated dof's of these forces will give evidence as to the place where the free motion is being interfered with. In the case of multi-point constraints, they should be able to act without developing opposing forces during rigid body deformation. So, by calling for MPCFORCES = ALL, there will be a report at only those points where forces arise in attempting to perform one of the six rigid body motions. If MPCFORCES are not zero, for any of the first six modes, this argues for reformulating the MPC so as to be free of opposition to rigid body motion.

The aforementioned four measures for detecting errors in modeling of free bodies are expensive and time consuming in that they are displayed only after an eigenvalue analysis has been performed. They should always be used, but not as the primary means of checking. There are ways, well upstream of the DPD module, to discover offenders against free motion. One way is to run through the GPWG (grid point weight generator) and exit in order to find the center of gravity (C.G.). Apply SPC's in the 3 displacement dof's at the C.G. and do static analyses with three subcases. The loading in each subcase is a one-g "GRAV" load in one of the 3 coordinate directions. Call for SPCF = ALL and MPCF = ALL, and call for displacements on opposite side of the C.G. Nonzero SPCF and MPCF at other than the C.G. will give direct evidence as to offenders. Displacement outputs will exhibit any tendency to rotate about the C.G. due to externals other than inertia effects. This is a much cheaper and much quicker way than running an eigenvalue analysis.

A useful but not too specific check is to look for a report of the epsilon sub E (ϵ_E) value that is reported immediately after condensation to the A-set. No report is issued if the residue is small. When the energy check computes to a value that is not small, NASTRAN reports its value. The message appears after the user information message 3023 about the value of parameters for the decomposition of K00.

There is a rigid body check in NASTRAN based on use of the R-set and deriving a rigid body transformation matrix based on the stiffness matrix.

$$DM = (-) [K_{11}]^{-1} [K_{1r}]$$

and calculates a net error check $\epsilon = \frac{\|X\|}{\|K_{rr}\|}$

which does not pinpoint trouble. Matrix $[X]$ is not output and would be difficult to use for locating trouble. This has useful applications especially when it is important to prescribe the rigid body coordinate directions. It is a good idea to get clean rigid body modes without the R-set first; then introduce SUPPORT cards in a final run.

If a static run precedes the eigenvalue analysis, a useful check occurs in module SSG3 if the analyst sets the parameter IRES. The residual matrix RUL' is output. It gives diagnostics for every dof in the L-set.

An even quicker and cheaper approach to diagnosing is to impose a rigid body test to the "K" (stiffness) matrix immediately after it has been generated. This method was called to the author's attention by Dr. Cheng Lin of the Aerospace Corp. By definition, a rigid body transformation "D" is one that is stress free. This implies that relative displacements are zero. If relative displacements are zero then the work computed by the product of stiffness into rigid body displacement

(K x D) is zero. If it is other than zero, local impediments to free body motion will cause local perturbations in displacements which in turn result in non-zero work. The beauty of this diagnostic tool is that it operates at the level of G-set so that its non-zero terms are direct locators. One needs to be sure to run with DIAG 21 & 22 turned on in order to correlate the location from internal sequence to external sequence. The method passed on by Cheng Lin needed implementing in NASTRAN. The rigid body transformation matrix "DM" in the normal NASTRAN static solution stream comes after the stiffness matrix is decomposed; i.e. $DM = (-)[K_{LL}]^{-1} \times [K_{LR}]$. The use of the "DM" matrix from this source is like sending the fox to guard the chicken coop. What is needed is a "D" matrix based solely on geometric relations rather than stiffness relations. New modules dealing with seismic analysis were delivered to COSMIC by the author during 1984. One of these named "RBTM" produces a "D" matrix based solely on geometry called "HAICH".

The output 'HAICH' from the RBTM module is the item around which a DMAP ALTER is written. The DMAP ALTER that follows operates under the conditional jumps associated with the three succeeding matrix partitions once the G-sized "K" and "D" matrices are generated. It calls for running a K x D check at the G-level, the N-level, the F-level and the A-level. The check on the G-level should catch any overconstrained GRID SPC's and grounded scalars. The check on the N-level should catch any improper MPC's. The check on the F-level should catch any GRID and general SPC's. The check on the A-level should provide a net check over all levels. The sequence in which the non-zero values appear in any of the partitioned products will tend to isolate what kind of constraint is causing interference. It is advisable to call for DIAG 21 & 22 so as to locate the external dof where non-zero terms in the KD product appear in the partitions for N, F, and A. Experience on the VAX computer has shown that all values in the KD product should be $< 10^{-8}$ to ensure no impediment to free motion. Whenever this criterion is met, all six frequencies of the rigid body modes compute to values $< 10^{-4}$. The ALTER packet for RF 3 of the APR 84 release of NASTRAN is included below. Note the module encircled. RBTM must be obtained from COSMIC to implement the DMAP packet.

```

ALTER 41
  (RBTM) BGPDT,CSTM,EQEXIN, ,USET/HAICH, ,HIRY6, /500/+2/*DIRECT* $
  MPYAD KGG,HAICH, /BALANCE/O/+1/O/O $ FOR STATIC CHECK
  MATPRN BALANCE,,,,// $ CHECK G-SIZE
ALTER 53
  VEC USET/NVEC/*G*/*N*/*COMP* $
  PARTN HAICH,,NVEC/NRIGID,,,/+1/O $
  MPYAD KNN,NRIGID, /NBALNC/O/+1/O/O $
  MATPRN NBALNC,,,,// $ CHECK N-SIZE
ALTER 57
  VEC USET/FVEC/*G*/*F*/*COMP* $
  PARTN HAICH,,FVEC/NRIGID,,,/+1/O $
  MPYAD KFF,FRIGID, /FBALNC/O/+1/O/O $
  MATPRN FBALNC,,,,// $ CHECK F-SIZE
ALTER 70

```

```

VEC      USET/AVEC/*G*/*A*/*COMP* $
PARTN    HAICH,,AVEC/ARIGID,,,/1/0 $
MPYAD     KAA,ARIGID,/ABALNC/0/+1/0/0 $
MATPRN    ABALNC,,,// $ CHECK A-SIZE
ENDALTER

```

The reason that it is useful to run a counter check on the A-sized matrices is two-fold. First, the effects on the "K" matrix of removing overconstraints and non-rigid constraints is reflected. It acts as a double check on the two previous partitions. Secondly, the A-sized matrices are passed to systems analysts who combine components of several structures into a comprehensive analysis. It serves as a public certification that the transmitted matrices truly satisfy rigid body requirements so that combined matrices can be free of cross-product terms between structures.

The KD diagnostic was applied to the 3 cases of the pilot model. Their results are tabulated.

MODEL	LARGEST VALUE OF			
	KDG	KDN	KDF	KDA
AS INTENDED	1.4-10		1.4-10	3.7-10
23(6) WARPED 24(6) SPC	1313.		3275.	199.0
23(6) WARPED 24(6) NO-SPC	1313.		2659.	88.0

In cases of high condensation the KDA results can be many orders higher in magnitude than KDG, KDN, or KDF, because, depending on the nature of the error and the nature of the condensation, the errors can be swept together and intensified. The advantages of the KD check are (A) that one can checkpoint and exit after each of the G, N, F, and A partitions then proceed economically without high investment in computer time; and (B) the trouble is located and cleared up well before entering eigenvalue analysis.

SUMMARY

This paper has come to the following conclusions that deal with problems in analysing free bodies.

1. Mechanisms that interfere with rigid body motion are:
 - Single point constraints (SPC'S)
 - A. Overconstrained, B. Canted, C. Out-of-plane
 - Multi-point constraints (MPC'S)
 - CELAS'S that are grounded.

2. Remedies for recovering rigid body motion are:
 - Eliminate SPC'S from an elastic path
 - Formulate MPC's so as to generate pure rigid body motion
 - Eliminate grounded scalars.

3. Detection of interference to rigid body motion from any of:
 - The appearance of a non-zero frequency for any of the first six modes.
 - Deformation that departs from rigid body motion in the candidate low frequency mode shapes.
 - Non-zero SPCFORCES for any mode.
 - Non-zero MPCFORCES for any of the first six modes
 - Non-zero SPCFORCES outside of the C.G. under static acceleration
 - Non-zero MPCFORCES outside of the C.G. under static acceleration
 - Epsilon elastic L-R rigid body check
 - Existence of an Epsilon sub E report following decomposition of K00 for condensation.
 - Non-zero values for the KD products in partitions G thru A.

It is recommended that the ALTER packet for the KD product be made standard practice when performing free body eigenvalue analyses. It is simple, effective, and the least expensive of all the checks that can be applied. Taking an exit after each partition of the four KD checks until each has a clean bill of health would prevent wasteful and costly condensations and eigenvalue analyses of defective models. When his model has passed the KD check, an analyst can have high expectations of recovering 6 clean rigid body modes from the eigenvalue analysis.

Even though the KD check was designed as a tool for diagnosing a model for free eigenvalue analysis, it can serve any other type of analysis if there is concern for overconstraints.

85-25888

NASTRAN ANALYSIS COMPARISON TO SHOCK TUBE
TESTS USED TO SIMULATE NUCLEAR OVERPRESSURES

Lt T. K. Wheelless
Nuclear Survivability Group
Analysis Support Branch
ASD/ENSSA
Wright-Patterson AFB, OH 45433

SUMMARY

This report presents a study of the effectiveness of the NASTRAN computer code for predicting structural response to nuclear blast overpressures. NASTRAN's effectiveness is determined by comparing results against shock tube tests used to simulate nuclear overpressures. Seven panels of various configurations are compared in this study. Panel deflections are the criteria used to measure NASTRAN's effectiveness. This study is a result of needed improvements in the survivability/vulnerability analyses capabilities of weapon systems subjected to nuclear blast.

INTRODUCTION

The objective of this project was to research NASTRAN's effectiveness in analyzing nuclear blast overpressure effects on panels as simulated by shock tube tests. Ultimately, this determines NASTRAN's effectiveness in predicting safe panel response to nuclear blast overpressure effects for survivability/vulnerability analysis. Accomplishment of this objective was achieved by comparing NASTRAN data to experimental shock tube test data which the Defense Nuclear Agency (DNA) collected with the Boeing Military Airplane Company under contract DNA-001-76-C-0084 and published in DNA report DNA-4278F, Volumes 1 through 4 (hereinafter addressed as reference 1). Shock tube tests are an accepted method for simulating the effects of nuclear blast overpressures. Therefore, comparing NASTRAN data to shock tube test data is an effective method for validating NASTRAN as an overpressure analysis technique.

NASTRAN is a finite element structural analysis computer code that is universally accepted in the structural analysis community. The version of NASTRAN used in the analysis for this report is COSMIC, a linear analysis valid only for predicting panel response to the yield point. Experimental data used for comparison with NASTRAN came from shock tube tests performed

upon seven panel configurations. These configurations varied in thickness, edge support constraints, magnitudes of subjected overpressures, geometry, and materials (see Table 2 and Figures 13 through 15). Magnitude of first deflection was the criterion used to measure NASTRAN'S effectiveness. Stress was not used as a criterion because deflection data in reference one is of more consistent quality. Deflection and stress exhibit a linear relationship in a material's elastic range. Therefore, deflection is a valid measure of NASTRAN's effectiveness for predicting sure safe panel response. This is discussed in further detail in the Discussion.

Shock tube test are performed by generating a shock wave that propagates down a tube and strikes a specimen. Experimental data used for comparison in this project was performed at Sandia Corporation's THUNDERPIPE shock tube in Albuquerque, New Mexico. The THUNDERPIPE shock tube generates a shock wave by primacord explosives. Figure 1 is taken from DNA report DNA-4278F and illustrates the dimensions of the Thunderpipe Shock Tube. The reader should realize that this is a relatively large test facility.

SHOCK TUBE TEST DATA

Researching NASTRAN's effectiveness for reproducing structural responses observed in shock tube tests required development of the data interpretation methodology introduced in this section. This development is divided into the two subsections: Data Interpretation and Error Effects. Large experimental data fluctuations required development of a data interpretation methodology. This methodology provides a consistent method of interpreting the pressure time history data reported in reference 1. The interpreted data is input into the NASTRAN model built to simulate the tested structure. Error Effects is a study of the effects upon NASTRAN analysis if data contains an inherent interpretational error.

Data Interpretation

Validating any numerical analysis technique requires accurate and consistent methods for reading experimental data used as analytical input data. The following is a methodology developed for reading experimental data of pressure time histories produced in the THUNDERPIPE shock tube. Ideal overpressure curves for reflected pressure time histories are the guidelines for data interpretations.

The reference used for ideal blast waves is: The Effects of Nuclear Weapons, compiled and edited by Samuel Glasstone and Phillip J. Dolan, 3rd edition, published by the United States Department of Defense and the Energy Research and Development Administration (hereinafter addressed as reference 2). Ideal curves for blast waves seldom correlate exactly to experimental shock tube data. Thus, it is emphasized that ideal curves are used only as guidelines. The methodology developed pertains to ideal curves for surface blast waves that strike normal to flat and curved panels. Figure 2 and Definitions of Terms will enhance the reader's understanding of the methodology.

Reflected pressure spikes are the most important consideration when interpreting pressure time history data. Spike peaks and widths are dependent upon post-reflected peaks. Therefore, interpreting experimental

reflected pressure data requires that post-reflected curves be determined first, followed by interpretation of spike peaks and then spike peak widths. Fitted curves will vary from one interpreter to another, but the differences will be negligible if the guidelines for this methodology are followed.

Post-Reflected Curves

Experimental shock wave data exhibits extreme fluxuations in the post-reflected pressure zone (see Figure 3). These fluxuations are due to the combined effects of multiple detonations during ignition of the primacord, close proximity of the test specimen to the explosive, and possible experimental data noise. A realistic approach to analysis requires this data be approximated as a smooth curve. Time steps required to analyse actual experimental data fluxuations would result in unnecessary expenditure of computer time. Selecting the post-reflected curve is accomplished by approximating a least squares fit to the experimental data in the post-reflected pressure zone. The method of least squares is a numerical analysis technique for selecting a particular curve to fit some given data. When approximating a least squares fit, the approach is to maintain an area under the fitted curve that equals the area under the experimental curve. The applicability of this approach to interpreting shock tube test data is verified in Figures 11 and 12 and discussed in Error Effects.

Large data fluxuations in the experimental shock wave data dictate the need for an approximated least squares fit instead of a computational fit. A major characteristic of the actual computational method of least squares is that it puts great emphasis on large fluxuations and little emphasis on small fluxuations. As a result, extreme fluxuations in the recording of data usually dominate the results.

Figure 3 is a typical plot of experimental post-reflected data fitted with the corresponding approximated least squares curve. Note the fitted post-reflected curve follows the general path of the experimental data, while ignoring large fluxuations. Ideal post-reflected curves characteristically exhibit a steady decline in pressure with time; however, experimental curves may decline more erratically as a result of test conditions. Whatever the post-reflected curve profile may be, post-reflected peaks (P_r) always occur at the initial stagnation time (t_s) of the post-reflected zone.

Figures 4 through 6 represent panels that have ideal stagnation times (t_s) of approximately .004 seconds (according to Glasstone calculations). Interpretations of Figures 4 through 6 yield experimental stagnation times (t_s) between .004 seconds and .007 seconds. Ideal stagnation times were used as guidelines to predict ranges where experimental stagnation times should occur.

Spike Peaks

Experimental spike peaks are dependent upon their associated post-reflected pressure peaks. Relationships between spike peaks and unreflected peaks are developed in detail in reference 2. This section develops the general applications of these ideal relationships as applied to experimental pressure data.

Reflected pressure spikes are characteristic of shock waves traveling non-parallel paths relative to the surface which they strike. Ideal spike peaks for reflected shock waves that strike at normal incidence to a flat surface are given by:

$$P_r = 2P(7P_0 + 4P)/(7P_0 + P)$$

Where: P_r = Reflected spike peak (psi)
 P_0 = Ambient pressure, ahead of the shock front (psi)
 P = Peak incident overpressure, behind the shock front (psi)

Peak incident overpressures were read from the experimental data labeled Tunnel Wall Incident Overpressure Time History. It was found that substituting post-reflected peaks (P_s) for peak overpressures (P) yields accurate results for reading the experimental data.

Table 1 lists P_r to P_s relationships within the range of the experimental data. These relationships are used to approximate spike peak magnitudes. Specific magnitudes are determined by the data profiles within the approximated regions. Examples of spike peak readings are given in Figures 4 through 6.

Spike Peak Widths

Reflected pressure spike peak widths are determined by experimental data profiles at the spike peak. Ideal blast waves do not exhibit spike peak widths; however, test conditions can induce this phenomenon. Spike peak magnitude and width are the most important data profiles to be read, since they initiate the greatest structural and material responses. Figures 4 through 6 exhibit data taken from various experimental plots. Corresponding notations define the approach applied in interpreting both spike peak magnitude and width.

Error Effects

Analytical deflections are dependent upon interpretations of the experimental reflected pressure time histories. The interpretation methodology developed in the previous sections is subject to variations from one interpreter to another. Considering these variations, the following study was made to gain some insight to the degree of error induced. This study consists of two approaches as follows: spike peak width variations, and complete displacement of the pressure time histories. Results of this study are covered in Discussion.

Spike peak width variations were analytically applied to a 22"x22"x.193" flat unstiffened panel with 2 sides clamped and 2 sides pinned. A pressure time history was developed for the first shot and the spike peak width was altered for the subsequent shots two and three. These curves were developed solely for the purpose of observation and do not necessarily represent ideal pressure time histories as developed by reference 2. The specific pressure time histories developed are listed with their corresponding plots in Figure 7. Resulting deflections are plotted in Figure 8.

Complete displacement of pressure time histories were studied to observe the effects of general variations in the interpretations of identical shock tube blasts. Actual interpretations were developed by the methodology covered in the section titled Data Interpretation. Ideal interpretations were developed from experimental data measured in the regions of the shock tube walls. These curves were developed for the sole purpose of providing various interpretations for identical shock tube blasts, and do not necessarily represent ideal pressure time histories as developed by reference 2. Two comparisons were made on 22"x22"x.192" flat unstiffened panels, one with all sides clamped and another with all sides hinged. The ideal versus actual interpretations are listed with their corresponding plots in Figures 9 and 11. Resulting deflections are plotted in Figures 10 and 12.

NASTRAN ANALYSIS

A total of seven NASTRAN models were developed to simulate structural response to shock tube overpressur-s. NASTRAN models were developed and compared against shock tube tests performed upon four flat panels, one flat stiffened panel, and one honeycomb panel. One curved panel was studied qualitatively since insufficient test data was provided for a quantitative study. The four flat panels and the curved panel were constructed with CQUAD2 elements. For the flat stiffened panel, CQUAD2 elements were used for the skin and CBAR elements were used for the stiffeners. CQUAD1 elements were used to construct the honeycomb panel. Refer to "The Nastran User's Manual" for detailed explanations of these elements. The seven NASTRAN models developed are presented in this section. Refer to Table 2 for general model specifications, Figures 13 through 15 for model geometry. Criterion for building NASTRAN models is simplicity of design. This assures that NASTRAN's effectiveness will be researched from both aspects of economy and accuracy.

Panel deflections are used as the criteria for comparisons between NASTRAN analysis and shock tube data. Stress was not used as a criterion because deflection data in reference one is of more consistent quality. Deflection and stress exhibit a linear relationship in a material's elastic range. Therefore, deflection is a valid measure of NASTRAN's effectiveness for predicting sure safe panel response. This is discussed in further detail in the section titled Discussion. Deflections are compared at panel centers. Tables 3 through 9 list the interpreted pressure time histories for each panel analyzed. Figures 18 through 24 plot the corresponding deflections for each panel. Results of the comparison are also covered in Discussion.

DISCUSSION

Results of the NASTRAN analysis and shock tube test comparisons are listed in Table 10. Results of the error effects studies are listed in Table 11 through 13. First deflections characteristically exhibit the largest deflection responses for aperiodic loading; therefore, magnitudes of first deflections are the comparison criteria. Times of deflections do not dictate stress levels and are therefore considered insignificant.

Percent error between magnitudes of first deflections was the measure of effectiveness in both the NASTRAN versus shock tube comparison and the error effects studies.

A hand calculation shows the correlation between deflection and stress response. The calculation determines edge stress for Panel 1 from NASTRAN's predicted deflection and compares this to edge stress data measured during the shock tube test. Equations are taken from Formulas For Stress and Strain, 5th Ed., Raymond J. Roark and Warren C. Young.

For rectangular plates, all edges fixed,
uniform load over entire plate: $\sigma_{EDGE} = \beta_1 q b^2/t^2$

$$Z_{MAX} = \alpha q b^4/Et^3$$

Where: $\beta_1 = 0.3078$ } Constants for a square plate with
 $\alpha = 0.0138$ } aspect ratio = 1.0
 $q =$ Uniform static load
 $b = 22.0$ in - long edge, all edges the same for panel 1
 $t = .192$ - plate thickness
 $E = 11.0 \times 10^6$ - Youngs modulus
 $\sigma_{EDGE} =$ Maximum stress at edge
 $Z_{MAX} = .219$ in (first deflection maximum).

First, calculate the equivalent static to dynamic uniform load:

$$q = Z_{MAX} E t^3/b^4 \alpha$$

$$q = (.219 \text{ in}) (11.0 \times 10^6 \text{ psi}) (.192 \text{ in})^3/(0.0138) (22.0 \text{ in})^4$$

$$q = 5.27 \text{ psi}$$

Second, calculate maximum stress at the edge:

$$\sigma_{EDGE} = \beta_1 q b^2/t^2$$

$$\sigma_{EDGE} = (-.3078) (5.27 \text{ psi}) (22.0 \text{ in})^2/ (.192 \text{ in})^2$$

$$\sigma_{EDGE} = 21297.18 \text{ psi}$$

Shock tube test edge stress measurements for panel 1 show a maximum value:

$$\sigma_{EDGE} = 25000 \text{ psi}$$

Thus:

$$\% \text{ ERROR} = \left| \frac{\text{NASTRAN} - \text{Test}}{\text{Test}} \right| \times 100$$

$$\% \text{ ERROR} = \left| \frac{21297.18 - 25000}{25000} \right| \times 100$$

$$\% \text{ ERROR} = 14.8$$

This corresponds to a 12.4% error in the deflection comparison for panel 1. Therefore, stress analysis does correlate very closely with deflection analysis, as is expected since stress and deflection exhibit a linear relationship within a materials elastic range.

Stress analysis with NASTRAN requires the appropriate model. Such a model should incorporate a center element and refined elements at the middle of the longest fixed edge of the panel. A center element is required to calculate stress at the panel center. Refined elements at the middle of the longest fixed edge are required to calculate the maximum stress for a fixed edge panel. The refinement of elements is necessitated by the sharp stress gradient that occurs at a panel's fixed edge. Deflection models do not require such element refinement, and therefore require less computer time than stress models. For these reasons deflection was used as the criterion for comparing NASTRAN results with the shock tube tests measurements.

Inherent errors of interpretations of pressure time histories taken from Boeing Military Airplane Company shock tube test data are a source of error in the NASTRAN analysis comparison. The Error Effects section studies two possible error effects. First, a study was conducted to observe the error effects of spike peak width variations. Second, a study was conducted to observe the error effects of completely displacing the pressure time history.

Table 11 list first and second deflections for shots 1, 2, and 3 of the spike peak width study. The term shot refers to a pressure time history. Figure 7 plots the three shots and list their corresponding pressure time histories. Corresponding deflection data is plotted in Figure 8. These are considered reasonable variations of interpretations for spike peaks represented by the Boeing Wichita shock tube test data.

Six possible error effects are taken from this study and the results are listed in Table 12. The procedure of this study observes each shot as an actual and measures the error effect of the two subsequent shots as ideals. Results of this study show that it is reasonable to expect approximately 20% error from a spike peak and 37.4% error in a worse case. It is emphasized here that not all of THUNDERPIPE's pressure time history data is subject to such inherent interpretational error.

Complete displacement of the pressure time history curve is the second error effect study. Figures 9 through 12 plot the pressure time histories and resultant deflections of the two cases. Table 13 list magnitudes for the first and second deflection peaks and their relative percent errors. Times of deflections are not listed since comparisons are made against identical NASTRAN models, which results in identical times of deflections.

Each case represents two interpretations for an identical shock tube test. Observing first deflections, a 39.2% error is found in the worse case.

While this does not represent a reasonable inherent interpretational error of the Boeing Military Airplane Company shock tube data, it is noteworthy in that it emphasizes the effect of the spike peak. Specifically, it takes relatively large variations in interpretations of complete displacements to produce the equivalent error resulting from small variations in interpretations of spike peak characteristics. This follows basic aspects of dynamic structural response for long pulse durations, such as those induced on the panels in this study. The general rule for long pulse durations, those twice the natural period of the oscillator, is that structural response depends primarily on peak pressure and becomes insensitive to impulse.

Results of the comparison between the NASTRAN analysis and shock tube test are listed in Table 10. Figures 18 through 24 plot the corresponding deflections. As aforementioned, percent errors between magnitudes of first deflections are the measurement criteria of effectiveness.

Panels 1 through 4 exhibit very close comparisons between NASTRAN data and shock tube test data -- ranging from 6.5 to 15.3% error. These four panels are flat and homogeneous. They differed in aluminum alloy, panel thickness, boundary constraints, and pressure time histories. Shock tube test data for these four panels were well defined by Boeing Military Airplane Company, and therefore considered to be correctly modeled by NASTRAN.

Trends for error due to modeling techniques cannot be deduced by comparing these four panels. By relating panel descriptions in Table 2 to relative percent errors in Table 10, it is determined that neither boundary constraints, panel thickness, or material properties are proportional to magnitude of error.

Panels 5 and 6 are flat nonhomogeneous panels. Panel 5 is a honeycomb construction and panel 6 is a stiffened panel. Shock tube test data for panel 5 was well defined by Boeing Wichita, and therefore considered to be correctly modeled by NASTRAN. Accordingly, panel 5 exhibits a very close comparison at 7.2% error. Panel 6 exhibits the worst case for deflection comparisons at 42.69% error.

Factors that may have affected the results of panel 6 are: incorrect boundary conditions, inherent interpretational error of the pressure time history, and exceeding the linear analysis capabilities of NASTRAN. This panel was modeled with boundary constraints as stated in the Boeing Wichita final report. Since deflection frequencies between the NASTRAN and shock tube test data coincide, it is assumed that boundary conditions are defined reasonably well. Inherent interpretational errors of pressure time histories have been addressed in the study on error effects and show that considerable error can be induced. NASTRAN uses linear finite element analysis, making it reliable in the elastic range of a material's response. Table 3 shows that panel 6 was subjected to a maximum reflected overpressure of 4.75 psi. Plastically yielding deflections during shock tube test exhibit substantially larger deflection magnitudes than NASTRAN, since NASTRAN continues linear past the yield point on the stress strain curve. Boeing Military Airplane Company documents that panel 6 plastically deformed during four shock tube tests. Figure 23 indicates that plastic deformation may have occurred during this shot; verifying the possibility that NASTRAN's elastic limits may have been exceeding.

Panel 7 is used for qualitative comparisons only, since there is no experimental deflection data available. It is a curved homogeneous panel which was subjected to a maximum overpressure of 10.5 psi -- the largest of all panels studied. Figure 24 shows the deflection response predicted by NASTRAN. The magnitude of the first deflection is relatively small, at .043 inches, for the size of reflected pressure experienced. This coincides reasonably with Boeing Military Airplane Company documentation that panel seven exhibited no permanent deformation after the test.

CONCLUSIONS

- (1) NASTRAN is an accurate analysis code for predicting elastic structural response to shock tube tests used to simulate nuclear blast overpressure effects.
- (2) Accurate pressure time histories of shock blast are extremely vital for accurate predictions of structural response.
- (3) NASTRAN's modeling flexibilities allow for greater analysis capabilities of nuclear blast overpressure effects than are allowed with present nuclear effects analysis codes.
- (4) NASTRAN's programming efficiency results in less computer time required than with present nuclear effects analysis codes.
- (5) NASTRAN's accuracy in overpressure analysis requires accurate model generation, which is dependent upon accurate structural and load input data.

P_s (psi)	P_r (psi)
.1	$2.01 \times P_s$
1	$2.06 \times P_s$
5	$2.28 \times P_s$
10	$2.53 \times P_s$

Table 1 - P_r to P_s relationships for approximating spike peak magnitudes.

	PANEL DESCRIPTION	ALUMINUM MATERIAL	DENSITY $\frac{\text{lb. sec}^2}{\text{in}^4}$	POISSON'S RATIO	MODULUS ELASTICITY (psi)	BOUNDARY CONDITIONS	YIELD STRENGTH (psi)	ULTIMATE STRENGTH (psi)
PANEL 1	22" x 22" x.192" Flat	6061-T6	2.54×10^{-4}	.33	11.0×10^6	4 Sides Clamped	40,350	44,820
PANEL 2	22" x 22" x.192" Flat	6061-T42	2.54×10^{-4}	.33	10.4×10^6	4 Sides Clamped	18,410	36,090
PANEL 3	22" x 22" x.193" Flat	6061-T6	2.54×10^{-4}	.33	10.9×10^6	2 Sides Clamped/ 2 Sides Pinned	40,500	45,200
PANEL 4	22" x 22" x.315" Flat	6061-T42	2.54×10^{-4}	.33	10.6×10^6	4 Sides Clamped	19,380	37,810
398 PANEL 5	22" x 22" x.333" Honeycomb	5052-0 Face Sheets (1)	2.54×10^{-4}	.33	12.3×10^6	4 Sides Pinned	13,270	30,300
PANEL 6	36" x 39" x.0625" Flat Stiffened	2024-T3511 Stiffeners 2024-T3 Skin (2)	2.59×10^{-4}	.33	10.6×10^6	2 Sides Clamped/ 2 Sides Pinned	52,230	66,320
PANEL 7	36" x 22.8" x.08" Curved	6061-T6	2.54×10^{-4}	.33	10.9×10^6	4 Sides Clamped	40,500	45,200

(1) Refer To Fig. 16

(2) Refer To Fig. 17

MODEL SPECIFICATIONS

TABLE 2

PANEL 1	
TIME (sec)	PRESSURE (psi)
0.0	0.0
0.0003	3.0
0.0015	3.3
0.0029	1.7
0.0042	1.6
0.0125	1.95
0.018	1.4
0.031	1.15
0.046	1.0

TABLE 3

PANEL 2	
TIME (sec)	PRESSURE (psi)
0.0	0.0
0.0002	1.2
0.002	0.6
0.006	0.5
0.0125	0.45
0.0212	0.42
0.0302	0.4
0.0352	0.4
0.0432	0.37

TABLE 4

PANEL 3	
TIME (sec)	PRESSURE (psi)
0.0	0.0
0.00025	1.3
0.002	0.98
0.0035	0.7
0.006	0.45
0.013	0.35
0.0225	0.35
0.0285	0.3
0.0395	0.25
0.044	0.2

TABLE 5

PANEL 4	
TIME (sec)	PRESSURE (psi)
0.0	0.0
0.0003	0.9
0.0017	2.0
0.003	1.0
0.0054	0.88
0.0115	0.75
0.017	0.67
0.025	0.63
0.031	0.6
0.04	0.6

TABLE 6

PANEL 5	
TIME (sec)	PRESSURE (psi)
0.0	0.0
0.0003	1.38
0.002	1.1
0.0035	0.8
0.0047	0.66
0.006	0.62
0.0095	0.58
0.0205	0.54
0.028	0.52
0.034	0.5

TABLE 7

PANEL 6	
TIME (sec)	PRESSURE (psi)
0.0	0.0
0.0002	2.4
0.0015	4.75
0.002	2.25
0.0045	1.4
0.012	1.2
0.026	1.0
0.04	0.09

TABLE 8

PANEL 7	
TIME (sec)	PRESSURE (psi)
0.0	0.0
0.0002	6.7
0.001	10.5
0.0029	5.9
0.0032	5.0
0.0044	4.4
0.015	3.7
0.027	2.9
0.033	2.5

TABLE 9

Tables 3 - 9:
Pressure Time Histories
input into NASTRAN
for Panels 1 - 7

1st and 2nd Peak Deflections

Panel/ Defl.	Magnitude (inches)			Time (sec)		
	NASTRAN	Test	% Error (1)	NASTRAN	Test	% Error (1)
1/1st	.219	.250	12.4	.0035	.0030	16.7
1/2nd	-.088	-.160	45.0	.0070	.0065	7.7
2/1st	.173	.150	15.3	.0060	.0044	36.4
2/2nd	-.040	-.065	38.5	.0130	.0090	44.4
3/1st	.113	.130	13.1	.0040	.0040	0.0
3/2nd	-.059	-.067	11.9	.0085	.0080	6.3
4/1st	.029	.031	6.5	.0025	.0030	16.7
4/2nd	-.012	-.009	33.3	.0050	.0055	9.1
5/1st	.154	.166	7.2	.0018	.0032	43.8
5/2nd	-.039	-.060	35.0	.0036	.0057	36.8
6/1st	.066	.115	42.6	.0025	.0032	21.9
6/2nd	-.042	-.030	40.0	.0060	.0055	9.1
7/1st	.043	(2)	—	.0025	(2)	—
7/2nd	-.015			.0045		

$$(1) \% \text{ Error} = \left| \frac{\text{NASTRAN} - \text{Test}}{\text{Test}} \right| \times 100$$

(2) Test Data Not Available

Table 10

Spike Peak
Width Effects
(1st and 2nd Deflection Peaks)

Shot/ Defl.	Time (sec)	Defl. (inches)
1/1st	.0039	.1412
1/2nd	.0084	-.0572
2/1st	.0039	.1779
2/2nd	.0084	-.0928
3/1st	.0045	.1940
3/2nd	.0086	-.1091

Table 11

Spike Peak
Width Effects
(1st Deflection)

Shot Ideal/Actual	% Error (1)
1/2	20.6
1/3	27.2
2/1	26.0
2/3	8.3
3/1	37.4
3/2	9.1

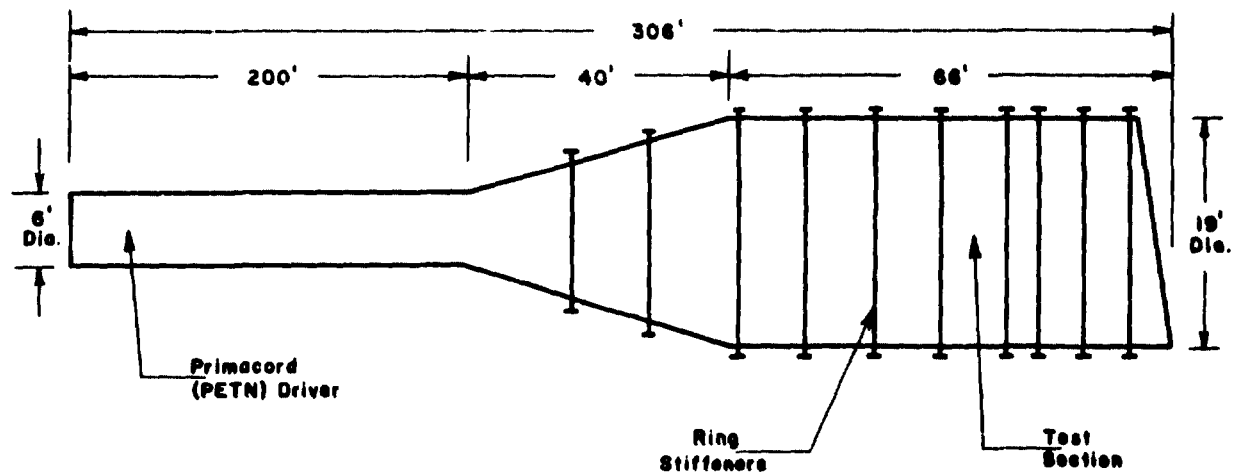
Table 12

Complete Displacement Effects
(1st and 2nd Deflections)

Case/ Defl.	Ideal Defl. (inches)	Actual Defl. (inches)	% Error (1)
1/1st	.2162	.219	1.3
1/2nd	-.0656	-.088	25.5
2/1st	.2408	.173	39.2
2/2nd	-.0739	-.040	84.8

Table 13

$$(1) \% \text{ Error} = \left| \frac{\text{Ideal} - \text{Actual}}{\text{Actual}} \right| \times 100$$



THUNDERPIPE SHOCK TUBE

Figure 1 - Sandia Corporation's THUNDERPIPE shock tube

DEFINITIONS OF TERMS

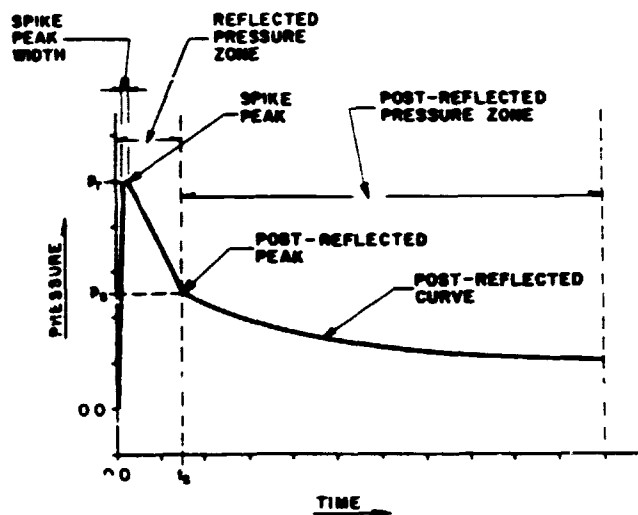
Reflected Pressure (P_r) - The initial pressure experienced by surfaces subjected to shock waves striking at non-parallel paths relative to the surface, resulting in a greater pressure experienced by the surface than is present at the shock front.

Reflected Pressure Time History - A numerical account (tabular or graphical) of the pressure as a function of time experienced by a surface subjected to shock waves traveling non-parallel paths relative to the surface. It is the addition of incident overpressure, dynamic pressure, and reflected pressure effects.

Stagnation Time (t_s) - The time at which reflected pressure effects subside, leaving only incident overpressure and dynamic pressure effects. It is a function of panel geometry and shock wave velocity. Ideal t_s is calculated from reference 2.

Stagnation Pressure (P_s) - The post-reflected peak pressure that corresponds to stagnation time (t_s).

Ideal Pressure Curve - Developed in reference 2. Major characteristics are an initial reflected pressure effect until time t_s , followed by a steady and more gradual decrease of the post-reflected pressure.



**TYPICAL REFLECTED PRESSURE
TIME HISTORY CURVE**

Figure 2 - A typical curve fitting of a reflected pressure time history from the Boeing Wichita shock tube test data.

ORIGINAL PAGE IS
OF POOR QUALITY.

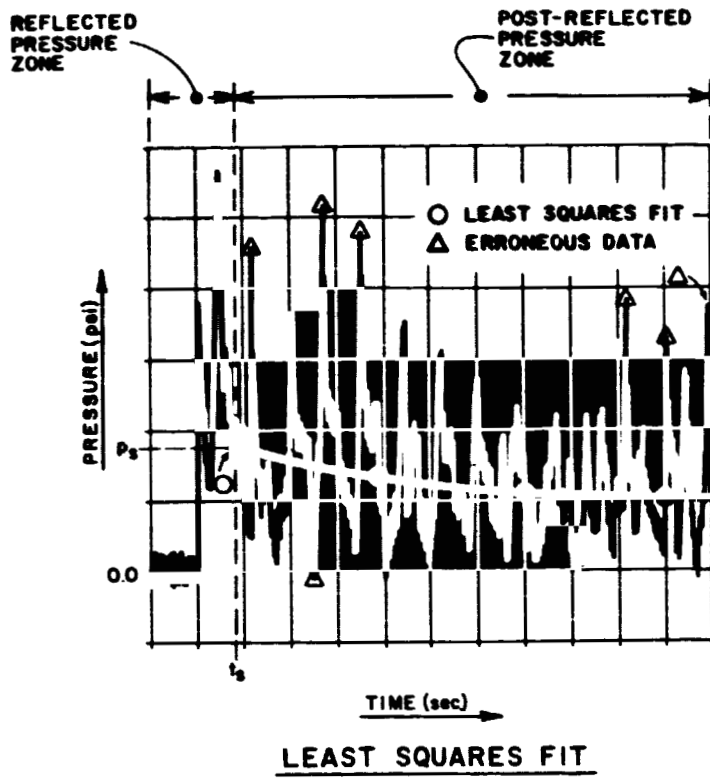
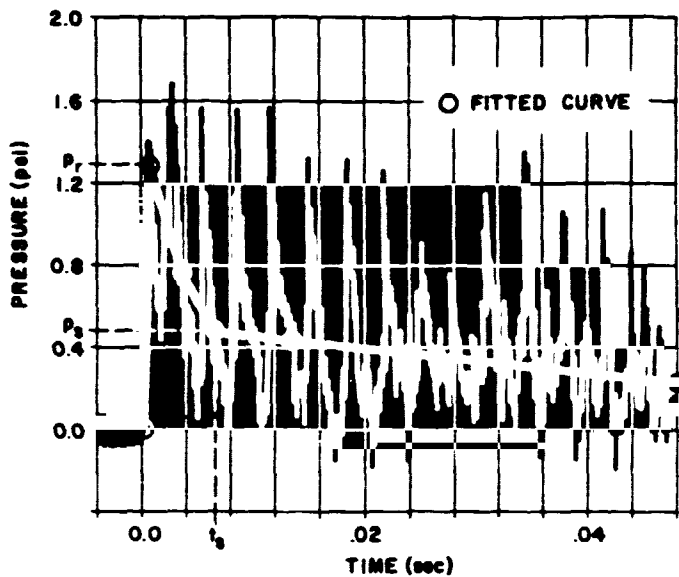


Figure 3 - Approximated least squares fit on a typical plot of experimental post-reflected data.

ORIGINAL PAGE IS
OF POOR QUALITY

INTERPRETATIONS



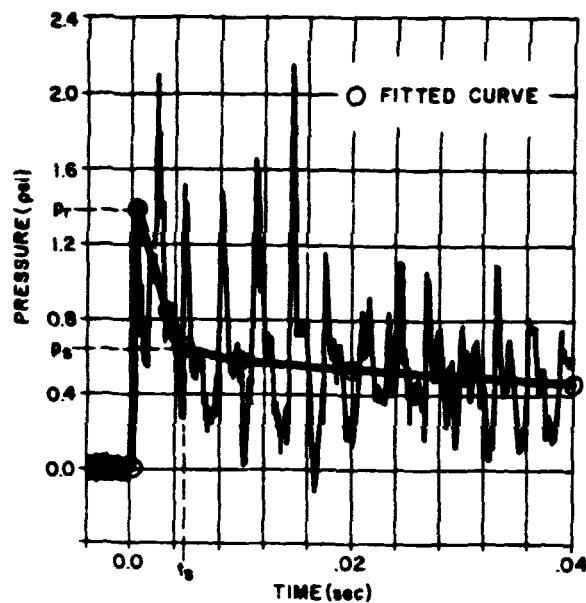
REFLECTED PRESSURE TIME HISTORY

Figure 4 - An example of data interpretation.

Curve Fitting for Figure 4

Apply a least squares approximation to curve fit post-reflected data. Note that experimental data fluxuations subside around .028 seconds, giving an indication of where the optimum approximated pressure levels are for the fitted curve. The post-reflected peak (P_s) is interpreted to be 0.5 psi at an experimental stagnation time (t_s) just over .006 seconds.

Table 1 indicates the reflected peak (P_r) is approximately 1.2 psi. Therefore, the initial experimental peak is taken as P_r at 1.3 psi and the second experimental peak is disregarded since it is well above the expected range of P_r . Fitting only one point in the range of P_r results in the absence of a spike peak width.



REFLECTED PRESSURE TIME HISTORY

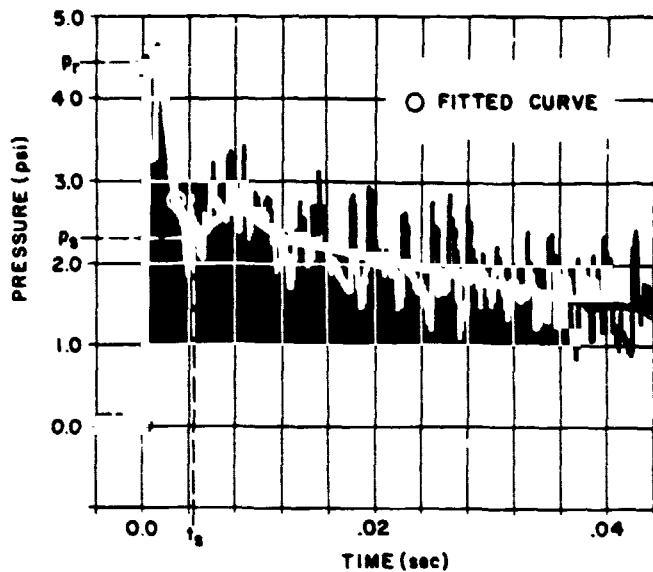
Figure 5 - An example of data interpretation.

Curve Fitting for Figure 5

Approximate a least squares curve to fit post-reflected data. Experimental data fluxuations subside around 0.022 seconds and 0.03 seconds, giving an indication of optimum fitted curve pressure levels. There are several data fluxuations before 0.016 seconds that are ignored. The post-reflected peak (P_s) is interpreted to be approximately .65 psi, corresponding to an experimental stagnation time (t_s) around .005 seconds.

Calculating the reflected peak yields P_r approximately equal to 1.3 psi - refer to Table 1. The initial experimental peak is recorded as P_r at 1.4 psi and the second experimental peak is disregarded since it is not within the expected range of P_r . There is no spike width because only one point is fitted in the range of P_r .

ORIGINAL SOURCE
OF POOR QUALITY



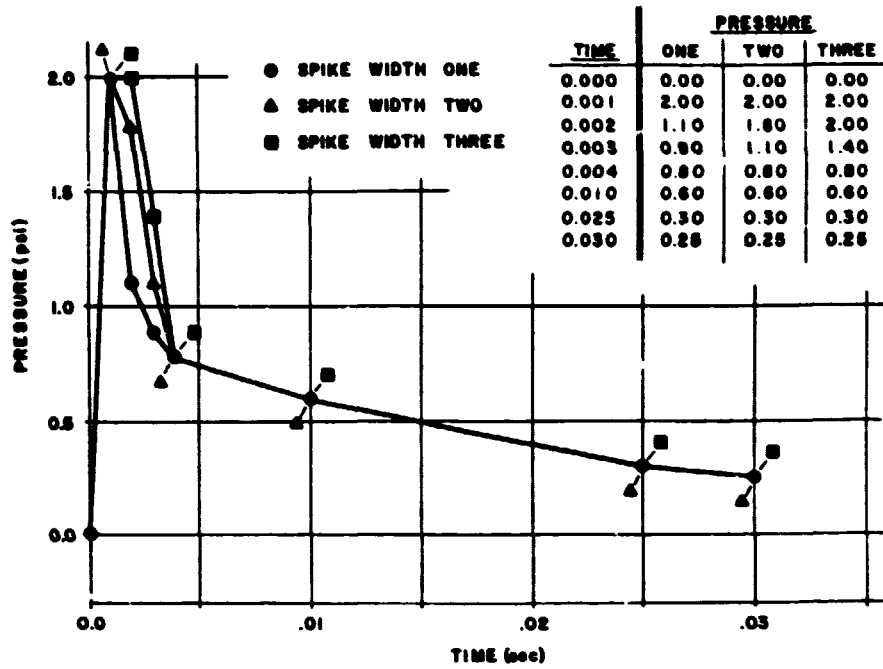
REFLECTED PRESSURE TIME HISTORY

Figure 6 - An example of data interpretation.

Curve Fitting for Figure 6

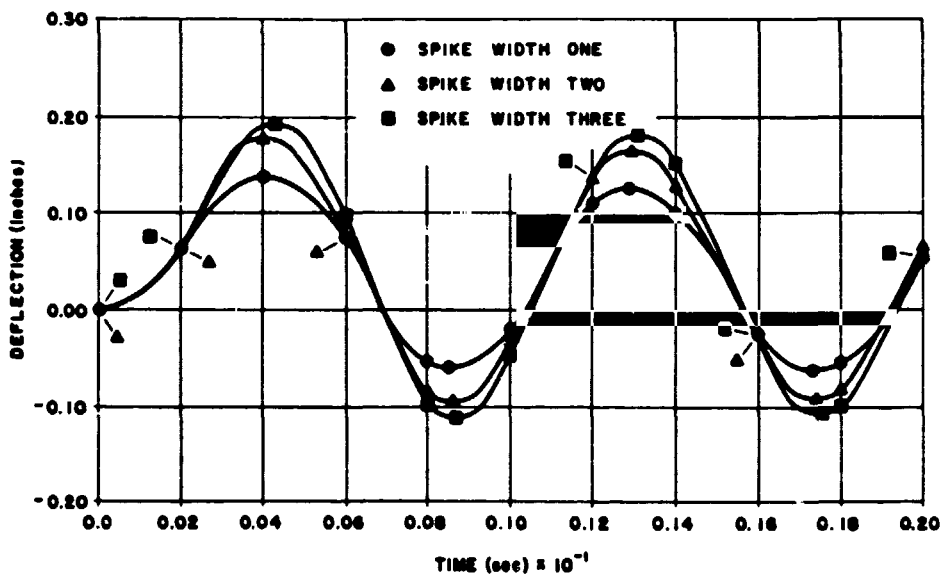
Curve fit the post-reflected data with a least squares approximation. Post-reflected data clearly deviates from theory between t_s and 0.012 seconds. This is shock tube phenomenon and is recorded as fitted data since project objectives are to validate NASTRAN against shock tube test. Near 0.032 seconds experimental data fluxuations subside, giving an indication of optimum approximate pressure levels for the fitted curve. The post-reflected peak (P_s) is interpreted to be approximately 2.3 psi, corresponding to an experimental stagnation time (t_s) .0045 seconds. Note that P_s is defined as the initial pressure of the post reflected curve.

Table 1 approximates the reflected peak P_r at 4.5 psi. Experimental data contains two points at this pressure range; therefore, a spike width does exist as indicated by the fitted curve. This deviates from the ideal but is recorded in order to duplicate shock tube phenomenon. Smooth spike peak widths are fitted and experimental data fluxuations at the peak are disregarded.



PRESSURE TIME HISTORIES

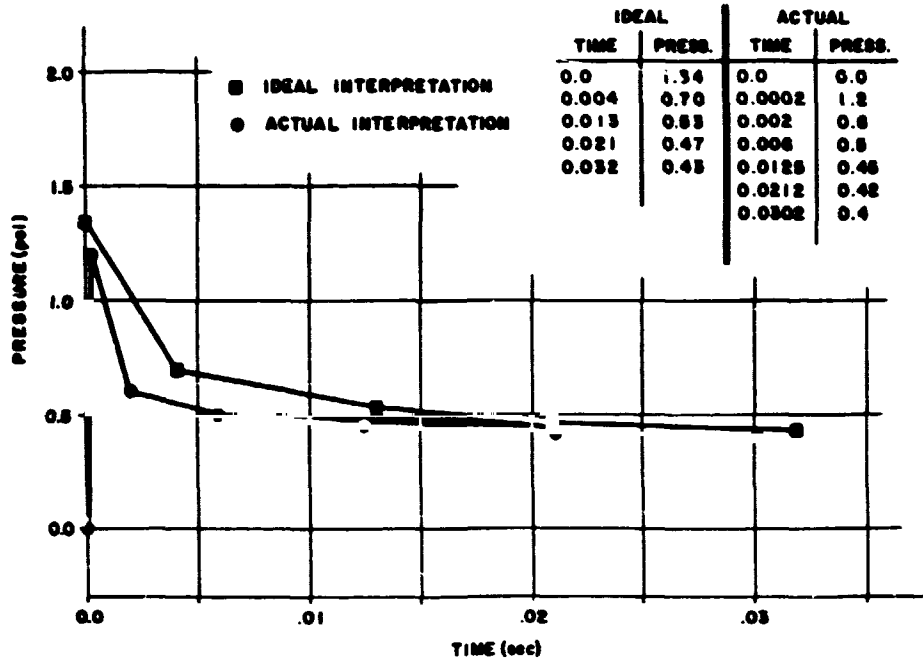
Figure 7 - Error Effects Study #1. Spike peak width interpretation variations.



SPIKE WIDTH DEFLECTION EFFECTS

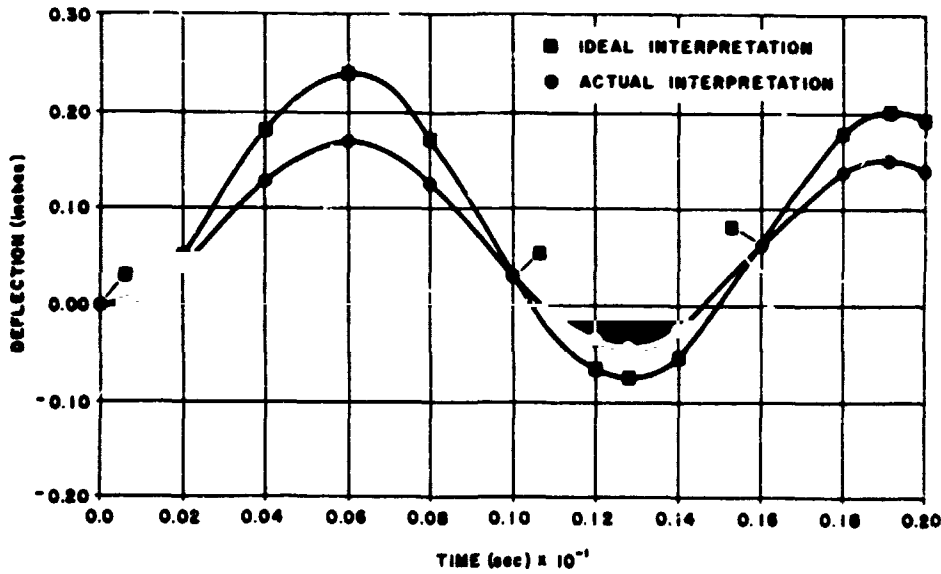
Figure 8 - Error effect study #1. Deflections resulting from pressures depicted in Figure 7.

ORIGINAL PAGE IS
OF POOR QUALITY



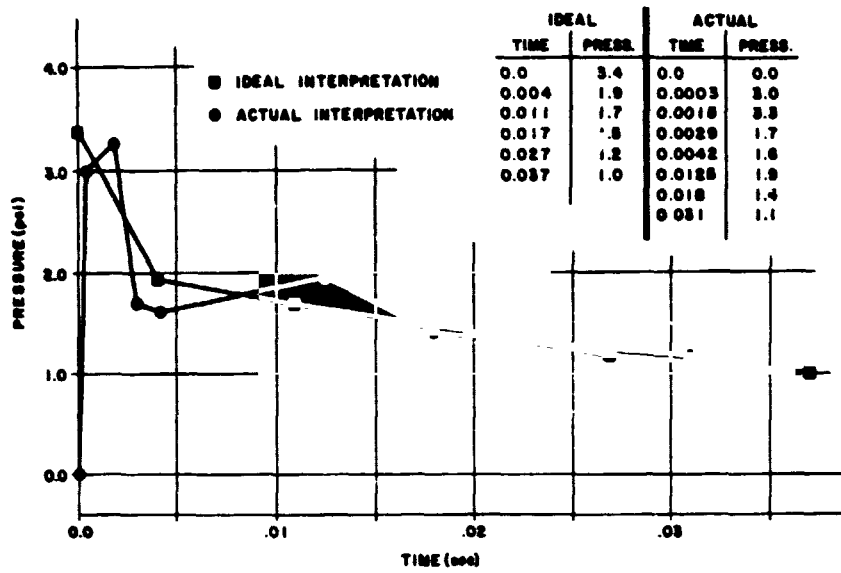
PRESSURE TIME HISTORIES

Figure 9 - Error effect study #2. Complete displacement interpretation variation.



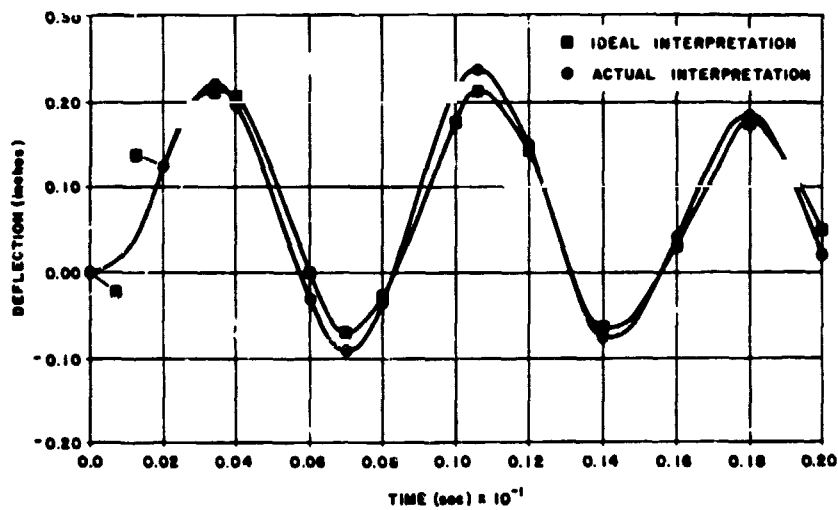
IDEAL vs. ACTUAL DEFLECTIONS

Figure 10 - Error effects study #2. Deflections resulting from pressures depicted in Figure 9.



PRESSURE TIME HISTORIES

Figure 11 - Error effects study #3. Complete displacement interpretation variation.



IDEAL vs. ACTUAL DEFLECTIONS

Figure 12 - Error effects study #3. Deflections resulting from pressures depicted in Figure 11.

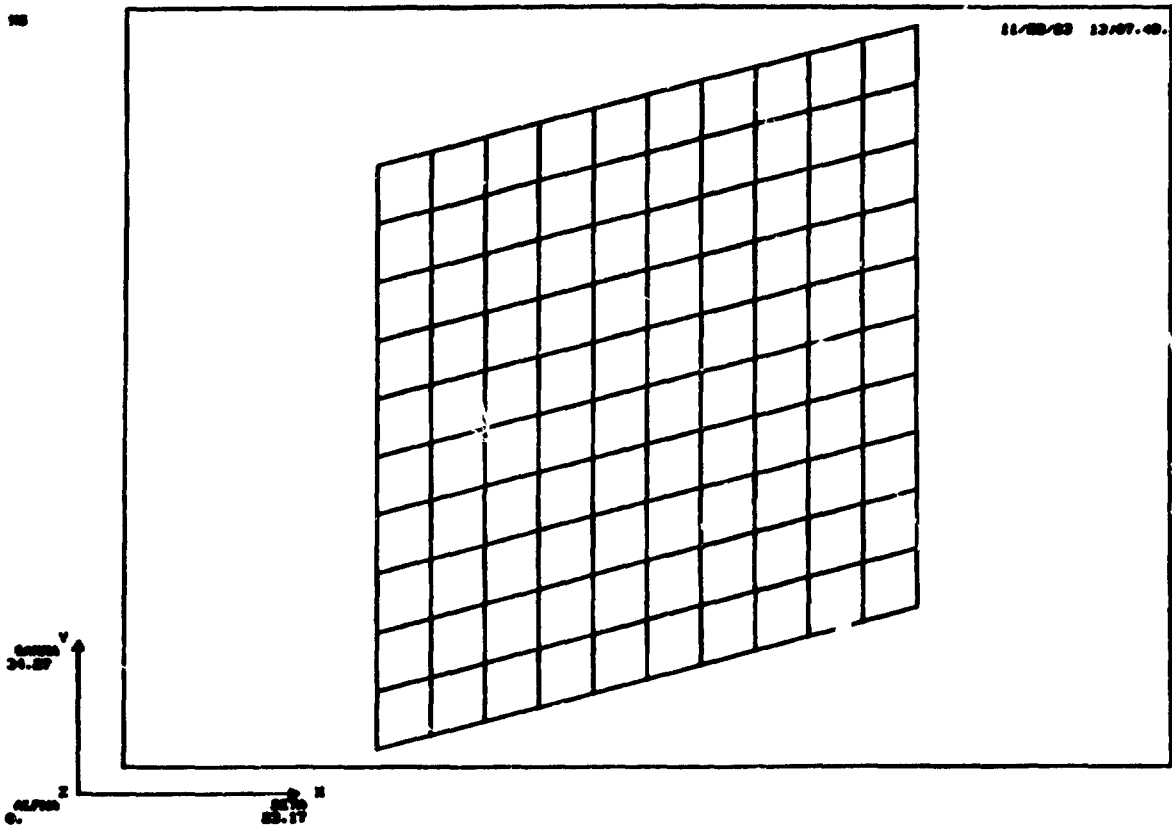


Figure 13 - NASTRAN finite element model for Panels 1 through 5. Refer to Table 2 for specific panel characteristics.

ORIGINAL PAGE IS
OF POOR QUALITY

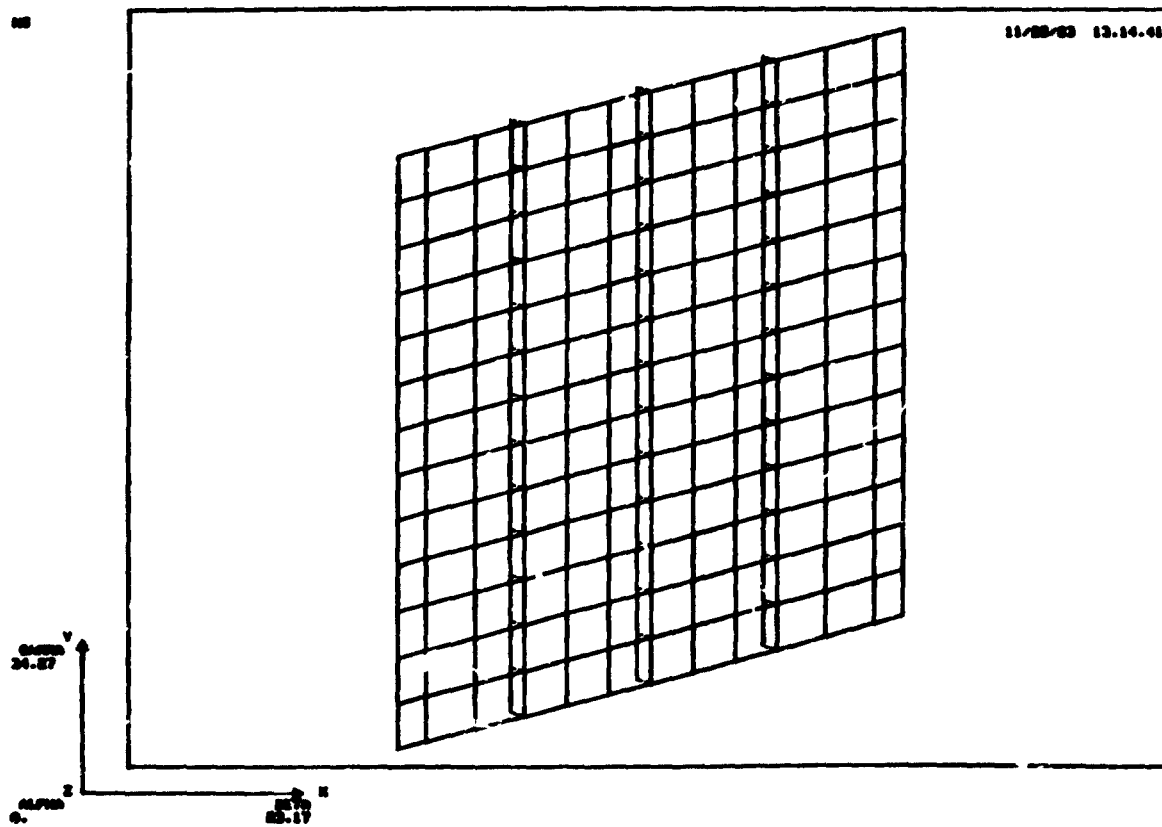


Figure 14 - NASTRAN finite element model for Panel 6, a flat stiffened panel. Refer to Table 2 for specific panel characteristics.

ORIGINAL PAGE IS
OF POOR QUALITY

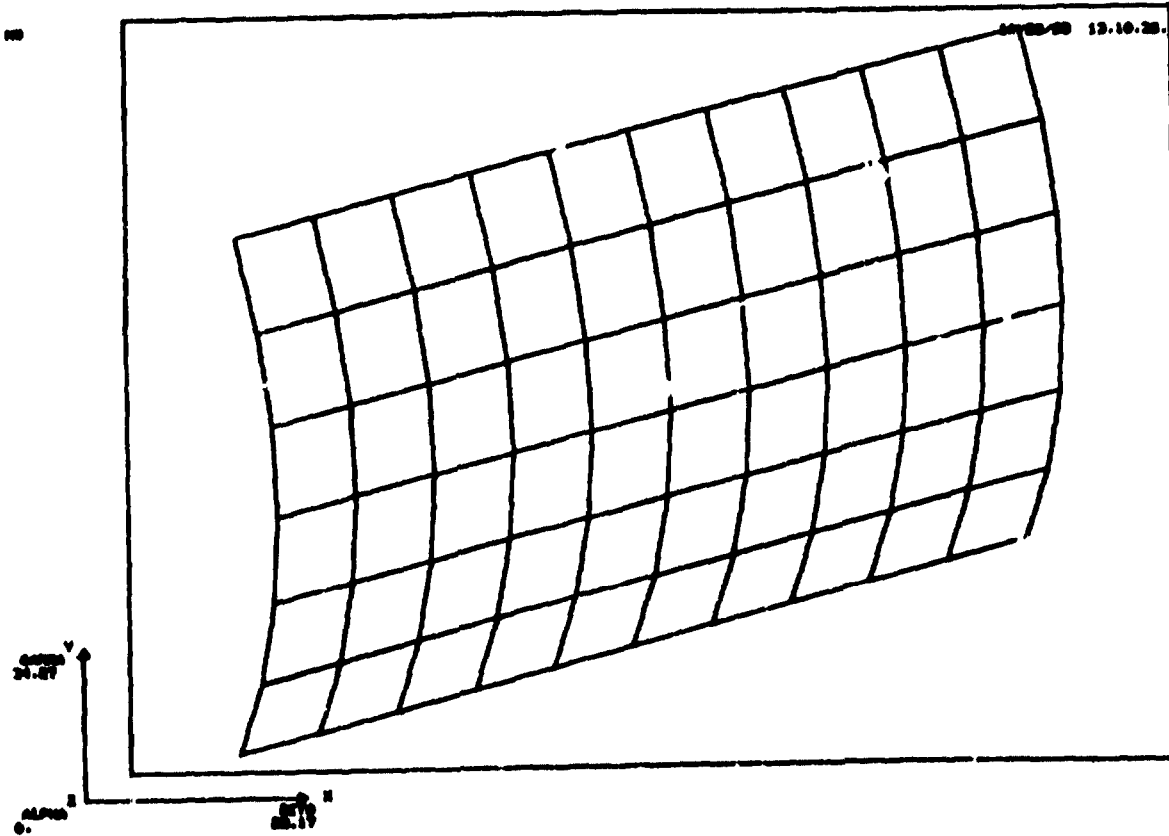
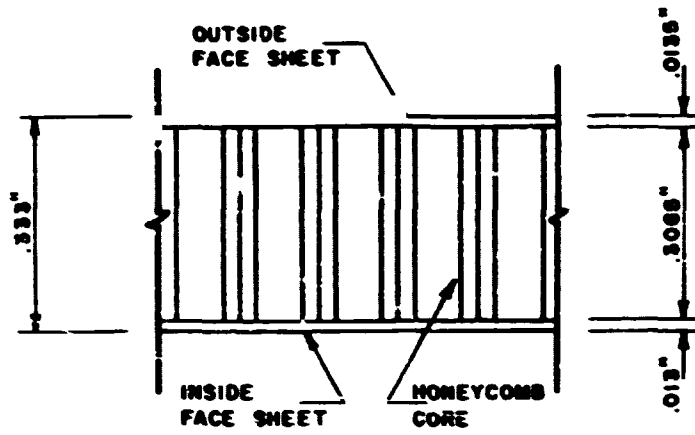
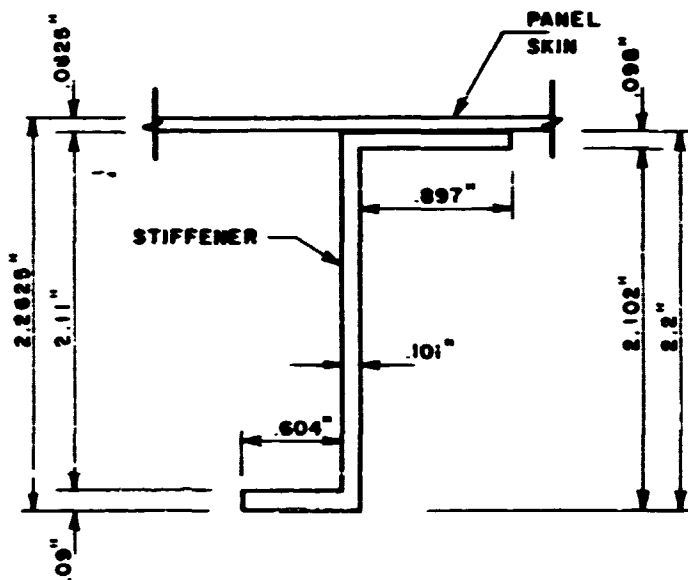


Figure 15 - NASTRAN finite element model for Panel 7, a curved panel. Refer to Table 2 for specific panel characteristics.



PANEL 5
CROSS SECTION

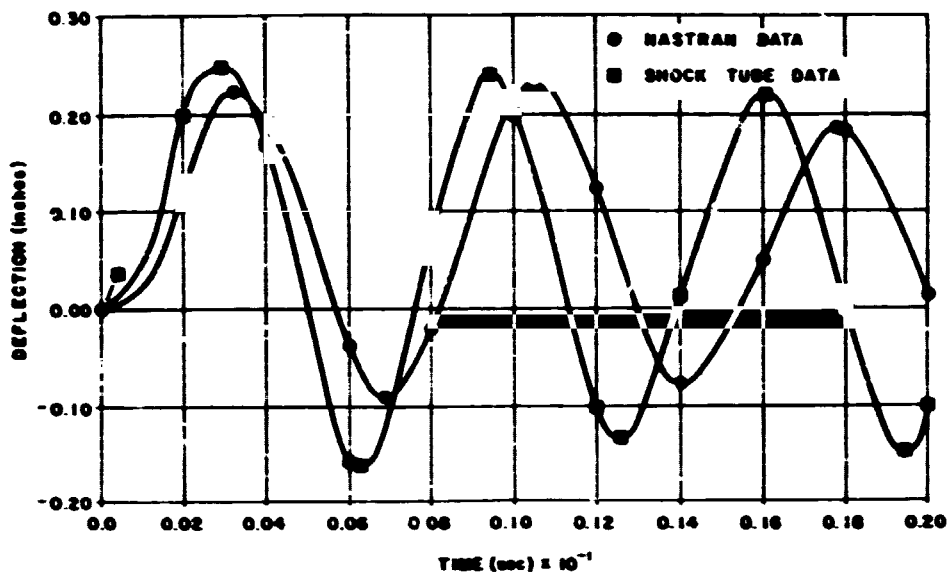
Figure 16



PANEL 6
STIFFENER CROSS SECTION

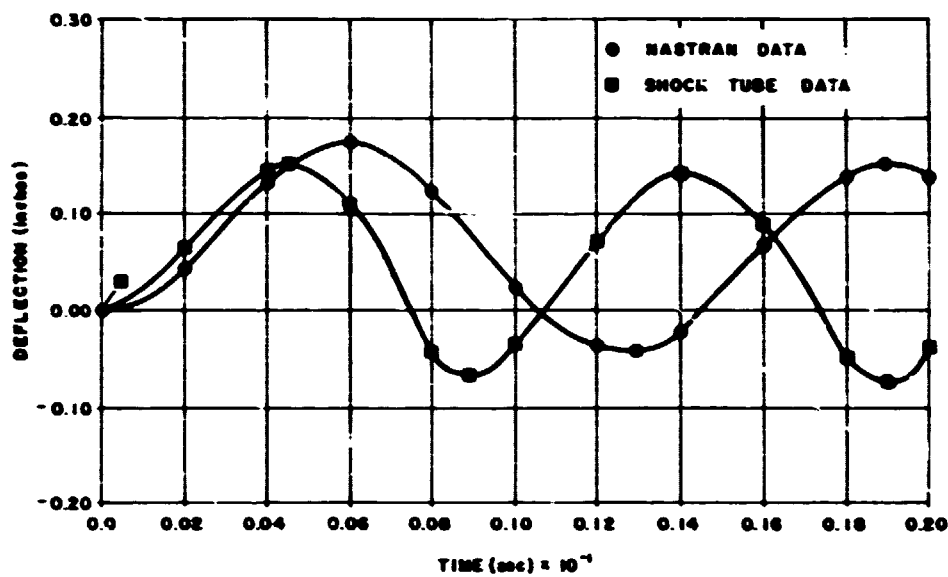
Figure 17

ORIGINAL PANEL 18
OF POOR QUALITY



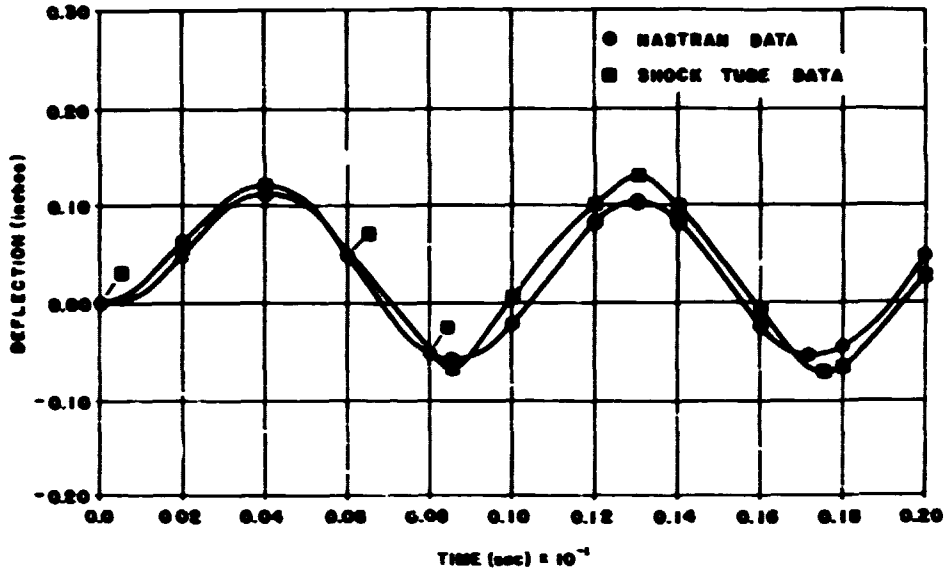
PANEL ONE

Figure 18 - NASTRAN versus shock tube deflections.



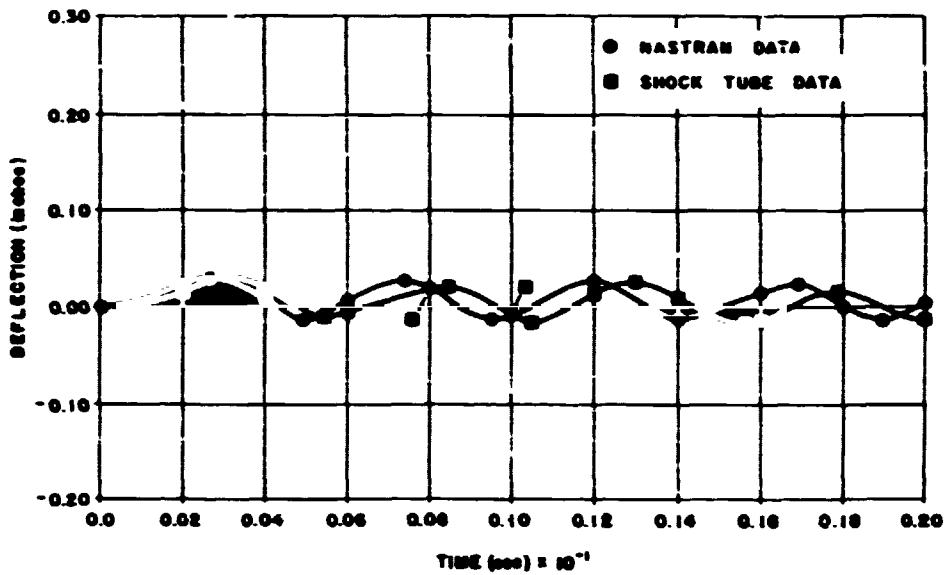
PANEL TWO

Figure 19 - NASTRAN versus shock tube deflections.



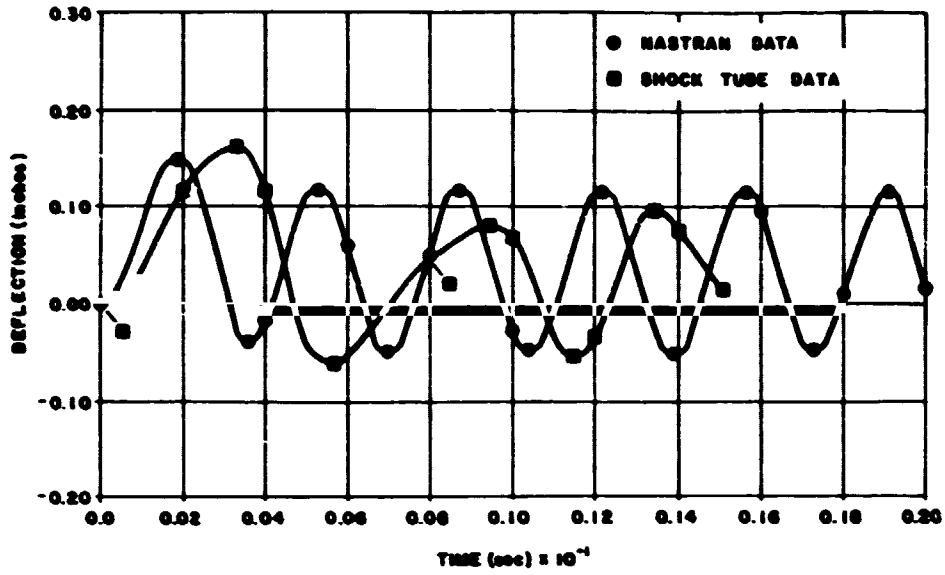
PANEL THREE

Figure 20 - NASTRAN versus shock tube deflections.



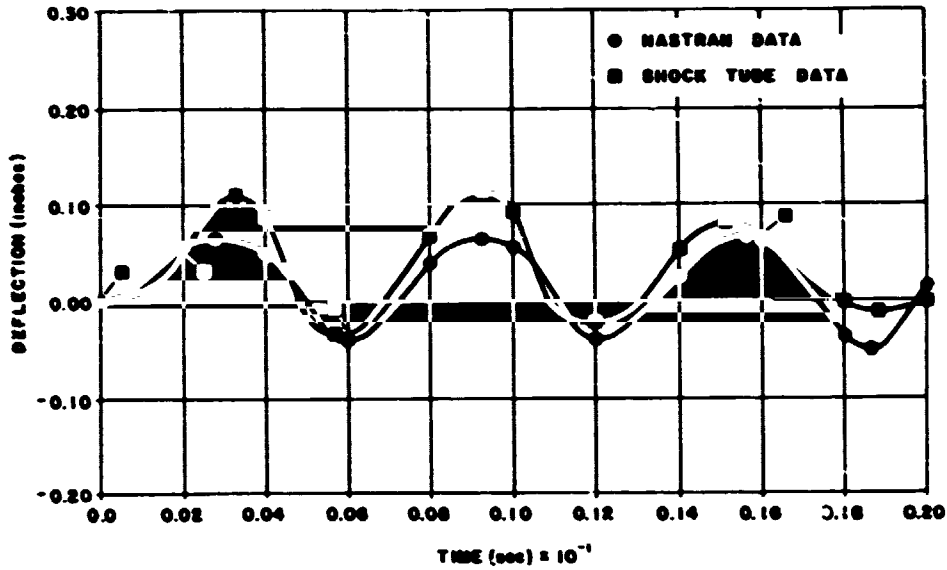
PANEL FOUR

Figure 21 - NASTRAN versus shock tube deflections.



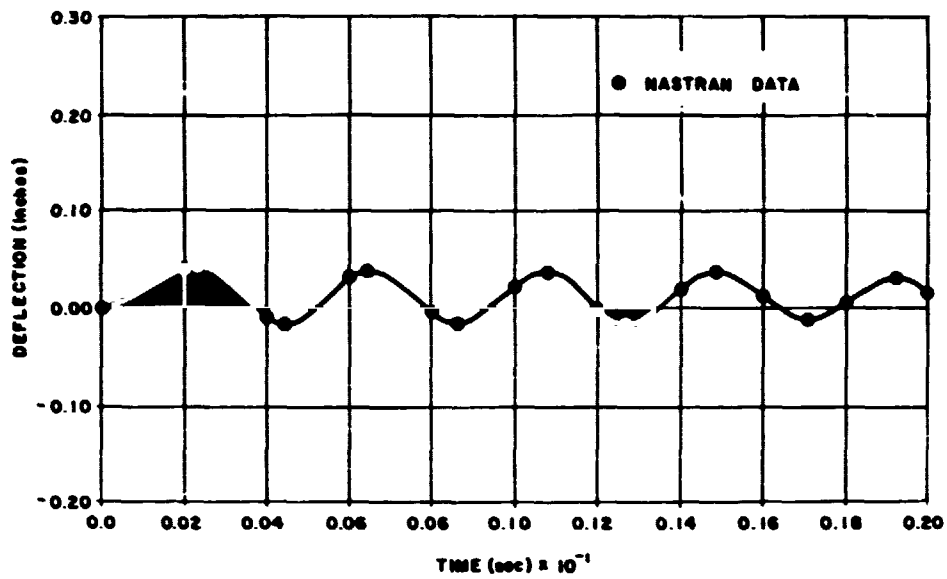
PANEL FIVE

Figure 22 - NASTRAN versus shock tube deflections.



PANEL SIX

Figure 23 - NASTRAN versus shock tube deflections.



PANEL SEVEN

Figure 24 - NASTRAN analysis deflection.

N85-25889

FINITE ELEMENT PREDICTION OF LOSS FACTORS FOR STRUCTURES
WITH FREQUENCY-DEPENDENT DAMPING TREATMENTS

Gordon C. Everstine and Melvyn S. Marcus

Numerical Mechanics Division
David Taylor Naval Ship R&D Center
Bethesda, Maryland 20084

ABSTRACT

A finite element procedure is described for calculating the loss factors for elastic structures to which frequency-dependent viscoelastic damping treatments have been applied. The frequency dependence of the viscoelastic damping material is treated by approximating its shear modulus with a second-order polynomial so that the stiffnesses associated with the constant, linear, and quadratic terms can be combined, respectively, with the stiffness, damping, and mass matrices assembled for the rest of the structure. A single complex eigenvalue analysis is then performed in which the eigenvalues are purely imaginary. The loss factor is computed by the modal strain energy (MSE) approach first formulated in 1962 by Ungar and Kerwin and recently recast in the finite element context by Johnson, Kienholz, and Rogers. In the MSE approach, the loss factor of a composite structure vibrating in one of its natural modes may be visualized as a weighted average of the loss factors of the component parts, with the relative stored energies as weighting constants. The finite element procedure, which can treat very general geometries, is illustrated for the case of a vibrating constrained-layer damped plate.

INTRODUCTION

Damping treatments are frequently applied to engineering structures to reduce both vibration and noise. For example, laminated plates composed of alternate layers of elastic and viscoelastic materials have been used as structural members which can dissipate vibratory energy as well as maintain the required structural integrity.

The finite element prediction of the dynamic response of such structures is complicated considerably by the frequency-dependence of the viscoelastic material properties. Because the structure's stiffness matrix is frequency-dependent, the finite element equations are nonlinear rather than linear, and conventional analysis cannot be used. For example, the calculation of time-harmonic forced response by a direct approach (in the physical, rather than modal, coordinates of the structure) would require the complete re-assembly and solution of the system equations for each drive frequency. Also, with most finite element codes, the overall damping characteristics of the structure cannot be determined by solving the complex eigenvalue problem since the frequency-dependence of the coefficient matrices results in a nonlinear eigenvalue problem.

This paper describes how constant coefficient matrices in finite element analysis can be restored so that the difficulties associated with frequency-dependent material properties can be reduced. In essence, a frequency-dependent material property is approximated by a polynomial quadratic in the circular frequency ω , and the coefficients of the first and second order terms of the

polynomial are combined with the system damping and mass matrices, respectively. The main requirements for this approach are (1) that the frequency-dependence can be adequately represented by a quadratic, and (2) that the finite element code can handle complex stiffness, damping, and mass matrices. NASTRAN, for example, allows these matrices to be complex.

This paper discusses two problems for structures to which frequency-dependent viscoelastic damping treatments have been applied:

1. forced time-harmonic response analysis using physical, rather than modal, coordinates (called "direct frequency response" in NASTRAN), and
2. prediction of the overall system loss factor (structural damping coefficient).

Convenient solution of the first problem requires only the quadratic polynomial approximation to the frequency dependence of the viscoelastic material properties. For the second problem, the approach taken here is to use the quadratic fit only for the real part of the viscoelastic modulus, and then to solve an undamped (but mathematically complex) eigenvalue problem and apply the modal strain energy (MSE) approach to extract the system loss factor.

APPROXIMATION FOR FREQUENCY-DEPENDENT MATERIALS

The formulation of a structural dynamics problem for finite element solution results, in the time domain, in the matrix equation

$$M\ddot{u} + B\dot{u} + Ku = F(t) \quad (1)$$

where M , B , and K are the mass, viscous damping, and stiffness matrices, respectively, u is the vector of unknown displacement components at the grid points, and F is the vector of applied forces at the grid points.

For time-harmonic loading,

$$F = F_0 e^{i\omega t} \quad (2)$$

$$u = u_0 e^{i\omega t} \quad (3)$$

where ω and F_0 are, respectively, the circular frequency and complex amplitude of the applied force, and u_0 is the complex amplitude of the displacement response. In that case, the time-harmonic form of Equation (1) is

$$(-\omega^2 M + i\omega B + K) u_0 = F_0 \quad (4)$$

Consider a structure made of one or more materials, only one of which is damped. Assume that the damped material (which may be anisotropic) is modeled mathematically by the complex modulus approach, in which the modulus of elasticity is the complex number $E(1+i\eta)$, where η is the loss factor for the material. Assume also that all moduli for that material have the same loss factor η and, hence, that the Poisson's ratios are real and frequency-independent. Since every term of the finite element material matrix D (which converts the strain vector to the stress vector for an element) is proportional to one of the elastic moduli, the frequency dependence can be factored out as a common dimensionless scalar factor:

$$D(\omega) = \alpha(\omega) D_0 (1 + i\eta(\omega)) \quad (5)$$

where D_0 is a real, frequency-independent reference material matrix, $\alpha(\omega)$ is a dimensionless factor which expresses the frequency dependence of the real part of the elastic moduli, and $\eta(\omega)$ is the frequency-dependent loss factor for the material. In effect, D_0 is the material matrix for some arbitrary frequency ω_0 , and αD_0 is the real part of the material matrix for some other frequency ω ; thus, $\alpha(\omega_0) = 1$. It therefore follows that the stiffness matrix K_d for the portion of the structure made of the damped material is of the form

$$K_d = \alpha K_0 (1 + i\eta) \quad (6)$$

where K_0 is the real part of K_d at the reference frequency ω_c . The stiffness matrix for the remainder of the structure (the undamped portion) will be denoted K_e .

With damping modeled using the complex modulus approach, M in Equation (4) is real, $B = 0$ (unless viscous damping is also present), and K is complex. The real part of K includes the contributions from all components and materials in the structure. However, if only one material has complex moduli, the imaginary part of the system stiffness matrix K arises only from the damped material, thus allowing the stiffness matrix for the damping material to be extracted from the overall system stiffness matrix. If the loss factor (structural damping coefficient) η for the damping material is specified as unity on the finite element material properties data card,

$$\alpha K_0 = \text{Im}(K_d) |_{\eta=1} = \text{Im}(K) |_{\eta=1} \quad (7)$$

The stiffness matrix K_e for the remainder of the structure (the undamped portion) is then obtained by subtracting from the system matrix K the contribution from the damping material:

$$K_e = \text{Re}(K) - \text{Im}(K) |_{\eta=1} \quad (8)$$

where K is the (complex) stiffness matrix for the entire structure assuming that $\eta = 1$ is specified for the damped portion.

It will be convenient to write Equation (6) in the form

$$K_d = K_0 (\alpha + i\beta) \quad (9)$$

where

$$\beta(\omega) = \alpha(\omega)\eta(\omega) \quad (10)$$

If the dependence of α and β on ω were quadratic, it is clear from Equation (4) that the frequency-dependent terms could be absorbed into the system's mass and viscous damping matrices, thereby transforming the problem into standard form (although with complex coefficient matrices).

Therefore, we attempt to approximate $\alpha(\omega)$ and $\beta(\omega)$ with the quadratic polynomials

$$\alpha(\omega) \cong \alpha_0 + \alpha_1\omega + \alpha_2\omega^2 \quad (11)$$

$$\beta(\omega) \cong \beta_0 + \beta_1\omega + \beta_2\omega^2 \quad (12)$$

The six unknown coefficients in Equations (11) and (12) can be determined by standard least-squares procedures (which are summarized in the next section).

With quadratic frequency-dependence of the damping material, the coefficient matrices M , B , and K in Equation (4) can be replaced by new complex matrices M^* , B^* , and K^* defined by the equality

$$-\omega^2 M + i\omega B + K_e + K_o[\alpha_o + \alpha_1\omega + \alpha_2\omega^2 + i(\beta_o + \beta_1\omega + \beta_2\omega^2)] = -\omega^2 M^* + i\omega B^* + K^* \quad (13)$$

where K_e is the system stiffness matrix for the undamped part of the structure, B is the damping matrix for the viscous dampers, if any, and M is the original mass matrix for the entire structure. Thus, by equating coefficients of like powers of ω in Equation (13), we obtain

$$K^* = K_e + (\alpha_o + i\beta_o)K_o \quad (14)$$

$$B^* = B + (\beta_1 - i\alpha_1)K_o \quad (15)$$

$$M^* = M + (-\alpha_2 - i\beta_2)K_o \quad (16)$$

where K_e is determined from Equation (8). In this form, the new coefficient matrices M^* , B^* , and K^* are complex and independent of frequency.

To summarize, the frequency dependence of the real and imaginary parts of the moduli of the viscoelastic material is replaced by a quadratic so that such dependence can be absorbed into the system mass and damping matrices. The principal assumptions made are (1) that the frequency dependence of the material can be described by a single scalar function, (2) that this function can be adequately represented by a quadratic polynomial, and (3) that the finite element code is general enough to allow complex coefficient matrices.

CURVE-FITTING

Let $y(x)$ represent one of the two frequency-dependent material property functions $\alpha(\omega)$ and $\beta(\omega)$ defined in Equation (9). Assume that $y(x)$ is known at n points (x_i, y_i) , $i=1, 2, \dots, n$. We wish to approximate $y(x)$ by the quadratic polynomial

$$p(x) = a_o + a_1x + a_2x^2 \quad (17)$$

in such a way that the residual

$$R = \sum_{i=1}^n w_i [y_i - (a_o + a_1x_i + a_2x_i^2)]^2 \quad (18)$$

is minimized, where w_i is the weighting factor for point i . This is the classical least squares problem. To minimize the squares of the absolute errors, $w_i = 1$. To minimize the squares of the relative errors, $w_i = 1/y_i^2$.

The polynomial coefficients which minimize the residual R are the solutions of the symmetric system [1]

$$\begin{bmatrix} \sum w_i & \sum w_i x_i & \sum w_i x_i^2 \\ \sum w_i x_i & \sum w_i x_i^2 & \sum w_i x_i^3 \\ \sum w_i x_i^2 & \sum w_i x_i^3 & \sum w_i x_i^4 \end{bmatrix} \begin{Bmatrix} a_0 \\ a_1 \\ a_2 \end{Bmatrix} = \begin{Bmatrix} \sum w_i y_i \\ \sum w_i x_i y_i \\ \sum w_i x_i^2 y_i \end{Bmatrix} \quad (19)$$

where all summations are from $i=1$ to n .

MODAL STRAIN ENERGY APPROACH TO DAMPING

The relationship between damping and energy concepts for nonhomogeneous structures was apparently first formulated by Ungar and Kerwin in 1962 [2]. In general terms, they showed that the loss factor of a composite structure may be computed as a weighted average of the loss factors of the component parts, with the relative stored energies as weighting factors. The Ungar-Kerwin ideas were recently recast in the finite element context by Johnson, Kienholz, and Rogers [3-5]. For completeness, we summarize (in a slightly different form) the aspects of this work needed here.

The complex Rayleigh quotient for a damped structure may be written in the form

$$\omega^2(1 + i\eta) = \phi_d^T(K_T + i\eta_d K_d)\phi_d / (\phi_d^T M \phi_d) \quad (20)$$

where K_T = stiffness matrix (real) for the entire structure
 K_d = stiffness matrix (real) for the part of the structure which is damped (i.e., the viscoelastic material)
 η_d = loss factor (real) for the viscoelastic material
 M = mass matrix (real) for the entire structure
 ϕ_d = complex eigenvector (mode shape) for a damped mode of the structure
 ω = circular natural frequency (real) for the mode
 η = composite loss factor (real) for the entire structure

For lightly damped structures, the damped mode shape ϕ_d may be approximated by the real eigenvector ϕ obtained by solving the real, undamped eigenvalue problem.

Using this approximation ($\phi_d = \phi$) and equating the imaginary parts of Equation (20) to each other yields

$$\eta = \eta_d (\phi^T K_d \phi) / (\omega^2 \phi^T M \phi) \quad (21)$$

Since the real eigenvector ϕ satisfies

$$\omega^2 \phi^T M \phi = \phi^T K_T \phi \quad (22)$$

we obtain

$$\eta = \eta_d (\phi^T K_d \phi) / (\phi^T K_T \phi) \quad (23)$$

or

$$\eta = \eta_d (k_d / k_T) \quad (24)$$

where k_T is the generalized stiffness of the mode, and k_d is the contribution of

the viscoelastic material to the generalized stiffness. Since the generalized stiffness for a mode is equal to twice the elastic strain energy in the mode, Equation (24) may be interpreted as stating that the ratio of the composite loss factor η to the loss factor of the viscoelastic material is equal to the fraction of the total strain energy contained in the damping material.

More generally, for structures containing several damping materials with individual loss factors $\eta_1, \eta_2, \eta_3, \dots$, the composite loss factor for the structure is

$$\eta = \eta_1(k_1/k_T) + \eta_2(k_2/k_T) + \dots \quad (25)$$

where k_i is the contribution of the i th damping material to the total generalized stiffness k_T .

Equation (24) is implemented within the finite element procedure by performing an undamped eigenvalue analysis and extracting for each mode the total strain energy $2k_T$ and the strain energy $2k_d$ contained in the viscoelastic material. In the undamped analysis, the damping material is modeled and assigned a zero loss factor.

NASTRAN IMPLEMENTATION

With NASTRAN analysis, the specification of quadratic frequency dependence for part of a structure requires that the stiffness matrix for that part be available and that various scalar multiples of that matrix be combined with the original stiffness, mass, and damping matrices for the entire system.

A convenient way to obtain the stiffness matrix for a subset of elements (the viscoelastic material) in a structure is to specify a unit material damping constant ($g = 1$) on the material card for that substructure. In that case, the reference elastic stiffness matrix K_0 for the damping material is merely the NASTRAN data block K4GG. Thus, from Equation (8), the elastic stiffness matrix K_e for the rest of the structure (all material except the damping material) is

$$K_e = KGGX - K4GG \quad (26)$$

where KGGX is the NASTRAN data block containing the real part of the complete system stiffness matrix. With the use of NASTRAN data block terminology, Equations (14) - (16) then become

$$K^* = KGGX + (\alpha_0 - 1 + i\beta_0) K4GG \quad (27)$$

$$B^* = BGG + (\beta_1 - i\alpha_1) K4GG \quad (28)$$

$$M^* = MGG + (-\alpha_2 - i\beta_2) K4GG \quad (29)$$

where the new complex matrices K^* , B^* , and M^* replace the original matrices KGGX, BGG, and MGG, respectively. This replacement is effected with an ALTER to the rigid format. The scalar multipliers in Equations (27) - (29) are defined in NASTRAN using three complex parameters:

$$\left. \begin{aligned} \text{PARMK} &= (\alpha_0 - 1, \beta_0) \\ \text{PARMB} &= (\beta_1, -\alpha_1) \\ \text{PARMM} &= (-\alpha_2, -\beta_2) \end{aligned} \right\} \quad (30)$$

where the α 's and β 's are the coefficients of the quadratic curve fits in Equations (11) and (12).

Forced Response

For the calculation of forced time-harmonic response (NASTRAN's Rigid Format 8), an ALTER to effect Equations (27) - (29) would be sufficient to enforce quadratic frequency dependence of the properties of one material. The DMAP ALTER which implements these changes is shown in Figure 1. The first section (ALTER 41) replaces the original coefficient matrices with the new matrices K^* , M^* , and B^* defined in Equations (27) - (29). The other three sections replace NASTRAN's functional modules SMP1 and SMP2, which perform the static condensation (Guyan reduction) on the stiffness, mass, and damping matrices. These replacements are needed because SMP1 and SMP2 do not allow complex input.

```

ALTER 41 $ APR 84, R.F. 8, FREQ-DEP MATL
PARAM /**MPY*/NOBG/1/1 $ YES BGG
PARAM /**MPY*/NOK4GG/1/-1 $ NO K4GG
ADD KGGX,K4GG/KBAR//C,Y,PARMK $ NEW K
ADD MGG ,K4GG/MBAR//C,Y,PARMM $ NEW M
ADD BGG ,K4GG/BBAR//C,Y,PARMB $ NEW B
EQUIV KBAR,KGGX//MBAR,MGG//BBAR,BGG $ NEW K,B,M
PURGE K4GG $
ALTER 78,78 $ REPLACE SMP1 FOR COMPLEX K
UPARTN USET,KFF/KAAB,KOA,,KOO/*F*/A/*O* $
SOLVE KOO,KOA/GO/1/-1 $
MPYAD KOA,GO,KAAB/KAA/1 $
DIAGONAL KAA/AVEC/*COLUMN*/0. $ VECTOR OF ONES
ADD AVEC,/PVEC/(0.0,0.0) $ VECTOR OF ZEROS (P-VEC)
MERGE KAA,, ,PVEC,/KAASYM/-1//6 $ DUMMY MERGE FOR K
EQUIV KAASYM,KAA $ KAA TRAILER NOW SYMMETRIC
ALTER 80,80 $ REPLACE SMP2 FOR COMPLEX M
UPARTN USET,MFF/MAAB,MOA,,MOO/*F*/A/*O* $
MPYAD MOO,GO,MAA/TEMP1/1 $
MPYAD GO,TEMP1,MAAB/TEMP2/1 $
MPYAD MOA,GO,TEMP2/MAA/1 $
MERGE MAA,, ,PVEC,/MAASYM/-1//6 $ DUMMY MERGE FOR M
EQUIV MAASYM,MAA $ MAA TRAILER NOW SYMMETRIC
ALTER 83,83 $ REPLACE SMP2 FOR COMPLEX B
UPARTN USET,BFF/BAAB,BOA,,BOO/*F*/A/*O* $
MPYAD BOO,GO,BOA/TEMP3/1 $
MPYAD GO,TEMP3,BAAB/TEMP4/1 $
MPYAD BOA,GO,TEMP4/BAA/1 $
MERGE BAA,, ,PVEC,/BAASYM/-1//6 $ DUMMY MERGE FOR B
EQUIV BAASYM,BAA $ BAA TRAILER NOW SYMMETRIC
ENDALTER $

```

Figure 1 - DMAP ALTER for Rigid Format 8 for Time-Harmonic Response of Structures with Frequency-Dependent Material Properties

To summarize, the NASTRAN procedure for calculating the time-harmonic response of a structure with one frequency-dependent damping material is as follows:

1. Perform a least squares quadratic fit to one of the elastic moduli to determine the α 's and β 's in Equations (11) and (12). For viscoelastic materials (e.g., rubber), the shear modulus G is usually used, in which case

$$G(\omega) = G_0 \alpha(\omega) \quad (31)$$

and $\beta(\omega)$ is defined in Equation (10). G_0 is the reference material property and may be taken to be 1 psi. In Equation (10), $\eta(\omega)$ is the loss factor for the viscoelastic material.

2. Specify the material damping constant $g = 1$ and reference elastic properties (e.g., shear modulus $G = G_0$) on the material card for the viscoelastic material; specify the mass density and Poisson's ratios correctly. Specify $g = 0$ on the material card for the undamped material.
3. Perform frequency response analysis (Rigid Format 6) with the DMAP ALTER of Figure 1 and the parameters defined in Equation (30).

Loss Factors

Forced response predictions for structures with one damping material require only the replacement of the original K , M , and B matrices with their complex counterparts K^* , M^* , and B^* defined in Equations (27) - (29). However, the same replacement cannot be used to solve the complex eigenvalue problem (Rigid Format 7) to obtain damping, because the assumed time dependence is different between Rigid Formats 7 and 8. Specifically, for forced response calculations, NASTRAN's time dependence is of the form $e^{i\omega t}$, whereas in the complex eigenvalue problem, the time dependence is of the form e^{pt} for complex p . The modal strain energy (MSF) approach is a means of avoiding this difficulty, since only undamped natural frequencies are computed, in which case

$$\beta_0 = \beta_1 = \beta_2 = 0 \quad (32)$$

in Equations (27) - (30). A complex eigenvalue analysis is still required, however, since the damping matrix B^* is purely imaginary; K^* and M^* are both real.

To complete the calculation of the composite loss factor η in Equation (24), we first note that Equation (24) is equivalent to

$$\eta = \eta_d(\alpha k_0)/(k_e + \alpha k_0) \quad (33)$$

where k_0 is the generalized stiffness for the damping material with some reference level of material properties chosen (e.g., shear modulus $G = 1$ psi), and k_e is the generalized stiffness for the remaining material. Since α is frequency-dependent, it is convenient to let NASTRAN compute k_e and k_0 for each mode and to use a post processor to compute η for each mode.

The DMAP ALTER which implements all these changes in NASTRAN's complex eigenvalue analysis (Rigid Format 7) is shown in Figure 2. The first section (ALTER 41) replaces the original coefficient matrices with the new matrices K^* ,

M^* , and B^* defined in Equations (27) - (29). The second section (ALTER 80,80) is the replacement for NASTRAN's static condensation module SMP2. The third section (ALTER 127) computes the generalized stiffnesses k_0 and k_e for each mode. These generalized stiffnesses as well as the list of eigenvalues (contained in data block CLAMA) are written on an OUTPUT2 file for postprocessing to evaluate η for each mode according to Equation (33).

To summarize, the NASTRAN procedure for calculating loss factors of structures with one frequency-dependent damping material is as follows:

1. Perform a least squares quadratic fit to one of the elastic moduli to determine the α 's in Equation (11). For damping materials (such as rubber), the shear modulus G is usually used; see Equation (31).
2. Specify the material damping constant $g = 1$ and reference elastic properties (e.g., shear modulus $G = G_0$) on the material card for the viscoelastic material; specify the mass density and Poisson's ratios correctly. Specify $g = 0$ on the material card for the undamped material.
3. Perform complex eigenvalue analysis (Rigid Format 7) with the DMAP ALTER of Figure 2. Use the parameters defined in Equation (30) with $\beta_0 = \beta_1 = \beta_2 = 0$. Retain the OUTPUT2 file (UT1).

```

ALTER 41 $ APR 84, R.F. 7, FREQ-DEP MATL
PARAM /*MPY*/NOBGG/1/1 $ YES BGG
PARAM /*MPY*/NOK4GG/1/-1 $ NO K4GG
DIAGONAL KGGX/IDENTG/*SQUARE*/0. $ G SET IDENTITY MATRIX
MPYAD IDENTG,KGGX,K4GG/KMAT2/1/1/-1 $
ADD,KGGX,K4GG/KBAR//C,Y,PARMK $ NEW K
ADD MGG ,K4GG/MBAR//C,Y,PARMM $ NEW M
ADD BGG ,K4GG/BBAR//C,Y,PARMB $ NEW B
EQUIV KBAR,KGGX//MBAR,MGG//BEAR,BGG $ NEW K,B,M
ALTER 80,80 $ REPLACE SMP2 FOR COMPLEX B
DIAGONAL KAA/AVEC/*C COLUMN*/0. $ VECTOR OF ONES
ADD AVEC,/PVEC/(0.0,0.0) $ VECTOR OF ZEROS (P-VEC)
UPARTN USET,BFF/BAAB,BOA,,BOO/*F*/A*/O* $
MPYAD BOO,GO,BOA/TEMP3/1 $
MPYAD GO,TEMP3,BAAB/TEMP4/1 $
MPYAD BOA,GO,TEMP4/BAA/1 $
MERGE BAA,,,PVEC,/BAASYM/-1//6 $ DUMMY MERGE FOR B
EQUIV BAASYM,BAA $ BAA TRAILER NOW SYMMETRIC
ALTER 127 $ GENERALIZED STIFFNESSES
SMPYAD CPHIP,K4GG ,CPHIP.,,/GKMAT1/3////1/1 $
SMPYAD CPHIP,KMAT2,CPHIP.,,/GKMAT2/3////1/1 $
DIAGONAL GKMAT1/K1 $
DIAGONAL GKMAT2/K2 $
MATFRN K1,K2,CLAMA,,$ $
OUTPUT2 K1,K2,CLAMA,,$ $
ENDALTER $

```

Figure 2 - DMAP ALTER for Rigid Format 7 for Loss Factors of Structures with Frequency-Dependent Material Properties

DISCUSSION

A finite element procedure has been described for predicting the loss factors of structures to which frequency-dependent viscoelastic damping treatments have been applied. This procedure, used on the simple test problem of a three-layer plate, yielded predictions similar to those of a generally-accepted analytical procedure for infinite plates.

The power of the finite element procedure, however, is that it is not restricted to such simple geometry but can readily handle such complications as different boundary conditions, variable plate thickness, and localized treatments. None of these effects can be treated by the infinite plate theory.

REFERENCES

1. Vandergraft, J.S., Introduction to Numerical Computations, second edition, Academic Press, New York, 1983.
2. Ungar, E.E., and E.M. Kerwin, Jr., "Loss Factors of Viscoelastic Systems in Terms of Energy Concepts," J. Acoust. Soc. of Amer., vol. 34, no. 7, July 1962, pp. 954-957.

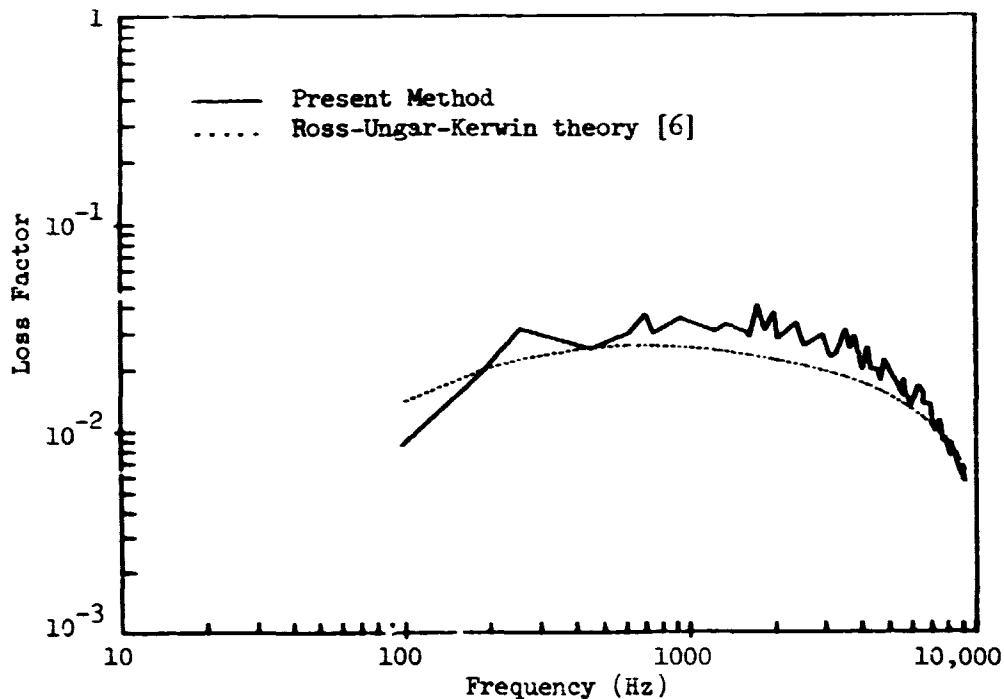


Figure 4 - Comparison of Loss Factors for Sandwich Plate as Predicted by Present Finite Element Method and by Ross-Ungar-Kerwin Theory [6]

4. With a postprocessor, read the UTL file and compute for each mode the loss factor η according to Equation (33).

EXAMPLE

The procedure for calculating composite loss factors will be illustrated for the three-layer sandwich plate shown in Figure 3. We assume that the shear modulus G and loss factor η for the middle layer are given by

$$G(f) = 10^4 + 9f \quad (\text{psi}) \quad (34)$$

$$\eta(f) = 0.5 - (4 \times 10^{-5})f \quad (35)$$

where f is frequency in Hz. These relations imply considerable frequency dependence, since between zero and 10,000 Hz, G varies by a factor of ten, and η varies by a factor of five. The top and bottom layers are made of steel.

The plate was modeled with three layers of 20-node isoparametric ("brick") finite elements. A $13 \times 5 \times 3$ mesh of elements was used. These elements were used rather than plate elements because of interest in fairly thick plates of variable thickness, in which case the engineering plate theory no longer applies. Guyan reduction was applied to this model in such a way that the only degrees of freedom retained were the normal translations at the corner nodes of each element on the top and bottom faces.

The composite loss factor computed using the finite element procedure described in the preceding sections is compared in Figure 4 with a calculation based on classical infinite plate theory presented by Ross, Ungar, and Kerwin [6]. That figure indicates a good agreement between the two predictions. The infinite plate theory is generally thought to provide a reasonably accurate prediction of the composite loss factor for plates with this simple geometry, and hence serves as a good check on the finite element result.

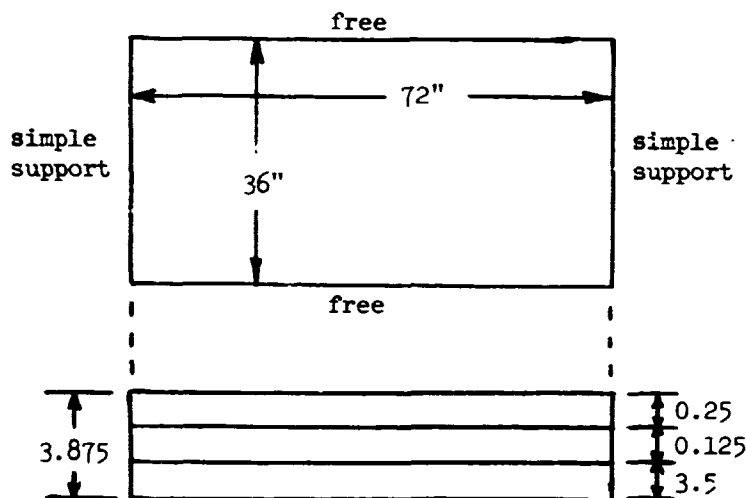


Figure 3 - Three-Layer Sandwich Plate Used for Calculating Loss Factors

3. Johnson, C.D., D.A. Kienholz, and L.C. Rogers, "Finite Element Prediction of Damping in Beams with Constrained Viscoelastic Layers," The Shock and Vibration Bulletin, bull. 51, part 1, May 1981, pp. 71-81.
4. Johnson, C.D., and D.A. Kienholz, "Finite Element Prediction of Damping in Structures with Constrained Viscoelastic Layers," AIAA J., vol. 20, no. 9, Sept. 1982, pp. 1284-1290.
5. Johnson, C.D., and D.A. Kienholz, "Prediction of Damping in Structures with Viscoelastic Materials," Proc. 1983 MSC/NASTRAN User's Conference, Los Angeles, California, March 1983.
6. Ross, D., E.E. Ungar, and E.M. Kerwin, Jr., "Damping of Plate Flexural Vibrations by Means of Viscoelastic Laminae," in Structural Damping, edited by J.E. Ruzicka, The American Society of Mechanical Engineers, New York, 1959, pp. 49-87.

DIRECT TRANSIENT ANALYSIS OF A FUZE ASSEMBLY BY AXISYMMETRIC SOLID ELEMENTS

Chung C. Dai and Jackson C. S. Yang*
Advanced Technology & Research, Inc.
Burtonsville, MD 20866

John Titus
Harry Diamond Laboratory
Adelphi, MD 20783

ABSTRACT

A fuze assembly, which consists of three major parts, i.e., nose, collar and sleeve, was designed to survive severe transverse impact giving a maximum base acceleration of 20,000 G. Experiments showed that hoop failure occurred in the collar after the impact. They also showed that by bonding the collar to the nose, the collar was able to survive the same impact. To find out the effectiveness of the bonding quantitatively, axisymmetric solid elements TRAPAX and TRIAAX were used in modelling the fuze and direct transient analysis was performed. The dynamic stresses in selected elements on the bonded and unbonded collars were compared. The peak hoop stresses in the unbonded collar were found to be up to three times higher than those in the bonded collar. NASTRAN results successfully explained the observed hoop failure in the unbonded collar. In addition, static and eigen value runs were performed as checks on the models prior to the transient runs. Their results are compared with experiments. Comments on the use of the MPCAX cards, the existence and contributors of the calculated first several nearly identical natural frequencies, are also addressed.

INTRODUCTION

The M732 E2 Artillery Proximity Fuze comprises an aluminum fuze body which houses a safety and arming module, detonator bulkhead, and power supply aft of a center bulkhead. Forward of the bulkhead is the fuze processor electronics and loop oscillator. The oscillator is housed in a 30% glass reinforced modified Polyphenylene Oxide (PPO) nose cone which is secured to the fuze body with a 30% glass reinforced PPO threaded retaining collar. See Figures 1 and 2.

When a projectile is fired from a gun, the fuze is subjected to side loads approaching 20,000 G's. In the laboratory, a machine was developed to simulate this loading. The fuze is secured to a rail guided steel fixture which is struck from the side by a steel weight. The impact is tailored to give a 20,000 G peak lateral acceleration with a 30 fps velocity change.

While fuzes at ambient temperature experienced no failures when subjected to the test, fuzes which were temperature conditioned at -40°C failed without exception. The major failure mode, named hoop failure, appeared to be hoop stress on the retaining collar causing a longitudinal crack from end to end. See Figure 3.

It was discovered that by solvent bonding the retaining collar to the nose cone during assembly, the low temperature failures could be avoided. Since the mechanism by which the solvent bond alleviated the problem was not well understood nor was the safety factor of the bond known, it was feared that future modifications to the fuze could not be evaluated with respect to the impact on the fuze joint integrity. Therefore, NASTRAN was used to model the forward section of the fuze in an attempt to better understand the behavior of the current design, and better predict the behavior of future designs.

NASTRAN MODEL

The given fuze forward section consists of three major parts, i.e., nose, collar and sleeve. As depicted in Figures 4a, 4b, and 4c, 105 TRAPAX and 9 TRIAAX elements were used to model this fuze and its interior electronic parts. These elements are inter-connected at 180 different rings or circles. Static and eigen value analyses were performed prior to the final transient runs. Numerical results from the static and eigen value runs were carefully examined and compared with the available experiment data. Constraint conditions and boundary conditions had been modified accordingly. We will discuss in more detail later.

TEST MODEL I

A cantilevered, hollow slender cylinder, as depicted in Figure 5a, was modelled by TRAPAX elements as a preliminary study. Stress analysis of this cylinder was performed. Axial pressure load or concentrated transverse tip loading was separately applied. Numerical results from these test cases provided basic understanding on TRAPAX's behavior and characteristics. Axial pressure loading condition was first considered, see Figure 5b. As expected, NASTRAN results showed that the cylinder's cross sections were displaced uniformly and axial stress was developed uniformly across each cross section.

Figure 5c shows the transverse tip loading condition. The cylinder was modelled by regular 8×2 , 16×2 , 32×1 , 32×2 , 64×1 meshes. Both the tip deflection and the bending stress at point A were checked for convergence with respect to mesh refinement. As noted in Table 1, with the same number of elements, 64×1 mesh gave better results than 32×2 mesh. Based on this observation, we used only one layer across the thickness of the real model.

TEST MODEL II

A cantilevered, hollow slender cylinder of different size (Figure 6) was used in the remaining preliminary studies. It was modelled also by TRAPAX elements but with 4×1 or 5×1 mesh. This model served for testing NASTRAN rigid formats 3, 9, and 12, simulating the prescribed base acceleration, and also for testing NASTRAN checkpoint and restart features.

Free vibration analysis was performed on the cantilevered hollow cylinder in Figure 6a. Different frequency ranges were specified requesting the extraction of natural frequencies and modes.

Given $V = 30$ ft/sec after the impact and the maximum acceleration of 20,000g, the duration of the impulse depends on the assumption of its shape. For a $\sin\omega t$ shaped impulse, the duration is about 70×10^{-6} sec. For a $\sin^2\omega t$ shaped impulse, the duration is about 90×10^{-6} sec. Impulses of both shapes were tested on Model II. However, only the $\sin^2\omega t$ shaped impulse was employed in the analysis of the real model because it simulates the real impulse more closely.

Several schemes to input the prescribed base acceleration $a(t)$ were also carefully examined. First, a nearly rigid layer with huge mass M was attached to the bottom of the original cylinder. Dynamic force $F(t) = Ma(t)$ was then applied to this layer in several ways to achieve the desired prescribed base motion. The dynamic force can be directly applied to the COSINE term of the ring No. 2 in Figure 6b. It can also be applied, using POINTAX cards, at selected points in the bottom layer. As observed in the test runs, both approaches gave the same results. The "POINTAX" approach was taken on the real model.

The appropriate E/ρ ratio was determined to be of the order of 10^{20} . This specific ratio gave an uniform base acceleration as desired. In addition, both CONEAX and TRAPAX elements were tested out as the base layer. The TRAPAX element was employed in the real model.

Modal transient analysis was performed on this test model. However, as noted from the eigen value analysis on the real model, there are a large number of natural modes in the low frequency range. Also, the impulse duration is so short that modes with extremely high frequencies are expected to participate in the dynamic response. Obviously, modal transient approach will not be accurate without using a large number of modes, which in turn will make it extremely time-consuming. Therefore, direct transient approach was taken for the analysis of real model.

STATIC ANALYSIS

Static analysis of both bonded and unbonded cases were performed as checks on the fuze model. The load condition considered was that of 100 lbs. transversely applied at node 9.

For this loading case, deflections at the load point and nodes 17, 21, are listed for different choices of harmonic terms. (See Table 2) Based on its convergence characteristics, AXIC = 3 was specified for the transient analysis. This means one constant and three harmonic functions were combined to describe the deformation field along the circumferential direction. Stress distribution in different parts were examined, and the MPCAX cards were modified accordingly to achieve appropriate constraints between nose, collar and plate.

In order to calibrate the model, simple experiments were devised to perform static tests on the fuze nose cones. A force gage was used to apply a static load onto the tip of the fuze. The fuze was mounted in a rigid base and a dial indicator was used to record the fuze deflection at the point of the load. The test setup is shown in Figure 7.

Loads were applied near the tip of the fuze, incrementing the load from 20 lbs. to 140 lbs. and recording the deflection of each increment. This test was performed for bonded sample of the fuze. Comparison of NASTRAN and experiment results is in Table 3. Note that the noticeable differences may have been caused by the fact that the tip of the force gage made a slight indentation in the surface of the nose cone.

EIGEN VALUE ANALYSIS

Eigen value analysis were performed to further check the appropriateness of the NASTRAN model. MPCAX conditions between nose-collar-plate were repeatedly examined and modified. The final arrangement of these conditions is listed in Table 4. This specific arrangement induces only relatively low stress in the plate while maintaining stability of the model. It is worth mentioning that in the seventh field of the MPCAX Card, the HID number should take the form of (Integer ≥ 0) instead of (Integer > 0). Otherwise, undesirable rigid body modes may be present in the model.

Ten fundamental frequencies and modes were extracted for both bonded and unbonded cases. As listed in Table 5, the first 9 eigen values of both cases are exactly the same. Also from Table 5, the lowest four frequencies are very close together at 30 cps. It was identified, very interestingly, that each harmonic contributed to one of them.

DIRECT TRANSIENT ANALYSIS

Transient responses from $t = 0$ sec to $t = 270 \times 10^{-6}$ sec, which was three times the impulse duration, were obtained for both bonded and unbonded cases. Solution convergence with respect to different time steps is listed in Table 6. $\Delta t = 2 \times 10^{-6}$ sec was chosen for the time increment in the analysis. The base displacement time history compared very well with the prescribed one. The dynamic stresses in the plane of impact in elements 104 and 105 were plotted and compared between both cases (see Figures 8-11).

Figures 8 and 10 show the hoop stress time histories of both cases. The peak hoop stress in unbonded collar is up to about three times higher than that in the bonded collar. This explains the hoop failure in the unbonded collar as was observed from experiments.

Figures 9 and 11 show the axial stress time histories of both cases. The peak axial stress in bonded collar is significantly higher than that in the unbonded collar.

CONCLUSION

The NASTRAN results presented in Figures 8 through 11 lead to the following conclusion:

By bonding the nose and the collar, the nose joint will take dynamic load mainly in the form of axial stress. The peak hoop stress experienced in the bonded collar will thusly be reduced by a factor of 4. Hence, the hoop failure was effectively avoided in the bonded collar.

TABLE 1. SOLUTION CONVERGENCE WITH RESPECT TO MESH REFINEMENT

MESH	ASPECT RATIO	TIP DEFLECTION	BENDING STRESS AT POINT A
8 x 2	7.5	0.001832	---
16 x 2	3.75	0.003029	798
32 x 1	0.94	0.003568	2151
32 x 2	1.875	0.003631	2085
64 x 1	0.47	0.003775	2314
ANALYTICAL	----	0.003918	2292

TABLE 2. CONVERGENCE OF LATERAL DEFLECTION
WITH RESPECT TO THE NUMBER OF HARMONICS (BONDED COLLAR)

NO. OF HARMONICS	LATERAL DEFLECTION		
	NODE 9	NODE 17	NODE 21
3	-0.00676	-0.00467	-0.00375
4	-0.00737	-0.00467	-0.00375
7	-0.00767	-0.00467	-0.00375

TABLE 3. COMPARISON OF STATIC RESULTS
(TRANSVERSE LOAD AT 0.27" FROM NOSE TIP)

CASE	EXPERIMENT	NASTRAN
BONDED	-0.014	-0.00676
UNBONDED	-0.020	-0.00821

TABLE 4. CONSTRAINT CONDITIONS ON HARMONICS
BETWEEN NOSE, COLLAR AND PLATE

CONSTRAINED RING PAIRS		BONDED			UNBONDED		
		r	θ	z	r	θ	z
35	235	0-3	0-3	0-3	0-3	0-3	0-3
37	237	0-3	0-3	0-3	0-3	0-3	0-3
40	240	0-3	0-3	0-3	0-3	0-3	0-3
43	243	0-3	0-3	0-3	0-3	0-3	0-3
46	246	0-3	0-3	0-3	0-3	0-3	0-3
49	249	0-3	0-3	0-3	0-3	0-3	0-3
52	252	0-3	0-3	0-3	0-3	0-3	0-3
55	255	0-3	0-3	0-3	0-3	0-3	0-3
58	258	0-3	0-3	0-3	0-3	---	0-3
60	260	0-3	0-3	0-3	0-3	---	0-3
63	263	0-3	0-3	0-3	0-3	---	0-3
64	364	---	---	0	---	---	0
65	365	0,1	---	0,1	0,1	---	0,1
70	370	---	---	0,1	---	---	0,1

EIGEN VALUE ANALYSIS BONDED NOSECONE

REAL EIGENVALUES

MODE NO.	EXTRACTION ORDER	EIGENVALUE	RADIAN FREQUENCY	CYCLIC FREQUENCY
1	6	3.611820E+04	1.900479E+02	3.024706E+01
2	5	3.626425E+04	1.904317E+02	3.030815E+01
3	7	3.642207E+04	1.908457E+02	3.037402E+01
4	4	3.648683E+04	1.910153E+02	3.040102E+01
5	2	9.198356E+04	3.032878E+02	4.326976E+01
6	1	1.029579E+05	3.208706E+02	5.106813E+01
7	3	1.211922E+05	3.481267E+02	5.540608E+01
8	9	2.205529E+05	4.686306E+02	7.474403E+01
9	10	3.234188E+05	5.686992E+02	9.051129E+01
10	9	3.374114E+05	5.808713E+02	9.244855E+01

EIGEN VALUE ANALYSIS UNBONDED NOSECONE

REAL EIGENVALUES

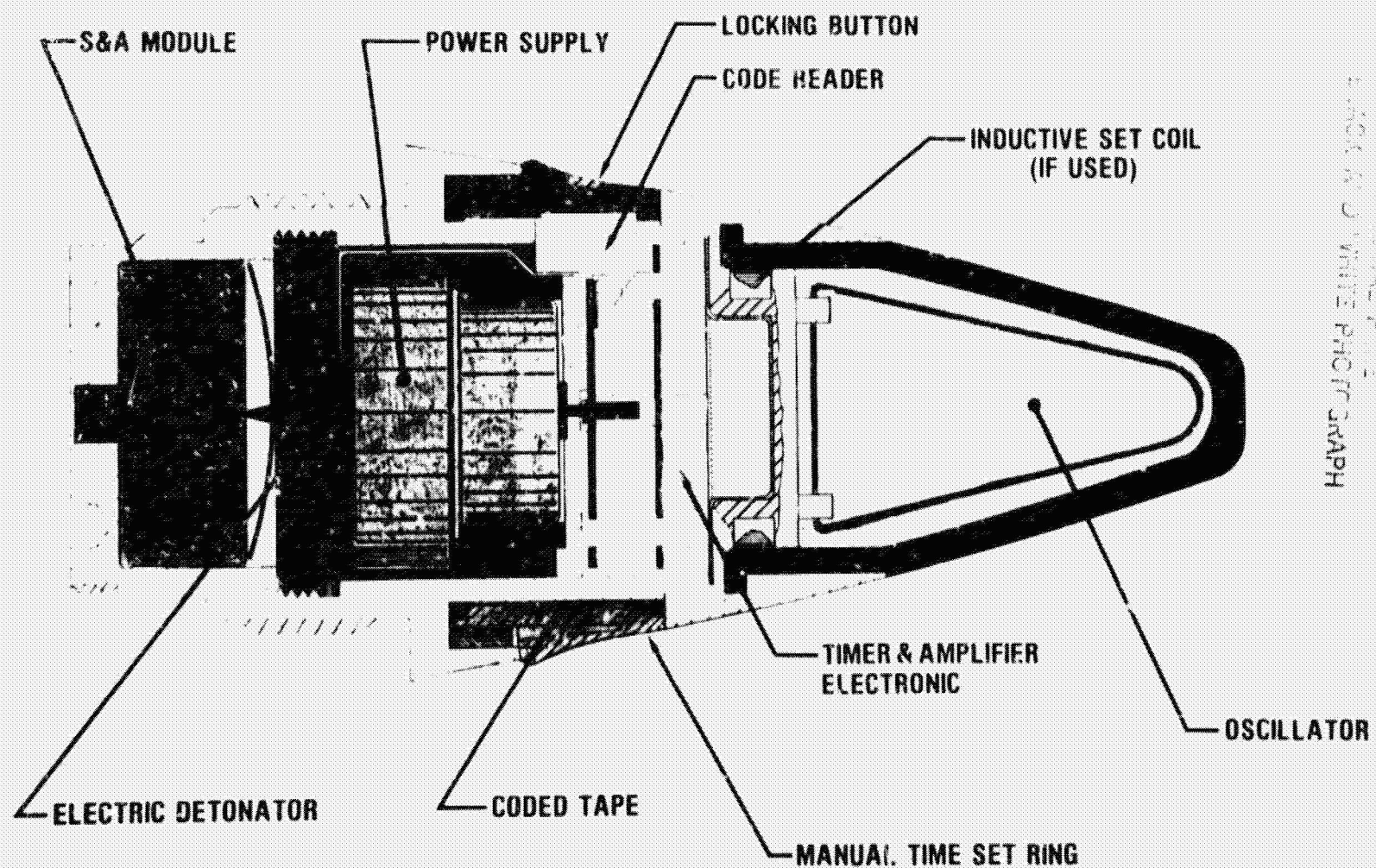
MODE NO.	EXTRACTION ORDER	EIGENVALUE	RADIAN FREQUENCY	CYCLIC FREQUENCY
1	6	3.611820E+04	1.900479E+02	3.024706E+01
2	5	3.626425E+04	1.904317E+02	3.030815E+01
3	7	3.642207E+04	1.908457E+02	3.037402E+01
4	4	3.648683E+04	1.910153E+02	3.040102E+01
5	2	9.198356E+04	3.032878E+02	4.326976E+01
6	1	1.029579E+05	3.208706E+02	5.106813E+01
7	3	1.211922E+05	3.481267E+02	5.540608E+01
8	9	2.205529E+05	4.686306E+02	7.474403E+01
9	10	3.234188E+05	5.686992E+02	9.051129E+01
10	9	3.246078E+05	5.697437E+02	9.067752E+01

TABLE 5. FIRST TEN NATURAL FREQUENCIES OF FUZE EXTRACTED FROM NASTRAN

TABLE 6. CONVERGENCE OF TRANSIENT SOLUTIONS WITH
RESPECT TO TIME STEP SIZE

BASE MOTION	$\Delta t = 4 \mu \text{ sec}$	$\Delta t = 2 \mu \text{ sec}$	$\Delta t = 1 \mu \text{ sec}$	$\Delta t = 0.5 \mu \text{ sec}$
Acceleration At:				
$t = 8 \mu \text{ sec}$	6.7×10^5	6.08×10^5	5.98×10^5	5.92×10^5
$t = 10 \mu \text{ sec}$	---	9.22×10^5	9.13×10^5	9.09×10^5
Displacement At:				
$t = 8 \mu \text{ sec}$	5.53×10^{-6}	3.77×10^{-6}	3.47×10^{-6}	3.4×10^{-6}
$t = 10 \mu \text{ sec}$	---	8.63×10^{-6}	8.17×10^{-6}	8.06×10^{-6}

FIGURE 1 ADVANCED PROX FUZE CONCEPT



440

ORIGINAL PHOTOGRAPH
BY
W. J. WHITE

ORIGINAL PAGE
COLOR PHOTOGRAPH

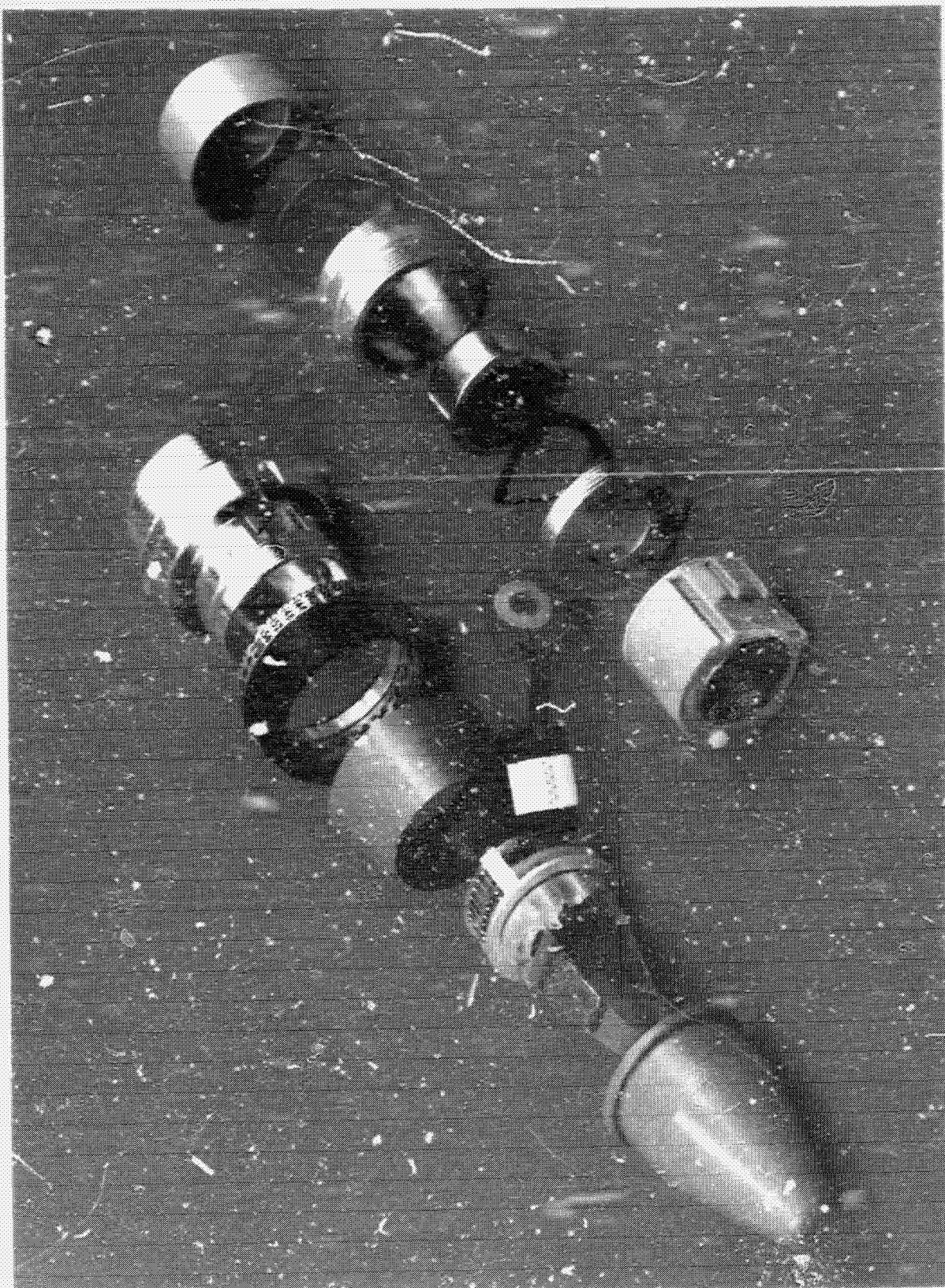


FIGURE 2

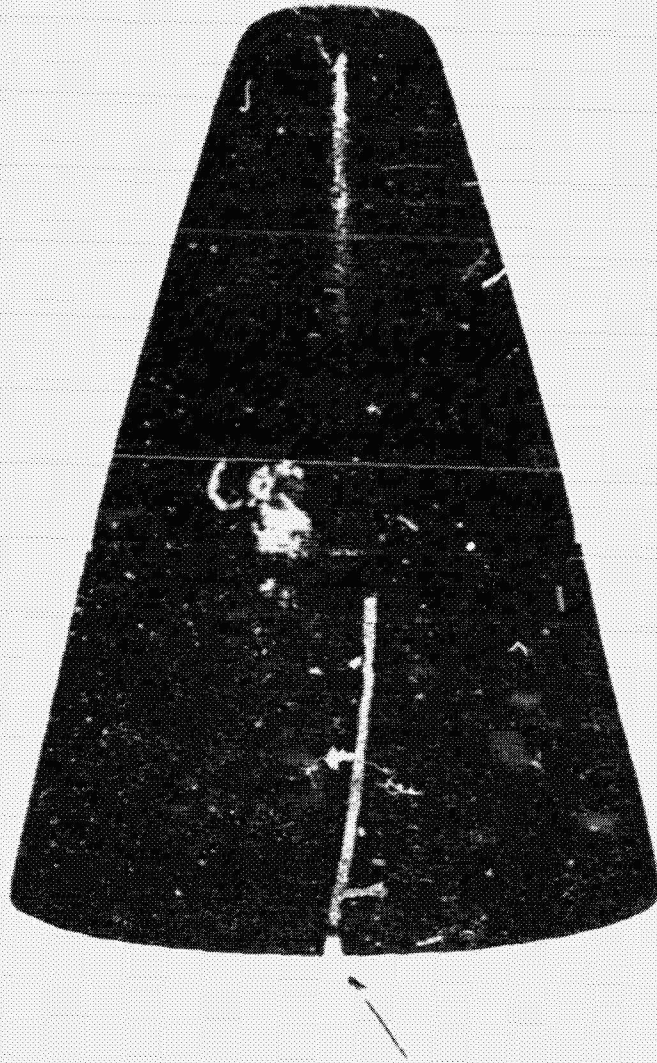


Figure 3 - Crack in the Retaining Collar

ORIGINAL PAGE
BLACK AND WHITE PHOTOGRAPH

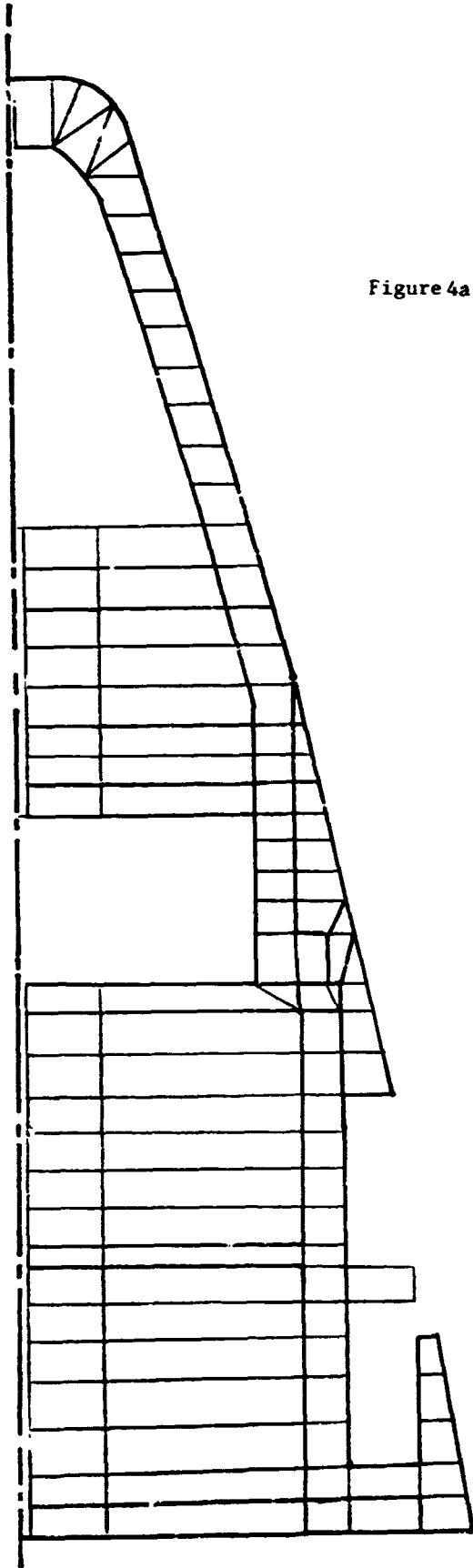


Figure 4a - Finite Element Mesh
Of The Fuze Assembly

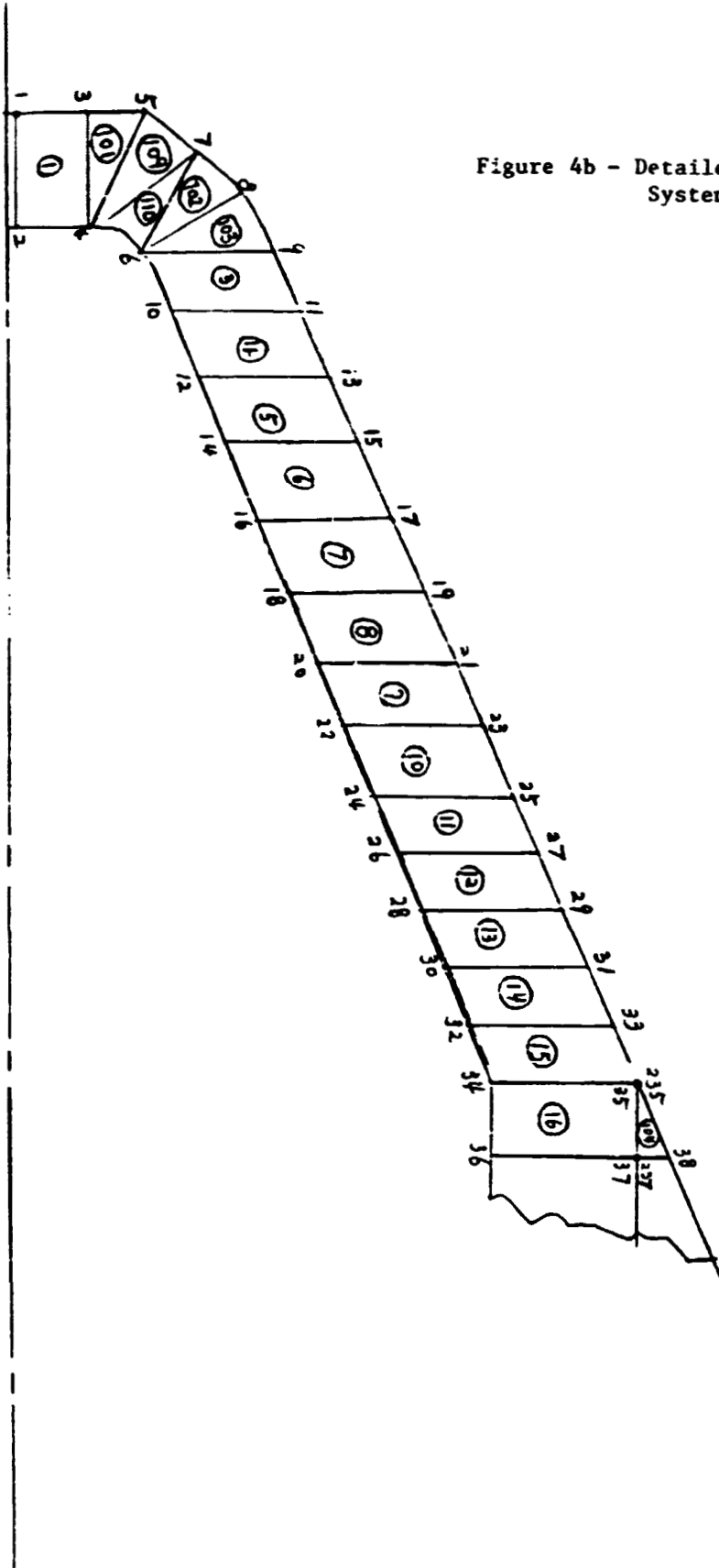
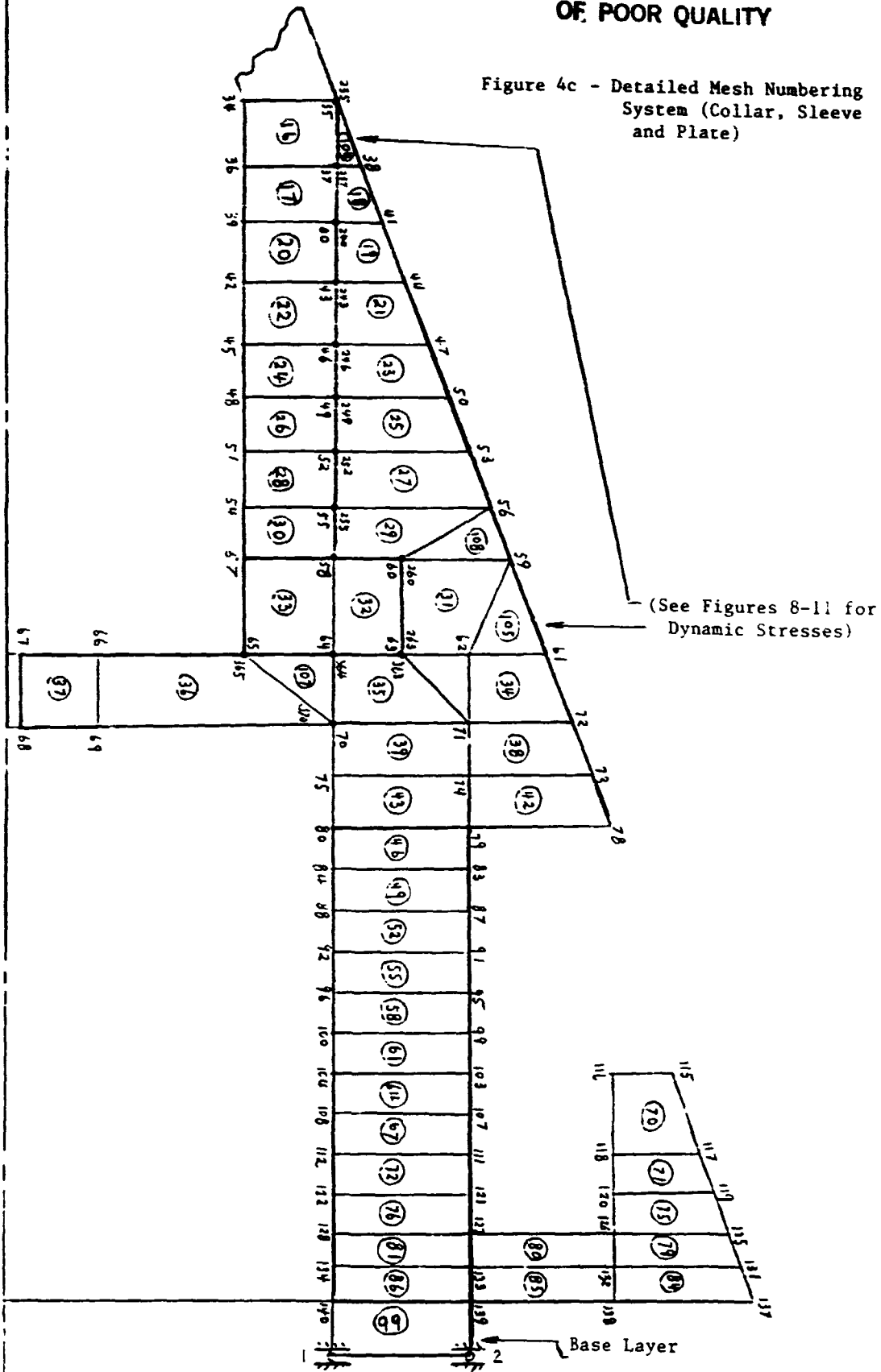


Figure 4b - Detailed Mesh Numbering System (Ncse)

ORIGINAL PAGE IS
OF POOR QUALITY

Figure 4c - Detailed Mesh Numbering
System (Collar, Sleeve
and Plate)



ORIGINAL PAGE IS
OF POOR QUALITY

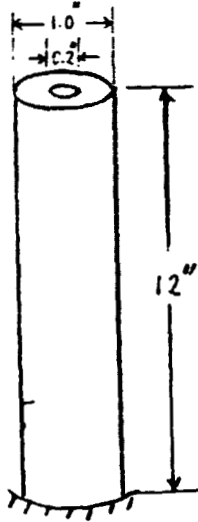


Figure 5a - Test Model I

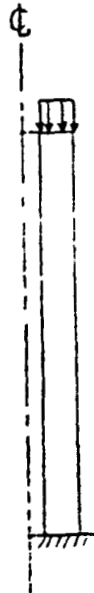


Figure 5b - Axial Pressure Loading
Condition

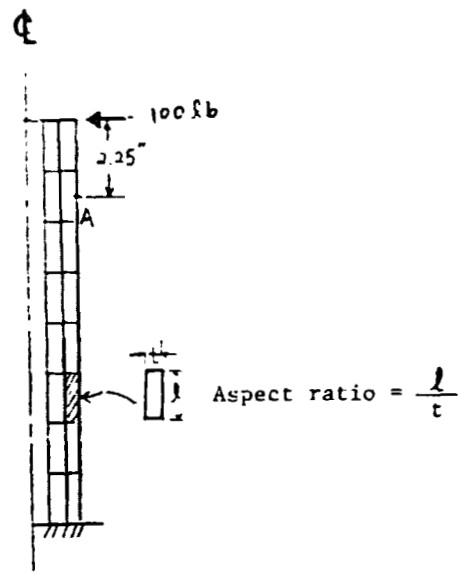


Figure 5c - Transverse Tip Loading
Condition (8 x 2 Mesh)

ORIGINAL PAGE IS
OF POOR QUALITY

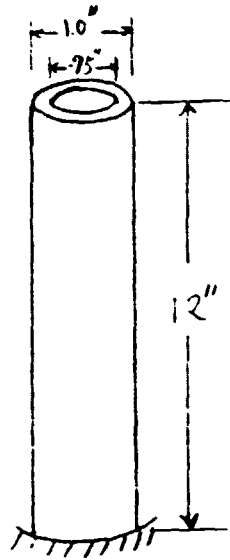


Figure 6 - Test Model II

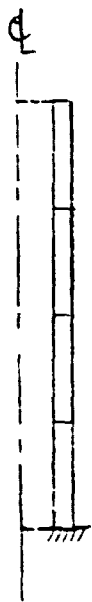


Figure 6a - FEM Model For
Free Vibration Analysis
(4 x 1 Mesh)

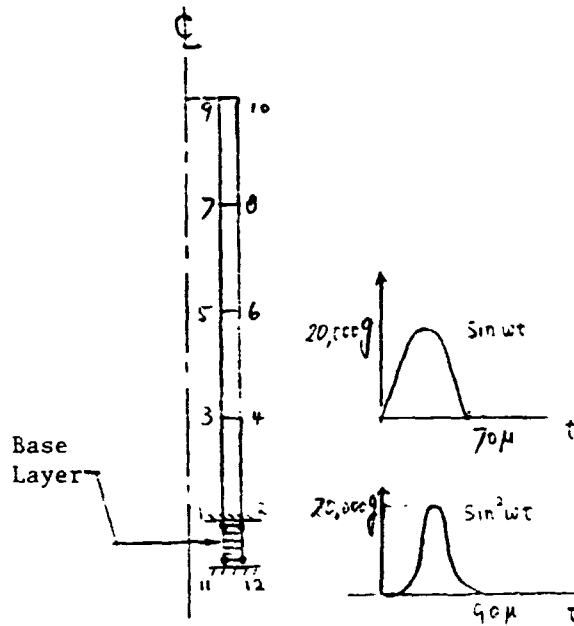


Figure 6b - FEM Model And Base
Excitations Transient Analysis
(5 x 1 Mesh)

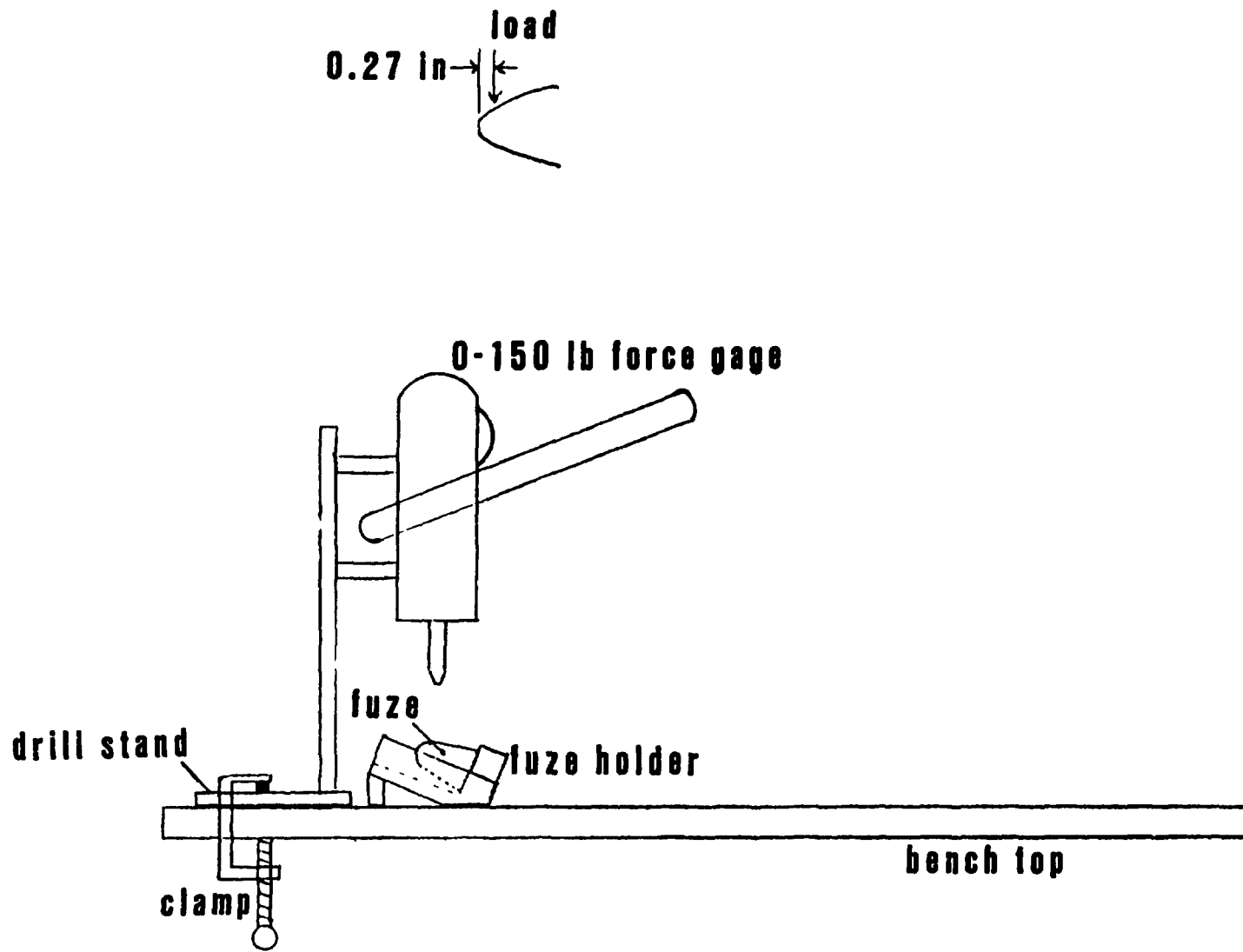


Figure 7. Test equipment setup

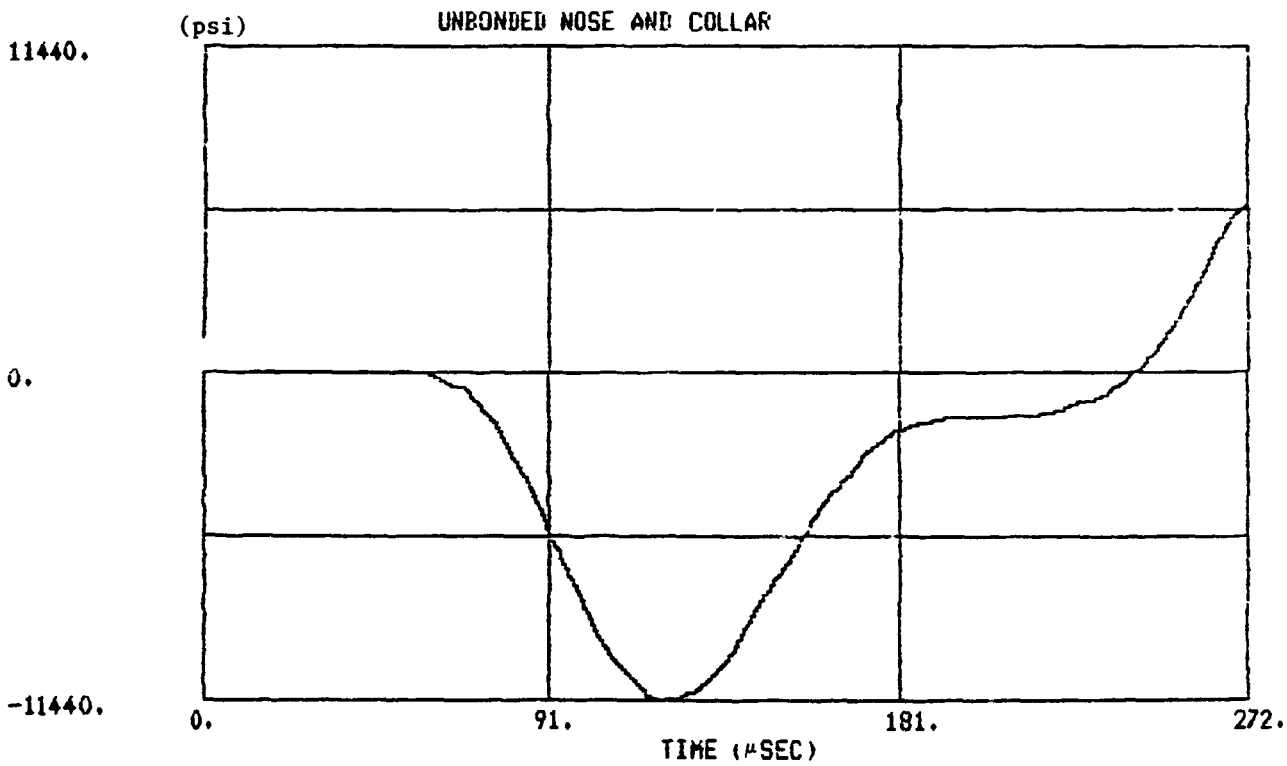
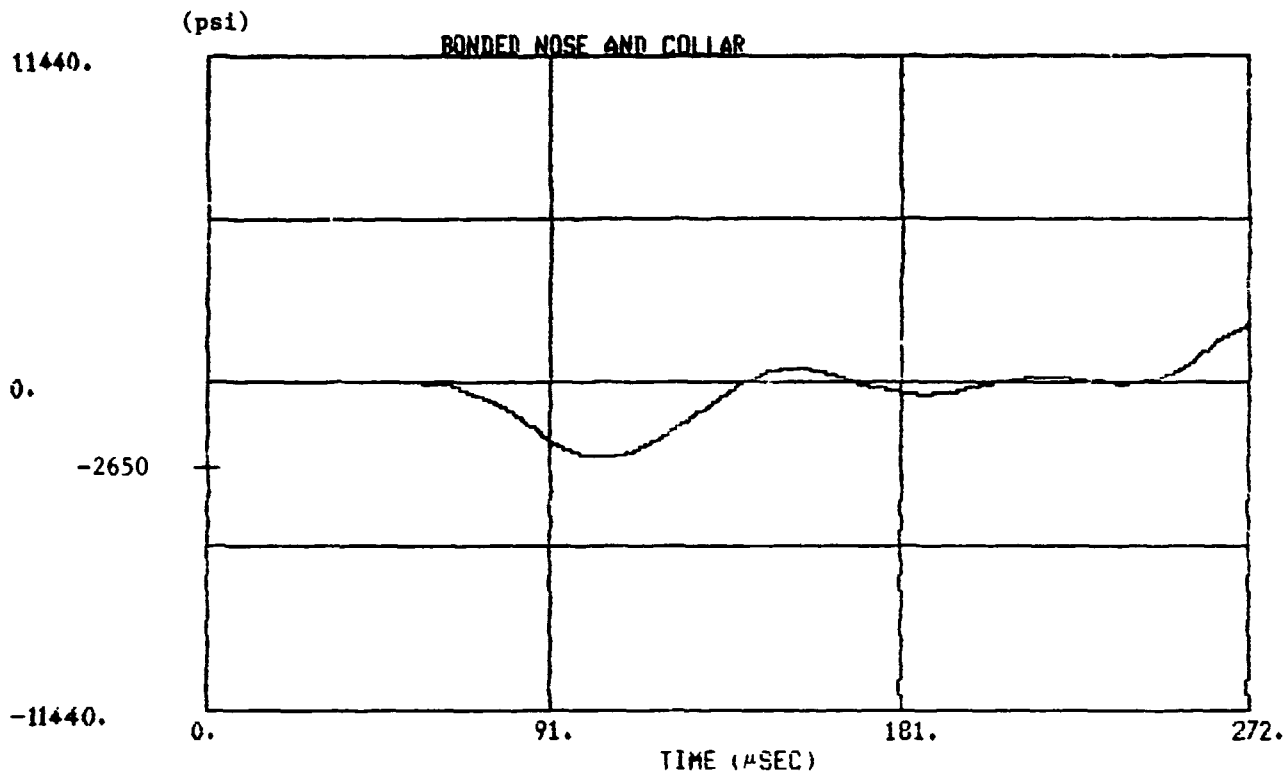


Figure 8 - Dynamic Hoop Stresses (Element 104)

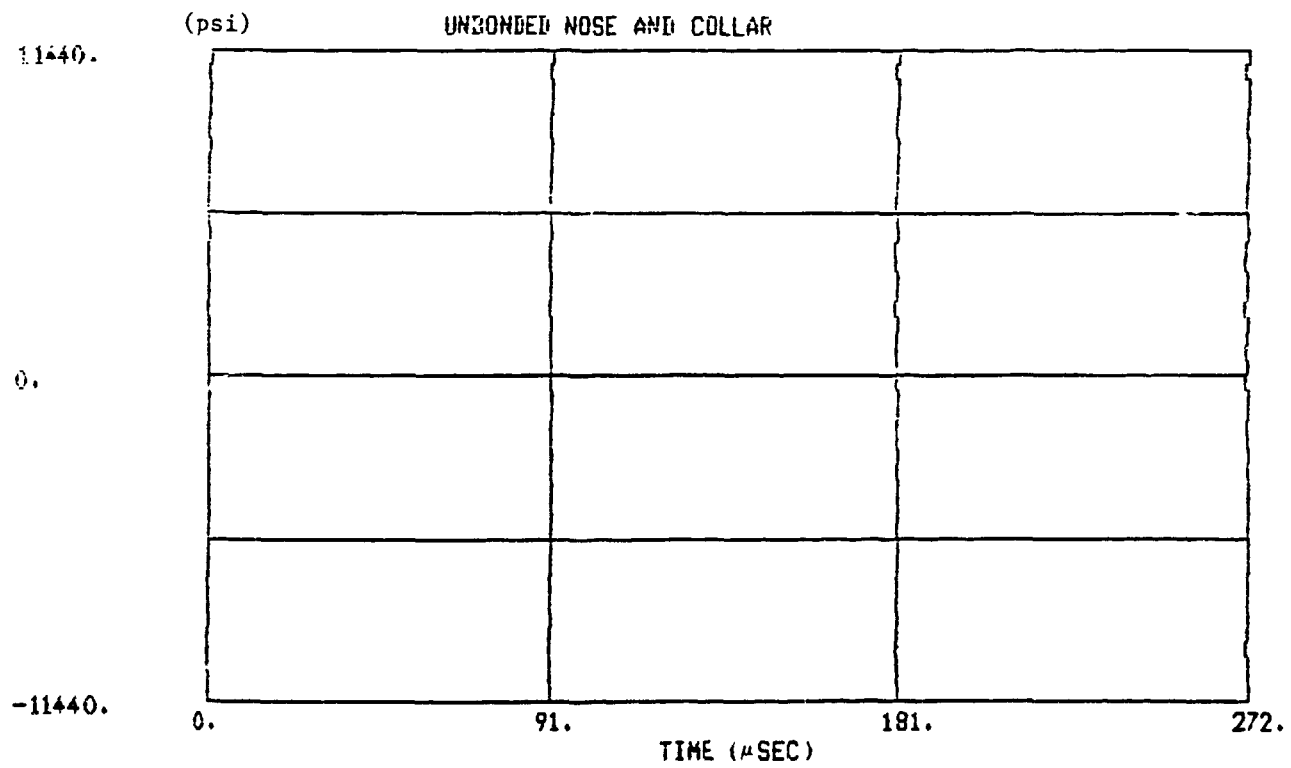
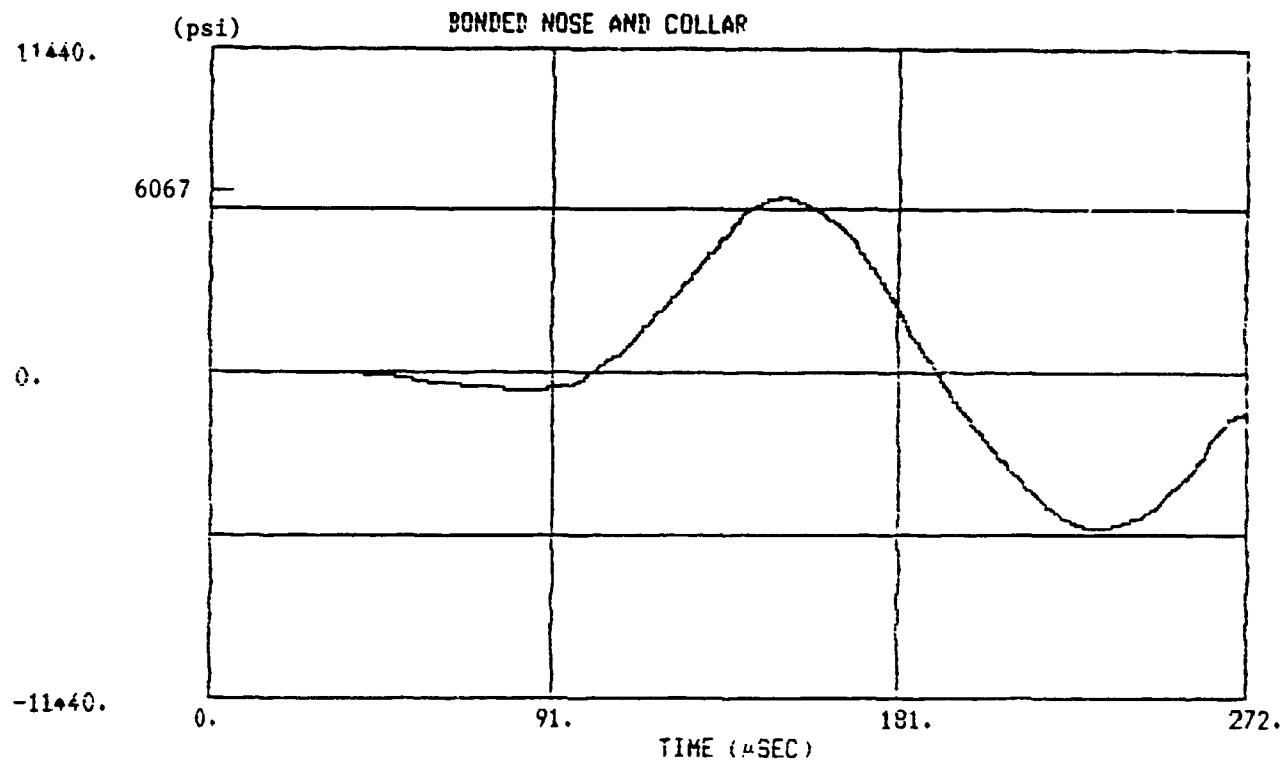


Figure 9 - Dynamic Axial Stresses (Element 104)

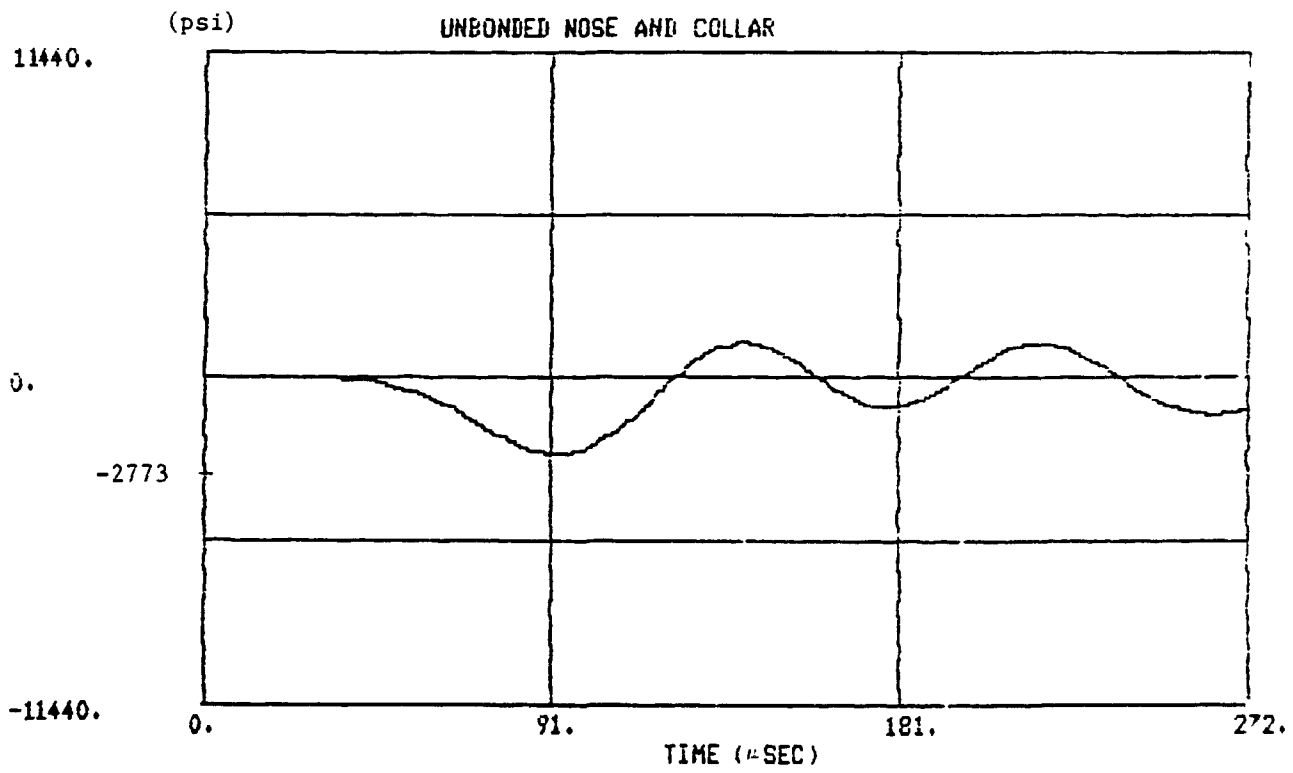
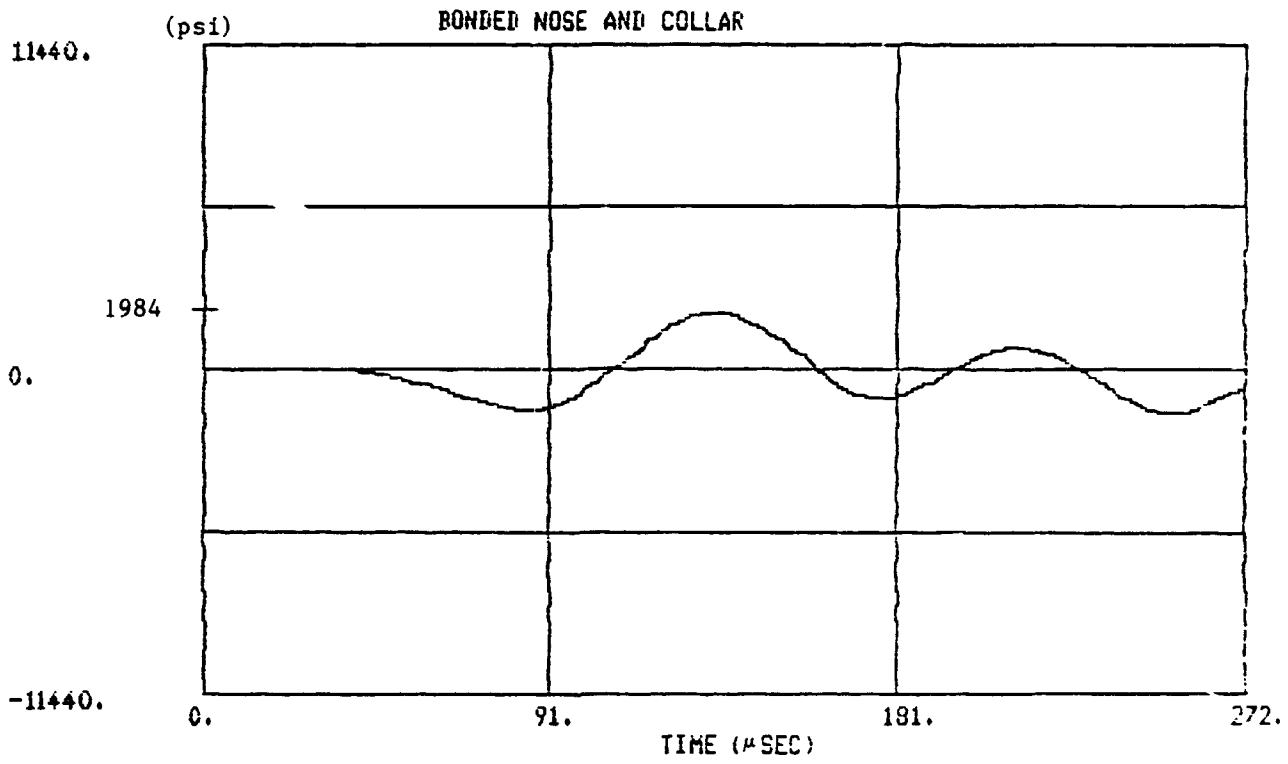


Figure 10 - Dynamic Hoop Stresses (Element 105)

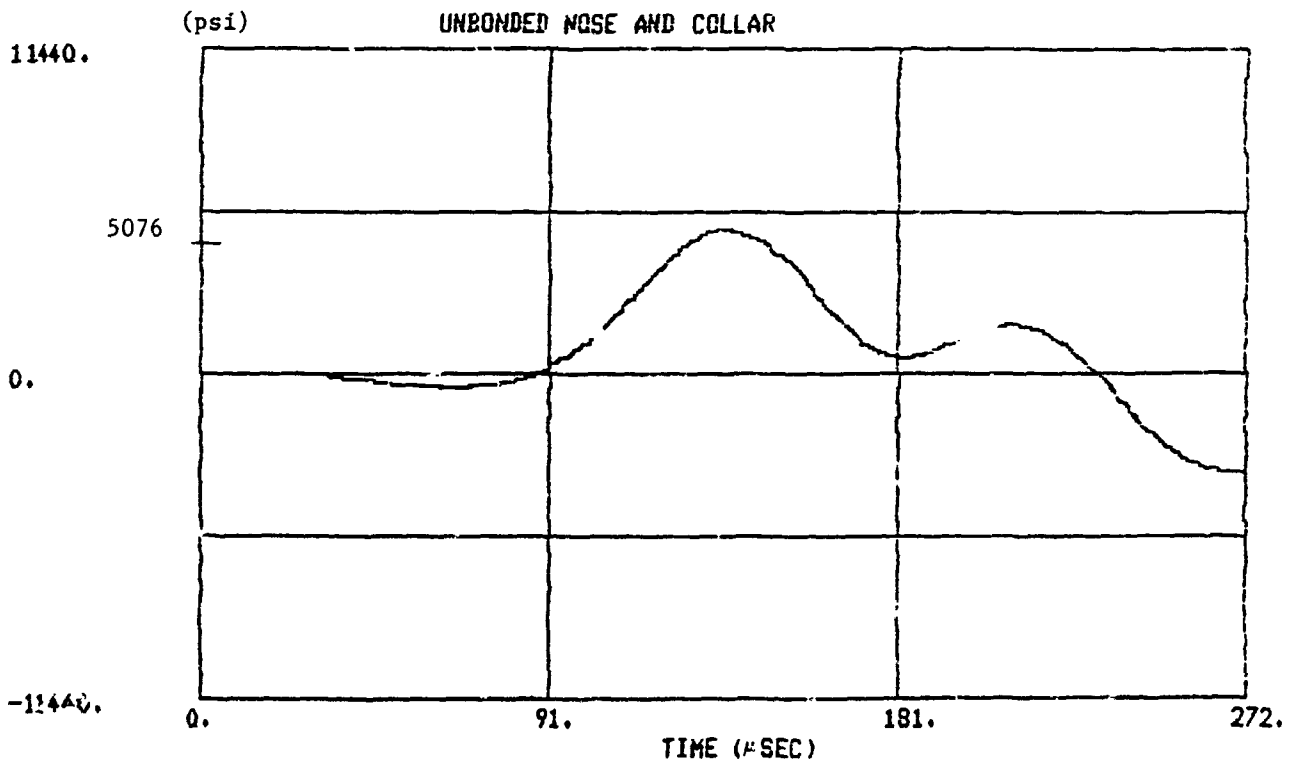
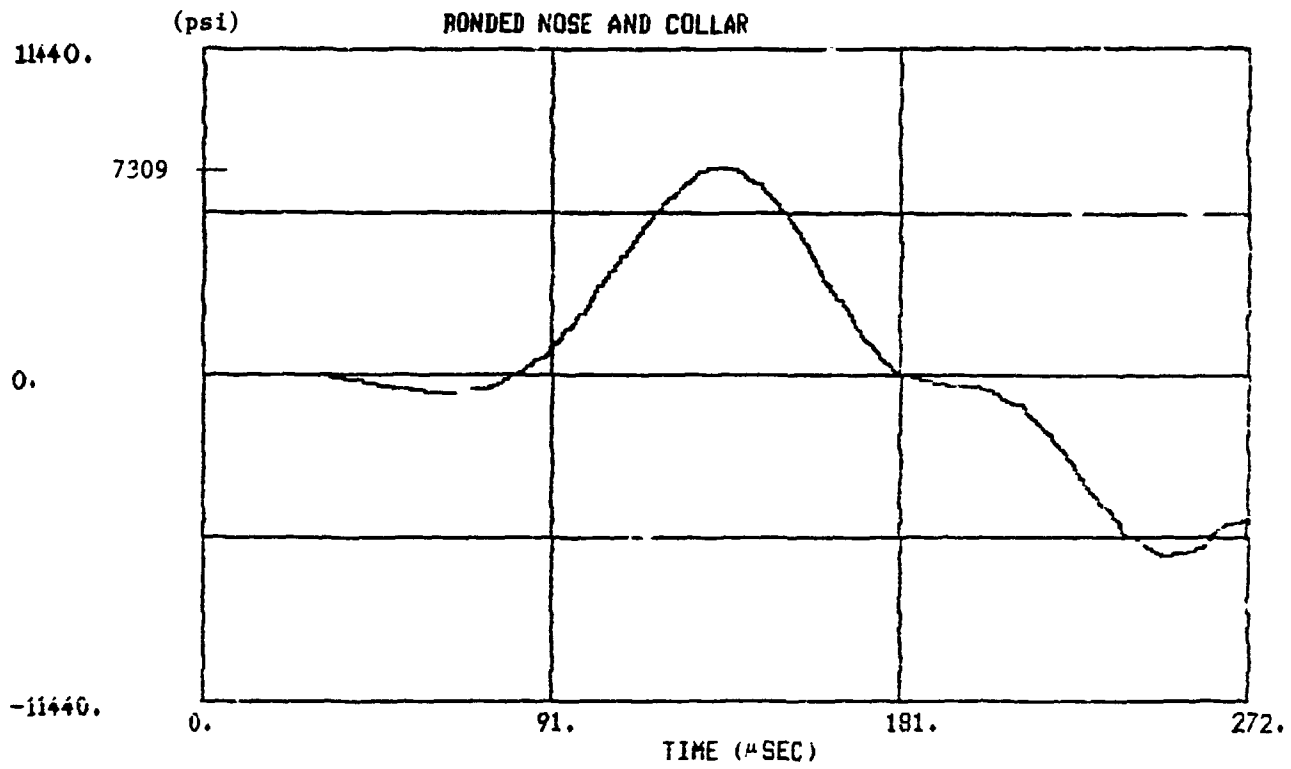


Figure 11 - Dynamic Axial Stresses (Element 105)

N85-25891

TRANSIENT ANALYSIS OF A MAGNETIC HEAT PUMP

Erwin A. Schroeder

**Numerical Mechanics Division
David W. Taylor Naval Ship R&D Center
Bethesda, Maryland 20084**

SUMMARY

An experimental heat pump that uses a rare earth element as the refrigerant is modeled using NASTRAN. The refrigerant is a ferromagnetic metal whose temperature rises when a magnetic field is applied and falls when the magnetic field is removed. The heat pump is used as a refrigerator to remove heat from a reservoir and discharge it through a heat exchanger. In the NASTRAN model the components modeled are represented by one-dimensional ROD elements. The analysis accounts for heat flow in the solids, heat transport in the fluid, and heat transfer between the solids and fluid. The problem is mildly nonlinear since the heat capacity of the refrigerant is temperature-dependent. One simulation run consists of a series of transient analyses, each representing one stroke of the heat pump. An auxiliary program was written that uses the results of one NASTRAN analysis to generate data for the next NASTRAN analysis. Computed results are compared with experimental data.

INTRODUCTION

An experimental heat pump being developed at the David W. Taylor Naval Ship R&D Center (DTNSRDC) uses one or more rare earth elements as the working substance. These elements are ferromagnetic metals whose temperature increases when a magnetic field is applied and decreases when the field is removed. This thermodynamic property is used in a two-stroke cycle to pump heat from a reservoir and discharge it into the surrounding air. Thus, a refrigeration cycle is implied and the heat pump will be referred to as a refrigerator. Using rare earth elements as the refrigerant makes possible magnetic refrigerators that discharge heat at room temperature and refrigerate to very low temperatures. Brown (Reference 1) gives considerations that are required to make magnetic refrigeration practical for such applications and (Reference 2) several configurations that have been proposed for magnetic heat pumps. In the apparatus developed at DTNSRDC, a regenerator serves as the reservoir from which heat is removed and discharged through a heat exchanger. Figure 1 is a schematic description of this test apparatus. Heat is carried by a fluid, compressed nitrogen, that moves through the refrigerator. The refrigerant is formed into thin bands that are wrapped around mandrels to form coils. These coils are formed with gaps between the layers through which fluid can

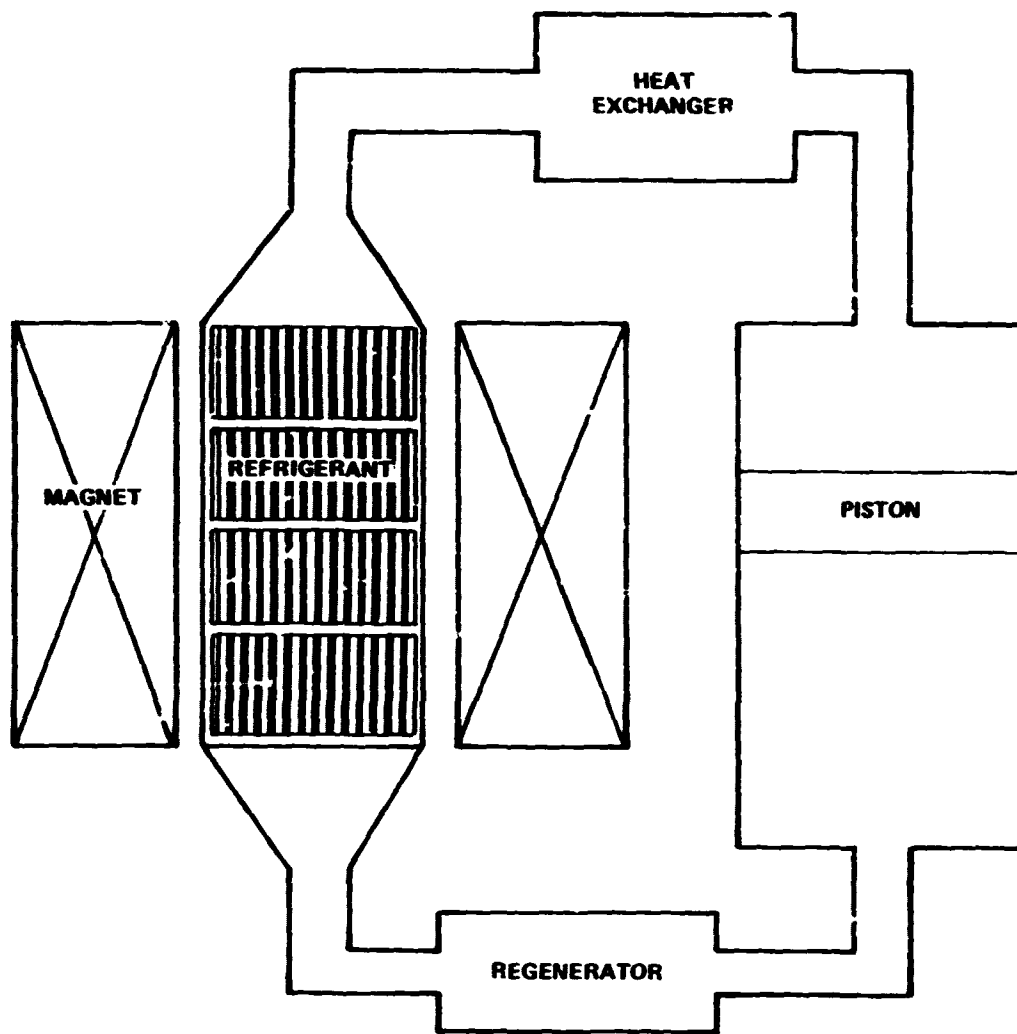


Figure 1. The Magnetic Refrigerator

flow. Several coils are stacked in a stainless steel chamber. The chamber is connected on the cool side to the regenerator and on the warm side to the heat exchanger. The fluid circuit is completed by a cylinder containing a piston that moves the fluid back and forth through the chamber, regenerator, and heat exchanger. The large magnetic field required through the refrigerant is provided

by a superconducting magnet.

The cooling cycle consists of two strokes which will be called the exhaust and intake strokes. During the exhaust stroke the magnetic field is applied to the refrigerant, raising its temperature, and fluid drawn through the cooled regenerator passes over and cools the refrigerant. The heat acquired by the fluid during the exhaust stroke is discharged by a heat exchanger. During the intake stroke, the magnetic field is removed; the temperature of the refrigerant falls, and fluid drawn through the heat exchanger and passing over the refrigerant in the opposite direction is cooled and in turn cools the regenerator.

To achieve very low temperatures, a refrigerator with several stages operating at progressively lower temperatures will be needed. Several rare earth elements or alloys of these elements will be used as refrigerants; each has a temperature range at which it works most effectively. One rare earth element, gadolinium, has its largest temperature change with a change in magnetic field at about 300 K which is near room temperature. Other rare earth metals that may be used are terbium and dysprosium which have largest temperature changes near 225 K and 180 K, respectively.

REQUIREMENTS FOR THE MATHEMATICAL ANALYSIS

Different designs for the refrigerator, using various materials must be tested to determine which configurations and material properties hold the most promise for effective and efficient operation. It is more efficient to model the refrigerator analytically and simulate its operation with different designs and materials than to make coils of various materials and then build and test experimental refrigerators.

Since DTNSRDC has considerable experience with the NASTRAN program, it was decided to use its heat transfer capability for this problem. However, several aspects of the problem make it a non-routine application. The material properties of the refrigerant are sufficiently temperature-dependent in the temperature range used to make the problem nonlinear. Also, each test run of the refrigerator consists of many strokes. Each stroke corresponds to a time segment in the solution with initial conditions different from, but determined, by the final conditions of the previous segment. NASTRAN provides for neither nonlinear material properties nor changing temperature values during a transient analysis. To accommodate these requirements, a sequence of NASTRAN analyses is used, one for each stroke. An auxiliary program HEATSTEP was developed that uses results from the NASTRAN analysis of the previous stroke, computes the initial conditions for the next stroke, and prepares data for the next NASTRAN analysis.

ASSUMPTIONS

A number of simplifying assumptions for the mathematical model keep the analysis manageable. Only the refrigerant, the chamber, and the fluid passing through the chamber are modeled, and a simple approximation is made of the heat capacity of the tubing leading from the chamber to the regenerator. Since the layers of refrigerant and fluid and the stainless steel chamber wall are thin, it is assumed that there is no significant temperature variation through these layers. It is also assumed that there is no significant temperature variation across the chamber. Therefore, the temperature of each type of material is assumed to vary only along the length of the refrigerant chamber, that is, the problem is one-dimensional. Since several seconds are required to apply and remove the magnetic field, it is assumed that at the beginning of each stroke the temperature of the fluid equals the temperature of the refrigerant at the same position. The temperature distribution in the chamber wall is assumed not to change while the magnetic field is changing. The refrigerant coils are stacked one on top of another, so there is a relatively small thermal connection between the coils, and it is approximated by a conductor with a relatively small thermal conductivity.

During the intake stroke the heat exchanger, and during the exhaust stroke the regenerator, are assumed to provide sources of fluid with constant temperatures. Therefore, during the intake stroke, the temperature of the fluid flowing into the refrigerant chamber equals the ambient temperature. Determining the temperature of the fluid entering the chamber during the exhaust stroke is not so straightforward. It is assumed that the temperatures of the fluid and the tubing on the cold side are equal and constant during the exhaust stroke, and at the beginning of the intake stroke the temperature of the cold side is the same as it was during the last exhaust stroke. Therefore, the temperature of the fluid entering the refrigerant chamber during the present exhaust stroke is computed by taking a weighted average of the average temperature of fluid entering the regenerator during the preceding intake stroke and the temperature of fluid leaving the regenerator during the preceding exhaust stroke. In computing the average, these temperatures are weighted by the values of the heat capacity of the fluid moved during one stroke and the heat capacity of the cool side of the apparatus, respectively. The temperature change during one stroke is at most a few degrees, so the temperature-dependent material properties are determined for the initial temperatures for each stroke and remain constant during the stroke.

THE EQUATIONS THAT DESCRIBE THE REFRIGERATOR MODEL

The partial differential equations that describe the temperature distribution in the refrigerant and the chamber wall are one-dimensional heat equations. A loading term on the right hand side represents film convection of heat to the fluid. These equations are of the form

$$\rho_m c_m \frac{\partial T_m}{\partial t} - k_m \nabla^2 T_m = \frac{A h}{V_m} (T_f - T_m)$$

where $m = r, s$ or f for refrigerant, stainless steel or fluid

ρ_m = density of material

c_m = heat capacity of material

k_m = conductivity of material

A_m = area of the surface between the material and fluid

V_m = volume of material

T_m = temperature of material

h = convection coefficient

The partial differential equation that describes the temperature distribution in the fluid is

$$\rho_f c_p \frac{\partial T_f}{\partial t} - k_f \nabla^2 T_f = -\rho_f c_p v \frac{\partial T_f}{\partial x} + \frac{A_r h}{V_f} (T_r - T_f) + \frac{A_s h}{V_f} (T_s - T_f)$$

The term containing $\partial T_f / \partial x$ represents transfer of heat due to the flow of the fluid. The two terms on the right hand side represent film convection to the refrigerant and stainless steel chamber wall. Boundary conditions for the one-dimensional heat equation consist of the initial temperature distribution in the chamber and specified temperatures or derivatives of the temperature at the ends of the chamber. The boundary conditions are provided by the initial temperatures and constraints contained in the NASTRAN input data.

THE FINITE ELEMENT MODEL

The problem is solved using the NASTRAN transient thermal analysis rigid format. The refrigerant, stainless steel, and fluid are modeled by NASTRAN one-dimensional ROD elements. The thermal contacts between the coils of refrigerant are represented by NASTRAN ELAS1 elements. Transfer of heat to and from the fluid from the refrigerant material and the stainless steel chamber is modeled using HBDY elements of type LINE. Figure 2 is a schematic representation of the finite element model.

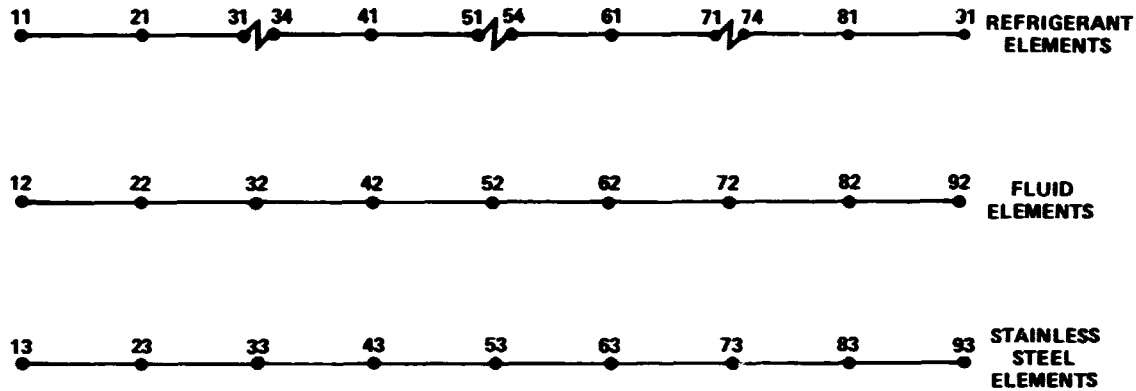


Figure 2. The Finite Element Model

The term in the fluid differential equation containing the spatial derivative of the fluid temperature is obtained by a finite difference approximation using a NASTRAN transfer function. This term is included in the differential equation by applying a load to the appropriate node using the capability for applying nonlinear loads. For example, to compute the finite difference approximation for the fluid node number 32, a value, u_{732} is assigned to an extra point, number 732, by the equation

$$Bu_{732} + A_1 u_{42} - A_2 u_{32} = 0$$

for $u_{732} = (u_{42} - u_{32}) / \Delta x$, where Δx is the distance between adjacent nodes, and u_{32} is the temperature at node number 32, so $B = \Delta x$, $A_1 = -1$, and $A_2 = 1$. The preceding approximation is for fluid flowing in the direction of increasing nodal identification numbers; for fluid flowing in the other direction the approximate value is

$$u_{732} = (u_{32} - u_{22}) / \Delta x$$

The term with $\partial T / \partial x$ is added in the form of a load using a NASTRAN NOLIN card where $u_{732} = \partial T / \partial x$ is the load and $\rho_f c_p v W$ is a scale factor.

The temperature of the fluid entering the chamber is maintained by a large source specified by a TLOAD1 card. The magnitude of this force multiplied by a large scale factor M is given on a DAREA card and applied to a scalar point. A large conductor from the scalar point to ground is specified by an ELAS4 element

that has conductivity equal to the scale factor M. Thus, the value assigned to the scalar point is constrained to equal the input temperature, and then the appropriate fluid grid point temperature is constrained by a multipoint constraint to equal this value. The temperature of the fluid entering the refrigerant chamber is maintained by attaching to the fluid node located where the fluid enters the chamber, a large linear conductor represented by a NASTRAN ELAS4 element, and applying to this node a source of heat with a magnitude that will enforce the required temperature.

THE PROGRAM HEATSTEP

The program HEATSTEP, developed at DTNSRDC, is run after each NASTRAN analysis to prepare data for the following NASTRAN run. To determine the temperatures at the end of the stroke and the average temperature of the fluid leaving the refrigerant chamber during an intake stroke, HEATSTEP reads the file of nodal temperatures produced by NASTRAN. Using this information it computes the temperature drop or rise at each refrigerant node depending on whether the preceding stroke was an intake or exhaust stroke. The program then determines the temperature of each refrigerant and stainless steel node for the beginning of the following stroke. The program also computes heat capacities for each refrigerant element.

HEATSTEP determines the temperature of the fluid that will be passing into the chamber on the following stroke, and selects the fluid grid point to which the incoming fluid temperature constraint is to be applied. This is accomplished by selecting the one of two MPCs which connects the appropriate fluid grid point to the scalar point whose temperature has been specified. For an intake stroke, the temperature of the fluid grid point nearest the heat exchanger is constrained to equal the ambient temperature. The rationale for this average is given in the section on Assumptions. The input temperature T_{IN} is given by the equation

$$T_{IN} = (C_F T_{OUT} + C_T T_{LAST}) / (C_F + C_T)$$

where C_F is the heat capacity of the volume of fluid moved during one stroke and C_T is the heat capacity of the tubing on the cold side; T_{OUT} is the average temperature of fluid leaving the chamber during the preceding intake stroke, and T_{LAST} is the temperature T_{IN} for the last exhaust stroke.

Finally, HEATSTEP prepares an input file for the next NASTRAN run that incorporates the new data it has computed.

RESULTS AND DISCUSSION

Several analyses were made using this method. Some of these analyses were made to get relative indications of the performance of proposed configurations. One analysis modeled the experimental device; results from this analysis are plotted in Figure 3.

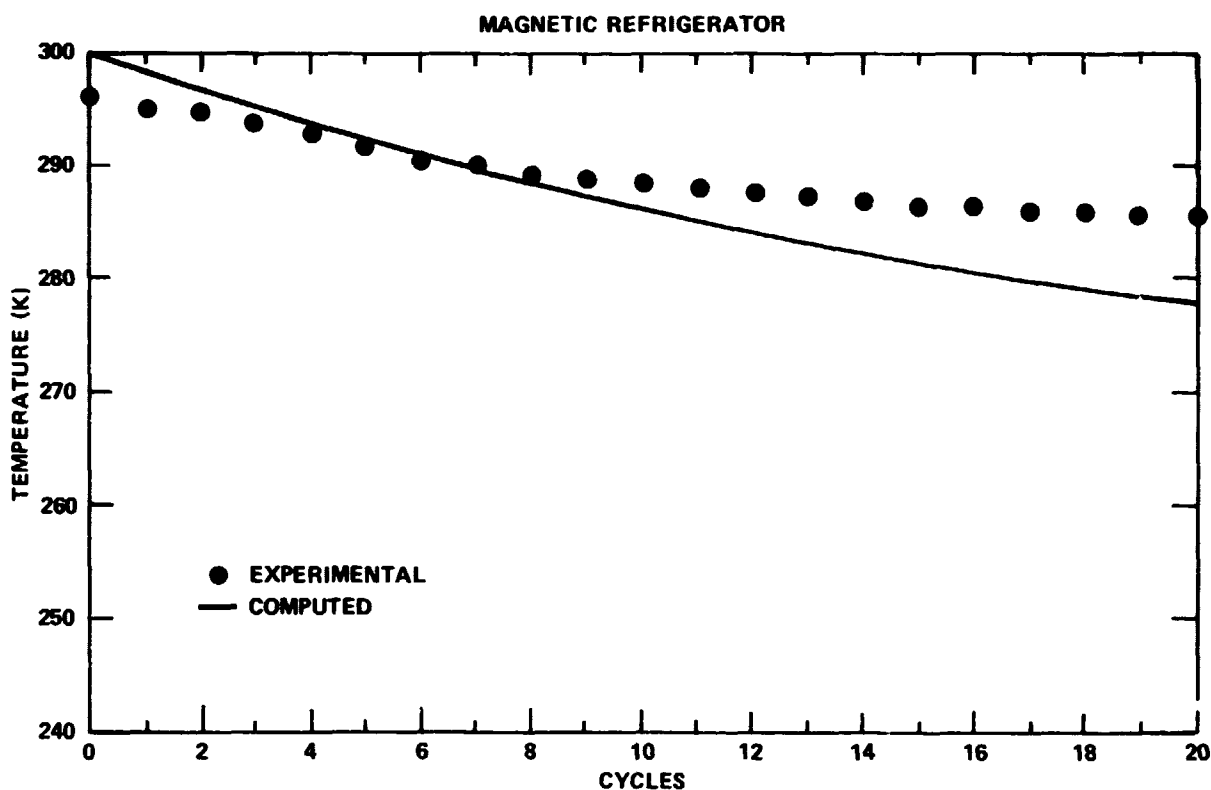


Figure 3. Comparison of Computed and Experimental Temperatures

Several factors may contribute to improving agreement between the computed and experimental results. To avoid penetrating the pressurized chamber, thermocouples were mounted on the outside surface of the stainless steel refrigerant chamber. Steps are being taken to move the thermocouples inside the chamber to more accurately record the temperature of the refrigerant and fluid. The finite element model uses a simple representation of the regenerator and probably its heat capacity is under represented; a larger heat capacity would likely slow the temperature

drop, producing better agreement in the results. It is also likely that better values may be obtained for the film convection coefficients and thermal conductivity of the contact between refrigerant coils. These improvements will be made during future work.

REFERENCES

1. Brown, G. V., "Magnetic Heat Pumping Near Room Temperatures," J. Appl. Phys., Vol. 47, pp. 3673-3680 (1976).
2. Brown, G. V., "Basic Principles and Possible Configurations of Magnetic Heat Pumps," ASHRAE Transactions, Vol. 87, Part 2, pp. 783-793 (1981).

1. Report No. NASA CP-2373	2. Government Accession No.	3. Recipient's Catalog No.	
4. Title and Subtitle Thirteenth NASTRAN® Users' Colloquium		5. Report Date May 1985	6. Performing Organization Code
		8. Performing Organization Report No.	10. Work Unit No.
7. Author(s)	9. Performing Organization Name and Address COSMIC, NASA's Computer Software Management and Information Center The University of Georgia Athens, GA 30602		11. Contract or Grant No.
12. Sponsoring Agency Name and Address National Aeronautics and Space Administration Washington, D.C. 20546			13. Type of Report and Period Covered Conference Publication
15. Supplementary Notes Available from COSMIC, Athens, GA 30602			
16. Abstract This publication is the proceedings of a colloquium, and it contains technical papers contributed during the Thirteenth NASTRAN® Users' Colloquium held in Boston, Massachusetts on May 6-10, 1985. The authors review general application of finite element methodology and the specific application of the NASA Structural Analysis System, NASTRAN, to a variety of static and dynamic structural problems.			
17. Key Words (Suggested by Author(s)) NASTRAN Structural Analysis Structures Finite Element Analysis Colloquium		18. Distribution Statement Unclassified - Unlimited Subject Category 39	
19. Security Classif. (of this report) Unclassified	20. Security Classif. (of this page) Unclassified	21. No. of Pages 462	22. Price A20